



THE STRENGTH OF SLENDER BRICK WALLS

by

D.C. Payne, B.E. (Hons.)

A Thesis presented to the Faculty of Engineering  
of the University of Adelaide for the  
Degree of Doctor of Philosophy

Civil Engineering Department  
University of Adelaide

January, 1982.

CONTENTS

	Page
LIST OF FIGURES	v
LIST OF TABLES	ix
SUMMARY	xi
DECLARATION	xiii
ACKNOWLEDGEMENTS	xiv
PRINCIPAL NOTATION	xv
CHAPTER 1 INTRODUCTION	1
CHAPTER 2 STRUCTURAL BRICKWORK — A SYNOPSIS	5
2.1 The Development of Structural Brickwork	5
2.2 Load Transmission in Structural Brickwork	10
2.3 A Study of a Structural Brickwork Building	13
2.4 Summary of the Principles of Structural Brickwork	15
2.5 Stability and Progressive Collapse of Structural Brickwork	16
2.6 The Behaviour of Brickwork Under Seismic Load	18
2.7 Reinforced Masonry	20
2.8 Economics of Structural Brickwork	20
CHAPTER 3 LITERATURE REVIEW	22
3.1 Clay Bricks	23
3.2 Masonry Mortar	29
3.3 Brick-Mortar Combination — Small Assemblages	44
3.3.1 Introduction	44
3.3.2 Compressive strength	44
3.3.3 Axial and flexural tensile strength across the bedjoints	66
3.3.4 Flexural strength across the perpend	72
3.3.5 Elastic properties of small assemblages	83
3.4 Analysis of Brick Walls and Panels	96
3.4.1 Analysis of columns with no tensile strength	96
3.4.2 Comparison of experiments with no-tension material column theory	108
3.4.3 Theory of panels simply-supported on four sides	112
3.4.3 Experiments on panels under vertical load	119
3.4.4 Summary	119
CHAPTER 4 THE ANALYSIS OF BRICKWORK WALLS IN ONE-WAY BENDING	121
4.1 Introduction	121
4.2 The Stiffness and Geometric Properties of Partially-cracked Brickwork Walls	121
4.3 Load-deflection Relationships and Equations of Equilibrium	141

	Page
4.4 Solution Procedure	149
4.5 Results of the Numerical Method	157
4.6 Summary and Conclusions	166
 CHAPTER 5 EXPERIMENTS ON WALLS IN ONE-WAY BENDING	 170
5.1 Stiffness Experiments	170
5.1.1 Experimental verification of curvature ratio factor, $\alpha$	170
5.1.2 An effective elastic modulus for uncracked brickwork under eccentric compression	172
5.1.3 The stiffness of partially-cracked brickwork	185
5.2 Wall Experiments	188
5.2.1 Tests on a slender steel block column	188
5.2.2 Tests on brickwork walls	196
 CHAPTER 6 THE ANALYSIS OF BRICKWORK PANELS IN TWO-WAY BENDING	 228
6.1 Introduction	228
6.2 The Stiffness of Partially-cracked brickwork panels	229
6.2.1 An analytical element for panels	229
6.2.2 Bending normal to the bedjoints	229
6.2.3 Bending parallel to the bedjoints	236
6.2.4 Torsion in brickwork	250
6.3 Equation of Equilibrium and Load-deflection relationships for a plate of varying thickness	260
6.3.1 The equation of equilibrium	260
6.3.2 Constitutive relationships	263
6.3.3 Finite difference formulation	267
6.3.4 Boundary conditions	269
6.4 Solution Procedure	273
6.5 Results of the Numerical Method	275
6.6 Summary and Conclusions	278
 CHAPTER 7 EXPERIMENTS ON BRICKWORK PANELS	 280
7.1 Introduction	280
7.2 Brickwork Panels subjected to Bending Parallel to the Bedjoints	280
7.3 A Simply-supported Panel in Two-way Bending	292
7.3.1 Introduction	292
7.3.2 Experimental apparatus	293
7.3.3 Brickwork material properties	305
7.3.4 Panel experiment results	309
7.3.5 Summary	322
 CHAPTER 8 COMPARISONS OF THEORETICAL RESULTS WITH DESIGN CODE SPECIFICATIONS	 324
8.1 Brickwork Walls -- PROGRAM PIER1	325
8.1.1 Walls loaded with equal end eccentricities in one-way bending	326

	Page
8.1.2 Walls loaded with unequal end eccentricities	330
8.1.3 Effect of initial imperfections	333
8.1.4 Summary	336
8.1.5 Brick-on-edge partition walls	338
8.2 Brickwork Panels in Two-way Bending – PROGRAM PANEL1	338
8.2.1 Panels loaded with equal load eccentricities	343
 CHAPTER 9 SUMMARY AND RECOMMENDATIONS	 346
 <u>APPENDICES</u>	
A The Brick Curvature Function, $\alpha$ (Equation (4.2))	351
B An Idealized Non-linear Mortar Subject to Eccentric Compression	355
C Brickwork Walls in One-way Bending – PROGRAM PIER1	369
D Brickwork Prism Tests and Non-linear Properties of Mortar (Section 5.2.2.4(b))	407
E Three-dimensional Finite Element PROGRAM MFYDCP	412
F Derivation of Panel Equations	447
G Brickwork Panels in Two-way Bending – PROGRAM PANEL1	456
 BIBLIOGRAPHY	 476

LIST OF FIGURES

<u>FIGURE</u>	<u>Page</u>
2.1 Conventional Load-bearing Brickwork	7
2.2 Structural Brickwork – Wall Arrangement	9
2.3 In-plane Shear Caused by Lateral Loads	9
2.4 Stresses in Wall Due to Vertical and Lateral Loads	12
2.5 Assumed Cantilever Action of High-rise Brickwork Structure	12
2.6 Floor Plan of Residential Blocks at the University of Essex	14
2.7 Quetta Bond	14
3.1 Relationship between Elastic Modulus and Compression Strength	28
3.2 Stress-strain Curve for Brick	28
3.3 Mortar Composition, Compressive Strength and Water Retentivity	35
3.4 Relationship between Mortar Composition, Average Compressive Strength and Water Retentivity	35
3.5 Mortar Mixes for Brickwork	36
3.6 Stress-strain Diagrams for Mortars	39
3.7 Stress-strain Curve for Mortar	39
3.8 Stress-strain and Poisson's Ratio-strain for Mortar	40
3.9 Compression Tests on Brickwork Prisms	40
3.10 Relationships between Mortar Strength and Elastic Modulus	42
3.11 Mortar Cube Strength Related to Dynamic Elastic Modulus	42
3.12 Strength Correction Factors for Brickwork Prisms	47
3.13 Relationship between Brick Strength and Strength of Brickwork Prisms	47
3.14 Stress Distribution in a Brickwork Prism	53
3.15 Values of Nonuniformity Coefficient, U	53
3.16 Failure Theory for Brickwork	55
3.17 Failure Envelope for Bricks	58
3.18 Failure Envelope for Brick Material	58
3.19 Graphical Solution for Brickwork Prism Compressive Strength	59
3.20 Brick and Mortar Stresses due to Applied Compressive Load	61
3.21 Theoretical Failure Envelope Relating Tensile and Compressive Stresses in Brick at Failure	61
3.22 Variation of Brickwork Prism Strength with Mortar Joint Thickness	64
3.23 Relationship between Mortar Strength and Curing Time	64
3.24 Effect of Water-Cement Ratio on Tensile Bond and Mortar Compressive Strength	69
3.25 Relationships between Tensile Bond Strength and Brick Suction (I.R.A.)	69
3.26 Relationship between Brickwork Shear Strength and Vertical Precompression	75
3.27 Failure Relationships for Combined Shear and Normal Compression along the Bedjoint	75
3.28 Failure Modes for Model Brickwork	77
3.29 Mechanism of Failure for Brickwork Subjected to Horizontal Bending	77
3.30 Strength Ratio Related to Bedjoint Bond Strength	81
3.31 Bending Tests on Model Brickwork Prisms	86
3.32 Bending Tests on Full-scale Brickwork Panels	86

	Page
<b>FIGURE</b>	
3.33 Bending Tests on Model Brickwork Panels	87
3.34 Stress-strain Curves for Brick and Brickwork Prisms	90
3.35 Stress-strain Relationships for Brickwork Piers	90
3.36 Average Stress-strain Curves in Shear for Brickwork Panels	94
3.37 A Column Without Tensile Strength	97
3.38 Assumed Stress-strain Relationship for Non-linear Material	97
3.39 Load-deflection Curves for Columns with Eccentric Load	102
3.40 Modes of Final Collapse	102
3.41 Column Deflection Immediately Prior to Collapse	104
3.42 Angles of Rotation of, and Edge Stresses in, a Wall having no Tensile Strength	107
3.43 Load Tests on Slender Walls	111
3.44 Plate Subjected to Uniform Compression	114
3.45 Buckling Loads of a Plate Simply-supported on Four Sides	114
3.46 Simply-supported Plate Subjected to Uniform Moments on Two Opposite Sides	116
4.1 Cracking on a Bedjoint Caused by the Position of the Vertical Load Resultant	122
4.2 Analysis of Cracked Brickwork	124
4.3 Flexural Stiffness Curves	127
4.4 Relationship between Curvature Ratio and Load Eccentricity	129
4.5 Relationship between Curvature Ratio and Brick Aspect Ratio	130
4.6 Stress Distribution for Load Eccentricity $d/3$	133
4.7 Mortar Stress Distributions for Load Eccentricity $d/3$	134
4.8 Stress-strain Relationship for an Axially-loaded Mortar Bedjoint	134
4.9 Stress and Strain Distributions for Cracked Non-linear Mortar	136
4.10 Stress and Strain Distribution for Uncracked Non-linear Mortar	136
4.11 Brickwork Curvatures	139
4.12 Effective Section Depth for No-tension Material Column	142
4.13 Column Loads, Reactions and Displacements	147
4.14 Wall Load and Support Conditions	150
4.15 Finite Difference Subdivision	151
4.16 Wall Load-displacement Curves (PROGRAM PIER1)	160-163
5.1 Test for Strain Profiles in Steel Blocks	171
5.2 Steel Block Compressed with Load Eccentricity $d/5$ (Nominal)	173
5.3 Steel Block Compressed with Load Eccentricity $d/3.5$ (Nominal)	174
5.4 Steel Block Compressed with Load Eccentricity $d/3$ (Nominal)	175
5.5 Steel Block Column Showing Martens Mirror Extensometer	176
5.6 Test Apparatus for Determining Brickwork Elastic Modulus	179
5.7 Brick and Mortar Prisms	182
5.8 Load-strain Curves for Brick and Mortar Prisms	183
5.9 Steel Block Column Loaded Inside Clear Acrylic Tube	190
5.10 Load Tests on Pin-end Steel Block Column	192
5.11 Load Tests on Fixed Base Steel Block Column	194
5.12 Brickwork Walls	198

	Page
<b>FIGURE</b>	
5.13 Grading Curve for Sand in Brickwork Walls	200
5.14 1416mm High Wall Tests	203
5.15 1416mm Wall Loaded Eccentrically at the Top (Base Fixed Against Rotation)	206
5.16 Load Displacement Relationships for 1416mm Height Fixed Base Walls (Wall No. 2)	207
5.17 Load-rotation Relationship for 1416mm High Wall with Fixed Base	208
5.18 Initial Displacement Profiles for 1416mm Walls with Fixed Base; Top Load Eccentricity $d/6$	210
5.19 Initial Displacement Profiles for 1416mm Walls with Fixed Base; Top Load Eccentricity $d/3$	211
5.20 Initial Displacement Profiles for 2714mm Walls with Fixed Base; Top Load Eccentricity $d/6$	213
5.21 Initial Displacement Profiles for 2714mm Walls with Fixed Base; Top Load Eccentricity $d/3$	214
5.22 Vertical Splitting Failure (Wall 6)	218
5.23 Spalling Failure (Wall 8)	218
5.24 Spalling Failure (Wall 4)	219
5.25 2714mm Walls Loaded at an Eccentricity of $d/6$	221
5.26 2714mm Walls Loaded at an Eccentricity of $d/3$	222
5.27 1416mm Walls Loaded at an Eccentricity of $d/6$	223
5.28 1416mm Walls Loaded at an Eccentricity of $d/3$	224
6.1 Brickwork Panel Module	230
6.2 Finite Element Details	232
6.3 Bedjoint Cracking in Panel Module	233
6.4 Panel Module Subjected to Bending Normal to the Bedjoints	234
6.5 Brickwork Dimensions	237
6.6 Bending of Panel Module Parallel to the Bedjoints	237
6.7 Relative Flexural Stiffness for Various Brick-Mortar Modular Ratios	239
6.8 Simulated Flexural Cracking at the Perpend Joint	242
6.9 Distribution of Flexural Stresses on X-Y Planes for Brickwork with Cracking on Perpend Only	243-247
6.10 Possible Combinations of Perpend and Bedjoint Cracking	249
6.11 Panel Module Subjected to Pure Twist	252
6.12 Subdivision of Brickwork into Panel Modules	254
6.13 Variation of Twisting Moments with Modular Ratio	256
6.14 Functions $F_1$ and $F_2$	256
6.15 Varying Thickness Plate Element	261
6.16 Finite Difference Mesh	268
6.17 Panel Loading Details	268
6.18 Finite Difference Mesh for Simply-supported Panel	271
6.19 Quadratic Extrapolation for Displacement of Corner Fictitious Node	271
6.20 Buckling Failure Loads of Cracked Brickwork Panels	277
7.1 Small Panel Details	284-285
7.2 Moment-curvature Relationship for Uncracked Brickwork Panels	286
7.3 Moment-curvature Relationships for Small Panel	288
7.4 Brickwork Panel Failure Mode	291
7.5 Full-scale Brickwork Panel Experiment	294-297
7.6 Method of Laying Bricks in Panel	300

	Page
<b>FIGURE</b>	
7.7	Grouting of Brickwork into Top Edge Channels 301
7.8	Jack Calibration Curves 303
7.9	Positions of Gauges on Brickwork Panel (East Elevation) 304
7.10	Instrumentation Block Diagram 306
7.11	Test for Brickwork Bond Strength 310
7.12	Comparison between Experimental and Calculated Lateral Displacements 312
7.13	Load — Central Displacement Curves for Brickwork Panel 314
7.14	Lateral Displacements of Brickwork Panel 316
7.15	Crack Patterns in Brickwork Panel 317
7.16	Lateral Displacement Contours Prior to Failure 318-319
7.17	Load Displacement Contours for Load 178N/mm 319
8.1	Failure Loads for Walls Loaded at Equal End Eccentricities 327
8.2	Failure Loads of Walls Loaded Eccentrically at the Top and Concentrically at the Base 332
8.3	Failure Loads of Fixed Base Brick-on-flat Walls Loaded Eccentrically at the Top 334
8.4	Failure Loads of Walls Loaded Eccentrically on Opposite Sides of the Wall Centreline 335
8.5	Failure Loads of Walls with Initial Imperfections 337
8.6	Failure Loads of Brick-on-edge Partition Walls 339
8.7	Modes of Failure for a Brickwork Panel 341
8.8	Failure Loads for Panels Simply-supported on Four Sides (Brick-on-edge Construction) 344
A.1	Scale Model of Function, $\alpha$ 354
B.1	Stress-strain Relationship for Non-linear Mortar (Bedjoint Cracked) 356
B.2	Stress-strain Relationship for Non-linear Mortar (Bedjoint Uncracked) 356
B.3	Partially Cracked Mortar Joint (Non-linear Mortar) 360
B.4	Partially Cracked Mortar Joint (Linear Mortar) 360
B.5	Uncracked Mortar Joint (Linear Mortar) 364
B.6	Uncracked Mortar Joint (Non-linear Mortar) 364
C.1	Cases which may be Solved by using PROGRAM PIER1 370
D.1	Brickwork Prism Subject to Eccentric Load 408
D.2	Failure of Brickwork Prisms in Axial Compression 408
E.1	Side Elevation of Panel Module 414
E.2	End Elevation of Panel Module 415
F.1	Varying Thickness Plate Element 448
G.1	Simply-supported Brickwork Panel showing Load Conditions for PROGRAM PANEL1 457



LIST OF TABLES

<u>TABLE</u>	<u>Page</u>
3.1 Mortar Mix Proportions	30
3.2 Optimum Sand Particle-size Distribution	32
3.3 Mortar Water-to-Cement Ratios	34
3.4 Brick and Mortar Combinations	52
3.5 Bond Strength in Brickwork Prisms	67
3.6 Elastic Modulus for Bending Across the Bedjoints	85
3.7 Elastic Modulus for Bending Across the Perpend	88
3.8 Column Failure Load Parameters for Equation (3.64)	99
3.9 Moments and Deflections for a Simply-supported Plate	117
4.1 Flexural Stiffness Values	128
4.2 Curvature Ratio, $\alpha$	128
4.3 Wall Properties for PROGRAM PIER1	158
4.4 Buckling Failure Loads for Pin-end Walls of Linear Material	165
4.5 Buckling Failure Loads for Fixed Base Walls of Linear Material	165
4.6 Buckling Failure Loads for Pin-end Walls of Non-linear Material	166
4.7 Check on Failure Loads of Brickwork Walls Computed by Different Versions of PROGRAM PIER1	167
5.1 Comparison of Curvature Factors, $\alpha$	177
5.2 Experimental Elastic Modulus for Brickwork	181
5.3 Calculated Elastic Modulus Values for Brickwork	184
5.4 Elastic Modulus Values for Brick Prisms	186
5.5 Elastic Modulus Values for Mortar Prisms	187
5.6 Relative Stiffness of Cracked and Uncracked Brickwork Prisms	188
5.7 Column End Conditions and Load Eccentricities	191
5.8 Buckling Failure Loads and Displacements of Pin-end Column	193
5.9 Buckling Failure Loads for Fixed Base Columns	195
5.10 Brickwork Wall Dimensions	197
5.11 Brick Elastic Modulus	201
5.12 Mortar Elastic Modulus	201
5.13 Brickwork Elastic Modulus	202
5.14 Changes in Slope at Top of 1416mm High Walls	209
5.15 Positions of Dial Gauges for Tall (2714mm) Walls	212
5.16 Changes in Slope at Top of 2714mm High Walls	215
5.17 Wall Failure Loads and Failure Modes	217
5.18 Experimental and Theoretical Failure Loads for Brick- work Walls	225
6.1 Stiffness of Brickwork Subject to Bending Normal to the Bedjoints	235
6.2 Flexural Stiffness of Brickwork Subject to Bending Parallel to the Bedjoints	240
6.3 Flexural Stiffness of Brickwork	241
6.4 Flexural Stiffness of Brickwork	248

TABLE

6.5	Panel Module Subjected to Pure Twist	255
6.6	Torsional Stiffness of Cracked Brickwork	258
6.7	Torsional Stiffness of Cracked Brickwork	260
6.8	Buckling Loads of Brickwork Panels and Walls	278
7.1	Brick Elastic Modulus	281
7.2	Mortar Elastic Modulus	282
7.3	Brickwork Compressive Strength	282
7.4	Ratio of Applied Moment: Curvature in Horizontal Plane	287
7.5	Relative Horizontal Stiffness of Brickwork Panel	289
7.6	Strengths of Brickwork Panels in Horizontal Bending	290
7.7	Brick Elastic Modulus	307
7.8	Mortar Elastic Modulus	307
7.9	Brickwork Elastic Modulus	308
7.10	Brickwork Prism Compressive Strength	308
7.11	Brickwork Flexural Bond Strength	309
8.1	Material Properties for Parametric Study on Brickwork Walls	325
8.2	Wall Support and Loading Conditions	331
A.1	Coefficients for Function $\alpha_1$	351
A.2	Coefficients for Function $\alpha_2$	352
D.1	Compression Failure of Brickwork Prisms	407
D.2	Constants in Equation (B.1) for Various Exponents, n	409

## SUMMARY

Brickwork is commonly used as a load-bearing component in both low-rise domestic buildings and high-rise structures. Analytical investigations conducted in the past on the strength of brick walls have been based on the assumptions that a brickwork wall or panel behaves as a column regardless of any vertical edge support conditions and that no tension stresses can exist in the assumed column. These simplifying assumptions do not reflect the actual behaviour of real brickwork and consequently have led to conservative predictions for wall strengths.

The work presented in this thesis has approached more closely the real behaviour of brickwork by observing that even for a stress distribution in which there are no tensile stresses at the brick-mortar interfaces, the stresses in the bricks themselves can be significant. For walls supported only at the top and bottom, equations are derived for an equivalent column of varying thickness by using a two-dimensional finite element method to calculate the bending stiffness of a brick-mortar module in which cracking may occur at the brick-mortar interfaces. It is assumed that the brick material is linearly elastic and the mortar is either linearly elastic or non-linear with a specified stress-strain relationship. For panels supported on four sides, equations are derived for an equivalent plate of variable thickness in which both the brick and mortar materials are assumed to be linearly elastic. The plate stiffness properties are determined by using a three-dimensional finite element method to analyse a brickwork module in which cracking may occur at the horizontal and vertical brick-mortar interfaces. Both the equivalent column equations and the

equivalent plate equations are written in finite difference form and are solved by using Newton-Raphson iteration.

Experiments conducted on a steel block column, brickwork prisms and a series of full-scale brickwork walls are described, and a full-scale test on a brickwork panel simply-supported on four sides is presented. All experimental results indicate that the numerical approach closely reflects the real behaviour of brickwork.

A brief review of Codes of Practice is given in which specified design loads are compared with load capacities calculated using the equivalent column and equivalent plate equations. The comparisons show that, generally for walls of high slenderness, Code requirements lead to conservative predictions of wall and panel strength. Further, it is demonstrated that the methods of analysis may be used as a basis for modifying existing Code recommendations related to the design of vertically-loaded slender brickwork walls and panels.

DECLARATION

This thesis contains no material which has been accepted for the award of any degree or diploma in any University and, to the best of the candidate's knowledge and belief, contains no material previously published or written by another person, except where due reference is made in the text.

David C. Payne

## ACKNOWLEDGEMENTS

The investigation described in this thesis was carried out in the Civil Engineering Department of the University of Adelaide.

The author wishes to acknowledge the assistance and advice he received from his supervisors Dr D.S. Brooks, Reader in Civil Engineering, and Dr G. Sved, Honorary Visiting Research Fellow in Civil Engineering. The work has been made possible through their dedicated interest in the project and their guidance during the preparation of the manuscript.

The experimental equipment was built in the Engineering Workshops of the University of Adelaide under the direction of Mr W.C. Hunter. Laboratory assistance was provided principally by Mr R. Taylor and Mr P. de Maria under the direction of the author and the laboratory manager, Mr H.F. Tabalotny.

The author also wishes to acknowledge the assistance given in the computing work by Dr M.F. Yeo, Senior Lecturer in Civil Engineering, and Mr R.C.L. Flint, a postgraduate student in Civil Engineering, who wrote some of the plotting software used in the panel experiment.

Mr S.D. Bushnell and Mr H. Middlemis developed the apparatus used for testing small brickwork panels subjected to combined horizontal bending and vertical compression as portion of an undergraduate project, directed by Dr D.S. Brooks.

PRINCIPAL NOTATION

b	Thickness of a mortar joint (Chapter 6), width of a wall (Chapter 3)
C	Compressive strength of a brick (MPa)
d	Thickness of an uncracked brickwork wall or panel
$d_c$	Depth of the uncracked part of a mortar-bedjoint (Chapter 4)
$d_p$	Distance of the vertical load resultant from the wall face at which the vertical compressive stress is a maximum (Chapter 4)
dx, dy	Dimensions of an equivalent plate element
D	Modulus of rigidity of plate = $\frac{Et^3}{12(1-\nu^2)}$
$e, e_c, e_o, e_0, e_1, e_2, e_n, e_N$	Effective vertical load eccentricity
$(e_o/d)$	Non-dimensional vertical load eccentricity for the brickwork wall module (Chapter 4)
E	Elastic modulus for a column or isotropic plate
$E'_x, E'_y, E''$	Elastic moduli for an orthotropic plate (Timoshenko <sup>(112)</sup> )
$E_b$	Elastic modulus for a brick
$E_{br}$	Initial tangent modulus for brickwork
$E_m$	Initial tangent modulus for mortar
$E_x, E_y$	Elastic moduli for an isotropic plate
$E_x(t), E_y(t)$	Elastic moduli for an equivalent plate of varying thickness
$(EI)_{eq}$	Equivalent stiffness of a brickwork wall module (Chapter 4)
$F_1, F_2$	Functions for brickwork subjected to uniform twist (Chapter 6)
$F'_m$	Brickwork compressive strength (Chapter 3)
G	Shear modulus for an isotropic plate
$G(t)$	Shear modulus for an equivalent plate of varying thickness
h	Height of a brickwork wall or panel

$h_b$	Height of a brick (Chapter 4)
$(h_b/d)$	Non-dimensional aspect ratio for a brick
$h_m$	Thickness of a mortar joint (Chapter 4)
H	Horizontal support reaction (Chapter 4); Height of a brick (Chapter 6)
$i, j$	Coordinates of finite difference mesh (Chapter 6)
I	Brickwork section second moment of area per unit length of wall = $\frac{d^3}{12}$
[J]	Jacobian matrix
K	Constant for non-linear mortar stress-strain relationship
$l$	Length of a brickwork panel; length of a finite difference element
L	Length of a brick (Chapter 6)
$(m-1), m, (m+1)$	Finite difference coordinates
$M_e$	Effective moment of the load resultant about the centre-line of the uncracked part of a bedjoint of a linear mortar
$M_x, M_y$	Bending moments per unit width of a plate
$M_{xy}, M_{yx}$	Twisting moments per unit width of a plate
$\bar{M}_{yz}, \bar{M}_{zy}$	Total twisting moments on the faces of a panel module (Chapter 6)
$n$	Exponent for non-linear mortar stress-strain relationship
$(n-1), n, (n+1)$	Finite difference coordinates
N	Number of finite difference elements in the wall analysis (Chapter 4)
$N_x, N_y, N_{xy}$	In-plane forces per unit width of a plate
$(N_y)_{cr}$	Critical load per unit length for a plate subjected to uniform vertical compression
p	Thickness of a perpend joint (Chapter 6)
P	Vertical load resultant per unit length of a wall
$P_f$	Vertical load resultant per unit length of a wall at failure



$P_{crit}$	Euler buckling load per unit length of a pin-end wall = $\frac{\pi^2 E_{br} d^3}{12h^2}$
$q$	Uniform lateral load acting on a plate or panel (Chapter 6)
$\left(\frac{1}{R}\right)_{av}$	Average curvature of brickwork wall module
$\left(\frac{1}{R}\right)_b$	Curvature of a brick
$\left(\frac{1}{R}\right)_m$	Curvature of a mortar bedjoint
$\left(\frac{1}{R}\right)_{nt}$	Curvature of a no-tension material
$[R]$	Matrix used for calculating function $\alpha$ (Equation (4.2))
$t$	Thickness of an equivalent plate of varying thickness (Chapter 6)
$u$	Displacement in the X-direction
$v$	Displacement in the Y-direction
$w$	Displacement in the Z-direction
$W$	Uniform vertical load per unit length of a brickwork panel
$X$	Principal axis
$X_n$	Distance of node $n$ from top of wall (Chapter 4)
$y$	Lateral displacements of a column
$Y$	Principal axis
$Z$	Principal axis
$\alpha, \alpha(e_o/d, h_b/d)$	Stiffness function for cracked brickwork (Chapter 4)
$\gamma_{xy}$	Shear strain in an isotropic plate
$\delta$	Prescribed lateral displacements for a brickwork wall
$\epsilon$	Normal strain
$\epsilon_x, \epsilon_y, \epsilon_z$	Normal strains in directions of principal axes
$\phi$	Prescribed rotations for brickwork modules (Chapter 4, Chapter 6)

$\{\eta\}$	Error vector in a brickwork wall analysis (Chapter 4)
$\{\xi\}$	Error vector in a brickwork panel analysis (Chapter 6)
$\sigma$	Normal stress
$\sigma_x, \sigma_y, \sigma_z$	Normal stresses in directions of principal axes
$\sigma_a$	Axial compression stress in a panel (Chapter 8)
$\sigma_b$	Bending stress normal to the bedjoints in a panel (Chapter 8)
$\sigma_{bt}$	Transverse bending strength of a brick
$\sigma'_{bt}$	Transverse bending strength of brickwork
$\sigma_c$	Mortar strength in triaxial compression; brickwork compressive strength (Chapter 4)
$\sigma_t$	Tensile strength of a brick
$\sigma_{45}$	Normal tensile stress at 45 degrees to the bedjoints (Chapter 7, Chapter 8)
$\tau$	Shear stress
$\nu$	Poisson's ratio for an isotropic plate
$\nu_{xy}, \nu_{yx}$	Poisson's ratios for an orthotropic plate
$\nu_b$	Poisson's ratio for a brick
$\lambda h$	Effective height of a brickwork wall (Chapter 3, Chapter 4)
$(\Omega l)$	Height of a finite difference element (Chapter 6)
$\rho$	Curvature ratio factor for a non-linear mortar (Appendix B)



## 1. INTRODUCTION

Brickwork has been a common form of building construction from the times of civilizations which existed several thousands of years B.C. Today it remains a popular material, particularly in residential construction because of its durability, its acoustic and insulation properties, its natural resistance to fire and its general aesthetic appeal.

In Australia, brickwork has been used extensively in both single-storey domestic construction and in multi-storey housing developments. In South Australia and Western Australia, many houses built since 1945 have internal partition walls with bricks laid on edge in order to save on material costs. These walls are relatively slender by comparison with walls constructed traditionally with bricks laid on flat. In some domestic buildings, the interior partition walls may be required to carry vertical loads arising from suspended floors, building services or roof loads when the roof structure is strutted off the interior brickwork. Although these loads may be relatively small, many building Codes place restrictions on the slenderness ratio of walls in load-bearing situations irrespective of the load levels in the walls. These restrictions are usually not unreasonable in view of the lack of knowledge of the behaviour of slender walls especially with respect to the unknown effects of imperfections in workmanship and difficulties associated with the definition of edge support conditions.

A number of investigations have previously been carried out to determine the load carrying capacities of various types of brick wall. In general, however, this work has been aimed at structures of relatively low slenderness ratios in which ultimate failure has been governed by a material failure rather than structural instability.

The aim of this thesis, therefore, is to fill the gaps left by previous researchers by investigating the behaviour of a wide range of brickwork walls with varying support conditions, making allowances for non-linearities in material behaviour and imperfections in workmanship. The effects of increasing the wall slenderness ratio are investigated in some detail.

In many of the previous research programmes, a considerable amount of effort has been directed towards the experimental testing of isolated brickwork walls and piers, possibly because brickwork, as an anisotropic and non-homogeneous material with its distinct planes of weakness in the mortar, appears not to be readily suited to mathematical analysis.

The few theories which have been developed have been applied to walls supported at the top and bottom edge which undergo one way bending. In general these theories assume that brickwork is a no-tension material, an assumption which may lead, in some cases, to conservative wall load capacities. In the investigation described in this thesis, it has been possible by allowing for the actual behaviour of the individual components of brickwork, that is, the bricks and mortar, to develop analytical procedures which permit general parametric studies to be carried out for many types of load-bearing brickwork.

In brickwork walls subjected to vertical loads, cracking may occur at discrete intervals at the brick-mortar interfaces, the extent of the cracking in the bedjoints depending on the position of the line of action of the resultant compression load relative to the wall centre-line. No cracking occurs in the brickwork when the resultant load acts inside the middle third of the wall section, the kern. However, if the brick-mortar tensile bond strength is small, cracking occurs when the resultant load acts outside the kern. Under such conditions the brickwork flexural stiffness is altered.

The approach adopted in this thesis is that the change in brickwork stiffness can be determined by using a two-dimensional finite element analysis to calculate the moment-rotation characteristics of a cracked brickwork module consisting of two half-height bricks plus one mortar bedjoint. The resulting characteristics are used to develop load-deflection relationships for a homogeneous isotropic varying-thickness column equivalent to the real brickwork. The load capacities of eccentrically-loaded brickwork walls are calculated from equivalent-column equations, written in finite difference form, by using a numerical Newton-Raphson method to solve the resulting equations. The method is checked by testing under eccentric load conditions a model slender steel block column and a series of brickwork walls having varying slenderness ratios.

The analytical methods have been extended to account for brickwork panels which are simply-supported on four sides and subjected to vertical load. The bending and torsion stiffnesses of a three-dimensional brickwork module are estimated from a three-dimensional finite element method of analysis. Load-deflection relationships are developed for an equivalent plate of varying thickness, analogous to the equivalent column of varying thickness for a wall, in order to represent the behaviour of a real brickwork panel. By writing the load-deflection equations in finite difference form, load capacities are calculated for eccentrically-loaded simply-supported brickwork panels. Results obtained from the numerical method are checked by testing several small panels and a full-scale slender brickwork panel simply-supported on four sides.

It is shown that the combination of finite element methods with finite difference solution procedures gives an efficient means of solving large non-linear load-bearing brickwork problems. Results obtained by

using the numerical methods indicate that the strengths of slender brickwork walls may be calculated for many different types of brickwork materials and wall support conditions. It is further demonstrated that the methods of analysis may be developed to revise some current Codes of Practice to allow, in some cases, the use of slender walls and panels in load-bearing situations not permitted at present.

To assist in the detailed understanding of the behaviour of brickwork, the following two chapters contain a general review of design procedures and construction practices used for structural brickwork, and a review of previous methods of analysis and relevant research results.

## 2. STRUCTURAL BRICKWORK - A SYNOPSIS

The concept of "structural brickwork" as a method of construction in masonry has evolved over many centuries. In this chapter, the development of construction methods using masonry is outlined together with current practices for the erection of structural brickwork. Design procedures are discussed and exemplified by considering the engineering details of a particular structural brickwork building. Attention is also given to the limitations of structural brickwork.

### 2.1 THE DEVELOPMENT OF STRUCTURAL BRICKWORK

The use of masonry in buildings other than low-rise domestic houses has developed from practices used in the construction of the major churches and cathedrals of medieval Europe. A paucity of contemporary documentation on the methods for both engineering design and the building construction has led modern writers such as Fitchen<sup>(1)</sup> and Heyman<sup>(2)</sup> to attempt a formulation of the respective procedures which might possibly have been adopted. Until the sixteenth century when the vector addition of forces was developed, all building proportions and dimensions appear to have been entirely dependent upon height-to-width ratios developed by arbitrary rules and perpetuated through masons' lodges. The notion of forces and their lines of action allowed design to progress in an analytical fashion.

At that time, the materials used for the construction of the major churches and cathedrals of Europe were not bricks as we know them, but large blocks of stone carefully finished to fit together closely without a need for mortar. The two design principles which appear to have been followed were that -

- (a) the compressive strength of the stone, for all practical purposes, was infinitely large, and
- (b) the resultant force in the stonework must lie within the middle third of the section.

Coulomb<sup>(3)</sup>, in 1773, proposed that the resultant force should never be outside the section otherwise failure would occur by the formation of a hinge at an outer edge and that this was the only possible mode of failure for masonry.

Brickwork differs from the stonework used in the large cathedrals in that it is an assemblage of bricks bonded together with mortar<sup>(4)</sup> to give uniform bearing between the relatively small and rough-faced brick units. Brickwork is commonly categorized into "Normal Brickwork" and "Structural Brickwork"; "Normal Brickwork" requires no engineering design while "Structural Brickwork" requires design for fully structural applications.

The methods used by the medieval builders evolved through to the nineteenth century into what has become known as conventional load-bearing brickwork. Each wall in a structure was treated as though it was independent of the rest of the building and hence relied on its own weight for its stability. Figure 2.1, (Francis<sup>(5)</sup>), shows that the brickwork was designed to be in compression under all likely load combinations by ensuring that the resultant forces acting on any cross-section would lie within the middle third of the section. This design philosophy, which had its roots in Renaissance Europe, proved to be grossly uneconomical in the late nineteenth century when steel and concrete framed structures were being developed. The Monadnock Building constructed in Chicago and completed in 1891 was a sixty-metre high tower block in which approximately 20 percent of the ground floor area was taken up by the load-bearing walls some 1650mm thick at



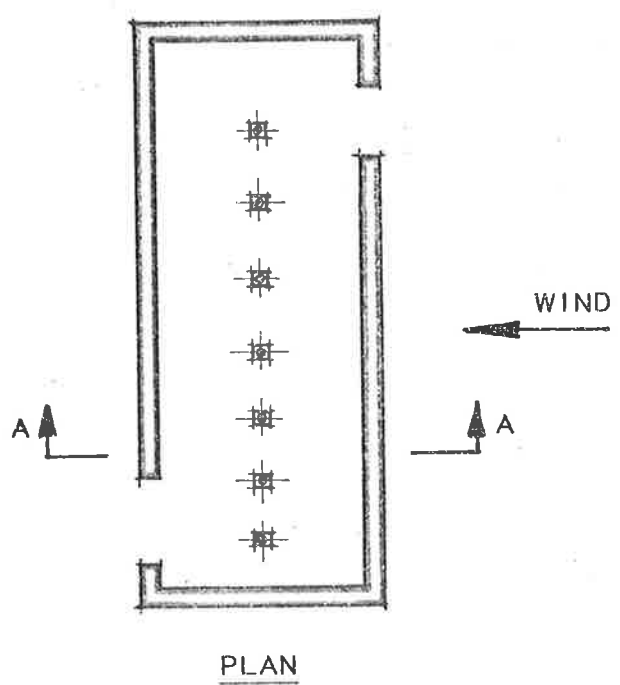
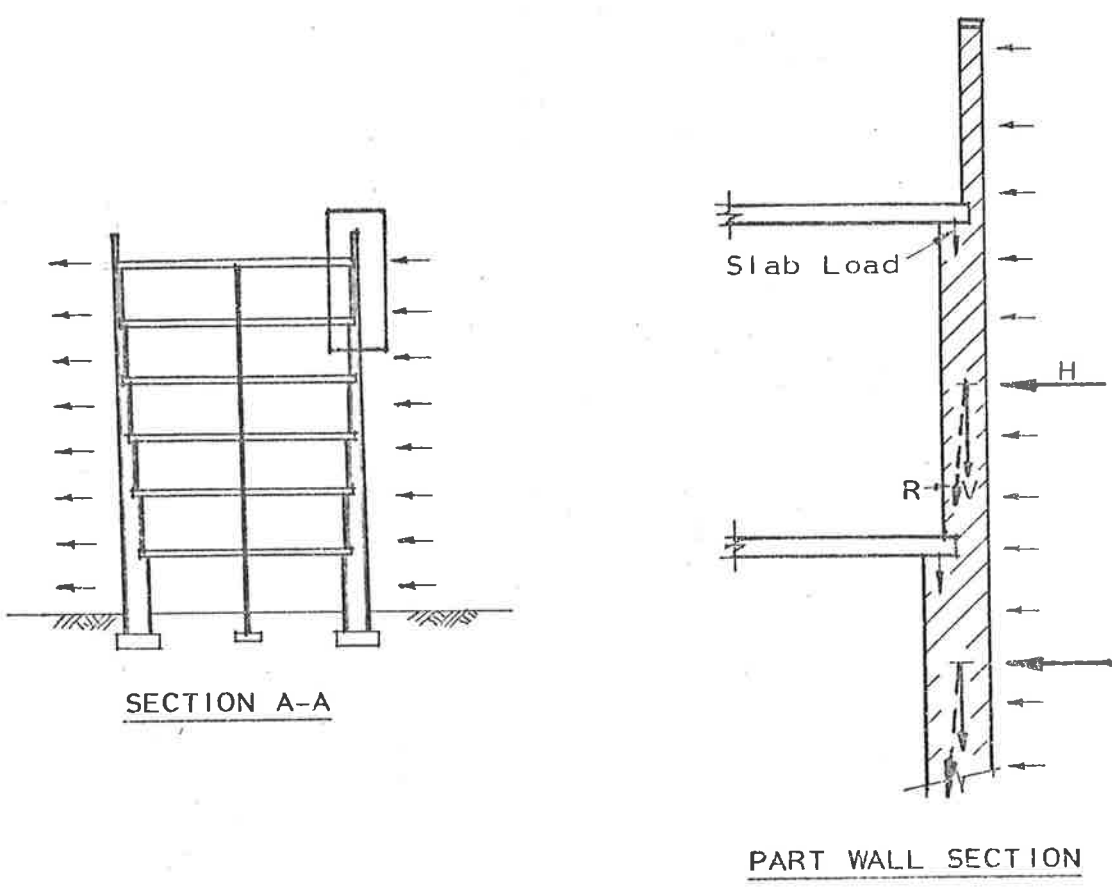


Figure 2.1<sup>(31)</sup>: Conventional Loadbearing Brickwork

street level. By the end of the nineteenth century, framed structures which were both economically more viable and architecturally more flexible were replacing masonry high-rise buildings.

In the 1950's, a new design approach for masonry was developed for high-rise residential buildings in Europe to cope with the post-war population problems in many countries. Haller<sup>(6)</sup>, in 1958, reported the construction of a number of nine-storey apartment houses and an eighteen-storey tower on the outskirts of Zurich. In the design, each wall was recognized as being an integral part of the whole building. The concrete floor slab at each level was assumed to be a diaphragm, rigid in its own plane, which constrained the walls to lateral translations which depended on the lateral translation and rotation in a horizontal plane of the floor slab. Simplified calculations were made to obtain the effective load eccentricities for each wall by taking into account the flexural stiffnesses of the concrete floor slabs. The improved efficiency of this approach over conventional load-bearing brickwork is evident in an eighteen-storey apartment house in Biel<sup>(7)</sup> in which the load-bearing walls at ground level are of the order of 150mm compared with 1650mm for the Monadnock Building, a structure of comparable height.

Figure 2.2<sup>(31)</sup> shows a diagrammatic layout of a modern structural brickwork building. The diaphragm-type action of the floors causes lateral loads, such as wind loads, to be transferred to ground as shear forces in the planes of the walls which are parallel to the direction of the resultant lateral force. It is this use of shear walls for the transfer of lateral loads to ground which differentiates structural brickwork from conventional load-bearing construction.

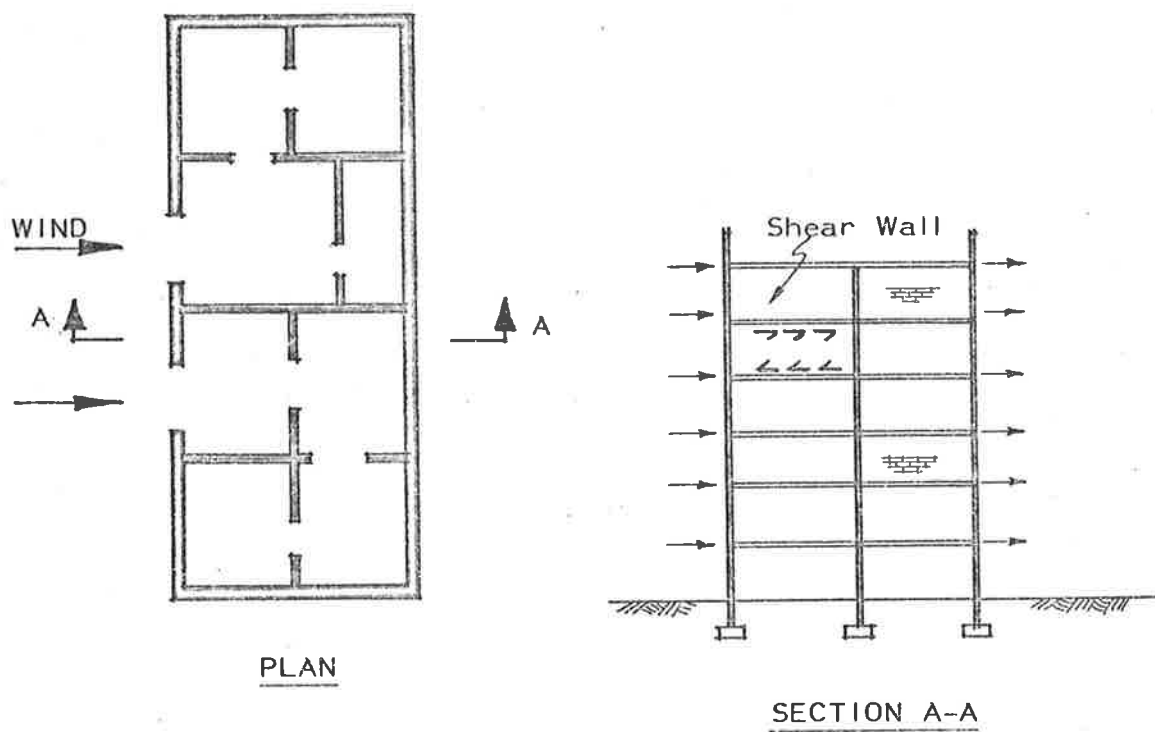


Figure 2.2<sup>(31)</sup>: Structural Brickwork  
- Wall Arrangement

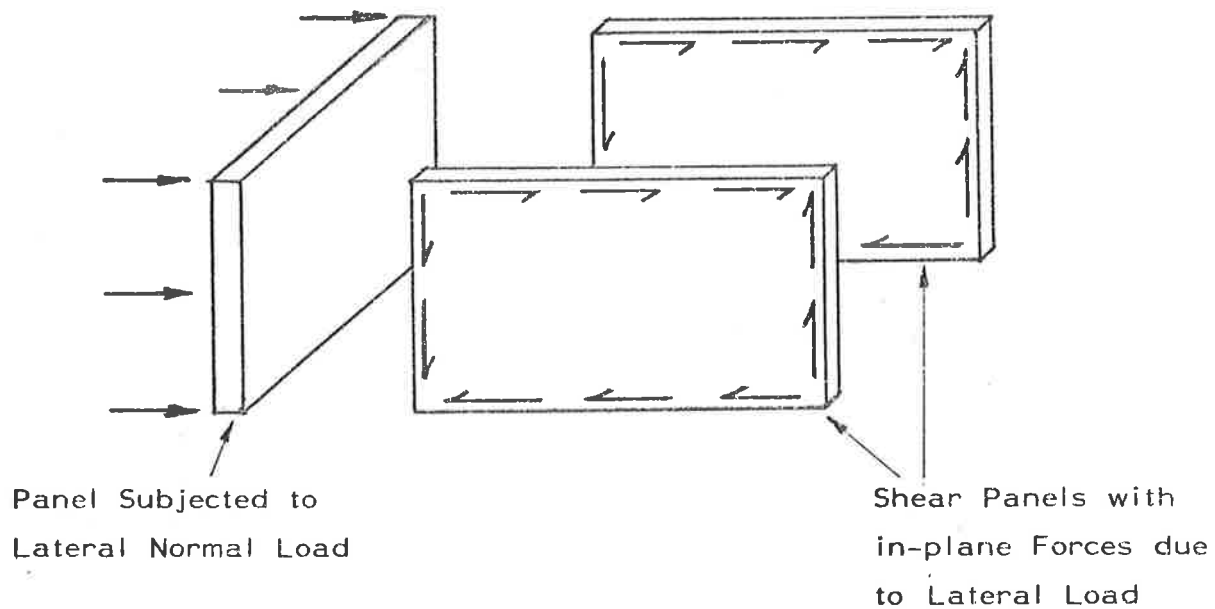


Figure 2.3: In-plane Shear Caused by Lateral Loads on a Brickwork Structure

## 2.2 LOAD TRANSMISSION IN STRUCTURAL BRICKWORK

The efficiency of structural brickwork is obtained by ensuring that the walls are aligned vertically throughout the height of the building. The walls serve multiple purposes. As well as carrying the vertical loads they provide the necessary separation between different rooms on each level and often provide the architectural finish as well. The concrete floors carry live loads at each level to the bearing walls and provide thermal and acoustic insulation between adjacent storeys of the building. The floors are usually of the order of 100mm to 150mm thick so that some degree of structural interaction between the floors and walls is possible because they are both of similar flexural rigidity. The bending effects produced by this interaction cause the walls to be loaded eccentrically so that the design of structural brickwork, even for vertical loads only, must take account of the possibility of failure not only under excess compression but also by instability. Methods of calculation which allow for interaction effects between crushing and instability will be discussed in Chapter 3.

The main effects of lateral loads on brickwork are shown in figure 2.3. The lateral forces which have a component normal to a wall cause transverse bending in that panel, and lateral forces which have a component parallel to a wall produce in-plane shear and normal stresses.

Hallquist<sup>(8)</sup>, Hendry<sup>(9)</sup>, Satti<sup>(10)</sup>, Baker<sup>(11)</sup>, Lawrence<sup>(12)</sup>, Bradshaw and Entwisle<sup>(13)</sup> and West<sup>(14)</sup> have investigated the effects of lateral loads on brickwork panels supported on both horizontal and vertical edges.

Extensive comparisons have been made between experimental results and theoretical predictions based on elastic plate behaviour, yield line collapse and a panel strip theory proposed by Baker<sup>(11)</sup> who

showed that good agreement between theory and practice may be obtained if the respective moduli of rupture are known for the directions both parallel to and normal to the bedjoint planes of the brickwork. Hendry<sup>(9)</sup> stated that for panels and walls without vertical precompression, none of the theoretical predictions are entirely satisfactory for calculating brickwork strength under lateral pressure. For this reason, Hendry has given empirical values for effective bending moment coefficients which are intended to give interim assistance in design. It is Hendry's stated opinion that the behaviour of walls with appreciable precompression has been thoroughly explored experimentally and theoretically<sup>(15)</sup>.

The transmission of lateral loads by in-plane shear is achieved by ensuring that enough walls are constructed parallel to the direction of the resultant lateral load. A residential-type plan provides this condition in most cases. The walls which are required to carry vertical loads are usually all that is required for transmitting lateral loads in shear and flexure to the foundation because the effective shear stresses are usually small. One design criterion usually observed is that tension induced by in-plane flexure in the structure must be less than any compression induced by superimposed gravity loads. This is shown schematically in figure 2.4.

A method which has been proposed for the design of walls which carry the lateral loads in shear assumes that the concrete floor slab at each level acts as a rigid horizontal diaphragm interconnecting the load-bearing walls. If the resultant of the lateral load acts through the centroid of the wall plan, all walls deflect horizontally by the same amount at any given level and consequently will share the applied lateral forces at that level in proportion to their relative stiffnesses about centroidal axes normal to the direction of the applied

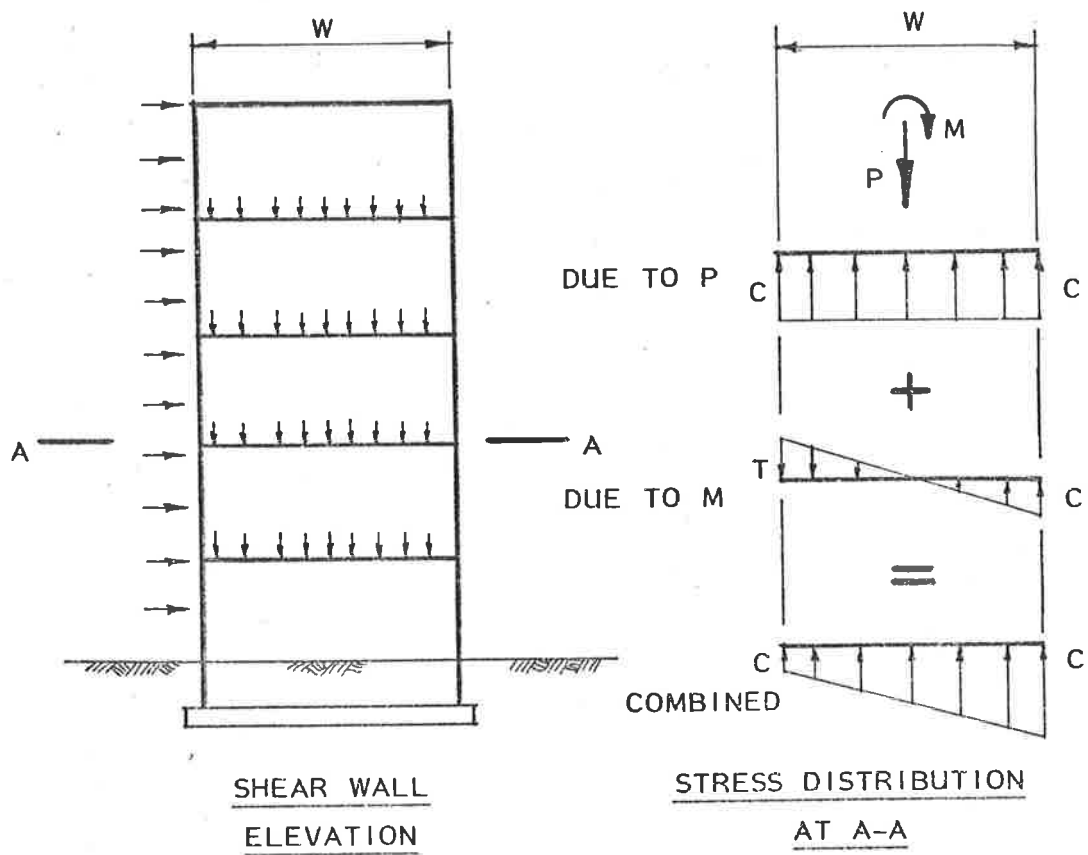


Figure 2.4<sup>(31)</sup>: Stresses in Wall Due to Vertical and Lateral Loads

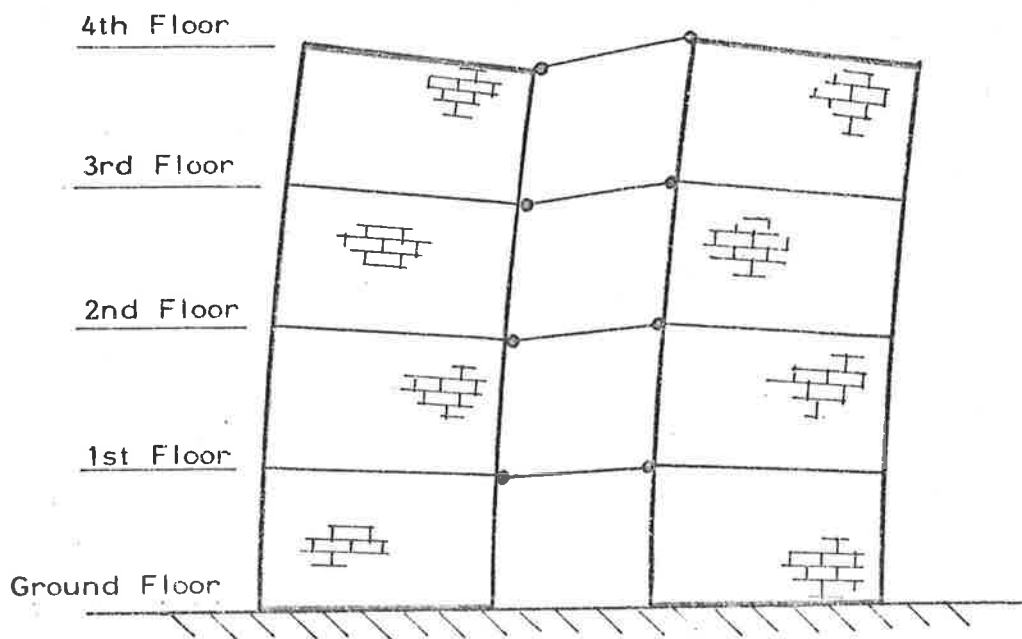


Figure 2.5: Assumed Cantilever Action of High-rise Brickwork Structure

force. If, however, the resultant of the lateral load causes a moment about the centroid of the wall plan, additional forces must be applied to all walls in proportion to their relative stiffnesses about centroidal axes radial from the centroid of the wall plan. In order to simplify the structural behaviour of a building, it may be assumed that the walls at each storey act as a series of tall cantilever columns interconnected by the floors at each level (figure 2.5).

Hendry<sup>(16)</sup> carried out several tests on one-sixth scale column structures and on a full-scale five-storey building to compare the results of different methods of analysis with experimental results. He concluded that the cantilever design method produced conservative results for the lateral displacements but did not give an accurate assessment of the stresses in the walls. However, it was noted that a design, based on the cantilever method, which indicated the stress levels to be acceptable, would always result in a satisfactory structure. Hendry further suggested that more refined calculations, such as a finite element analysis, might be used as a check on the cantilever design method. The super-elements developed by Leung<sup>(17)</sup> for the analysis of high-rise buildings might be suitable for brickwork buildings in which lateral loads are critical to the design. However, the choice of elastic modulus may be difficult because, as Hendry reported, this parameter varies with the degree of precompression in the walls. The elastic moduli of brickwork will be discussed in Chapter 3.

### 2.3 A STUDY OF A STRUCTURAL BRICKWORK BUILDING

Many high-rise residential structural brickwork buildings have been constructed in the world in the past twenty years. The group of fourteen-storey Residential Blocks at the University of Essex<sup>(18)</sup> is an early example of structural brickwork in tall buildings in

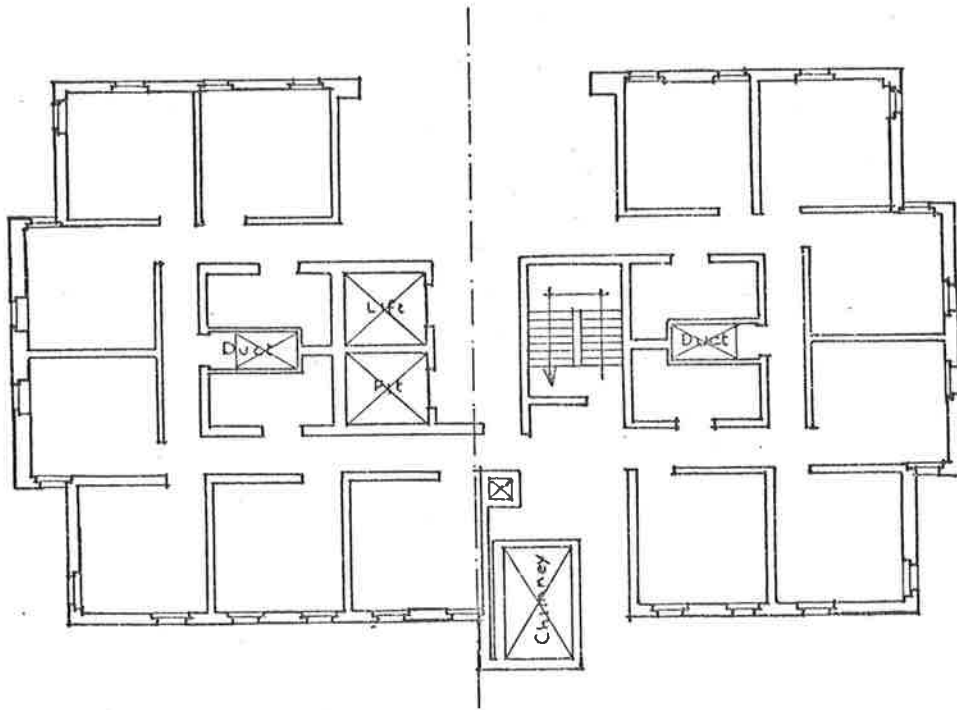


Figure 2.6: Floor Plan of Residential Blocks at the University of Essex. (Typical for Load-bearing Structural Brickwork.)

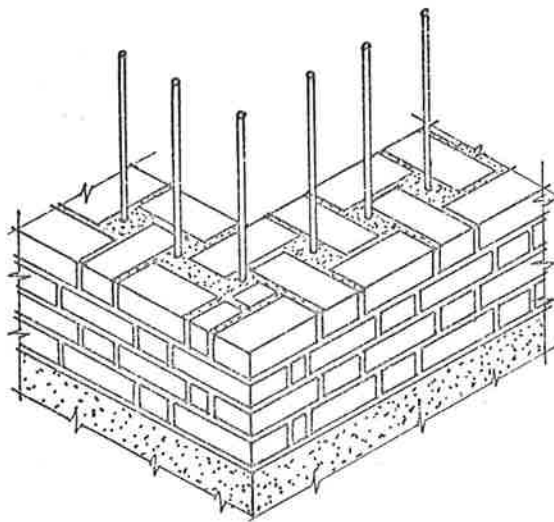


Figure 2.7: Quetta Bond.



Britain. Figure 2.6 shows a typical wall plan of a Residential Block. Load-bearing brickwork was chosen because it presented an economical solution to the problem of student accommodation. The brickwork is fair-faced internally for reasons of economy and ease of maintenance.

The structure relies basically on 11" (280mm) cavity external walls and 9" (230mm) solid internal walls for its strength and stability. However, some 15½" (390mm) cavity walls and 13½" (340mm) solid walls are utilized up to the eighth storey. All floors are insitu reinforced concrete 4" (100mm) thick, except in the communal area where they are 5" (125mm). Each wall was assumed to be an independent cantiliver linked to the structure by pin-ended connections at each floor level. This design approach showed that some tension might occur at the lower levels, so that a Quetta bond (figure 2.7) was used with vertical reinforcement in the grout-filled cavities.

Results of research by Hendry<sup>(16)</sup> and Soane<sup>(19)</sup> into the interaction between the various wall groups and the floors allowed the designers to omit the vertical tensile reinforcement in the walls of the third and fourth towers, and it was eventually decided to use 9" (230mm) solid and 11" (280mm) cavity construction for the load-bearing elements.

#### 2.4 SUMMARY OF THE PRINCIPLES OF STRUCTURAL BRICKWORK

In order to achieve efficiency and hence economy with structural brickwork, there are several principles which should be observed. Some of these are of an architectural nature but are nevertheless important from an engineering point of view. Krantz<sup>(20)</sup> states that two fundamental principles are:

1. All loads must be distributed as evenly as possible among the load-bearing elements.

2. Vertical loads must be transferred to ground by the shortest possible route.

A corollary of these two principles is that an identical floor plan must be used at each level and be such that areas of floor supported by each wall are approximately equal. In residential buildings this can be attained without gross penalty to the function of the building.

An important architectural aspect to be considered is the ability of the floor slabs to span between the walls without the aid of beams or piers. Beams cause concentration of loading on the walls and isolated piers, may be susceptible to accidental damage which could lead to progressive collapse of large sections of the structure. It is preferable, therefore, to span all slabs in two-way action between continuous brick walls so that in the event of the removal of part of a wall, say by gas explosion, the slab can still remain, albeit in a distressed but uncollapsed state, to support loads from above which may include some sections of load-bearing walls.

## 2.5 STABILITY AND PROGRESSIVE COLLAPSE OF STRUCTURAL BRICKWORK

The stability of structural brickwork has become a mandatory design issue since the partial collapse of a block of flats at Ronan Point, Canning Town, London in 1966. Following the accident, a considerable amount of work was carried out in the United Kingdom to assess the possibility of bearing wall structures failing by progressive collapse. The "Fifth Amendment" to the English Building Regulations, published in 1970, required all buildings over four storeys to remain stable under specified loading conditions, with a reduced loading factor, in the event of a defined structural member or portion thereof

being removed. Limits of damage were specified so that if a member, such as a wall, could not be removed because of its importance in the design, that member must be designed to resist the effects of a pressure of 34KPa in any direction. The intention of the amendment was that structural failure and progressive collapse could not be tolerated as a result of damage by a gas explosion. Hendry<sup>(21)</sup> has summarized an investigation carried out by Morton<sup>(22)</sup> in which nineteen designs for existing buildings between three and sixteen storeys were examined. Under the requirements of the Fifth Amendment all the high-rise buildings were acceptable with the low-rise ones up to four storeys not being affected by the Act. However, Hendry reported that a number of low-rise school buildings with relatively large floor spans would be susceptible to extensive collapse upon application of the Fifth Amendment design requirements. Sutherland<sup>(23)</sup> supported Hendry's conclusions and observed that high-rise masonry structures are generally not subject to stability failure or progressive collapse. He noted that low-rise structures such as classrooms, hospital wards or assembly halls, in which modified domestic detailing has been used, are the most likely to suffer a stability failure. The likelihood of progressive collapse in a multistorey masonry building, when designed according to what might be regarded as good practice, is remote even for those buildings designed prior to the Fifth Amendment. In addition, Hendry suggested that in current designs failure by instability under expected impact loads is of such a low probability that specific design allowances need not be made.

The British Code of Practice<sup>(24)</sup> for the structural use of masonry incorporates the following three methods for complying with the Fifth Amendment:

- (i) By considering the removal, one at a time, of vertical and horizontal elements, unless each is capable of withstanding a lateral pressure of 34KPa with a partial safety factor of 1.05 on the material.
- (ii) By providing ties between vertical and horizontal elements capable of resisting certain specified impact loads and then considering the removal, one at a time, of the vertical elements.
- (iii) By incorporating in the structure horizontal and vertical ties to resist specified impact loads.

The Australian Code<sup>(4)</sup> places the responsibility on the designer to the extent that if there is a possibility that certain walls in a storey may become structurally ineffective due to impact damage, an ultimate load design must be used for the floors, using yield line theory if appropriate. In addition, a reduced load factor and only a fraction of the design floor live load may be used to check that there is an adequate margin of safety against local collapse vertically above and below the walls initially destroyed.

## 2.6 THE BEHAVIOUR OF BRICKWORK UNDER SEISMIC LOADS

Research into the effects of seismic loads on unreinforced masonry structures has been reported only recently at conferences such as VIBMAC in 1979. Design Codes have been based on experiences gained throughout the seismic zones of the world and have been framed in terms of the extent of damage which may be tolerated after an earthquake of known intensity. According to Bubb<sup>(25)</sup>, the Uniform Building

Code (U.B.C.) of the United States, which is empirically based, sets minimum standards with regard to public safety and is updated every three years according to any new information obtained from earthquakes and earthquake damage anywhere in the world.

The Australian Earthquake Code<sup>(26)</sup> prescribes equivalent static design forces for various structure classes which depend upon the likelihood of regional seismic activity and the degree of post-yield ductility of the structural material. The return period of the design earthquake for most structures is assumed to be sixty years and therefore unreinforced masonry structures, which may be long-standing residential and commercial buildings, can be expected to experience at least one design earthquake in their lifetime. The Design Code recognizes that unreinforced masonry structures are essentially brittle and have very little post-yield ductility. It therefore specifies a horizontal force factor which is deemed to be sufficient to ensure that the masonry does not fail in a design earthquake. The U.B.C. specifies the factor  $K$  as 4.0, while the Australian Earthquake Code allows  $K$  to be 3.2. A further restriction placed on unreinforced masonry structures is that they must not be constructed in an area designated as Zone 3 (a zone having the greatest earthquake intensity) and are only permitted in Zone 2 if they are not required as post-disaster function buildings.

The Meckering earthquake<sup>(27)</sup> of 1968 in Western Australia was felt in Perth 130km away. Although the vibrations felt in Perth registered 6.75 on the Richter Scale, no structural damage was evident in load-bearing walls in high-rise buildings. This was partly due to high precompression from vertical loads. Masonry infill panels, however, did show cracking, while many old brick buildings with conventional free-standing walls and timber floors were badly

cracked. It is apparent from that earthquake and others of similar intensity, that where unreinforced masonry structures are permitted, great care must be taken with structural details particularly in wall-elements with little or no precompression such as a wall connected to a roof or a parapet wall.

The Australian Design Code<sup>(26)</sup> states that all masonry structures in Zone 3 must be reinforced. The philosophy is that the steel reinforcement increases the post-yield ductility of a masonry structure and decreases the likelihood of major structural damage in an expected design earthquake. Mayes and Clough<sup>(28)</sup> have summarized the behaviour of reinforced masonry under cyclic loads.

## 2.7 REINFORCED MASONRY

Structural masonry reinforced with steel bars or mesh is used if a designer requires the characteristic strength and behaviour of reinforced concrete but with the appearance of masonry. Plummer and Blume<sup>(29)</sup> and Davey and Thomas<sup>(30)</sup> have reported extensively on the behaviour of reinforced brick masonry. As a structural system it is a hybrid form of construction brought about by a compromise between concrete and masonry, and as such will not be dealt with in detail in this thesis.

## 2.8 ECONOMICS OF STRUCTURAL BRICKWORK

The relative economy of structural brickwork compared with other forms of construction is dependent upon the type of structure and the general prevailing economic climate. Page<sup>(31)</sup> reported costs which were applicable in 1970 but these costs certainly have altered since that time. In South Australia in 1981, structural brickwork is reported

to be commercially competitive with concrete-framed structures clad with precast concrete panels in buildings costing less than  $\$ \frac{1}{2}$  million, but for more expensive structures, the concrete construction is preferred. The cost of external cavity-wall fair-faced brickwork in Adelaide in 1981 is approximately  $\$50/\text{m}^2$  of which  $\$24/\text{m}^2$  is brick cost,  $\$30/\text{m}^2$  is labour cost and  $\$6/\text{m}^2$  is associated material cost. The cost of internal single-leaf walls is approximately  $\$30/\text{m}^2$ . The corresponding cost of external precast concrete non-load-bearing panels is approximately  $\$70/\text{m}^2$ , but cost savings may be made, compared with structural brickwork, because of possible reductions in construction time.

Overall, the economics of structural brickwork is extremely sensitive to local building practice and therefore each structure must be evaluated economically in terms of local conditions.

### 3. LITERATURE REVIEW

This chapter presents a study of the strength and stress-strain characteristics of the materials of brickwork, the clay bricks and the mortar, and describes theories of analysis for the load-deformation behaviour of slender brick walls and panels. For the purpose of this thesis, a wall is defined to be a brickwork assemblage which spans only between its base and top and a panel is defined to be a wall which is supported additionally on its two vertical edges. A slender brick wall or panel is defined to be a brickwork assemblage subject to vertical load in which the effects of out-of-plane deformations on the brickwork stresses may be significant.

The characteristics of brickwork as a structural material are reviewed initially in terms of the properties of the component materials and particular references are made to standard methods of determining material properties as specified by Australian Codes of Practice. Results of experiments on brickwork assemblages are presented which relate the strength of brickwork to the strengths of the component materials and theoretical studies of the strength of brickwork are also described. Stress-strain characteristics of structural brickwork, determined by experiment, are presented and methods proposed for the analysis of brickwork columns subject to vertical load are described; results of experiments on brickwork walls are compared with calculated wall behaviour. The chapter concludes with a review of the theory of thin plates, the basis of a method proposed in Chapter 6 for the analysis of slender brickwork panels.



### 3.1 CLAY BRICKS

#### 3.1.1 Introduction

Australian Standards define three categories of brick. Clay bricks must comply with AS1225-1980<sup>(32)</sup>, "Burnt Clay and Shale Building Bricks", calcium silicate bricks with AS1653-1974<sup>(33)</sup>, "Calcium Silicate Bricks" and concrete bricks with AS1346-1974<sup>(34)</sup>, "Concrete Building Bricks". The investigations presented in this thesis consider only clay bricks to AS1225-1980<sup>(32)</sup> and will not necessarily include calcium silicate and concrete bricks.

#### 3.1.2 Manufacture and Specification

The ancient art of brickmaking has been refined by modern manufacturing methods so that it is now possible to obtain clay bricks of high strength and improved durability. Most importantly, these modern processes have minimized the variation in brick properties caused by variability of the raw materials such as clays and shales.

In Australia, clay bricks are made by shaping a mass of clay and/or shale material made plastic by the addition of water. The bricks are oven-dried and are subsequently heated to temperatures which may vary from 750°C to 1300°C. During the heating process, often referred to as "firing", any water remaining after drying is evaporated, any combustible materials are oxidized and a process known as vitrification takes place in which the individual soil particles fuse together.

The shaping of the clay mass is usually done in one of three ways; the clay may be semi-dry pressed, stiff-plastic pressed or extruded and wire-cut. The semi-dry pressed method involves compressing the clay powder with 10 to 12 percent moisture content in

a steel mould, while the stiff-plastic pressed method uses a clay of 14 to 17 percent moisture content which is pressed in two stages. Pressed bricks are manufactured with a depression in one face, known as a "frog", which allows the formation of a shear key in the bedjoint mortar. Extruded bricks are formed from a clay with a moisture content of 18 to 25 percent and are cut from a continuous extruded column of clay using single-filament wire strands. Extruded bricks may be solid but are often perforated to reduce weight, improve firing efficiency and to provide a shear key for the bedjoint mortar.

Australian Standard AS1226-1980<sup>(35)</sup>, "Methods of Sampling and Testing Burnt Clay and Shale Building Bricks", specifies that for small projects, tests must be carried out on a random sample of forty bricks chosen from each consignment of either 30,000 bricks, or part thereof. For large projects, forty bricks must be chosen for each consignment of 100,000 bricks, or part thereof. For the determination of compressive strength, twelve bricks are taken at random from the forty brick sample and are halved along the largest dimension. One half-brick from each of the twelve bricks is saturated, placed in the same orientation as in the completed wall and compressed between single sheets of nominal 4mm thickness plywood. The minimum compressive strength, C, of a brick batch is the least value for the twelve test specimens expressed in megapascals.

The initial rate of absorption (I.R.A.), sometimes referred to as the suction, is measured using six bricks from the forty-brick sample. Australian Standard AS1226-1980 specifies the calculation of I.R.A. as a gain in weight per minute of a brick placed in 3mm of water corrected on the basis of a bed-face area of 25000mm<sup>2</sup> and has as its units gm/25000mm<sup>2</sup>/min. The bricks must be tested in the orientation in which they are finally used.

The transverse strength of a batch of bricks is assessed by a central point load bending test on each of six bricks from the forty-brick sample. The transverse strength is often referred to as the modulus of rupture.

Australian Standard AS1226-1980 does not specify a method for the measurement of the elastic properties of bricks.

### 3.1.3 Brick Properties

The properties of brick which have important influences on the behaviour of brickwork are compressive strength, tensile strength, the elastic modulus and the I.R.A. The last property influences the bond between mortar and brick, as does the surface texture of the brick-mortar interface.

#### 3.1.3.1 Compressive strength

Tests which are deemed to measure the compressive strength of bricks actually measure the load capacity under uniaxial compression in which failure is governed by the lateral tensile strength of the specimen. The load capacity, or "compressive strength" of bricks from any batch varies because of differences in raw materials, manufacturing processes, degree of burning and the brick shape and size. The method of testing can also influence the test results. Grimm<sup>(36)</sup> reported that specimens which are square in a plane perpendicular to the direction of compressive stress were stronger than rectangular specimens. The compressive strength was generally found to be higher for units made of shale by the stiff mud process and burned at high temperatures.

Compression tests on plaster-capped bricks give higher values for the load capacity than tests on bricks whose surfaces are not laterally restrained by friction on the platens of a test machine.

Grenley<sup>(37)</sup> reported the results of tests in which the bricks were relatively unrestrained by the insertion of teflon pads between the brick and the machine platens. The apparent compressive strength was found to be between 25 and 67 percent of the conventional restrained value.

It has been recognized since the turn of the century that the degree of saturation affects brick compressive strength<sup>(38)</sup>. Bricks tested in a dry condition may be up to 15 percent stronger than the same bricks tested in a saturated state.

The Australian Standard AS1226-1980 specifies a method for testing the compressive strength of bricks using plywood capping, so that results obtained using AS1226-1980 cannot be compared directly with research results in which other types of capping have been used. However, although there is little information on the strength of bricks laid on edge,\* the strength of Australian clay bricks commonly varies between 30MPa and 80MPa in a brick-on-flat orientation. AS1226-1980 does not refer to bricks with perforations or cores, but Shellbach<sup>(41)</sup> has reported that as long as coring of bricks does not exceed 35 percent of the cross-sectional area perpendicular to the load, then a brick is as strong as if it were solid. The improved firing achieved by coring is responsible for the increase in nett-area strength, although, as West<sup>(42)</sup> has indicated, brick strength is dependent upon the coring pattern as well as the size and shape of the cores. A few large round cores are preferable to many small cores or cores with sharp re-entrant corners. The British Code BS3921:1965<sup>(43)</sup> recognizes the increase in strength of cored bricks due to improved firing by specifying that all bricks with less than 25 percent by volume perforations are "solid" for design purposes.

---

\* A practice followed in some States of Australia for domestic buildings and partition walls.

### 3.1.3.2 Initial rate of absorption

The initial rate of absorption is a measure of the degree to which a brick has an affinity for the moisture in a mortar. A reduction in the water content of a mortar affects the adhesion or bond between the brick and mortar to the detriment of the brickwork as a whole. Sahlin<sup>(44)</sup> has reported that the I.R.A. shows a strong relationship to brick strength, especially the modulus of rupture, and that brick suction varies inversely with brick density.

### 3.1.3.3 Transverse strength

According to Nevander,<sup>(45)</sup> the transverse strength or modulus of rupture of solid brick varies between 14 and 32 percent of the compressive strength for strengths ranging from approximately 20MPa to approximately 50MPa (2750psi to 7150psi). Hilsdorf<sup>(46)</sup> has given this percentage ratio as either 11, 15 or 17 percent for three types of uncured solid bricks, and S.C.P.R.F.<sup>(47)</sup> tested three types of cored bricks for percentage ratios of 11, 10 and 10 percent respectively. The standard deviation for Hilsdorf's tests was about 25 percent and, for the S.C.P.R.F. results, the standard deviation was between 5 and 20 percent.

### 3.1.3.4 Modulus of elasticity

Glanville and Barnett<sup>(48)</sup> measured the modulus of elasticity for a representative sample of bricks available in Great Britain in 1927; the bricks were compressed between sheets of plywood. Figure 3.1 shows the relationship between modulus of elasticity and compressive strength for all bricks tested. In each sample of twelve bricks, the strength variation was  $\pm 50$  percent of the mean and Glanville and Barnett stated that the results could not be used to give a meaningful statistical analysis. If, however, the results for pressed bricks are discounted, a regression analysis gives the relationship -

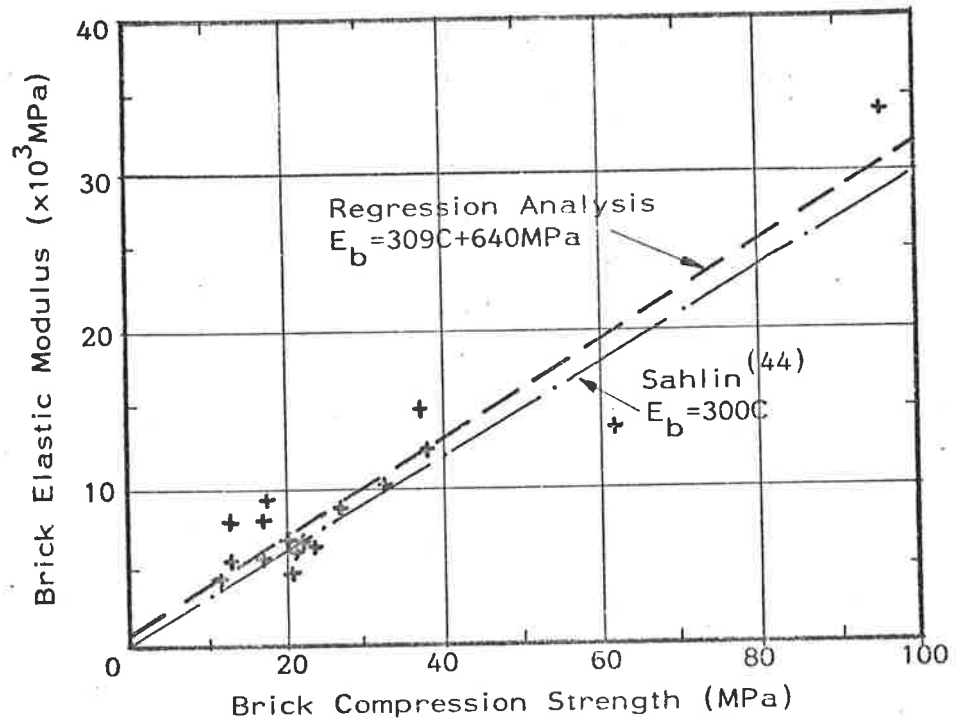


Figure 3.1: Relationship between Elastic Modulus and Compression Strength

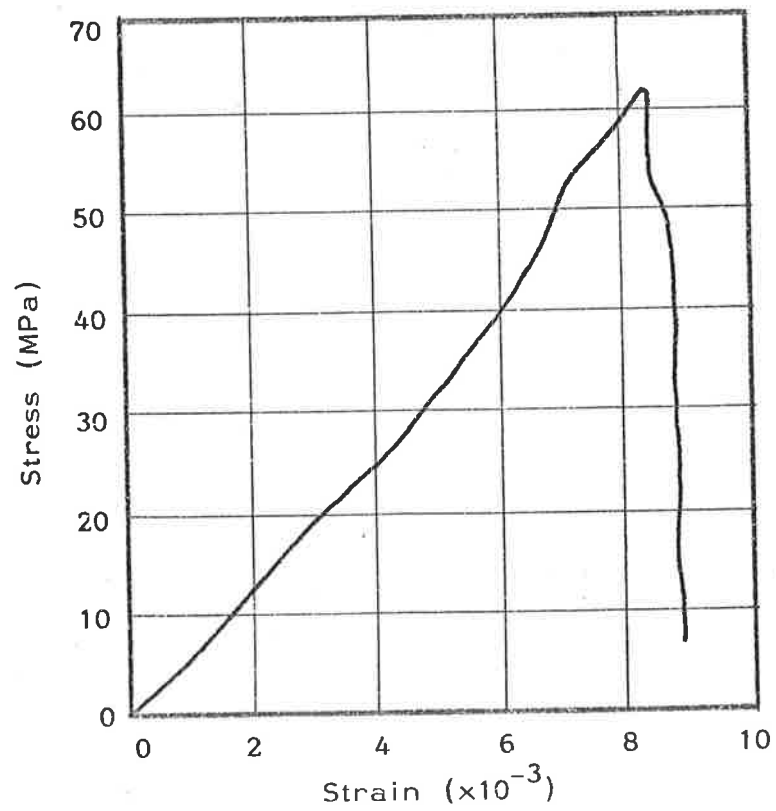


Figure 3.2: Stress-Strain Curve for Brick

$$E_b = 309C + 640\text{MPA} \quad (3.1)$$

in which  $E_b$  is the brick elastic modulus

$C$  is the brick compressive strength

The correlation coefficient is 0.94.

Sahlin<sup>(44)</sup> gave the relationship for the same points as

$$E_b = 300C \quad (3.2)$$

Psaltis<sup>(49)</sup> has investigated the dynamic measurement of elastic modulus on solid bricks using sonic techniques and has reported a correlation of 0.99 between sonic and mechanical test results. The variation of elastic modulus within individual bricks was of the order of 10 to 15 percent for the specimens tested.

Scrivener and Williams<sup>(50)</sup> have given a complete stress-strain curve for a brick prism (figure 3.2) in which the linear-elastic behaviour of the brick material and its brittle failure characteristic are clearly shown.

Plowman<sup>(51)</sup> has summarized the relationship between brickwork modulus and brick strength but has not given results for the elastic modulus of the bricks themselves. The modulus of brickwork is discussed further in Section 3.3.

## 3.2 MASONRY MORTAR

### 3.2.1 Introduction

A masonry mortar must fulfil certain requirements during brick-laying and also be well suited as a load-carrying material when in its hardened state. A wet mortar must have good workability so that all joints can be filled easily and it must have an early rigidity so that excessive rocking movements cannot occur as new courses of bricks are laid. The ability of a mortar to retain its moisture, even if the

brick suction is high, is also important because the mortar relies on the moisture for complete hydration of the cementitious materials. Factors which affect mortar strength, workability, water retentivity as well as other important properties will be discussed in the following sections.

### 3.2.2 Mortar Specification

Mortar mixes have traditionally been based on paste-sand ratios which vary from  $1:2\frac{1}{4}$  to  $1:3$  by volume. This is based to some extent on the approximate amount of paste which is required to fill the voids between the sand particles. Australian Standard AS A123-1963 "Mortar for Masonry Construction"<sup>(52)</sup> states that all mortars which are specified by proportion, rather than by compressive strength, must comply with Table 3.1 for the appropriate mortar type.

Proportion Cement:Lime:Sand	Parts by Volume		
	Portland Cement	Hydrated Lime or Lime Putty	Fine Aggregate
Cement Mortar 1:1/10:3	1	1/10	3
Composition { Mortars {	1:1:6	1	6
	1:2:9	1	9
	1:3:12	1	12
Lime Mortar 0:1:3	0	1	3

Table 3.1: Mortar Mix Proportions

A mortar may also be specified by compressive strength, in which case the parts by volume of aggregate in the mortar must not be less than  $2\frac{1}{2}$  times the total volume of the cementitious material used. For Australian masonry mortars the aggregate used is sand which complies with AS1465-1974<sup>(53)</sup>, "Dense Natural Aggregates for Concrete", with



the added stipulation that the material passing a No. 200 B.S. test sieve shall not exceed 10 percent<sup>(52)</sup>. The Brick Development Research Institute<sup>(54)</sup> has indicated, however, that 10 percent of such fine material may result in excessive shrinkage cracking. For a natural sand, ASTM Standard ASTM144<sup>(55)</sup> allows no material to pass a 200 sieve while the British Standard<sup>(56)</sup> calls for not more than 3 percent passing.

Cementitious materials must comply with AS1315-1973<sup>(57)</sup>, "Portland Cement" or AS1672-1974<sup>(58)</sup>, "Building Limes". Lime putty may also be used provided it complies with AS A123-1963<sup>(52)</sup>.

The water retentivity of a mortar, which is a measure of its ability to retain water against suction from the bricks, is tested in accordance with the provisions of ASTM C91, "Specifications for Masonry Cement".<sup>(59)</sup> The flow of a mortar, tested in accordance with ASTM C91,<sup>(59)</sup> is related to workability. Both water retentivity and flow will be discussed in Section 3.2.3.2.

### 3.2.3 Mortar Properties

#### 3.2.3.1 Effects of type of aggregate

A graded sand which is within the limits prescribed by AS A123-1963<sup>(52)</sup> gives an overall aggregate density which requires a minimum amount of cementitious material for a given strength. Monk<sup>(40)</sup> has reported that the compression and tensile strengths decrease as the sand varies from a uniform coarse sand to a uniform fine sand, while a blend of coarse and fine particles gives the maximum strength because the void ratio is a minimum.

Filling of the voids is thus achieved with a minimum of cementitious material. Mayes and Clough<sup>(28)</sup> have indicated that natural

sands have void ratios which vary from 25 to 40 percent. Experimentally, the lowest void ratio achieved is about 16.8 percent using a mixture of particles as in Table 3.2.

Particle	% total volume	Relative diameter
Coarse	70	50.5
Medium	20	8.0
Fine	10	1.0

Table 3.2: Optimum Sand Particle-size Distribution<sup>(28)</sup>

Natural sands vary from the gradation required for optimal packing and therefore will not generally produce mortars of optimum strength. Creep and shrinkage are also minimized if the void ratio in the sand particles can be kept to a minimum.

### 3.2.3.2 Effects of variations in cementitious material

Mortars traditionally were composed of sand and lime, either hydrated lime or lime putty, and depended upon atmospheric carbon dioxide for carbonation and strength development. It was found that naturally-occurring cements and Portland cement proved to be compatible with the lime and produced a workable, early-setting mortar which led to stronger brickwork and permitted more rapid construction. As the need for faster construction rates developed, the acceptance of Portland cement increased, until at the present time, sand-lime mortars are seldom used and are not permitted for structural brickwork.

The performance of cement-lime mortars and cement mortars is largely dependent on the proportion of cement in them. Tricalcium silicate and tricalcium aluminate are the two compounds which contribute to high early-strength development. After mixing, the cement

hydration begins immediately with hydration of the tricalcium aluminate and is followed progressively by hydration of the tricalcium silicate which is the more important in terms of the final mortar strength. The hardening process is quite different from the carbonation of a lime mortar.

The workability of a mortar is usually controlled by the use of lime although plasticizers other than lime may be interground with the Portland cement. Plasticizers such as clay and limestone and air-entraining agents provide mortars with increased workability, but are not permitted by AS A123-1963<sup>(52)</sup> as a replacement for the lime content of any mortar-type covered by that specification. Isberner<sup>(60)</sup> has described workability as a complex rheological property which includes adhesion, cohesion, density, flow-ability, plasticity and viscosity. In the laboratory, the evaluation of mortars is often made using mortars which have the same flow, which is a measurable quantity related approximately to workability. In the standard flow test, a truncated cone of mortar is subjected to twenty-five one-half inch (12mm) drops of a standard flow table. The diameter of the disturbed sample is compared with the original diameter of the conical mortar sample and the ratio of the disturbed diameter to the original diameter, expressed as percent, is called the mortar flow. Monk<sup>(40)</sup> has given the water:cement ratios, shown in Table 3.3, required to produce a desirable workability in a mortar using an average brick-layer's sand; the flow values are also given.

An important property of a mortar, which is related to workability and flow, is water retentivity which is a measure of its ability to retain water and prevent it from being drawn into bricks with high suction. Sahlin<sup>(44)</sup> has reported that there are conflicting claims among researchers regarding the effect which water retentivity

Mortar Type	Proportion by Volume Cement:Lime:Sand	Water:Cement Ratio (by Weight)	Average Flow
M	1: $\frac{1}{4}$ :3	0.74	124.3
S	1: $\frac{1}{2}$ :4 $\frac{1}{2}$	1.13	130.2
N	1:1:6	1.64	122.7

Table 3.3: Mortar Water-to-Cement Ratios

has on mortar strength and adhesion, with Höberg<sup>(61)</sup> claiming that low water retentivity gives better adhesion to very absorbent materials and Palmer and Parsons<sup>(62)</sup> claiming that the opposite is true. Water retentivity is usually measured in the laboratory by comparing the flow of a mortar sample after being subjected to a vacuum of 50mm of mercury for one minute with the original flow of the mortar. Australian Standard AS A123-1963<sup>(52)</sup> specifies that a mortar must have a minimum flow after suction of not less than 70 percent of the original flow.

Hoath<sup>(63)</sup> has plotted the curves shown in figure 3.3, derived from results obtained by Ritchie and Davison<sup>(64)</sup>, in which mortars were prepared to conform with types M, S, N, O and K as designated by the ATSM C270-68<sup>(65)</sup>.

Results obtained from mortars made from seven different types of lime and a standard sand are shown in figure 3.4. All tests were in accordance with the British Draft Standard 68/3502<sup>(66)</sup>. The results for figure 3.4 were obtained by Gillard and Lee.<sup>(67)</sup>

Davey and Thomas<sup>(30)</sup> reported that the compressive strength of mortar depends on the cement:lime ratio and the proportion of cementitious material to sand (figure 3.5), and recommended three mortar mixes for low, medium and high-strength bricks. From figure

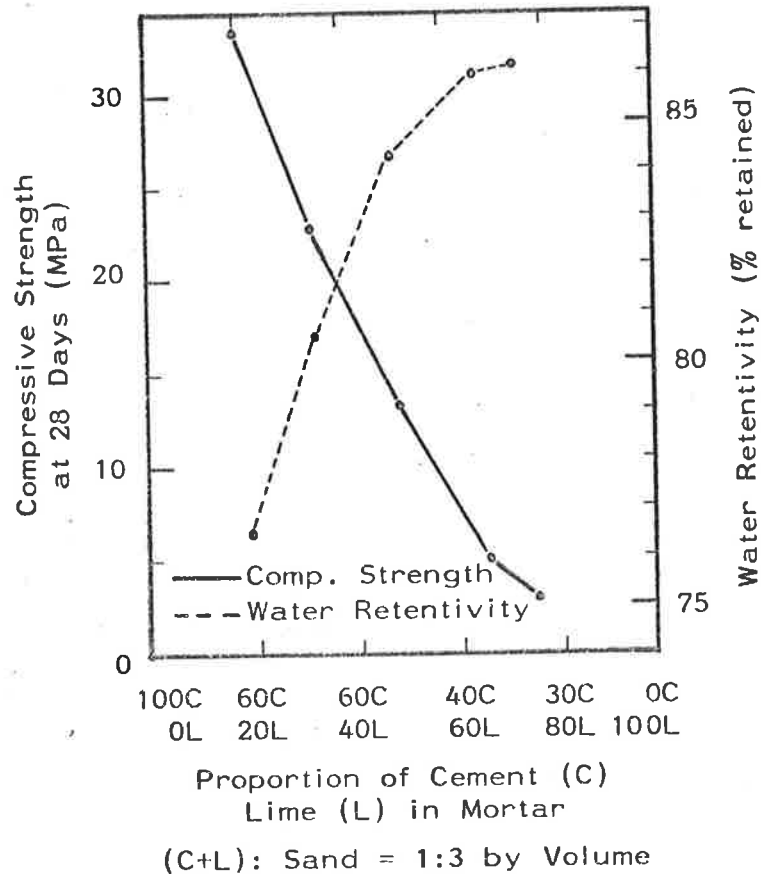


Figure 3.3: Relationship between Mortar Composition, Compressive Strength and Water Retentivity

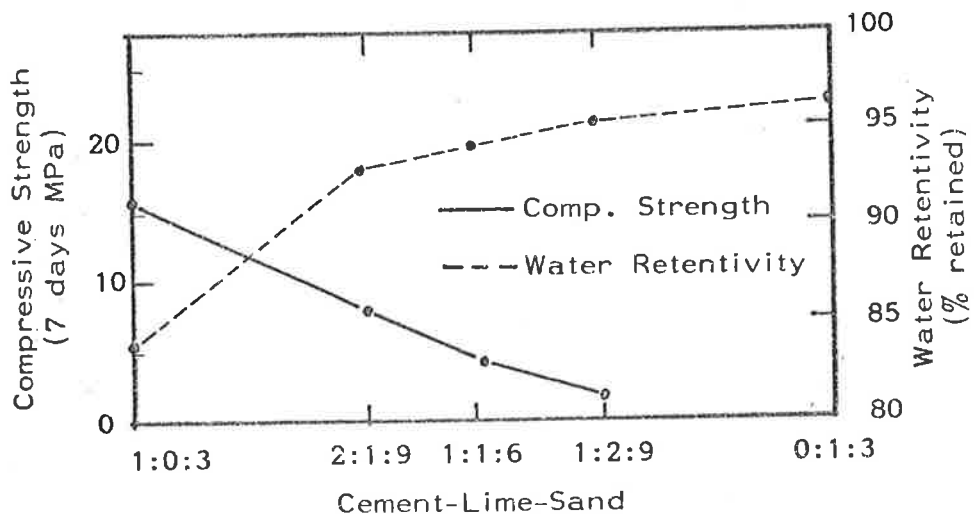


Figure 3.4: Relationship between Mortar Composition, Average Compressive Strength and Water Retentivity

Recommended Mixes for Brickwork: (30)

Mix A for low-strength bricks (10MPa)

Mix B for medium-strength bricks (20MPa to 30MPa)

Mix C for higher strength bricks (> 30MPa)

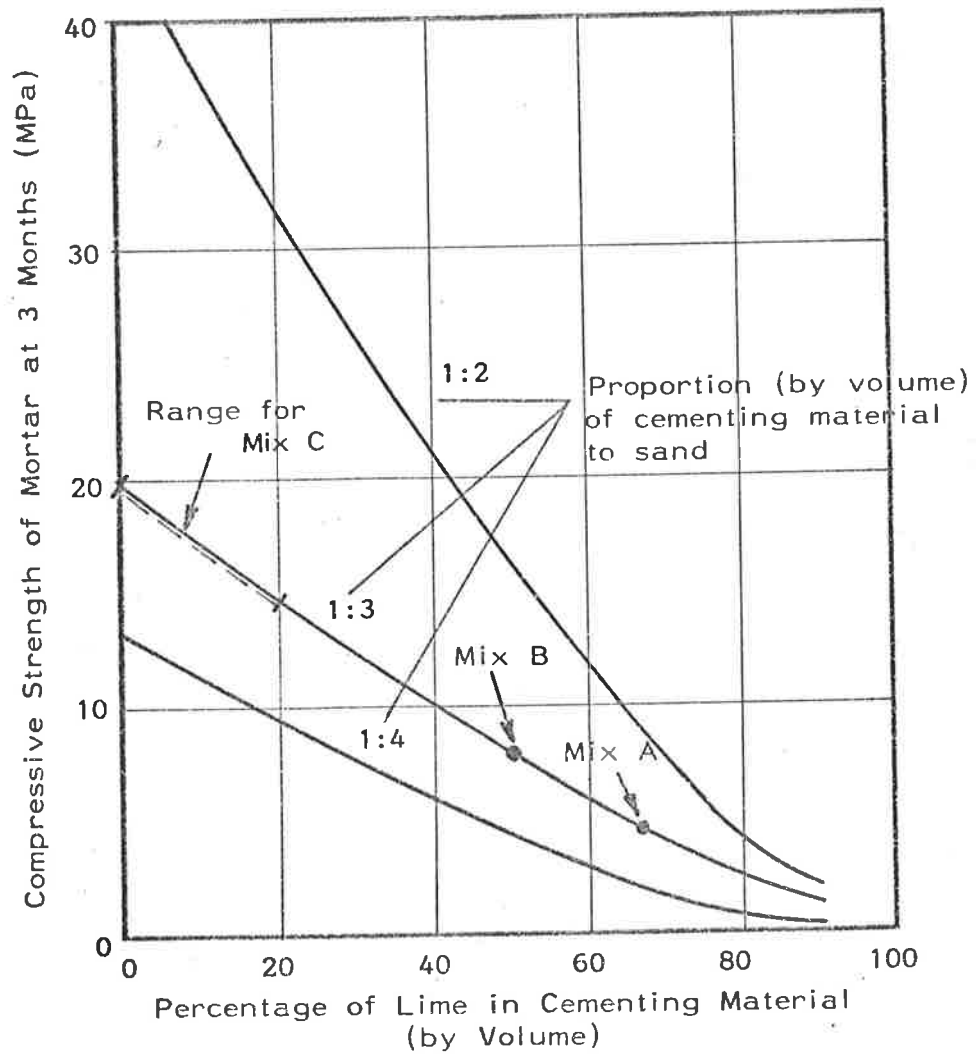


Figure 3.5: Mortar Mixes for Brickwork (30)

3.5, for ratios of cementing material to sand 1:3 by volume, pure lime mortars have compressive strengths of about 0.1 to 1.0MPa and pure cement mortars 15 to 20MPa when tested in uniaxial compression.

Lenczner<sup>(68)</sup> tested batches of 1:1:6 mortar mixes in which the water content was varied to give a range of workabilities used in common trade practice. The mortar mixes were cast into both 76mm cubes and 115mm diameter by 230mm long cylinders. The strengths of the 76mm mortar cubes, tested in uniaxial compression, varied between 2.8MPa and 6.3MPa and increased with a decrease in water:cement ratio.

Grimm<sup>(36)</sup> has summarized the experimental results of many researchers and has found that the compressive strength of mortar as measured by standard methods may be approximated by the expression —

$$f_c = 22.4 S\alpha\beta T [554\delta + \gamma (130-F)] \times 10^{-3} \quad (3.3)$$

$f_c$  is uniaxial compressive strength in MPa

$S$  is a shape factor

$\alpha$  is a moisture curing factor

$\beta$  is an air-content factor

$T$  is plastic mortar age factor

$\delta$  is mortar type factor for mortars to ASTM

$F$  is initial flow as a percent

$\gamma$  is a factor dependent upon the volumetric ratio of Portland cement:lime in mortar.

The water:cement ratios typically varied from 0.74 to 1.64. Grimm found that the higher water:cement ratios reduced mortar compressive strength but increased mortar-to-brick bond strength.

The flexural tensile strength of conventional mortar does not usually control the flexural strength of brickwork because the tensile strength of the mortar generally exceeds the tensile bond strength between mortar and brick (Section 3.3). Grimm<sup>(36)</sup> has given an approximation for flexural tensile strength, taken from results presented by Monk<sup>(40)</sup>, as -

$$f_t = 2.13 \times 10^{-3} f_c (80.75 - f_c) \quad (3.4)$$

$f_t$  is the flexural tensile strength of the mortar in MPa

$f_c$  is the compressive strength of the mortar in MPa.

Monk's results showed that for normal mortars, the flexural tensile strength is approximately 10 to 15 percent of the compressive strength.

### 3.2.3.3 Modulus of elasticity

Stress-strain diagrams from observations of different types of mortars, as reported by Hilsdorf<sup>(46)</sup> (figure 3.6), show that the tangent modulus of elasticity at zero stress varies widely for different cement/lime ratios: the highest modulus of elasticity, obtained with a cement mortar, is approximately two hundred times that of a lime mortar. Therefore if the modulus of elasticity is important, as can be the case for slender walls,<sup>(44)</sup> then the mortar used in the brickwork must be chosen with care.

Scrivener and Williams<sup>(50)</sup> determined a complete stress-strain curve for mortar cylinders (figure 3.7) and, using a stress-strain curve for lateral strains, they calculated Poisson's Ratio for a mortar bed-joint tested in a short brick pier under uniaxial loading (figure 3.8).

The value of Poisson's ratio, which is the absolute value of the ratio of the lateral strain to the longitudinal strain, had a constant value of 0.22 until the stress reached 75 percent of its maximum value



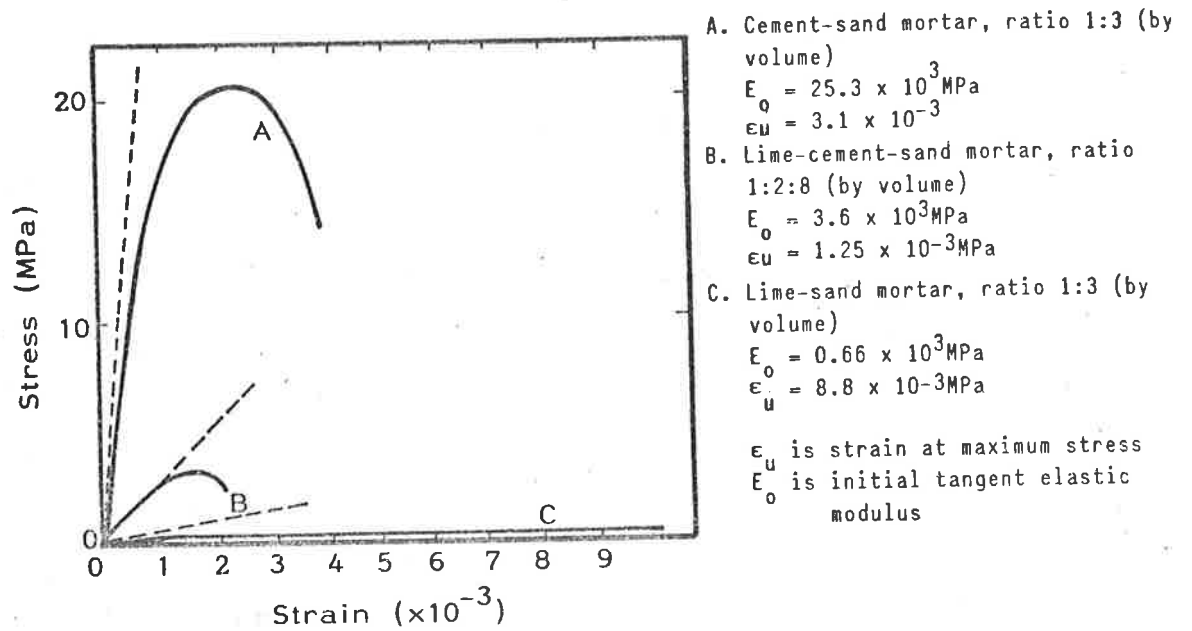


Figure 3.6: Stress-strain Diagrams for Mortars  
 (Hilsdorf<sup>(46)</sup>)

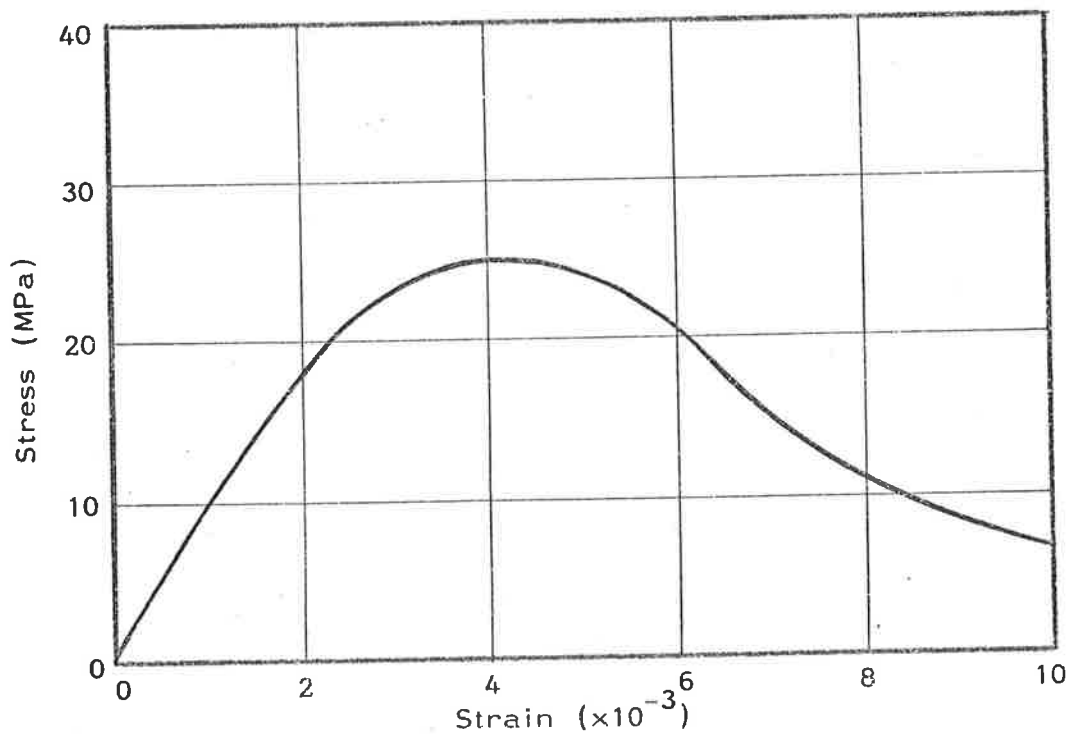


Figure 3.7: Stress-strain Curve for Mortar  
 (Scrivener and Williams<sup>(50)</sup>)

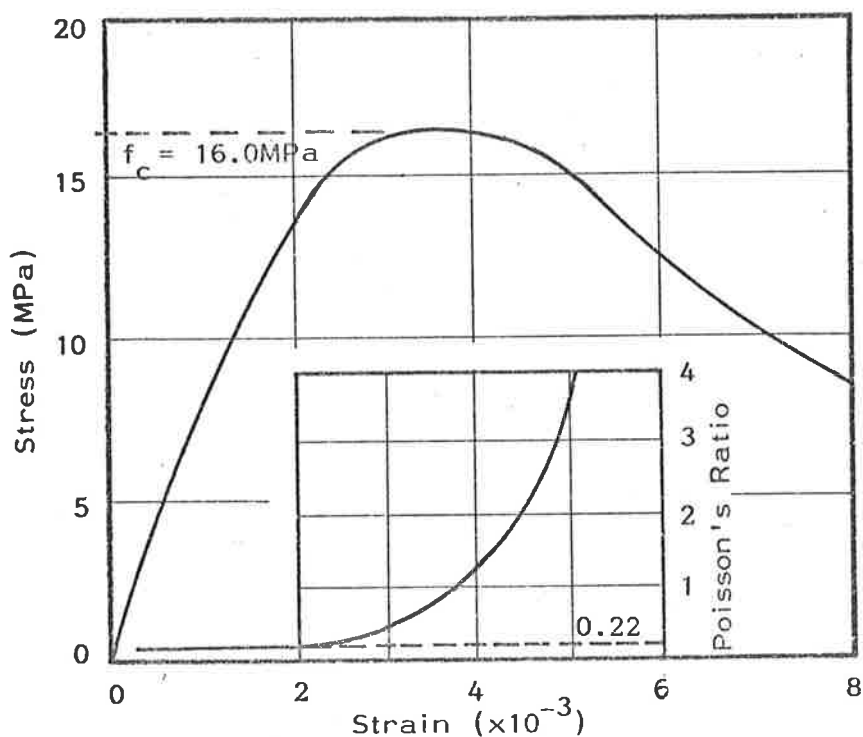


Figure 3.8: Stress-strain and Poisson's Ratio-strain for Mortar  
(Scrivener and Williams<sup>(50)</sup>)

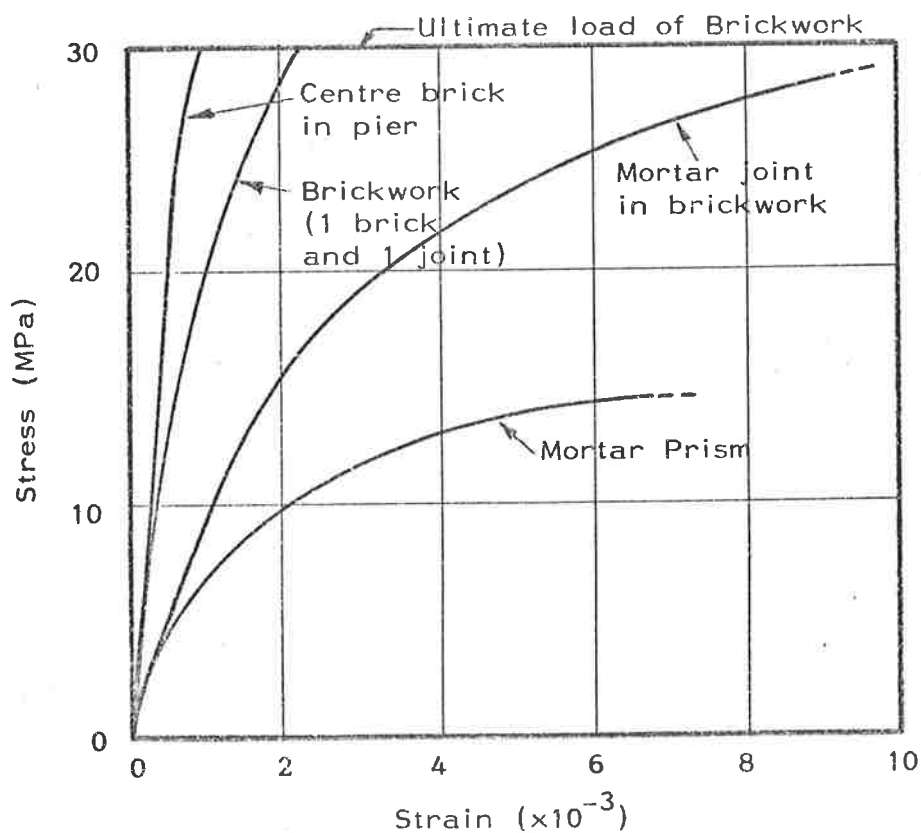


Figure 3.9: Compression Tests on Brickwork Prisms  
(Base and Baker<sup>(69)</sup>)

and then increased with increasing stress. At a stress of 98 percent maximum stress, Poisson's ratio reportedly reached a value of 0.50. As the stress level decreased after the maximum stress was reached, the ratio of lateral strains to longitudinal strains reportedly increased to a value of 3.0 at a lateral strain of approximately 0.5 percent.

Base and Baker<sup>(69)</sup> measured the strains in a mortar bedjoint as well as in the adjacent brick using DEMEC gauges and showed for their case that the strains in the mortar were very much larger than in the bricks. They also presented results (figure 3.9) which indicated the difference between the behaviour of mortar in a joint under triaxial stress conditions and its uniaxial behaviour in a mortar prism. The triaxial behaviour of mortar will be discussed in Section 3.4.

Sahlin<sup>(44)</sup> has attempted to relate mortar elastic properties to prism strength and has given the relationship shown in figure 3.10. The equations are not based on the physical material properties but are approximations deduced from tests on concrete specimens with strengths between 15MPa and 45MPa, that is, outside the range of most mortars used in practice.

The equations used by Sahlin are -

$$E_m = 1000f_c \quad (3.5)$$

$$E_m = 43 \times 10^{-3} \cdot \omega^{1.5} \cdot \sqrt{f_c} \quad (3.6)$$

$$E_m = 12.4 \times 10^3 + 500f_c \quad (3.7)$$

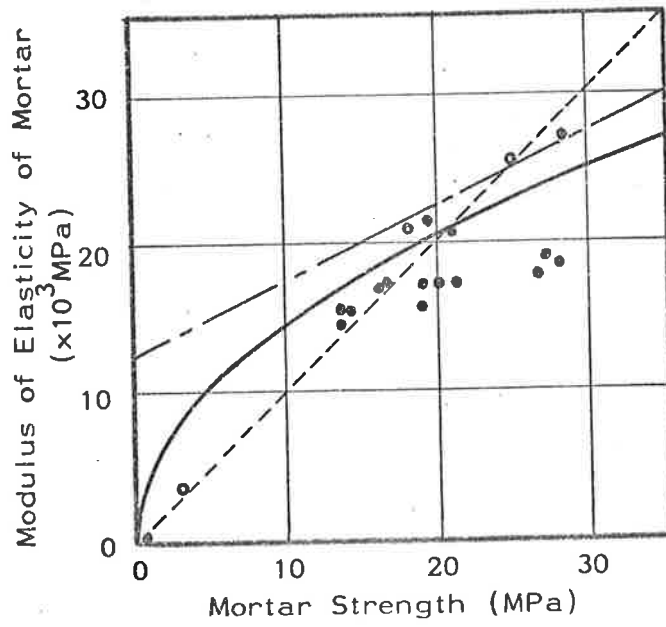
in which  $E_m$  is the mortar elastic modulus

in MPa

$f_c$  is the mortar uniaxial compressive strength

in MPa

$\omega$  is the mortar density ( $\text{kg/m}^3$ ) =  $2300\text{kg/m}^3$ .



- Glanville and Barnett (48)
- Hilsdorf (46)

Figure 3.10: Relationships between Mortar Strength and Elastic Modulus

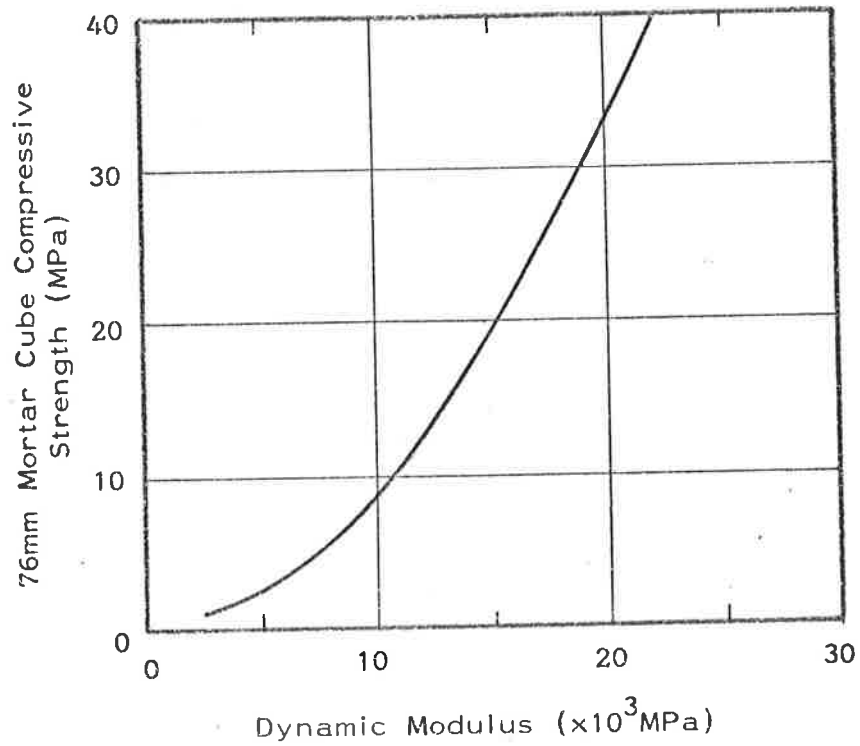


Figure 3.11: Mortar Cube Strength Related to Dynamic Elastic Modulus

None of the equations gives a particularly good approximation for the modulus of elasticity - strength relationships of mortars as tested by Glanville and Barnett<sup>(48)</sup> and by Hilsdorf.<sup>(46)</sup>

Leczner<sup>(68)</sup> tested mortar cylinders of 115mm diameter and 230mm long and determined the static elastic modulus using a compression testing machine and the dynamic elastic modulus using sonic methods. He showed that both methods of measurement gave the same results for elastic modulus and that the 28 day compressive strength of a 76mm mortar cube varied approximately as the square of the dynamic modulus (figure 3.11).

#### 3.2.4 Summary

This section has presented results which indicate that the compressive strength of a mortar depends upon the ratio of cementitious material to sand, the sand gradation and the water-to-cement ratio. Test results<sup>(68)</sup> also indicate that mortar elastic modulus may be a function of the mortar compressive strength. However, mortar test results have been obtained from various methods of testing so that quantitative comparisons between sets of data may not be made. In particular, no relationship has been established between mortar-type and the elastic properties required for the analysis of slender brick walls.<sup>(44)</sup> At this stage, therefore, a mortar elastic modulus must be determined for each case by test using either static or dynamic methods<sup>(68)</sup>. A method for determining the elastic modulus of a mortar will be discussed in Chapter 5.

### 3.3 BRICK-MORTAR COMBINATION – SMALL ASSEMBLAGES

#### 3.3.1 Introduction

In considering the general behaviour of walls and panels, it is necessary to investigate the properties of small assemblages, or units, of brickwork. Factors such as the compressive strength under loads normal to the bedjoints, the tensile strength both parallel to and normal to the bedjoints, the shear strength with simultaneous vertical compression and the elastic properties of the brickwork may all influence significantly the behaviour of brickwork either spanning vertically only or supported on more than two sides. Previous research has involved both experimental programs and theoretical analyses based on the assumption of elastic behaviour up to the point of failure. This section reviews the reported behaviour of small assemblages up to failure.

#### 3.3.2 Compressive Strength

Many investigations have been carried out on the compressive strength of brickwork loaded uniformly in a direction normal to the bedjoints. Because of the many possible combinations of bricks and mortars, the range of strengths can vary from 1MPa for very weak bricks and lime mortars up to 50MPa for very strong bricks and cement mortars.

##### 3.3.2.1 Mechanism of failure

The failure mechanism most frequently observed in structural brickwork loaded in uniform compression normal to the bedjoints is a splitting failure produced by the formation of vertical cracks through the bricks and bedjoints. Scrivener and Williams<sup>(50)</sup> observed that the first visible signs of failure were in the crushing of the mortar in the bedjoints at loads near the maximum load. The crushing of the mortar

was accompanied by very large lateral strains in the bedjoints until eventually the bricks failed in tension under the lateral expansion. In all cases the failure load was larger than the uniaxial compressive strength of the mortar as determined from mortar cylinders, but less than the compressive strength of the bricks. The increased mortar strength is related to the differential lateral expansions of the brick and the mortar. At loads near to failure, a triaxial state of stress is induced in the brickwork so that, at the brick-mortar interface, the brick material is subjected to uniaxial compression and bilateral tension; the mortar is in triaxial compression.

Monk<sup>(40)</sup> reported tests which showed that the splitting failure mechanism is consistent with the assumed stress-strain state at the brick-mortar interface if the mortar is less stiff than the bricks, Gypsum blocks, jointed by either aluminium or polythene sheets were tested in compression. When the joint material was stiffer than the blocks, as in the case of the aluminium sheet, a shear failure occurred in the gypsum which was similar to the failure of a brick tested between steel platens. However, for the polythene joint material, which was much less stiff than the blocks, a tensile splitting failure occurred. The failure load associated with shear failure was consistently higher than the failure load produced by vertical splitting of the blocks. Monk noted that in brickwork built with lime mortars, spalling and crushing of the mortar forced material from the joints at loads well below failure, but in brickwork built with cement mortars, spalling of the bricks occurred immediately prior to failure.

### 3.3.2.2 Methods of determining compressive strength

Many factors can affect the compressive strength of brickwork and it has been found that a good estimate of the load bearing capacity of a wall or panel can be made by testing small brickwork

prisms constructed from the materials to be used in the actual structure. For example, a good estimate of the strength of a single-leaf wall can be obtained by testing a statistically-significant number of single-leaf brickwork prisms constructed from the materials to be used in the wall.

Plummer and Blume<sup>(29)</sup> investigated the extent to which a testing machine with stiff bearing platens can affect the failure loads of brickwork prisms by varying the height-to-thickness ( $h/d$ ) ratio of the brickwork prisms. The compressive strengths of prisms of very low  $h/d$  ratios were affected by the stiffness of the machine platens and strength correction factors were proposed so that the splitting type of failure load in a wall could be estimated from the results of brickwork prism tests. The correction factors increase with the  $h/d$  ratio until the latter reaches a value of 6, beyond which the factors remain essentially constant for  $h/d$  ratios up to 12 (figure 3.12).

Anderson<sup>(74)</sup> compared the results of full scale wall tests conducted by Base<sup>(73)</sup> with other measures of brickwork strength and showed that prism tests gave failure loads up to 33 percent higher than those measured in full scale wall tests.

### 3.3.2.3 The effect of brick strength

It is not known whether there exists a relationship between the strength of brickwork as determined by prism strengths and the compressive strength of the brick and mortar components, although attempts have been made to relate brickwork strength to both individual brick strength and mortar prism strength. Sahlin<sup>(44)</sup> reported tests conducted by S.C.P.R.F.<sup>(47), (70), (71)</sup> which showed a non-linear relationship between brickwork strength and brick strength for various types of mortar, and tests by Nevander<sup>(45)</sup> gave a series of relationships of the form —



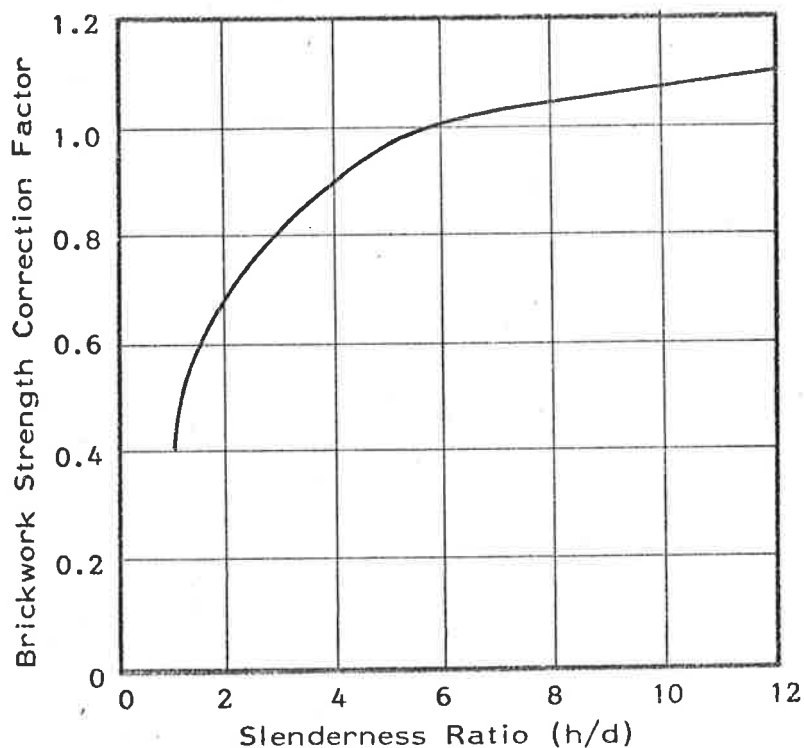
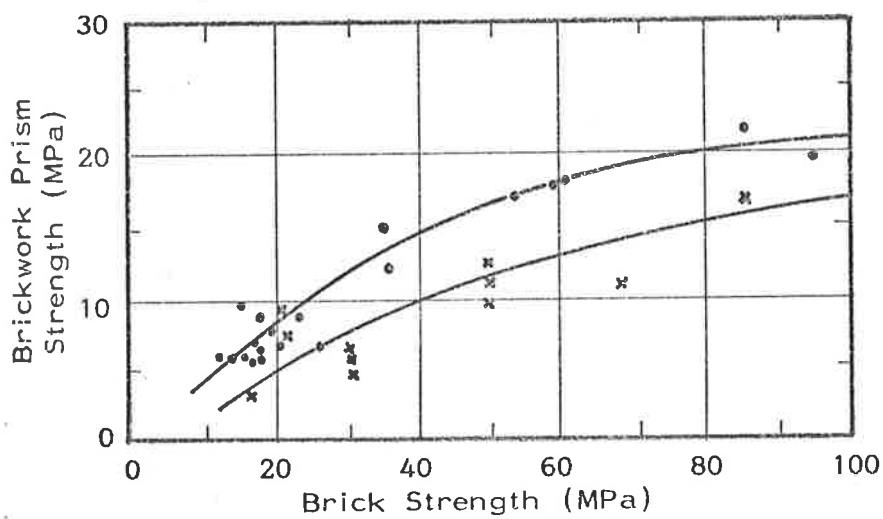


Figure 3.12: Strength Correction Factors for Brickwork Prisms <sup>(29)</sup>



- Brickwork built with 1:3 Cement-Sand Mortar of Strength 14MPa to 20MPa
- x Brickwork built with Mortar of Strength less than 3.5 MPa

Figure 3.13: Relationship between Brick Strength and Strength of Brickwork Prisms  
(Davey and Thomas <sup>(30)</sup>)

$$F'_m = kC^n \quad (3.8)$$

in which  $F'_m$  is the brickwork compressive strength

$C$  is the brick strength

$k, n$  are constants which depend on the brick strength and mortar type.

Davey and Thomas<sup>(30)</sup> related the strength of 18" x 18" x 8'-0" (460mm x 460mm x 2440mm) brickwork piers to the strength of the individual bricks when combined with either weak mortar having a prism strength less than 3.5MPa or strong mortar with a strength between 14MPa and 20MPa (figure 3.13). The experimental relationships between pier strength and brick strength for the two mortars generally follow the form of equation (3.8).

Lenczner<sup>(66)</sup> investigated the strength of 9" (230mm) brickwork cubes and found that the dry density of the bricks was directly related to cube strength and further suggested that brick dry density could be a useful criterion for estimating the strength of brickwork for a given mortar type.

The compressive strength of brickwork built with cored bricks rather than solid bricks is affected by a number of additional parameters, not all of which are fully understood. Nevander<sup>(45)</sup>, in tests which included solid bricks, bricks which were cored with 19 holes and bricks cored with 78 holes showed that there was a significant decrease in strength when the cored bricks were combined with a weak lime mortar, but the 19-hole bricks gave the same or higher strength than solid bricks when laid in a medium-strength lime-cement mortar.

Schellbach<sup>(41)</sup> tested cored bricks in a mortar with proportions 1:2:8 (cement:lime:sand by volume) and found that optimum utilization

could be made of the brick material if the bricks had a core space ratio of about 38 to 43 percent, provided that stress concentrations were avoided by using cores with no sharp or re-entrant corners.

#### 3.3.2.4 Effect of mortar properties

The effect of mortar properties on the strength of 9 inch (230mm) brickwork cubes was studied by Lenczner<sup>(68)</sup> who related the 28-day mortar strength, determined from 76mm cubes loaded in uniaxial compression, to the brickwork cube strength. The general relationship between the brickwork cube strength and mortar strength was taken to be --

$$F'_m = k (f_c)^{0.25} \quad (3.9)$$

where  $F'_m$  is brickwork cube strength

$k$  is constant of proportionality

$f_c$  is mortar cube strength in uniaxial compression.

Stang, Parsons and McBurney<sup>(72)</sup> also proposed an exponential relationship between wall strength and mortar strength of the form

$$F'_m = k (f_c)^{0.33} \quad (3.10)$$

in which  $F'_m$  is brickwork compressive strength.

The compressive strength of brickwork has also been found to depend upon the thickness of the mortar joint. Sahlin<sup>(44)</sup> concluded that brickwork strength is decreased by approximately 15 percent for every 1/8 inch (3.2mm) increase in bedjoint thickness from a mean value of joint thickness of 3/8 of one inch (9.5mm). He also stated that if the bedjoint thickness is decreased from this mean value, a 15 percent increase in compressive strength for each 1/8 inch (3.2mm) decrease in joint thickness may be expected. Scrivener and Williams<sup>(50)</sup>

reported a less significant bedjoint thickness effect in which, for both a weak lime-cement mortar and a richer cement mortar, specimens with  $\frac{1}{4}$  inch (6.3mm) joint thickness only had compressive strengths approximately 10 percent greater than specimens with  $\frac{1}{2}$  inch (12.7mm) thickness. The degree of change in strength with change in bedjoint thickness was also reported by Lenczner<sup>(68)</sup> to be approximately 10 percent per  $\frac{1}{8}$  inch (3.2mm) change in bedjoint thickness. Methods which may be used to calculate the effect of bedjoint thickness on compressive strength of brickwork will be reviewed in Section 3.3.2.6.

### 3.2.2.5 Brickwork strength related to brick and mortar interaction

The compressive strength of brickwork is dependent upon both the brick and mortar properties and not upon each independently of the other as implied by the results reviewed in the previous two sections. However, the interactive influences of the two materials are very difficult to assess. Bröcker<sup>(75)</sup> proposed the empirically-based relationship -

$$F'_m = C^{0.5} \cdot f_c^{0.33} \quad (3.11)$$

where  $F'_m$  is the compressive strength of brickwork

$C$  is brick compressive strength

$f_c$  is uniaxial mortar compressive strength.

Schellbach<sup>(41)</sup> reported tests on walls constructed with 1:2:8 mortar and either solid or cored bricks which showed good agreement with equation (3.11) especially when the brick strengths were above 25MPa and the void ratio for the cores did not exceed 35 percent of the brick area.

By analysing experimental data from a large number of tests, Grimm<sup>(36)</sup> suggested that the interactive effect of brick and mortar properties on the compressive strength of brickwork could be expressed by equation (3.12).

$$F'_m = 298 \times 10^{-6} \xi \eta C (f_c^2 + 450)(1 + \epsilon)^{-1} \quad (3.12)$$

in which  $F'_m$  is compressive strength of masonry in MPa

$\epsilon$  is workmanship factor

= 0 for inspected work

= 0.012 (83 - C) for uninspected work in which

$C < 83\text{MPa}$

or assume  $C = 83\text{MPa}$  if  $C > 83\text{MPa}$

$C$  is average compressive strength of bricks in MPa  
(ASTM67<sup>(76)</sup>)

$\xi$  is a brickwork prism slenderness factor

$$= 0.0178 \{57.3 - [h_s/t_s - 6]^2\}$$

where  $h_s/t_s$  is the prism slenderness ratio (height-to-

least lateral dimension) in which  $2 < h_s/t_s < 6$

$\eta$  is material size factor

$$= 0.0048 \{273 - [h_u/t_j - 14]^2\}$$

where  $h_u/t_j$  is the ratio of the brick height to mortar

bed thickness in which  $2.5 < h_u/t_j < 10$

$f_c$  is the compressive strength of mortar in MPa determined

from mortar prism tests.

Grimm stated that equation (3.12) applied to brickwork prisms with compressive strengths in the range of approximately 1.7MPa to 45MPa (250psi to 6500psi). He did not give any confidence limits on results using equation (3.12), but implied that brickwork strength is proportional to brick strength for a given mortar strength, a premise which is not supported by results reviewed in Section 3.3.2.3.

For practical purposes, Davey and Thomas<sup>(30)</sup> recommended the combinations of brick strength and mortar type, given in Table 3.4, to obtain both efficiency and economy.

Brick Strength		Mortar Mix (C:L:S by volume)
psi	MPa	
< 1500	< 10.4	1:2:9
3000 to 4000	20.7 to 27.6	1:1:6
> 4000	> 27.6	1: $\frac{1}{4}$ :3

Table 3.4: Brick and Mortar Combinations

They gave no recommendation for brick strengths between 10.4MPa and 20.7MPa (1500psi and 3000psi) although 1:1:6 mortar would be suitable for bricks in that low to medium strength range.

### 3.3.2.6 Theoretical prediction of compressive strength

Hilsdorf<sup>(77)</sup>, Khoo and Hendry<sup>(118)</sup> and Francis et al.<sup>(78)</sup> have attempted to predict the compressive strength of brickwork analytically by evaluating the interaction of the materials up to failure. Hilsdorf assumed that the stress distribution in a brickwork pier could be idealized as in figure 3.14.

Shellbach<sup>(41)</sup> found experimentally that the failure load of brickwork made of high strength bricks (100MPa) could be increased by up to 80 percent if the normally-irregular brick faces were ground flat. Surface and material irregularities caused the stresses,  $\sigma_y$ , in the direction of the external load to be non-uniform so that stress concentrations could be present to cause premature failure of the brickwork. Hilsdorf expressed the ratio of the maximum normal stress to the average normal stress by a term, U, called the non-uniformity coefficient.

Experiments by Base and Baker<sup>(69)</sup> showed that U varied between 1.10 and 1.49 depending on the brickwork sample and the stress level,

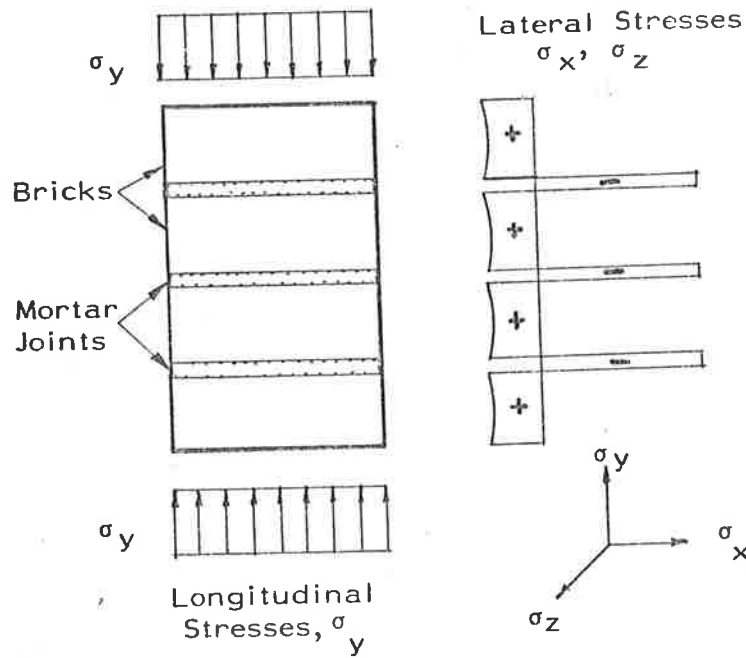


Figure 3.14: Stress Distribution in a Brickwork Prism (Hiltsdorf<sup>(77)</sup>)

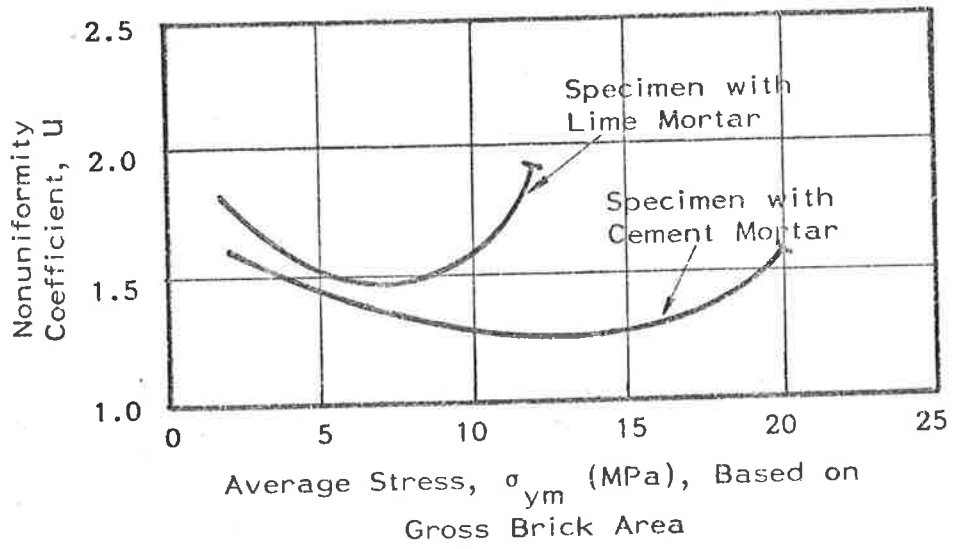


Figure 3.15: Values of Nonuniformity Coefficient,  $U$ . (Hiltsdorf<sup>(77)</sup>)

and Hilsdorf found experimentally that  $U$  varied as in figure 3.15. Figure 3.16 shows how the combination of stresses could vary in a single brick within a brickwork unit subjected to axial compression.

For the purpose of constructing the diagram, it is assumed that the lateral tensile stresses,  $\sigma_x$  and  $\sigma_z$ , are equal and that the critical compressive stress,  $\sigma_y$ , is equal to the average stress,  $\sigma_{ym}$ , multiplied by the non-uniformity coefficient  $U$ . With reference to figure 3.16, line A represents the assumed failure criterion for a brick subjected to uniform compression and biaxial tension, and the development of internal stresses under increasing load is assumed to be given by a stress path, such as line  $B_1$ . Hilsdorf assumed that the intersection of line  $B_1$  would produce only local cracking in the brick and would not cause total failure because the triaxial stress state in the mortar for that loading condition would not constitute a failure state in the mortar (line C). Failure of the brickwork was assumed to occur at a triaxial stress condition represented by the point at the intersection of line A and line C in figure 3.16. Hilsdorf assumed that the strength of mortar under triaxial compression was similar to the strength of concrete under triaxial compression. Richart et al. (81) had found that, for a small range of concrete strengths, the triaxial strength of concrete could be approximated by —

$$f_1 = f_c + 4.1 \sigma_2 \quad (3.13)$$

in which  $f_1$  is the compressive strength of a laterally confined concrete cylinder

$f_c$  is the uniaxial compressive strength of a concrete cylinder

$\sigma_2$  is the lateral confinement pressure on the cylinder.

Hilsdorf further assumed, for simplicity, that the lateral stresses were uniformly distributed throughout the height of each brick and



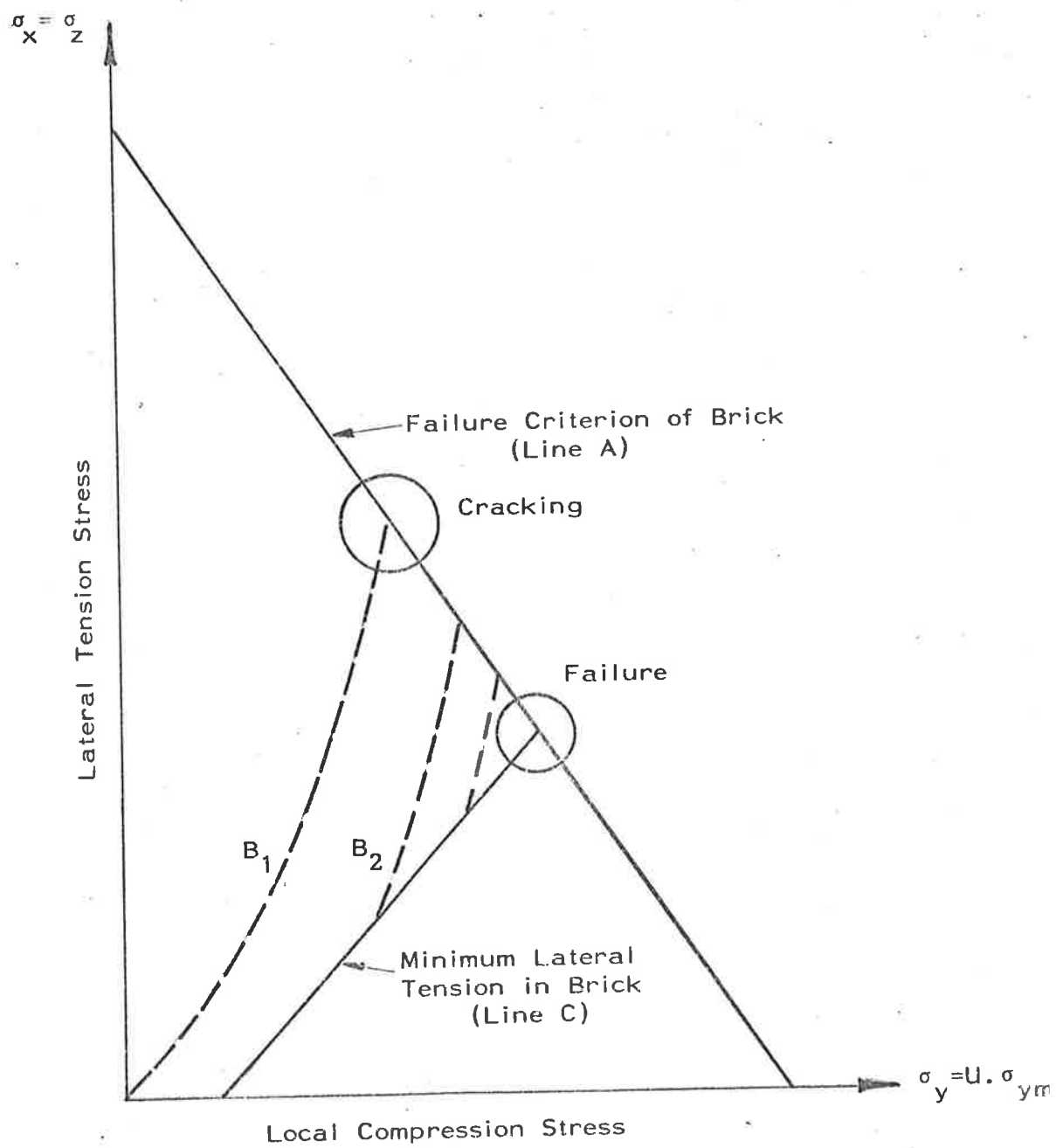


Figure 3.16: Failure Theory for Brickwork  
(Hilsdorf<sup>(77)</sup>)

each mortar joint. The expression Hilsdorf obtained for the axial strength of masonry was -

$$F'_m = \frac{C}{U_u} \cdot \frac{f_{bt} + r_{jb} \cdot f_c}{f_{bt} + r_{jb} \cdot C} \quad (3.14)$$

in which  $F'_m$  is brickwork strength

$U_u$  is value of non-uniformity at failure

$f_{bt}$  is uniaxial brick tensile strength

$f_c$  is uniaxial mortar compressive strength

$r_{jb}$  is the ratio proportional to joint thickness/brick height

$$= \frac{j}{4.1 b} \quad \text{where } j \text{ is joint thickness}$$

$b$  is brick height

$C$  is the brick uniaxial compressive strength.

The non-uniformity coefficient  $U_u$  was not constant but depended on a number of parameters including joint thickness and mortar strength.

Khoo and Hendry<sup>(117)</sup> investigated the behaviour of brick material in a state of biaxial tension and uniaxial compression and the behaviour of mortar subjected to triaxial compression. They established that the strength envelope for brick, which Hilsdorf assumed to be linear (figure 3.16), could be represented by the relationship

$$\left( \frac{\sigma'_{ym}}{C} \right) = 1 - \left( \frac{\sigma'_t}{f_{bt}} \right) 0.546 \quad (3.15)$$

in which  $\sigma'_{ym}$  is the average compressive stress at failure

$C$  is the uniaxial brick compressive stress

$\sigma'_t$  is the tensile stress at failure

$f_{bt}$  is the uniaxial brick tensile strength.

Equation (3.15) is shown in figure 3.17 and was based on the results of tests on a large number of specimens of bricks ranging in crushing strength from 31.6MPa to 92.7MPa. The concave shape of the failure curve shows that the compressive strength of a brick may be severely reduced by the presence of orthogonal tensile stresses.

Khoo and Hendry also investigated the triaxial compressive strength of 1:¼:3 and 1:1:6 mortars using a triaxial test cell. (118) The principal stress relationship was found to be

$$\frac{f_1}{f_c} = 1 + 2.91 \cdot \left(\frac{\sigma_2}{f_c}\right)^{0.805} \quad (3.16)$$

in which  $f_1$  is the compressive strength of the laterally confined mortar

$f_c$  is the uniaxial strength of the mortar

$\sigma_2$  is the lateral confinement pressure on the mortar.

Equation (3.16) gives lower strengths for mortar in a triaxial stress state than does equation (3.13) proposed by Hilsdorf. On the basis of their test results, Khoo and Hendry (117), (119) proposed a failure theory for brickwork (figure 3.18).

As the vertical compression acting on a brickwork increases, the state of stress in the brick may change as represented by the dashed line OA in figure 3.18. Failure should occur in the brick when the curve OA intersects the failure envelope at point A, so that the compressive strength of the brickwork prism would be given by the stress ordinate at that point. The stress path depends upon the characteristics of the mortar joint under triaxial compression, so that for a weaker mortar, whose lateral strain may be greater under vertical load, the stress path could be represented by the curve OB. In this case, the point B on the failure envelope would define the compressive strength of the brickwork prism. Hendry indicated that

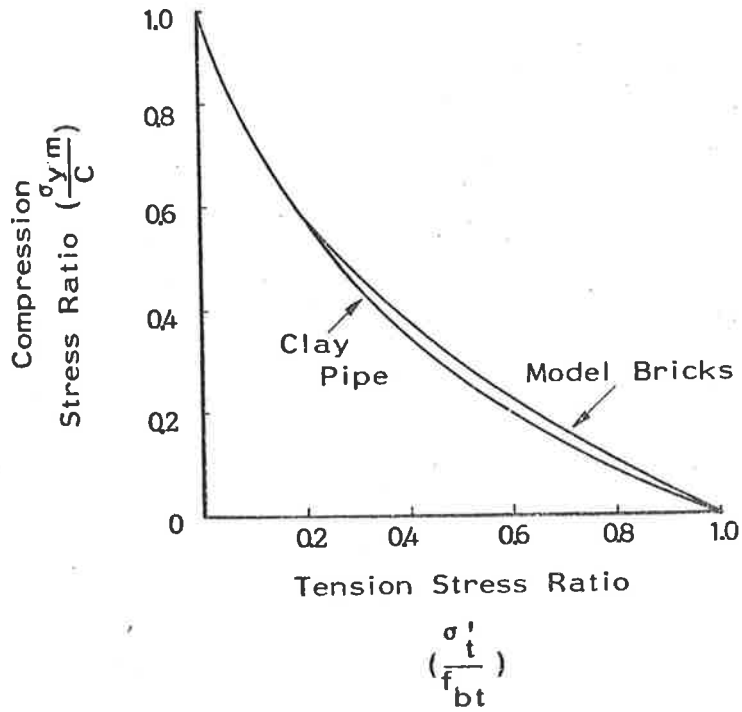


Figure 3.17: Failure Envelope for Bricks (Khoo and Hendry<sup>(117)</sup>)

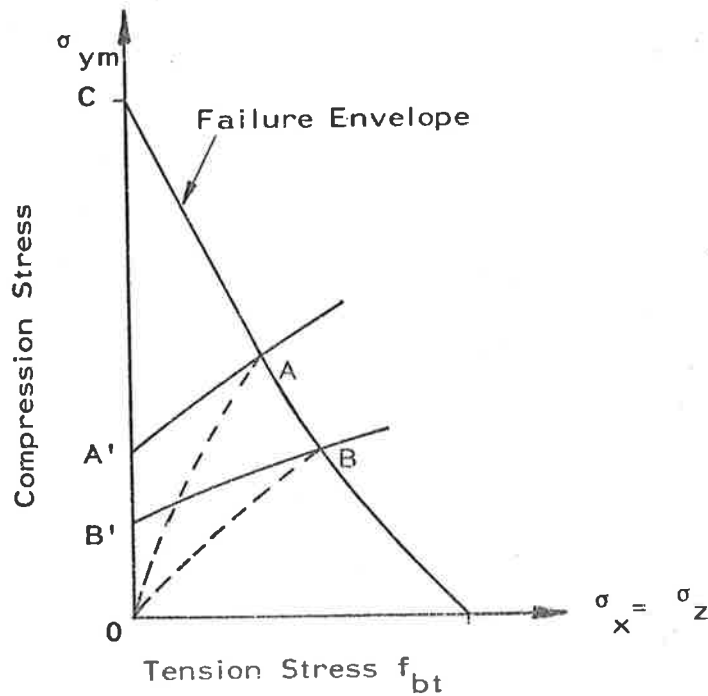


Figure 3.18: Failure Envelope for Brick Material (Khoo and Hendry<sup>(120)</sup>)

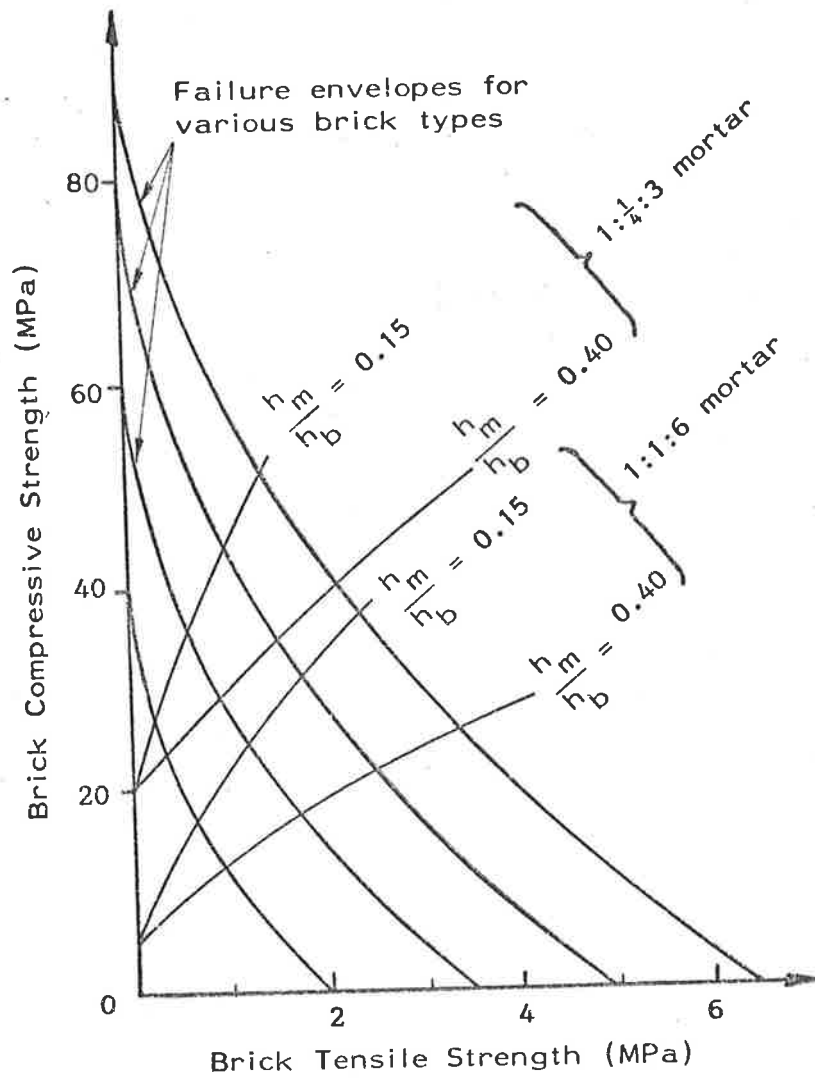


Figure 3.19: Graphical Solution for Brickwork Prism Compressive Strength (Hendry<sup>(120)</sup>)

it is not necessary to determine the stress paths OA and OB in figure 3.18 because the stresses in the brick at the brick-mortar-interface can be represented by superimposing on the brick failure envelope a curve derived from the triaxial compressive strength relationship for the mortar. Curves for various mortars have been determined by Khoo<sup>(118)</sup> and are shown in figure 3.19 superimposed on the brick failure envelope (curves AA' and BB'). Hendry<sup>(120)</sup> reported that the brickwork prism strengths calculated using graphs such as figure 3.19 compare well with experimental results.

Francis et al.<sup>(78)</sup> assumed that the stress distribution in a stack-bonded prism could be as shown in figure 3.20. The prism is subjected to an axial compressive stress  $\sigma_y$  so that the lateral stresses induced in a central brick and in the mortar joint above and below it may be represented as in figure 3.20(b). The failure envelope assumed for the brick was the linear relationship between tensile and compressive stresses shown in figure 3.21. It can be shown that the failure compressive stress  $\sigma_{ult}$  is related to the lateral tensile stress  $\sigma_{xb}$  induced in the brick by a linear expression of the form –

$$\sigma_{xb} = \frac{1}{\phi} \cdot (\sigma'_{ult} - \sigma_{ult}) \quad (3.17)$$

$$\text{in which } \phi = \frac{\sigma'_{ult}}{\sigma'_t}$$

and  $\sigma'_t$  is the lateral tensile strength of the brick.

With reference to figure 3.20, the strains in the brick in the x and z directions may be calculated as follows:

$$\epsilon_{xb} = \frac{1}{E_b} [\sigma_{xb} + \nu_b (\sigma_y - \sigma_{zb})] \quad (3.18)$$

$$\epsilon_{zb} = \frac{1}{E_b} [\sigma_{zb} + \nu_b (\sigma_y - \sigma_{xb})] \quad (3.19)$$

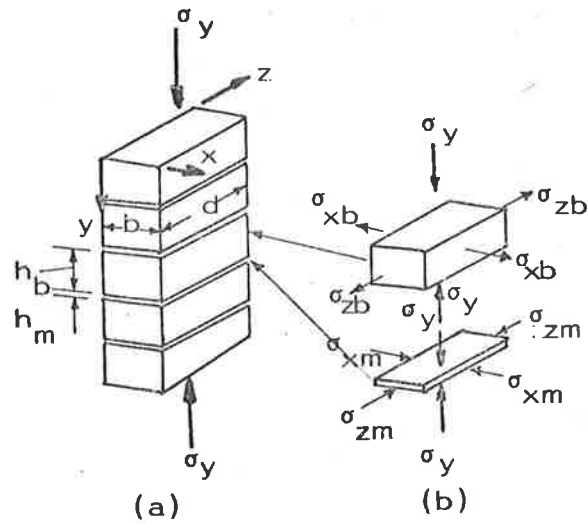


Figure 3.20: Brick and Mortar Stresses due to Applied Compressive Load (Francis et al. (78))

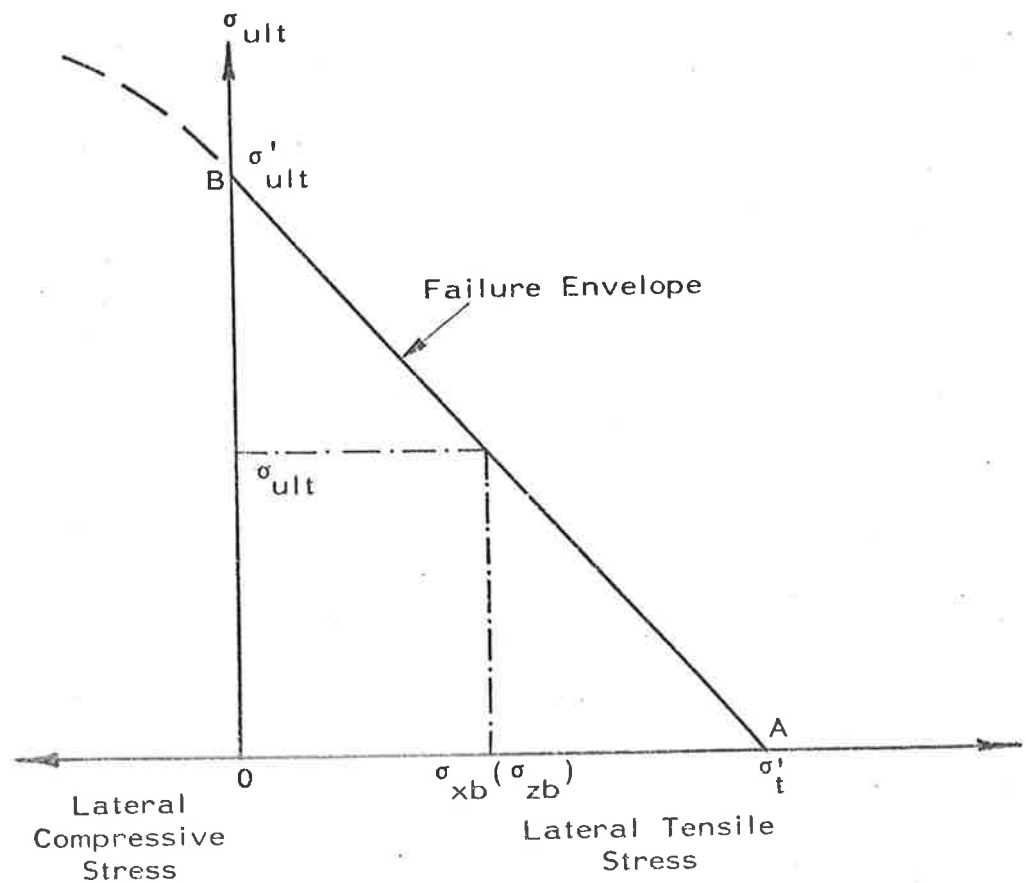


Figure 3.21: Theoretical Failure Envelope Relating Tensile and Compressive Stresses in Brick at Failure (Francis et al. (78))

Similarly, in the mortar joints

$$\epsilon_{xm} = \frac{1}{E_m} [-\sigma_{xm} + \nu_m (\sigma_y - \sigma_{zm})] \quad (3.20)$$

$$\epsilon_{zm} = \frac{1}{E_m} [-\sigma_{zm} + \nu_m (\sigma_y - \sigma_{xm})] \quad (3.21)$$

In the above equations  $E_b$  and  $E_m$  are the elastic moduli of the brick and mortar respectively and  $\nu_b$  and  $\nu_m$  are the corresponding Poisson's ratios.

For equilibrium, the total lateral tensile force in the brick is equal to the total lateral compressive force in the mortar, so that if the ratio of brick height-to-mortar thickness is denoted by  $(\frac{h_b}{h_m})$ , then -

$$\sigma_{xm} = \frac{h_b}{h_m} \cdot \sigma_{xb} \quad (3.22)$$

$$\text{and } \sigma_{zm} = \frac{h_b}{h_m} \cdot \sigma_{zb} \quad (3.23)$$

For compatibility of displacements at the brick-mortar interface,

$$\epsilon_{xb} = \epsilon_{xm}$$

$$\text{and } \epsilon_{zb} = \epsilon_{zm} \quad (3.25)$$

Therefore, from equations (3.18) and (3.20), (3.19) and (3.21), (3.22), (3.23), (3.24) and (3.25), it can be shown that -

$$\sigma_{xb} = \sigma_{zb} = \frac{\sigma_y \cdot \left( \frac{E_b}{E_m} \cdot \nu_m - \nu_b \right)}{1 + \frac{h_b}{h_m} \cdot \frac{E_b}{E_m} - \nu_b - \frac{h_b}{h_m} \cdot \frac{E_b}{E_m} \cdot \nu_m} \quad (3.26)$$



Substituting for  $\sigma_{xb}$  in equation (3.26) using equation (3.17), and neglecting the term  $(1 - \nu_b)$  gives the result

$$\frac{\sigma_{ult}}{\sigma'_{ult}} = \frac{1}{1 + \left\{ \frac{\phi \left( \frac{E_b}{E_m} \cdot \nu_m - \nu_b \right)}{\frac{h_b}{h_m} \cdot \frac{E_b}{E_m} (1 - \nu_m)} \right\}} \quad (3.27)$$

Francis conducted experiments to test results from equation (3.27) by using two types of brick, one solid and the other cored, together with 1:1:6 mortar and showed that the reduction in brickwork prism strength caused by mortar joint thickness could be predicted to an acceptable degree of accuracy as shown in figure 3.22. However, the assumption that mortar is linearly elastic up to failure is not supported by experimental evidence (Section 3.2) and test results presented by Khoo and Hendry do not support either Hilsdorf's or Francis' proposition that a Tresca-type failure criterion is applicable to brick material. Francis used a Poisson's ratio for mortar of 0.25, and although its value was important to the result, it was estimated and not measured. Therefore, of the three methods described in this section, the graphical approach proposed by Khoo and Hendry (figure 3.19), based upon experimental tests on brick and mortar materials, appears to give the best estimate available at this stage of the compressive strength of a brickwork prism.

### 3.3.2.7 The effect of time on compressive strength

The curing time of the cement and lime in the mortar in the joints affects the compressive strength of brickwork in a manner similar to that for the cement in concrete. Sahlin<sup>(44)</sup> reported the increase in mortar prism strength with time, based on data presented by Davis<sup>(79)</sup> as shown in figure 3.23.

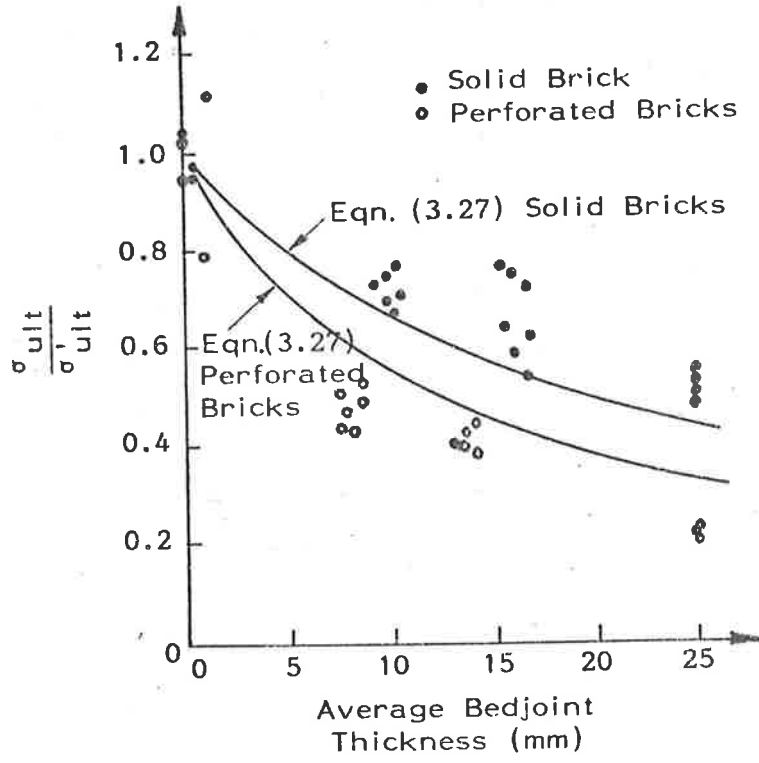


Figure 3.22: Variation of Brickwork Prism Strength with Mortar Joint Thickness (Francis et al.<sup>(78)</sup>)

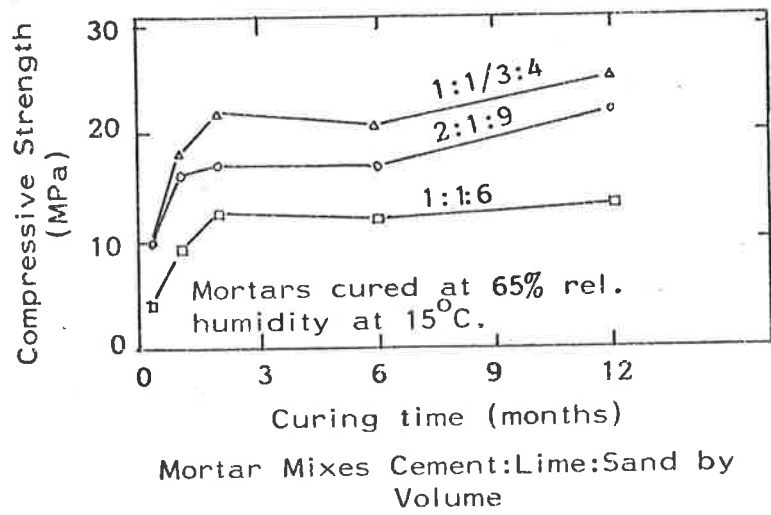


Figure 3.23: Relationship between Mortar Strength and Curing Time (Sahlin<sup>(44)</sup>)

It was shown in the previous section that the strength of brickwork is related to the triaxial compressive strength of the mortar so that it may be assumed that the increase in brickwork strength with time is similar in a qualitative sense to the increase with time of mortar prism strength as shown in figure 3.23. That is, compressive strength increases significantly up to approximately two months after construction after which no significant change in strength is apparent. From the results shown in figure 3.23, the 28-day uniaxial compressive strength of a mortar is approximately 70 percent of the long-term strength.

#### 3.3.2.8 Effect of bond patterns

Monk<sup>(40)</sup> described several investigations on both piers and walls in which different bond patterns were used. No significant difference in compressive strengths was observed among the various methods of bonding. Sinha and Hendry<sup>(80)</sup> reached the same conclusion after tests on model brickwork walls using several different bonding systems. The differences which may occur between single-leaf walls and multiple-leaf walls will not be discussed here.

#### 3.3.2.9 Summary

The compressive strength of brickwork depends upon the strength of the mortar in triaxial compression and the brick material in vertical compression and biaxial lateral tension. Empirical studies based on the uniaxial strengths of both the brick and mortar materials have resulted in proposed formulae which may be used to obtain approximate values of brickwork strength, for example equation (3.12) (Grimm<sup>(36)</sup>). Khoo and Hendry<sup>(118)</sup> have proposed an analytical approach by which the compressive strength of brickwork may be predicted using a graphical method as shown in figure 3.19. The compressive strength

of brickwork may be calculated using their method once the mortar type, the brick uniaxial compressive strength and the ratio of the mortar thickness to brick height are known.

### 3.3.3 Axial and Flexural Tensile Strength Across the Bedjoints

Tensile failure, or cracking along the bedjoints, can be produced either by pure axial tension or by tension caused by flexure. Structural brickwork is often constructed from relatively high strength bricks and medium-to-high strength mortars so that the most frequent mode of tensile failure across the bedjoints results from a bond failure at a brick-to-mortar interface. Mortars which are modified by organic bonding agents can develop exceptionally high bond so that failure may occur in the bedjoint mortar, and possibly in the brick adjacent to the mortar-brick interface. However, normal Portland cement mortars which use only lime as a plasticizer do not usually experience material tensile failure. The factors which influence the strength of the bond between the bedjoint mortar and the bricks are reviewed in the following sections.

#### 3.3.3.1 A comparison between axial and flexural bond

Plummer and Blume<sup>(29)</sup> assessed results obtained by Davis<sup>(79)</sup> who reported differences between the bond strength of brickwork when measured in axial tension and in flexure across the bedjoints. (Bond strength measured by a test which induces flexure tension with no axial tension is usually referred to as the modulus of rupture of brickwork.) In the tests, all bricks were wet prior to laying and axial tensile bond was determined using couplets of crossed bricks. The modulus of rupture was determined using a line load on a cantilever brickwork pier which spanned in a direction normal to the bedjoints. Comparisons between the axial tensile bond strength and the modulus

of rupture for three types of brick and three types of mortar can be made from the results summarized in Table 3.5. Davis concluded that the axial tensile strength, determined from a test on a cross-brick couplet, is less than the modulus of rupture. Further tests were conducted and the results indicated that bond is approximately 25 percent less between mortar and smooth brick surfaces than between mortar and roughened surfaces. Table 3.5 shows that in all cases, the axial tensile bond strengths were less than the moduli of rupture and in no instance was the bond strength greater than 20 percent of the mortar compressive strength.

	Brick Designation (a)								
	A			B			C		
Mortar Type (b)	1	2	3	1	2	3	1	2	3
Axial Tensile Bond (MPa)	0.45	0.56	0.23	0.43	0.60	0.19	0.59	0.45	0.34
Modulus of Rupture (MPa)	1.19	1.23	0.66	1.57	0.72	0.79	2.36	1.14	1.39

(a) Brick A; C = 20.9MPa  
 Brick B; C = 26.7MPa  
 Brick C; C = 53.2MPa

(b) Mortar 1; 1:1/3:4;  $f_c = 20.2\text{MPa}$   
 Mortar 2; 1:1/2:4 1/2;  $f_c = 17.0\text{MPa}$   
 Mortar 3; 1:1:6;  $f_c = 11.7\text{MPa}$

Table 3.5: Bond Strength in Brickwork Prisms

Grimm<sup>(36)</sup> reported results of flexural tensile strength and direct tensile strength tests measured according to ASTM E149<sup>(82)</sup>. He showed that the flexural tensile strength ranged from 0.34MPa to 3.4MPa (50psi to 500psi) and typically was as much as twice the value of the direct tensile strength. The larger values of flexural tensile strength

(modulus of rupture) agreed with the results in Table 3.5 given by Davis, but neither Davis nor Grimm offered an explanation for the flexural bond strength being greater than axial tensile strength.

### 3.3.3.2 Factors which affect bond.

The bond of conventional Portland cement mortar to brick is primarily a mechanical keying of the mortar into the brick surface rather than a molecular bond<sup>(36)</sup>. Therefore, the mortar paste must flow into the surface voids of the brick so that three factors which affect brick-mortar bond are flow of the mortar, water retentivity of the mortar and brick suction (I.R.A.). Tests reported by Isberner<sup>(60)</sup> indicated that the addition of water to a mortar which raised its flow from 100 to 135 percent produced a decrease in compressive strength but increased the tensile bond strength (figure 3.24).

The increase in bond strength with increased water-to-cement-ratio possibly was caused by the increased ability of the mortar to flow into the brick surface irregularities.

Youl and Foster<sup>(83)</sup> suggested, as a result of experiments on miniature brickwork panels, that optimum bond, as measured by a flexural bond test, could be achieved with a mortar flow of 130 percent and water retentivity not less than 80 percent.

Plummer and Reardon<sup>(84)</sup> reported that the tensile bond strength decreased rapidly as the brick suction (I.R.A.) increased, particularly for strong cement mortars (figure 3.25). The removal of water from the mortar by the brick causes incomplete hydration of the cement at the brick-mortar interface and thereby leads to reduced mortar strength.

Other researchers<sup>(36), (72)</sup> found that brickwork specimens which were made with bricks which had been "wet" prior to laying developed

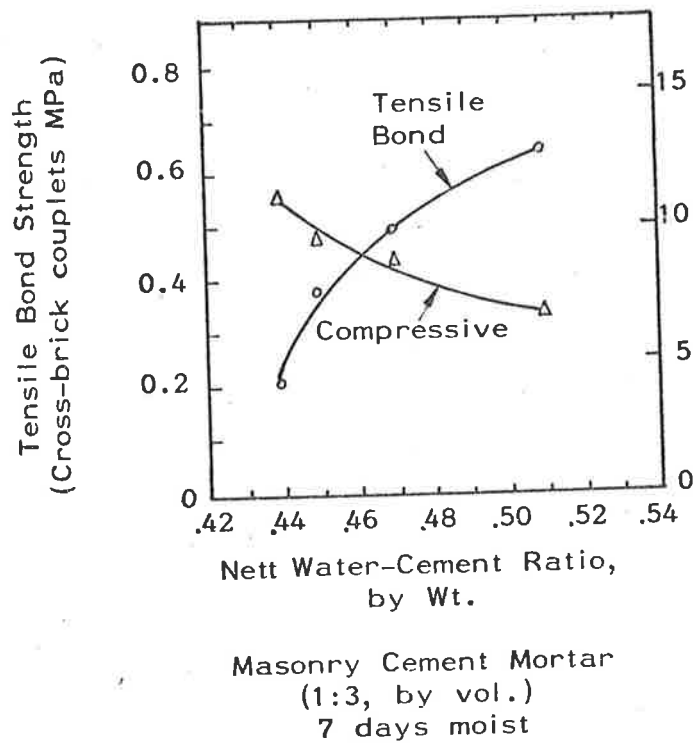


Figure 3.24: Effect of Water-Cement Ratio on Tensile Bond and Mortar Compressive Strength (Isberner<sup>(60)</sup>)

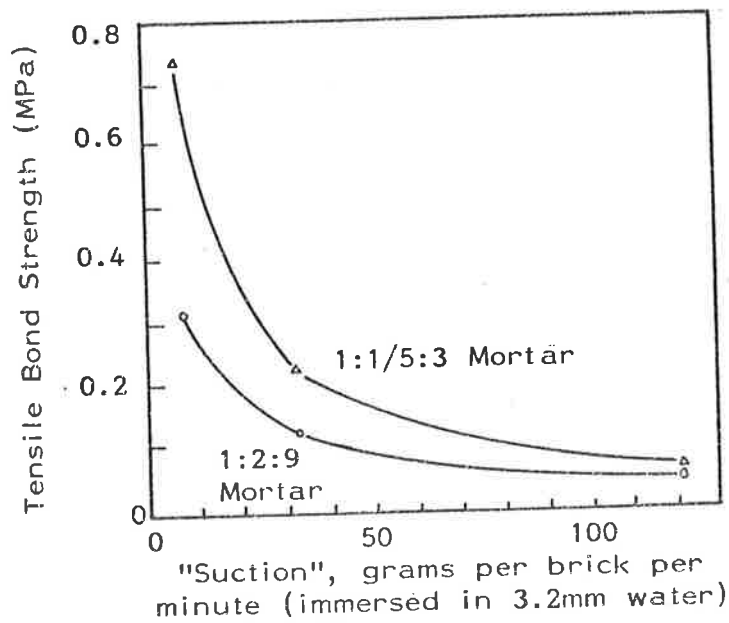


Figure 3.25: Relationships between Tensile Bond Strength and Brick Suction (I.R.A.) (Plummer and Reardon<sup>(84)</sup>)

substantially higher bond strengths than those which were laid dry, and that a suitable method for achieving optimum brick suction involved saturating the bricks but allowing the surface to dry immediately before laying. A brick in this condition is often referred to as being saturated surface-dry. Grimm<sup>(36)</sup> stated that the time interval between spreading and laying the brick should not exceed one minute and that each brick should be tapped into place once only, using the trowel, into a full-bedjoint so that the mortar is forced into the brick surface without any separation of the mortar constituents. Subsequent to the laying process, the method of curing can be critical to bond strength and it has been found<sup>(60)</sup> that moist-curing of tensile bond specimens produces considerably higher bond strengths compared with stored-in-air prisms.

Grimm<sup>(36)</sup> proposed experimentally-based expressions for both direct tensile bond strength (equation (3.28)) and flexural tensile strength (equation (3.29)) for brickwork constructed with normal Portland cement mortar as follows –

(a) Direct Tensile Bond Strength

$$f_b = 35 \times 10^{-6} \cdot [1.8 + (F - 105)^{0.5}] (40 - A) (124 - t_m) \quad (3.28)$$

in which  $f_b$  is bond strength of mortar to brick in MPa (ASTM E149<sup>(82)</sup>]

$F$  is initial flow of mortar ( $105\% < F < 135\%$ )

$A$  is air content in mortar by volume where  $A < 30\%$

$t_m$  is mortar exposure time ( $t_m < 120$  seconds) which is the time taken between laying the mortar and laying the brick.



## (b) Flexural Tensile Bond Strength

(Modulus of Rupture across Bedjoints)

$$f_t = 0.026 \phi f_b \cdot (28 - t_j) \left[ 3.8 + \left( \frac{C_v}{L} - 1 \right)^{0.5} \right] \quad (3.29)$$

in which  $f_t$  is flexural tensile strength in MPa

$\phi$  is workmanship constant for masonry in flexure

= 1 for inspected work (all joints filled)

= 0.8 for uninspected work (joints partially filled)

$f_b$  is bond strength according to equation (3.28) in MPa

$t_j$  is mortar bedjoint thickness in mm where  $t_j < 19$

$\left( \frac{C_v}{L} \right)$  is cement:lime ratio by volume in mortar where

$1 \leq \frac{C_v}{L} \leq 4$  ( $\frac{C_v}{L} = 4$  for type M mortar, 2 for S

and 1 for N).

Typically, for type N mortar and inspected work and 10mm (3/8 inch) bedjoints, equation (3.29) becomes

$$f_t = 1.85 f_b \quad (3.30)$$

Grimm quoted the coefficient of variation on the data used to derive equation (3.23) as 21 percent.

The effects of other factors such as sand-to-cement ratio, sand gradation, sand particle shape and the chemical properties of the cement and lime on the bond strength of brickwork have not been studied. The long-term characteristics of bond strength also have not been investigated, and although the short-term effects on bond of mortar flow, water retentivity and brick suction are understood, it is possible that the long-term strength of brickwork may depend not only on bond at the bedjoints but also on frictional shear at the brick-mortar interfaces. These shear aspects of brickwork are discussed in the next section.

### 3.3.4 Flexural Strength Across the Perpend

The behaviour of small brickwork assemblages subject to bending parallel to the bedjoints is complicated by the fact that the common stretcher bond pattern causes horizontal bending to be transmitted in part by a complex torsional shear in the bedjoints. A review of research into the simpler problem of in-plane shear on the bedjoints, both with and without compression normal to the bedjoints, is therefore useful in assessing the parameters which affect the flexural behaviour of brickwork under horizontal bending.

#### 3.3.4.1 In-plane shear on the bedjoints

The shear strength of masonry has been reported<sup>(36)</sup> to be a function of both the bond strength of the mortar to the brick and also the frictional resistance at the brick-mortar interface which itself depends on the compression forces normal to the bedjoints. If the brickwork is constructed with cored bricks, then the shear strength is increased by the mortar intrusions into the brick cores, since failure in that case also relies on a shear failure in the mortar intrusion. Grimm<sup>(36)</sup> recognized that there was no specified method for testing the ultimate shear strength of brickwork with a compression stress and suggested that the following equation could be used:

$$f_s = 1.4 f_b + \theta f_p \quad (3.31)$$

where  $f_s$  is shear strength of brickwork in MPa

$f_b$  is bond strength in MPa

$\theta$  is coefficient of friction

$f_p$  is axial compression stress in MPa and  $f_p > f_s$ .

A recommended practical value for the coefficient of friction,  $\theta$ , was 0.68, and typical values for the shear strength of brickwork were reported as ranging from 0.42MPa to 4.7MPa (60psi to 680psi).

Haller<sup>(7)</sup> gave the following expressions, which represented fitted curves to experimental data —

(a) Normal Quality Brickwork (Cement-Lime Mortar)

$$\bar{\tau} = 2.9 \sqrt{\bar{\sigma} + 1.93} - 3.73 \text{MPa} \quad (3.32)$$

(b) Special Quality Brickwork (Cement Mortar)

$$\bar{\tau} = 2.9 \sqrt{\bar{\sigma} + 0.90} - 1.73 \text{MPa} \quad (3.33)$$

In both equations (3.32) and (3.33),

$\bar{\tau}$  is the in-plane shear strength in MPa

$\bar{\sigma}$  is the compressive stress normal to the bedjoint in MPa.

For the cases in which  $\bar{\sigma}$  is zero,  $\bar{\tau}$  for Normal Quality Brickwork from equation (3.32) is 0.30MPa and for Special Quality Brickwork,  $\bar{\tau}$  from equation (3.33) is 1.02MPa.

Sinha and Hendry<sup>(85)</sup> related the shear bond strength, as distinct from the frictional shear strength, to the tensile bond strength, after they had tested specimens, built with cement mortar, to which no compressive stress was applied. Their proposed relationship was

$$\tau_o = 0.73 \sqrt{\sigma_{tb}} \quad (3.34)$$

in which  $\tau_o$  is the shear bond strength in MPa

$\sigma_{tb}$  is the tensile bond strength in MPa.

Murthy and Hendry<sup>(86)</sup> had reported previously, from a similar set of experiments, that the relationship could be expressed in the form —

$$\tau_o = 2.3 \sigma_{tb} \quad (3.35)$$

Equation (3.35) was similar to the relationship proposed by Polyakov<sup>(92)</sup> and subsequently used by Mayes and Clough<sup>(28)</sup>, which was

$$\frac{\tau_o}{\sigma_{tb}} = 2.25 - 5 \cdot \sigma_{tb} \quad (3.36)$$

in which  $\sigma_{tb}$  was expressed in MPa and was less than 0.18MPa.

Both Sinha<sup>(85)</sup> and Murthy<sup>(86)</sup> concluded that when vertical pre-compression is present the total shear strength of brick couplets could be expressed in terms of bond shear and frictional resistance in the form -

$$\tau = \tau_o + f\sigma_c \quad (3.37)$$

in which  $\tau$  is the in-plane shear strength on the bedjoints

$\tau_o$  is the bond shear strength

$f$  is the coefficient of friction at the brick-mortar interface

$\sigma_c$  is the compressive stress normal to the bedjoints.

The coefficients of friction calculated by the two authors<sup>(85), (86)</sup> from test results were 0.74 and 0.725 respectively.

Hendry<sup>(120)</sup> reported more recent tests on model and full-scale structures conducted to establish a relationship of the form of equation (3.37). The shear strength for the type of brickwork tests was found to be given by the expression

$$\tau = 0.3 + 0.5 \sigma_c \quad (3.38)$$

Equation (3.38) fitted the experimental data well for values of the vertical precompression,  $\sigma_c$ , less than 2.0MPa (figure 3.26). Hendry<sup>(120)</sup> also summarized experimental results which indicate that the value of bond shear strength,  $\tau_o$ , may vary between 0.14MPa and

- × Model structures: single shear panel
- Model structures: double shear panel
- Full-scale structures: double shear panels
- ▼ Full-scale structures: without openings
- + Full-scale structures: complete tests

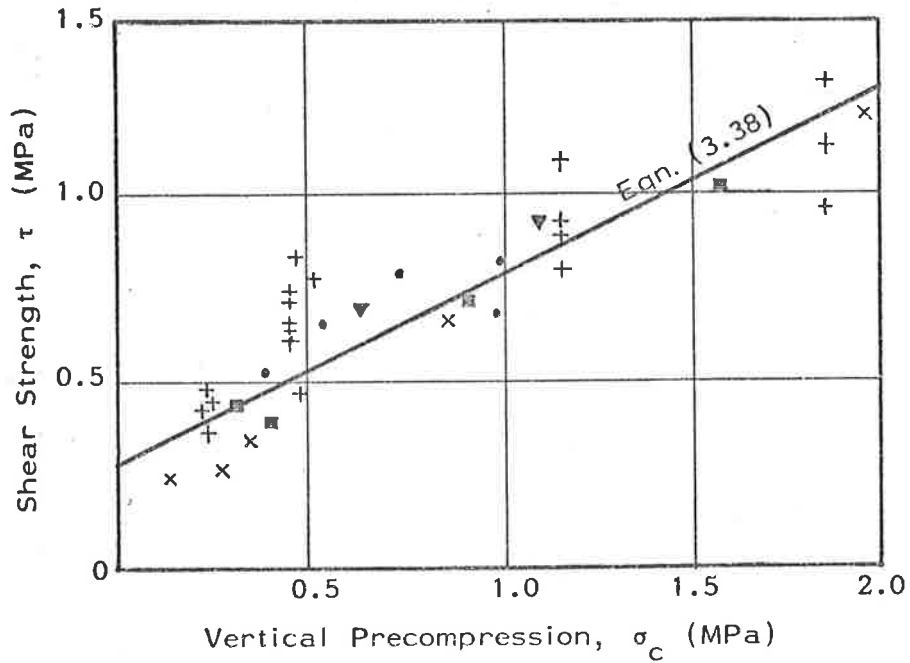


Figure 3.26: Relationship between Brickwork Shear Strength and Vertical Precompression (Hendry<sup>(120)</sup>)

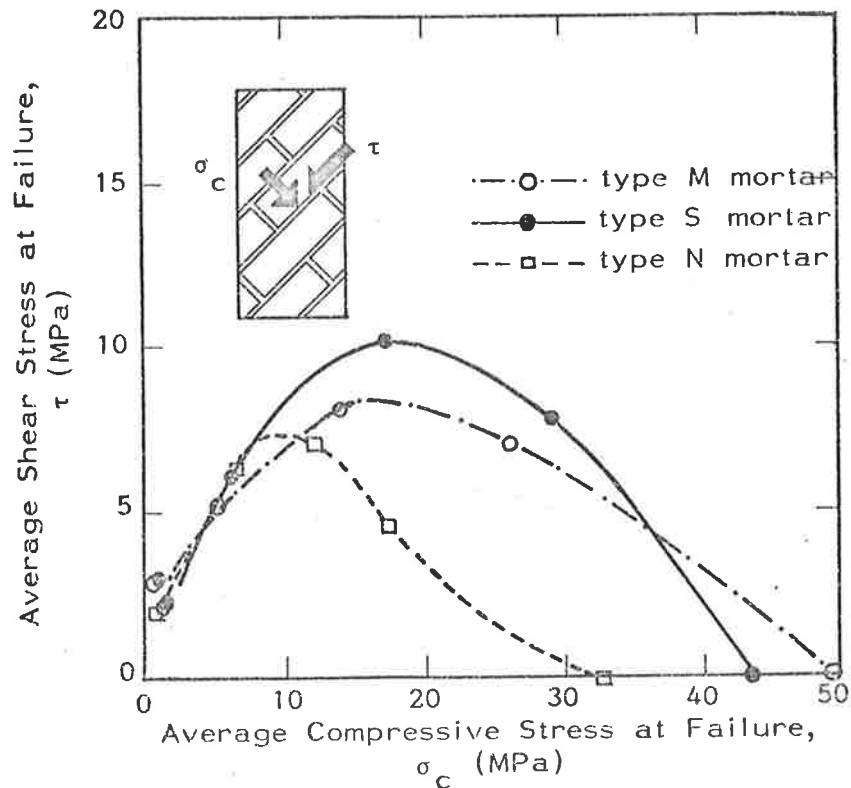


Figure 3.27: Failure Relationships for Combined Shear and Normal Compression along the Bedjoint (Hamid and Drysdale<sup>(87)</sup>)

0.3MPa for practical combinations of brick and mortar and that the coefficient of friction,  $f$ , may vary between 0.3 and 0.84 for different types of brickwork.

Hamid and Drysdale<sup>(87)</sup> indicated that the strength of brickwork in combined shear and compression on the bedjoints may be sensitive to the ratio of normal compressive stress to the in-plane shear stress along the bedjoints, particularly at relatively high normal stresses. Their experiments on brickwork specimens showed that the interaction of compressive stress and shear stress caused the strength of the brickwork to vary as shown in figure 3.27. They concluded that the mortar type did not have any effect on the capacity of the brickwork as long as the shear-slip mode of failure was predominant by comparison with a vertical splitting failure characteristic of excessive normal compressive stress (Section 3.3.2).

#### 3.3.4.2 Torsional shear on the bedjoints

Any combination of loads which causes a brickwork panel, restrained at its vertical edges, to translate out of its unloaded plane, produces bending stresses parallel to the bedjoints and consequently induces torsional shear in the bedjoint mortar. Base and Baker<sup>(69)</sup> described the failure modes of small brickwork assemblages, built with model bricks, which experienced bending stresses across the perpendicular joints (figure 3.28).

The three types of failure observed were a bending failure in the bricks (figure 3.28(a)), a failure of bond in bending on a perpendicular joint (figure 3.28(b)) and failure of the bedjoints in torsional shear (figure 3.28(c)). Base stated that torsional shear failure was associated with a bond failure, but the research reviewed in Section 3.3.4.1 suggested that, for in-plane shear, a frictional component was

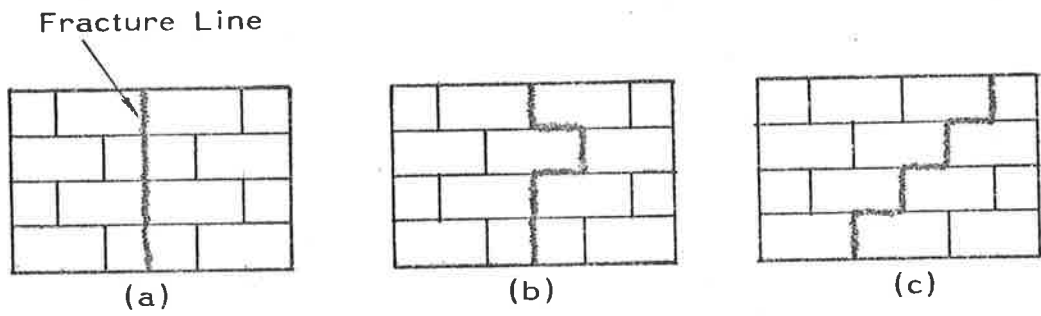


Figure 3.28: Failure Modes for Model Brickwork  
(Base and Baker<sup>(69)</sup>)

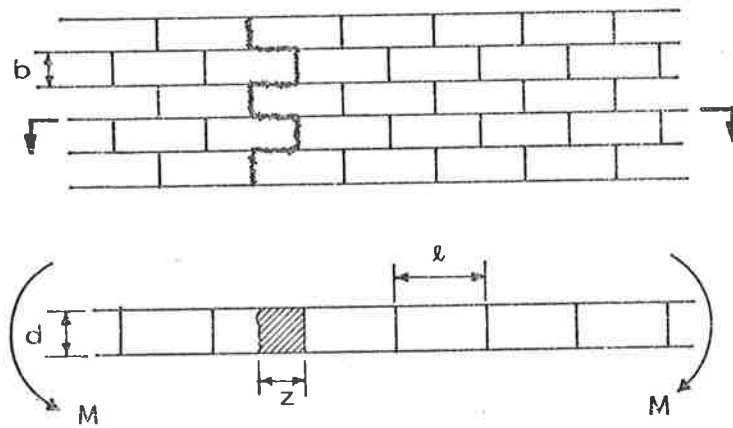


Figure 3.29: Mechanism of Failure for Brickwork Subjected to  
Horizontal Bending (Sahlin<sup>(44)</sup>)

also present, so that it seems reasonable to assume that there could also be a frictional component in torsional shear.

Sahlin<sup>(44)</sup> summarized a theoretical approach by Royen<sup>(88)</sup> who described the mechanism of flexural action across the perpend by assuming that the shear stress over the area  $(d \times z)$  (figure 3.23) had a maximum value  $\tau$ . The maximum moment carried by that area, by the membrane analogy<sup>(89)</sup> (for a fully plastic type shear stress distribution) is thus

$$M = \frac{\tau d^2}{2} \cdot \left(z - \frac{d}{3}\right) \quad (3.39)$$

where  $M$  is the maximum moment capacity of the area  $(d \times z)$  in figure 3.29.

Royen assumed that the shear stress was mobilized solely by friction and not by brick-mortar bond, and that the moment capacity per unit height of wall could be expressed as

$$\bar{m} = \frac{\mu \sigma d^2}{2b} \cdot \left(z - \frac{d}{3}\right) \quad (3.40)$$

in which  $\bar{m}$  is the moment capacity per unit height of wall

$\mu$  is the coefficient of friction

$\sigma$  is the compressive stress normal to the bedjoints.

Royen also considered a non-uniform distribution of vertical stress over the friction area so that when the axial force was applied outside the kern at an effective eccentricity of  $e$  from the section centreline, the friction area was reduced from  $(d \times z)$  to

$$\frac{3}{2} \cdot (d - 2e) \cdot z \quad (3.41)$$

The stress  $\sigma$  was assumed then to be a uniform average stress over the reduced effective area given by equation (3.41).

Sahlin<sup>(44)</sup> proposed that an upper limit for  $\bar{m}$  could be taken as the moment which caused a bending failure with cracks through



the bricks and perpendicular mortar joints. That is,

$$\text{(Failure)} \quad \bar{m} = \frac{d^2 \sigma'_{bt}}{6} \quad (3.42)$$

in which  $\sigma'_{bt}$  is a transverse bending strength for the brickwork.

Therefore from equation (3.40),

$$\bar{m} \leq \frac{\mu \sigma d^2}{2b} (z - d/3) \leq \frac{d^2 \sigma'_{bt}}{6} \quad (3.43)$$

In equation (3.43),  $z \geq d$ ,  $l \geq 2z$  (figure 3.29) and  $\mu$  may be assumed to be approximately 0.5 to 0.7 at a clay brick-mortar interface<sup>(44)</sup>.

Royen's theory did not include the continuity of the bedjoint mortar nor the stress-carrying capacity of the perpends which could be significant. No research has been carried out to compare any theory on torsional shear with experimental evidence. Comparisons have been made, however, between the flexural strength of stretcher-bond brickwork across the perpends and across the bedjoints, but the complex nature of bedjoint torsional shear has not been investigated. Instead, research has been directed towards an overall appreciation of bending across the brickwork perpends. Some of the results which compare flexural strengths in the two principal directions in brickwork are presented in the next section.

#### 3.3.4.3 Comparisons of flexural strengths across perpends and bedjoints

Experiments designed to establish a predictable ratio of flexural strength across brickwork perpends to flexural strength across bedjoints for brickwork built in stretcher bond have produced ratios which vary from approximately 1.5 to 9.5<sup>(90)</sup> over a range of brick and mortar types.

Lawrence<sup>(91)</sup> investigated the flexural strength of brickwork normal to and parallel to the bedjoints, without the influence of

on-plane compressive forces, and used the results together with data from the researchers, to obtain the relationship –

$$R = \frac{2.17}{\sqrt{B}} \quad (3.44)$$

in which R is the ratio of flexural strength across the perpend to flexural strength across the bedjoints in MPa

B is the flexural strength across the bedjoints in MPa.

A plot of equation (3.44) together with the experimental data is given in figure 3.30.

Lawrence stated that the correlation coefficient was 0.94 which indicated that the ratio R was highly dependent on the bond strength achieved by the brick-mortar combination. Lawrence also claimed that the results shown that the ratio R was independent of whether failure occurred in the brick or as a torsional shear failure in the bedjoints. Equation (3.44) was subsequently modified by Lawrence<sup>(121)</sup> as a result of more experimental data being available to be –

$$R = \frac{1.75}{\sqrt{B}} \quad (3.45)$$

The difference between equations (3.44) and (3.45), resulting from the amount of test data available, indicates that there may not be a useful relationship of that form for brickwork. However, Hendry<sup>(120)</sup> has reported that West<sup>(122)</sup> showed that statistically there exists a relationship between flexural strength across the perpend and brick section (I.R.A.), a factor which influences the flexural bond at the bedjoints (Section 3.3.3.2).



#### 3.3.4.4 Summary

In-plane shear strength of brickwork may be calculated by using equation (3.37) provided that the normal compression stress,  $\sigma_c$ , is less than 2.0MPa. In equation (3.37), the bond strength,  $\tau_o$ , may vary between 0.14MPa and 0.3MPa depending on the type of brick and mortar and the coefficient of friction,  $f$ , may vary between 0.3 and 0.84<sup>(120)</sup>. At normal stresses greater than 2.0MPa the shear strength may depend upon the normal compressive stress in a non-linear fashion<sup>(87)</sup> (figure 3.27).

Equation (3.43) gives a method of calculating the moment capacity of brickwork subject to bending across the perpends. However, Sahlin<sup>(44)</sup> gave no value for the transverse bending strength for brickwork,  $\sigma_{bt}^I$ . Possibly for brickwork in common stretcher bond,  $\sigma_{bt}^I$  may lie in the range

$$0.5 \sigma_{bt} \leq \sigma_{bt}^I \leq \sigma_{bt} \quad (3.46)$$

in which  $\sigma_{bt}$  is the transverse bending strength of a brick (Section 3.1.3.3).

The relationship between flexural strength across the bedjoints and the flexural strength across the perpends, as determined by Lawrence<sup>(121)</sup> (equations (3.44), (3.45)), may not be acceptable because the relationship appears to depend upon the sample size for its form. In addition, the effects of time on the bond at the brick-mortar interface has not been assessed in the test data used for the development of equations (3.44) and (3.45) (Section 3.3.3.2).

### 3.3.5 Elastic Properties of Small Assemblages

#### 3.3.5.1 Elastic Modulus, E

Base and Baker<sup>(69)</sup> calculated effective elastic moduli for brickwork both normal to and parallel to the bedjoints assuming that both the brick and mortar materials were linearly elastic as follows:

- (i) for a stack-bonded prism in axial compression normal to the bedjoints,

$$E_C = E_b \cdot \left[ \frac{H + b}{H + \left(\frac{b}{E_m}\right) \cdot b} \right] \cdot \frac{A_n}{A_g} \quad (3.47)$$

in which  $E_C$  is the brickwork elastic modulus for compression normal to the bedjoints

$E_b$  is the brick modulus

$E_m$  is the mortar modulus

$H$  is the brick height

$b$  is the bedjoint thickness

$A_n$  is the nett area of the bricks, reduced from the gross area  $A_g$  by coring of the bricks.

- (ii) for a stack-bonded prism in bending across the bedjoints,

$$E_B = E_b \cdot \left[ \frac{(H + b)}{H + \left(\frac{b}{E_m}\right) \cdot b} \right] \cdot \frac{I_n}{I_g} \quad (3.48)$$

in which  $E_B$  is the elastic modulus for bending across the bedjoints

$I_n$  is the second moment of area of the brick nett section about an axis parallel to the bedjoints

$I_g$  is the corresponding second moment of area for the gross brick section.

(iii) for a wall subject to bending across the perpend,

$$E_p = \frac{E_1 H + E_m b}{(H + b)} \quad (3.49)$$

in which  $E_p$  is the elastic modulus for bending across the perpend

$E_1$  is an equivalent modulus for bending defined as

$$E_1 = E_b \cdot \left[ \frac{(L + p)}{L \cdot \left(\frac{I'_g}{I'_n}\right) + \left(\frac{E_b}{E_m}\right) \cdot p} \right] \quad (3.50)$$

in which  $L$  is the brick length

$p$  is the mortar perpend thickness

$I'_g$  is the second moment of area of the brick gross section about an axis normal to the bedjoints

$I'_n$  is the corresponding second moment of area for the nett brick section.

(iv) for a wall subjected to bending across the bedjoints,

$$E_s = E_2 \cdot \left[ \frac{(H + b)}{H + \left(\frac{E_2}{E_m}\right) \cdot \left(\frac{I'_g}{I'_n}\right) \cdot b} \right] \quad (3.51)$$

in which  $E_s$  is the elastic modulus for bending across the bedjoints

$E_2$  is an equivalent modulus for bending defined as

$$E_2 = \left[ \frac{E_b \cdot \left(\frac{I'_n}{I'_g}\right) \cdot L + E_m \cdot p}{(L + p)} \right] \quad (3.52)$$

If the perpend thickness,  $p$ , in equation (3.52) is insignificant relative to the brick length,  $L$ , equation (3.51) gives approximately the same result for a wall as does equation (3.48) for a stack-bonded prism.

Base and Baker tested the theoretical results by bending small brickwork assemblages both normal to the parallel to the bedjoints. The load-deflection curves for tests on model brick piers in flexure across the bedjoints when loaded over a 330mm span with line loads 95mm apart, placed symmetrically, are shown in figure 3.31.

Base and Baker reported that the curves in figure 3.31 were typical for all tests conducted, the results of which are summarized in Table 3.6.

Brick Type	$E_b$ ( $\times 10^3$ MPa)	$E_m$ ( $\times 10^3$ MPa)	Elastic Modulus ( $\times 10^3$ MPa)			
			Experimental			Calculated
			Min.	Max.	Average	
Solid (12 tests)	26.6	8.76	17.3	25.0	21.4	21.4
17-hole (1 test)	26.6	8.76	-	-	21.0	20.4

Table 3.6: Elastic Modulus for Bending Across the Bedjoints

Base and Baker also tested both full-sized and model brickwork in bending across the perpend, with no compression normal to the bedjoints.

The results showed that the load-deflection characteristics were initially linear and agreed well with theoretical predictions as indicated in Table 3.7.

However, a distinct change in brickwork stiffness was noted during the experiments (figure 3.32). Base and Baker attempted to explain the change in brickwork stiffness by testing several small panels constructed from "model bricks" in which the perpend were greased so that the brick-mortar bond on the perpend could be neglected (figure 3.33). They concluded that the displacements for the

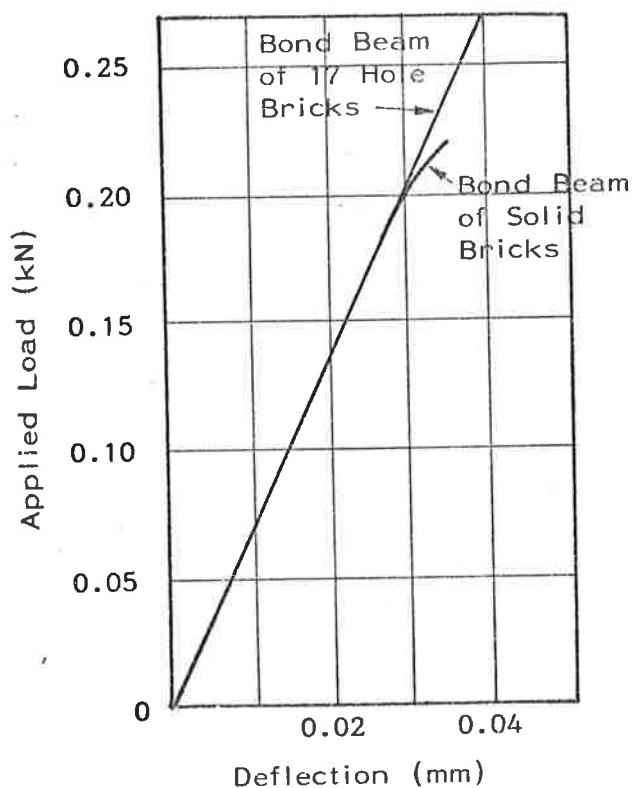


Figure 3.31: Bending Tests on Model Brickwork Prisms (Base and Baker<sup>(69)</sup>)

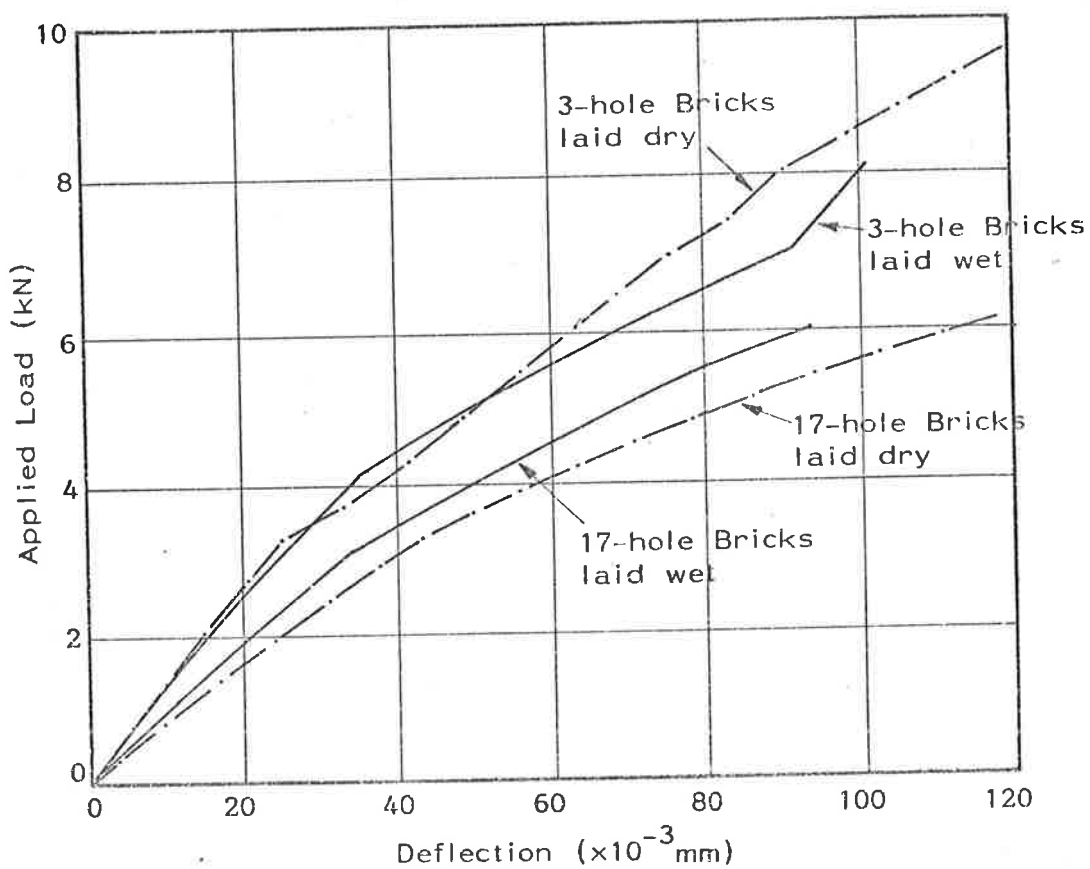


Figure 3.32: Bending Tests on Full-scale Brickwork Panels (Base and Baker<sup>(69)</sup>)



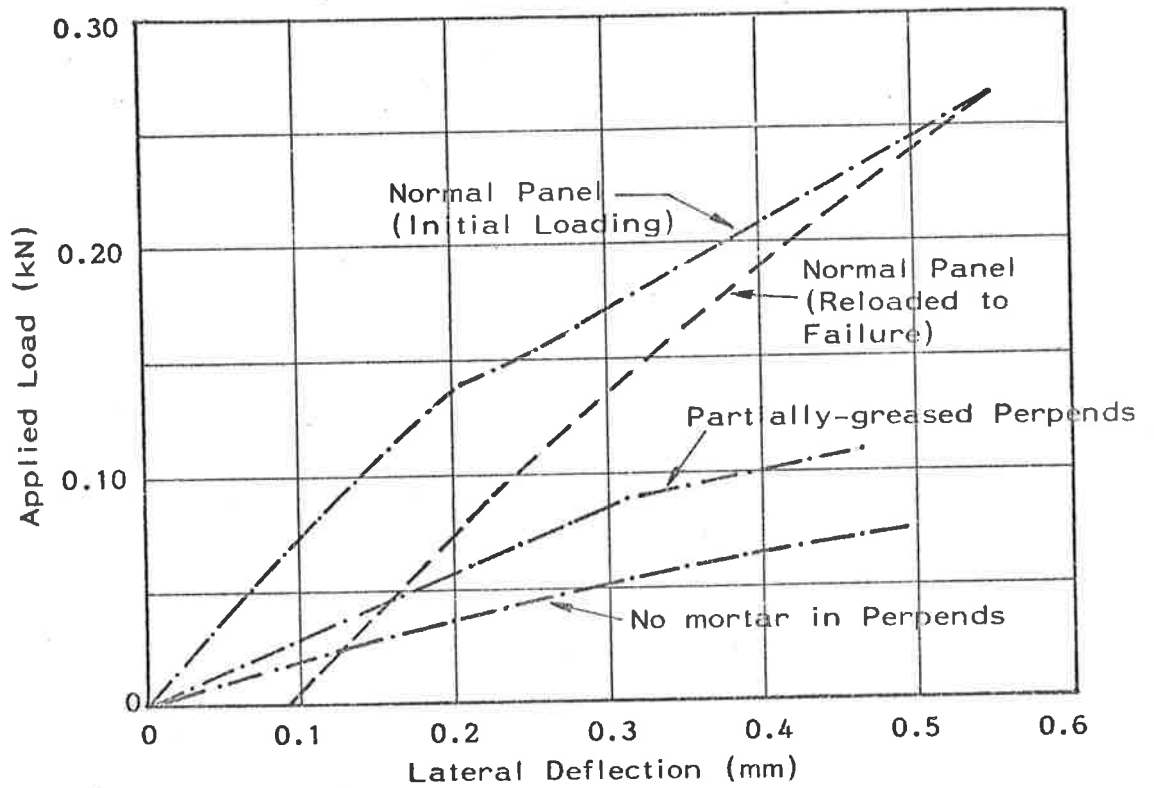


Figure 3.33: Bending Tests on Model Brickwork Panels  
(Base and Baker (69))

Brick Type	$E_b$ ( $\times 10^3$ MPa)	$E_m$ ( $\times 10^3$ MPa)	Elastic Modulus ( $\times 10^3$ MPa)			
			Experimental			Calculated
			Min.	Max.	Average	
Solid (13 tests)	26.6	8.76	19.3	23.4	21.3	22.6
17-hole (1 test)	26.6	8.76	-	-	15.8	17.3

Table 3.7: Elastic Modulus for Bending Across the Perpend

panels with greased perpend were sufficiently different from those of a normal brickwork panel that the changes in slope shown in figure 3.32 could not be caused by cracking in the perpend. However, they were unable to propose an alternative explanation.

Lawrence and Morgan<sup>(12)</sup> investigated the properties of small brickwork panels in bending across the perpend and concluded that there was a distinct change in flexural stiffness at approximately 40 to 50 percent of the ultimate bending moment. The relationship between the reduced stiffness and the initial stiffness was approximated, using a least-squares analysis, as

$$E_2 = 0.57E_1 - 50\text{MPa} \quad (3.53)$$

in which  $E_2$  is the reduced modulus of elasticity in MPa  
 $E_1$  is the initial modulus of elasticity in MPa.

The correlation coefficient was reported as 0.90. Lawrence stated that the significant correlation coefficient showed that the ratio  $E_2:E_1$  was an intrinsic property of the brickwork. He suggested that the reduction in stiffness could have been caused by partial cracking in the perpend but did not obtain direct experimental evidence to confirm such behaviour.

Scrivener and Williams<sup>(50)</sup> reported axial compression tests on small brick prisms in which the stress-strain relationships were recorded. A complete stress-strain curve for the brick prism with 10mm (3/8 inch) mortar joints is shown in figure 3.34, together with the stress-strain curve for the brick. Scrivener reported that the secant modulus obtained from the ascending portion of the curve at the point where the strain was half the strain,  $\epsilon_0$ , at maximum stress was  $7.5 \times 10^3$  MPa and at maximum stress,  $\epsilon_0$  was 0.0063.

The maximum strain obtained by Scrivener, while relatively high compared with concrete, was not supported by experiments by Powell and Hodgkinson<sup>(93)</sup> who tested brick piers in compression beyond the maximum stress levels. Figure 3.35 shows typical stress-strain graphs.

The tests were conducted on small brickwork piers built from four different types of bricks and 1:¼:3 mortar. The initial tangent modulus in all cases was greater than the secant modulus calculated for two-thirds maximum stress, and the ratio of the moduli varied from 1.33 for type C bricks to 1.53 for type A bricks. Although the brickwork prisms showed non-linear elastic material behaviour at stresses near failure, the stress-strain behaviour was close to linear elastic at low stresses, especially for higher-strength brick types A, B and D. Hendry<sup>(120)</sup> has reported that by plotting the four stress-strain curves on dimensionless axes, the curves are of the same form and may be expressed as

$$\left(\frac{\sigma}{\sigma_f}\right) = 2 \cdot \left(\frac{\epsilon}{\epsilon_f}\right) - \left(\frac{\epsilon}{\epsilon_f}\right)^2 \quad (3.54)$$

in which  $\sigma$  is stress normal to the bedjoints

$\sigma_f$  is the maximum stress

$\epsilon$  is strain normal to the bedjoints

$\epsilon_f$  is the strain at maximum stress.

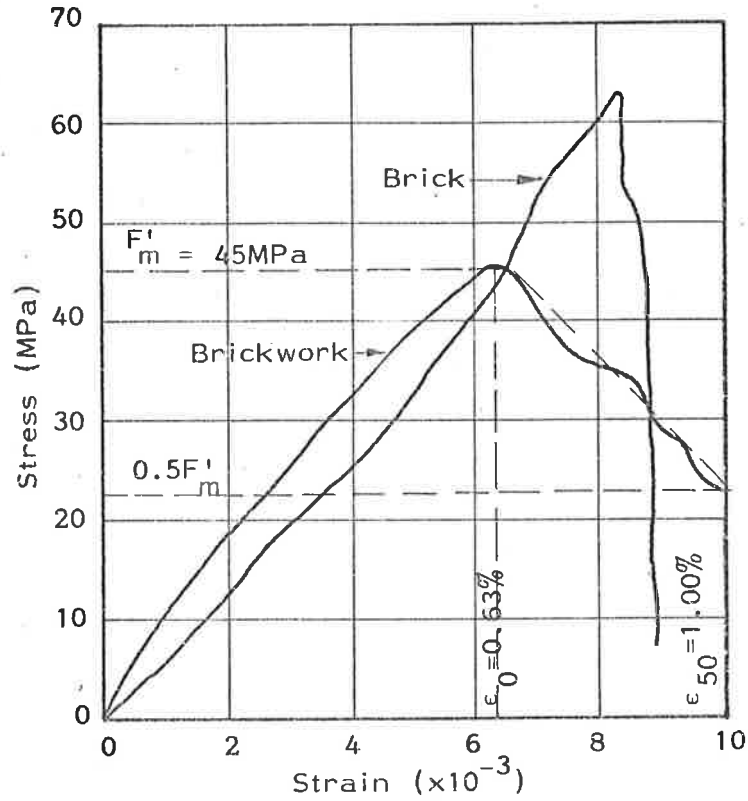
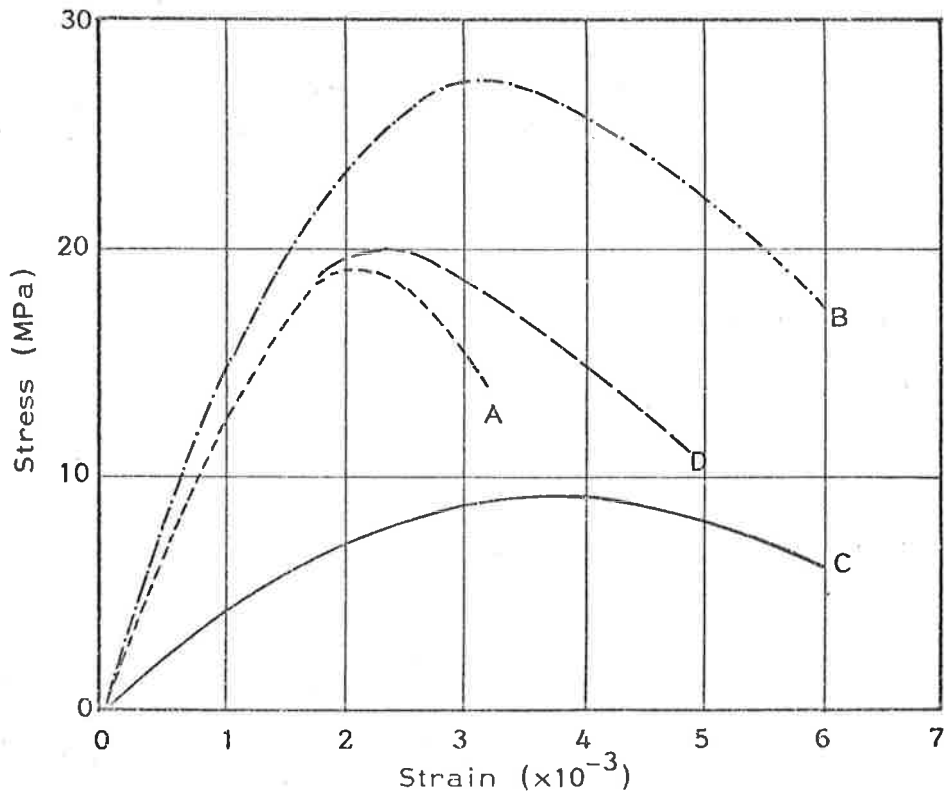


Figure 3.34: Stress-strain Curves for Brick and Brickwork Prisms



(Mortar 1:1/4:3 by Volume)

Figure 3.35: Stress-strain Relationships for Brickwork Piers (Powell and Hodgkinson<sup>(93)</sup>)

From the parabolic stress-strain relationship given by equation (3.54), the initial tangent modulus for the brick is

$$E_{br} = 2 \cdot \frac{\sigma_f}{\epsilon_f} \quad (3.55)$$

The maximum stress for all piers occurred at a strain of 0.38 percent or less compared with a strain of 0.63 percent reported for tests conducted by Scrivener and Williams (figure 3.34).

Walstein and Allen<sup>(94)</sup> conducted tests on forty-five walls using one batch of solid bricks and one type of mortar. They reported stress-strain relationships for brickwork similar to the curves shown in figure 3.35.

Other research on the elastic modulus of brickwork has been concentrated on results from compressive tests on brick prisms and has attempted to relate brickwork modulus to the compressive strength normal to bedjoints. Base and Baker<sup>(69)</sup> (equations (3.48), (3.49), (3.50), (3.51), (3.52)) showed that the elastic modulus of brickwork was dominated by the brick modulus and Sahlin<sup>(44)</sup> reported that the elastic modulus of a brick was approximately proportional to its strength (equation (3.2), Section 3.1.3.4). However, in Section 3.3.2, it was shown that brickwork compressive strength is not directly proportional to brick strength, and therefore brickwork compressive strength is unlikely to be related directly to its elastic modulus. However, in order to present the results of past research, some relationships which have been proposed as measures of elastic modulus are given below (including corrections to Plowman's paper<sup>(51)</sup>).

(a) Plowman<sup>(51)</sup>:

$$(i) E_{br} = (\text{Brickwork Strength (MPa)} - 0.7) \times 10^3 \text{MPa} \quad (3.56)$$

$$(ii) E_{br} = \left( \frac{\text{Brick Strength (MPa)}}{5.0} \pm 4.1 \right) \times 10^3 \text{MPa} \quad (3.57)$$

(b) Plummer and Blume<sup>(29)</sup>:

$$700 F'_m \leq E_{br} \leq 1200 F'_m \quad (3.58)$$

(c) Anderson<sup>(74)</sup>:

$$E_{br} = 1250 F'_m \quad (3.59)$$

for 1:1:6 mortar

and bricks  $51\text{MPa} \leq C \leq 112\text{MPa}$

(d) Sahlin<sup>(44)</sup>:

$$400 F'_m \leq E_{br} \leq 1000 F'_m \quad (3.60)$$

but  $E_{br} = 700 F'_m$  at low stresses

(e) Grimm<sup>(36)</sup>:

$$E_{br} + 6.25 F'_m (80 + h_s/t_s) \quad (3.61)$$

in which  $h_s/t_s$  is a slenderness height-to-thickness ratio of test pier

and  $h_s/t_s < 45$ ,  $F'_m \leq 21\text{MPa}$

In equations (3.56) to (3.61),

$F'_m$  is brickwork compressive strength

$E_{br}$  is initial tangent brickwork modulus normal to the bedjoints

$C$  is brick compressive strength.

With relation to equation (3.60), Sahlin<sup>(44)</sup> reported that the tangent modulus of elasticity decreased as the stress increased with the rate of decrease depending upon the type of mortar used. He indicated that because the tangent modulus varied with stress, the buckling load of a brickwork column would depend upon the variation of modulus. In addition, Nylander<sup>(45)</sup> indicated that a stress-strain

relationship obtained from a concentrically-loaded prism might not be suitable for calculating the buckling load of an eccentrically-loaded column because the stress, and hence elastic modulus, varies across the column section. Nevertheless, analytical methods proposed by other researchers for predicting the failure of walls and panels will be discussed in Section 3.4.

### 3.3.5.2 Modulus of rigidity, G

So far, investigations in brickwork have been concerned essentially with the modulus of rigidity as it applies to in-plane shear. Page<sup>(95)</sup> conducted experiments on small one-half scale brickwork panels loaded in combined compression and shear and calculated average stress-strain curves for shear for each of the brickwork types shown in figure 3.36. In each case, the shear stress and the normal stress were assumed to be uniformly distributed along the bedjoint so that each curve represents average values for all tests at each stress level. Page concluded that the shear deformations were not sensitive to the degree of compression normal to the bedjoint, although the stress-strain curves themselves were not linear.

Hendry<sup>(16)</sup> conducted tests on one-sixth scale single-storey structures and concluded that the shear modulus of brickwork increased very rapidly at precompression loads within the range of working stresses. This result is a contradiction to Page's conclusions above, possibly because the modulus relationships were determined using two different experimental approaches.

In practical design applications, the elastic moduli in the two principal directions, say X and Y, are sufficiently close to each other<sup>(69)</sup>, so that the following approximation is possible<sup>(122)</sup> —

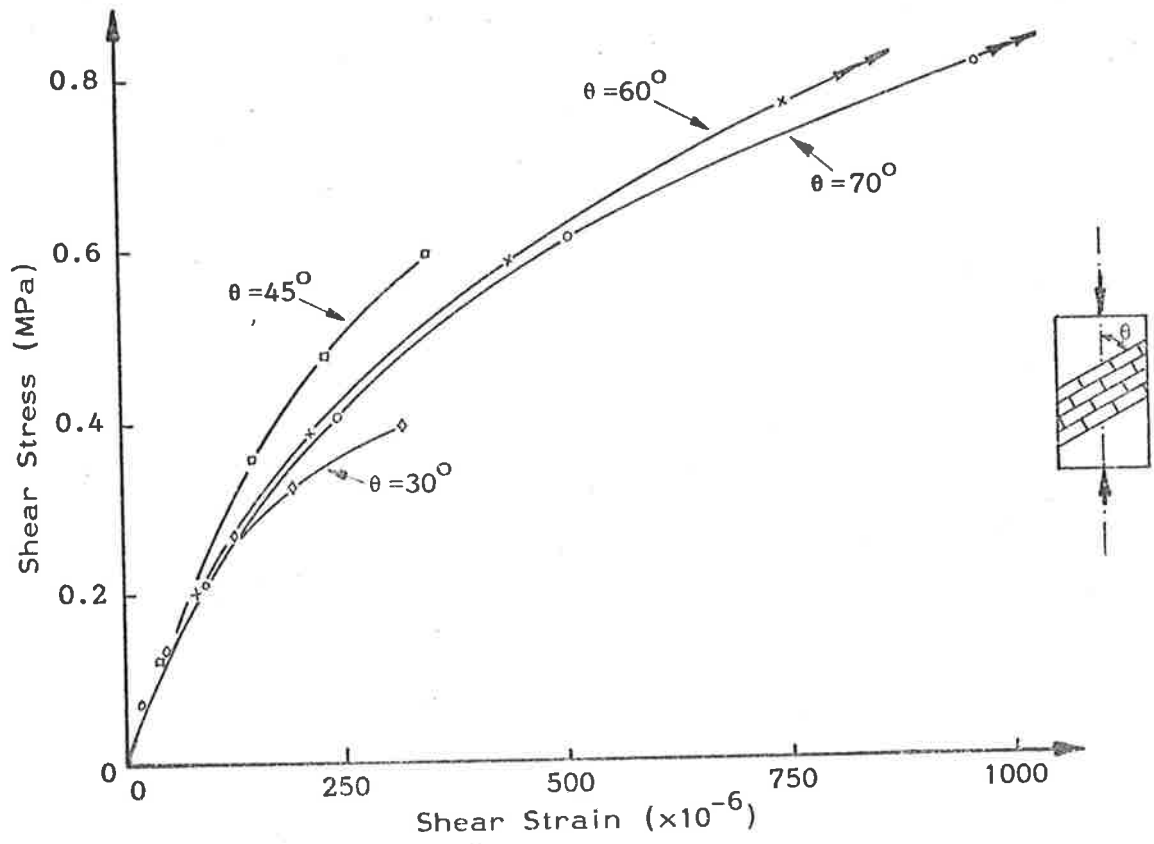


Figure 3.36: Average Stress-strain Curves in Shear for Brickwork Panels (Page<sup>(95)</sup>)



$$G = \frac{(E_x \cdot E_y)^{\frac{1}{2}}}{2 \cdot (1 + \nu)} \quad (3.62)$$

in which  $G$  is the modulus of rigidity of brickwork

$E_x, E_y$  are the elastic moduli parallel to, and normal to, the bedjoints at low stresses

$\nu$  is an average Poisson's ratio for brickwork which may be taken as 0.2<sup>(50)</sup>, (120)

Equation (3.62) is derived from an equation developed by Timoshenko<sup>(112)</sup> for the modulus of rigidity of an orthotropic plate.

### 3.3.5.3 Creep in brickwork

Long-term behaviour of brickwork can be affected by creep both in the mortar bedjoints and in the bricks. Plowman<sup>(51)</sup> reported that the degree of creep in a mortar can depend upon the following factors:

- (a) Water content of the mortar after moisture absorption by the bricks
- (b) Type of sand
- (c) Proportions of the mortar mix
- (d) Stress level
- (e) Air humidity

Plowman concluded from experimental evidence that the creep of brickwork may be assumed to be approximately 20 to 25 percent that of concrete under similar conditions of stress and environment. He suggested that a value of  $100 \times 10^{-6}$  for creep after ten years could apply to all strengths of brickwork. The behaviour of walls and panels in which creep is not significant is reviewed in the following section.

### 3.4 ANALYSIS OF BRICK WALLS AND PANELS

This section reviews the theories which predict the behaviour of brick walls and panels subjected to vertical load either concentric or eccentric with respect to the wall or panel middle surface. For the purposes of this section, the collapse mode of a wall or panel is assumed to be characterized by a buckling failure rather than a brickwork material failure (Section 3.3).

#### 3.4.1 Analysis of Columns with No Tensile Strength

Most theories adopted for brick walls assumed that the material had no tensile strength. Consequently, the theories do not apply strictly to brickwork because the brick units themselves can resist significant tensile stresses. That is, the bricks remain intact while discrete cracks may appear in the mortar joints or at the brick-mortar interfaces<sup>(69)</sup>. Angervo<sup>(96)</sup> considered an eccentrically compressed homogeneous column, initially straight (figure 3.37) with a cross-section symmetrical with respect to the plane of deflection. The region of the section in compression is the shaded area in figure 3.37. The centroid of the compressed area differs from the centroid of the full section in those parts of the column in which a part of the section is ineffective, that is, in zones that would be subject to tensile stresses if the material had tensile strength. Angervo extended the Bernoulli-Navier hypothesis for uncracked columns by assuming that for columns with no tensile strength, planes which were perpendicular to the centroidal axis of the column prior to loading remained plane in their compressed parts and perpendicular to the original centroidal axis.

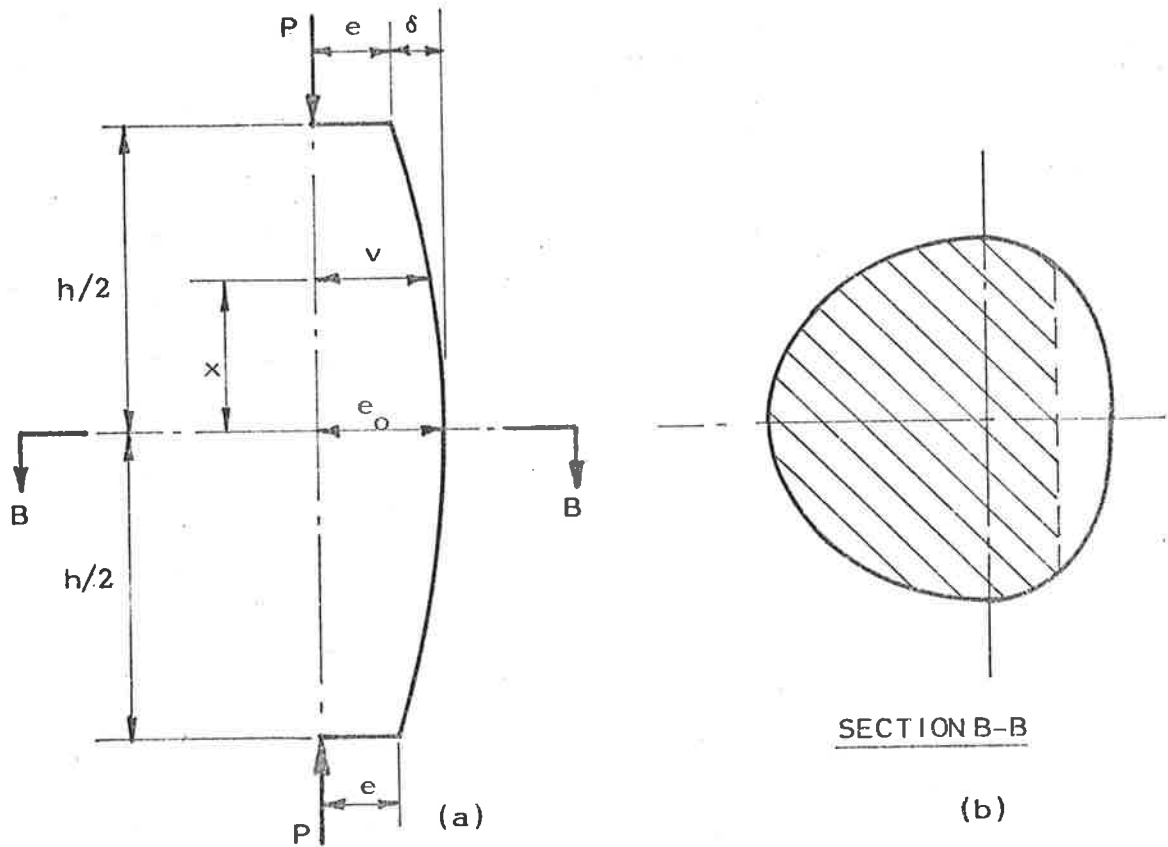


Figure 3.37: A Column Without Tensile Strength (Angervo<sup>(96)</sup>)

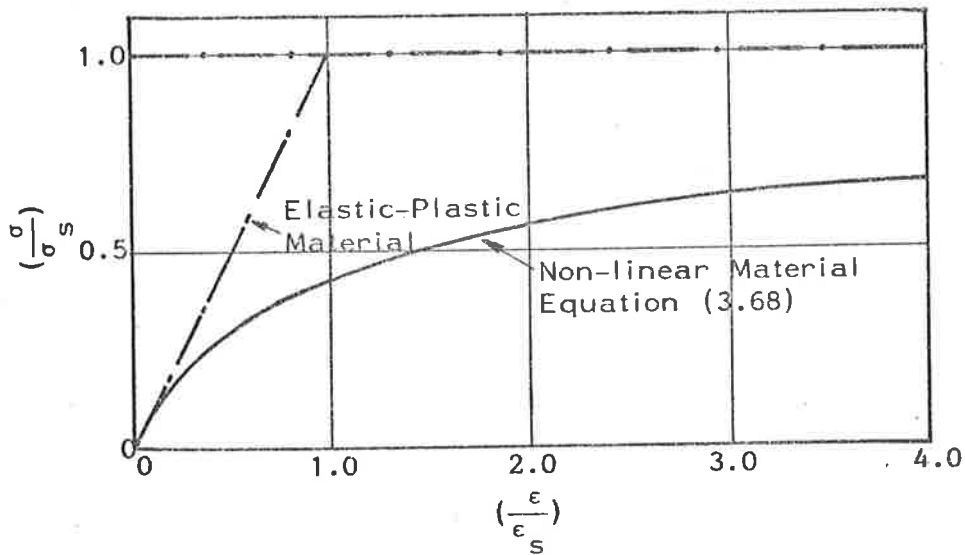


Figure 3.38: Assumed Stress-strain Relationship for Non-linear Material (Angervo<sup>(96)</sup>)

The strain at each fibre is thus proportional to the distance from the neutral axis at that fibre. If the column is divided into small elements along its height, the planes at the ends of an element intersect at the centre of curvature for the original centroidal axis, and hence the compression face, for that element. Angervo calculated the failure loads for pin-ended columns of constant rectangular section and linear-elastic material as

$$P_f = \mu \frac{EI}{h^2} \quad (3.63)$$

in which  $P_f$  is the column failure load

$E$  is the Young's Modulus in compression

$I$  is the full-section second moment of area

$h$  is the column height

$\mu$  is the factor which depends upon the end eccentricity of the load as follows —

- (i) if the load is applied at the same eccentricity at both ends such that the load acts outside the kern at both ends, then Angervo showed that the constant  $\mu$  may be approximated as

$$\mu = 9.44 \left(1 - \frac{m}{3}\right)^3 \quad (3.64)$$

$$\text{in which } m = \frac{6e}{d} \quad (3.65)$$

where  $e$  is the load eccentricity at both ends measured from the centroid of the full section

$d$  is the section thickness.

- (ii) if the load is applied at both ends with equal eccentricity but within the kern, it is possible for the line of action of the load to be inside the kern for the end parts of the column and outside the kern near the midheight. In this case, Angervo showed that—

$$\mu = 4 \cdot \left\{ (1-p)^{1.5} \cdot \left[ \frac{p^{0.5}}{(1-p)} + \frac{1}{2} \cdot \ln \left( \frac{1+p^{0.5}}{1-p^{0.5}} \right) \right] + \arcsin \left( \frac{1-p}{1+3p} \right)^{0.5} - \arcsin \left[ m \cdot \left( \frac{1-p}{1+3p} \right)^{0.5} \right] \right\}^2 \quad (3.66)$$

in which the parameter,  $p$ , is defined by—

$$p = \frac{3e_o}{d} - \frac{1}{2} \quad (3.67)$$

where:  $e_o$  is the maximum effective eccentricity of the load at failure (figure 3.37)

$d$  is the section thickness

$m$  is as defined for equation (3.65).

The value of the parameter,  $p$ , at column failure may be solved by trial by calculating the value of  $p$  for which equation (3.66) tends to a maximum value for  $\mu$ .

Angervo gave values of  $p$  and  $\mu$  for various end eccentricities of the load (Table 3.8).

$m$ (eqn.(3.65))	$p$	$\mu$
0	0	$\pi^2$
0.10	0.0815	8.75
0.25	0.147	7.36
0.50	0.234	5.48
0.75	0.312	3.98
1.00	0.388	2.80

Table 3.8: Column Failure Load Parameters for Equation (3.64)

Angervo showed further that values of  $\mu$  calculated using equation (3.65) with values of  $m \leq 1$  (end load inside the kern) were within 5 percent of values of  $\mu$  calculated using equation (3.66). He suggested, therefore, that the buckling failure loads for all cases of end load eccentricity could be calculated approximately using equations (3.64) and (3.65).

Many materials do not possess stress-strain characteristics which can be represented adequately by a simple mathematical model. In order to investigate the behaviour of a non-linear material with no tensile strength, Angervo suggested one particular form of constitutive relationship as follows -

$$\left(\frac{\sigma}{\sigma_s}\right) = 1 - \frac{1}{\sqrt{\frac{2E}{\sigma_s} \cdot \epsilon + 1}} \quad (3.68)$$

in which  $\sigma_s$  is the maximum stress sustained by the material

$E$  is the initial tangent elastic modulus

$\sigma$  is the stress

$\epsilon$  is the strain.

Equation (3.68), plotted in figure 3.38, was selected because the resulting differential equations for the column deformations could be solved readily.

Powell's<sup>(93)</sup> experiments (Section 3.3.5, figure 3.35) showed, however, that the stress-strain relationships for brickwork were considerably different from the relationship proposed by Angervo, so that any non-linear analysis for brickwork behaviour based on equation (3.68) could result in significant errors.

Chapman and Slatford<sup>(97)</sup> analysed the elastic buckling of columns both without tensile strength and with limited tensile strength and considered the following cases;

- (i) the column was pinned and concentrically loaded at each end. Initially the column was assumed to be deformed in the shape of two linear segments such that the imperfection was a maximum at column mid-height.
- (ii) the column was clamped at each end and was deformed initially as in (i) above.
- (iii) the column was initially straight and was loaded with equal eccentricity at each end.

The column section was assumed to be rectangular for all three conditions and the investigation was essentially focussed on the problem of the initially straight column with equal end eccentricities. The material was assumed to be without tensile strength but to behave according to Hooke's Law. The load against central deflection curves for these eccentrically loaded columns were calculated and are shown in figure 3.39.

It is important to note that in real columns, the unstable equilibrium condition, indicated by the falling load-deflection characteristic in figure 3.39, is not attained and column buckling failure occurs at the maximum load. (The assumption is made throughout this section that material failure does not occur prior to buckling failure.)

Chapman and Slatford further stated that for an eccentrically loaded column in which the load was applied outside the kern, the maximum load may be calculated approximately by the expression —

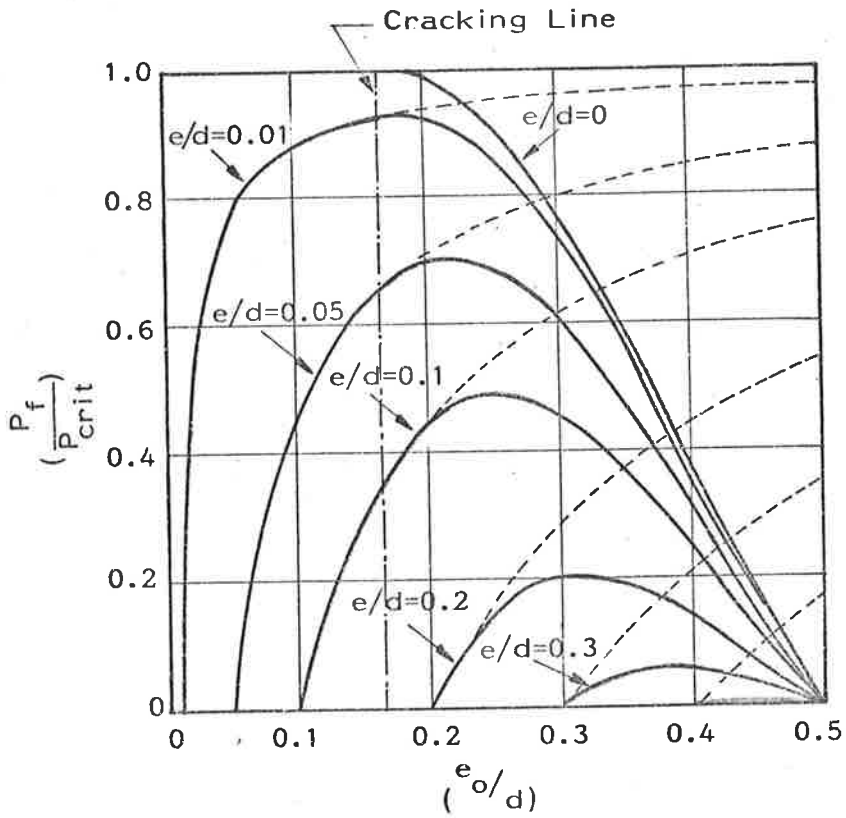
$$\frac{P_f}{P_{crit}} = 7.65 \left( \frac{1}{2} - \frac{e}{d} \right)^3 \quad (3.69)$$

in which  $P_f$  is the buckling failure load

$P_{crit}$  is the Euler load for the full section

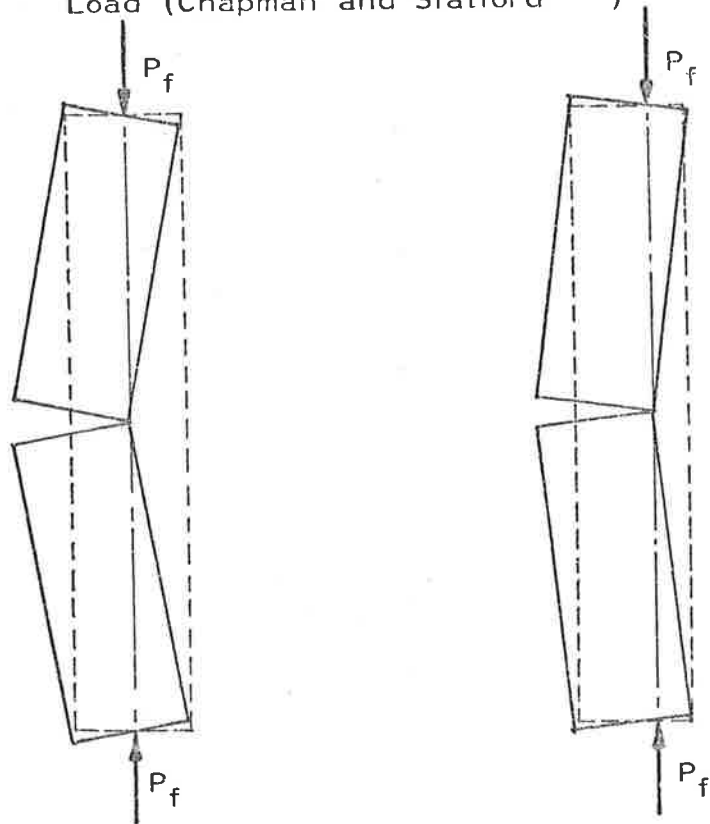
$e$  is the load end-eccentricity

$d$  is the section thickness.



(Note:  $e_o$  in this diagram is defined in figure 3.37)

Figure 3.39: Load-deflection Curves for Columns with Eccentric Load (Chapman and Slatford<sup>(97)</sup>)



(a) Concentric Load

(b) Eccentric Load

Figure 3.40: Modes of Final Collapse (Chapman and Slatford<sup>(97)</sup>)



They also stated that equation (3.69), which can be reduced to equation (3.63) when combined with equation (3.64), gave the maximum load with fair accuracy for eccentricities less than  $d/6$ , although the limiting value for  $\frac{P_f}{P_{crit}}$  at  $e$  equal to zero was 0.95 instead of 1.00.

Chapman and Slatford attempted to explain the failure mechanism of a column without tensile strength by means of the diagrams shown in figure 3.40. They stated that at the moment of final collapse in the pin-ended columns, the effective depth of the section due to cracking at the centre of the column was reduced to zero (figure 3.40(a) and figure 3.40(b)) so that a hinge was formed and each half of the column momentarily became straight.

At that instant, the centre of the compression face of the column was said to coincide with the line of the thrust. In fact, the cases described are unrealistic cases of unstable equilibrium achieved only if the external load is zero, since there must be some bending in the column if the load is non-zero. The situation shown in figure 3.40(b) say, can only occur if the eccentrically-loaded column is in the state at which  $\left(\frac{e_0}{d}\right)$  in figure 3.39 is equal to 0.5. In real columns under eccentric load, at the maximum load the effective section is reduced to some thickness at which column equilibrium is at a transition from a stable to an unstable condition (figure 3.41). If the deflection at column mid-height increases beyond that point, then equilibrium cannot be attained at the load level and the column fails. At no stage does a real column exist in the state described by Chapman and Slatford in figure 3.40(a) and 3.40(b).

An important phenomenon which Chapman and Slatford did not consider, particularly when testing their theory against experimental results, was the increase in compression stresses which might occur

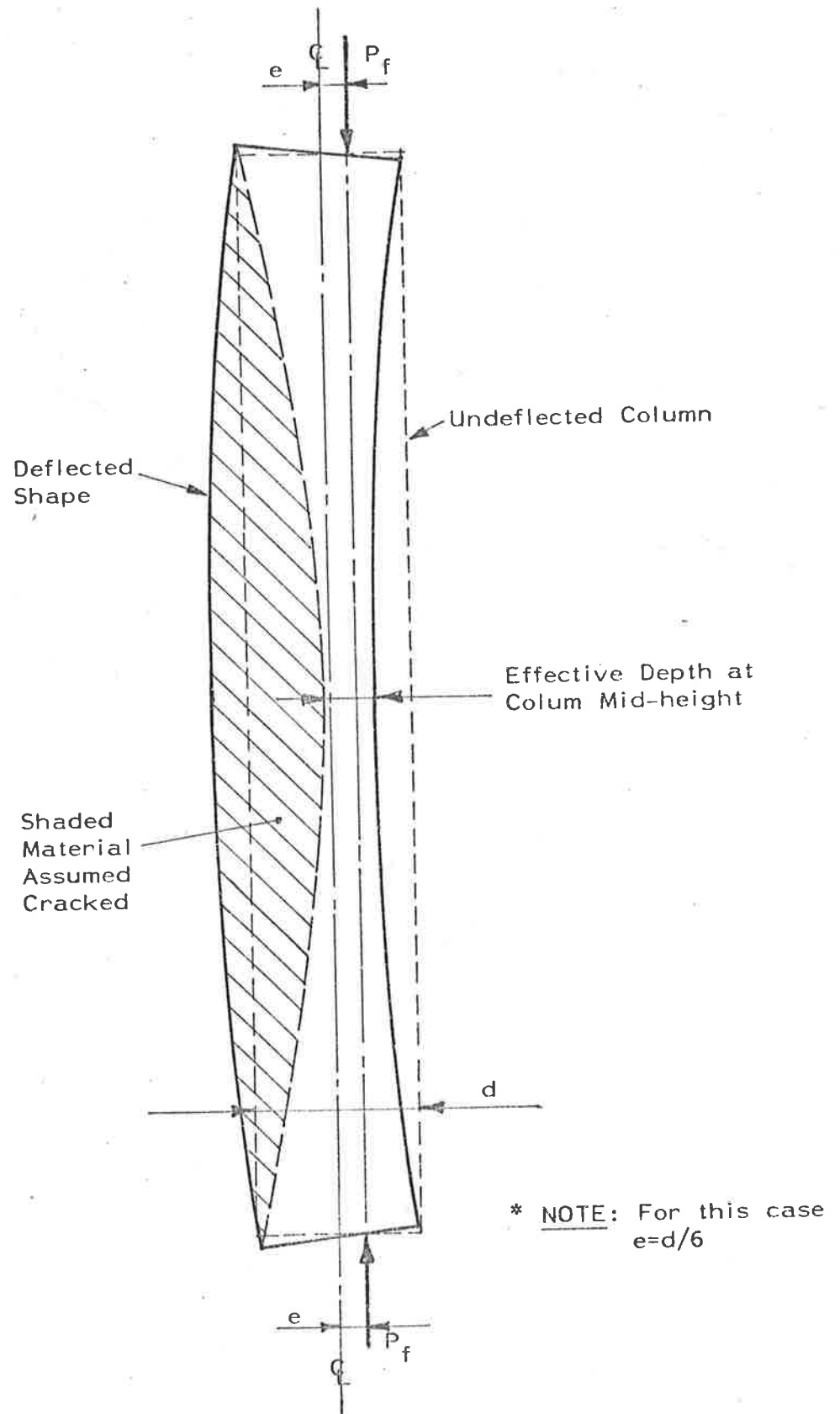


Figure 3.41: Column Deflection Immediately Prior to Collapse

if the load is maintained as the column fails. Chapman and Slatford's experimental results will be discussed further in Section 3.4.2.

Yokel<sup>(98)</sup> used the same assumptions as Angervo and Chapman and Slatford, but considered only pin-ended columns loaded with identical end eccentricities outside the kern. The form of Yokel's equation was —

$$P_f = 0.64 \cdot \frac{\pi^2 E b u_1}{h^2} \quad (3.70)$$

in which  $P_f$  is the failure load

$E$  is Young's Modulus

$b$  is column width

$u_1$  is distance from load to compression face at the ends

$h$  is column height.

Yokel also calculated that provided the load was outside the kern at the ends, the deflection at mid-height immediately before failure was given by

$$\frac{u_0}{u_1} = 0.625 \quad (3.71)$$

in which  $u_0$  is the distance from the line of action of the load to the compression face at column mid-height

$u_1$  is the distance from the line of action of the load to the compression face at the ends.

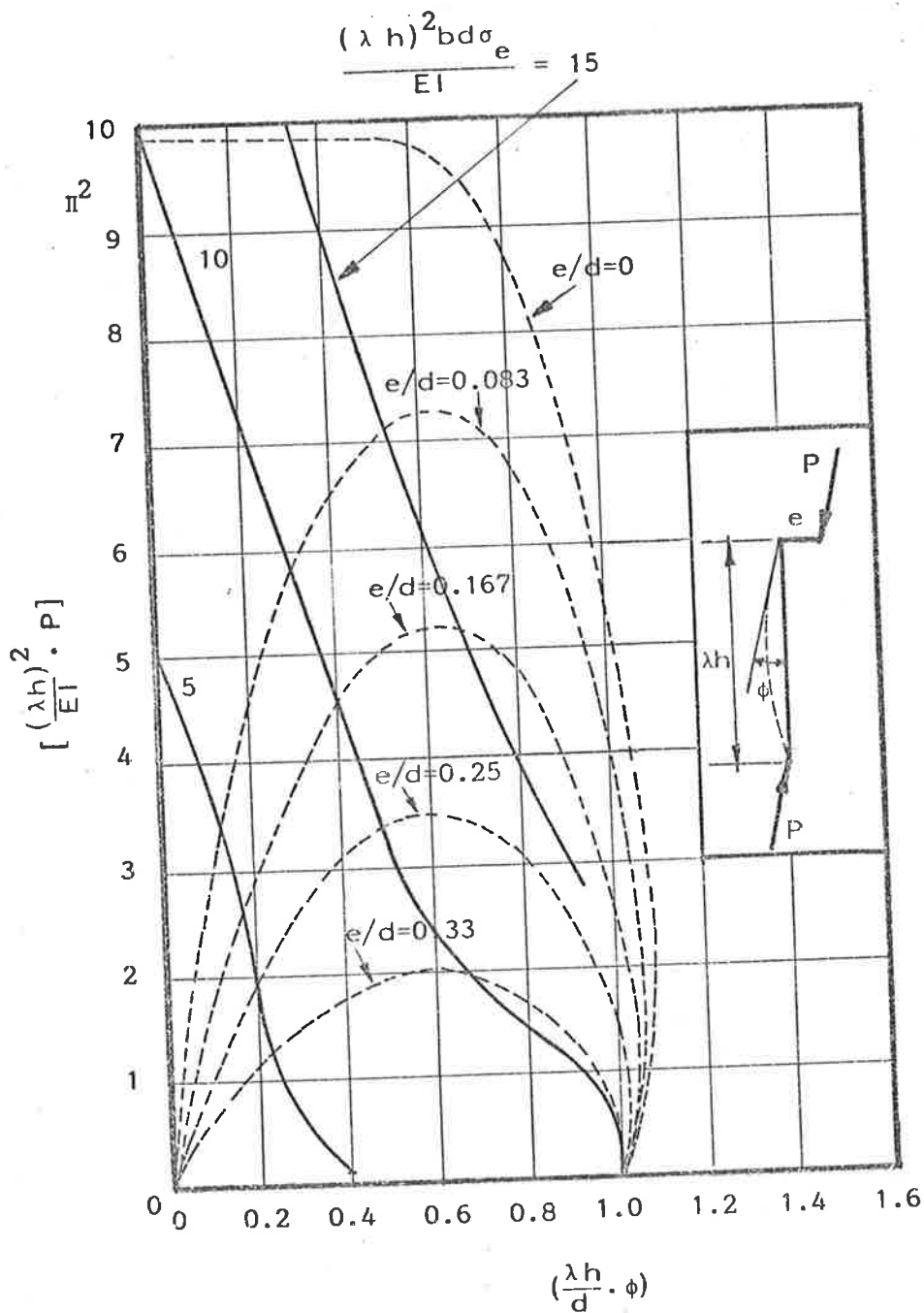
Equation (3.70) can be reduced to the same forms proposed by Angervo and Chapman and Slatford. Sahlin<sup>(44)</sup>, Frisch-Fay<sup>(99), (100)</sup>, Chen<sup>(101)</sup>, Haller<sup>(7)</sup>, Monk<sup>(102)</sup> and Risager<sup>(103)</sup> have also derived expressions which are essentially of the same form as equations (3.63), (3.69) and (3.70).

Sahlin also extended the results to columns in which the load is eccentric at one end only. The results, summarized in figure 3.42, may be used to calculate the buckling load of fixed-base columns provided that the effective height,  $\lambda h$ , is known. In practice, the effective height is not easily calculated.

Yokel indicated that the no-tensile strength theory was inadequate for brickwork because the real tensile strength would alter the equilibrium conditions and the load capacities would be larger than those predicted by a brittle-material theory. He stated that this was the case particularly for walls of very high slenderness ratios and high load eccentricities. He also pointed out that the brick units, with their greater strength and stiffness than the mortar joints, would cause stress distributions in the brickwork which might be much more complex than the idealized linear stress distribution assumed in the no-tension solution. The distribution of stresses in the bricks and its effects on the behaviour of brickwork will be discussed in Chapter 4.

Tesfaye and Broome<sup>(104)</sup> investigated the effect of wall self-weight on the failure load of eccentrically loaded columns and showed that, for single-leaf slender brick walls, the effect was negligible.

Cranston and Roberts<sup>(105)</sup> tested solid concrete blocks under vertical eccentric load and developed a theory which included an approximate method for analysing the tension-stiffening associated with the tensile strength of the blocks. However, they did not indicate how the theory could be implemented and most of their results were obtained from small-scale tests on blockwork couplets. The block aspect ratio, height-to-thickness, used in the couplet tests differed substantially from the aspect ratio of the full-sized blocks, so that the moment-rotation characteristics used by Cranston and Roberts are of questionable value.



Contaldo et al.<sup>(106)</sup> used finite difference techniques to model the linear-elastic problem solved by Angervo<sup>(96)</sup> and also to simulate the results obtained on brickwork piers by Powell and Hodgkinson<sup>(93)</sup>, by assuming that the stress-strain relationship for brickwork was of the form

$$\sigma = E\epsilon - K\epsilon^n \quad (3.72)$$

in which  $E$  is Young's Modulus at zero stress

$K, n$  are constants

Contaldo et al. reported that Powell and Hodgkinson's results showed that the exponent,  $n$ , was approximately equal to 2. However, the formulation did not distinguish between the different behaviour of the brick and mortar components, and therefore the results cannot be applied generally. Contaldo et al. did show that the finite difference method is quite an accurate method for modelling pin-ended brittle columns particularly if at least eight elements are used. The use of finite difference techniques in modelling no-tension material columns as well as slender brick walls will be discussed in more detail in Chapter 4.

#### 3.4.2 Comparison of Experiments with No-tension Material Column Theory

Chapman and Slatford<sup>(97)</sup> compared the experimental results reported by Davey and Thomas<sup>(30)</sup> with their own no-tension material column theory and reported that, subject to corrections on the assumed end conditions and assuming that the columns failed by lateral buckling, the experiments agreed well with theory. However, in the discussion on their paper on brickwork, Davey and Thomas<sup>(30)</sup> reported that the only buckling failure among all the walls they had tested had been induced artificially by using plywood in the bedjoints.

Therefore, effectively, Chapman and Slatford compared their results from a no-tension material column theory with experimental failure loads resulting from material failure. Any conclusions drawn from such a comparison are clearly invalid.

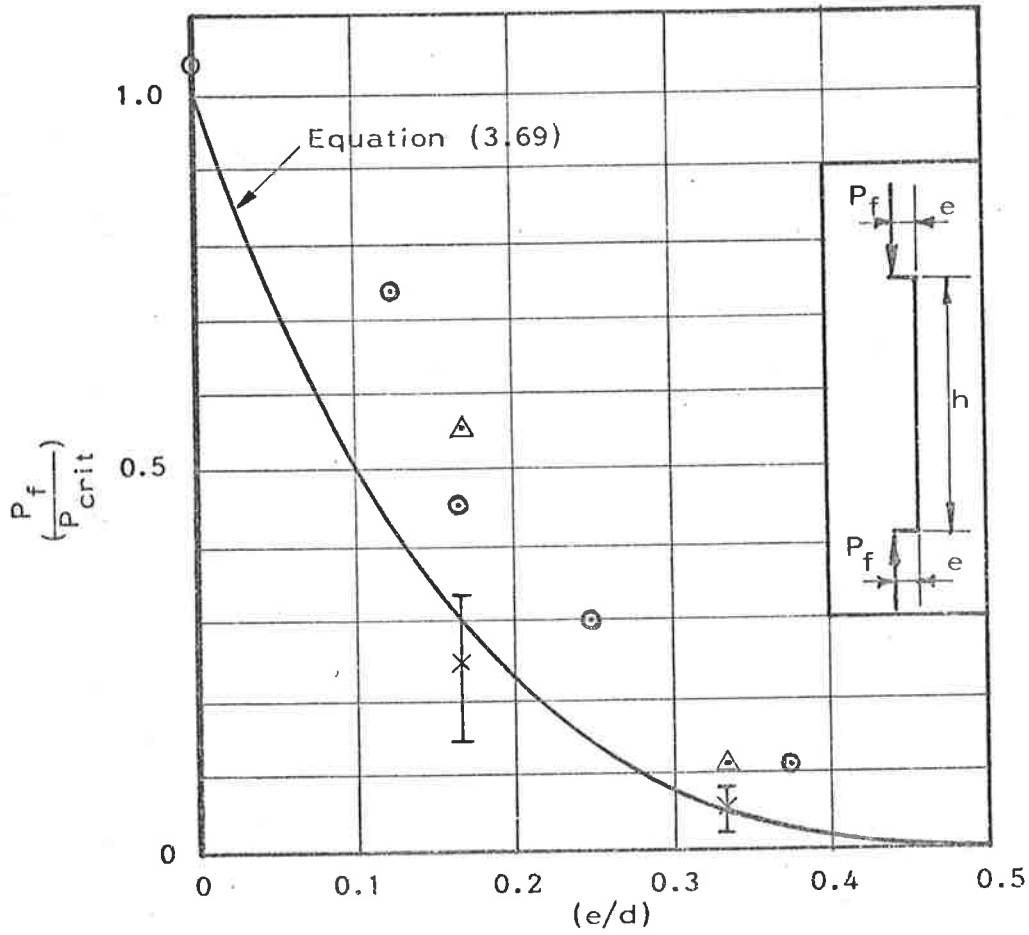
Chapman and Slatford also tested their brittle-column theory by constructing a column of thirty-three, two-inch high (50.8mm) by one-inch thick (25.4mm), aluminium blocks and compressing the column between knife-edges both axially and eccentrically. However, because of the relatively high aspect ratio, or height-to-thickness ratio of the blocks, they did not test precisely a no-tension material column, but one which could crack only at widely-spaced intervals. The end faces of the blocks were reported to have been machined flat and parallel to within  $\pm 0.0003$  inches (0.008mm). However, it is probable that after column failure, damage would have been incurred at the block edges because of the very large increase in compression stresses at failure (Section 3.4.2), particularly since the blocks were of aluminium. The initial slopes of the experimental load-deformation curves differed markedly from the theoretical curves, consistent with a hypothesis of damage, so that even although the experimental failure loads were reported to agree with the theoretical failure loads, the experiments did not establish the validity of the theory. Chapman and Slatford's experiments have been repeated by the author using steel blocks and the results, which differ from those of Chapman and Slatford, are discussed in Chapter 5.

James<sup>(107), (108), (109)</sup> and Martin and Nettle<sup>(110)</sup> tested storey-height brick walls, three bricks long, with slenderness ratios up to 32 so that all walls failed by elastic buckling. James tested walls of bricks laid on flat while Martin and Nettle used bricks on edge throughout, and the loads were applied through knife edges at

identical eccentricities top and bottom. James' results (figure 3.43) which show considerable spread at each load eccentricity, are from ten tests at each eccentricity and Martin and Nettle's results are each from one test only. The elastic modulus values for James' experiments have been calculated from load-deflection data. On the other hand, Martin and Nettle obtained modulus values from tests on small mortar and brick prisms, but they noted that the Young's modulus values were of questionable accuracy because of the small number of prisms tested from each mortar batch.

Hasan and Hendry<sup>(123)</sup> reported tests on one-third scale model brickwork walls supported top and bottom and loaded concentrically and at equal end eccentricities of  $d/6$  and  $d/3$ . The height-to-thickness ratios (slenderness ratios) of the walls varied between 6 and 25. All walls loaded concentrically reportedly failed by vertical splitting or brick spalling as did walls of slenderness ratio up to 18 loaded at  $d/6$ . However, walls of slenderness ratio 25 failed by lateral buckling when loaded at  $d/6$ . All walls loaded at  $d/3$  (slenderness ratios 6, 12, 18 and 25) reportedly failed by lateral buckling. By using an elastic modulus, calculated from the test results of  $5.26 \times 10^3 \text{MPa}$ , the failure load ratios for the walls which failed by buckling may be calculated as shown in figure 3.43; the failure load ratio for an eccentricity of  $d/3$  is the mean of the ratios for walls with slenderness ratios 18 and 25. Hasan and Hendry stated that the buckling mode of collapse occurred as a result of bond failure at a brick-mortar interface, thereby explaining the higher-than-predicted failure loads (figure 3.43) because Chapman and Slatford's theory (equation 3.69) assumes that the bond strength is negligible. Hasan and Hendry's test results may indicate, therefore, that model brickwork should not be





- △ Hasan and Hendry<sup>(123)</sup>
- ⊙ Martin and Nettle<sup>(110)</sup>  
Each point 1 test (brick-on-edge)
- ⊥ James<sup>(107), (108), (109)</sup>  
⊗ Showing mean and range of 10 tests (brick-on-flat)

NOTE:  $P_{crit} = \frac{\pi^2 EI}{h^2}$

Figure 3.43: Load Tests on Slender Walls

used for testing slender walls because the bond strength, which may not be zero, cannot be scaled in the same way as are all the wall dimensions.

West, Hodgkinson and Davenport<sup>(42)</sup> tested walls at eccentricities of  $d/8$  but, because no Young's Modulus values were obtained, comparison with no-tension material column theory cannot be made.

The failure load of slender walls may also be affected by workmanship<sup>(111)</sup> and initial imperfections, but these effects have not been incorporated into any of the theories for columns of no-tension material subjected to eccentric loading. The possible reduction in the load-carrying capacity of slender walls due to these effects, even when constructed within limits prescribed by Codes of Practice, will be discussed in Chapter 8.

### 3.4.3 Theory of Panels Simply-supported on Four Sides

Timoshenko<sup>(112)</sup> described the equation of equilibrium for an isotropic plate loaded both by lateral loads and forces in the middle plane of the plate. By using Timoshenko's conventions for the calculation of forces, moments and displacements, the equation of equilibrium on a plate element can be expressed as -

$$\frac{\partial^2 M_x}{\partial x^2} - 2 \cdot \frac{\partial^2 M_{xy}}{\partial x \partial y} + \frac{\partial^2 M_y}{\partial y^2} = - (q + N_x \cdot \frac{\partial^2 w}{\partial x^2} + N_y \cdot \frac{\partial^2 w}{\partial y^2} + 2N_{xy} \cdot \frac{\partial^2 w}{\partial x \partial y}) \quad (3.73)$$

$w$  is the plate displacement in the Z direction

$N_x$  is the force per unit width of plate in the X direction

$N_y$  is the force per unit width of plate in the Y direction

$N_{xy}$  is the shear force per unit width of plate

$q$  is the uniform lateral pressure

$M_x$  is the bending moment per unit width of plate caused by normal stresses in the X direction

$M_y$  is the bending moment per unit width of plate caused by normal stresses in the Y direction

$M_{xy}$  is the twisting moment per unit width of plate

$N_x, N_y$  are positive for tension.

Substitution of the constitutive relationships

$$M_x = -D \cdot \left( \frac{\partial^2 w}{\partial x^2} + \nu \frac{\partial^2 w}{\partial y^2} \right) \quad (3.74(a))$$

$$M_y = -D \cdot \left( \frac{\partial^2 w}{\partial y^2} + \nu \frac{\partial^2 w}{\partial x^2} \right) \quad (3.74(b))$$

$$M_{xy} = D \cdot (1 - \nu) \cdot \frac{\partial^2 w}{\partial x \partial y} \quad (3.74(c))$$

in which, for an isotropic plate of constant thickness, D is constant and equal to  $\frac{Eh^3}{12 \cdot (1 - \nu^2)}$  (3.75)

where E is the elastic modulus

h is the plate thickness

$\nu$  is Poisson's ratio

gives equation (3.73) in the form –

$$\frac{\partial^4 w}{\partial x^4} + 2 \cdot \frac{\partial^4 w}{\partial x^2 \partial y^2} + \frac{\partial^4 w}{\partial y^4} = \frac{1}{D} \cdot \left( q + N_x \cdot \frac{\partial^2 w}{\partial x^2} + N_y \cdot \frac{\partial^2 w}{\partial y^2} + 2N_{xy} \cdot \frac{\partial^2 w}{\partial x \partial y} \right) \quad (3.76)$$

If  $N_x, q$  and  $N_{xy}$  are zero, and  $N_y$  is compression and constant throughout the plate (figure (3.44)) then equation (3.76) becomes –

$$\frac{\partial^4 w}{\partial x^4} + 2 \cdot \frac{\partial^4 w}{\partial x^2 \partial y^2} + \frac{\partial^4 w}{\partial y^4} = \frac{1}{D} \cdot \left( -N_y \cdot \frac{\partial^2 w}{\partial y^2} \right) \quad (3.77)$$

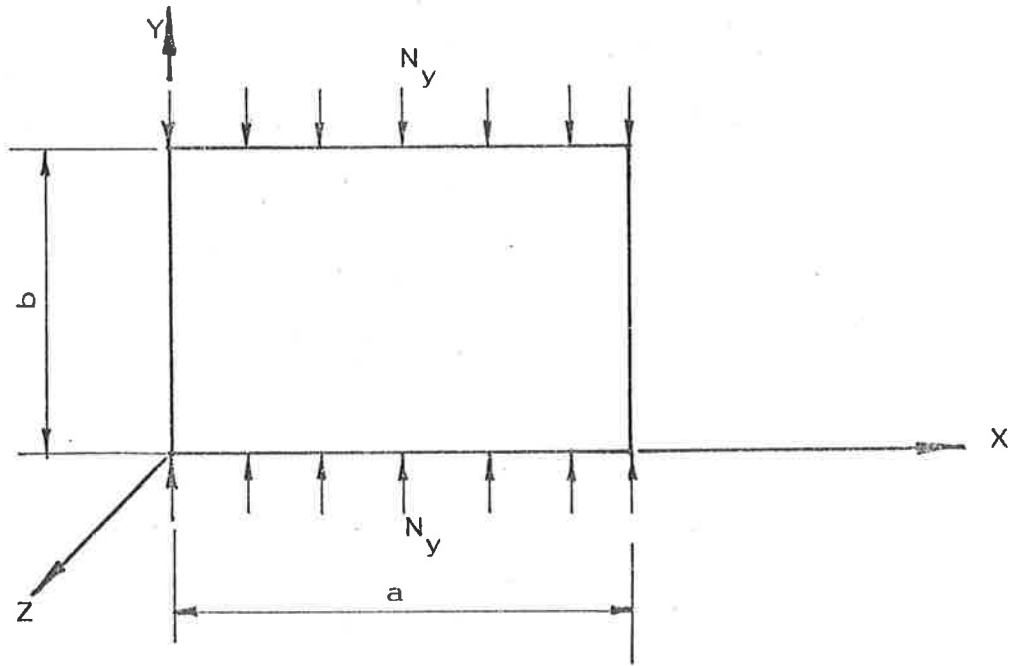
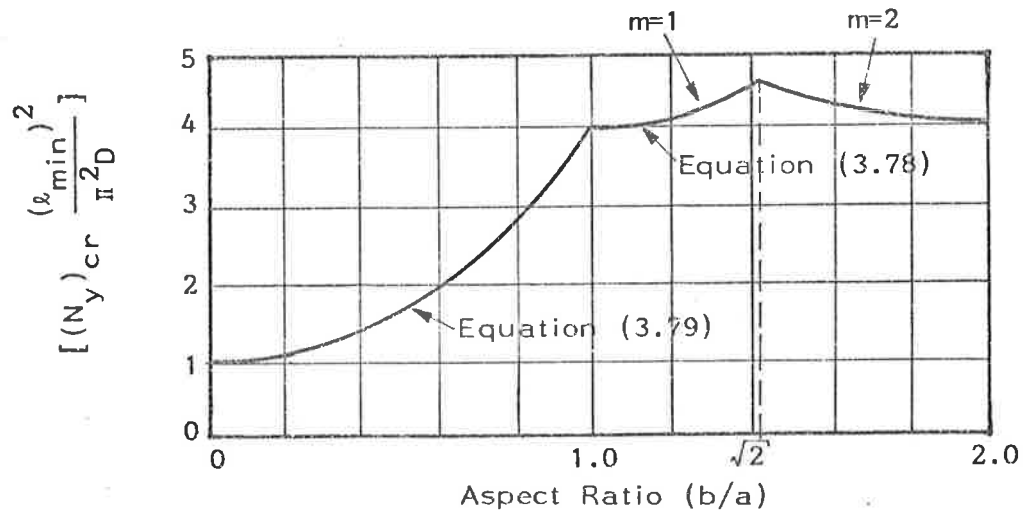


Figure 3.44: Plate Subjected to Uniform Compression



NOTE:  $l_{min}$  is the smaller of  $b$  and  $a$

Figure 3.45: Buckling Loads of a Plate Simply-supported on Four Sides

Timoshenko showed that the critical buckling load,  $(N_y)_{cr}$ , for such a plate simply-supported on four sides, is given by

$$(N_y)_{cr} = \frac{\pi^2 D}{a} \left( \frac{ma}{b} + \frac{b}{ma} \right)^2 \quad (3.78)$$

in which  $m$  is the number of half-sine waves into which the plate buckles.

The variable  $m$  is an integer and must be chosen to make  $(N_y)_{cr}$  in equation (3.78) a minimum. For aspect ratios  $(b/a) < 1$ ,  $m$  is unity and equation (3.78) becomes

$$(N_y)_{cr} = \frac{\pi^2 D}{b^2} \left[ 1 + \left( \frac{b}{a} \right)^2 \right]^2 \quad (3.79)$$

The critical buckling load  $(N_y)_{cr}$  is plotted non-dimensionally against the aspect ratio  $(b/a)$  in figure 3.45. The buckling load for a square plate simply-supported on four sides is four times the buckling load of the plate if supported top and bottom only.

The lateral displacements of a plate loaded only by a constant force,  $N_y$ , which is eccentric with respect to the middle plane of the plate, can be approximated by the expressions obtained by Timoshenko<sup>(112)</sup> for a plate with moments uniformly distributed along two opposite edges, provided that the load is small compared with the critical buckling load (figure 3.46).

The solution for the lateral displacements in the plate is

$$w = \frac{2M_0 a^2}{\pi^3 D} \sum_{m=1,3,5,\dots}^{\infty} \frac{1}{m^3 \cosh \alpha_m} \left\{ \left( \alpha_m \cdot \tanh \alpha_m \cdot \cosh \left( \frac{m\pi y}{a} \right) - \left( \frac{m\pi y}{a} \right) \sinh \left( \frac{m\pi y}{a} \right) \right) \cdot \sin \frac{m\pi x}{a} \right\} \quad (3.80)$$

$$\text{in which } \alpha_m = \frac{m\pi b}{2a} \quad (3.81)$$

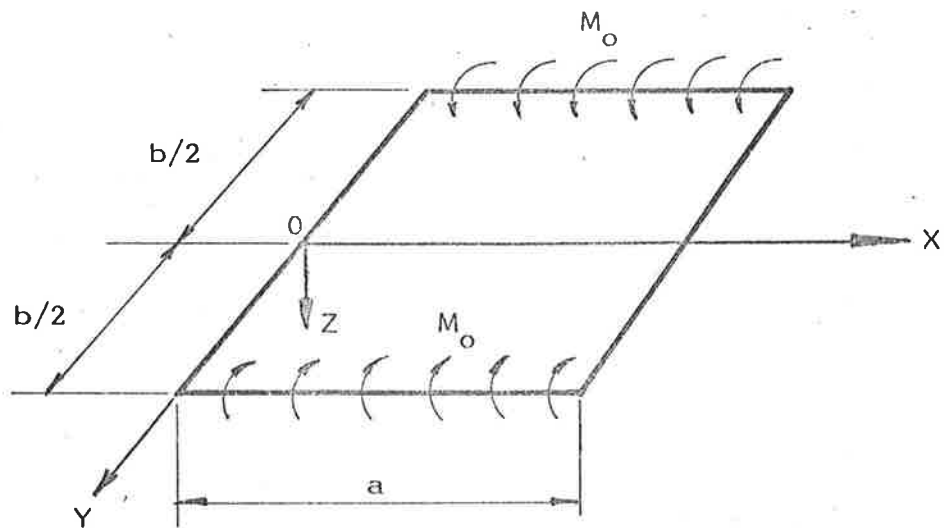


Figure 3.46: Simply-supported Plate Subjected to Uniform Moments on Two Opposite Sides

Along the axis of symmetry,  $y=0$ , the lateral displacements are given by

$$(w)_{y=0} = \frac{2M_0 a^2}{\pi^3 D} \sum_{m=1,3,5,\dots}^{\infty} \frac{1}{m^3} \cdot \alpha_m \cdot \frac{\tanh \alpha_m}{\cosh \alpha_m} \cdot \sin \frac{m\pi x}{a} \quad (3.82)$$

and for any given ratio  $(b/a)$ , the lateral deflection at  $x=a/2$ ,  $y=0$  is

$$(w)_{y=0, x=a/2} = \frac{M_0 ab}{\pi^2 D} \sum_{m=1,3,5,\dots}^{\infty} (-1)^{\frac{(m-1)}{2}} \cdot \frac{1}{m^2} \cdot \frac{\tanh \alpha_m}{\cosh \alpha_m} \quad (3.83)$$

Values for these deflections and bending moments per unit width for a plate for which Poisson's ratio  $\nu$ , is 0.3 are shown in Table 3.9.

$(b/a)$	$(\frac{wD}{M_0})$	$(M_x/M_0)$	$(M_y/M_0)$
0	$0.1250b^2$	0.300	1.000
0.50	$0.0964b^2$	0.387	0.770
0.75	$0.0620b^2$	0.424	0.476
1.00	$0.0368a^2$	0.394	0.256
1.50	$0.0280a^2$	0.264	0.046
2.00	$0.0174a^2$	0.153	-0.010

Table 3.9: Moments and Deflections for a Simply-supported Plate

The central deflection of a strip length  $\underline{b}$  unsupported on its edges is approximately  $3\frac{1}{2}$  times that of a square plate of edge dimensions  $\underline{b}$ , simply-supported on four sides; the moment  $M_y$  at the centre of the strip is equal to the end moment  $M_0$ , while  $M_y$  decreases in a square plate from  $M_0$  at the edges to a smaller value at the centre of the plate. Timoshenko stated that the change in moment  $M_y$  was due to a "damping effect" of the edges  $x=0$  and  $x=a$  which are not subject to a moment couple.

It is important to note that the critical buckling load for a solid isotropic plate subjected to a uniform edge moment on two opposite sides is given by equations (3.78) and (3.79).

Timoshenko also described the analysis of rectangular plate, isotropic in material properties but variable in thickness, and concluded that provided there was no abrupt variation in thickness the expressions for bending and twisting moments derived for plates of constant thickness (equations (3.74(a)), (3.74(b)) and (3.74(c))) could be applied with sufficient accuracy. However, because the flexural rigidity,  $D$ , was no longer a constant but was a function of the  $x$  and  $y$  coordinates, the equilibrium equation (3.73) became—

$$\begin{aligned} D\Delta\Delta w + 2\frac{\partial D}{\partial x}\frac{\partial(\Delta w)}{\partial x} + 2\frac{\partial D}{\partial y}\frac{\partial(\Delta w)}{\partial y} + \Delta D\Delta w \\ - (1-\nu)\left(\frac{\partial^2 D}{\partial x^2}\frac{\partial^2 w}{\partial y^2} - 2\frac{\partial^2 D}{\partial x\partial y}\frac{\partial^2 w}{\partial x\partial y} + \frac{\partial^2 D}{\partial y^2}\frac{\partial^2 w}{\partial x^2}\right) \\ = q + N_x\frac{\partial^2 w}{\partial x^2} + N_y\frac{\partial^2 w}{\partial y^2} + 2N_{xy}\frac{\partial^2 w}{\partial x\partial y} \end{aligned} \quad (3.84)$$

$$\text{in which } \Delta = \frac{\partial^2}{\partial x^2} + \frac{\partial^2}{\partial y^2}$$

Olsson<sup>(113)</sup> used equation (3.84) to solve the particular case for which the flexural rigidity was given by —

$$D = D_0 + D_1 y \quad (3.85)$$

and the lateral load  $q$  by —

$$q = q_0 \left(1 + \frac{D_1}{D_0} y\right) \quad (3.86)$$

In equations (3.85) and (3.86)  $D_0$ ,  $D_1$  and  $q_0$  are constants.

Nakagawa<sup>(114)</sup> obtained a finite difference solution for equation (3.84) applied to the plate problem defined by Olsson in equations (3.85) and (3.86). For a plate of dimensions  $(b/a) = 1.0$  and a mesh



of (6 x 6) internal grid points, the finite difference results were very close to Olsson's results.

#### 3.4.4 Experiments on Panels Under Vertical Load

Sinha and Hendry<sup>(115)</sup> tested brickwork panels loaded axially both top and bottom, both full scale and one-third scale, with the height-to-length ratios between 0.8 and 5.6; the height-to-thickness slenderness ratios varied between 8 and 32. Sinha and Hendry concluded that, because failure was produced by vertical splitting of the brickwork in all cases, walls with stiffened returns with slenderness ratios up to 32 behaved in a similar manner to walls without end returns. However, they did not test the panels under eccentric loading, nor were any panels with height-to-length aspect ratios less than 0.8 investigated.

In real structural brickwork, the height-to-length ratio can be expected to vary between 0.3 and 1.0 or more, and, to the author's knowledge, experiments have not been conducted on panels of low aspect ratios subject to either concentric or eccentric vertical loading.

#### 3.4.5 Summary

The theories which have hitherto been applied to structural brickwork were derived for no-tension material columns. In structural brickwork, the brick units themselves can take significant tensile stresses, so that the equations of equilibrium derived by Angervo, Chapman and Slatford and others do not strictly apply to brickwork. Contaldo et al. showed that finite difference techniques can be used effectively on no-tensile material columns, but they did not give a detailed description of the means by which the finite difference technique could be applied to brickwork columns. Nakagawa showed that

plates of variable thickness, at least for the cases governed by equations of the type similar to equations (3.85) and (3.86), can be analysed using finite difference.

A method which combines a finite element procedure with finite differences to analyse brickwork columns is proposed in Chapter 4 and several experimental case studies are presented in Chapter 5.

The analysis of slender brickwork panels simply-supported on four sides, based on finite element and finite difference techniques, is presented in Chapter 6 and in Chapter 7 an experimental case study is presented of a slender brickwork panel subjected to an eccentric load both top and bottom. The results of the full-scale experiment are compared with Timoshenko's plate theory and the proposed theory for slender brickwork panels.

## 4. THE ANALYSIS OF BRICKWORK WALLS IN ONE-WAY BENDING

### 4.1 INTRODUCTION

It was shown in Chapter 3 that the stress-strain characteristics of a fired clay solid brick under axial compression could be assumed as linear (Section 3.1), whereas a mortar joint may deform in a non-linear manner (Section 3.2). In the following sections, the load-deformation characteristics of the brick and mortar materials under eccentric load are described and the behaviour of a combination of brick and mortar is investigated. A numerical method for calculating the failure of brick walls in one-way bending in which discrete cracking may occur at the brick-mortar interfaces is developed for both linear and non-linear mortar. (Linear brick properties are assumed throughout.) Comparisons are made with results calculated from wall theories described in Section 3.4. The numerical calculations, using PROGRAM PIER1, show that the no-tension material theories<sup>(96)(97)</sup>, which make no allowance for material failure, do not predict the failure of walls in which the compression stresses in the bedjoints are a significant fraction of the mortar failure stress,  $\sigma_c$ .

### 4.2 THE STIFFNESS AND GEOMETRIC PROPERTIES OF PARTIALLY-CRACKED BRICKWORK WALLS

#### 4.2.1 Cracking in the Bedjoints

The extent of bedjoint cracking in one-way bending of brickwork depends on the position of the line of action of the resultant compression load with respect to the wall centreline when the tensile bond strength between brick and mortar at the bedjoint is small. No cracking on the bedjoints occurs if the resultant vertical load acts

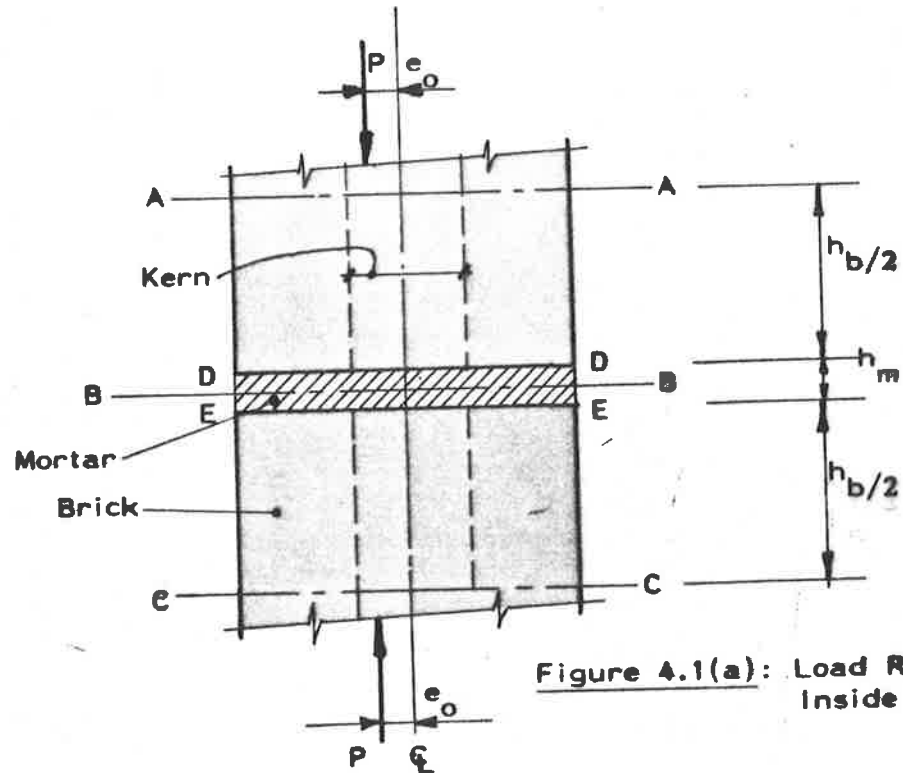


Figure 4.1(a): Load Resultant Inside Kern

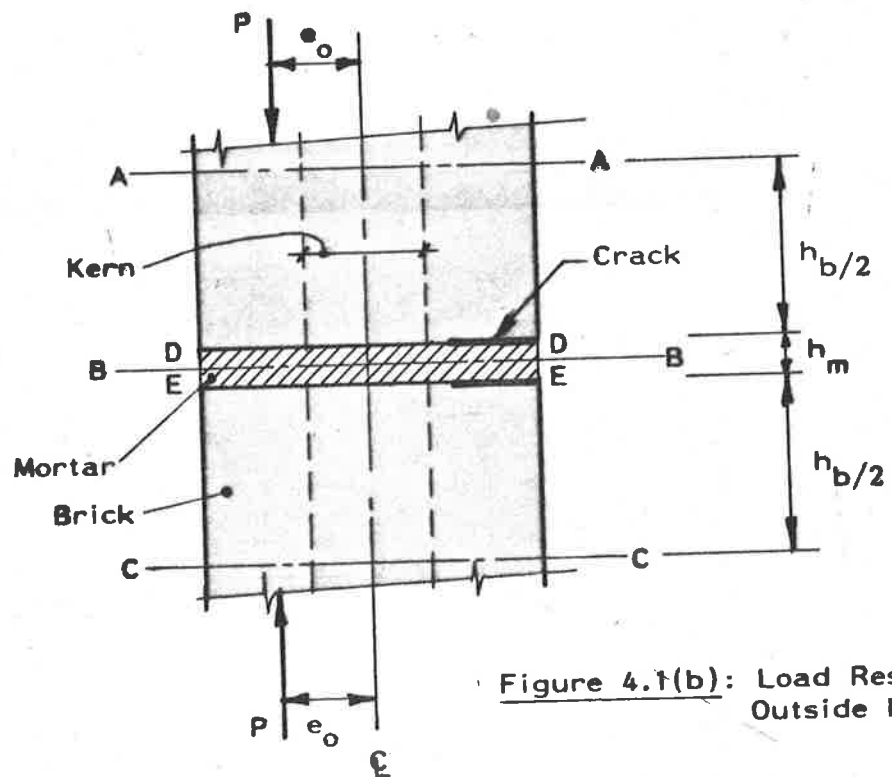


Figure 4.1(b): Load Resultant Outside Kern

Figure 4.1: Cracking on a Bedjoint Caused by the Position of the Vertical Load Resultant

within the kern (figure 4.1(a)). However, when the resultant load acts outside the kern, a crack forms at one or both of the brick-mortar interfaces (figure 4.1) and the brickwork stiffness is altered.

In the analysis which follows, it is assumed that, by symmetry, plane sections remain plane at the brick half-height planes AA and CC (figures 4.1(a), 4.1(b)) and that the plane section BB remains plane at the bedjoint mid-height. The calculations may be simplified considerably by assuming further that the compressed parts of the interfaces between brick and mortar on planes DD and EE remain plane during bending. As a result of this simplifying assumption, the deformations of the brick and mortar components may be calculated separately and then combined to determine the overall behaviour of the brickwork unit AACC.

#### 4.2.2 Solid Bricks under Eccentric Compression Load

It has been shown (Section 3.1.3.4) that the brick material can be assumed linear, that is, stress is proportional to strain. The flexural stiffness of solid bricks under eccentric vertical load may be calculated using two half-height bricks, without the mortar bedjoint, as shown in figure 4.2(a). The cases for which the resultant load acts within the kern are trivial because there is no cracking and therefore the flexural stiffness of the full section remains unaffected. However, the effective flexural stiffness of a brick subjected to vertical compression such that the line of action of the resultant lies outside the kern differs from the stiffness of the full section and may be calculated by using a finite element technique (figure 4.2(b)).

In both figures 4.2(a) and 4.2(b),  $P$  is the load per unit length of brick and  $e_0$  is the eccentricity of the resultant,  $P$ , from the brick centreline. The relative end rotation of the brick mid-planes AA and CC is denoted by  $\phi$ .

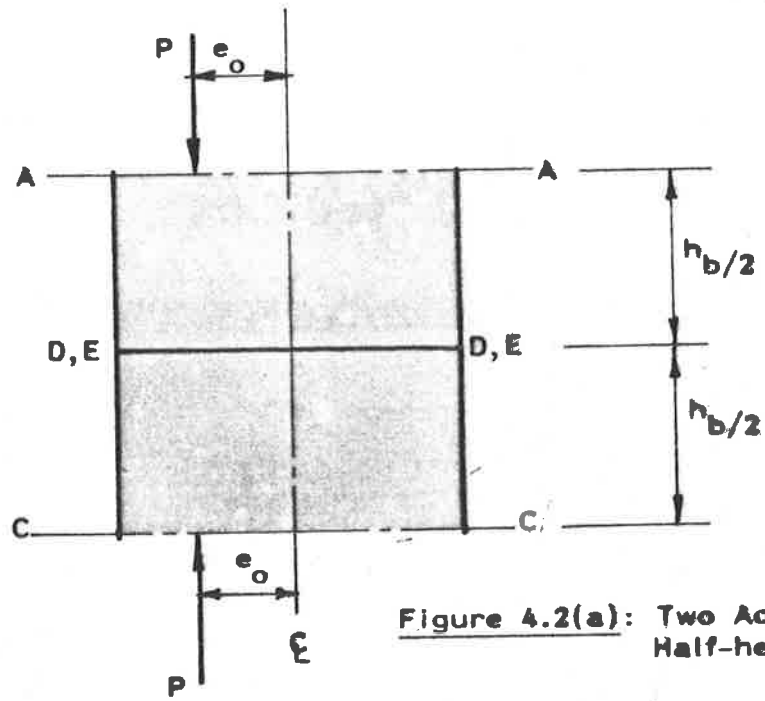


Figure 4.2(a): Two Adjacent Half-height Bricks

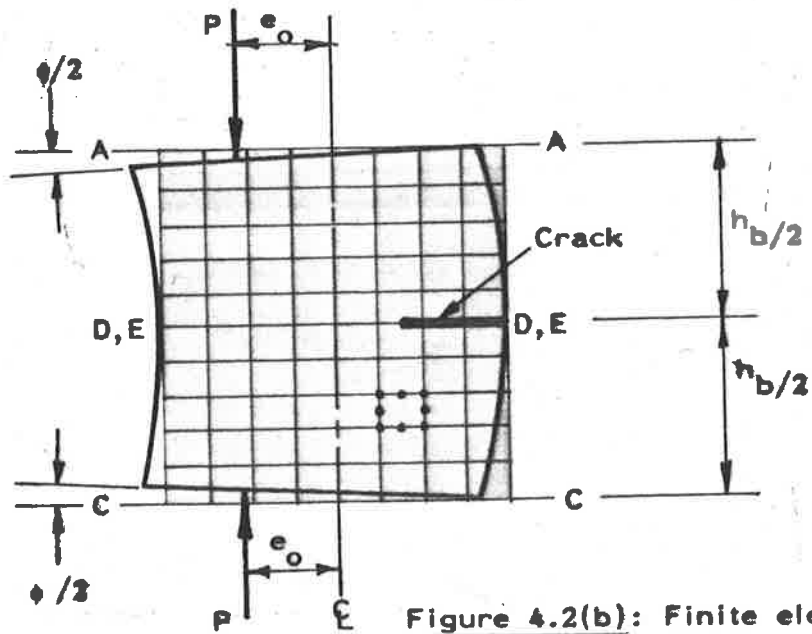


Figure 4.2(b): Finite element Sub-division Showing Typical Eight-noded Element

Figure 4.2: Analysis of Cracked Brickwork

All elements in the analysis are eight-noded isoparametric plane-stress elements, chosen because the non-uniform nature of the loading precludes the use of four-noded rectangular elements unless a very large number is used. Cracking between the brick units may be simulated by uncoupling the element nodes on plane DD(EE) in figure 4.2(b) at intervals of one-sixteenth of the section depth as described in the following section.

#### 4.2.2.1 Solution procedure

An iterative solution procedure is necessary because equivalent nodal loads cannot be calculated, initially, on planes AA and CC of the finite element mesh shown in figure 4.2(b) unless the stress distributions are known. The solution procedure is as follows. The (element) nodes on plane CC in figure 4.2(b) are restrained against translation in the direction of the applied load. The effective eccentricity of the load resultant and the magnitude of the load per unit length,  $P$ , are chosen. A set of nodal loads, statically equivalent to the chosen eccentric force, is applied on the plane AA; the resultant of the reactions on the plane CC will be statically equivalent to the reaction force shown in figure 4.2(b). The opposite forces to the reactions on plane CC are then applied at the nodes of plane AA and a new set of reactions is calculated on plane CC. Cracking between the brick units may be simulated during the iteration procedure by uncoupling nodes on plane DD(EE) so that no normal tension stresses occur on that plane. In the calculations, the nodal reactions on plane CC were found to be closely equal to the applied nodal loads on plane AA after four cycles. The resulting set of nodal forces may be applied in a finite element analysis of the model shown in figure 4.2(b) and the end rotations  $\phi/2$  may be calculated (the rotation of plane AA in the nodal load iteration procedure described above is for practical

purposes equal to  $\phi$ ). The flexural stiffness of the brick units may be calculated once the relative end rotation,  $\phi$ , is known.

#### 4.2.2.2 Results from the finite element analysis

The finite element software package ACES<sup>(125)</sup> was used to calculate the deformations and stress distributions for bricks of height-to-thickness aspect ratios of 0.691 (standard brick-on-flat), 1.447 (standard brick-on-edge) and 2.00. The relative rotations of the planes AA and CC (figure 4.1(b)) are summarized in Table 4.1 in non-dimensional form for the various brick aspect ratios and for a range of load eccentricities. Relative rotations are also given for a no-tension material and a non-cracking material.

In Table 4.1,  $e_0$  is the eccentricity of the load resultant from the brick centreline

$d$  is the brick thickness

$h_b$  is the brick height

$E_b$  is the brick Young's Modulus

$P$  is the load per unit length

$\phi$  is the relative rotation of planes AA and CC in figure 4.1(b).

The results given in Table 4.1 are plotted in figure 4.3. The ratio of the curvature of a no-tension material to the curvature of a solid brick, if both are loaded equally at the same eccentricity, can be calculated from the results summarized in Table 4.1. The ratio of curvatures may be denoted by a factor,  $\alpha$ , such that

$$\alpha = \left(\frac{1}{R}\right)_{nt} / \left(\frac{1}{R}\right)_b \quad (4.1)$$

in which  $\left(\frac{1}{R}\right)_{nt}$  is the curvature of a no-tension material

and  $\left(\frac{1}{R}\right)_b$  is the curvature of a solid brick.



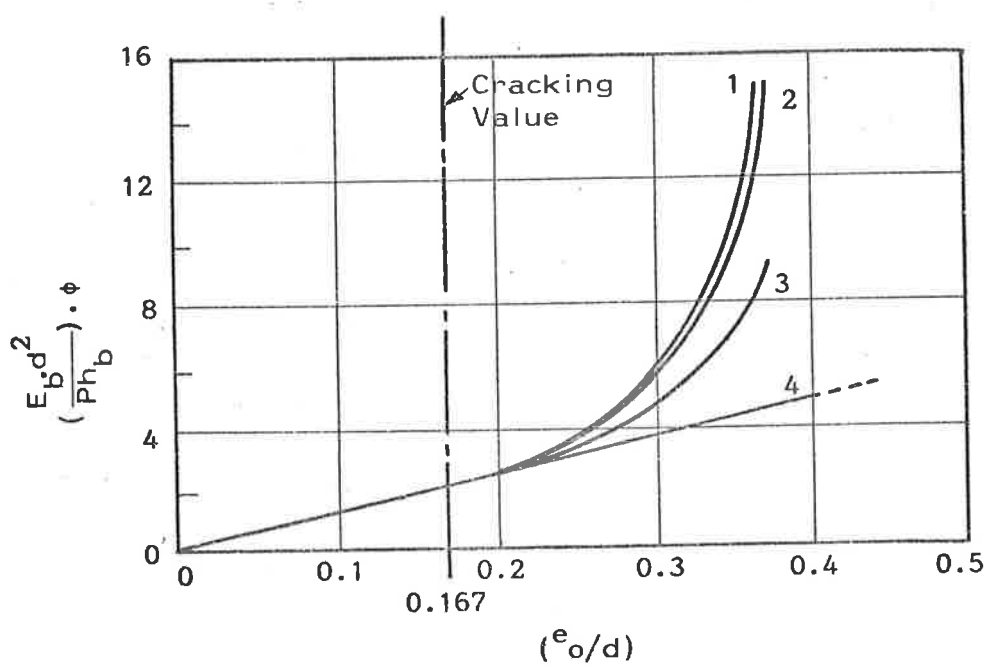


Figure 4.3: Flexural Stiffness Curves

Load Eccentricity ( $e_0/d$ )	Non-dimensional Relative End-plane Rotation ( $\phi \cdot \frac{E_b \cdot d^2}{Ph_b}$ )				
	Non-cracking	No-tension	$h_{b/d}=0.691$	$h_{b/d}=1.447$	$h_{b/d}=2.00$
0.167	2.00	2.00	2.00	2.00	2.00
0.208	2.50	2.61	2.57	2.53	2.52
0.250	3.00	3.56	3.45	3.24	3.17
2.292	3.50	5.12	4.90	4.30	4.07
0.333	4.00	8.00	7.45	5.98	5.42
0.375	4.50	14.22	12.43	8.89	7.65

Table 4.1: Flexural Stiffness Values

Values of  $\alpha$  for various load eccentricities and brick height-to-thickness aspect ratios are given in Table 4.2.

Load Eccentricity ( $e_0/d$ )	Curvature Ratio, $\alpha$			
	No-tension	$h_{b/d}=0.691$	$h_{b/d}=1.447$	$h_{b/d}=2.00$
0.167	1.000	1.000	1.000	1.000
0.208	1.000	1.016	1.032	1.036
0.250	1.000	1.032	1.099	1.123
0.292	1.000	1.045	1.191	1.258
0.333	1.000	1.074	1.338	1.476
0.375	1.000	1.144	1.600	1.859

Table 4.2: Curvature Ratio,  $\alpha$ 

The relationships between the curvature ratio,  $\alpha$ , and load eccentricity are shown in figure 4.4 and between the curvature ratio,  $\alpha$ , and brick aspect ratio in figure 4.5.

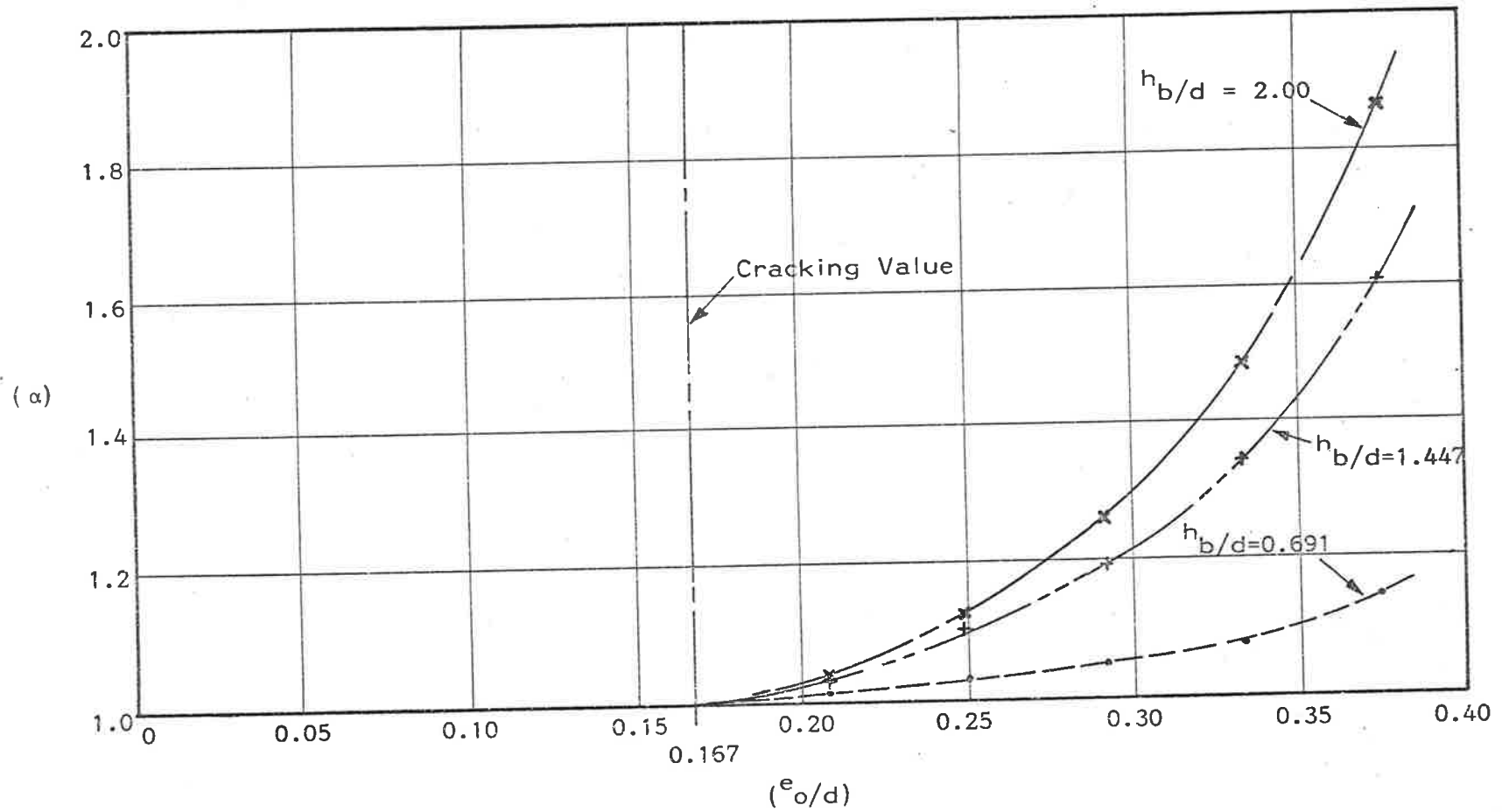


Figure 4.4: Relationship between Curvature Ratio and Load Eccentricity

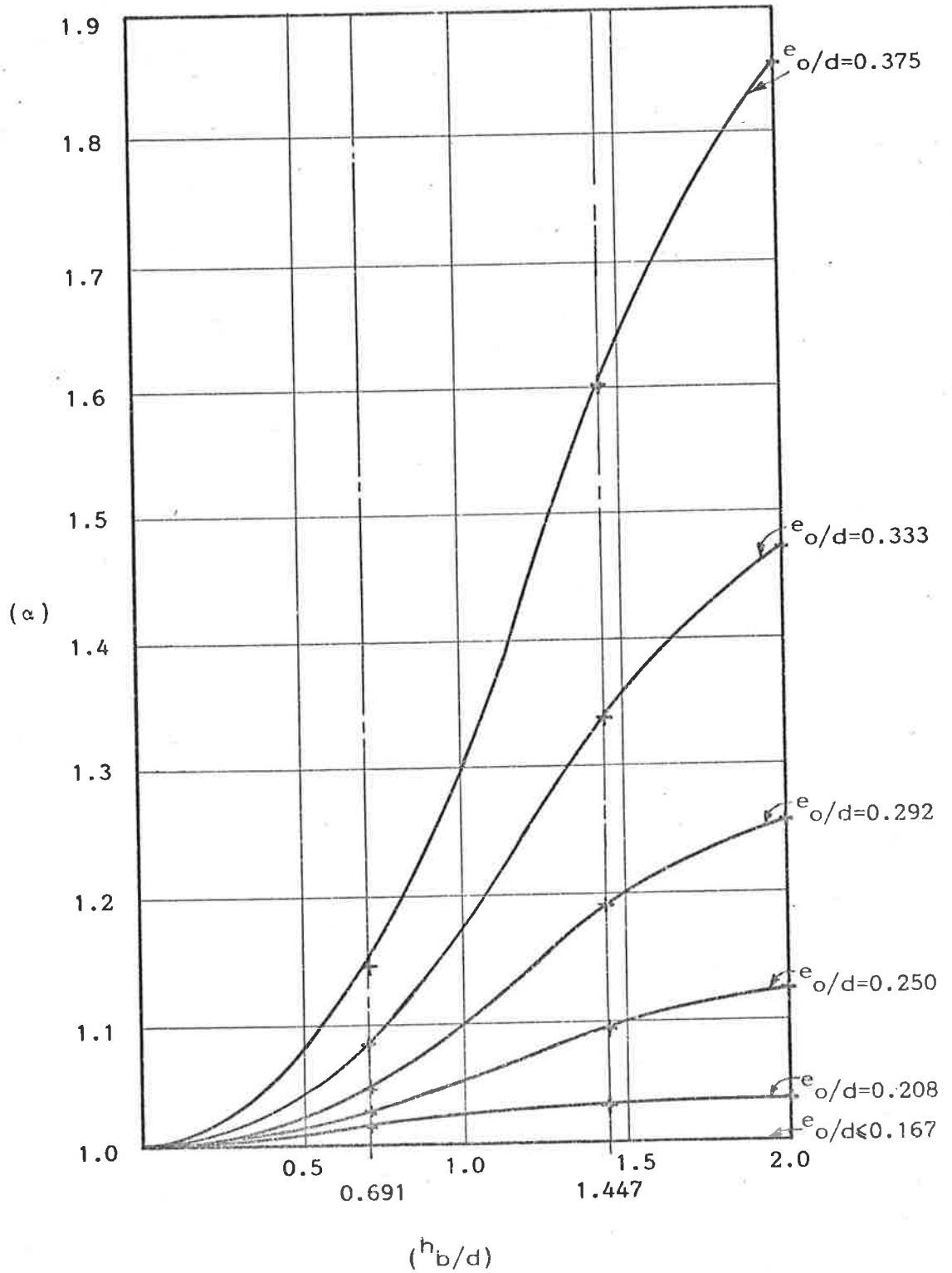


Figure 4.5: Relationship between Curvature Ratio and Brick Aspect Ratio

$\alpha$  may be represented as a function of  $(e_o/d)$  and  $(h_b/d)$  by using a least-squares approximation to the data in Table 4.2 (Appendix A), so that -

$$\alpha (e_o/d, h_b/d) = [1(e_o/d)(e_o/d)^2 (e_o/d)^3] [R] \begin{Bmatrix} 1 \\ (h_b/d) \\ (h_b/d)^2 \\ (h_b/d)^3 \end{Bmatrix} \quad (4.2)$$

in which  $[R]$  is a 4 x 4 matrix, and is given by -

$$[R] = \begin{bmatrix} 1.03 & -1.18 & 0.794 & -0.187 \\ -0.326 & 14.4 & -9.47 & 2.32 \\ 1.22 & -54.1 & 31.3 & -7.98 \\ -1.39 & 61.0 & -18.5 & 4.79 \end{bmatrix} \quad (4.3), \quad (A.9)$$

In the ranges  $0 \leq h_b/d \leq 2.0$ ,  $0.167 \leq e_o/d \leq 0.375$ , equations (4.2) and (4.3) give values for the curvature ratio,  $\alpha$ , to within 1 percent of the finite element values at all  $(h_b/d)$  and  $(e_o/d)$  points used to obtain  $[R]$ .

As a check on equations (4.2) and (4.3), a brick with an aspect ratio 1.0 and an effective load eccentricity  $(e_o/d)$  of 0.26 may be taken as an example. The finite element analysis gave a curvature ratio,  $\alpha$ , of 1.071, while equations (4.2) and (4.3) yielded a value for  $\alpha$  of 1.067. The results may be seen to agree to an acceptable degree of accuracy.

Normal stress distributions for both brick-on-edge ( $h_b/d = 1.447$ ) and brick-on-flat ( $h_b/d = 0.691$ ) configurations are shown in figures 4.6(a) and 4.6(b) respectively, and the stresses at the brick mid-height are compared with values calculated for both no-tension and non-cracking materials. The results show that the stress distribution at the brick mid-height depends upon the brick aspect ratio ( $h_b/d$ ), and that the stresses in a brick laid on flat are similar to the stresses in a no-tension material.

#### 4.2.3 Mortar Bedjoints Subject to Eccentric Compression

The behaviour of mortar bedjoints subject to eccentric compression can be investigated using a similar method to that described for solid bricks in Section 4.2.1. Results obtained for a linear mortar using the finite element method with a mesh of eighty elements (figure 4.2(b)) show that the flexural stiffness of a 10mm thick mortar joint is approximately equal to that of a no-tension material. That is, the curvature ratio,  $\alpha$ , defined in Section 4.2.2, may be taken to be unity for a mortar bedjoint. A typical stress distribution calculated by the finite element method is shown in figure 4.7.

However, the stress-strain relationship for a mortar bedjoint can be non-linear, particularly at stresses greater than the uniaxial compression strength (Section 3.2.3.3). An expression which may be used for the non-linear relationship is (106) –

$$\sigma = E_m \cdot (\epsilon - K\epsilon^n) \quad (B.1)$$

in which  $E_m$  is the initial tangent modulus

$\sigma$  is normal stress on the bedjoint

$\epsilon$  is normal strain on the bedjoint

$K, n$  are constants.

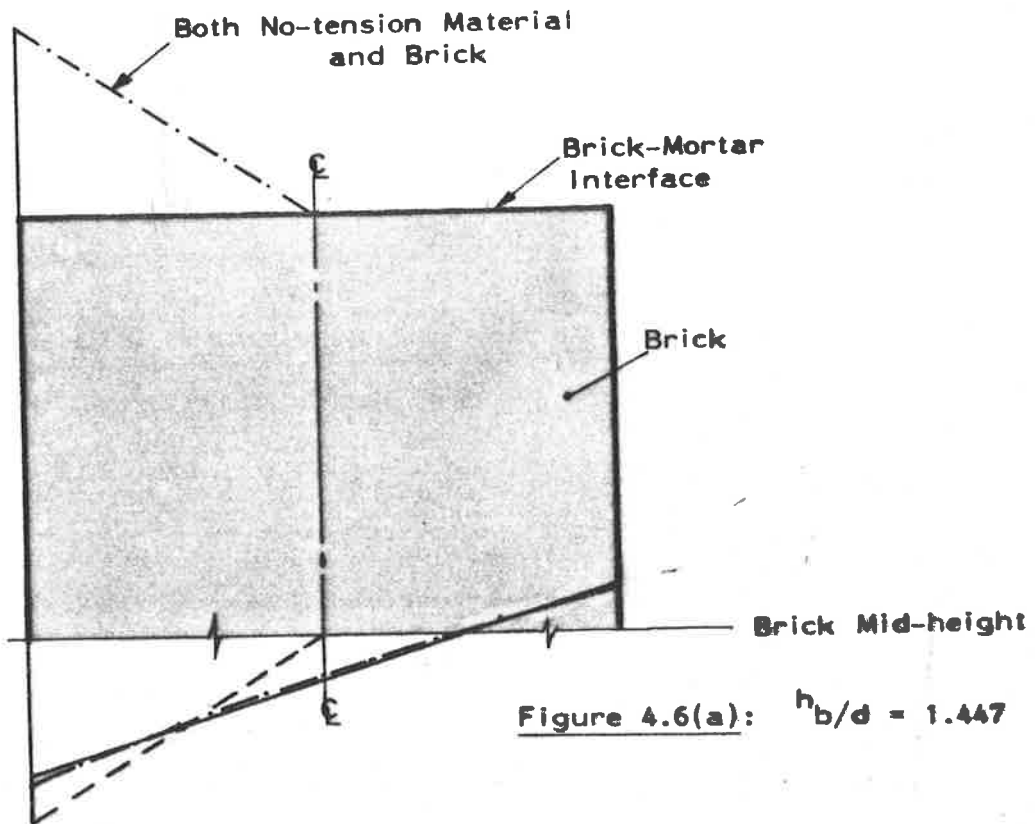


Figure 4.6(a):  $h_b/d = 1.447$

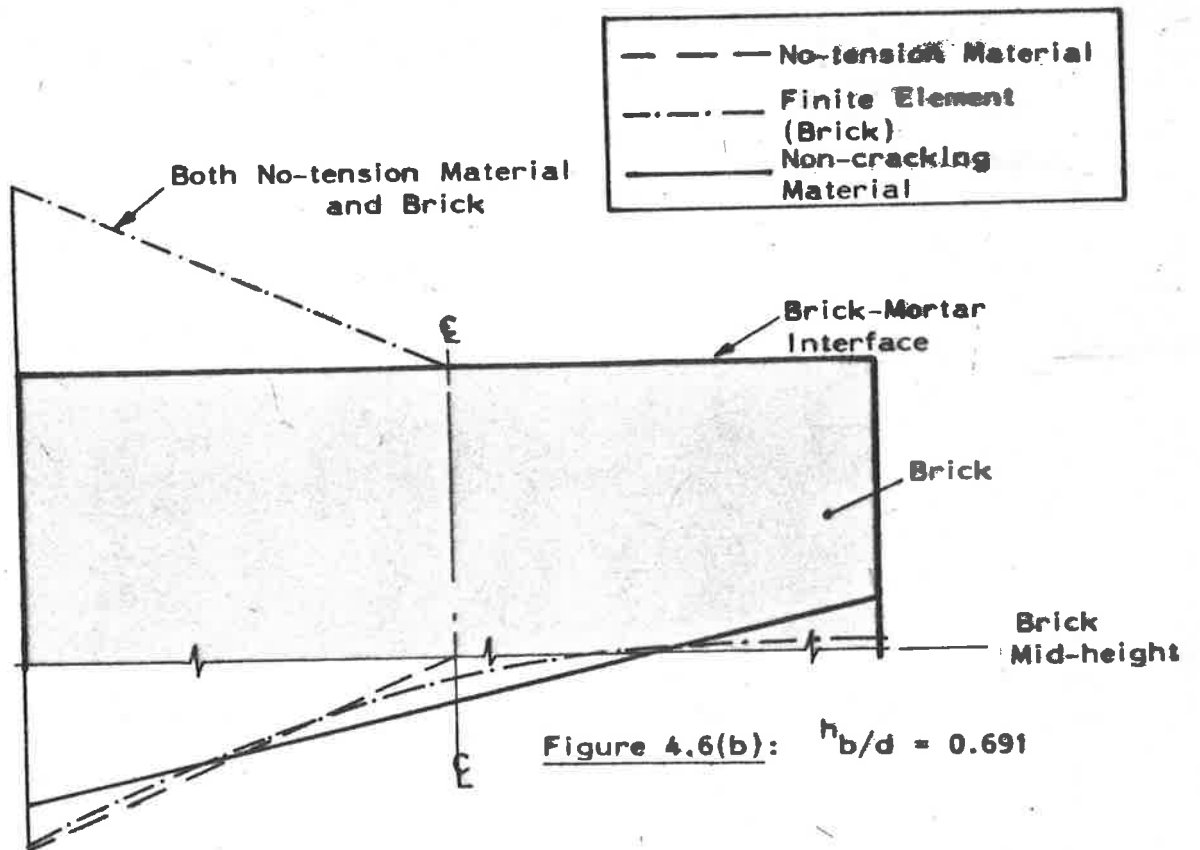


Figure 4.6(b):  $h_b/d = 0.691$

Figure 4.6: Stress Distribution for Load Eccentricity  $d/3$

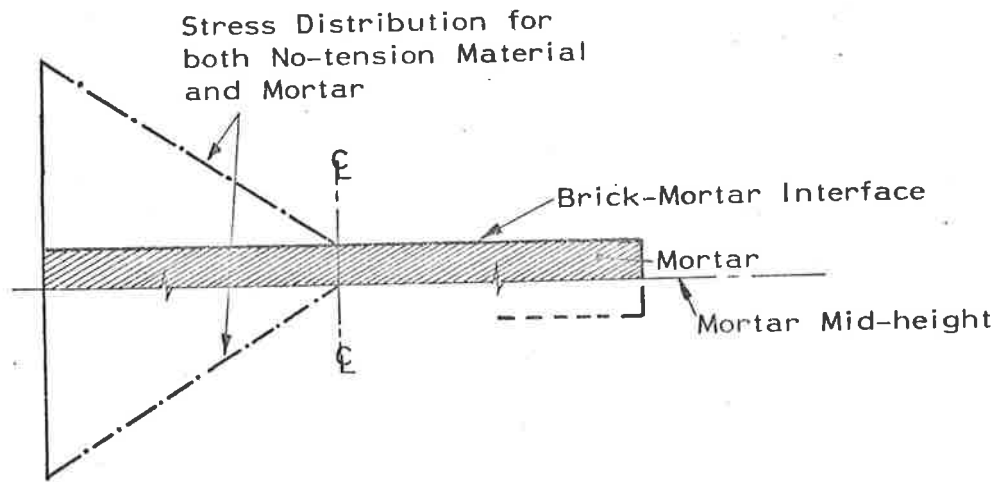


Figure 4.7: Mortar Stress Distributions for Load Eccentricity  $d/3$

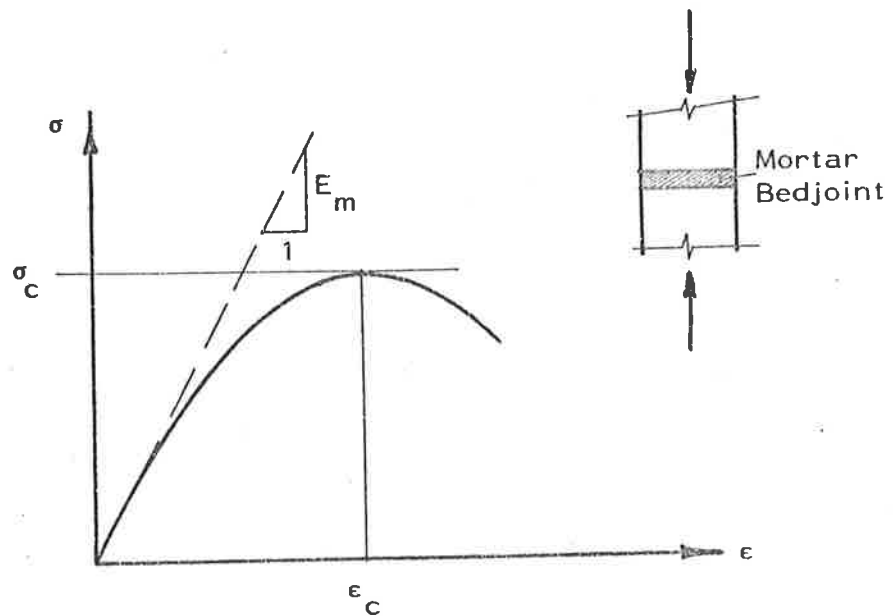


Figure 4.8: Stress-strain Relationship for an Axially-loaded Mortar Bedjoint



Equation (B.1) is shown in figure 4.8. The maximum normal stress,  $\sigma_c$ , attained by the mortar in a state of triaxial compression occurs at a strain  $\epsilon_c$ . The initial tangent elastic modulus is  $E_m$ . Moment-curvature relationships for such a non-linear mortar can be compared with the relationships for a linear mortar as follows.

Consider the case in which the brickwork is partially cracked through the bedjoint at the brick-mortar interface and for which the maximum strain at the compression face is  $\epsilon_1$  and the corresponding stress is  $\sigma_1$  (figure 4.9).

It is shown in Appendix B that, provided the load resultant is outside the kern of the full section, the ratio,  $\rho$ , of the curvature of a bedjoint with a non-linear mortar to that of a bedjoint having a linear mortar, subjected to similar load conditions, is given by—

$$\rho = \frac{9}{2} \cdot \frac{\epsilon_1}{d_c} \cdot \frac{d_p^2}{P} \cdot E_m \quad (\text{B.21})$$

in which  $\epsilon_1$  is the maximum compression strain in the non-linear mortar in the cracked bedjoint

$d_c$  is the depth of the uncracked part of the non-linear mortar bedjoint

$d_p$  is the distance from the compression face to the load resultant

$P$  is the load per unit length

$E_m$  is the initial tangent modulus of the non-linear mortar and is equal to the elastic modulus of the linear mortar.

It is also shown in Appendix B that for a non-linear mortar described by equation (B.1), cracking can occur at a brick-mortar interface in cases in which the load resultant acts within the kern as determined for a linear elastic material. For this condition, the

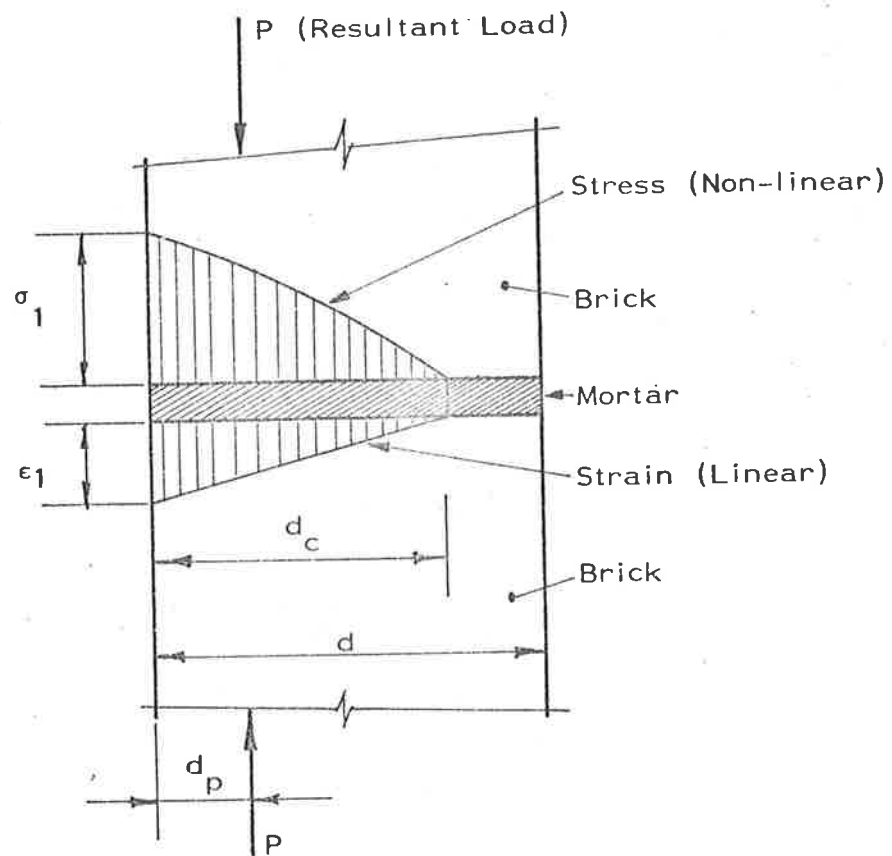


Figure 4.9: Stress and Strain Distributions for Cracked Non-linear Mortar

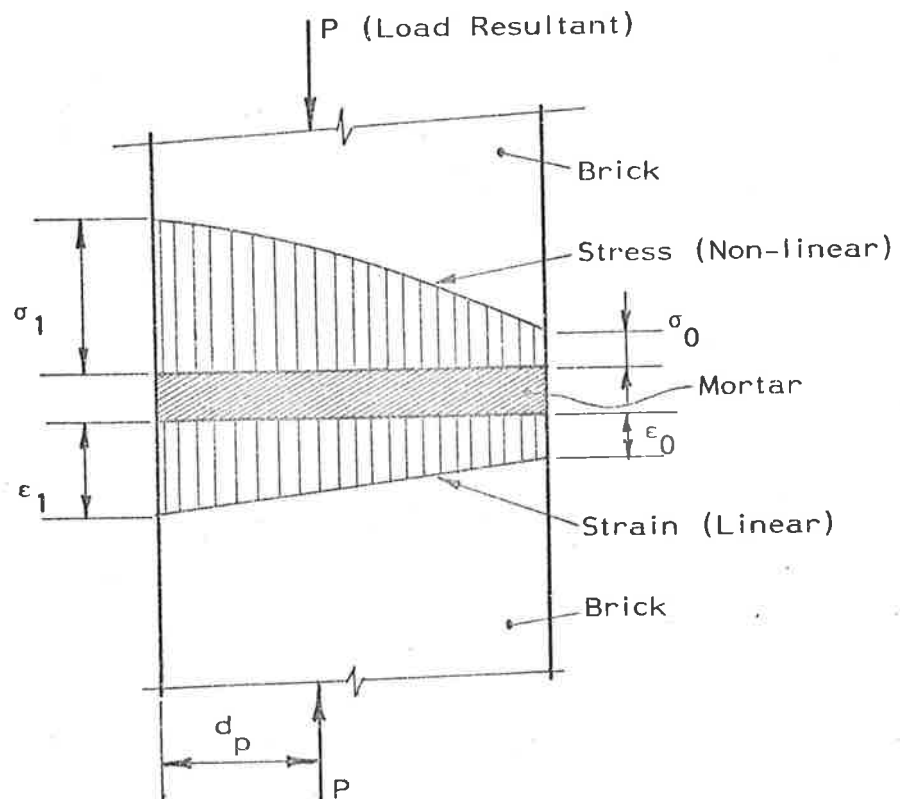


Figure 4.10: Stress and Strain Distribution for Uncracked Non-linear Mortar

ratio  $\rho$ , is -

$$\rho = \frac{\epsilon_1}{d_c} \cdot \frac{d^3}{12P} \cdot \left(\frac{d}{2} - d_p\right)^{-1} \cdot E_m \quad (\text{B.24})$$

A third condition for the brickwork is that in which the mortar bedjoint is uncracked. The maximum compression strain in the mortar,  $\epsilon_1$ , and the minimum mortar compression strain,  $\epsilon_0$ , occur simultaneously with stresses  $\sigma_1$  and  $\sigma_0$  respectively (figure 4.10).

It is shown in Appendix B that the curvature ratio,  $\rho$ , is -

$$\rho = \frac{d^2}{12P} \cdot (\epsilon_1 - \epsilon_0) \cdot \left(\frac{d}{2} - d_p\right)^{-1} \cdot E_m \quad (\text{B.33})$$

The strain,  $\epsilon_1$ , and the uncracked depth of the mortar,  $d_c$ , in equations (B.21) and (B.24) must be calculated by an iteration procedure described in Appendix B.  $\epsilon_1$  and  $\epsilon_0$  in equation (B.33) must also be found by using a similar iteration technique.

#### 4.2.4 Brickwork Subjected to Eccentric Compression Load

The results presented in Sections 4.2.2 and 4.2.3 may be used to calculate the flexural stiffness of brickwork subjected to eccentric compression load. The assumptions made in Sections 4.2.2 (figure 4.1(b)) and 4.2.3 are reiterated below as an introduction to this section.

- (i) By symmetry, plane sections AA and CC remain plane after bending.
- (ii) Planes DD and EE at the brick-mortar interfaces remain plane in the compressed part of the bedjoint after bending.
- (iii) The brick elastic modulus,  $E_b$ , is constant.
- (iv) The mortar elastic modulus is  $E_m$  for a linear mortar and for a non-linear mortar  $E_m$  is the initial tangent modulus. For

a non-linear mortar, the stress-strain relationship is assumed to be

$$\sigma = E_m (\epsilon - K\epsilon^n) \quad (B.1)$$

Assumption (ii), as mentioned in Section 4.2.1, simplifies the calculation of the effective brickwork flexural stiffness; the method of calculation is as follows.

It is assumed that the radius of curvature of each half-brick, calculated from the relative relations of planes AA and DD (CC and EE), is  $R_b$ . Assume also that the radius of curvature of the mortar joint, calculated from the relative rotations of planes DD and EE, is  $R_m$ . The geometry of the unit AACC may be represented by figure 4.11(a) if  $R_b > R_m$  and by figure 4.11(b) if  $R_b < R_m$ . The case for which  $R_b = R_m$  is trivial.

Let the average radius of curvature for the whole brick-mortar unit AACC be denoted by  $R_{av}$ . The equivalent uniform curvature for the unit AACC, shown by the dashed circular curve in each of figures 4.11(a) and 4.11(b), differs from the true displaced shape, but provided that  $R_b$ ,  $R_m$  and  $R_{av}$  are all much greater than  $h_b/2$  and  $h_m$ , the difference is small. The end slopes corresponding to the equivalent curvature unit are identical to those for the actual unit AACC. The average radius of curvature,  $R_{av}$ , is related to the radii of curvature of the brick and mortar,  $R_b$  and  $R_m$  respectively, as follows -

$$R_{av} = (h_b + h_m) \cdot \left( \frac{R_b R_m}{R_b h_m + R_m h_b} \right) \quad (4.4)$$

provided that

$$\begin{aligned} R_b &\gg (h_b + h_m) \\ R_m &\gg (h_b + h_m) \\ R_{av} &\gg (h_b + h_m) \end{aligned}$$

Figure 4.11(a):

$$R_b > R_m$$

$$R_b = MD = NE$$

$$R_m = RE = RD$$

$$R_{av} = AQ = QC$$

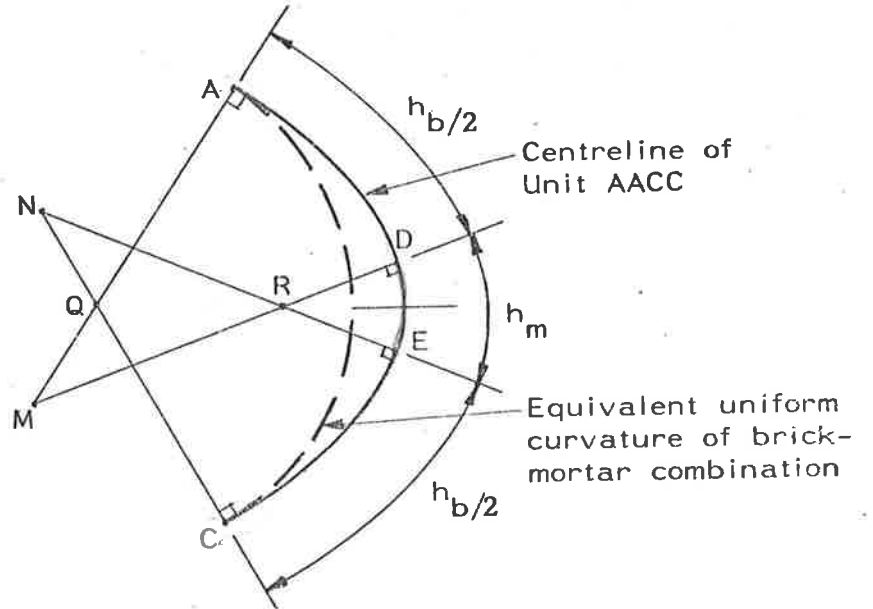


Figure 4.11(b):

$$R_b < R_m$$

$$R_b = MD = NE$$

$$R_m = RD = RE$$

$$R_{av} = AQ = QC$$

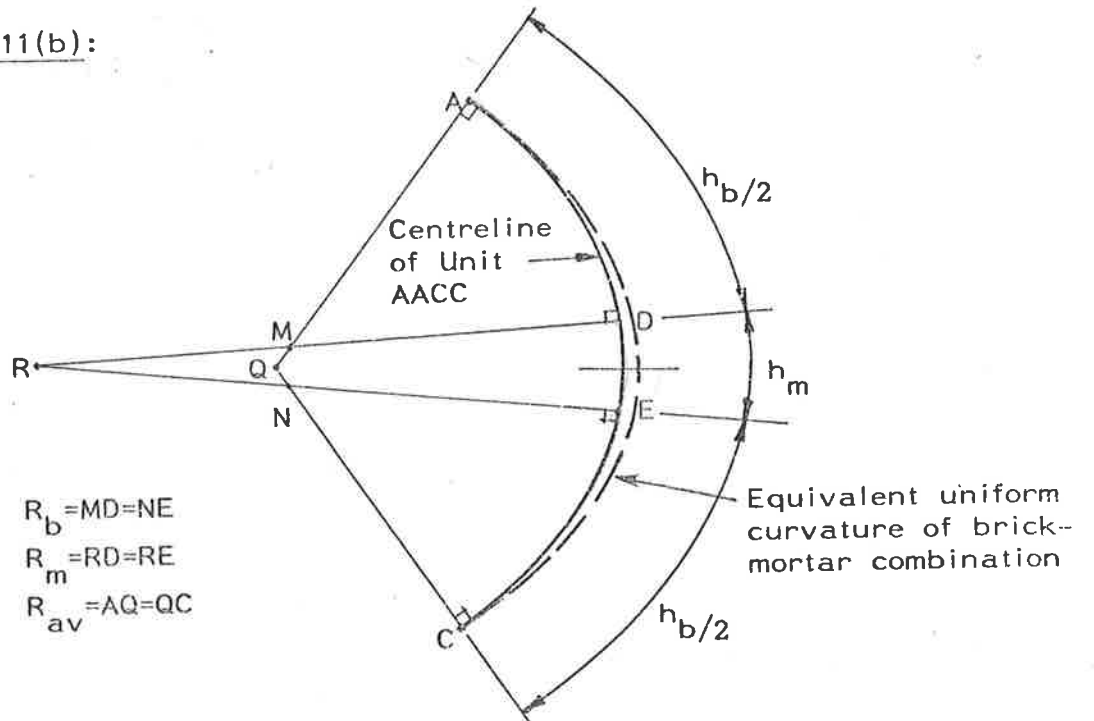


Figure 4.11: Brickwork Curvatures

In order to simplify calculations, the behaviour of a brickwork wall may be related to the behaviour of a homogeneous no-tension material column. Therefore, by using the relationship between the radius of curvature of a brick and a no-tension material with same material properties (equation (4.1)) and the curvature ratio factor for mortars,  $\rho$  (Appendix B), equation (4.4) may be written as –

$$\left(\frac{1}{R}\right)_{av} = \frac{\frac{1}{\alpha} \cdot \left(\frac{1}{R}\right)_{nt} \cdot h_b + \rho \left(\frac{1}{R}\right)_m \cdot h_m}{(h_b + h_m)} \quad (4.5)$$

in which  $\left(\frac{1}{R}\right)_{nt}$  is the curvature of a no-tension material with identical elastic properties to the brick

$\left(\frac{1}{R}\right)_m$  is the curvature of a linear mortar

$\alpha$  is a curvature ratio factor for the brick defined in Section 4.2.2.2

$\rho$  is a curvature ratio factor for the mortar defined in Section 4.2.3; for the linear mortar,  $\rho = 1.0$  (Appendix B)

$h_b$  is the brick height

$h_m$  is the mortar bedjoint thickness.

#### 4.2.5 Summary

This section has presented relationships between the curvature of brickwork subjected to eccentric compression and the curvatures of the brick and mortar components, both for linear and non-linear mortars. The results of a finite element analysis of the brick and mortar components show that the stress distributions in bricks and mortar (both with linear stress-strain characteristics) depend upon the height-to-thickness aspect ratio. A curvature relationship for

brickwork (equation 4.5)) has been presented which relates the curvature of brickwork to the curvature of a column of no-tension materials. Equation (4.5) has been derived from geometry and the results of finite element calculations (factor  $\alpha$ ).

#### 4.3 LOAD-DEFLECTION RELATIONSHIPS AND EQUATIONS OF EQUILIBRIUM

In the following sections, relationships are examined between the moments and associated curvatures in a no-tension material column. By using the resulting equations, further relationships are established between moments and associated curvatures for actual brickwork in which discrete cracking may occur on the bedjoints.

The equations of equilibrium for walls are investigated and a finite difference method of solution is described which takes into account initial imperfections and various end support conditions.

##### 4.3.1 Load-Deflection Relationships for a Linear No-Tension Material Column

Initially, it is assumed that a no-tension material column is subjected to eccentric compression and that the lateral deformations of the column are negligible. The no-tension material is taken to have a linear stress-strain relationship and plane sections are assumed to remain plane during loading. The effective depth of section of such a column depends upon the eccentricity of the resultant load per unit length,  $P$  (figures 4.12(a), 4.12(b)). The column section depth is  $d$  if the load resultant acts within the kern (figure 4.12(a)) and if the load resultant acts outside the kern the section depth is —

$$d_c = 3d_p \quad (4.6)$$

in which  $d_p$  is defined in figure 4.12(b).

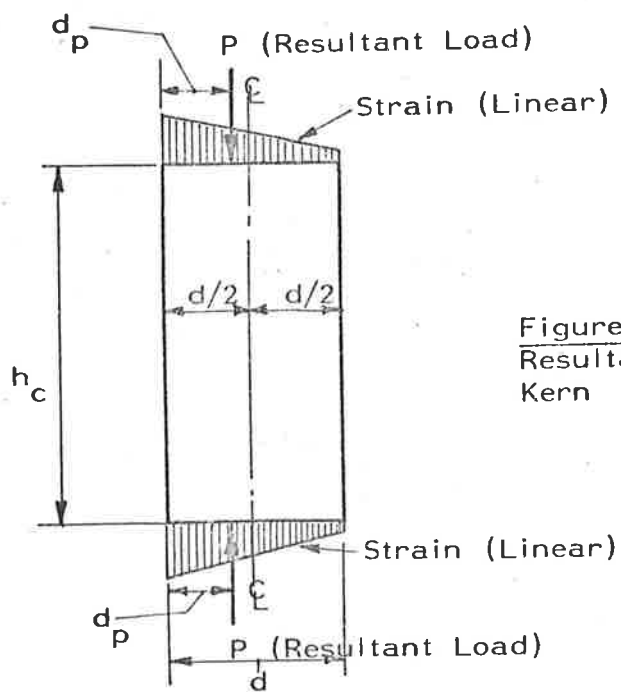


Figure 4.12(a):  
Resultant Load Within Kern

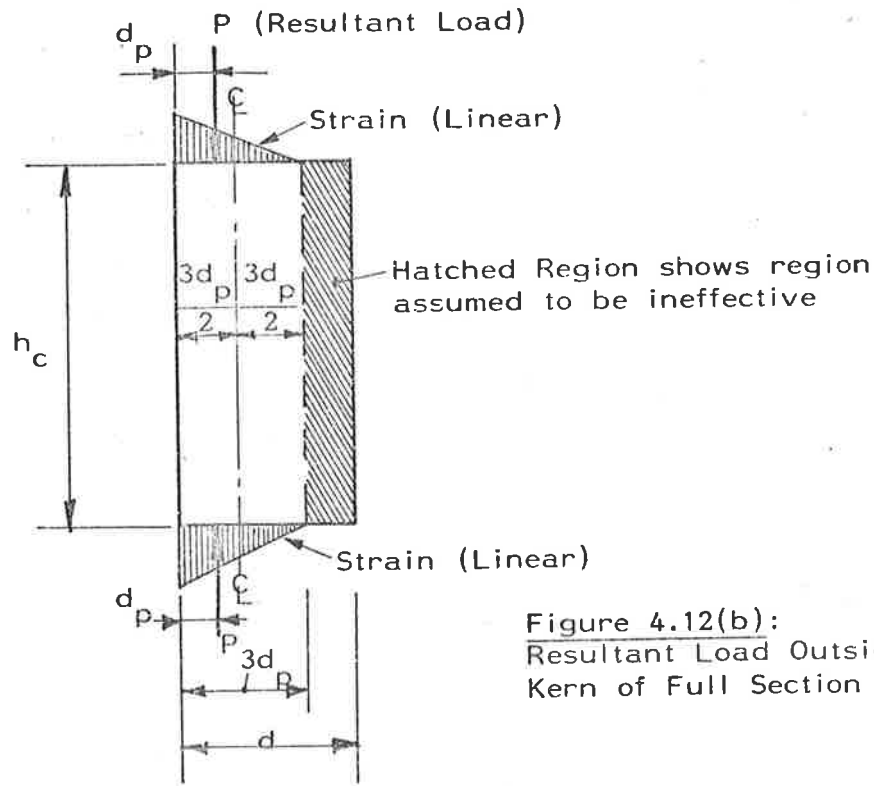


Figure 4.12(b):  
Resultant Load Outside Kern of Full Section

Figure 4.12: Effective Section Depth for No-tension Material Column



The effective moment,  $M_{eu}$ , of the resultant load about the column centreline of the uncracked section (figure 4.12(a)) is –

$$M_{eu} = P(d/2 - d_p) \quad (4.7)$$

By geometry, for small lateral deformations, the curvature of the no-tension material column is –

$$\left(\frac{1}{R}\right)_u = \frac{M_{eu}}{(EI)_u} \quad (4.8)$$

in which  $(EI)_u$  is the flexural stiffness per unit length of the column calculated as follows –

$$(EI)_u = \frac{Ed^3}{12} \quad (4.9)$$

where  $E$  is the elastic modulus of the no-tension material.

Equation (4.5), written for uncracked brickwork in which  $\alpha$  is unity (Section 4.2.2.2), is –

$$\left(\frac{1}{R}\right)_{av} = \frac{\left(\frac{1}{R}\right)_{nt} \cdot h_b + \rho \left(\frac{1}{R}\right)_m \cdot h_m}{(h_b + h_m)} \quad (4.5(a))$$

From equations (4.8) and (4.9), the curvature of a no-tension material column with the elastic properties of a brick is –

$$\left(\frac{1}{R}\right)_{nt} = \frac{M_{eu}}{(E_b \cdot \frac{d^3}{12})} \quad (4.10)$$

and the curvature of a no-tension material column with the elastic properties of a linear mortar is –

$$\left(\frac{1}{R}\right)_m = \frac{M_{eu}}{(E_m \cdot \frac{d^3}{12})} \quad (4.11)$$

By using equations (4.10) and (4.11), equation (4.5(a)) may be written as –

$$\left(\frac{1}{R}\right)_{av} = \frac{M_{eu}}{(EI)_{eq,u}} \quad (4.12)$$

in which  $(EI)_{eq,u}$  is the equivalent flexural stiffness of uncracked brickwork and may be calculated as follows —

$$(EI)_{eq,u} = E_b \left[ \frac{h_b + h_m}{h_b + \rho h_m \cdot \left(\frac{E_b}{E_m}\right)} \right] \cdot \frac{d^3}{12} \quad (4.13)$$

The effective moment,  $M_{ec}$ , of the resultant load,  $P$ , about the centreline of the uncracked part of a no-tension material column in which the load acts outside the kern is —

$$M_{ec} = \frac{Pd_p}{2} \quad (4.14)$$

By geometry, for small lateral deformations, the curvature of this no-tension material column is —

$$\left(\frac{1}{R}\right)_c = \frac{M_{ec}}{(EI)_c} \quad (4.15)$$

in which  $(EI)_c$  is the flexural stiffness per unit length of the column calculated as follows —

$$(EI)_c = \frac{(3d_p)^3}{12} = \frac{9}{4} \cdot d_p^3 \quad (4.16)$$

From equations (4.15) and (4.16), the curvature of a no-tension material column with the elastic properties of a brick is —

$$\left(\frac{1}{R}\right)_{nt} = \frac{M_{ec}}{\left(\frac{9}{4} \cdot E_b \cdot d_p^3\right)} \quad (4.17)$$

and the curvature of a no-tension material with the elastic properties of a linear mortar is —

$$\left(\frac{1}{R}\right)_m = \frac{M_{ec}}{\left(\frac{9}{4} \cdot E_m \cdot d_p^3\right)} \quad (4.18)$$

By using equations (4.17) and (4.18), equation (4.5) may be written as -

$$\left(\frac{1}{R}\right)_{av} = \frac{M_{ec}}{(EI)_{eq,c}} \quad (4.19)$$

in which  $(EI)_{eq,c}$  is the equivalent flexural stiffness of cracked brickwork and may be calculated as follows -

$$(EI)_{eq,c} = E_b \cdot \left[ \frac{h_b + h_m}{\frac{h_b}{\alpha} + \rho h_m \cdot \left(\frac{E_b}{E_m}\right)} \right] \cdot \frac{9}{4} \cdot d_p^3 \quad (4.20)$$

Equations (4.12) and (4.19) may be written generally as -

$$\left(\frac{1}{R}\right)_{av} = \frac{M_e}{(EI)_{eq}} \quad (4.21)$$

in which  $\left(\frac{1}{R}\right)_{av}$  is an average curvature for brickwork over a height of two half-bricks and one mortar joint

$M_e$  is the effective moment of the load resultant about the centreline of the uncracked part of a bed-joint of linear mortar

$(EI)_{eq}$  is the equivalent flexural stiffness of brickwork and may be calculated as follows -

$$(EI)_{eq} = E_b \cdot \left[ \frac{h_b + h_m}{\left(\frac{h_b}{\alpha}\right) + \rho h_m \cdot \left(\frac{E_b}{E_m}\right)} \right] \cdot l_{eq} \quad (4.22)$$

$$\text{in which } l_{eq} = \begin{cases} \frac{9}{4} \cdot d_p^3 & \text{for } 3d_p < d \\ \frac{d^3}{12} & \text{for } 3d_p \geq d \end{cases} \quad (4.23(a))$$

$$(4.23(b))$$

### 4.3.2 Equations of Equilibrium

Figure 4.13 shows the initial and deflected shapes of the centre-line of the full-depth column, together with coordinate axes used in the subsequent analysis. At the mid-height of a mortar bedjoint, at section N-N, say, assume that the initial deviation from the X-coordinate axis is  $\delta_n$  and that the subsequent lateral deflection due to load P per unit length, is  $y_n$ . The "effective eccentricity" of the load at the section N-N with respect to the centreline of the full section column is -

$$e_n = \frac{M_n}{P} = \frac{P(e_1 + \delta_n + y_n) - HX_n}{P} \quad (4.24)$$

in which  $M_n$  is the bending moment at section N-N also taken about the centreline of the full-section column.

The horizontal end reactions, H per unit length of column (figure 4.13), are zero if the applied load eccentricities at both ends are equal.

If the vertical load acts within the kern at section N-N, then

$$|e_n| \leq d/6 \quad (4.25(a))$$

$$\text{and } 3d_p \geq d \quad (4.25(b))$$

The expression  $|e_n|$  is taken to be the absolute value of the effective eccentricity,  $e_n$ , calculated by using equation (4.24). For this case, the effective moment,  $M_e$ , defined in the previous section, is

$$M_e = P \cdot e_n \quad (4.26)$$

However, if the load acts outside the kern at section N-N (figure 4.13) then -

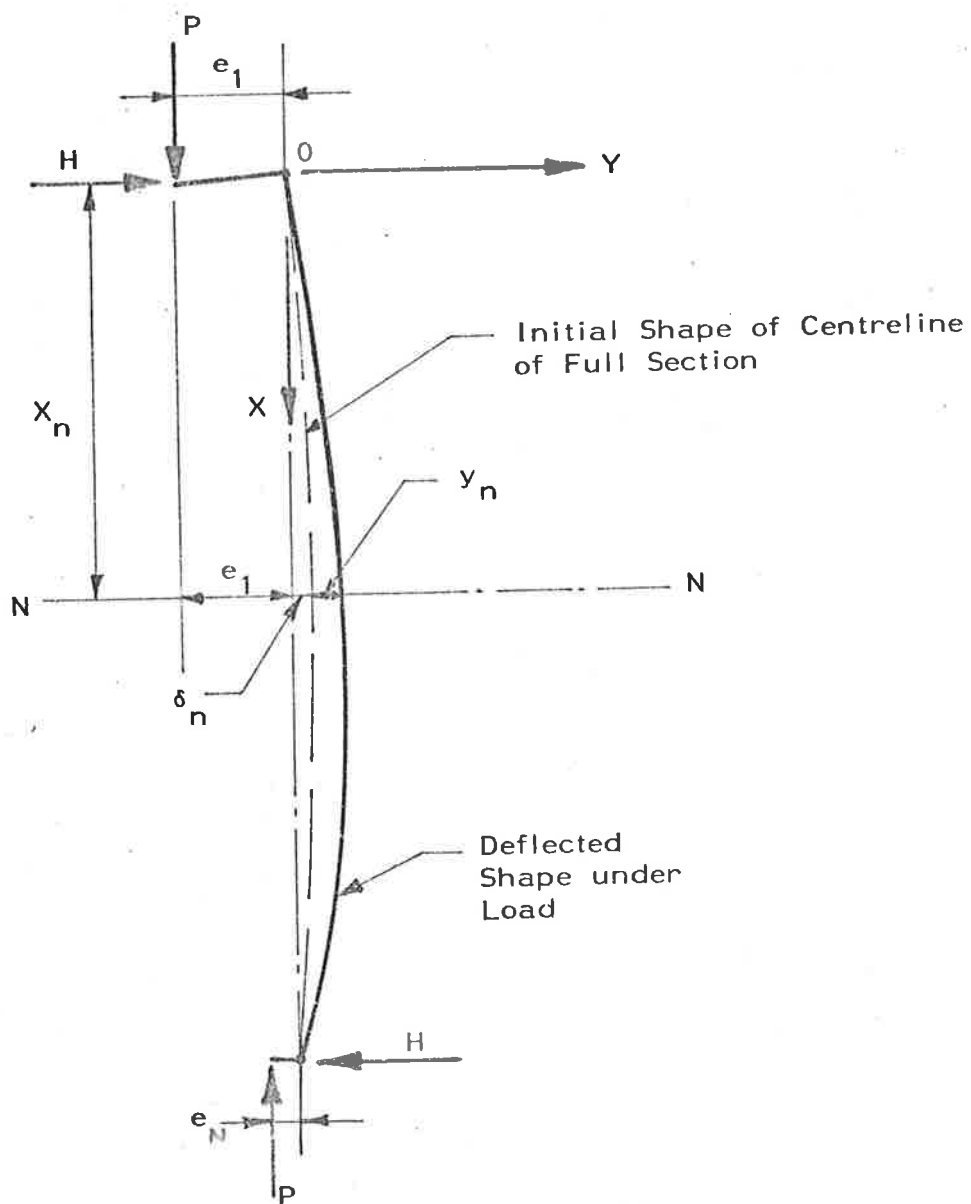


Figure 4.13: Column Loads, Reactions and Displacements

$$|e_n| > d/6 \quad (4.27(a))$$

$$\text{and } 3d_p < d \quad (4.27(b))$$

For this case, the column section N-N, at a mortar joint, is cracked and the effective moment,  $M_e$ , is (Section 4.3.1) -

$$M_e = (\text{sgn } e_n) \cdot \frac{P}{2} \cdot \left(\frac{d}{2} - |e_n|\right) \quad (4.28)$$

$$\text{in which } (\text{sgn } e_n) = \begin{cases} +1 & \text{if } e_n \text{ is positive} \\ -1 & \text{if } e_n \text{ is negative} \end{cases}$$

#### 4.3.3 Finite Difference Formulation

For small deflections, the average curvature of brickwork may be expressed as -

$$\left(\frac{1}{R}\right)_{av} = -\frac{d^2y}{dx^2} \quad (4.29)$$

Equations (4.21) and (4.29) together give the displacements of the column in finite difference form as -

$$\frac{d^2y}{dx^2} = \left[ \frac{y_{n+1} - 2y_n + y_{n-1}}{(\Delta x)^2} \right] = -\frac{M_e}{(EI)_{eq}} \quad (4.30)$$

in which  $y_{n+1}$ ,  $y_n$ ,  $y_{n-1}$  are the deflections at the (n+1)th, nth and (n-1)th joints respectively and  $\Delta x = (h_b + h_m)$  is the axial distance between neighbouring bedjoints.

From equations (4.24) and (4.30) it follows that if  $e_n > d/6$ ,

$$y_{n+1} - 2y_n + y_{n-1} = -\frac{(\Delta x)^2}{2(EI)_{eq}} \cdot [P(d/2 - e_1 - \delta_n - y_n) + HX_n] \quad (4.31)$$

and if  $e_n < -d/6$ ,

$$y_{n+1} - 2y_n + y_{n-1} = - \frac{(\Delta x)^2}{2(EI)_{eq}} \cdot [-P(d/2 + e_1 + \delta_n + y_n) + HX_n] \quad (4.32)$$

For  $|e_n| \leq d/6$ ,

$$y_{n+1} - 2y_n + y_{n-1} = - \frac{(\Delta x)^2}{(EI)_{eq}} \cdot [P(e_1 + \sigma_n + y_n) - HX_n] \quad (4.33)$$

#### 4.3.4 Boundary Conditions

As examples, consideration is given to two types of boundary conditions which correspond to a pinned base and a perfectly fixed base respectively (figures 4.14(a) and 4.14(b)). The top support is a "pin-and-roller" for both examples.

(a) for a wall with pinned supports top and bottom (figure 4.14(a))

$$(1) \ y_1 = 0 \quad (2) \ y_N = 0 \quad (3) \ H = \frac{P}{h} (e_1 - e_N) \quad (4.34)$$

(b) for a wall pinned at the top and fixed at the base (figure 4.14(b))

$$(1) \ y_1 = 0 \quad (2) \ y_N = 0 \quad (3) \ \left(\frac{dy}{dx}\right)_N = 0 \quad (4.35)$$

The end slope condition (3) may be simulated by introducing a fictitious node (N+1) at a distance  $(\Delta x)$  below the base such that  $y_{N+1} = y_{N-1}$ .

#### 4.4 SOLUTION PROCEDURE

Figure 4.15 shows a brick wall as it is represented for the finite difference equations (4.31), (4.32) or (4.33) with the governing equation at each node,  $n$ , depending on the equilibrium conditions (Section 4.3). Once the column starts to crack at a mortar joint (node

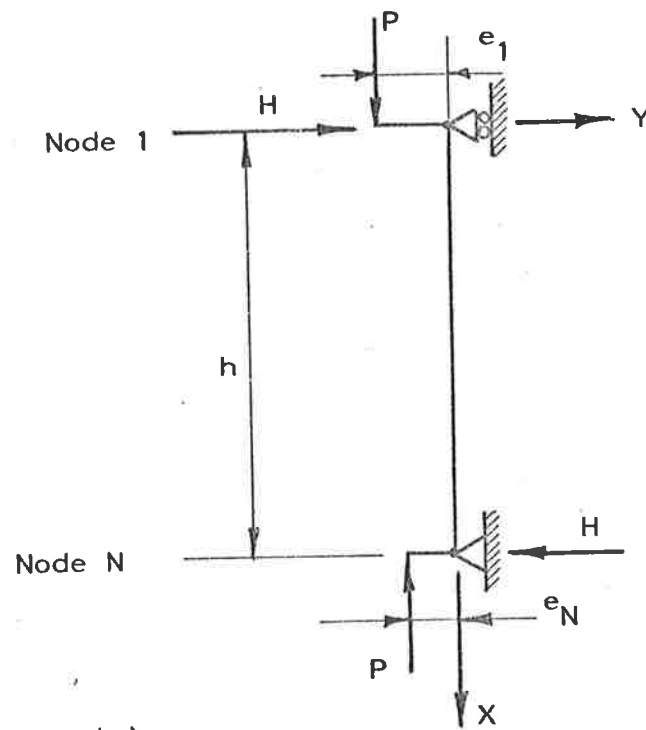


Figure 4.14(a):  
Pin-ended Wall

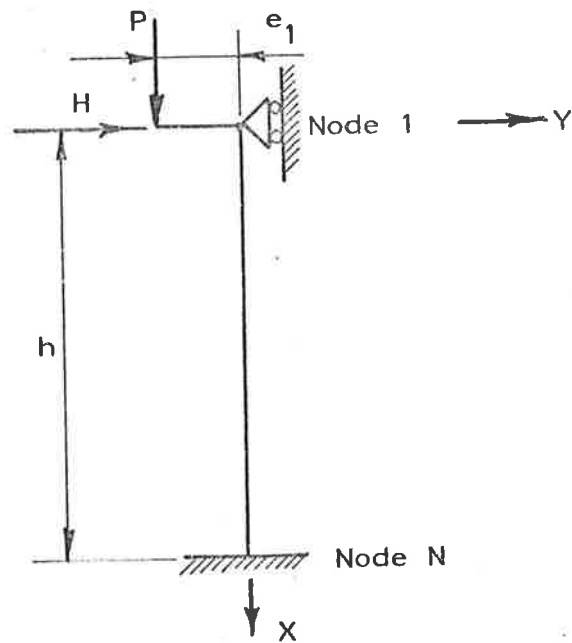


Figure 4.14(b):  
Fixed Base Wall

Figure 4.14: Wall Load and Support Conditions



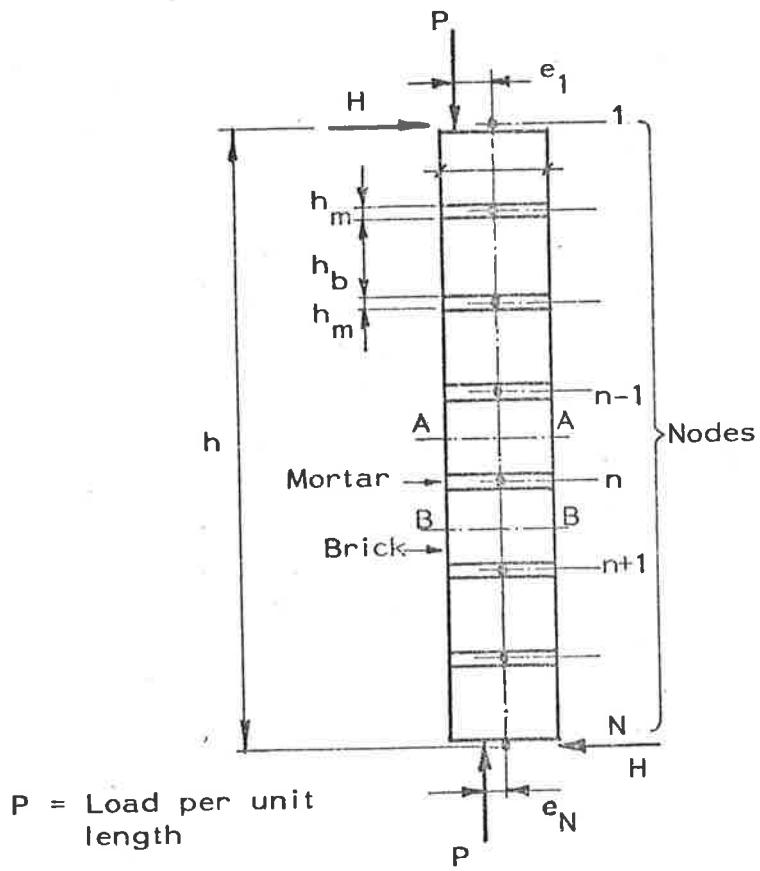


Figure 4.15: Finite Difference Subdivision

n),  $(EI)_{eq,n}$  changes with the depth of the cracked section and for a fixed-base wall the ratio  $H/P$  also changes. The set of simultaneous equations generated for the  $(N-2)$  nodes away from the ends, plus the three boundary equations (Section 4.3.4) are therefore non-linear and direct solutions cannot be obtained. In the solution method proposed, the load,  $P$ , is applied incrementally and at each load increment, a Newton-Raphson technique is used to find a consistent set of values for the deflections ( $y$ ), the stiffnesses  $((EI)_{eq})$ , and for a fixed-base wall the horizontal reaction,  $H$ , such that the equations are satisfied to within a prescribed error limit. Load-displacement graphs can be plotted for various brick and mortar combinations, for both linear and non-linear mortars, allowing for initial imperfections, support conditions and load eccentricity. As the ratio of displacement increment to load increment increases, the magnitude of the load increment can be decreased. Column buckling is deemed to have occurred if no displacement configuration can be found for the incremental load.

#### 4.4.1 Matrix Formulation

If the wall is divided into  $N-1$  elements and has  $N$  nodes, as shown in figure 4.15, equations (4.31), (4.32), (4.33), applied at each node, together with the boundary conditions, may be written as the equation system —

$$[A] \left\{ \frac{y}{H} \right\} = \{B\} \quad (4.36)$$

in which —



$$\{B\} = \begin{Bmatrix} B_2 \\ \cdot \\ \cdot \\ \cdot \\ \cdot \\ B_{N-1} \\ B_N \end{Bmatrix} \quad \text{with } B_j = \begin{cases} -\frac{P(\Delta x)^2}{2(EI)_{eq,j}} \cdot (d/2 - e_1 - \delta_j - y_j) & \text{if } e_j > d/6 \\ -\frac{P(\Delta x)^2}{(EI)_{eq,j}} \cdot (e_1 + \delta_j + y_j) & \text{if } |e_j| \leq d/6 \\ +\frac{P(\Delta x)^2}{2(EI)_{eq,j}} \cdot (d/2 + e_1 + \delta_j + y_j) & \text{if } e_j < -d/6 \end{cases}$$

$$\text{and } B_N \begin{cases} \text{as } B_j, j = N, \text{ for fixed base.} \\ \text{absent for pinned base.} \end{cases}$$

The dependent variables are  $y_2$  to  $y_{N-1}$  for a pinned base wall and, additionally,  $H$  for a fixed base wall; correspondingly there are  $N-2$  and  $N-1$  equations respectively.

#### 4.4.2 Solution of Equations

Calculations may be started with a small value of  $P$  so that by setting  $y_j = 0$  wherever it appears in  $B_j$  (on the right hand side of equation (4.36)), stiffnesses  $(EI)_{eq,j}$  may be calculated using equation (4.22). Equation (4.36) is then solved. From the resulting values of  $y$  and  $H$ , new values of  $(EI)_{eq,j}$  may be calculated at all nodes,  $j$  (equation (4.22)) and after substitution of the current values of  $y_j$ ,  $H$  and  $(EI)_{eq,j}$  in all relevant places, an "error vector" may be calculated as follows:

$$\{\eta\} = \{B\} - [A] \left\{ \frac{y}{H} \right\} \quad (4.37)$$

A simple geometrical interpretation can be attributed to this error vector. Each term is proportional to the difference between two curvatures: the first is calculated from the loads, the current deflections and the consistent stiffness values; the other curvature is calculated geometrically from the current deflection values by finite differences. The components of the error vector are -

$$\eta_j = \left[ \frac{M_e}{(EI)_{eq,j}} - \frac{y_{j+1} - 2y_j + y_{j-1}}{(\Delta x)^2} \right] \cdot (\Delta x)^2 \quad (4.38)$$

It has been found by trial that if no component of  $\{\eta\}$  exceeds in absolute value a limit selected to be  $1.0 \times 10^{-6}$ , the calculated values of  $y$  and  $H$  may be accepted.

#### 4.4.3 Newton-Raphson Correction

If any component of  $\{\eta\}$  exceeds the prescribed limit Newton-Raphson corrections are applied until the desired accuracy is reached.

For a function of a single variable  $y = f(x)$ , it is well known that an approximate solution  $(x_1)$  of equation  $f(x) = 0$ , giving  $y_1 - f(x_1) = \Delta y_1$ , is generally improved by calculating—

$$x_2 = x_1 - \Delta x_1 = x_1 - \frac{\Delta y_1}{f'(x_1)} \quad (4.39)$$

and evaluating  $y_2 = f(x_2)$ .

The corresponding Newton-Raphson correction for the simultaneous equations (4.36) for the  $i^{\text{th}}$  iteration can be calculated from—

$$[J]_i \cdot \left\{ \frac{\Delta y}{\Delta H} \right\}_i = - \{ \eta \}_i \quad (4.40)$$

$$\text{and setting } \left\{ \frac{\Delta y}{\Delta H} \right\}_{i+1} = \left\{ \frac{y}{H} \right\}_i + \left\{ \frac{\Delta y}{\Delta H} \right\}_i \quad (4.41)$$

In equation (4.40),  $[J]$  is the "Jacobian" of  $\{ \eta \}$ , that is, a square matrix formed from the partial derivatives of the components of  $\{ \eta \}$ , with respect to the components of the solution vector,  $\left\{ \frac{y}{H} \right\}$ . If  $\eta_j$  denotes the  $j^{\text{th}}$  component of the error vector and  $a_k$  denotes the  $k^{\text{th}}$  component of the solution vector,  $\left\{ \frac{y}{H} \right\}$ , then the components of the "Jacobian" matrix are given by—

$$J_{jk} = \frac{\partial \eta_j}{\partial a_k} \quad (4.42)$$

Elements of the "Jacobian" matrix can be evaluated numerically by incrementing successively the components of the solution vector by approximately 0.01 percent and calculating the increments of the error vector, giving—

$$J_{jk} \approx \frac{\Delta \eta_j}{\Delta a_k} \quad (4.43)$$

One complication encountered was an oscillatory behaviour, well known in the one-dimensional problem and associated with an inflection point (or slope-discontinuity) at or near the solution point. Such a

slope-discontinuity is encountered in the present problem whenever cracking starts. In such cases the load-increment was altered, but generally closure was obtained in less than ten cycles.

An alternative approach is to use "regula falsi" in such cases, using the arithmetic or a weighted mean of successive oscillatory solutions.

#### 4.5 RESULTS OF THE NUMERICAL METHOD

##### 4.5.1 Results from PROGRAM PIER1

PROGRAM PIER1, documented in Appendix C, has been used to investigate several problems, summarized in Table 4.3, which illustrate the type of results which may be obtained using the numerical method. A more detailed set of results in the form of a parametric study is given in Chapter 8.

The brick Young's modulus is  $16 \times 10^3$  MPa in all cases and the mortar initial tangent modulus is  $8 \times 10^3$  MPa. Each of the eight walls is analysed for three cases:

- (i) linear bricks and mortar, both of no-tension material.
- (ii) linear bricks and mortar, with the brick unit capable of sustaining tension stresses.
- (iii) linear bricks and non-linear mortar, with the brick unit able to sustain tension stresses. The crushing strength of the mortar,  $\sigma_c$ , is assumed to be 30MPa and  $n$  is assumed to be 3 so that  $\epsilon_c = 5.625 \times 10^{-3}$  and  $K = 10535$  (Appendix B, equations (B.2) and (B.3)).

The results of all the computed load-deflection characteristics for points on the respective columns which sustain maximum deflection

Wall No.	A	B	C	D	E	F	G	H
Wall height, h	2400	2400	2408	2408	2400	2400	2408	2408
Thickness, d	76	76	110	110	76	76	110	110
Slenderness Ratio, h/d	32	32	22	22	32	32	22	22
Brick height, $h_b$	110	110	76	76	110	110	76	76
Mortar thickness, $h_m$	10	10	10	10	10	10	10	10
No. of courses	20	20	28	28	20	20	28	28
Base support	F	F	F	F	P	P	P	P
Top support	PR	PR	PR	PR	PR	PR	PR	PR
Eccentricity, (e/d)	0.250	0.0833	0.250	0.0833	0.250	0.0833	0.250	0.0833

- (i) All length dimensions are mm
- (ii) F denotes perfectly-fixed support
- (iii) P denotes pinned support (figure 4.14)
- (iv) PR denotes pin-roller support (figure 4.14)

Table 4.3: Wall Properties for PROGRAM PIER1

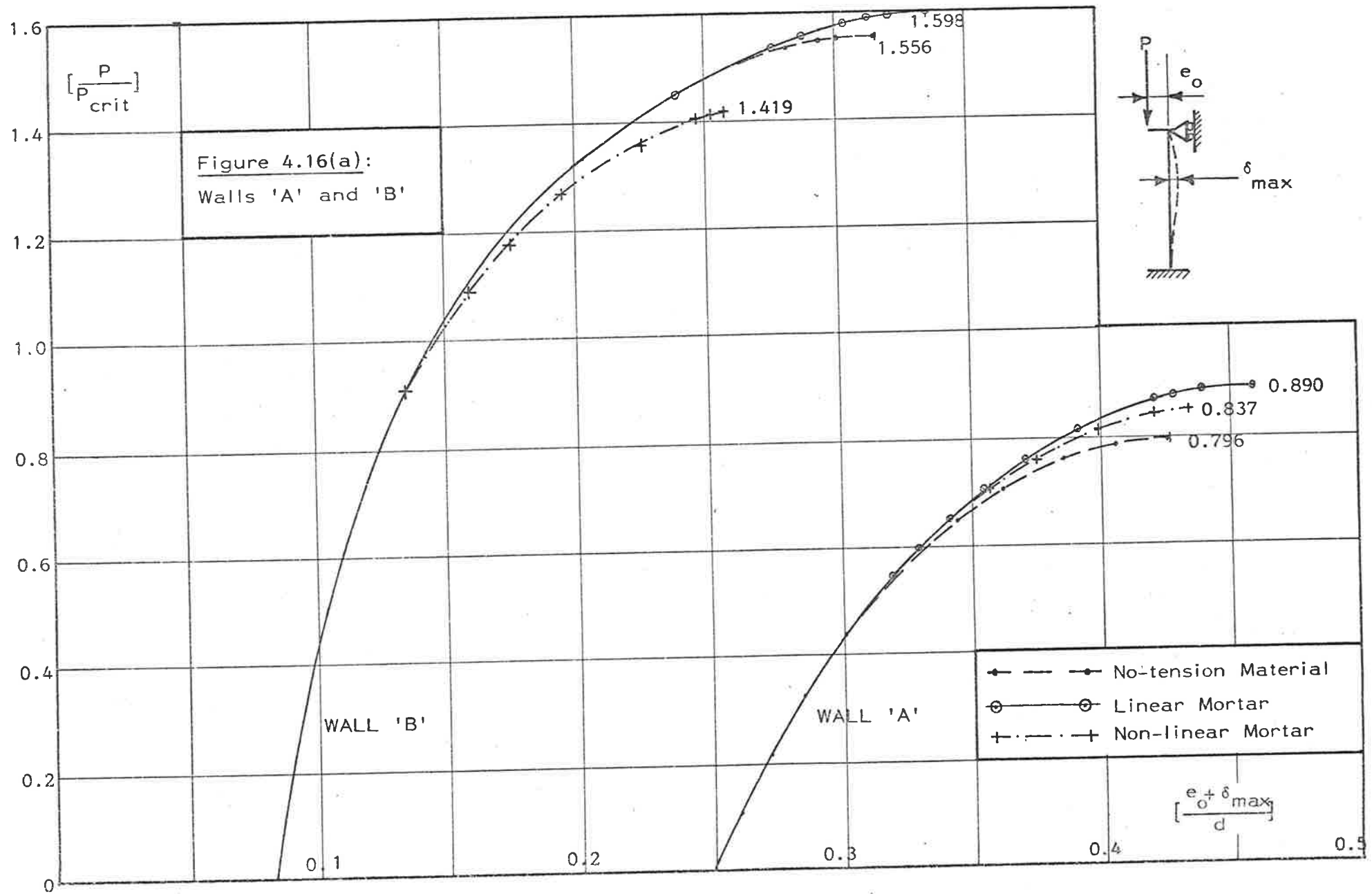


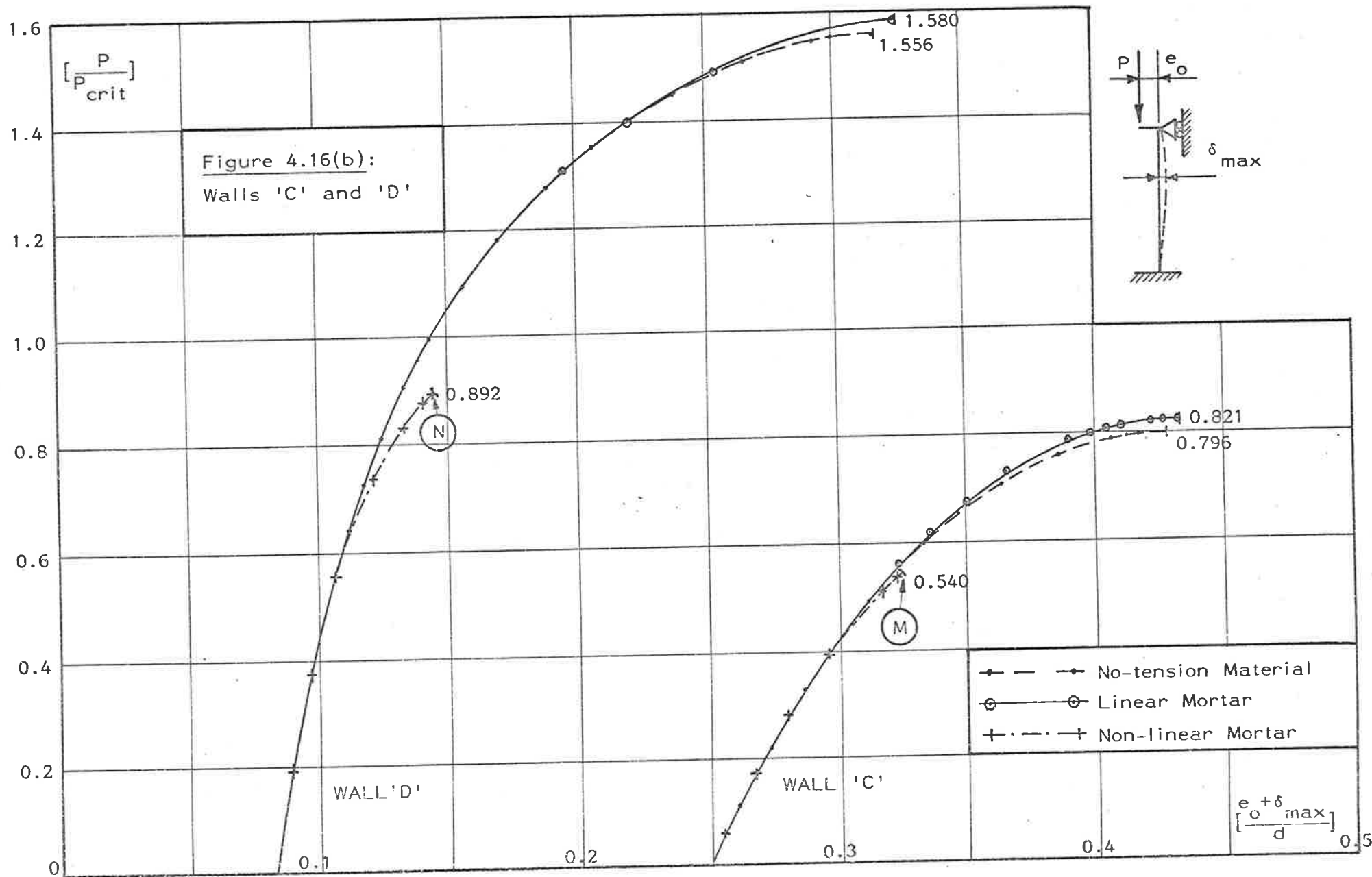
are presented in figures 4.16(a) to (d). The buckling failure load for each of the eight walls with linear mortar is less for a no-tension material wall than for a wall in which the bricks take tension stresses. The difference in buckling failure load is less than 5 percent between brick-on-flat brickwork and corresponding no-tension material walls (walls C, D, G and H, figures 4.16(b) and 4.16(d)). However, the buckling failure load of a wall of brick-on-edge construction, when loaded eccentrically at each end at  $d/4$ , is approximately 30 percent higher than the buckling failure load of the same wall given by a no-tension theory (figure 4.16(c)).

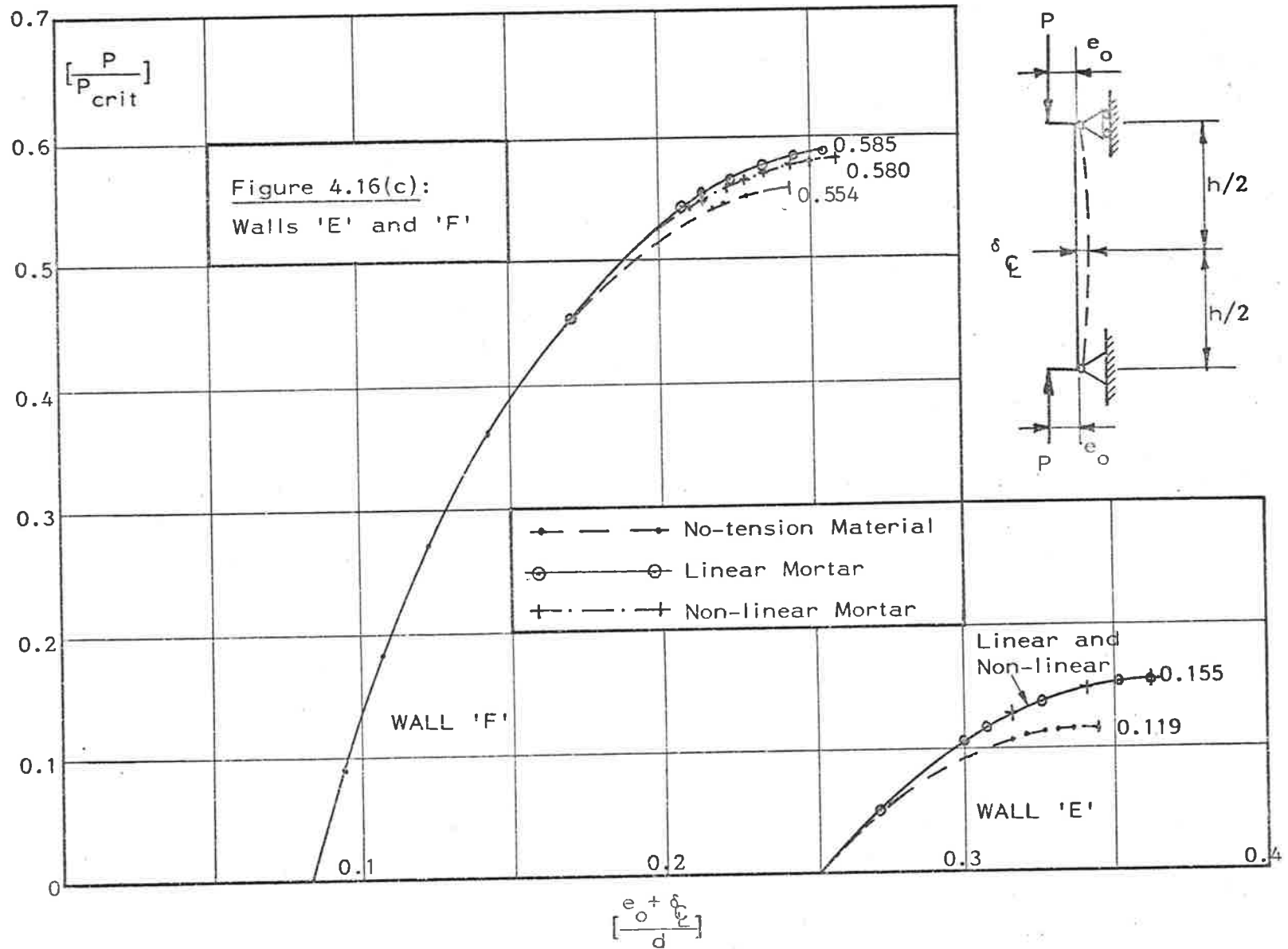
The maximum wall loads for the linear and non-linear mortars are within 6 percent of one another for pin-ended walls load at end eccentricities of  $d/12$  and are within less than 1 percent for an eccentricity of  $d/4$  (figures 4.16(c), 4.16(d)). However, the maximum wall loads for the fixed base walls with the non-linear mortar are less than the corresponding maximum loads for the linear mortar walls (figures 4.16(a), 4.16(b)). The percentage difference in maximum loads is greater for walls loaded at an eccentricity of  $d/12$  than at  $d/4$ .

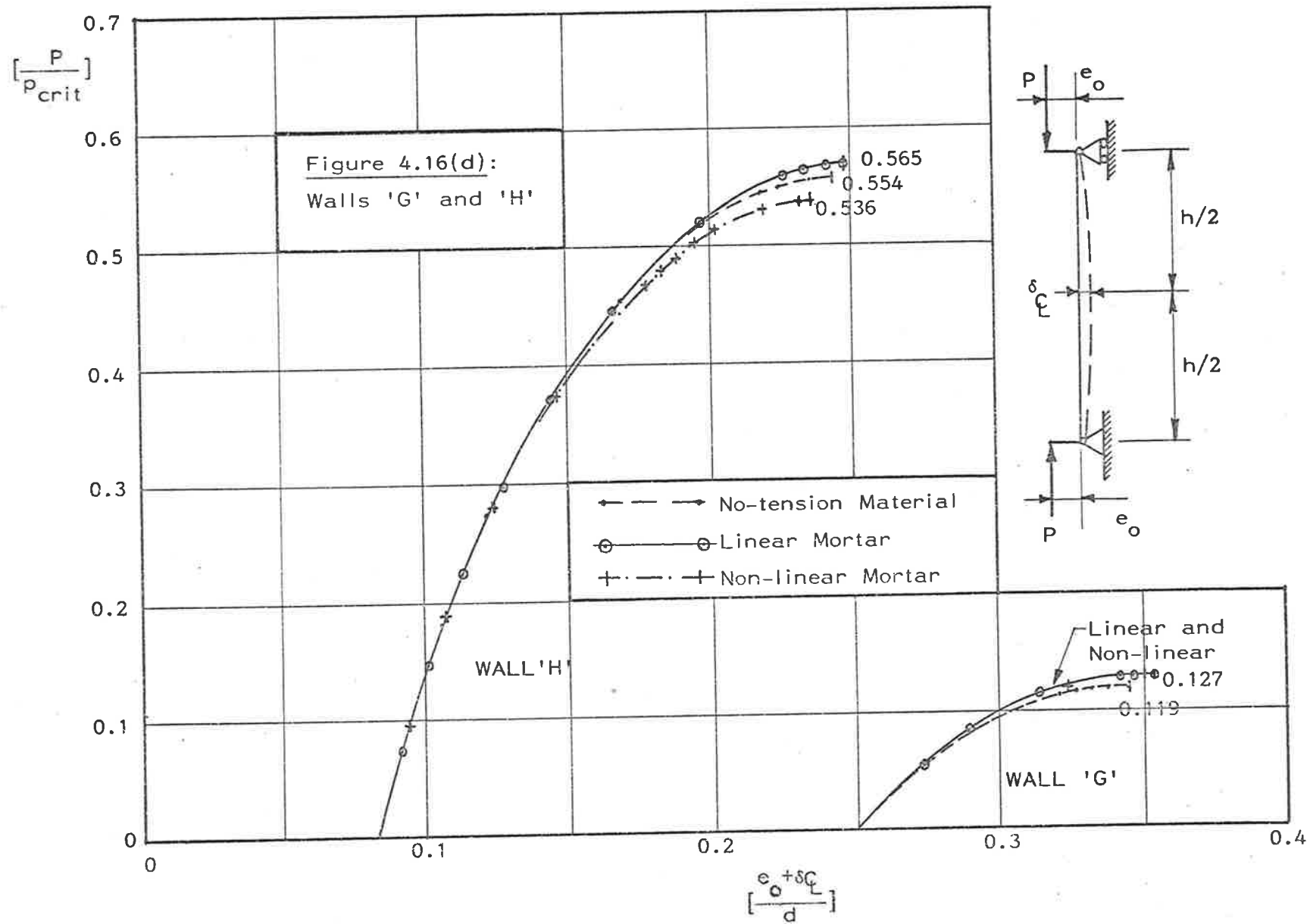
The points 'M' and 'N' in figure 4.16(b) (walls C and D respectively) indicate the loads at which the maximum stress in the mortar is equal to  $\sigma_c$ , the mortar failure stress in triaxial compression (figure 4.8). That is, points 'M' and 'N' represent the loads at which theoretical stress-related failure of the walls occurs by crushing of the mortar and splitting of the brickwork due to large lateral strains<sup>(117)</sup>.

Stress-related failure in brickwork may also occur at stresses less than  $\sigma_c$ , particularly in the case of low-strength bricks whose strengths in compression and biaxial tension may be less than









the mortar strength in triaxial compression. However, combinations of high-strength mortar and low-strength brick are not permitted in structural brickwork<sup>(4)</sup> and therefore are not considered further.

The non-linear mortar parameters  $n$  and  $\sigma_c$  assumed in this section may vary from values suitable for real brickwork. This aspect of an idealized non-linear mortar is considered, in conjunction with experimental data, in Chapter 5.

#### 4.5.2 Results of the Numerical Method Compared with Other Results

Results obtained for no-tension walls by using PROGRAM PIER1 (Appendix C) are compared in this section with results calculated from the no-tension material column theories reviewed in Section 3.4.1. The cases reviewed are as follows:

- (i) Pin-ended walls loaded with equal end eccentricities; the results are compared with the no-tension material column theory proposed by Angervo<sup>(96)</sup> (Table 4.4).
- (ii) Walls pinned at the top with perfectly fixed bases; the results are compared with results from a method proposed by Sahlin<sup>(44)</sup> (figure 3.42, Section 3.4.1). The effective heights,  $\lambda h$ , of the walls are assumed to be the values calculated by PROGRAM PIER1 (Table 4.5).
- (iii) Pin-ended walls of non-linear homogeneous material, described by equation (B.1), and loaded with equal end eccentricities. The results are compared with graphical results published by Confaldo et al.<sup>(106)</sup> (Table 4.6).

Wall No. (Table 4.3)	Load Eccentricity ( $e_o/d$ )	$(P_f/P_{crit})$		$(e_c/d)$	
		Angervo	PIER1	Angervo	PIER1
E, G	0.250	0.120	0.119	0.344	0.344
F, H	0.0833	0.555	0.554	0.244	0.242

$P_f$  is the computed buckling failure load

$P_{crit}$  is the Euler critical load for a pin-end column

$e_c$  is the maximum load eccentricity immediately before failure

Table 4.4: Buckling Failure Loads for Pin-end Walls of Linear Material

Wall No. (Table 4.3)	Load Eccentricity at top ( $e_o/d$ )	$(P_f/P_{crit})$	
		Sahlin <sup>(a)</sup>	PIER1
A, C	0.250	0.785	0.796
B, D	0.0833	1.55	1.56

(a) From PROGRAM PIER1,

$$\text{for } (e_o/d) = 0.250, \lambda \approx 0.67$$

$$\text{for } (e_o/d) = 0.0833, \lambda \approx 0.69$$

Table 4.5: Buckling Failure Loads for Fixed Base Walls of Linear Material

PROGRAM PIER1 has been written with the facility that if the vertical compression load is known, end eccentricities may be calculated at which either stress-related failure or buckling occurs (Section 4.5.1). The walls may be either pin-ended or pinned at the top with perfectly fixed bases (Appendix C).

Case No.	Wall Slenderness (h/d)	Load Eccentricity ( $e_o/d$ )	[[ $P_f/(\sigma_c \cdot d)$ ]]	
			Contaldo <u>et al.</u>	PIER1
1	25	zero	0.25	0.248
2	15	1/18 = 0.0556	0.41	0.413
3	15	1/3 = 0.333	0.025	0.0253

For the three cases,

- (i) Initial central deflection is  $h/1000$ , where  $h$  is the wall height.
- (ii)  $\frac{\sigma_c}{E} = 0.0038$ , where  $\sigma_c$  is the material failure stress  
 $E$  is the initial tangent modulus
- (iii) Both top and base are pinned.

Table 4.6: Buckling Failure Loads for Pin-end Walls of Non-linear Material

This aspect of PIER1 has been used to check results which cannot be compared with the theories reviewed in Section 3.4.1. An indication of the order of accuracy obtained by the numerical method can be assessed from the results summarized in Table 4.7. For all cases investigated, the agreement is closer than 0.5 percent.

#### 4.6 SUMMARY AND CONCLUSIONS

This chapter describes a finite difference method of analysis of brickwork walls which includes the effect of discrete cracking on the bedjoints. As examples of the method, the following types of wall and loading conditions have been considered –



Wall No. (Table 4.3)	Brick Orientation	Mortar Type	End Supports		Load Increment Method		Eccentricity Increment Method	
			Top	Base	Chosen ( $e_o/d$ )	Computed ( $P_f/P_{crit}$ )	Chosen ( $P_f/P_{crit}$ )	Computed ( $e_o/d$ )
C	On Flat	NL	PR	F	0.250	0.540	0.540	0.250
E	On Edge	L	PR	P	0.250	0.155	0.155	0.250
H	On Flat	NL	PR	P	0.0833	0.535	0.535	0.0831

NL denotes non-linear mortar  
 L denotes linear mortar  
 P denotes pin support  
 PR denotes pin-roller support  
 F denotes perfectly fixed support

} (figure 4.14)

Table 4.7: Check on Failure Loads of Brickwork Walls Computed by Different Versions of PROGRAM PIER1

- (i) a pin-end wall under eccentric end load with either equal or unequal end eccentricity. The end eccentricities are chosen and the load is incremented to failure.
- (ii) a wall with a perfectly fixed base and a pin-roller top support, loaded eccentrically at the top. The load eccentricity is chosen and the load is incremented to failure.
- (iii) a pin-end wall under loads with equal eccentricities at each end. The load is chosen and the end eccentricity is incremented to failure.
- (iv) a wall with a perfectly fixed base and a pin-roller top support. The load is chosen and the load eccentricity at the top is incremented to failure.

For each of the four cases above, the mortar stress-strain relationship can either be linear or non-linear of the form  $\sigma = E_m \cdot (\epsilon - K\epsilon^n)$ ;  $K$  and  $n$  are constants and  $E_m$  is the initial tangent modulus (Appendix B). Comparisons of results from PROGRAM PIER1 with the results of no-tension theories have shown that the finite difference method can be used to calculate the behaviour of columns of no-tension material. Results obtained using PROGRAM PIER1 (Table 4.7) show that flexural stiffening due to the tension field effect in the bricks may be determined by a finite element method. This stiffening can be incorporated into a finite difference method for the calculation in brickwork walls of the displacements and stresses at any specified load, so that with a knowledge of the brickwork material properties, the finite difference method can be used to predict the loads that would cause either stress-related failure or buckling of the brickwork. An important feature of the incremental procedure used in PROGRAM PIER1 is that the equilibrium configuration calculated at any load level (or value of

eccentricity if the load is specified) is independent of the path chosen for the analysis.

PROGRAM PIER1 may also be used to investigate the effects of initial deviations from vertical straightness (figure 4.13) due to, say, poor workmanship. This aspect of brickwork walls is considered in Chapter 8 in a comparison between a set of results obtained from PROGRAM PIER1, in the form of a parametric survey, and design criteria specified by current Codes of Practice.

## 5. EXPERIMENTS ON WALLS IN ONE-WAY BENDING

Experiments described in this chapter were designed to test the stiffness results obtained from the finite element analysis of eccentrically compressed bricks (Chapter 4), and to check the results of calculations using PROGRAM PIER1. The results of Chapman and Slatford<sup>(97)</sup> were checked by testing a steel column, similar to their aluminium column (Section 3.4.2), and comparisons are presented between the test results and results calculated by PROGRAM PIER1. In addition, displacements and failure loads calculated using PROGRAM PIER1 are compared with results from experiments on eight brickwork walls.

### 5.1 STIFFNESS EXPERIMENTS

#### 5.1.1 Experimental Verification of Curvature Ratio Factor, $\alpha$

A program of experiments was undertaken to measure accurately both the strain profiles and also the magnitude of the curvature ratio factor,  $\alpha$ , in replica mild steel blocks under eccentric load.

In order to check the strain profiles calculated by the finite element analysis, a column comprising five steel blocks, each nominally 50mm x 50mm x 25mm, was placed in a testing machine (figure 5.1(a)) and loaded eccentrically at each end. Electrical resistance strain gauges of 2mm gauge length were fixed to the 50mm x 50mm faces of the central steel block as shown in figure 5.1(b). The block thickness was measured to be 24.9mm. Loads were applied through knife edges at nominal eccentricities of  $d/5$ ,  $d/3.5$  and  $d/3$ , but the actual eccentricities were measured to be 5.16mm ( $d/4.83$ ), 7.19mm ( $d/3.46$ ) and 8.29mm ( $d/3.00$ ) respectively. For each eccentricity value, two load tests were carried out, each with the load on opposite sides of the

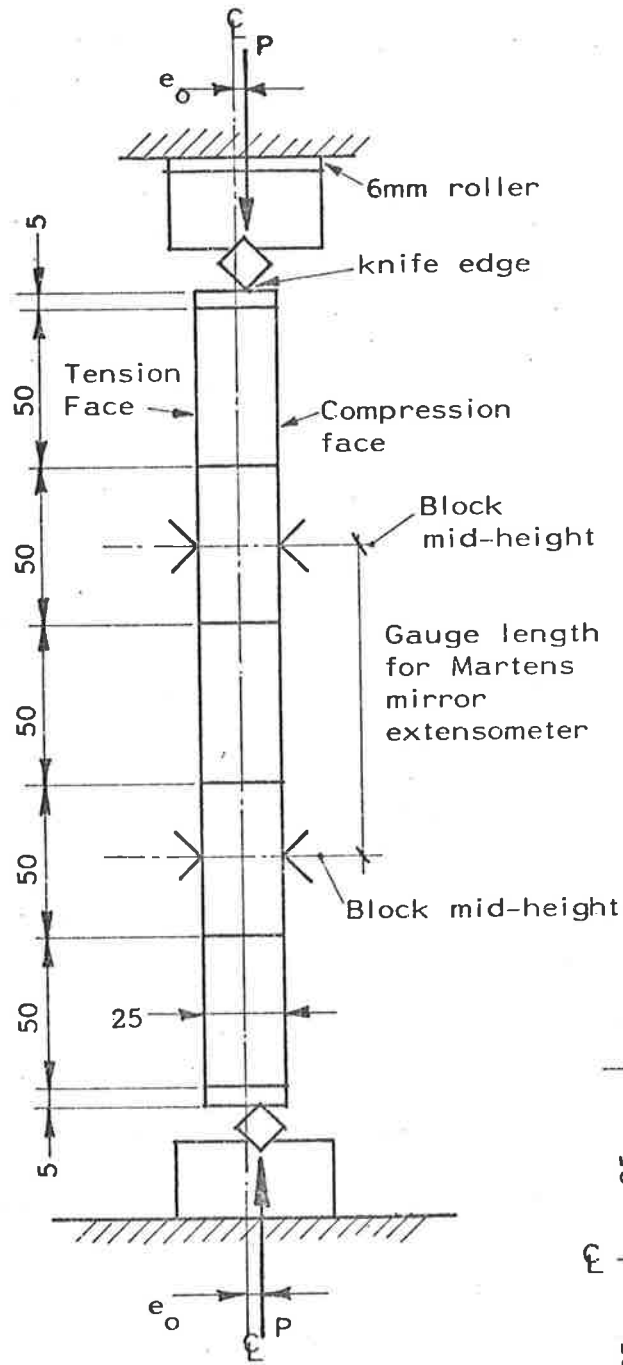


Figure 5.1(a):  
Steel Block Column

Figure 5.1: Test for Strain Profiles in Steel Blocks

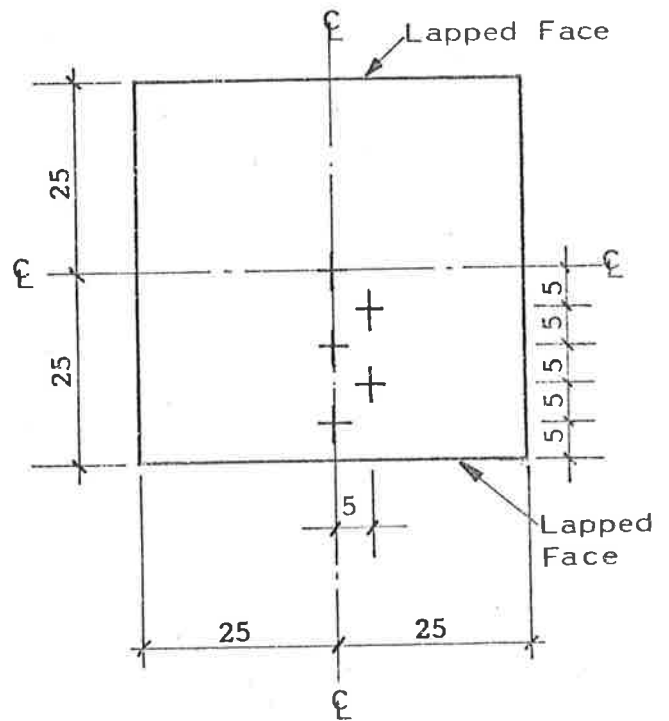


Figure 5.1(b): Steel Block Showing Positions of Strain Gauges (all Dimensions Nominal)

column centreline. Plots of the experimental and calculated strain profiles are shown in figures 5.2 to 5.4, the experimental points being the mean of two tests. The agreement between computed and experimental strain profiles was very close.

A column of five steel blocks (figure 5.5) was set up with a pair of Martens mirror extensometers fixed to opposite faces of two blocks separated by the centre block (figure 5.1(a)). The curvature ratio factors,  $\alpha$  (Section 4.2.2), were determined for various load eccentricities by measuring the relative rotations of the midplanes of the blocks, the resolution of the extensometers giving an angle of resolution of  $50 \times 10^{-6}$  radians. To define precisely the line of action of the load relative to the centreline of the column, dial gauges were used to measure lateral displacement. The mating surfaces of the blocks were hand-lapped to remove excessive irregularities and to allow intimate contact of the bearing surfaces. The elastic modulus of the steel was determined by tension tests on a solid bar of the same stock material as the blocks, strains being calculated from both Martens mirror extensometers and by electrical resistance strain gauges. The experimental Young's Modulus of the blocks given by both sets of measurements was  $203 \times 10^3$  MPa. The experimental values of factor  $\alpha$  and the values of  $\alpha$  calculated using equations (4.2) and (4.3) (Section 4.2.2) are summarized in Table 5.1. The agreement in the factors  $\alpha$  is within 3 percent.

#### 5.1.2 An Effective Elastic Modulus for Uncracked Brickwork under Eccentric Compression

Base and Baker<sup>(69)</sup> calculated effective elastic moduli for brickwork assuming that both the brick and mortar materials were linearly elastic and there was no cracking at the brick-mortar interfaces

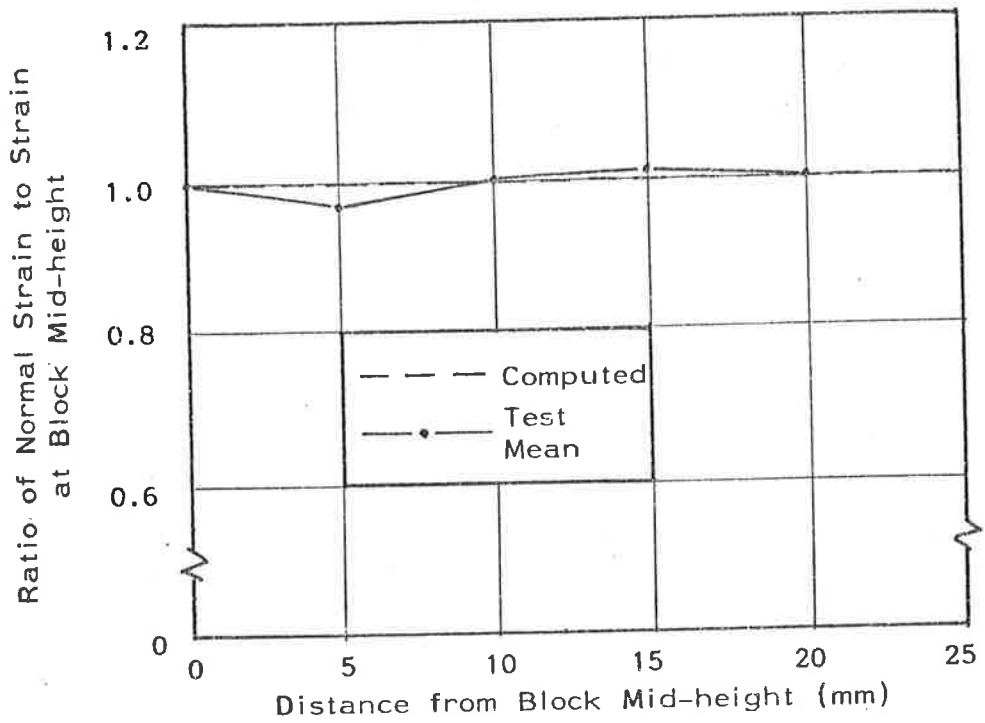
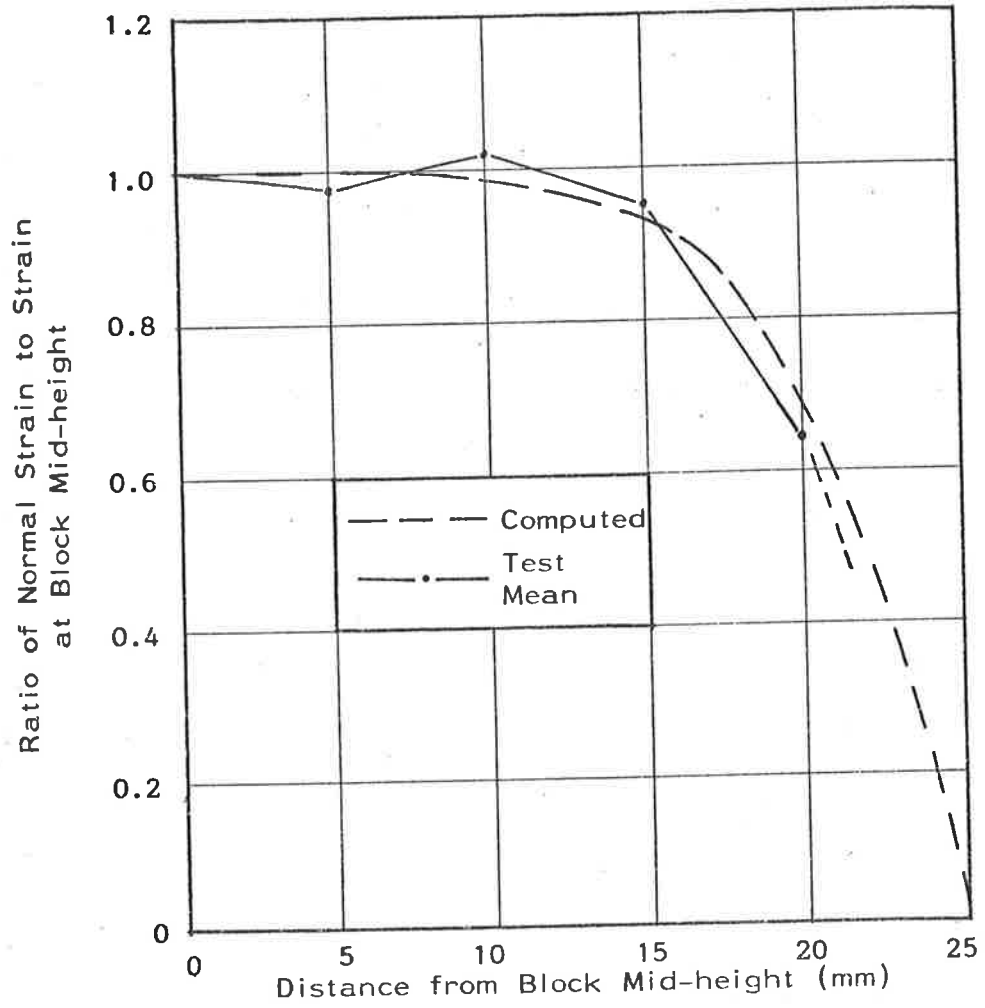


Figure 5.2: Steel Block Compressed with Load Eccentricity  $d/5$  (Nominal)

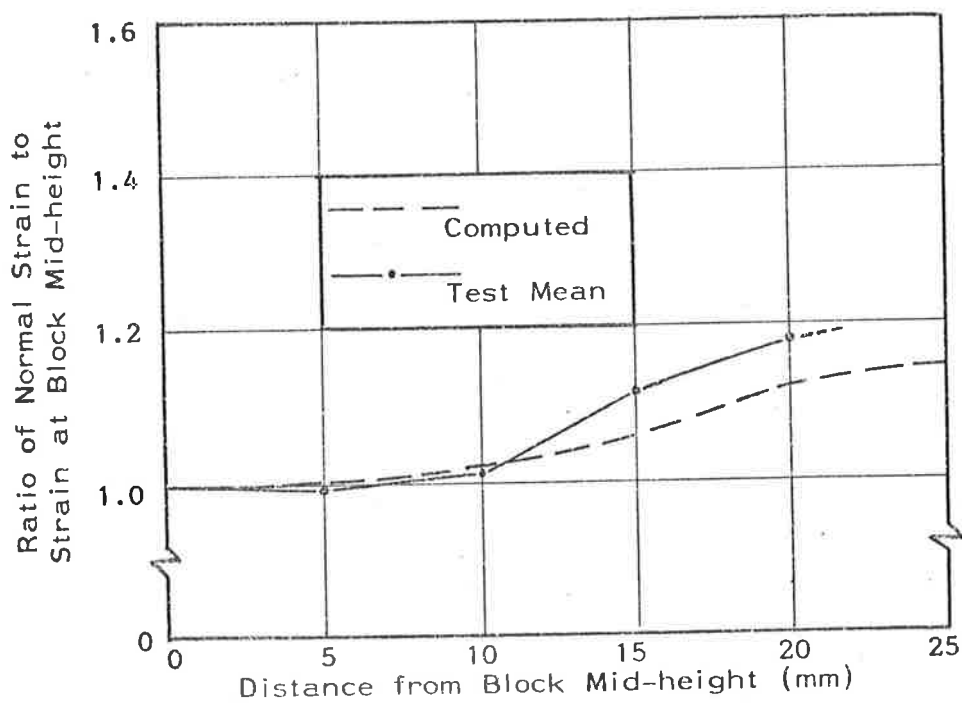
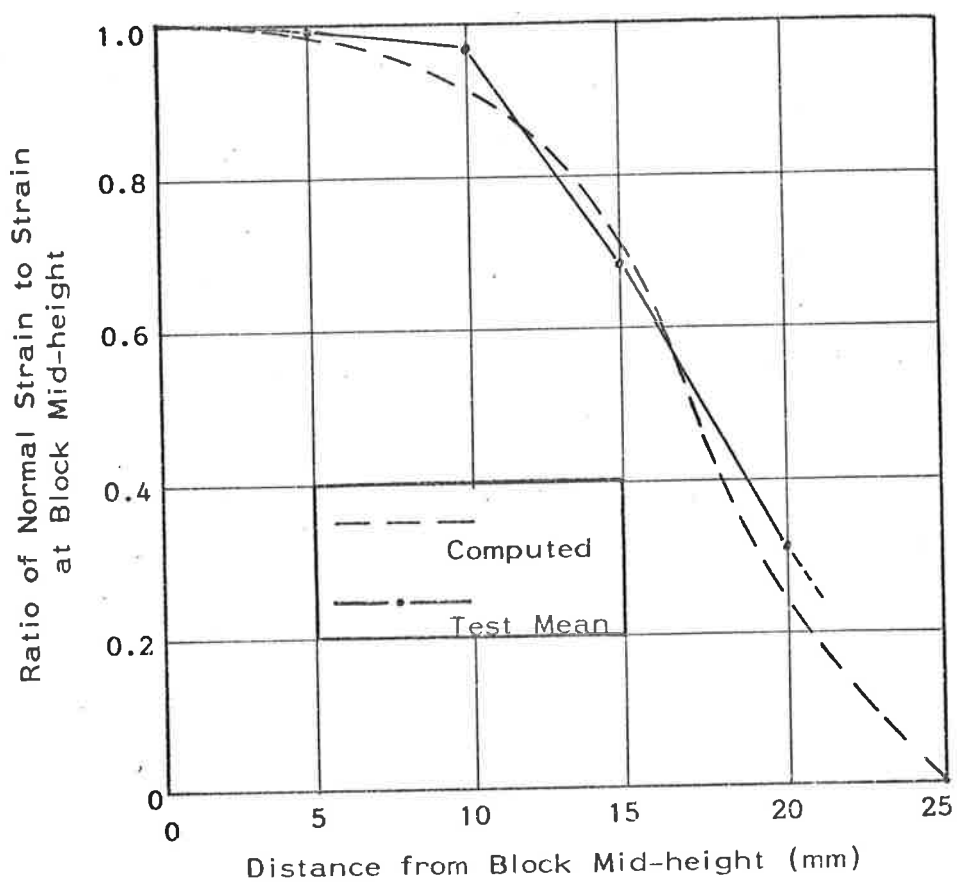


Figure 5.3: Steel Block Compressed with Load Eccentricity  $d/3.5$  (Nominal)



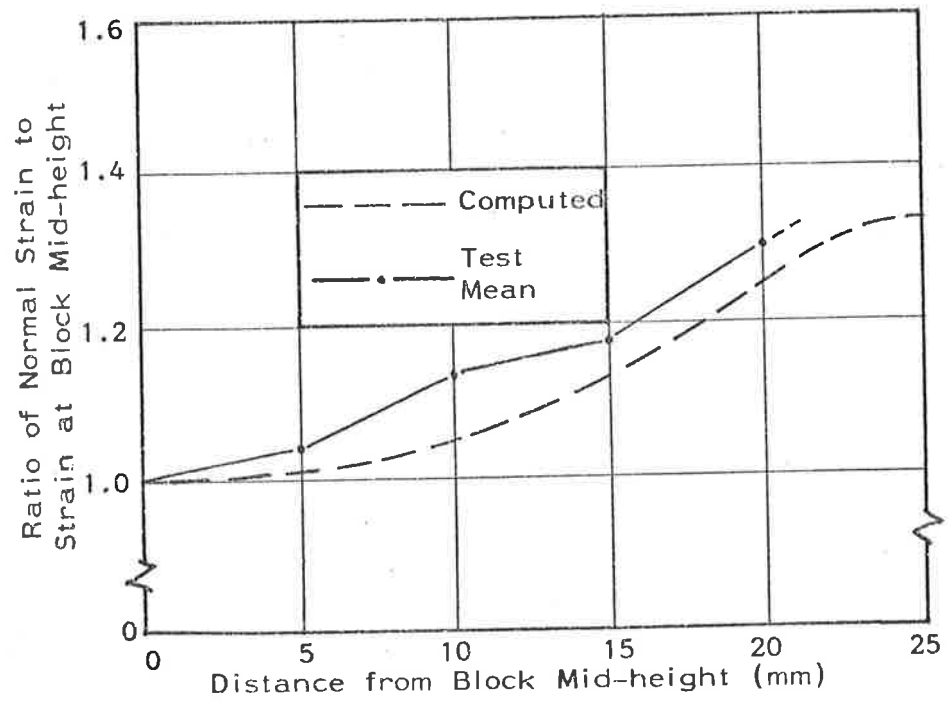
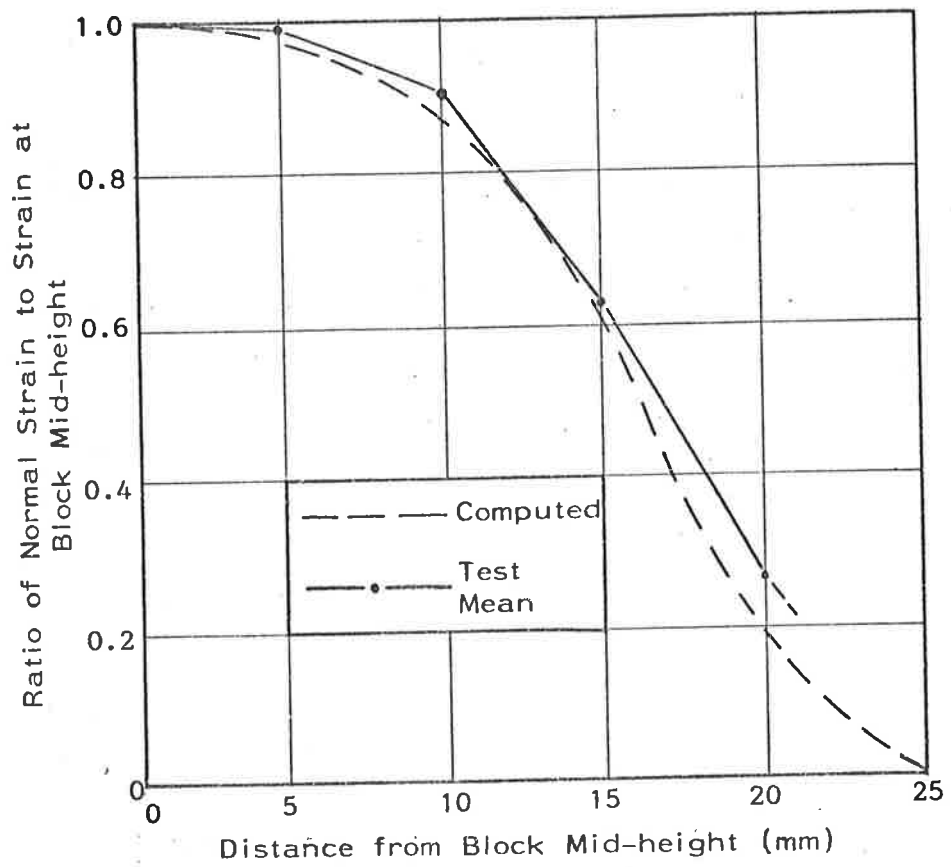
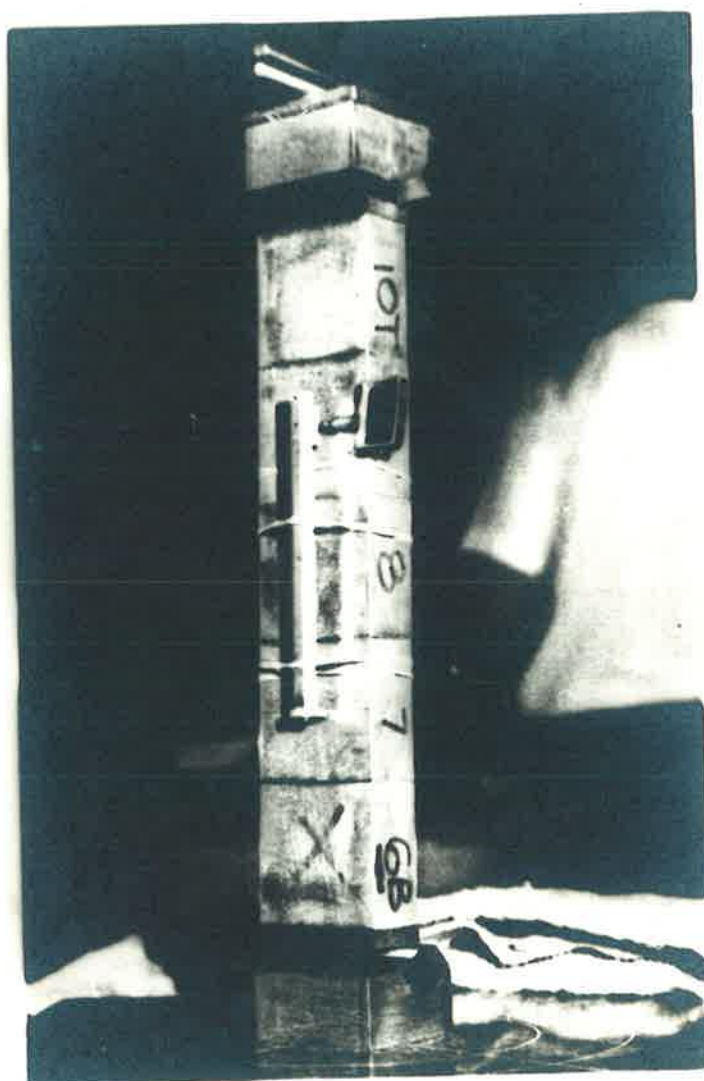


Figure 5.4: Steel Block Compressed with Load Eccentricity  $d/3$  (Nominal)



**Figure 5.5: Steel Block Column Showing  
Martens Mirror Extensometer**

Nominal Load Eccentricity	Load Eccentricity ( $e_0 + \delta_c$ ) (mm)	Curvature factor, $\alpha$		Ratio $\frac{\alpha \text{ (experimental)}}{\alpha \text{ (calculated)}}$
		Experimental	Calculated (Equations (4.2), (4.3))	
d/5	5.23	1.01	1.04	0.97
d/3.5	7.33	1.21	1.24	0.98
d/3	8.45	1.43	1.48	0.97

Table 5.1: Comparison of Curvature Factors,  $\alpha$ 

(Section 3.3.5.1). The theoretical results were tested by bending bond-beam specimens, loaded with line loads placed symmetrically on the span. For the group of twelve tests on solid bricks in brickwork piers, the agreement between theoretical and practical results was close (Table 3.6). However, tests were not conducted to determine the elastic modulus of brickwork under eccentric compression loading. Consequently, as a part of the test program on the measurement of brickwork stiffness, six brickwork prisms were tested to determine whether the measured flexural properties of uncracked brickwork depend upon either the load eccentricity or the method of measurement. The tests were conducted to determine also whether the brickwork modulus of elasticity determined under conditions of eccentric compression agreed with calculated values using results obtain by Base and Baker<sup>(69)</sup> (equations (3.47), (3.48)).

Each prism comprised six bricks and five mortar joints and was built in a steel frame to achieve vertical alignment on one face. All bricks were without perforations and were selected for uniformity, their dimensions being 228mm x 108mm x 75mm closely. The mortar proportions by volume were 1 cement:1 hydrated lime:6 sand with the water:cement ratio 1.41 by weight and the ratio of water:cementitious

materials (cement and lime) was 1.03 by weight. All bricks were laid in a saturated surface-dry condition and in a brick-on-edge orientation with 10mm bedjoints. The prisms were cured subsequently under polythene sheet for 21 days and under ambient conditions until tested at a minimum 28 days after construction.

The experimental apparatus (figure 5.6) was designed so that all lateral displacements could be measured relative to a plane defined by the end-pin supports.

Three of the brickwork prisms were loaded at an eccentricity of 12.5mm ( $d/6$ ) at each end and the remaining three at an eccentricity of 25mm ( $d/3$ ). Effective elastic modulus values for each prism were determined by the following methods -

1. The lateral displacements of each mortar joint relative to the ends of the prism were measured and a circular-curve approximation to the displaced shape was made using a least-square-error method. An effective elastic modulus was calculated from the relationship -

$$E_{br} = \frac{MR}{I} \quad (5.1)$$

in which  $E_{br}$  is an effective elastic modulus for uncracked brickwork

$M$  is the moment about the prism centre plane

$R$  is the radius of the best-fit circular curve approximation to lateral displacements

$I$  is the section second moment of area about the centre plane.

In equation (5.1), the moment,  $M$ , was assumed constant along the prism height.

2. The rotations of the ends of the prisms were measured with bubble micrometers having a sensitivity of  $2 \times 10^{-5}$  radians. An effective

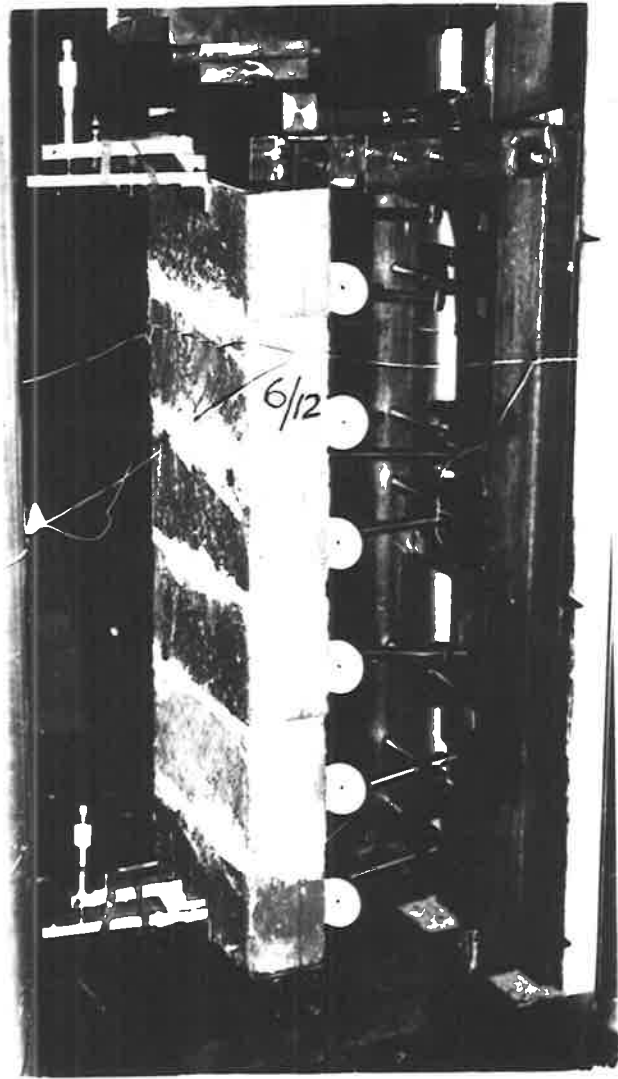


Figure 5.6(a):

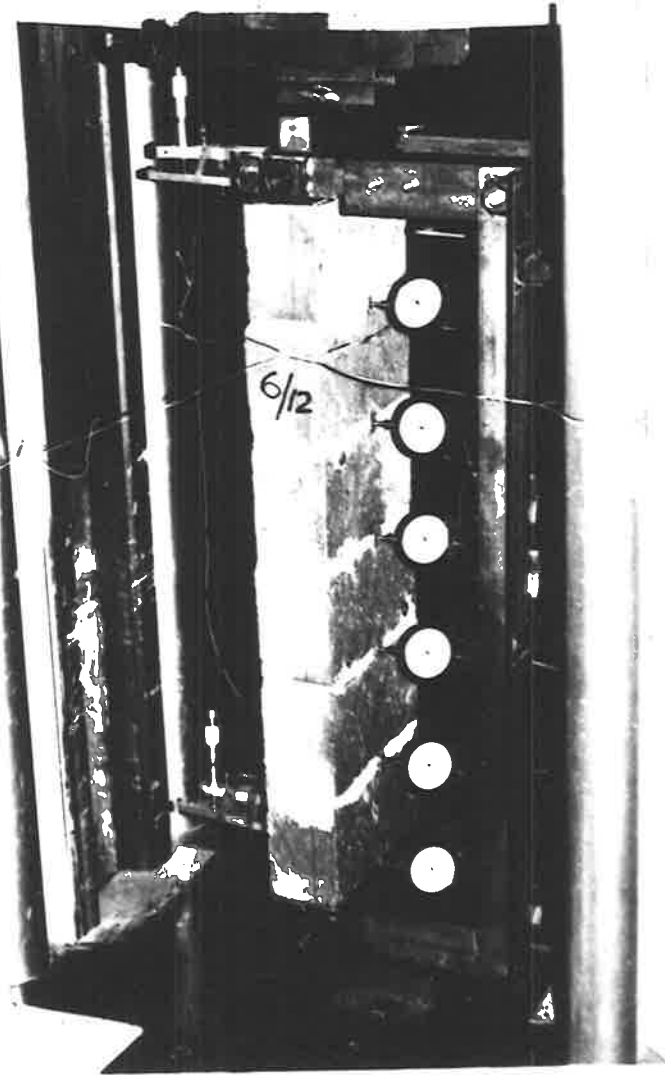


Figure 5.6(b):

Figure 5.6: Test Apparatus for Determining Brickwork Elastic Modulus

elastic modulus for each of the prisms was calculated from the relationship -

$$E_{br} = \frac{Mh}{\phi I} \quad (5.2)$$

in which  $E_{br}$ ,  $M$  and  $I$  are as defined for equation (5.1)

$h$  is the distance between the bubble micrometers

$\phi$  is the relative end rotation caused by the moment  $M$ .

3. DEMEC points were used on each prism face to measure the axial shortening of each of the brickwork prisms. An effective elastic modulus was calculated from -

$$E_{br} = \frac{Ph_D}{A\delta} \quad (5.3)$$

in which  $E_{br}$  is an effective elastic modulus for uncracked brickwork

$P$  is the load on the prism

$\delta$  is the mean axial shortening between DEMEC points

$A$  is the section area of the prism

$h_D$  is the DEMEC gauge length.

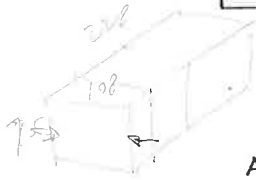
The effective elastic modulus values calculated using equations (5.1), (5.2) and (5.3) are summarized in Table 5.2.

In all six prisms, the differences between measured lateral displacements and the respective best-fit circular curves were less than 10 percent of the measured displacements, with an average absolute difference of 3.8 percent.

A two-way statistical analysis of variance on the results in Table 5.2 showed that there was no significant difference (at the 5 percent significance level on a two-tailed test) among effective elastic modulus values calculated by the three methods at the two different load eccentricities.

Brickwork Prism No.	Load Eccentricity (mm)	Effective Elastic Modulus (x10 MPa)		
		Displacements Eq. (5.1)	Rotations Eq. (5.2)	DEMEC Eq.(5.3)
1	12.5	9.5	10.0	9.3
2	12.5	12.0	11.6	11.9
3	12.5	13.2	12.2	11.5
4	25.0	10.7	9.8	10.8
5	25.0	9.0	9.8	9.4
6	25.0	10.5	10.2	10.2

Table 5.2: Experimental Elastic Modulus for Brickwork



A fourth method of estimating an effective elastic modulus for uncracked brickwork was also investigated. Six bricks from the batch used for the piers were saw-cut to give, from each brick, two sample prisms 75mm x 25mm x 108mm. The twelve prisms were tested in axial compression (figure 5.7(a)) and estimates of elastic modulus for the bricks were made from an average of the two prisms from each brick. Six mortar prisms, 25mm x 25mm x 50mm, cast from the mortar batch used for the piers were also tested in axial compression (figure 5.7(b)). Typical stress-strain curves for the brick and mortar prisms are given in figures 5.8(a) and 5.8(b) respectively. The mortar prisms showed non-linear behaviour when loaded in uniaxial compression and the brick material behaved linearly in agreement with the results obtained by Scrivener and Williams<sup>(50)</sup> (Section 3.1.3.4).

Six estimates (Table 5.3) of brickwork elastic modulus were obtained by combining at random the initial tangent elastic modulus values for the six bricks and six mortar prisms using the equation –

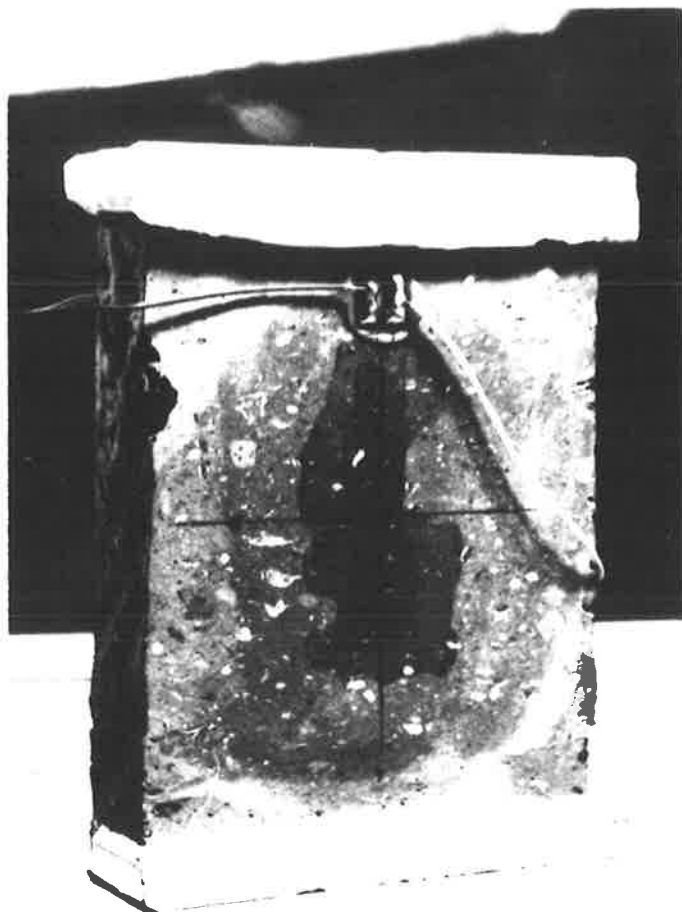


Figure 5.7(a): Brick Prism Showing Sulphur Capping and Strain Gauge

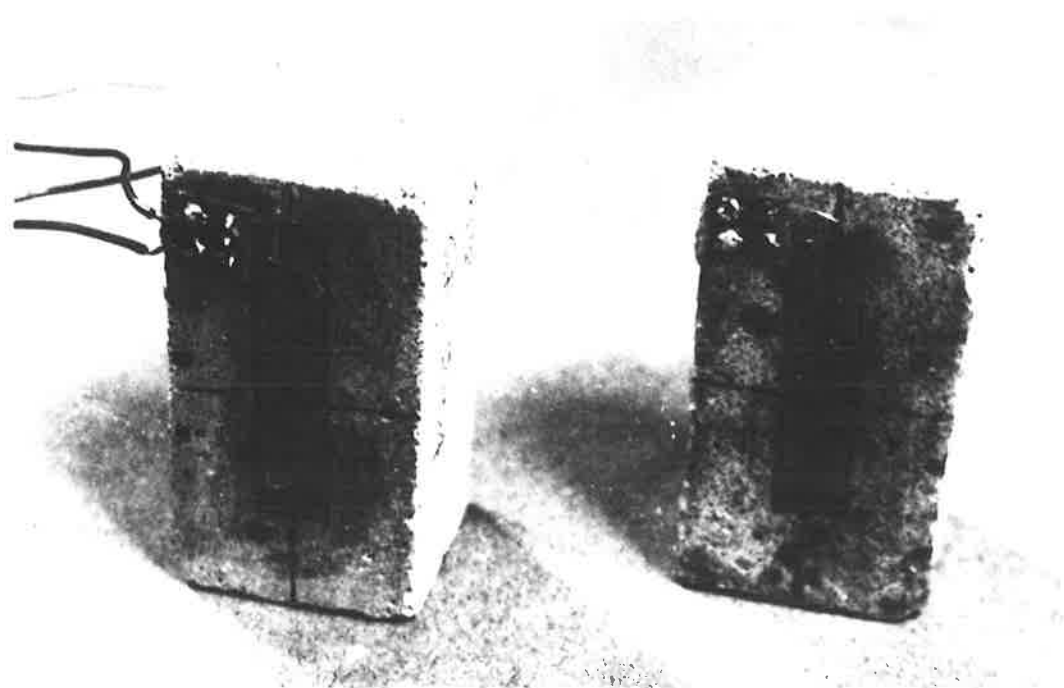


Figure 5.7(b): Mortar Prisms Showing Strain Gauges

Figure 5.7: Brick and Mortar Prisms



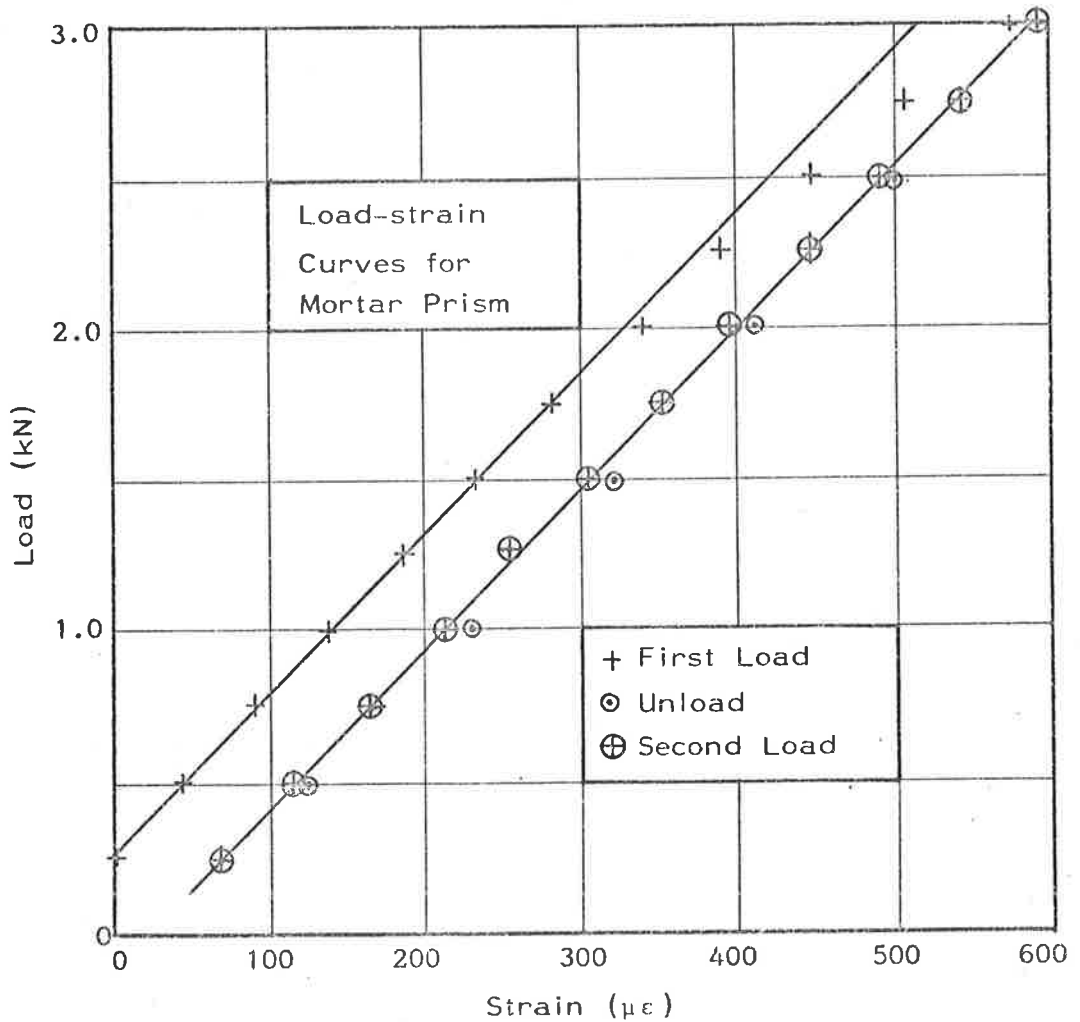
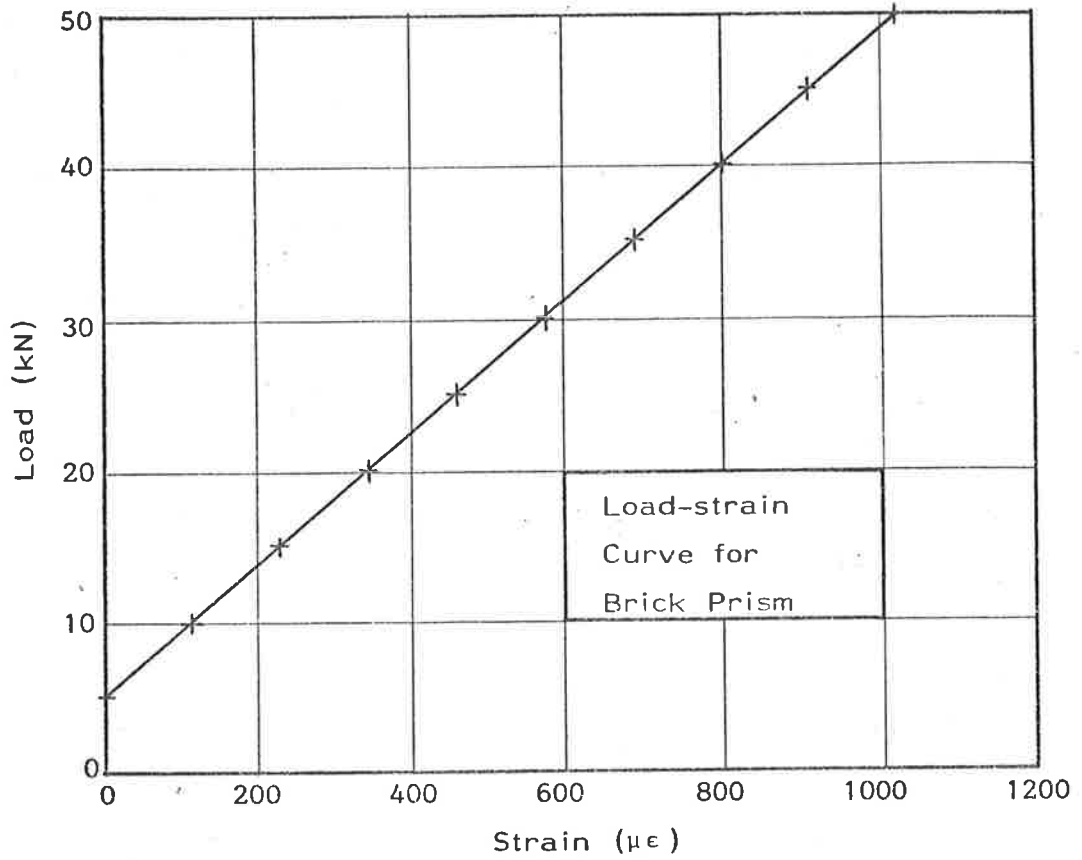


Figure 5.8: Load-strain Curves for Brick and Mortar Prisms

$$E_{br} = E_b \cdot \left[ \frac{(h_b + h_m)}{h_b + \left(\frac{E_b}{E_m}\right) \cdot h_m} \right] \quad (5.4)$$

in which  $E_{br}$  is an effective elastic modulus for uncracked brickwork

$E_b$  is a calculated brick initial tangent modulus

$E_m$  is a calculated mortar initial tangent modulus

$h_b$  is the brick height (108mm)

$h_m$  is the bedjoint thickness (10mm).

Equation (5.4) is similar to equation (3.48) proposed by Base and Baker<sup>(69)</sup> (Section 3.3.5.1).

Estimate No.	Effective Elastic Modulus ( $\times 10^3$ MPa)
1	9.4
2	12.6
3	8.3
4	7.6
5	9.0
6	10.5

Table 5.3: Calculated Elastic Modulus Values for Brickwork

A one-way statistical analysis of variance incorporating a method of planned comparisons was used to compare the results of Table 5.2 with the modulus values in Table 5.3. Calculations showed that there was no significant difference between the effective elastic modulus values obtained by any of the four methods, when tested at the 5 percent level on a two-tailed test.

From the experiments on brickwork prisms and brick and mortar prisms, it may be concluded that all of the four methods of measurement give statistically equivalent estimates of the elastic modulus of uncracked brickwork under eccentric compression loading. The stress-strain relationship for a mortar prism under uniaxial compression (figure 5.8(b)) became linear once the specimen had been loaded and unloaded, although possible non-linear behaviour in triaxial compression at stresses beyond the uniaxial failure stress was not investigated. The behaviour of uncracked brickwork in the non-linear range of the materials will be considered in Section 5.2.2.

### 5.1.3 The Stiffness of Partially-cracked Brickwork

A relationship between the average curvature of brickwork in eccentric compression and the curvatures of the component materials was given in Section 4.2.4.1 as —

$$\left(\frac{1}{R}\right)_{av} = \frac{\frac{1}{\alpha} \cdot \left(\frac{1}{R}\right)_{nt} \cdot h_b + \rho \left(\frac{1}{R}\right)_m \cdot h_m}{h_b + h_m} \quad (4.5)$$

and also as

$$\left(\frac{1}{R}\right)_{av} = \frac{M_e}{(EI)_{eq}} \quad (4.21)$$

in which, for linear elastic materials ( $\rho = 1$ , Appendix B),

$$(EI)_{eq} = E_b \cdot \left[ \frac{h_b + h_m}{\left(\frac{h_b}{\alpha}\right) + h_m \cdot \left(\frac{E_b}{E_m}\right)} \right] \cdot I_{eq} \quad (5.5)$$

$I_{eq}$  in equation (5.5) is defined by equations (4.23) in Section 4.3.1.

In order to check equation (5.5) against experimental results, six brickwork prisms of six bricks and five mortar joints were constructed as for the tests conducted to determine elastic modulus values. In addition, six bricks from the batch were saw-cut to give twelve sample prisms each 75mm x 25mm x 108mm which were tested in compression using pairs of 30mm long strain gauges to determine strains. The brick elastic modulus values are shown in Table 5.4.

Brick No.	Elastic Modulus ( $\times 10^3$ MPa)	
	Sample 1	Sample 2
1	9.30	9.87
2	14.40	12.33
3	8.22	8.46
4	7.22	7.79
5	10.05	8.05
6	11.56	9.70

Table 5.4: Elastic Modulus Values for Brick Prisms

The mean elastic modulus was  $9.75 \times 10^3$  MPa with a coefficient of variation of 21 percent.

Six mortar prisms, 25mm x 25mm x 50mm, were cast to determine the mortar elastic modulus in uniaxial compression (Table 5.5). The main elastic modulus was  $8.3 \times 10^3$  MPa with a coefficient of variation of 5 percent.

Each of the brickwork prisms was tested in a 1000KN compression machine, as described in Section 5.1.2, and to eliminate problems of material variability, each prism was tested initially at an eccentricity of 12.5mm ( $d/6$ ) and subsequently at 25.0mm ( $d/3$ ). The former test did not produce cracking at the brick-mortar interfaces so that in equation (5.5), the curvature ratio,  $\alpha$ , for the bricks should be unity.

Mortar Prism No.	Elastic Modulus ( $\times 10$ MPa)
1	7.84
2	7.87
3	8.28
4	8.72
5	8.34
6	8.84

Table 5.5: Elastic Modulus Values for Mortar Prisms

In Section 5.1.2, it was shown that measurement of relative end rotations of a brickwork prism gave a statistically reliable estimate of the brickwork stiffness. Consequently, the stiffness of a cracked brickwork prism loaded at  $d/3$  was compared with the uncracked prism stiffness. Before testing each prism, a load was applied at an eccentricity of 25mm ( $d/3$ ) to ensure that the brick-mortar interfaces were debonded, but the load was chosen so that cracking would occur without causing distress in the compression regions of the mortar joints.

The end rotations per unit load for the brickwork prisms are summarized in Table 5.6. The load rotation graphs were all essentially linear for the range of loads selected.

From equation (5.5), with  $h_b = 108\text{mm}$ ,  $h_m = 10\text{mm}$  and the corresponding elastic modulus values given in Tables 5.4 and 5.5, the theoretical ratio of the end rotation rates is 3.08. The average of the experimental values in Table 5.6 is 2.82 with a coefficient of variation of 3 percent. The difference between the theoretical and experimental results could be attributed, in part, to some degree of tension across the brick-mortar interface because of incomplete debonding and also some small residual friction effects in the pin joints through which the load was applied.

Brickwork Prism No.	Relative End Rotation Rate ( $\times 10^{-6}$ rad/KN)		Ratio of Rotation Rates [ $\frac{\text{Rotation (d/3)}}{\text{Rotation (d/6)}}$ ]
	Eccentricity = d/6	Eccentricity = d/3	
1	91.6	274	2.99
2	94.6	268	2.83
3	84.6	236	2.79
4	94.2	256	2.72
5	80.8	224	2.77
6	87.0	244	2.80

Table 5.6: Relative Stiffness of Cracked and Uncracked  
Brickwork Prisms

## 5.2 WALL EXPERIMENTS

### 5.2.1 Tests on a Slender Steel Block Column

#### 5.2.1.1 Introduction

The method of analysis of a linear elastic brickwork column, described in Chapter 4, was checked experimentally by loading a steel column 50mm x 25mm in cross-section consisting of thirty-three blocks each of 50mm length. The experimental program was similar to the tests of Chapman and Slatford<sup>(97)</sup> except that steel blocks were used instead of the original aluminium blocks.

The matching faces of the blocks were ground and hand-lapped so that intimate contact could be achieved and the blocks were stacked in the same order for all tests such that minimum deviation from straightness was obtained. The column was precompressed for the purpose of handling by two 6mm diameter high-tensile rods and placed

inside a clear acrylic rectangular tube. The rods were removed prior to testing when the column was loaded through knife edges in a compression testing machine (figure 5.9).

Column failure occurred by lateral buckling, so that confinement of the column in a clear acrylic tube was necessary to prevent damage to the steel blocks and the loading knife edges by falling on hard surfaces after failure.

#### 5.2.1.2 Boundary conditions

The column was loaded with two types of end support conditions —

(a) restrained from lateral translation but free to rotate both at the top and at the base (pinned end condition).

(b) restrained from lateral translation and free to rotate at the top only (fixed base condition).

The load eccentricity was nominally either one-fifth or one-tenth the section thickness, the load being applied successively on either side of the column centreline as a test of the symmetry of the set up. A summary of the test conditions is given in Table 5.7.

#### 5.2.1.3 Instrumentation

Lateral deflections were measured by dial gauges at column mid-height for the pin-end column tests and at third points for the fixed base column tests. Deflections at the column supports were also checked in all tests and the loads were measured by a hydraulic load cell at the column base (figure 5.9).

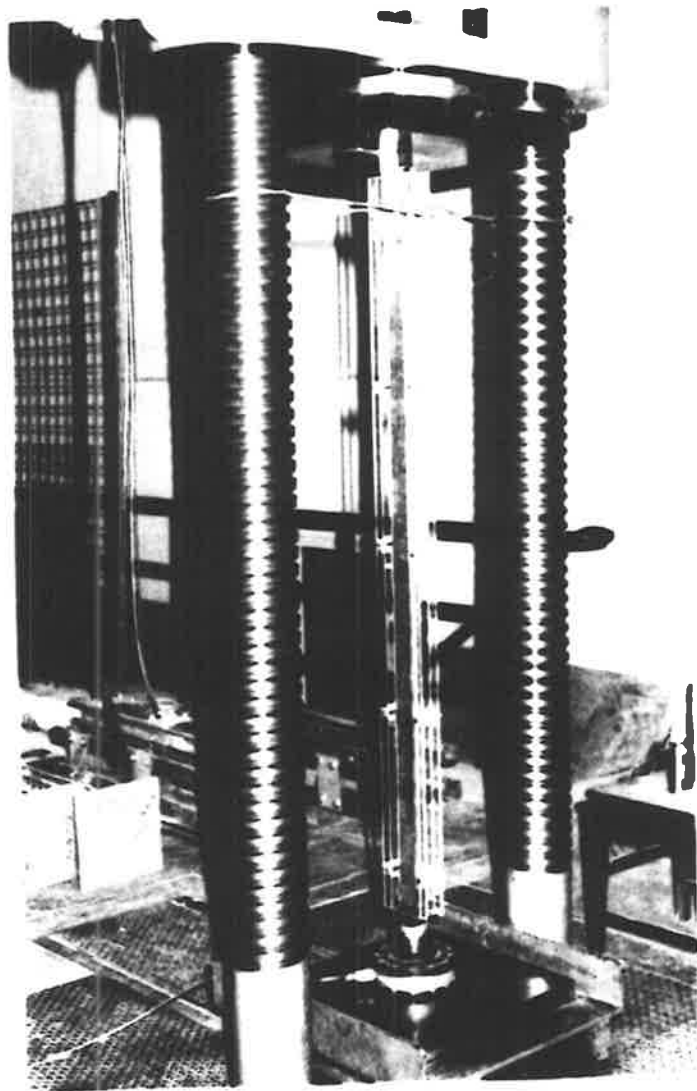


Figure 5.9(a): Steel Block Column  
Inside Clear Acrylic Tube

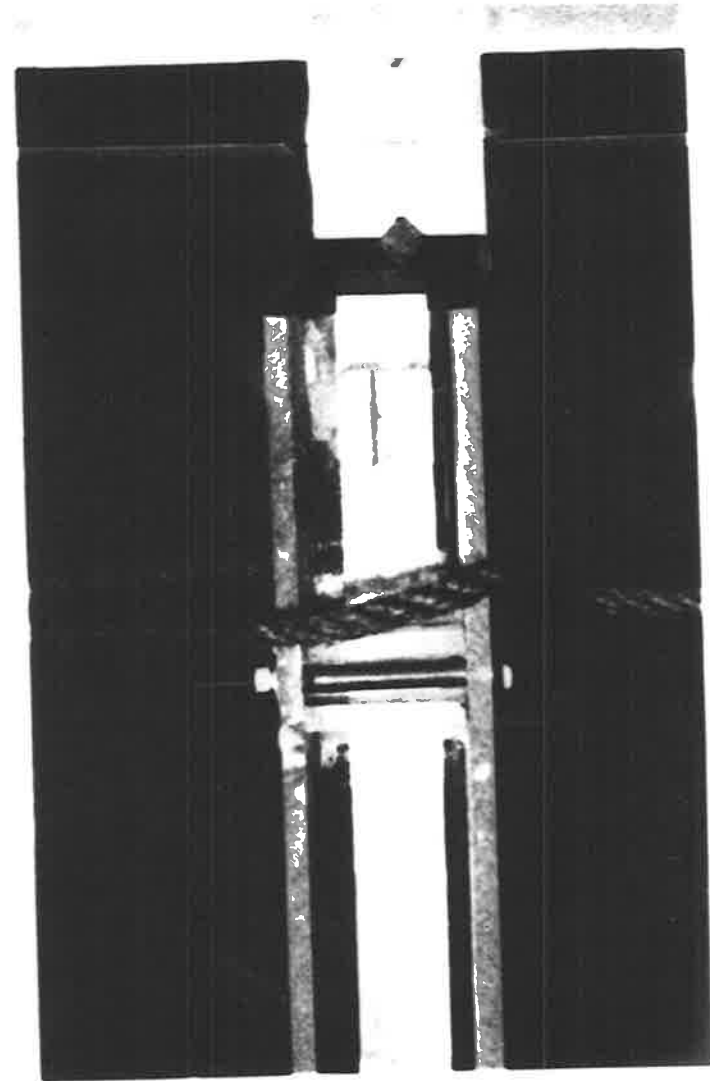


Figure 5.9(b): Knife-edge Loading  
at Top of Steel Column

Figure 5.9: Steel Block Column Test



Test No.	Boundary Conditions (refer to text)	Load Eccentricity (a), (b)	
		Top	Base
1	Case (a)	+d/ 4.83	+d/ 4.83
2	Case (a)	-d/ 4.83	-d/ 4.83
3	Case (a)	+d/10.6	+d/10.6
4	Case (a)	-d/10.6	-d/10.6
5	Case (b)	+d/ 4.83	Fixed
6	Case (b)	-d/ 4.83	Fixed
7	Case (b)	+d/10.6	Fixed
8	Case (b)	-d/10.6	Fixed

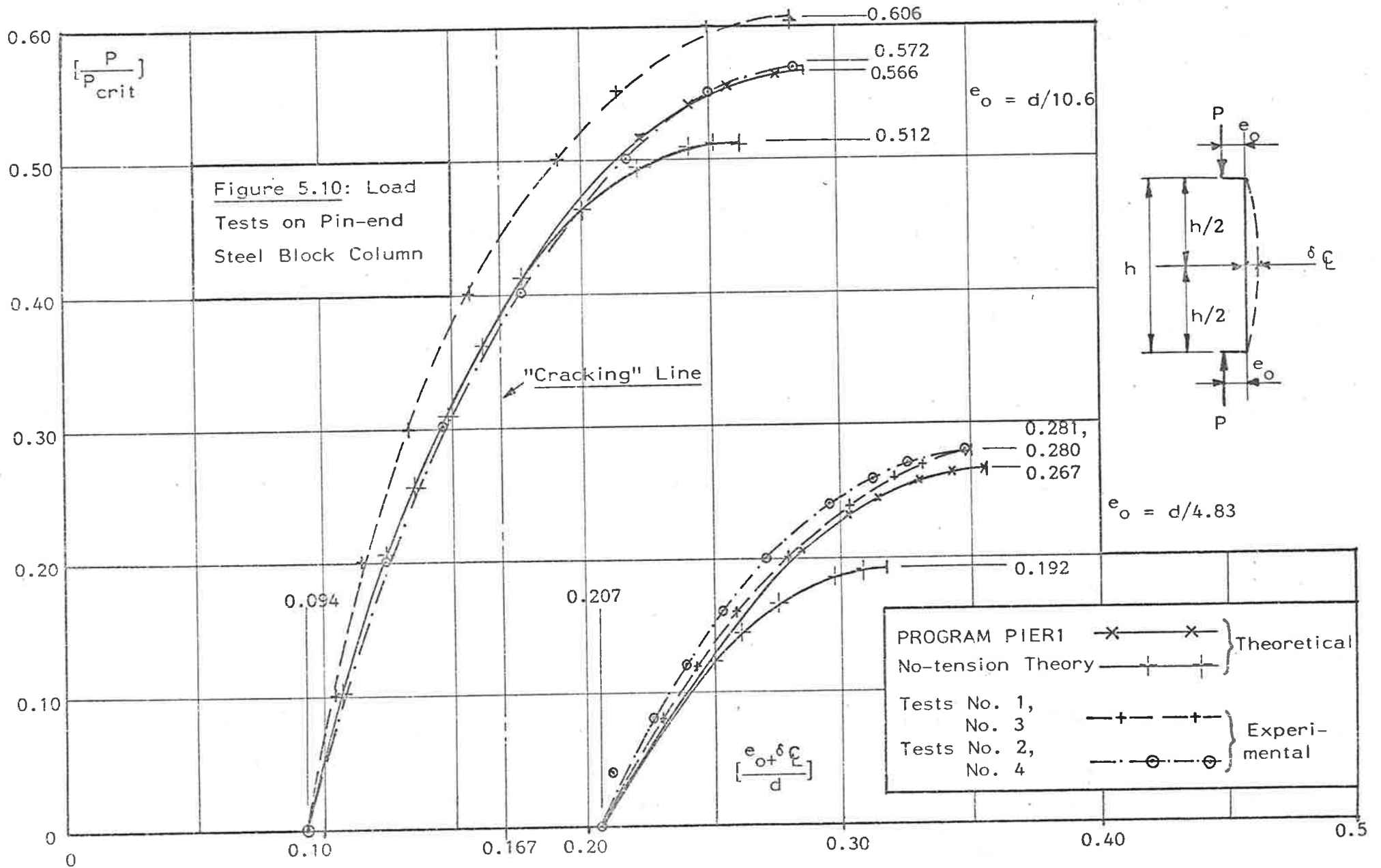
(a) "+" and "-" refer to loading on opposite sides of column centreline

(b) d is column thickness (nominally 25mm)

Table 5.7: Column End Conditions and Load Eccentricities

#### 5.2.1.4 Experimental results

The results of the pin-end column tests were compared with the load-displacement characteristics calculated by PROGRAM PIER1 (Appendix C) and the no-tension theory of Chapman and Slatford<sup>(97)</sup> (figure 5.10). From the differences in the initial slopes of the theoretical and experimental curves, it was evident that there was some lack of straightness in the column, possibly caused by mismatch at the steel block interfaces. Nevertheless, the test failure loads and maximum central deflection prior to failure were more closely predicted by PROGRAM PIER1 than by the no-tension theory, particularly at the greater load eccentricity (Table 5.8). The average of the two experimental curves is very close to the predicted curve of PROGRAM PIER1 (figure 5.10).



Load Eccentricity (mm)	Failure Load $(P/P_{crit})^{(a)}$			Max. Centre Displacement Prior to Failure $(\delta_C/d)^{(c)}$		
	Test <sup>(b)</sup>	No-tension	PIER1	Test <sup>(b)</sup>	No-tension	PIER1
$d/10.6^{(c)}$	0.589	0.512	0.566	0.28	0.246	0.284
$d/4.83^{(c)}$	0.280	0.192	0.267	0.35	0.317	0.355

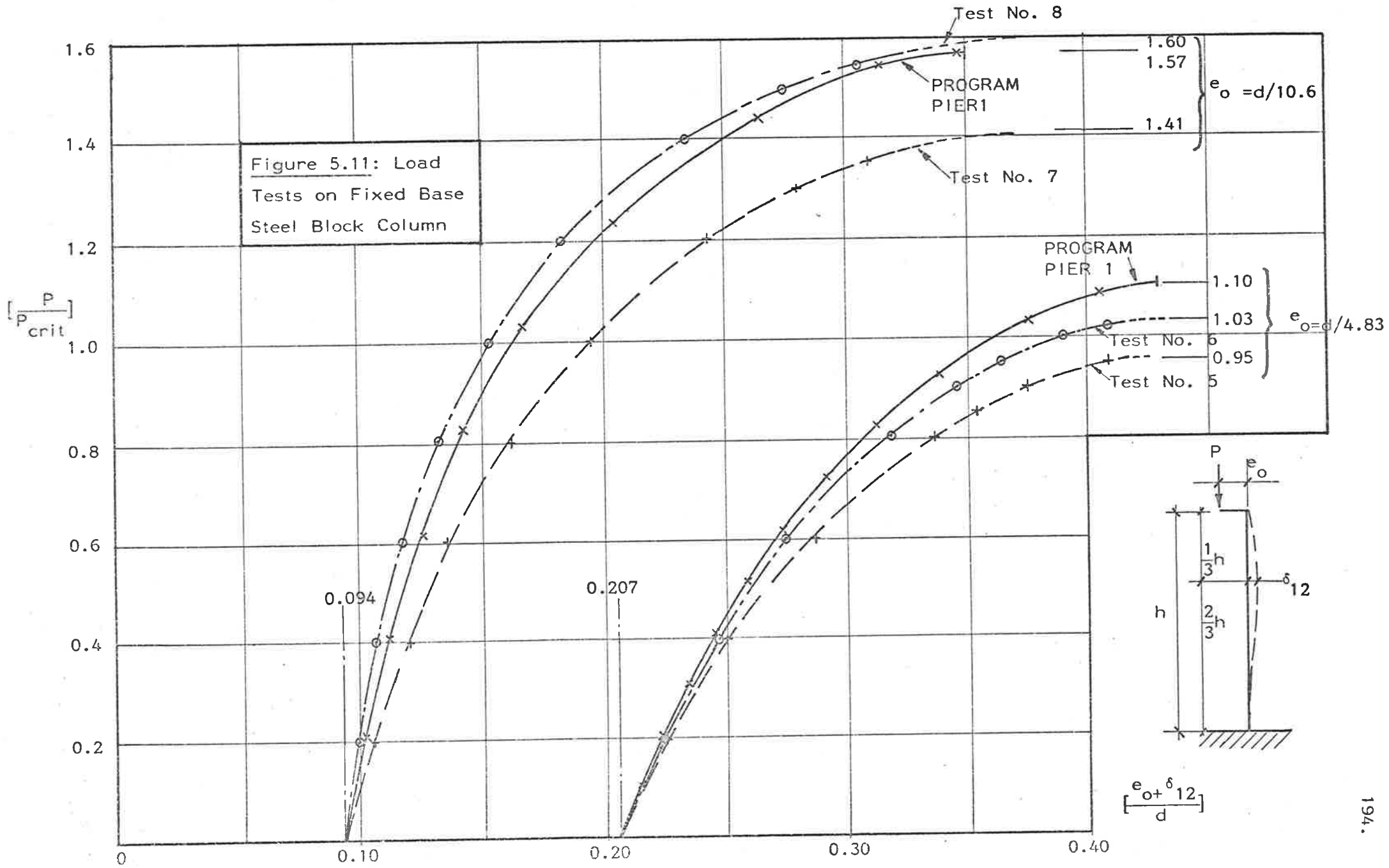
(a)  $P_{crit}$  is the Critical Buckling Load of a pin-end column.

(b) Average of 2 tests – pin-end columns.

(c)  $d$  is column thickness (nominally 25mm)

Table 5.8: Buckling Failure Loads and Displacements of Pin-end Column

The results of the fixed base tests were compared with the calculated results from PROGRAM PIER1 (figure 5.11). Again, the lack of straightness in the column was evident in the differences between initial slopes of the theoretical and experimental curves. However, the agreement between experimental and theoretical failure loads was close. Failure loads calculated by a no-tension material theory<sup>(44)</sup> (figure 3.42) agree closely with the experimental results provided that a suitable estimate is made of the column effective height,  $\lambda h$  (Table 5.9). This indicates that the tension field stiffening effect of the blocks is not as significant in a fixed base column as in a column with pinned ends (Table 5.8). Although the two estimates of  $\lambda$  in Table 5.9 give good agreement with the tests, in most practical design cases the column effective length cannot be calculated easily for the fixed base column.



Load Eccentricity (mm)	Non-dimensional Failure Load ( $P_f/P_{crit}$ ) <sup>(a)</sup>			
	Test <sup>(b)</sup>	No-tension <sup>(d)</sup>		PROGRAM PIER1
		$\lambda=0.67$	$\lambda=0.70$	
$d/10.6$ <sup>(c)</sup>	1.50	1.58	1.45	1.57
$d/4.83$ <sup>(c)</sup>	0.99	0.98	0.90	1.10

(a)  $P_{crit}$  is the critical buckling load of a column with pinned ends.

(b) Mean of two tests.

(c)  $d$  is column thickness (nominally 25mm).

(d)  $\lambda=0.67$  from PROGRAM PIER1

$\lambda=0.70$  from column theory<sup>(44)</sup>

Table 5.9: Buckling Failure Loads for Fixed Base Columns

### 5.2.1.5 Conclusions on steel column tests

The experimental results presented by Chapman and Slatford as "confirmation" of the validity of no-tension theory for brickwork did not agree with the calculations produced by the more rigorous finite element model contained in PROGRAM PIER1. Repetition of the experiments using an articulated steel column showed that the reported results obtained with the aluminium column were not repeated. As has been stated (Section 3.4.3), irregularities in the contact surfaces of the original aluminium blocks could have caused the differences between the initial slopes of Chapman and Slatford's experimental results and the no-tension theory curves. Moreover, in Chapman and Slatford's tests<sup>(97)</sup>, the maximum column displacements immediately prior to failure were closer to those predicted by PROGRAM PIER1 than by the no-tension theory (Table 5.8). Therefore, the experiments on a pin-end steel block column have shown that the results of Chapman

and Slatford's experiments cannot be used as confirmation of the validity of the no-tension theory of brickwork.

In contrast, results of tests on both pin-end and fixed-base steel block columns agree closely with results obtained using PROGRAM PIER1 thus indicating that the finite element model incorporated into PROGRAM PIER1 is a better predictor of the behaviour of a linear elastic column under eccentric load than the no-tension theories proposed by Chapman and Slatford and Sahlin.

## 5.2.2 Tests on Brickwork Walls

### 5.2.2.1 Introduction

In Section 4.5, a parametric study was made on brickwork walls which were restrained against lateral translation at the top and base and either free to rotate at both the top and the base or free to rotate at the top but restrained against rotation at the base. Walls included in the parametric study were considered to be laid in either brick-on-flat or brick-on-edge configuration and the mortar properties were either linear or non-linear in the form given by equation (B.1), Appendix B. In this section, the results of a series of experiments are presented to assess the adequacy of the numerical predictions of PROGRAM PIER1 as applied to fixed base brickwork walls loaded eccentrically at the top. All brickwork material properties required for use in PROGRAM PIER1 were determined during the tests.

Although the number of tests was, of necessity, small, it is possible to make comparisons, both qualitative and quantitative, between the calculated displaced shapes, failure loads and failure modes and the respective experimental values.

### 5.2.2.2 Wall construction

Each of a total of eight walls was constructed against a timber frame to achieve a wall with one face as close as possible to a plane (figures 5.12(a), 5.12(b)). The wall dimensions are summarized in Table 5.10.

Wall No.	No. of Courses	Wall Dimension (mm)			Slenderness Ratio, h/d
		Height	Length	Thickness	
1	23	2714	714	75.0	36.2
2	12	1416	718	74.5	19.0
3	23	2714	711	74.9	36.2
4	12	1416	714	74.9	18.9
5	23	2714	710	75.1	36.1
6	12	1416	713	75.0	18.9
7	23	2714	714	74.2	36.6
8	12	1416	714	74.4	19.0
Mean		-	714	74.8	-

Table 5.10: Brickwork Wall Dimensions

The bricks for the walls were extruded, wire-cut and without performations and were selected with dimensions closely 108mm x 75mm x 228mm. They were also chosen for uniformity of colour and texture because the degree of vitrification, which may affect the brick material properties, is related to brick colour, texture and dimensions (Section 3.1). All bricks in the walls were laid in a saturated, surface-dry condition in an "on-edge" configuration, the base course being constructed in a 900mm length of 127 x 64 rolled channel section to allow transportation to the compression testing machine.

The mortar was 1 cement:1lime:6 sand by volume with a water-to-cement ratio of 1.41 by weight; the ratio of water-to-cementitious

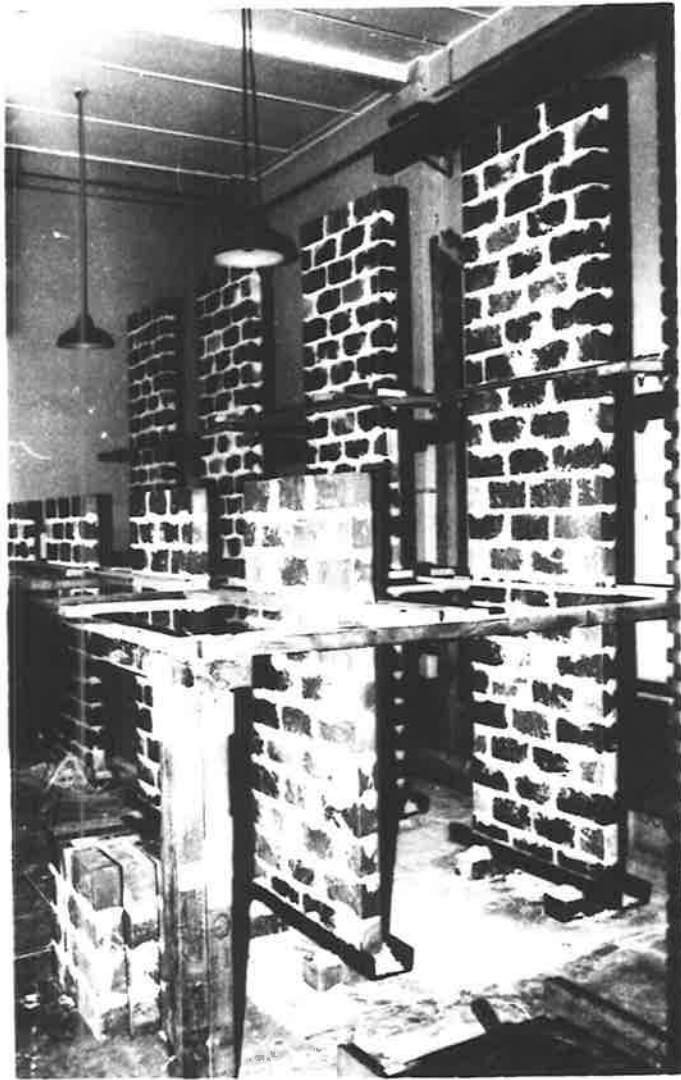


Figure 5.12(a): Eight Brickwork Walls

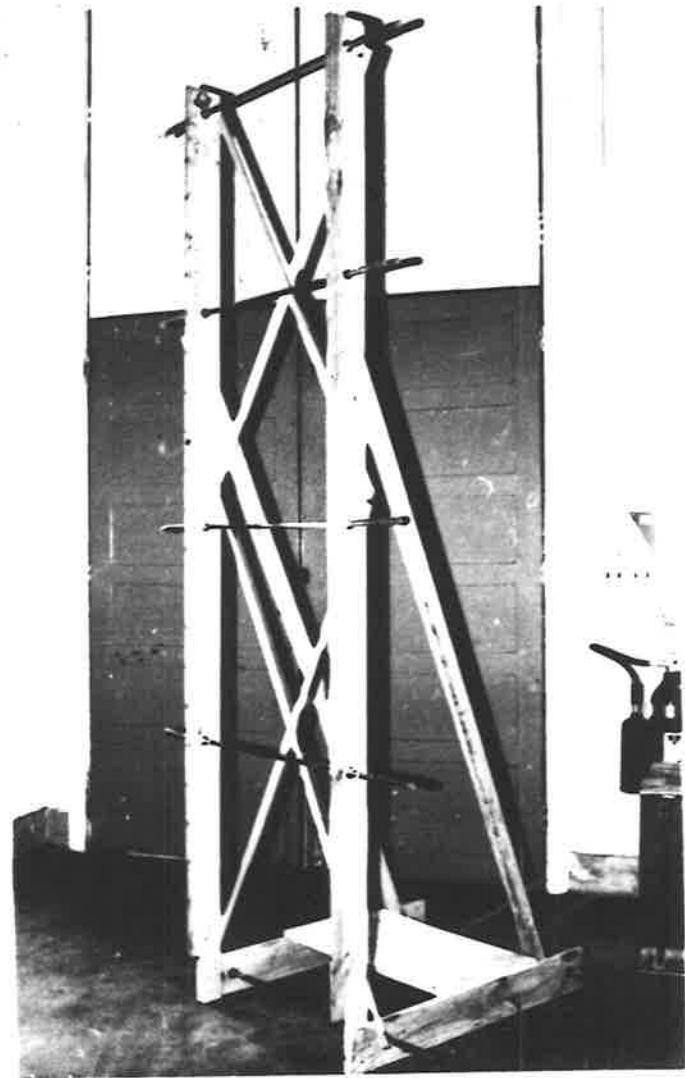


Figure 5.12(b): Timber Construction Frame

Figure 5.12: Brickwork Walls



material was 1.02 by weight. Hydrated lime powder and Portland Type A cement were used from fresh bags and the sand was oven-dried for 48 hours and sieved through a B.S. No. 7 sieve (2.40mm mesh). The sand grading curve is shown in figure 5.13.

The mortar was mixed in 15kg batches which remained workable for the  $1\frac{1}{2}$  hours required to lay twelve courses without the addition of water. Each of the tall walls was constructed in two sessions using two mortar batches on the one day, and three mortar prisms, each 25mm x 25mm x 50mm, were cast for each mortar batch at approximately three-quarters of an hour after construction commenced.

All walls were cured for 21 days covered with polythene sheeting and subsequently under ambient conditions. Six brickwork prisms, each four bricks high (figure 5.12(a)) were constructed simultaneously with the walls for measurement of the brickwork compressive strength. The method of curing was identical for the walls, mortar prisms and brickwork prisms.

### 5.2.2.3 Elastic modulus tests

#### (a) Bricks and Mortar

Six bricks were selected at random from the batch used for the walls and two prisms, approximately 25mm thick, were cut from each brick, as described in Section 5.1.3. ERS gauges were fixed to the prisms and the load-strain characteristics measured and plotted. The experimental elastic modulus values for the twelve prisms are given in Table 5.11.

The mean elastic modulus was  $18.2 \times 10^3$ MPa, with a coefficient of variation among bricks of 11.3 percent.

All mortar prisms cast were tested at a minimum 28 days in axial compression, as described in Section 5.1.3. The experimental initial

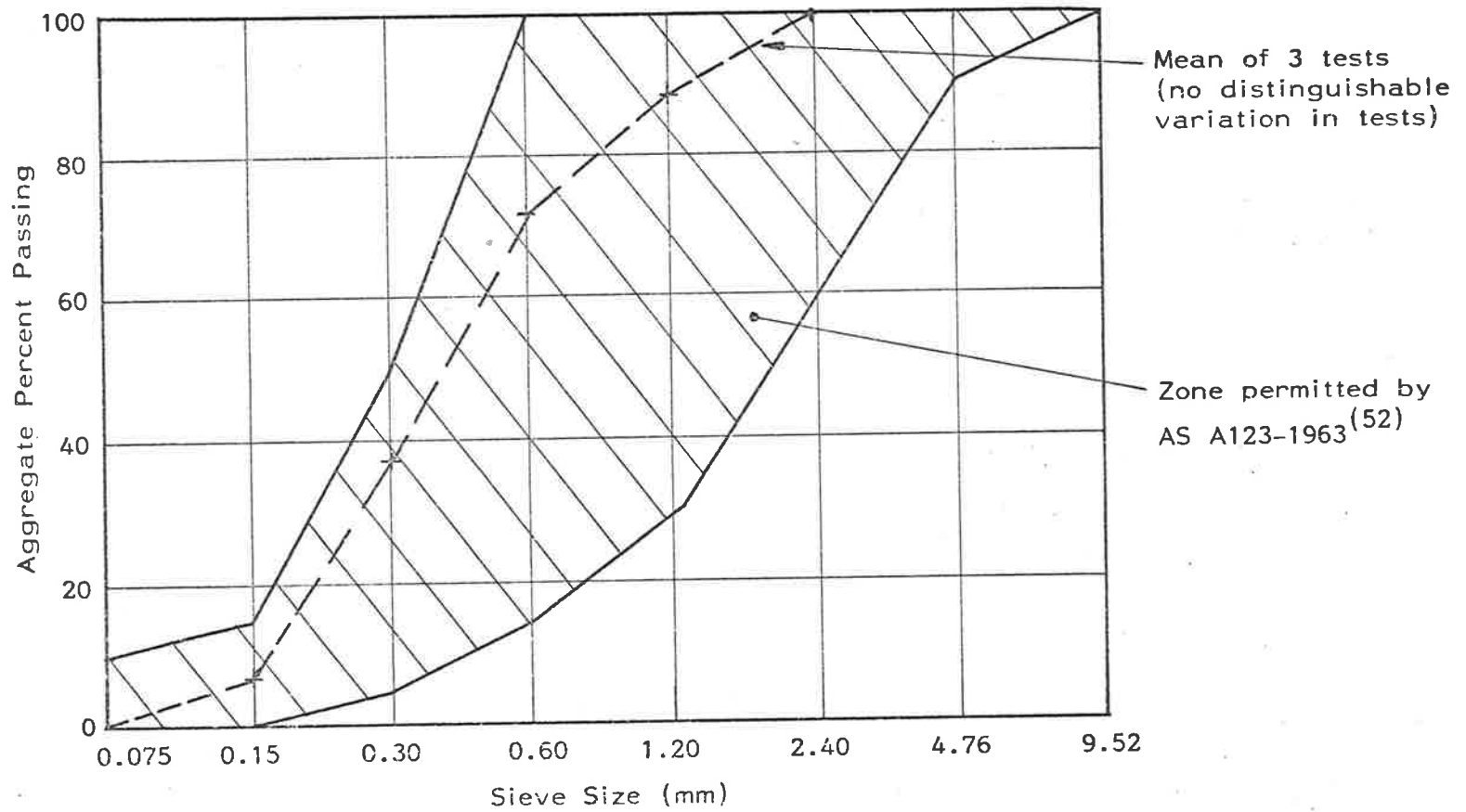


Figure 5.13: Grading Curve for Sand in Brickwork Walls

Brick No.	Elastic Modulus, $E_b$ ( $\times 10^3$ MPa)		
	Prism No. 1	Prism No. 2	Average
1	21.3	20.9	21.1
2	16.1	17.2	16.6
3	19.4	19.4	19.4
4	20.7	19.3	20.0
5	16.4	14.6	15.5
6	17.0	16.3	16.6

Table 5.11: Brick Elastic Modulus

tangent modulus values are summarized in Table 5.12. The average initial tangent modulus was  $8.29 \times 10^3$  MPa and the coefficient of variation among mortar batch averages was 17 percent. The coefficient of variation among prisms in any batch was less than 13 percent.

Mortar Batch	Wall No.	Elastic Modulus, $E_m$ ( $\times 10^3$ MPa)				C.V. %
		Prism 1	Prism 2	Prism 3	Average	
1	1	8.51	8.08	8.44	8.34	3.6
2		5.44	5.41	6.06	5.64	4.0
3	2	6.33	6.44	6.38	6.38	0.7
4	3	6.99	8.81	6.72	7.51	12.4
5		9.63	9.72	8.60	9.32	4.8
6	4	6.42	6.29	6.12	6.28	2.0
7	5	9.78	8.96	8.09	8.94	7.7
8		9.40	10.43	8.34	9.39	9.1
9	6	10.00	9.75	8.86	9.54	5.1
10	7	9.36	9.25	7.23	8.61	11.4
11		9.75	9.62	9.22	9.53	2.4
12	8	11.20	8.94	9.75	9.96	9.4

Table 5.12: Mortar Elastic Modulus

(b) Tests on Walls

All walls were capped with a 900mm length of 127 x 64 M.S.C. bedded in a high alumina grout to permit early testing of the walls. For all walls, the base channel was restrained against rotation by bedding it into a thin layer of freshly mixed "Plasti-bond" polyester resin spread on the rigid base platen of a 5000KN capacity compression testing machine. Four sets of steel blocks with machined and greased pins, each 100mm long, were placed centrally along the top of each wall as shown in figure 5.14, and the wall was loaded up to 100KN in 10KN increments. At each load increment, the axial shortening was measured and an effective elastic modulus for the wall was calculated. With reference to figure 5.14, the gauge length for the 12-course walls (walls 2, 4, 6 and 8) was nine courses (1062mm) and for the 23-course walls (walls 1, 3, 5 and 7) was ten courses (1180mm). The relationship between load and axial shortening was linear for each wall; a summary of the calculated effective brickwork moduli is given in Table 5.13. The average value of effective brickwork modulus was  $15.0 \times 10^3$  MPa with a coefficient of variation of 3.5 percent.

Wall No.	Gauge Length (mm)	Brickwork Modulus $E_{br}$ ( $\times 10^3$ MPa)
1	1180	14.5
2	1062	14.3
3	1180	14.7
4	1062	14.4
5	1180	15.6
6	1062	15.1
7	1180	15.5
8	1062	15.6

Table 5.13: Brickwork Elastic Modulus

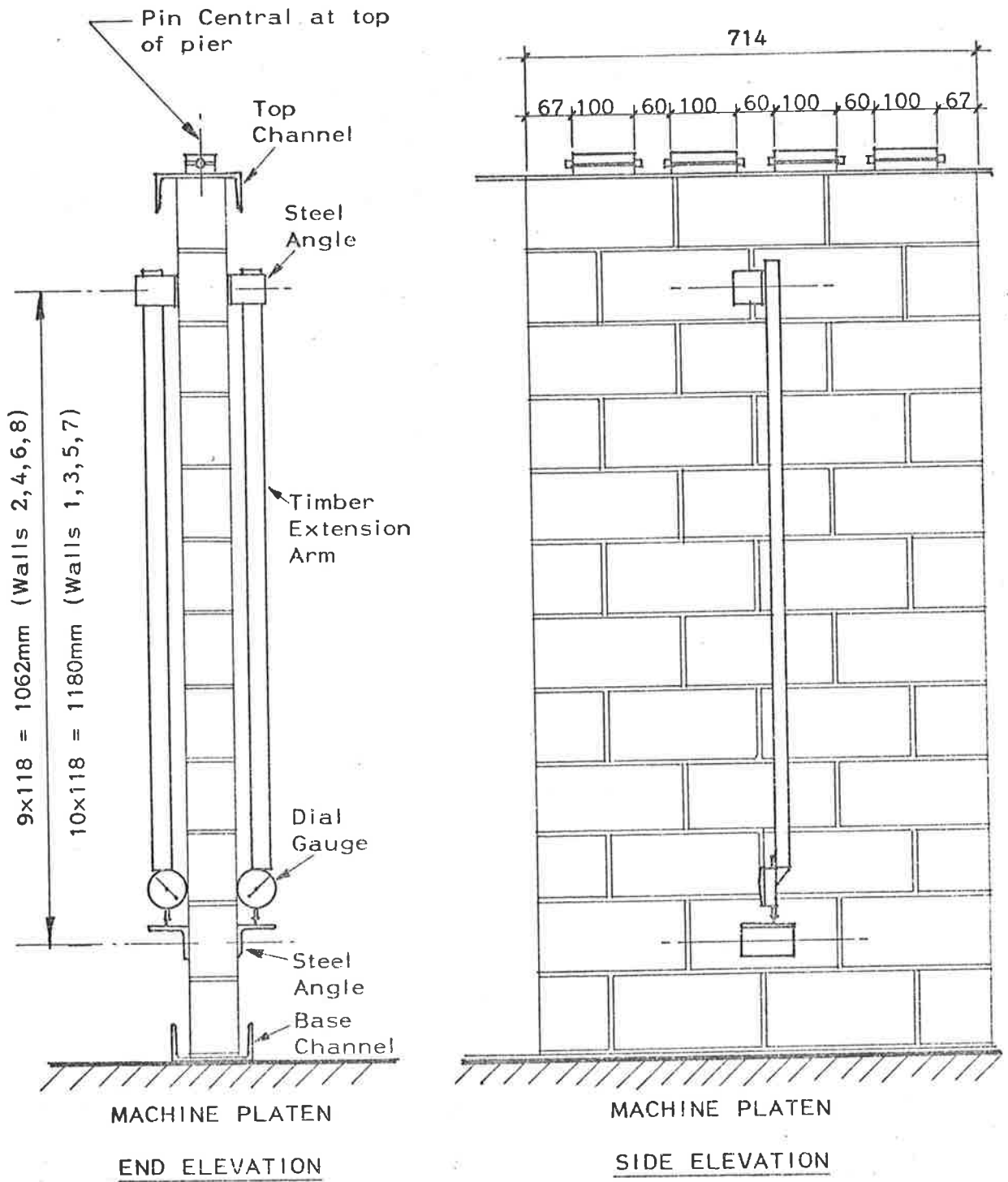


Figure 5.14: 1416mm High Wall Showing Apparatus for Determination of Brickwork Elastic Modulus (Typical for 2714mm Walls)

(c) Summary of Elastic Modulus Tests

From the experimental results summarized in Tables 5.11 and 5.12, the effective elastic modulus for brickwork, according to equation (5.4), should be  $16.5 \times 10^3$  MPa. This value, calculated from the separate moduli of the bricks and mortar, is approximately 10 percent higher than the effective modulus obtained directly from brickwork wall tests (Table 5.13). However, the two calculated means of the effective elastic modulus values for brickwork are within one standard deviation of the brick modulus values (Table 5.11), so that the two sets of modulus values may be assumed to be from the same statistical population of means.

The large variation in mortar modulus (Table 5.12) did not cause large variations in the overall brickwork modulus in comparison with that caused by the variation in brick modulus. Equation (5.4) shows that the mortar modulus does not exert a major influence on the brickwork elastic modulus for the cases in which brick and mortar moduli are approximately equal. Therefore, the experimental results (Tables 5.11, 5.12 and 5.13) indicate that a sample size of six bricks was insufficient to obtain a good estimate of the mean brick elastic modulus of the batch.

Consequently, in the following section, in which eccentric load tests on the walls are described and compared with the calculated results of PROGRAM PIER1, a brickwork elastic modulus of  $15.0 \times 10^3$  MPa is used in PROGRAM PIER1. Values of brick and mortar moduli consistent with equation (5.4) and the results of tests on brick and mortar prisms, as well as the brickwork walls, have been chosen to be  $16.2 \times 10^3$  MPa and  $8.3 \times 10^3$  MPa respectively.

#### 5.2.2.4 Eccentric Load Tests on Fixed Base Walls

##### (a) Non-destructive Load Tests

Experiments were first conducted on the eight walls (Section 5.2.2.2) to check under eccentric loading the correlation between the lateral displacements calculated by PROGRAM PIER1 and the measured wall profiles.

Each of the four short piers (1416mm) was placed in a 5000KN compression testing machine and loaded through pin blocks as shown in figure 5.15. Lateral displacements were measured by dial gauges, placed as shown, and end rotations were measured close to the top and base steel channel sections by bubble micrometers as in previous tests (Section 5.12, figure 5.6). The out-of-plane imperfections on the face built against the timber construction frame were measured and found to be less than 1.0mm. Each wall was loaded successively at eccentricities of 12.5mm ( $d/6$ ) and 25mm ( $d/3$ ) at the top, the base being rigidly fixed against rotation. The wall was loaded to 100KN; at every 10KN increment the lateral displacements and end rotations were recorded. The set of load-displacement results for wall 2 (figure 5.16) showed that for loads up to 20KN there was some settling in the wall, possibly caused by shrinkage in the mortar joints (Sahlin<sup>(44)</sup>) and end supports, but, between 20KN and 100KN, the lateral displacements varied almost linearly with the load. Linear load-displacement relationships were observed for all short walls tested.

A plot of load against rotation at the top of wall 2 (figure 5.17) showed that, between loads of 20KN and 100KN, the rotation varied linearly with the applied load. Figure 5.17 shows only the results for a 25mm load eccentricity on wall 2, but the load-rotation relationships were essentially linear for all short walls at both test load eccentricities when the loads were between 20KN and 100KN.

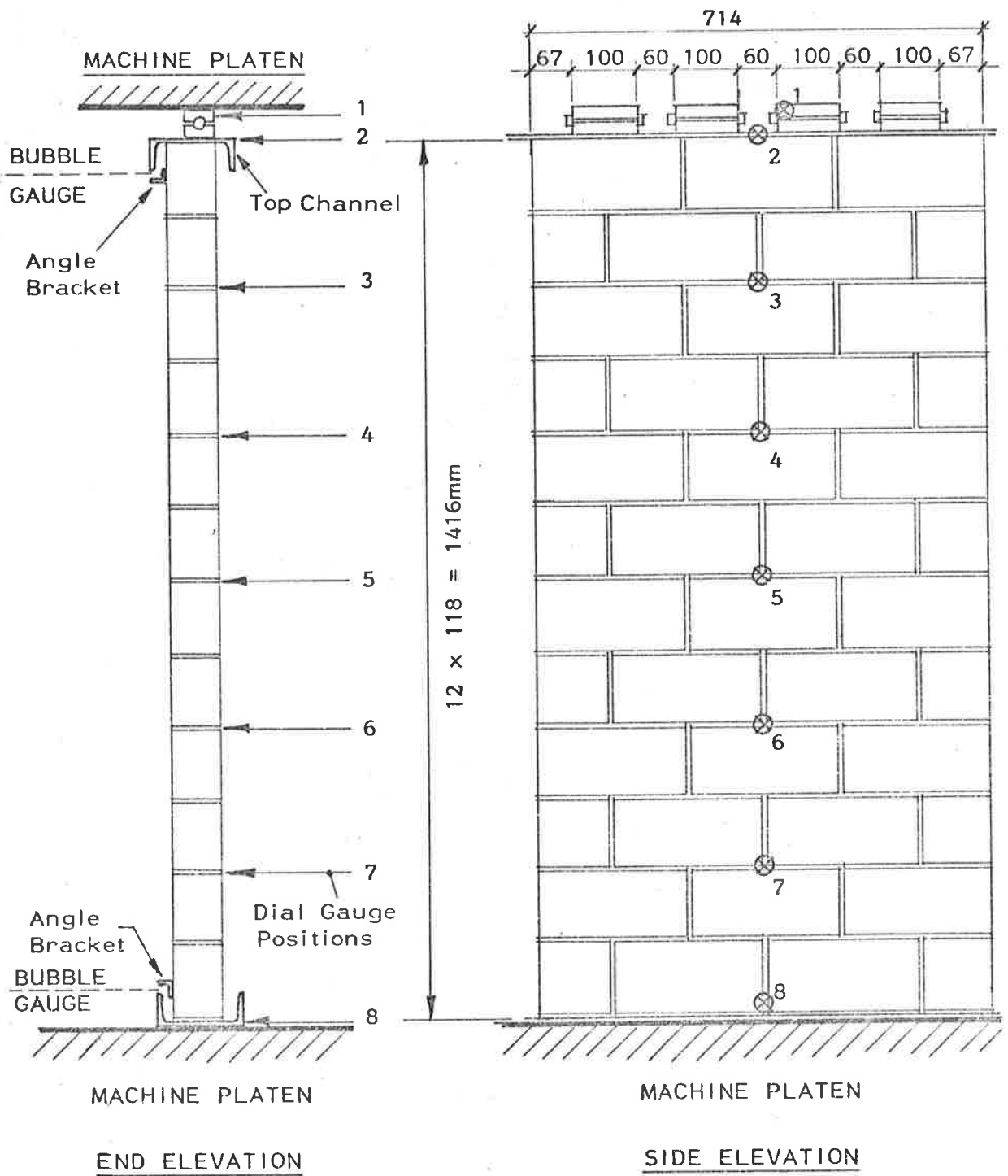


Figure 5.15: 1416mm Wall Loaded Eccentrically at the Top (Base Fixed Against Rotation)



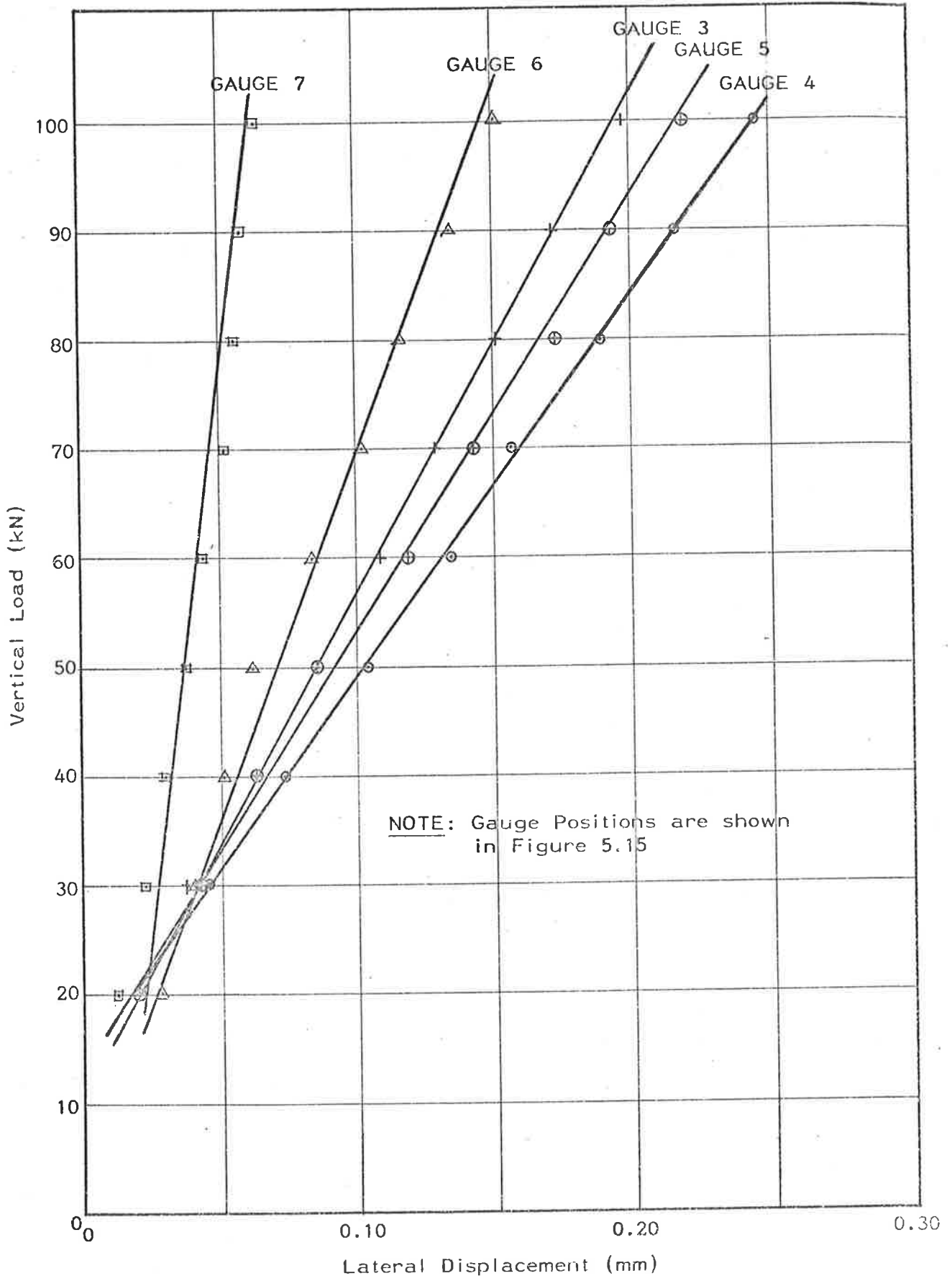


Figure 5.16: Load Displacement Relationships for 1416mm Height Fixed Base Walls (Wall No. 2)

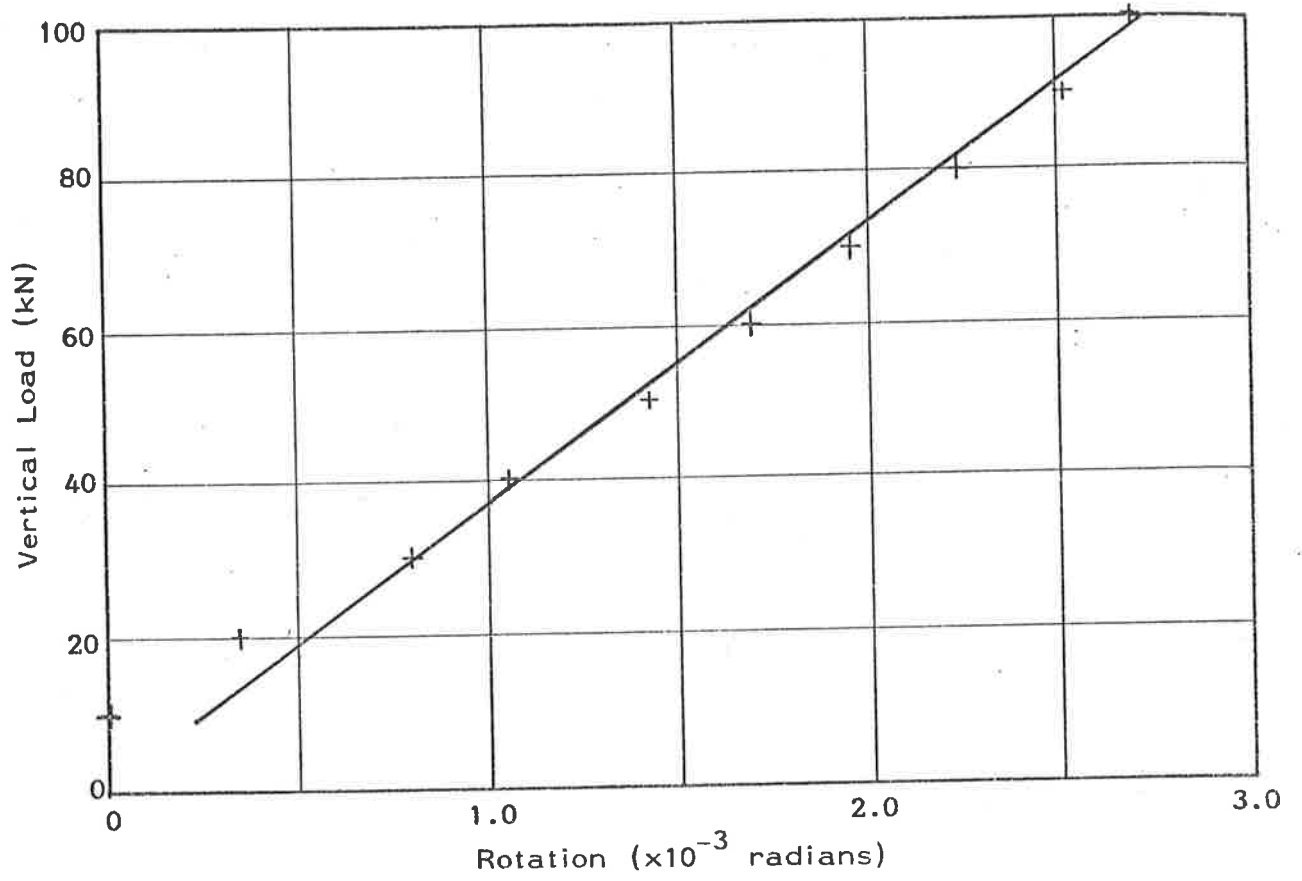


Figure 5.17: Load-Rotation Relationship for 1416mm High Wall with Fixed Base

Graphs of the lateral displacement profiles for the short walls are shown in figures 5.18 and 5.19 in which the average profile is compared with a theoretical displaced shape computed using PROGRAM PIER1 and the material properties in Section 5.2.2.3. The spread of experimental results is more pronounced for the lower load eccentricity, but overall, the theoretical and experimental displacement profiles are comparable, the differences being consistent for the two load eccentricities. Several possible reasons for the differences are discussed later in this section.

The changes in slope at the top of each of the short (1416mm) walls as the load increased from 20KN to 100KN are summarized in Table 5.14.

Wall No.	Change in Slope ( $\times 10^{-3}$ rad/80KN)	
	Eccentricity 12.5mm	Eccentricity 25mm
2	1.31	2.14
4	1.41	2.35
6	1.25	2.30
8	0.90	1.85
Average	<u>1.22</u>	<u>2.16</u>
C.V.	15.8%	9.0%
PROGRAM PIER1	<u>0.94</u>	<u>2.12</u>

Table 5.14: Changes in Slope at Top of 1416mm High Walls

The change in slope at the base of each short wall was found to be insignificant.

Each of the four tall walls (2714mm) was tested in the same way as the short walls. The dial gauge positions were as in Table 5.15.

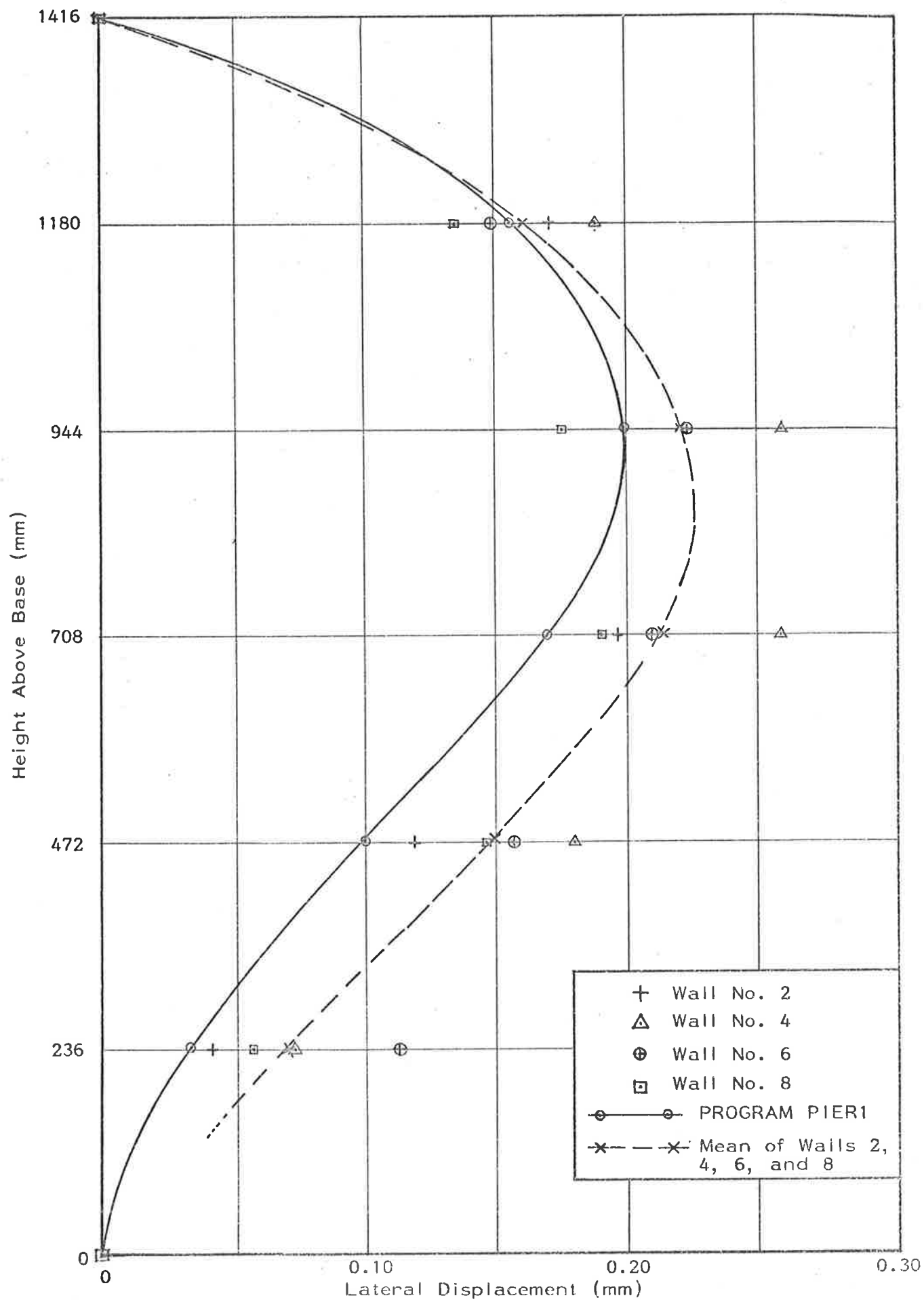


Figure 5.18: Initial Displacement Profiles for 1416mm Walls with Fixed Base; Top Load Eccentricity  $d/6$

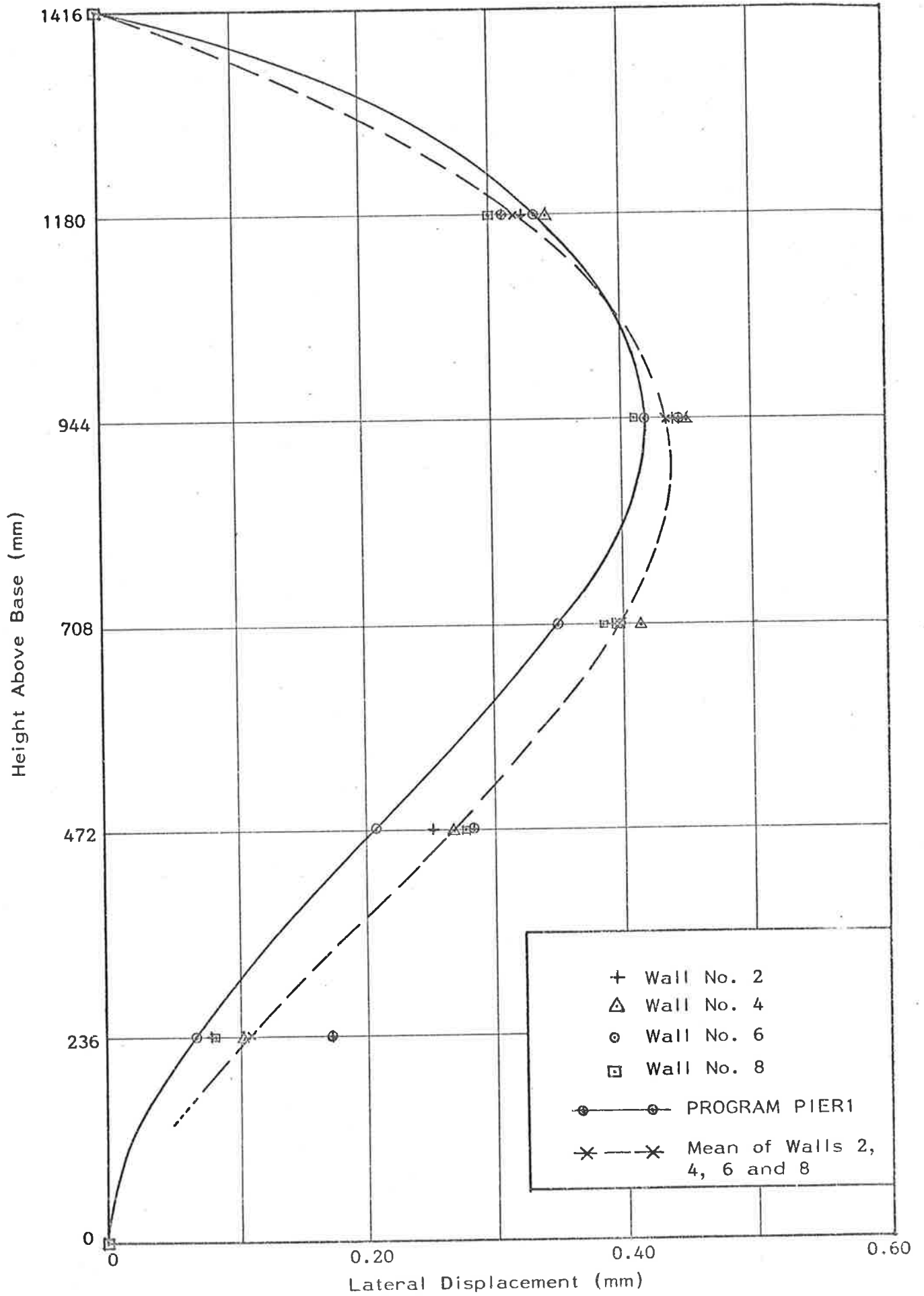


Figure 5.19: Initial Displacement Profiles for 1416mm Walls with Fixed Base; Top Load Eccentricity  $d/3$

Gauge No. (ref. figure 5.15)	Height Above Wall Base (mm)
1	top platen
2	2714
3	2242
4	1770
5	1298
6	826
7	354
8	zero

Table 5.15: Positions of Dial Gauges for Tall  
(2714mm) Walls

The out-of-plane imperfections on the face built against the timber construction frame were measured and found to be less than 1.0mm. The base of each wall was restrained against rotation, as described in Section 5.2.2.3, and each wall was loaded successively at eccentricities of 12.5mm ( $d/6$ ) and 25mm ( $d/3$ ) as for the short (1416mm) walls.

The wall was loaded to 100kN; at every 10kN increment the lateral displacements and end rotations were recorded. For all tall walls, the load-lateral displacement relationships were essentially linear for loads between 20kN and 100kN. Graphs of the lateral displacement profiles for the tall walls are given in figures 5.20 and 5.21 for load eccentricities of 12.5mm and 25mm respectively, and the average profile is compared with the theoretical displacement profile computed by PROGRAM PIER1 using the material properties specified in Section 5.2.2.3. The results for wall 1 were not included in the average profile because the method used for fixing the wall base did not restrain adequately the base of the wall from rotation (figure

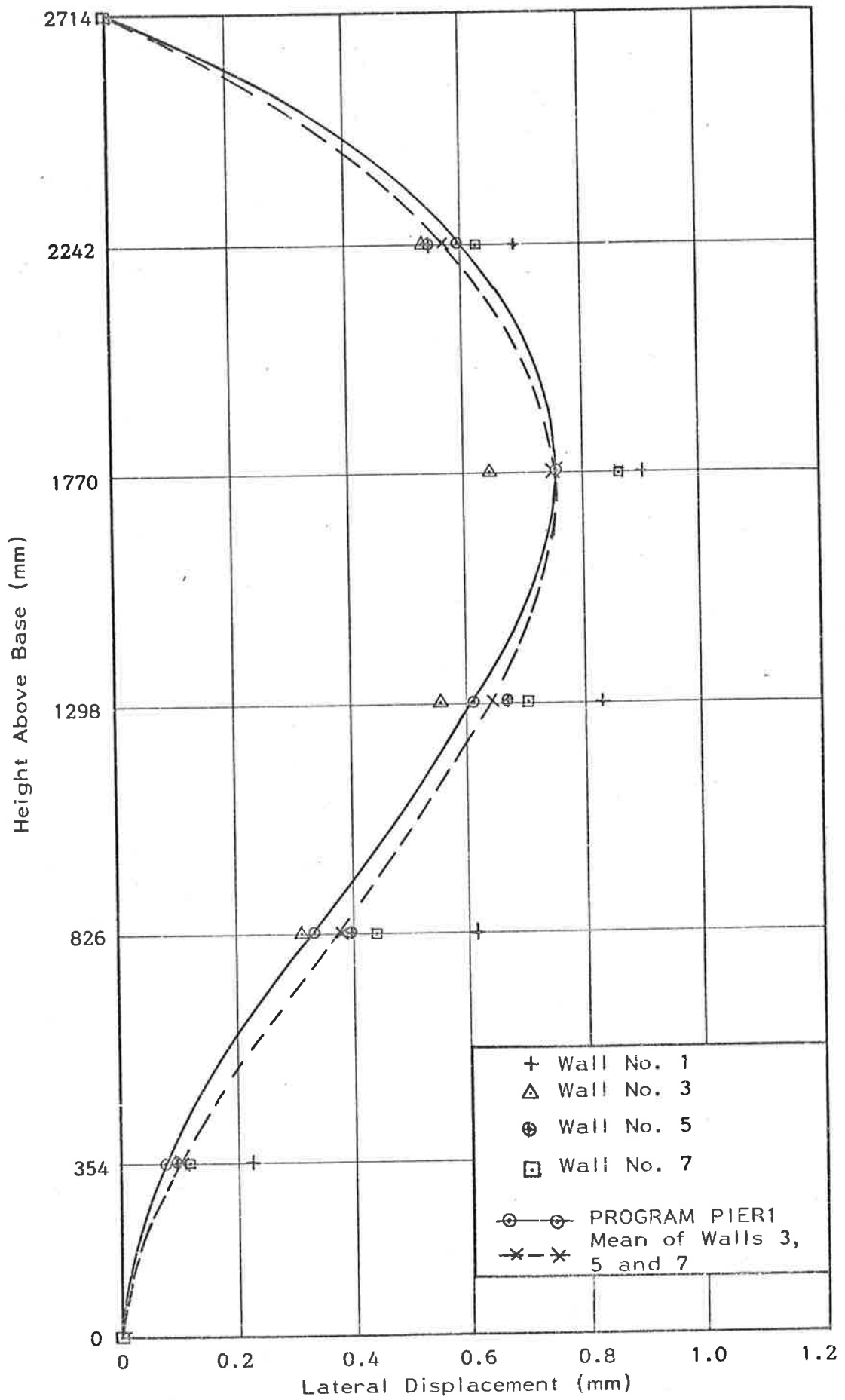


Figure 5.20: Initial Displacement Profiles for 2714mm Walls with Fixed Base; Top Load Eccentricity  $d/6$

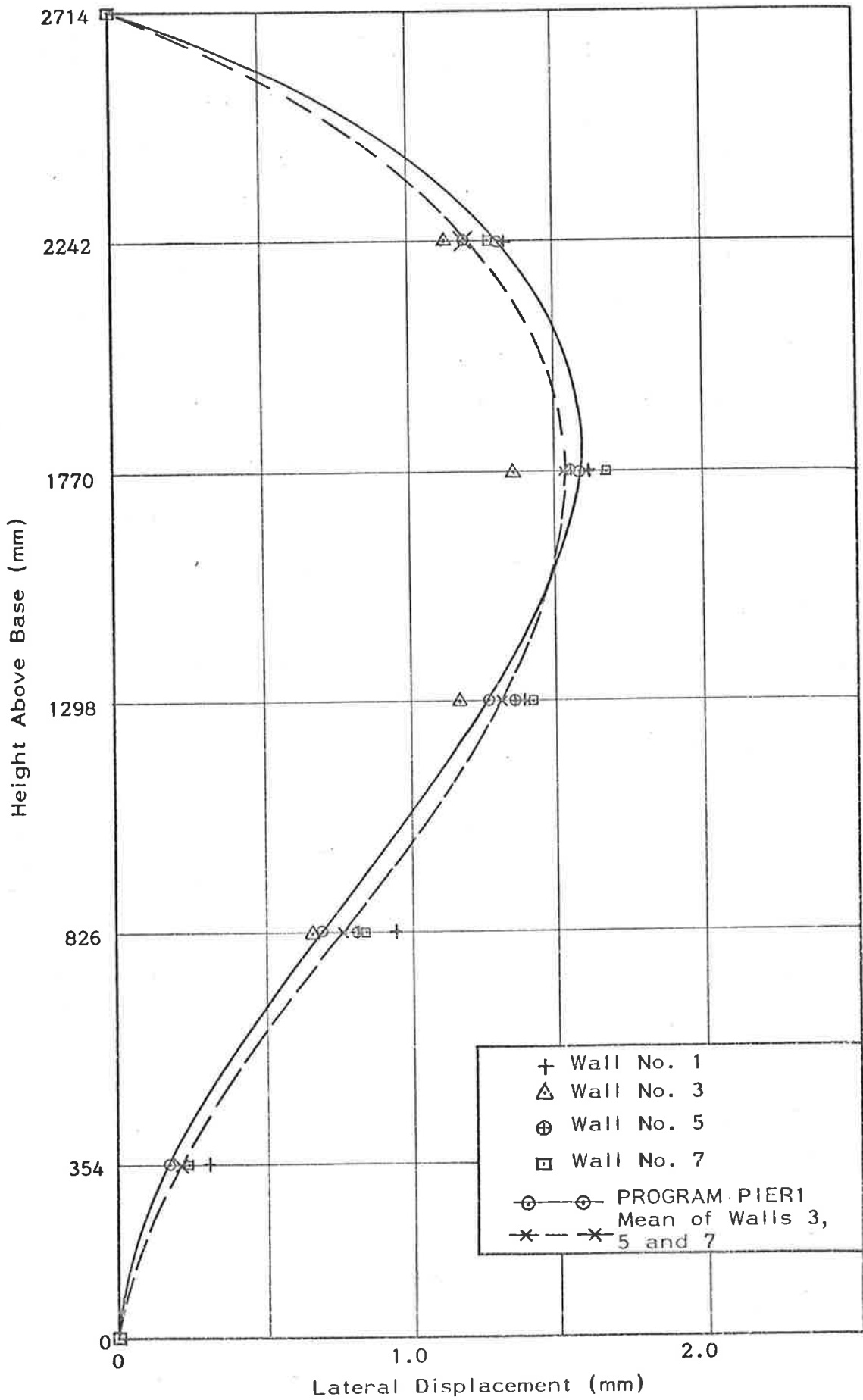


Figure 5.21: Initial Displacement Profiles for 2714mm Walls with Fixed Base; Top Load Eccentricity  $d/3$



5.20). The spread of results for walls 3, 5 and 7 was similar for both load eccentricities, and for both loading cases the theoretical and average experimental profiles were closely comparable. The change in slope at the top of each tall wall between loads of 20KN and 100KN is summarized in Table 5.16. For all tall walls, the change in slope at the base was insignificant.

In wall 1, for loads greater than 20KN, the change in slope at the base was small, but there was significant rotation at low load. This behaviour may have been caused by a low grout strength at the time of first testing.

Wall No.	Change in Slope ( $\times 10^{-3}$ rad/80KN)	
	Eccentricity 12.5mm	Eccentricity 25mm
1	2.30	5.13
3	2.12	4.31
5	2.13	4.22
7	1.74	4.40
Average <sup>(a)</sup>	<u>2.00</u>	<u>4.31</u>
C.V. <sup>(a)</sup>	9.1%	1.7%
PROGRAM PIER1	<u>1.86</u>	<u>4.35</u>

(a) Statistics on walls 3, 5, 7 only (refer to text).

Table 5.16: Changes in Slope at Top of 2714mm High Walls

In summary, the non-destructive tests on the eight fixed base walls at load eccentricities of 12.5mm ( $d/6$ ) and 25mm ( $d/3$ ) showed linear relationships between load and displacements, including end rotations.

Small initial movements at the wall base, which effectively would result from a partial release of full rotational fixity, would have produced the differences between experimental and theoretical displacement profiles and end rotations, particularly in the short walls (figures 5.18, 5.19). Small errors in placing the eccentrically-located pin blocks also could have led to differences between experimental and theoretical results, particularly at the 12.5mm eccentricity ( $d/6$ ).

In general, however, the tests showed an acceptable degree of agreement with displacements and rotations calculated by PROGRAM PIER1 (Tables 5.14, 5.16) using the material properties specified in Section 5.2.2.3. In all computations, the mortar was assumed linear because the stress levels were low and because the axial load tests on the walls (Section 5.2.2.3) did not indicate that the mortar was non-linear at loads up to 100KN. However, for the subsequent wall tests to failure, the theoretical predictions were based on PROGRAM PIER1 with an assumed non-linear mortar behaviour.

(b) Load Tests to Failure

For the load tests to failure, the rotations at the top of the walls and the lateral movements of the top and base supports were measured on the assumption that the wall behaviour could be assessed satisfactorily by comparing only the measured and calculated end rotations. This assumption was based on test results given in Sections 5.1.2 and 5.1.3. A summary of the load eccentricities, failure loads and failure modes is given in Table 5.17.

Three modes of failure were observed. All the tall walls (1, 3, 5 and 7) collapsed by lateral buckling; no visible distress was evident in either of the brick or mortar materials prior to collapse. However, the two modes of failure displayed by the short walls were —

Wall No.	Height (mm)	Load Eccentricity (mm)	Failure Load $P_f$ (KN)	Failure Mode
1	2714	12.5	503	Lateral Buckling
2	1416	12.5	780	Vertical Splitting
3	2714	25.0	293	Lateral Buckling
4	1416	25.0	584	Brick Spalling on Comp. Face
5	2714	12.5	550	Lateral Buckling
6	1416	12.5	800	Vertical Splitting
7	2714	25.0	290	Lateral Buckling
8	1416	25.0	765	Brick Spalling on Comp. Face

Table 5.17: Wall Failure Loads and Failure Modes

(a) a vertical splitting failure (Section 3.3), shown in figure 5.22 and (b) a brick spalling failure at the compression face of the wall (figures 5.23 and 5.24) for walls 8 and 4 respectively.

The second type of failure was not noted in a review of the literature. It differed from previously reported spalling due to bearing in which the mortar, usually of very low strength, had spalled by itself<sup>(44)</sup>. In the tests on walls 4 and 8, the spalling failure was preceded by a "powdering" of the mortar at the wall compression face, indicating that total failure of the mortar had occurred at the compression face of the joint. In wall 4, the spalling occurred at the third bedjoint (354mm) from the top and in wall 8 at the first (118mm) from the top. The brick spalling was probably precipitated by large lateral strains in the mortar at the compression face. The maximum thickness of the wedge-shaped pieces of brick which spalled off was

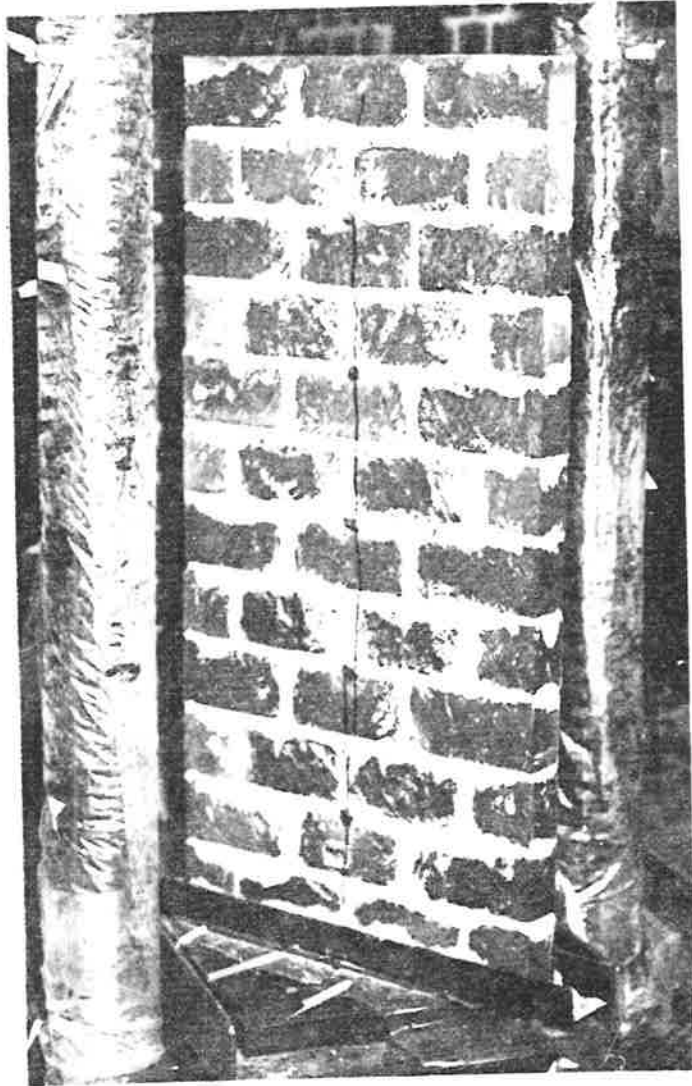


Figure 5.22: Vertical Splitting Failure (Wall 6)

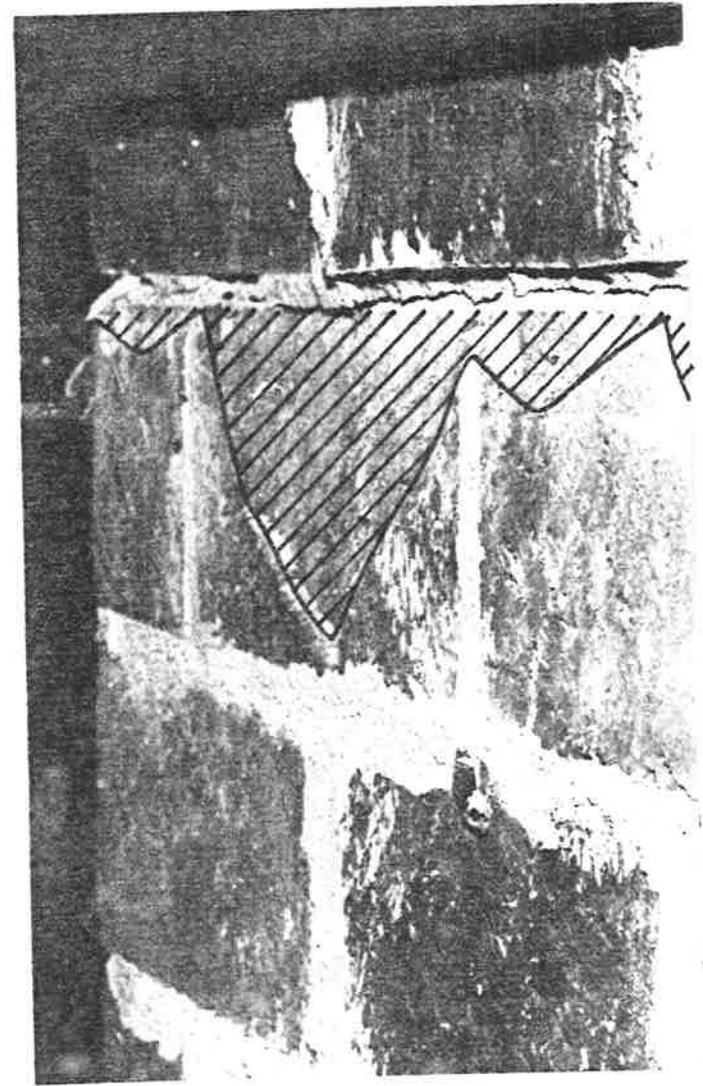


Figure 5.23: Spalling Failure (Wall 8)  
Showing Spalled Brick Hatched



Figure 5.24(a)

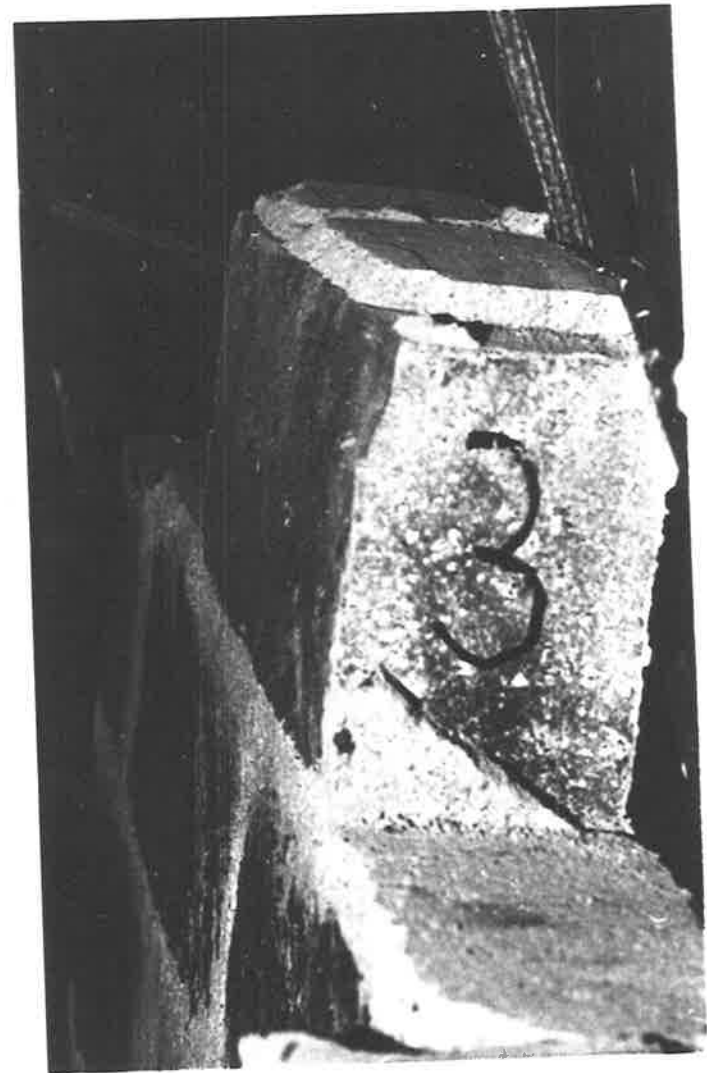


Figure 5.24(b)

Figure 5.24: Spalling Failure (Wall 4)

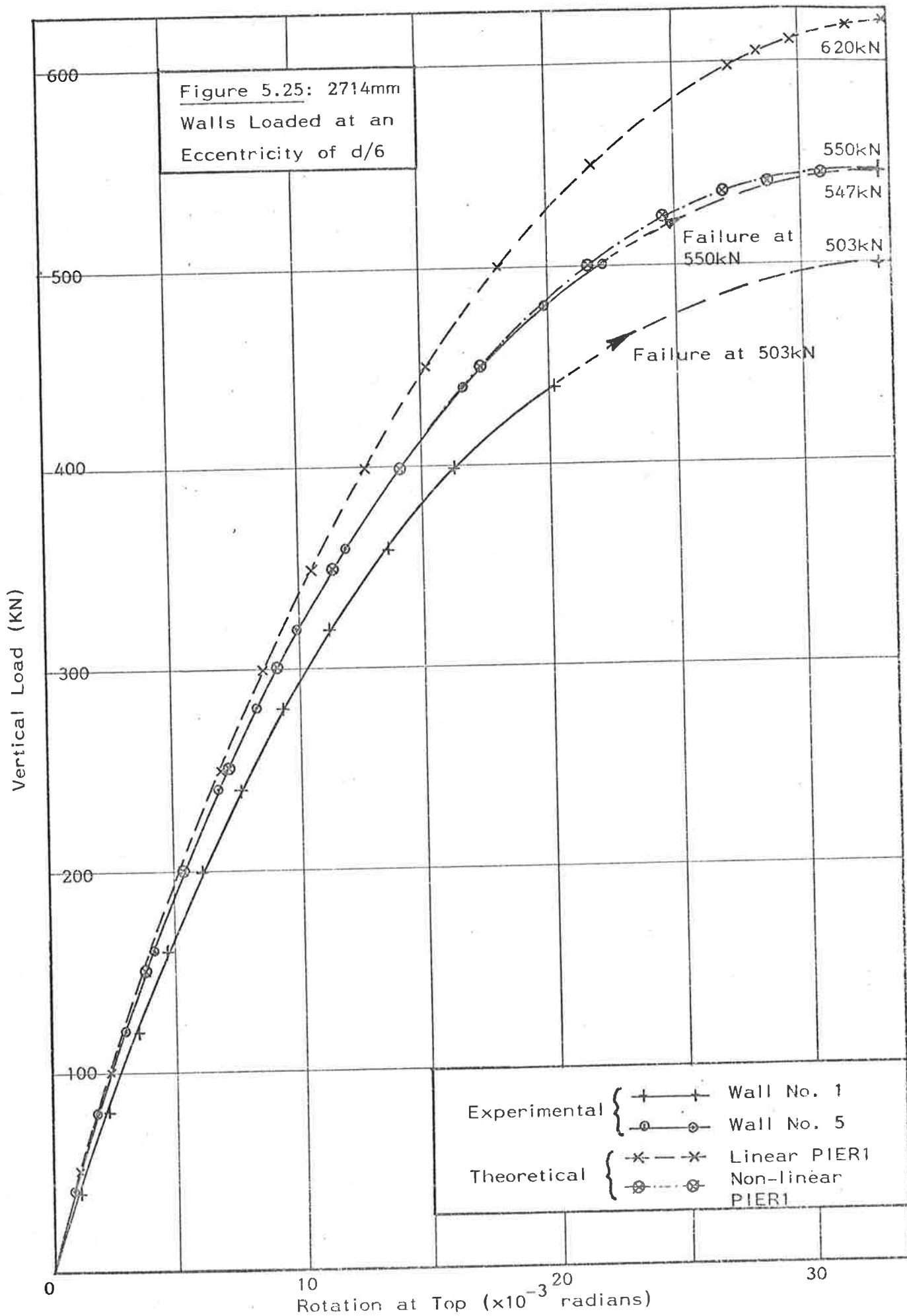
approximately 6mm at the mortar joint (figures 5.23, 5.24). Wall 2 showed a vertical splitting failure at 780KN; however, the load could be further increased to 1112KN before the wall collapsed. The actual mode of failure could not be determined because the wall disintegrated instantaneously at collapse. Wall 6, which was tested similarly to wall 2, was not loaded beyond the vertical splitting stage, deemed to be wall failure, for reasons of safety. Plots of load against top rotation for all walls are given in figures 5.25, 5.26, 5.27 and 5.28 together with theoretical end rotations calculated by PROGRAM PIER1. In the calculations, the brick elastic modulus was  $16.2 \times 10^3$ MPa and the linear mortar elastic modulus was  $8.3 \times 10^3$ MPa (Section 5.2.2.3).

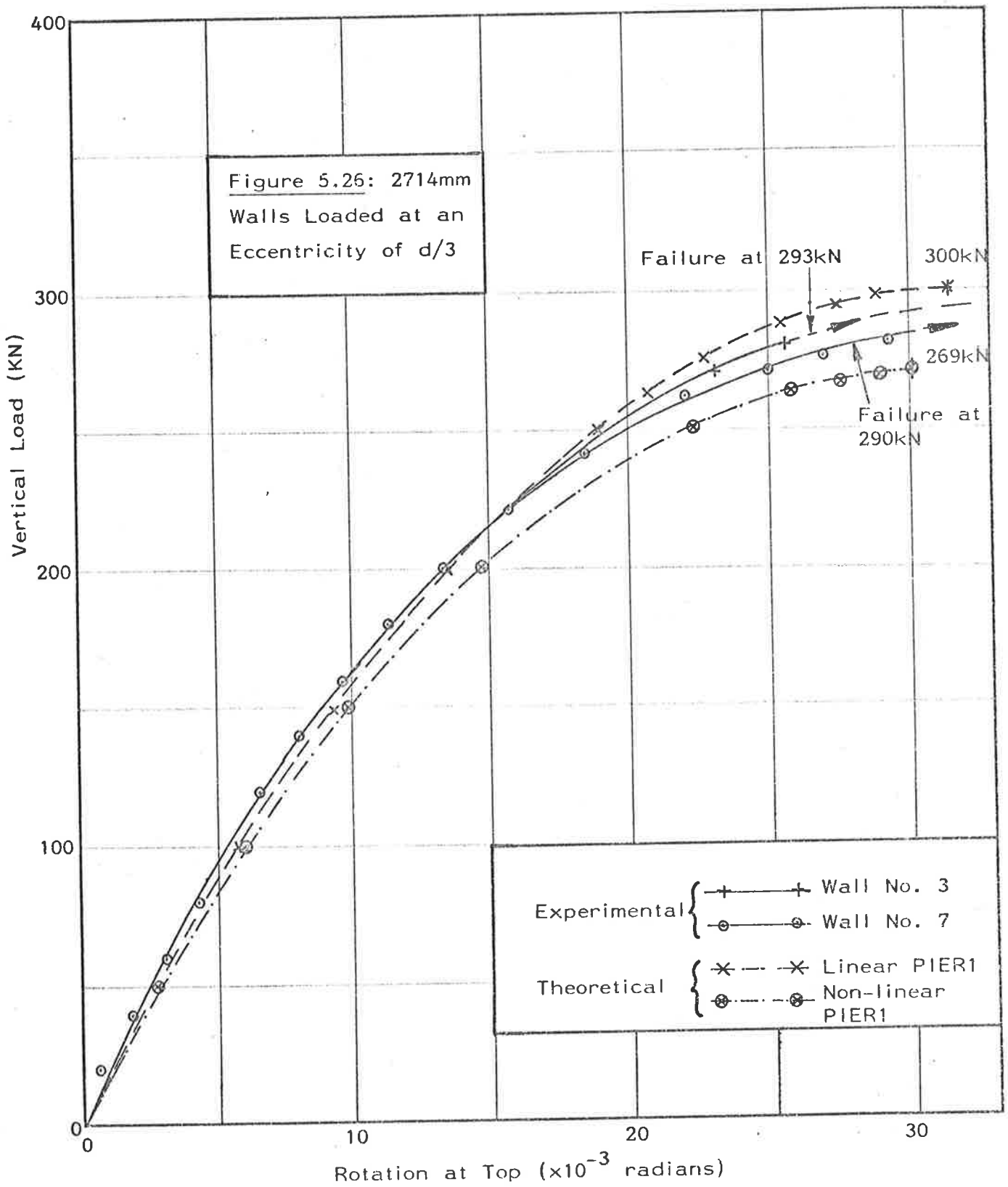
Also shown in figures 5.25 to 5.28 are theoretical wall top rotations calculated by using PROGRAM PIER1 with a non-linear mortar with the stress-strain relationship –

$$\sigma = 8.3 \times 10^3 (\epsilon - 6.104 \epsilon^{1.5}) \quad (5.6)$$

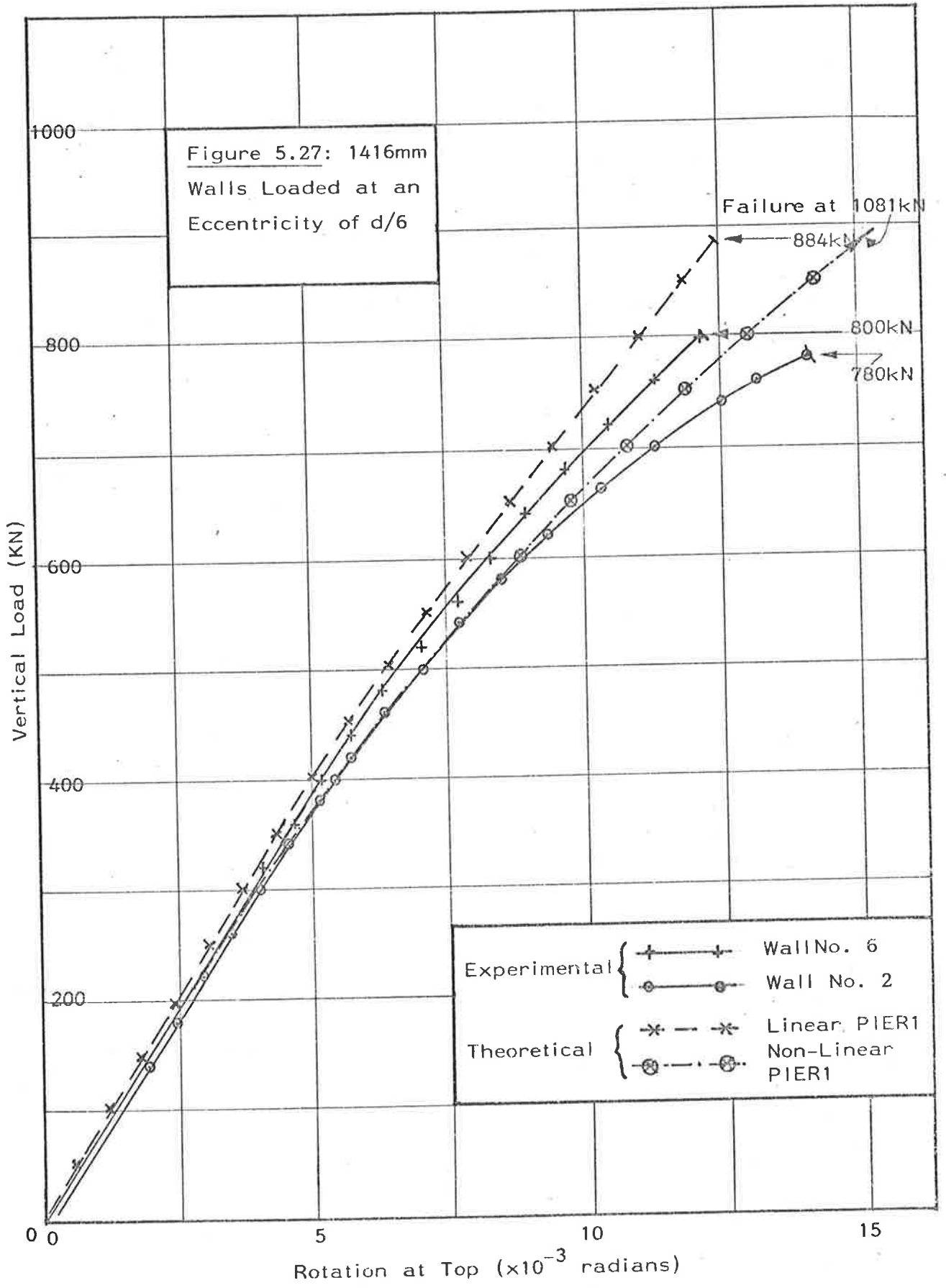
Equation (5.6) was obtained from the general equation given in Appendix B, using  $n = 1.5$  and  $\sigma_c = 33.0$ MPa. This value of  $\sigma_c$  was determined from axial compression tests on four-brick prisms constructed with the walls (figure 5.12(a); Appendix D).

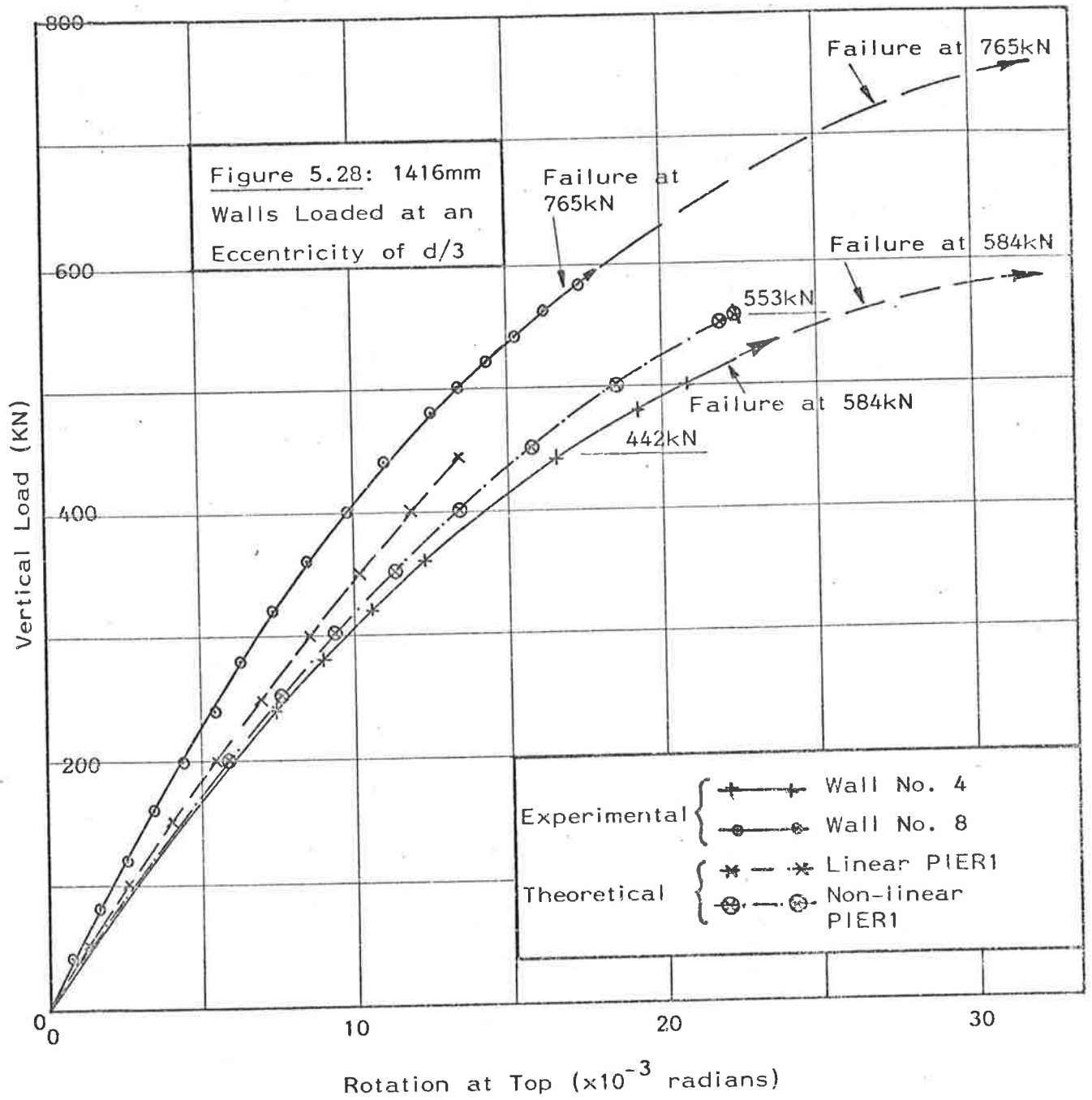
A parametric study was made to investigate the effect on the wall failure loads of using exponents,  $n$ , in equation (B.1) of 1.2, 1.5, 2.0 and 3.0. The results are summarized in Table 5.18 together with failure loads calculated by PROGRAM PIER1 using a linear material analysis.











Wall Height (mm) (Slenderness, h/d)	Load Eccentricity (mm)	Failure Load, $P_f$ (KN)					
		Expt. (a)	Theoretical				
			Linear <sup>(d)</sup> Mortar	Non-Linear Mortar			
				n = 3.0	n = 2.0	n = 1.5	n = 1.2
2714 (36)	12.5 (d/6)	{ 503 550 }	620	604	583	547	469
2714 (36)	25.0 (d/3)	{ 290 293 }	300	295	286	269	230
1416 (19)	12.5 (d/6)	{ 780 } <sup>(b)</sup> { 800 }	884	1050	1068	1081	1025
1416 (19)	25.0 (d/3)	{ 584 } <sup>(c)</sup> { 765 }	442	525	537	553	555

- (a) Each pair of loads is from two tests      (b) Ultimate failure load for wall 2 was 1112KN  
(c) Initial Slopes of Load-rotation Curves varies considerably between walls (figure 5.28)  
(d) Failure Stress 33.0MPa (Appendix D).

Table 5.18: Experimental and Theoretical Failure Loads for Brickwork Walls

(c) Summary of Failure Load Tests

The top rotations and the buckling failure loads of the tall walls 1, 3, 5 and 7 (slenderness ratio 36) agreed closely with the calculated values from PROGRAM PIER1 (figures 5.25 and 5.26). The computations used a brick elastic modulus,  $E_b$ , of  $16.2 \times 10^3$  MPa (Section 5.2.2.3) and a non-linear mortar with the stress-strain relationship -

$$\sigma = 8.3 \times 10^3 (\epsilon - 6.104\epsilon^{1.5}) \quad (5.6)$$

By using equation (5.6), the maximum stress attainable in the calculations was 33MPa, the minimum axial compressive failure stress for the brickwork (Appendix D).

The top rotations of the short walls 2, 4 and 6 (slenderness ratio 19) were calculated closely by PROGRAM PIER1 using a non-linear mortar in the analysis given by equation (5.6). The failure load of short wall 4, which failed by brick spalling, was calculated by PROGRAM PIER1 using a non-linear mortar (equation (5.6)) to within 6 percent of the experimental value (figure 5.28, Table 5.18). Possible errors in the test set up of wall 8 produced significant differences between experimental and theoretical values of top rotation and failure load (figure 5.28).

A linear analysis using PROGRAM PIER1 predicted closely the vertical splitting failure loads in walls 2 and 6 (figure 5.27, Table 5.18) and the ultimate failure load for wall 2 (1112KN) was calculated by using a non-linear mortar analysis (equation (5.6)) in PROGRAM PIER1. The difference between the failure loads calculated by the linear and non-linear analyses was less than 30 percent of the larger value.

It appears, therefore, that in a more general investigation into the behaviour of brickwork walls, a series of brickwork prism tests, similar to tests described in Appendix D, could be used to determine whether the vertical splitting mode of failure is more likely to occur for a specified load eccentricity than failure by brick spalling. If the splitting mode of failure is predominant, the corresponding failure stress could be specified as an upper limit on wall load in a linear material analysis using PROGRAM PIER1. However, if wall failure might occur by lateral buckling or brick spalling, a non-linear mortar could be used in the analysis. Results summarized in Table 5.18 for a range of non-linear mortars (Appendix D) indicate that the exponent,  $n$ , for a non-linear mortar with a stress-strain characteristic described by equation (B.1) might not be critical to the values of wall failure loads calculated by such an analysis.

A large number of experiments is required before the general utility of PROGRAM PIER1 for brickwork walls can be assessed on a statistical basis. However, the experiments summarized in this section indicate that PROGRAM PIER1 has a number of advantages over previous methods of analysis in providing more accurate predictions for both the load deformation behaviour and the failure loads of eccentrically-loaded brickwork walls.

## 6. THE ANALYSIS OF BRICKWORK PANELS IN TWO-WAY BENDING

### 6.1 INTRODUCTION

A brickwork structure is generally non-homogeneous and non-isotropic, as it is built up from bricks, separated by layers of mortar. In general the relative amounts of brick and mortar along a horizontal section is different from that along a vertical section.

In Chapter 4, it was shown that a brick column can be analysed as an equivalent homogeneous isotropic column of varying thickness; the thickness varies with the effective eccentricity of the load, which in turn depends on the initial eccentricity and the deflection. The relationship between the thickness to be used in the calculations and the effective eccentricity was established using a two-dimensional finite element analysis by making the moment-rotation characteristic for a module of this equivalent column, which was one brick height plus one mortar thickness in length, equal to the corresponding characteristics of the real column. Although the stresses in the real column and the equivalent column are not equal at all sections, once the deflections have been calculated the stresses in the real column can be computed.

In this chapter it is proposed that a similar equivalent plate of varying thickness can be analysed to find the deflection of a brickwork panel supported on four sides and loaded by in-plane eccentric compression forces. Brick-mortar units of appropriate size are analysed by three-dimensional finite element methods to calculate the bending and torsion stiffness of the equivalent homogeneous plate which can be used in the calculations.

## 6.2 THE STIFFNESS OF PARTIALLY-CRACKED BRICKWORK PANELS

### 6.2.1 An Analytical Element for Panels

The arrangement of bricks and mortar in conventional stretcher bond is shown in figure 6.1(a).

If the panel in figure 6.1(a) is subjected to uniform bending or in-plane forces, a small volume of the panel, defined by the planes AAAA, BBBB, CCCC and DDDD, and referred to in this chapter as a panel module, can be used to analyse the behaviour of the whole panel (figure 6.1(b)). The dimensions of the panel module given in figure 6.1(b) refer to the particular bricks used in the construction of an experimental panel to be described in Chapter 7. In the following sections, the stiffness of the panel module is calculated for both uncracked brickwork and cracked brickwork in which there is bond in shear but no tensile bond between the brick and mortar components. Bending of the panel module is defined to be normal to the bedjoints if the moment is associated with stresses normal to the bedjoints and bending is defined to be parallel to the bedjoints if the moment is associated with stresses parallel to the bedjoints.

### 6.2.2 Bending Normal to the Bedjoints

The extent of bedjoint cracking in walls supported only at the top and base depends on the position of the in-plane force resultant acting normal to the bedjoints (Section 4.2). The effect of load eccentricity on the cracking and stiffness of complete panels supported on three or four sides may be investigated by the finite element method in which the panel module, defined in the previous section, is divided into ninety twenty-node isoparametric three-dimensional prism elements. A system of eight-noded elements was found to be unsatisfactory

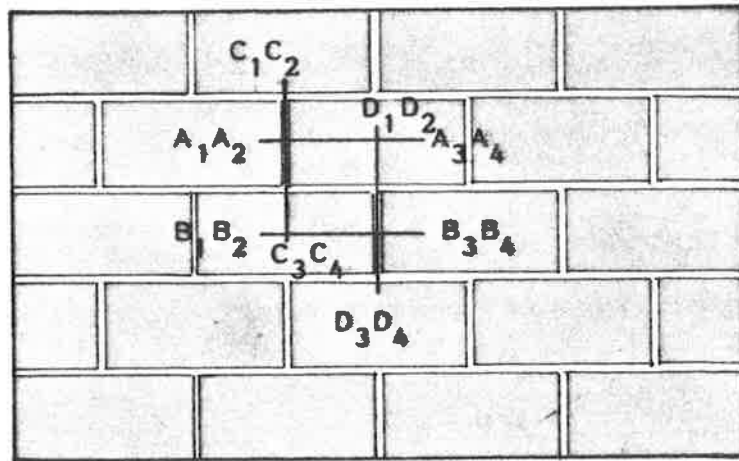


Figure 6.1(a): Elevation of Brickwork in Stretcher Bond

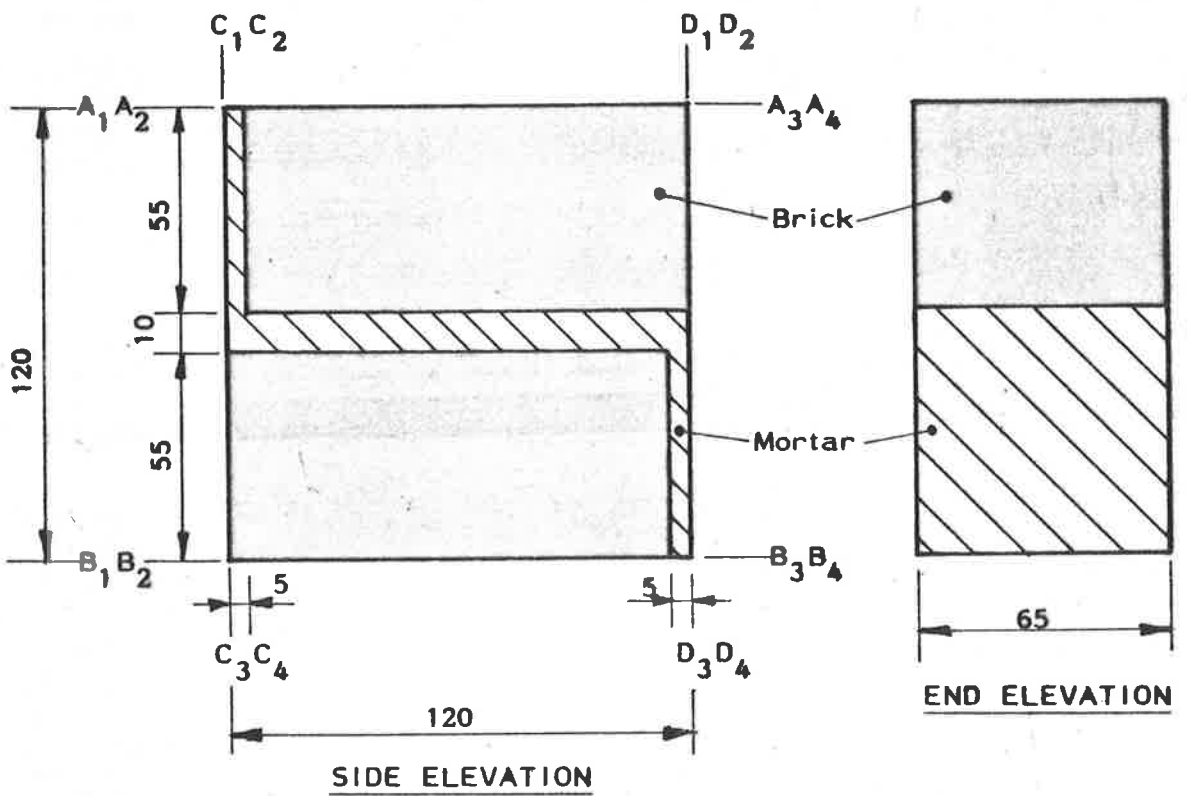


Figure 6.1(b): Details of Panel Module

Figure 6.1: Brickwork Panel Module



because of the large number of elements required to model the brickwork adequately in bending. A typical twenty-node element is shown in figure 6.2(a) and the finite element grid for the complete panel module in figure 6.2(b). Details of the panel module subdivision are given in Appendix E.

If the panel module is compressed by a vertical load whose resultant acts within the kern, there is no cracking on the bedjoint. When the resultant load acts outside the kern, a crack forms at one or both of the brick-mortar interfaces on the bedjoint depending on the position along the bedjoint (figures 6.3(a), 6.3(b), 6.3(c)).

The stiffness of the brickwork varies as a result of the cracking at the bedjoint brick-mortar interfaces. The results obtained for one-way bending (Section 4.2) were compared with calculations based on the panel module, shown in figure 6.1(b), for various values of brick and mortar moduli. With reference to figures 6.1(a), 6.1(b), the planes  $AAAA_{1234}$  and  $BBBB_{1234}$  are taken to remain plane for bending normal to the bedjoints and similarly, planes  $CCCC_{1234}$  and  $DDDD_{1234}$  are assumed to remain plane. In order to calculate the flexural rigidity of the panel module, planes  $AAAA_{1234}$  and  $BBBB_{1234}$  may be rotated by a chosen angle, say  $\phi$ , and the length of the middle surface  $EEEE_{1234}$  may be decreased by a chosen amount, say  $\delta$  (figure 6.4).

The nodes of elements at the horizontal brick-mortar interfaces, on planes  $MMMM_{1234}$  and  $NNNN_{1234}$  in figure 6.4, can be uncoupled where tension normal to the interface could be developed.

The problem can be solved using a finite element program such as PROGRAM MFYDCP (Appendix E). The position and magnitude of a resultant load required to deform the panel module into the shape specified can be calculated from the reactions on the faces  $AAAA_{1234}$  and  $BBBB_{1234}$ . The effective flexural stiffness of the panel module may be defined as —

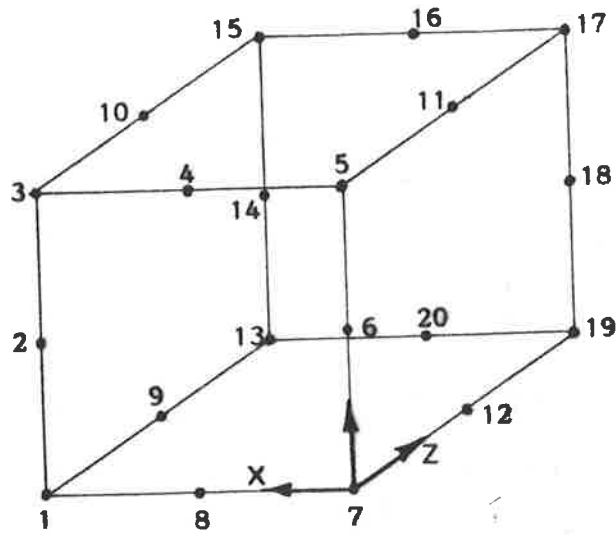


Figure 6.2(a): Twenty-node Isoparametric Element

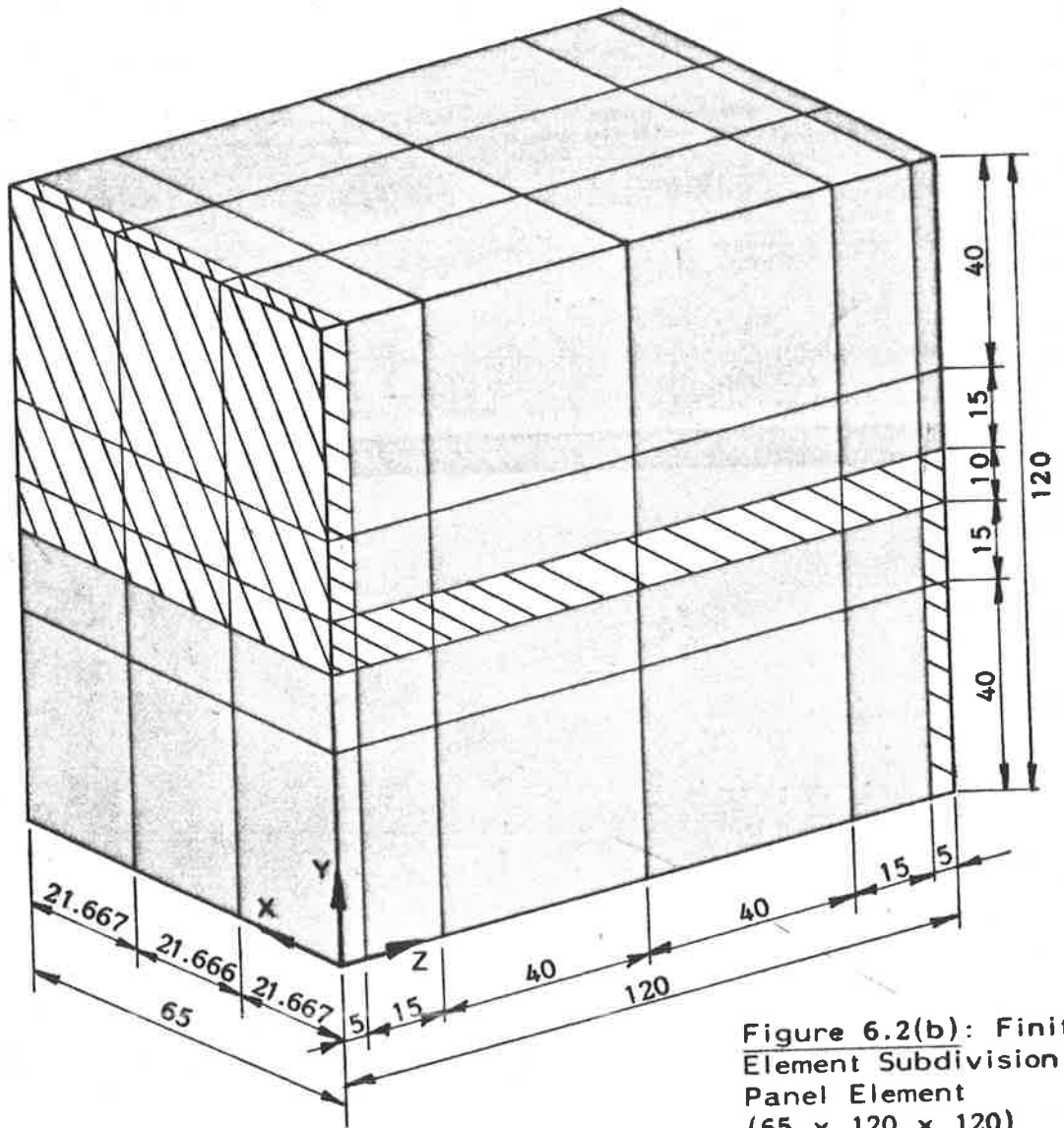


Figure 6.2(b): Finite Element Subdivision of Panel Element (65 x 120 x 120)

Figure 6.2: Finite Element Details

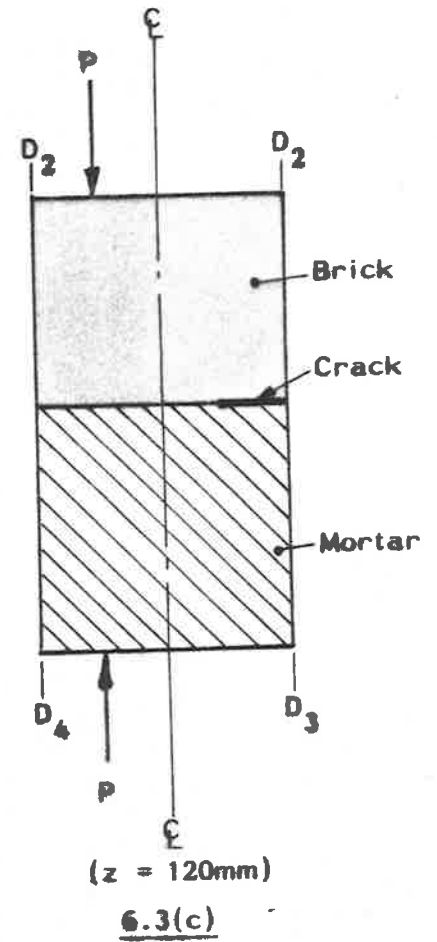
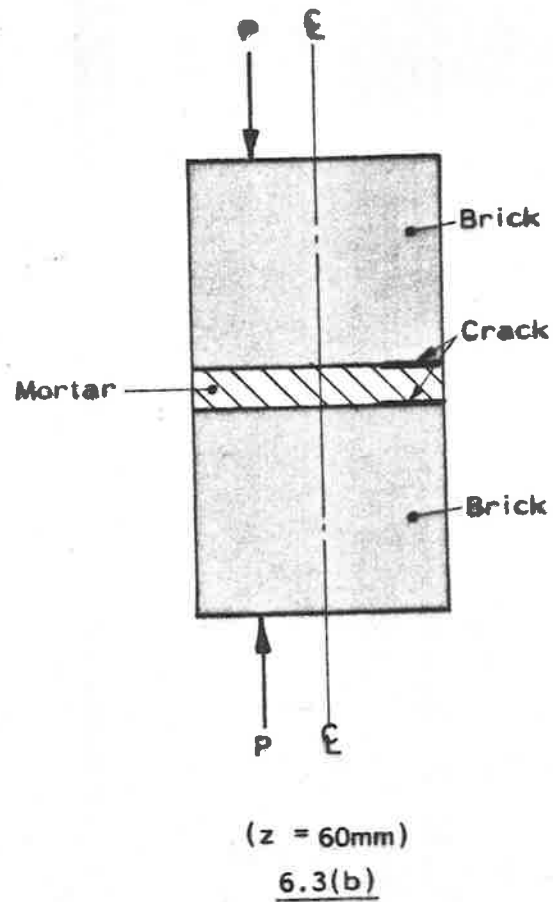
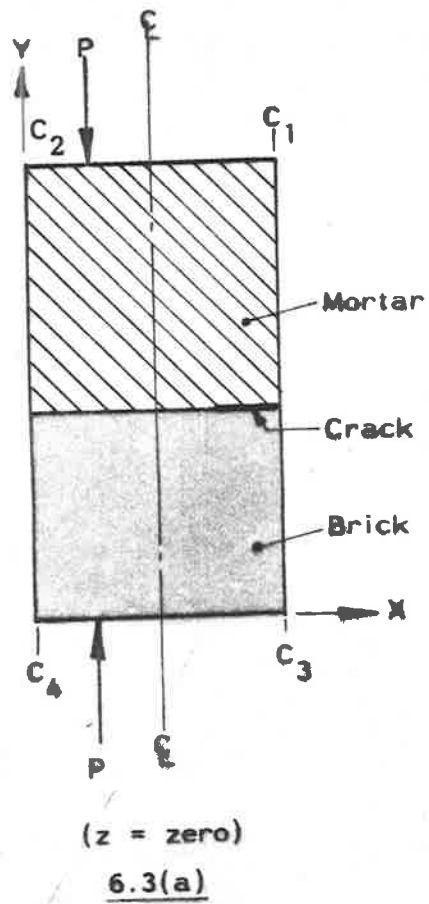


Figure 6.3: Bedjoint Cracking in Panel Module

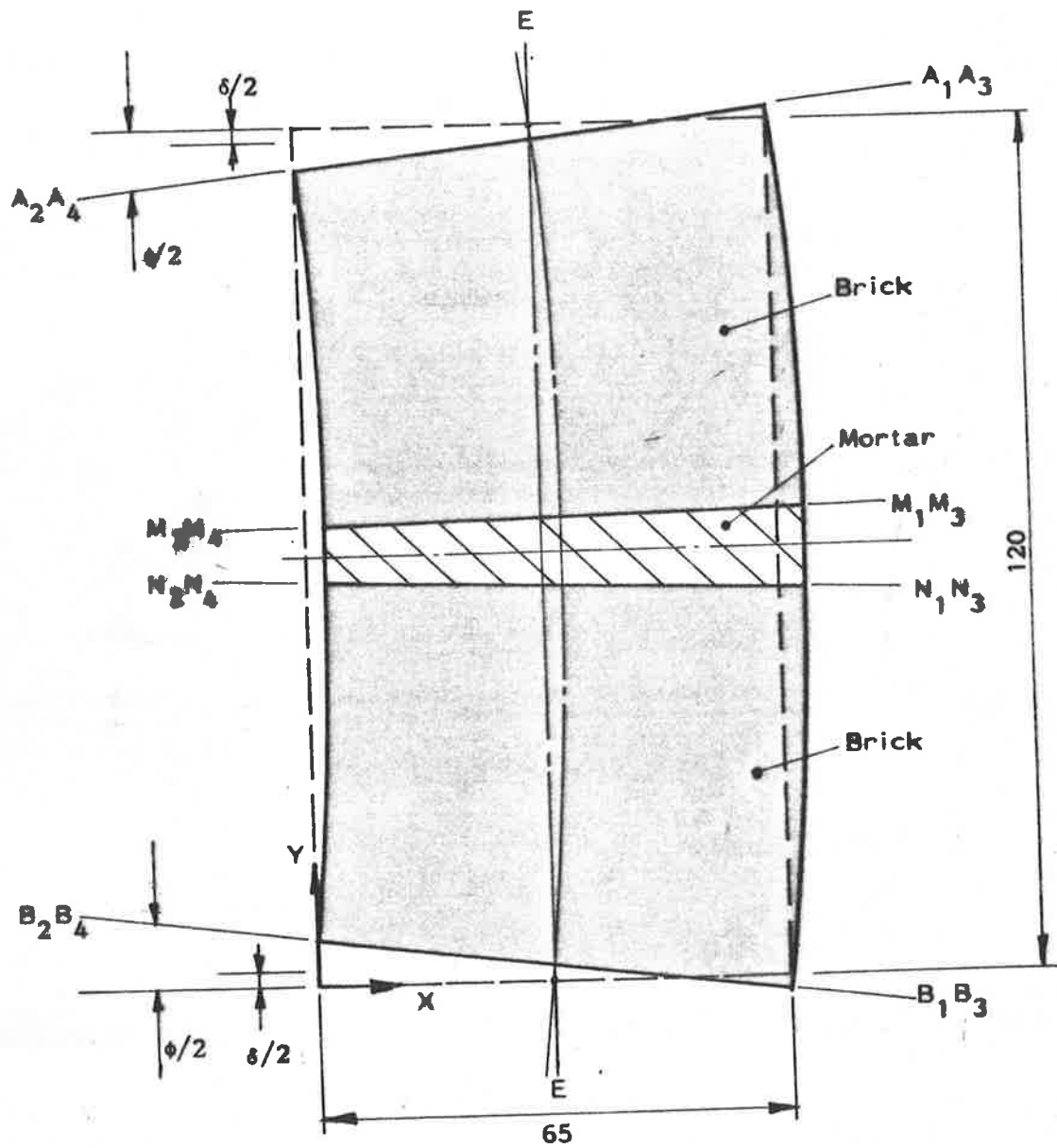


Figure 6.4: Panel Module Subjected to Bending Normal to the Bedjoints

$$(EI)_{eq} = \frac{P \cdot e}{\phi} (h_b + h_m) \quad (6.1)$$

in which  $P$  is the total resultant load

$e$  is the eccentricity of the resultant load

$\phi$  is the specified relative rotations of planes AA and

BB

$h_b$  and  $h_m$  are as defined in Chapter 4.

The calculated results showed that, for solid brickwork with dimensions given in figure 6.1(b), PROGRAM MFYDCP gave solutions which agreed closely with the results calculated using equation (4.1) for brickwork in one-way bending (Table 6.1).

Brick:Mortar Modular Ratio <sup>(a)</sup>	Calculated Effective Eccentricity ( $e/d$ ) <sup>(b)</sup>	Ratio of Effective Flexural Stiffness <sup>(c)</sup>
1.0	0.32	0.99
2.0	0.32	0.99
4.0	0.31	0.97
10.0	0.30	0.95

(a) Brick Modulus is  $20 \times 10^3$  MPa for all cases.

(b)  $\phi = 1.0 \times 10^{-3}$  radians,  $\delta = 0.02$  mm (figure 6.4) for all cases.

(c) Ratio  $\left[ \frac{(EI)_{eq} \text{ calculated by Equation (6.1)}}{(EI)_{eq} \text{ calculated by Equation (4.21)}} \right]$

Table 6.1: Stiffness of Brickwork Subject to Bending Normal to the Bedjoints

That is, the effective flexural stiffness of a brickwork panel cracked on the bedjoints by an eccentric compression force, uniform along the

panel length, can be calculated using the curvature ratio factor,  $\alpha$ , derived in Chapter 4 for brickwork in one-way bending.

### 6.2.3 Bending Parallel to the Bedjoints

When a brick panel (figure 6.1(a)) is subjected to bending moments parallel to the bedjoints, tension stresses can develop at the vertical joints, or perpends. If the bond strength at the perpends is negligible, cracking in the perpend occurs, and the flexural stiffness of the brickwork is reduced below that for uncracked brickwork.

#### 6.2.3.1 Uncracked brickwork

As a preliminary investigation for calculating the reduction in stiffness, PROGRAM MFYDCP was used to calculate the stiffness of uncracked brickwork for bending parallel to the bedjoints. An effective stiffness for uncracked brickwork was calculated by Base and Baker<sup>(69)</sup> (Section 3.3.5) in the form—

$$(EI)_p = E_b \cdot \left[ \frac{H(L+p)}{\left(L + \left(\frac{E_b}{E_m}\right)p\right)} + \frac{b}{\left(\frac{E_b}{E_m}\right)} \right] \cdot \frac{d^3}{12} \quad (6.2)$$

in which  $(EI)_p$  is the effective flexural stiffness, per unit height, for uncracked brickwork

$E_b$  is the elastic modulus for the bricks

$E_m$  is the elastic modulus for the mortar

$L, H, p, b,$  are dimensions defined in figure 6.5

$d$  is the panel thickness.

Equation (6.2) was checked by using the panel module shown in figure 6.1(b). The brickwork panel shown in figure 6.1(a) was assumed to be subject to uniform bending parallel to the bedjoints.

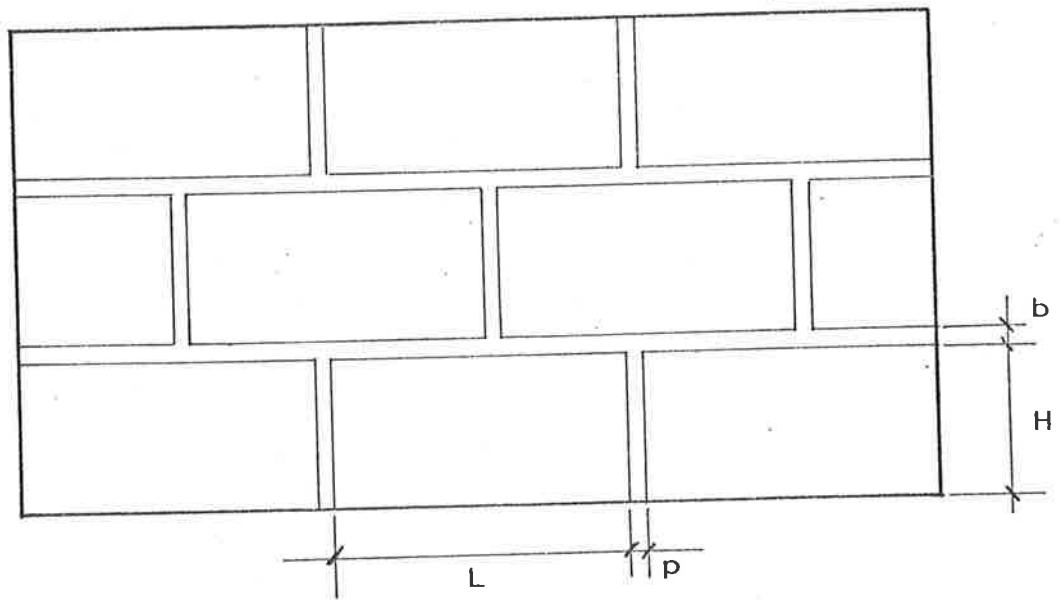


Figure 6.5: Brickwork Dimensions

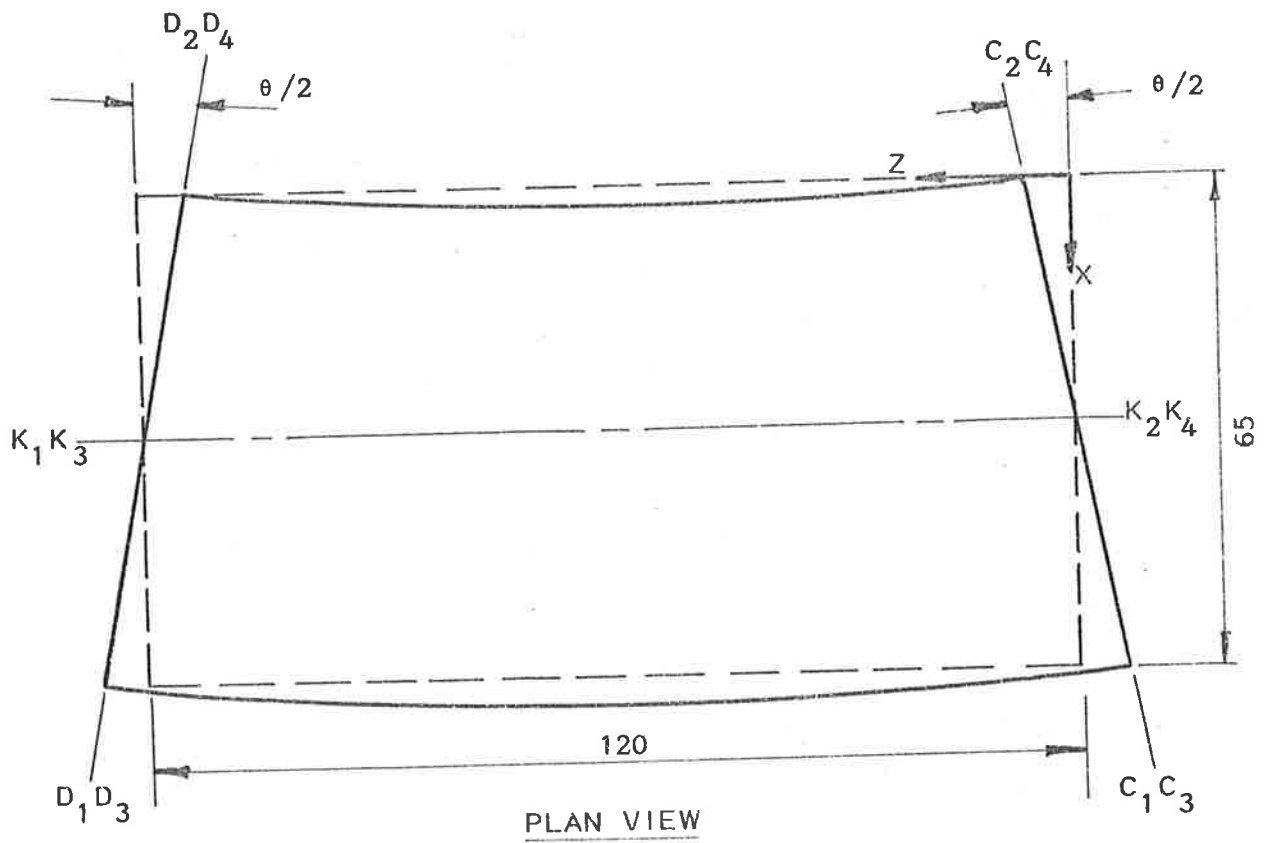


Figure 6.6: Bending of Panel Module Parallel to the Bedjoints

It was also assumed that the plane boundaries  $A_{1234}A_{1234}$ ,  $B_{1234}B_{1234}$ ,  $C_{1234}C_{1234}$  and  $D_{1234}D_{1234}$  remained plane during bending. PROGRAM MFYDCP was used with a subdivision of ninety elements (Appendix E), and the planes  $C_{1234}C_{1234}$  and  $D_{1234}D_{1234}$  were "rotated" by prescribing the displacements of all nodes on planes  $C_{1234}C_{1234}$  and  $D_{1234}D_{1234}$  (figure 6.6). Planes  $A_{1234}A_{1234}$  and  $B_{1234}B_{1234}$  were restrained against out-of-plane translations.

The finite element solution indicated that there was no change in length of the middle surface,  $K_{1234}K_{1234}$ . The bending moment required to achieve the prescribed end rotations was calculated from the reactions at the nodes on planes  $C_{1234}C_{1234}$  and  $D_{1234}D_{1234}$ . Because there are no resultant forces parallel to the bedjoint on the planes  $C_{1234}C_{1234}$  and  $D_{1234}D_{1234}$  (figure 6.6), an effective flexural stiffness per unit height for the panel module may be calculated from the equation -

$$(EI)_p = \left(\frac{M_p}{\phi_p}\right) \cdot \left(\frac{L+p}{b+H}\right) \quad (6.3)$$

in which  $M_p$  is the resultant moment of the end forces on planes  $C_{1234}C_{1234}$  and  $D_{1234}D_{1234}$  about the middle surface,  $K_{1234}K_{1234}$ ,

$\phi_p$  is the relative rotation of planes  $C_{1234}C_{1234}$  and  $D_{1234}D_{1234}$ ,

$L$ ,  $H$ ,  $b$ ,  $p$  are defined in figure 6.5.

A summary of calculated relative stiffnesses for selected brick:mortar modular ratios is given in Table 6.2 and figure 6.7.

The calculated results, summarized in figure 6.7 and Table 6.2, agreed closely with equivalent stiffnesses proposed by Base and Baker for various brick and mortar moduli provided that the brick:mortar modular ratios were less than 5.0. For a modular ratio of 5.0, the difference in relative stiffnesses calculated by equation (6.2) and PROGRAM MFYDCP, was approximately 5 percent, with equation (6.2) giving the lower value. Base and Baker assumed that plane sections, normal to a neutral axis along the brickwork, remained plane (Section



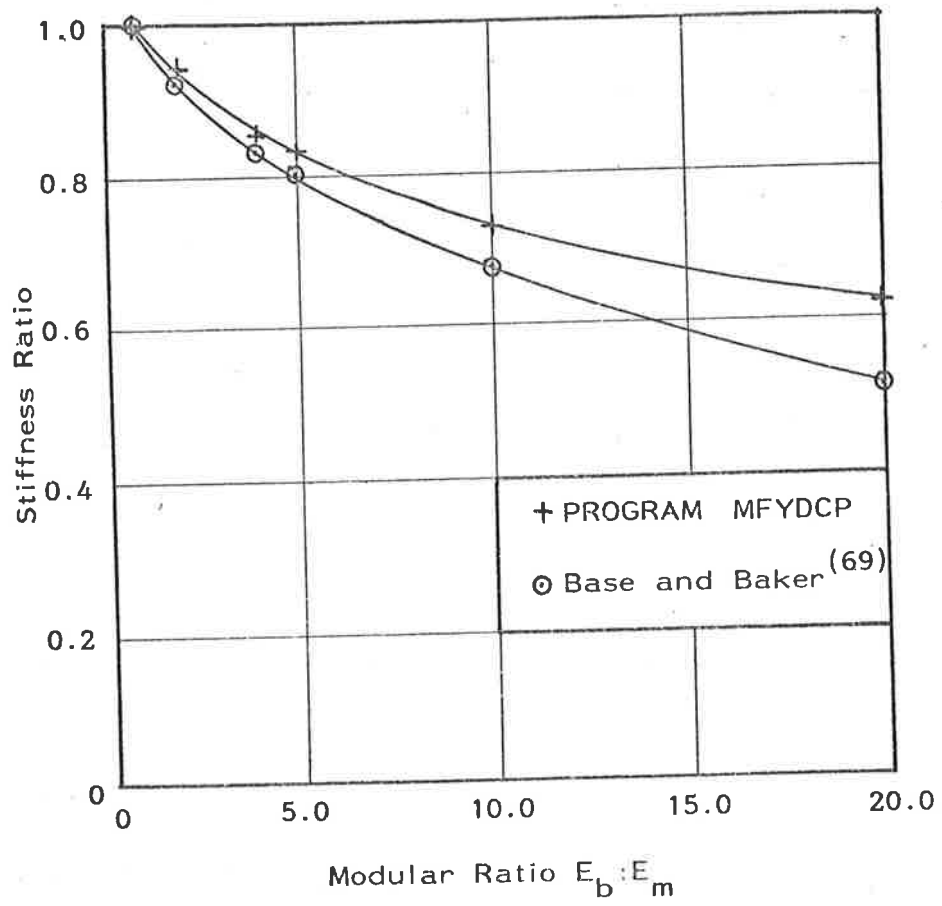


Figure 6.7: Relative Flexural Stiffness for Various Brick-Mortar Modular Ratios

Modular Ratio ( $E_b/E_m$ )	Relative Stiffness <sup>(a)</sup>	
	Base and Baker <sup>(69)</sup>	PROGRAM MFYDCP
1.0	1.00	1.00
2.0	0.92	0.94
4.0	0.83	0.85
5.0	0.80	0.83
10.0	0.67	0.73
20.0	0.51	0.62

(a) Bending stiffness relative to brickwork with modular ratio  $E_b/E_m = 1.0$ .

Table 6.2: Flexural Stiffness of Brickwork Subject to Bending Parallel to the Bedjoints

3.3.5), and hence that brickwork subjected to bending parallel to the bedjoints deflects into a cylindrical circular surface. However, the results from PROGRAM MFYDCP showed that, in general, brickwork did not deflect into such a cylindrical shape and that there were significant twisting moments and shear stresses on the bedjoints, particularly for modular ratios greater than 5.0. These differences between the deformed shape assumed by Base and Baker and the shape predicted from the more accurate numerical model account for the differences in the flexural stiffnesses calculated by the two methods.

#### 6.2.3.2 Brickwork with cracked perpend

The effective flexural stiffness in horizontal bending for brickwork with no tensile bond strength on the perpend was calculated using the panel module shown in figure 6.1(b). The planes defined by  $AAAA_{1234}$ ,  $BBBB_{1234}$ ,  $CCCC_{1234}$  and  $DDDD_{1234}$  were assumed to remain plane during horizontal bending. PROGRAM MFYDCP was used with ninety elements (Appendix E) and planes  $CCCC_{1234}$  and  $DDDD_{1234}$  were "rotated" about their

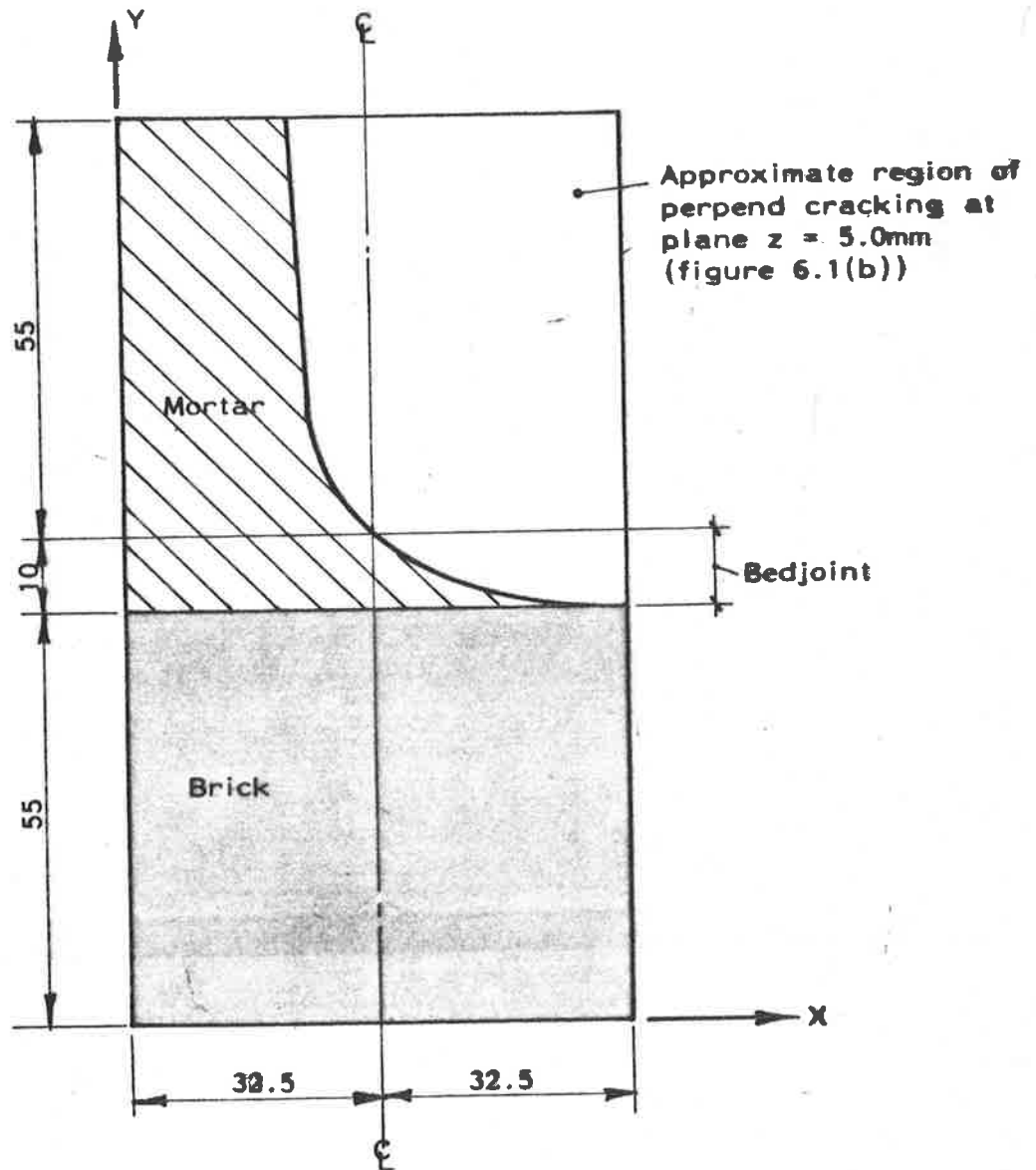
respective vertical centrelines by prescribing the displacements of all nodes on planes  $\underset{1\ 2\ 3\ 4}{CCCC}$  and  $\underset{1\ 2\ 3\ 4}{DDDD}$ . The planes  $\underset{1\ 2\ 3\ 4}{AAAA}$  and  $\underset{1\ 2\ 3\ 4}{BBBB}$  were restrained against out-of-plane translation. By trial, elements whose edges defined the perpend brick-mortar interfaces were uncoupled at all nodes at which tension normal to the interfaces could develop. A profile of the simulated perpend "cracking", shown in figure 6.8, represents an approximation to the real perpend cracking because of the coarseness of the finite element mesh and because of the assumption of materials with linear stress-strain relationships. In real brickwork, the extent of perpend cracking varies with increasing rotations on planes  $\underset{1\ 2\ 3\ 4}{CCCC}$  and  $\underset{1\ 2\ 3\ 4}{DDDD}$  because of non-linear material behaviour and the restraint of in-plane deformations in the horizontal direction. PROGRAM MFYDCP was used with the simulated cracked perpend (figure 6.8) and with various brick:mortar modular ratios (Table 6.3) to calculate the effective stiffness of brickwork subjected to bending parallel to the bedjoints.

Modular Ratio $E_b : E_m$	Relative Stiffness <sup>(a)</sup> PROGRAM MFYDCP
1.0	0.768
2.5	0.766
10.0	0.765

(a) Bending stiffness of cracked brickwork relative to uncracked brickwork with the same modular ratio (perpend cracking only).

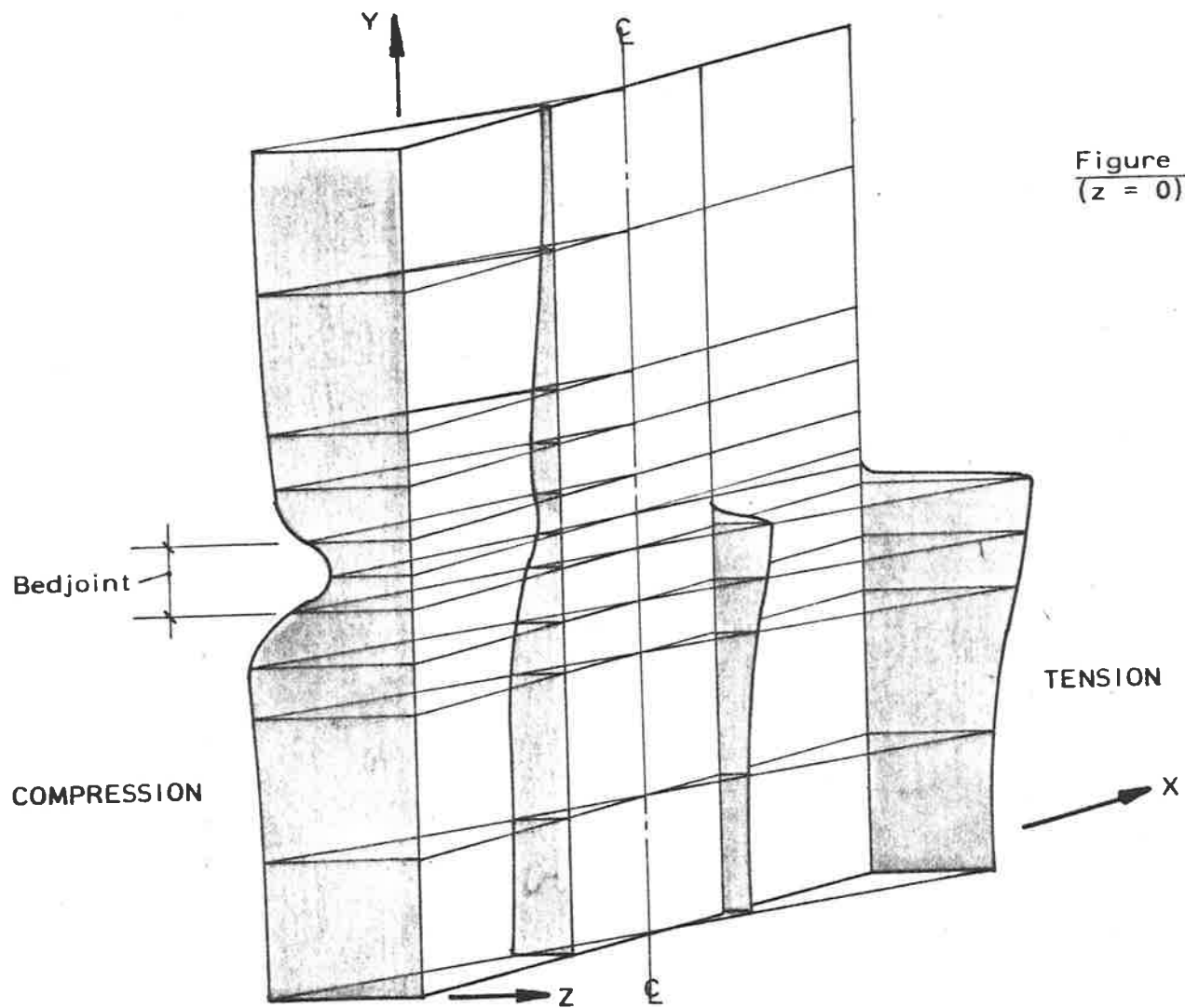
Table 6.3: Flexural Stiffness of Brickwork

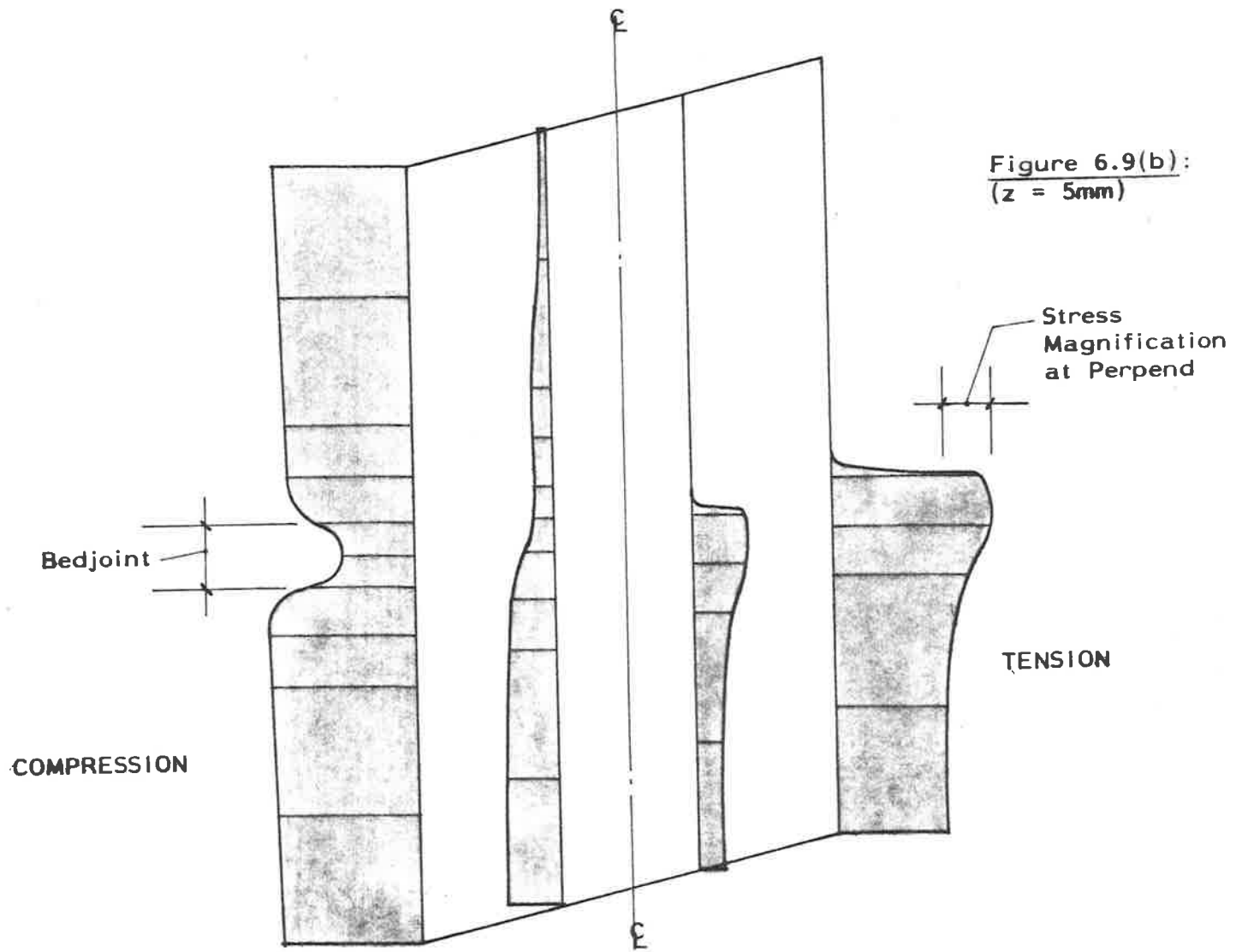
Plots of stress distributions at selected cross-sections for brickwork with a modular ratio of 2.5 are given in figure 6.9. Relatively large normal stresses at the junction of a bedjoint with a perpend



**Figure 6.8: Simulated Flexural Cracking at the Perpend Joint**

Figure 6.9: Distribution of Flexural Stresses on X-Y Planes for Brickwork with Cracking on Perpend Only





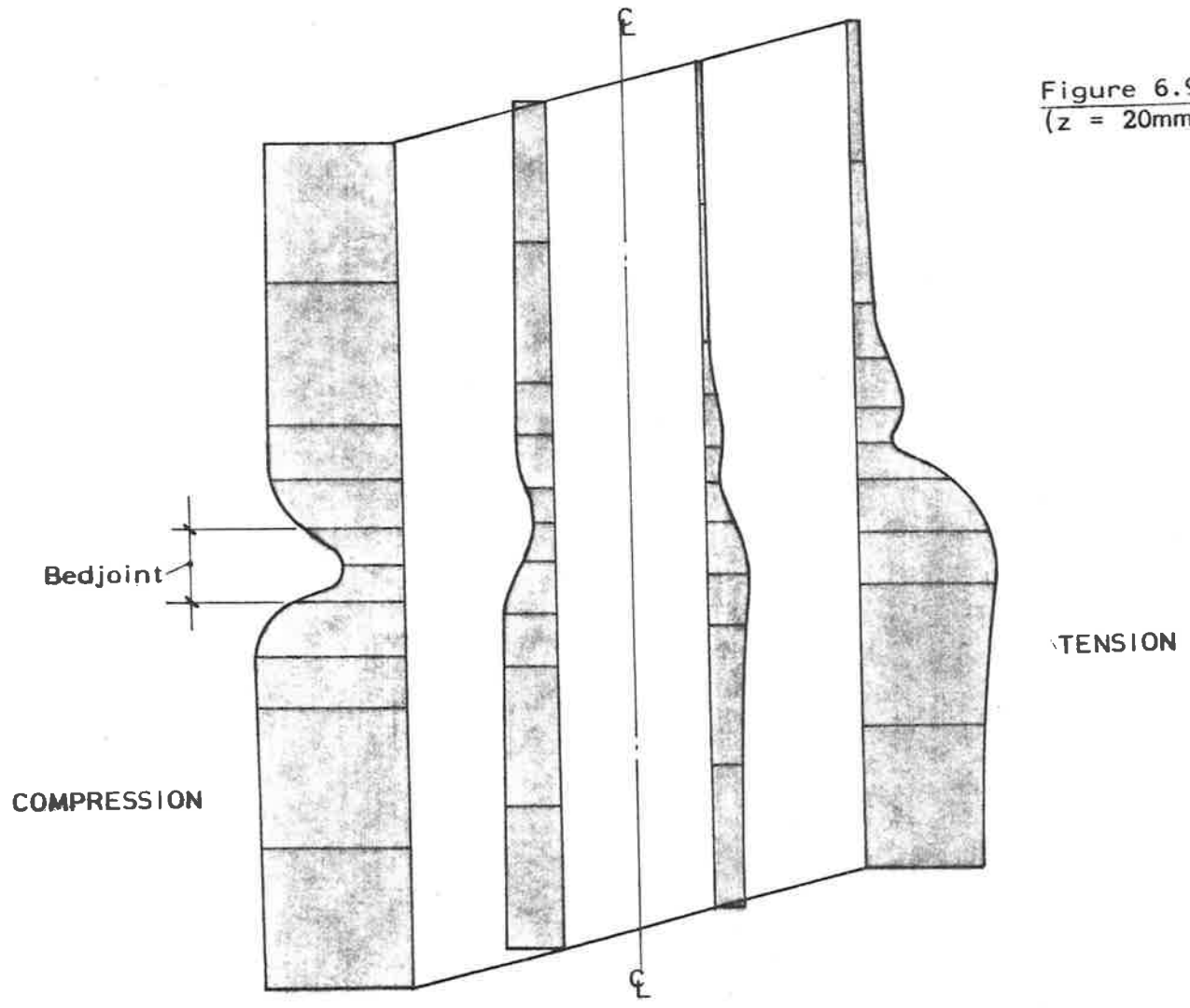


Figure 6.9(c):  
 $(z = 20\text{mm})$

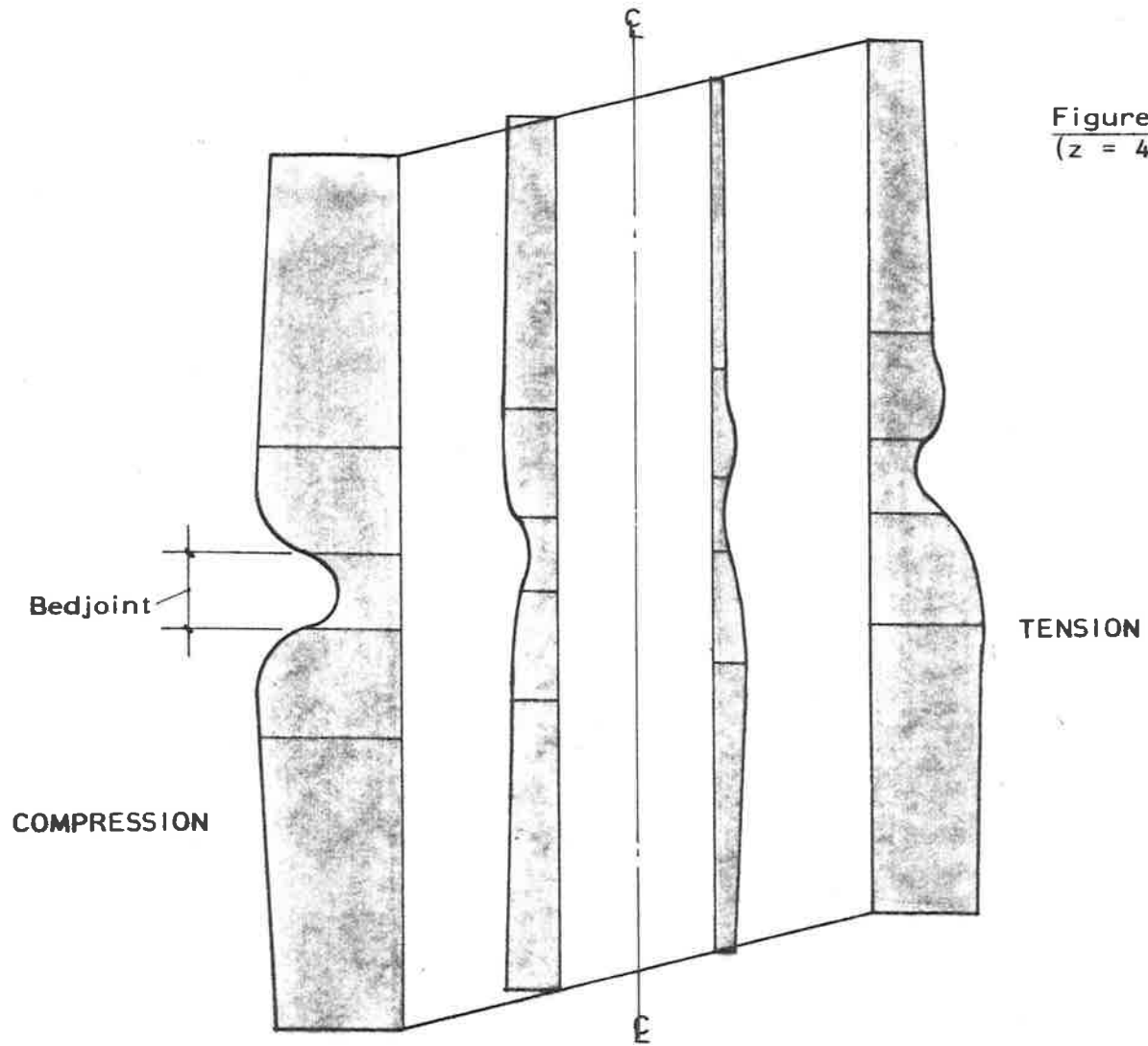
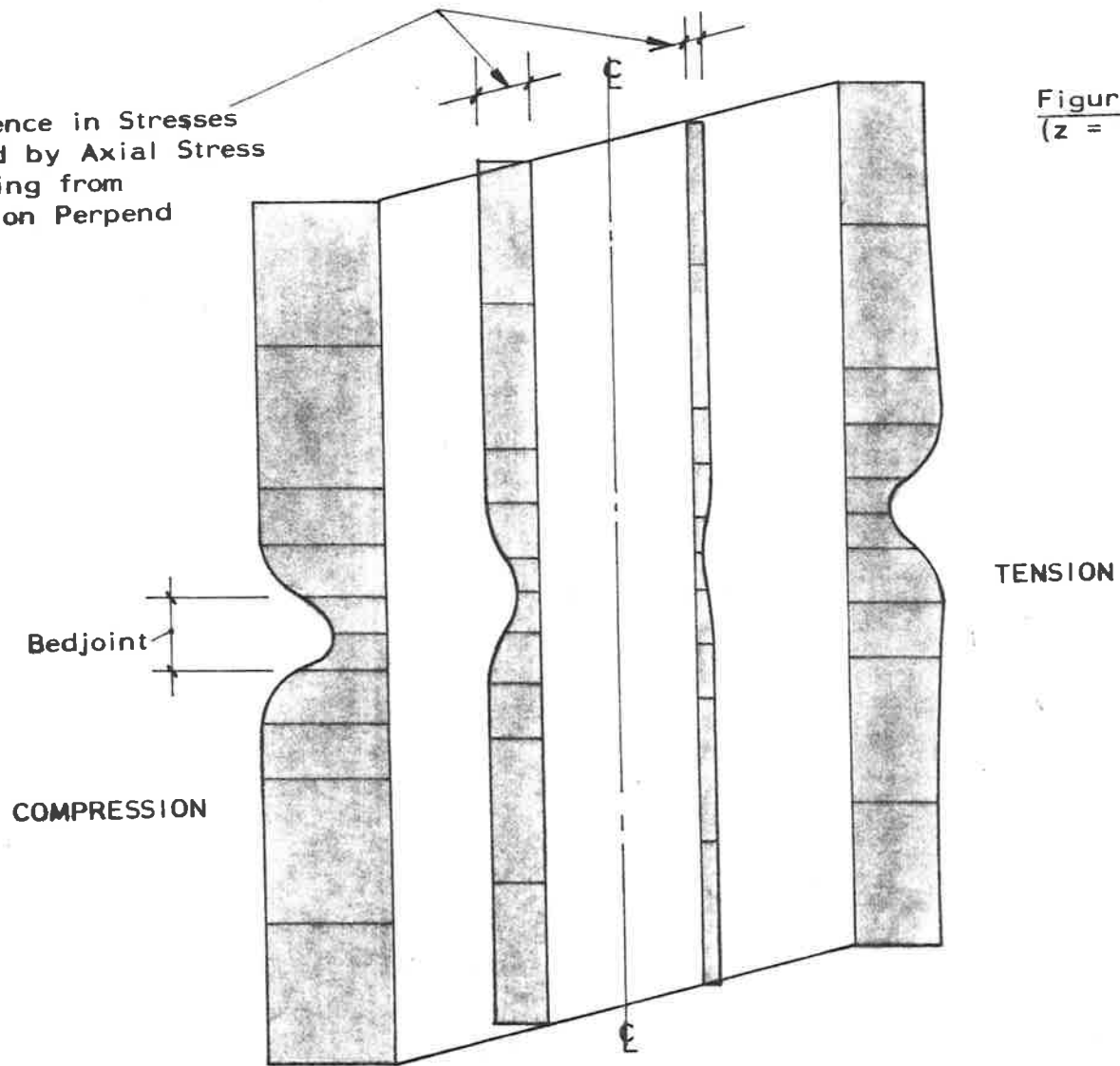


Figure 6.9(d):  
( $z = 40\text{mm}$ )



**NOTE:** Difference in Stresses  
Caused by Axial Stress  
Resulting from  
Crack on Perpend



**Figure 6.9(e):**  
(z = 60mm)

may indicate that tensile failure of the bricks could be expected at a perpend-bedjoint intersection in a case of excess bending parallel to the bedjoints.

### 6.2.3.3 Brickwork with cracked perpends and cracked bedjoints

Eccentric vertical compression loads applied simultaneously with bending parallel to the bedjoints can produce cracking on both the perpend and bedjoint brick-mortar interfaces. The cracking on the bedjoints can take place either on the same panel face as the perpend cracking (figure 6.10(a)) or the bedjoint and perpend cracking can occur on opposite faces of a panel (figure 6.10(b)). In this thesis, the only cases considered are those in which perpend and bedjoint cracking occur on the same panel face (figure 6.10(a)).

PROGRAM MFYDCP was used with simulated cracked perpends and bedjoint cracking up to one-half the panel thickness (Appendix E) and the relative flexural stiffness for horizontal bending of cracked brickwork were calculated for selected brick:mortar modular ratios as shown in Table 6.4.

Relative Stiffness <sup>(a)</sup> – PROGRAM MFYDCP			
Modular Ratio $E_b:E_m$	Depth of Bedjoint Crack <sup>(b)</sup>		
	d/6	d/3	d/2
1.0	0.751	0.724	0.699
2.5	0.745	0.718	0.691
10.0	0.733	0.705	0.676

(a) Bending stiffness of cracked brickwork relative to uncracked brickwork with the same modular ratio (Section 6.2.3.1).

(b) Perpend and bedjoint cracks on same panel face.

Table 6.4: Flexural Stiffness of Brickwork

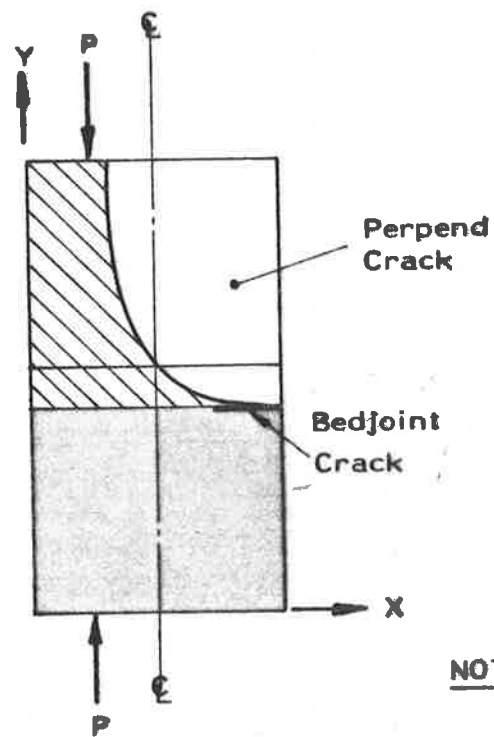


Figure 6.10(a)

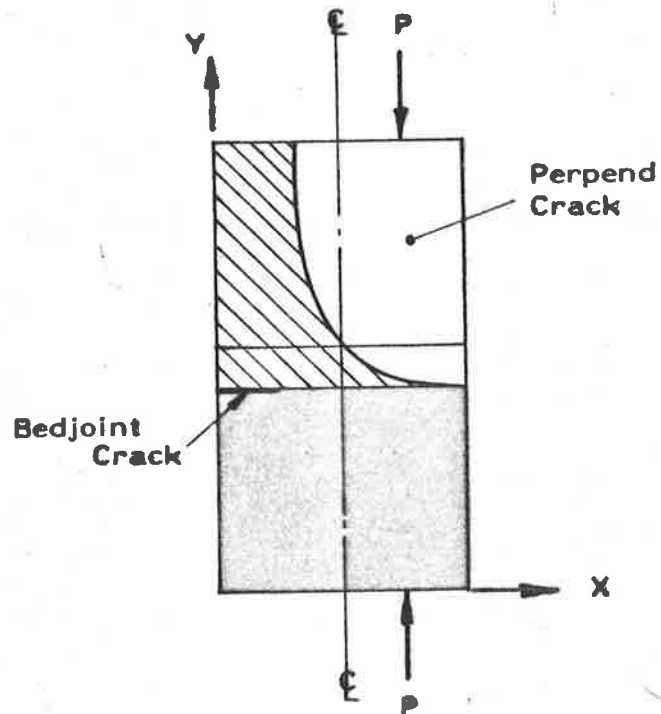


Figure 6.10(b)

**Figure 6.10: Possible Combinations of Perpend and Bedjoint Cracking**

#### 6.2.3.4 Summary

The calculated relative stiffness values (Table 6.3) showed that the stiffness of the brickwork studied (figure 6.1(a), 6.1(b)); when subjected to bending parallel to the bedjoints and cracked on the perpends only, was approximately three-quarters of the uncracked stiffness. Simultaneous cracking of the bedjoints with the perpend reduced the relative stiffness, depending upon the depth of the bedjoint crack and the brick-mortar modular ratio, as shown in Table 6.4.

#### 6.2.4 Torsion in Brickwork

##### 6.2.4.1 Uncracked brickwork

Timoshenko<sup>(112)</sup>, as mentioned in Section 3.3.5.2, showed that an effective shear modulus for orthotropic plates could be calculated by using the expression —

$$G = \frac{\sqrt{E_x \cdot E_y}}{2(1 + \sqrt{\nu_{xy} \cdot \nu_{yx}})} \approx \frac{\sqrt{E_x \cdot E_y}}{2(1 + \nu)} \quad (6.4)$$

in which  $G$  is an effective shear modulus

$E_x, E_y$  are elastic moduli in the principal directions of an orthotropic plate

$\nu_{xy}, \nu_{yx}$  are effective Poisson's ratios for an orthotropic plate in the respective principal directions  $x$  and  $y$

$\nu$  is an effective Poisson's ratio for the plate.

PROGRAM MFYDCP (Appendix E) was used to analyse the panel moduli (Section 6.2.1, figure 6.1(b)) to determine whether an expression similar to equation (6.4) might be developed for uncracked brickwork. For this purpose, it was assumed that the panel module may be subjected to pure twist by applying twisting moments on the

surfaces AA, BB, CC and DD (figure 6.11). As in the case of pure bending, the dimensions of the module given in figure 6.11 refer to the particular bricks used in the experimental panel to be described in Chapter 7.

If the elastic properties of the brick and mortar materials are similar and are assumed to be linear, the displacements of the middle surface of the panel module (parallel to the Y-Z plane of the module in its undeflected state) may be given by the equation –

$$\bar{x} = k(y-60)(z-60) \quad (6.5)$$

in which k is a constant.

The displacements of the panel module middle surface in the Y direction ( $\bar{y}$ ) and in the Z direction ( $\bar{z}$ ) may be taken as all zero.

It may be assumed that any line normal to the middle surface remains normal to that surface after deformations occur due to pure twist. In such a case, the displacements of any point P(x,y,z) within the module, associated with the total twisting moment couples  $\bar{M}_{yz}$  and  $\bar{M}_{zy}$  (figure 6.11) are given by the following equations –

$$\bar{x}_P = \bar{x} = k(y-60)(z-60) \quad (6.6(a))$$

$$\bar{y}_P = -\frac{\partial \bar{x}}{\partial y} (x-32.5) = -k (x-32.5)(z-60) \quad (6.6(b))$$

$$\bar{z}_P = -\frac{\partial \bar{x}}{\partial z} (x-32.5) = -k (x-32.5)(y-60) \quad (6.6(c))$$

Therefore the displacements of any point Q( $x_1, y_1, z_1$ ) on the boundary faces AA, BB, CC and DD (figure 6.11) may be calculated as –

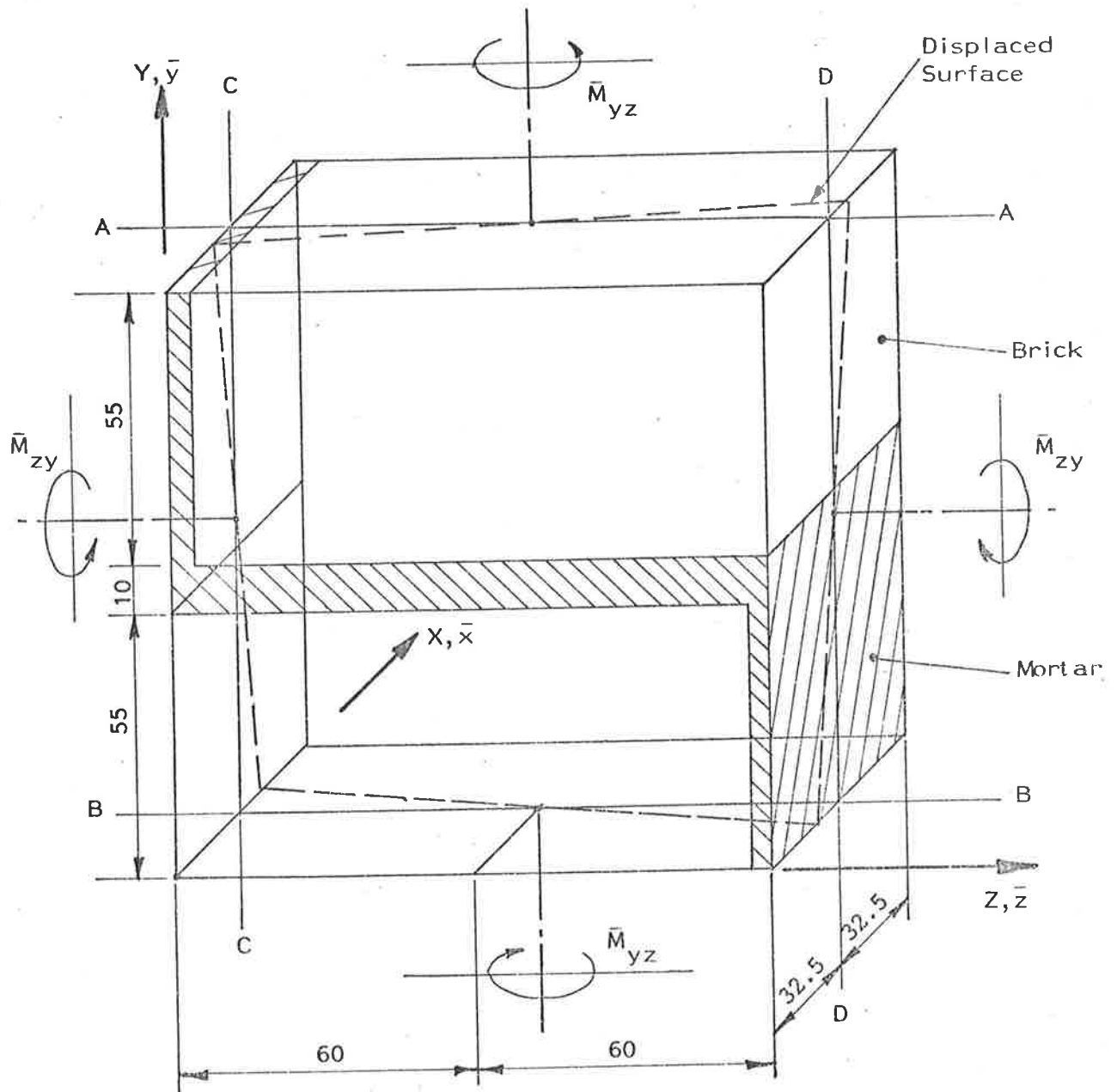


Figure 6.11: Panel Module Subjected to Pure Twist

(i) Boundary face AA( $y_1=120$ )

$$\bar{x}_Q = 60k(z_1-60)$$

$$\bar{y}_Q = -k(x_1-32.5)(z_1-60)$$

$$\bar{z}_Q = -60k(x_1-32.5)$$

(6.6(d))

(ii) Boundary face BB( $y_1=0$ )

$$\bar{x}_Q = -60k(z_1-60)$$

$$\bar{y}_Q = -k(x_1-32.5)(z_1-60)$$

$$\bar{z}_Q = 60k(x_1-32.5)$$

(6.6(e))

(iii) Boundary face CC( $z_1=0$ )

$$\bar{x}_Q = -60k(y_1-60)$$

$$\bar{y}_Q = 60k(x_1-32.5)$$

$$\bar{z}_Q = -k(x_1-32.5)(y_1-60)$$

(6.6(f))

(iv) Boundary face DD( $z_1=120$ )

$$\bar{x}_Q = 60k(y_1-60)$$

$$\bar{y}_Q = -60k(x_1-32.5)$$

$$\bar{z}_Q = -k(x_1-32.5)(y_1-60)$$

(6.6(g))

It should be noted that brickwork in common stretcher bond may be subdivided into modules, as shown in figure 6.12, in which any chosen module is surrounded by four modules, all of which are mirror images of the given module. If all modules are subjected to the same set of twisting moments (figure 6.12), then, in order that deformations at the boundaries of adjacent modules might be compatible, irrespective of the elastic modulus of the brick and mortar materials, any initially-straight line on a module boundary must remain straight after deformations have occurred. That is, for all values of brick and mortar elastic moduli, the displacements at the boundaries of a panel module may be given by equations (6.6(d)), (6.6(e)), (6.6(f)) and (6.6(g)).

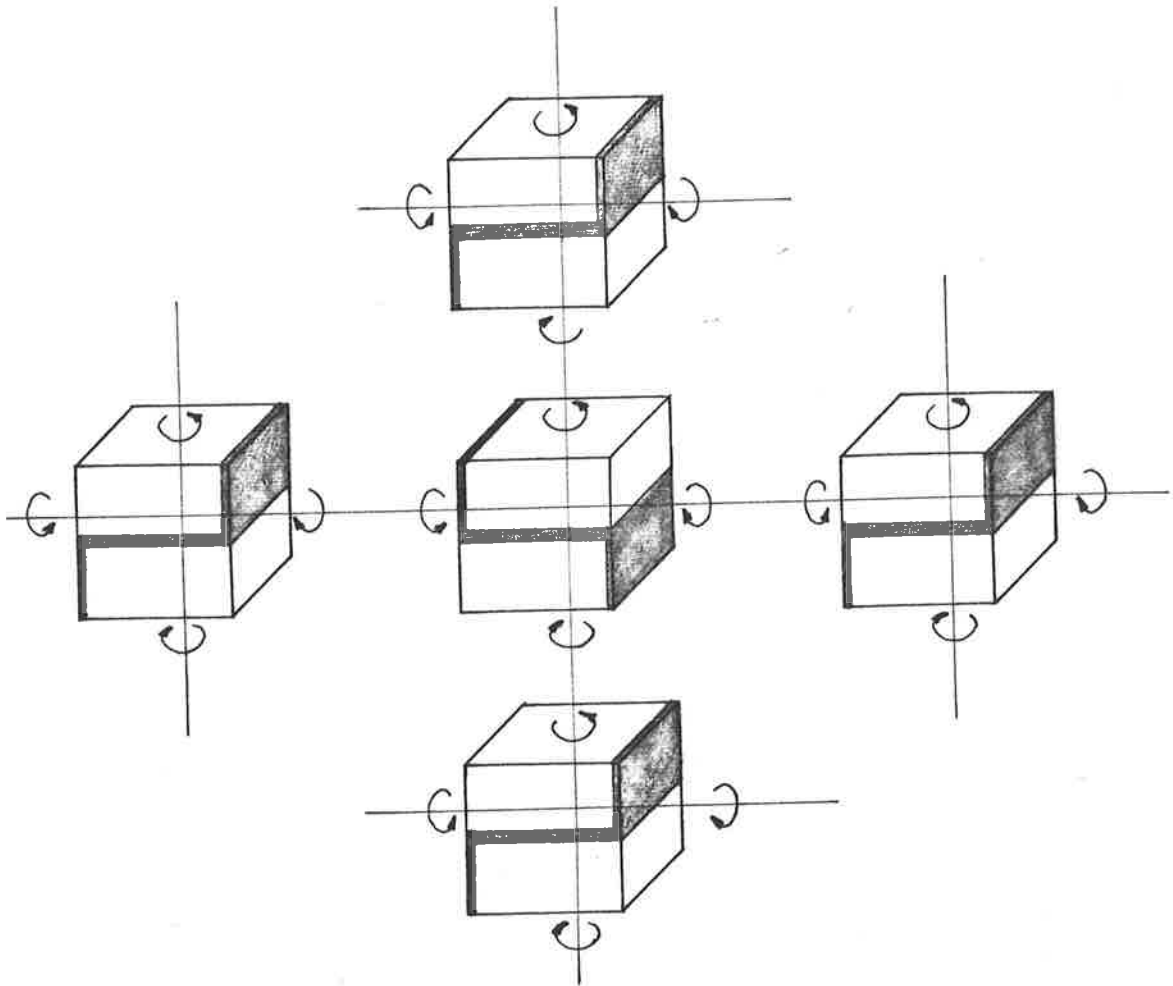


Figure 6.12: Subdivision of Brickwork into Panel Modules  
(showing Twisting Moments)



These equations may be regarded as displacement functions for the boundaries of a brickwork panel module subjected to pure twist; the internal deformations may be calculated subsequently by using a finite element method such as in PROGRAM MFYDCP. As a check on the computed displacements within the panel module shown in figure 6.11, equations (6.5) and (6.6) must hold for the line for which  $y = 60$  and  $z = 60$ , that is  $\bar{x} = 0$ ,  $\bar{x}_p = 0$ ,  $\bar{x}_Q = 0$ .

For all calculations involving PROGRAM MFYDCP, the brick modulus was chosen as  $20 \times 10^3 \text{MPa}$  and the brick:mortar modular ratio was varied between 1.0 and 10.0. For equations (6.6), the constant,  $k$ , was chosen to be  $100 \times 10^{-6}$  so that the maximum displacements  $\bar{x}_Q$ ,  $\bar{y}_Q$  and  $\bar{z}_Q$  were 0.360mm, 0.195mm and 0.195mm respectively. The resulting twist on the panel module (figure 6.11) was  $100 \times 10^{-6} \text{rad/mm}$ . The total twisting moments  $\bar{M}_{yz}$  on faces AA and BB and  $\bar{M}_{zy}$  on faces CC and DD were calculated from the nodal reactions (Table 6.5, figure 6.3). According to Timoshenko<sup>(112)</sup>, the total twisting moment for an isotropic plate with the properties and dimensions of the panel module, when subjected to a twist of  $100 \times 10^{-6} \text{rad/mm}$ , are  $4.776 \times 10^6 \text{Nmm}$

Modular Ratio $E_b : E_m$ (a)	Total Twisting Moments <sup>(b)</sup> ( $\times 10 \text{ Nmm}$ )	
	Faces AA, BB ( $\bar{M}_{yz}$ )	Faces CC, DD ( $\bar{M}_{zy}$ )
1.0	4.78	4.77
2.0	4.65	3.95
5.0	4.39	2.84
10.0	4.10	2.23

(a)  $E_b$  is  $20 \times 10^3 \text{MPa}$

(b) Twist is  $100 \times 10^{-6} \text{rad/mm}$

Poisson's ratio is 0.15.

Table 6.5: Panel Module Subjected to Pure Twist

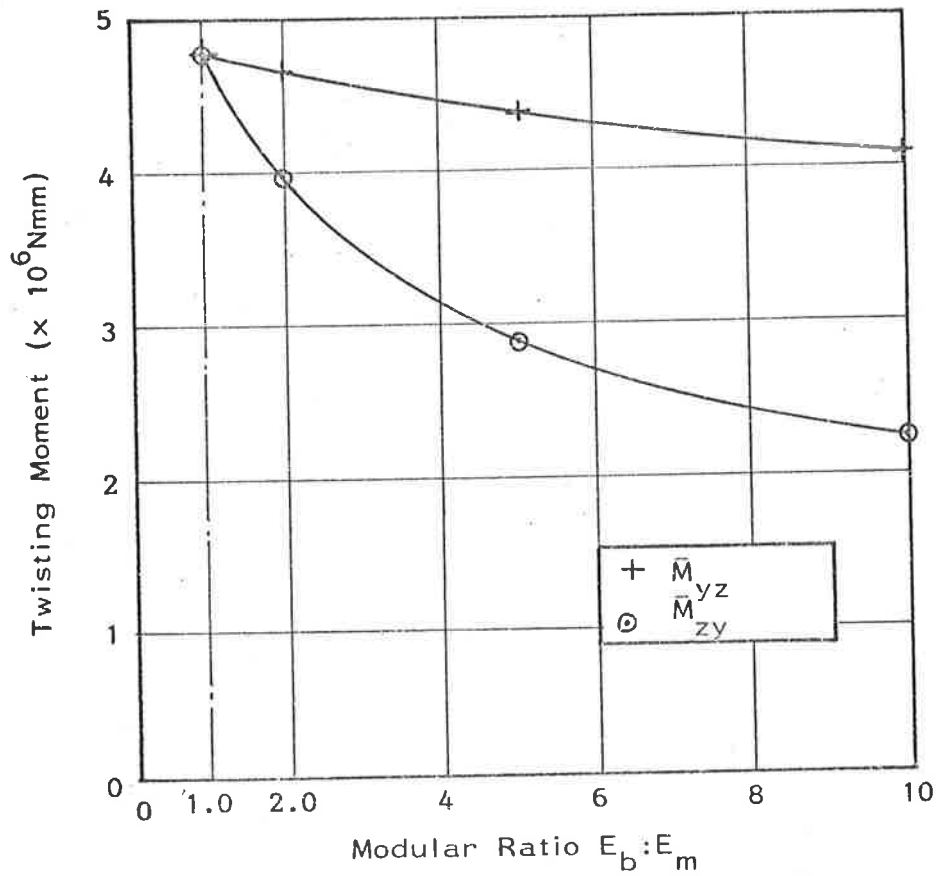


Figure 6.13: Variation of Twisting Moments with Modular Ratio

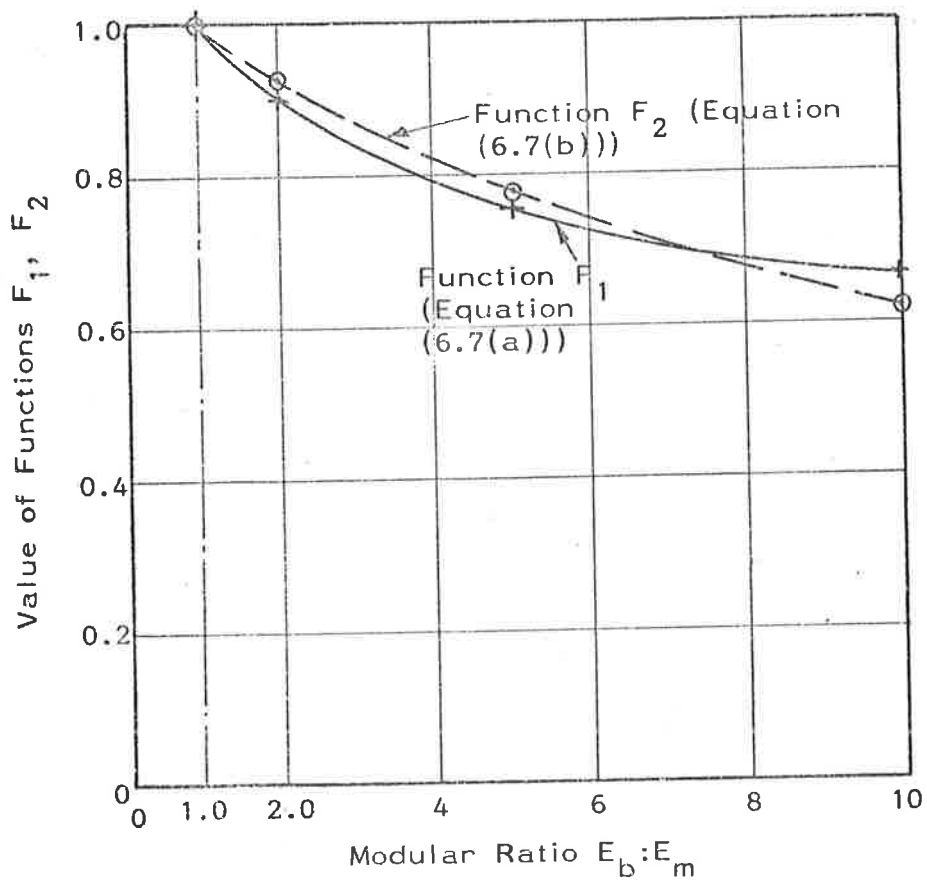


Figure 6.14: Functions F<sub>1</sub> and F<sub>2</sub>

on each face. This compares closely with the values computed for  $\bar{M}_{yz}$  and  $\bar{M}_{zy}$  given in Table 6.5 for a modular ratio of 1.0. As the modular ratio increases, the total twisting moments on faces CC and DD ( $\bar{M}_{zy}$ ) decrease more rapidly than the moments on faces AA and BB ( $\bar{M}_{yz}$ ). This may be attributed in part to the fact that the relative magnitude of the shearing stresses in the perpendicular mortar decreases with increasing modular ratio.

Equivalent elastic moduli  $E_y$  and  $E_z$  may be calculated for the panel module by using equations (4.21) (Section 4.3.1) and (6.2) (Section 6.2.3.1) respectively. By using the results summarized in Table 6.5 and the calculated values of  $E_y$  and  $E_z$ , the following two functions may be plotted (figure 6.14).

$$F_1 (E_b : E_m) = \frac{1}{2} \left( \frac{\bar{M}_{yz} + \bar{M}_{zy}}{\bar{M}} \right) \quad (6.7(a))$$

in which  $\bar{M} = \bar{M}_{yz} = \bar{M}_{zy}$  for a modular ratio of 1.0

$$F_2 (E_b : E_m) = \left[ \frac{E_y \cdot E_z}{E_b \cdot E_b} \right]^{\frac{1}{2}} \quad (6.7(b))$$

in which  $E_b$  is the brick elastic modulus.

It can be shown (Appendix F) that because functions  $F_1$  and  $F_2$  are approximately equal for modular ratios between 1.0 and 10.0, an effective shear modulus for the uncracked brickwork module may be represented by the expression—

$$G = \frac{\sqrt{E_y \cdot E_z}}{2(1 + \nu_b)} \quad (6.8)$$

in which  $E_y$  is an equivalent elastic modulus for bending normal to the bedjoints (equation (4.21))

$E_z$  is an equivalent elastic modulus for bending parallel to the bedjoints (equation 6.2))

$\nu_b$  is Poisson's ratio for the brick only.

By inspection, equation (6.8) is similar to equation (6.4) proposed by Timoshenko<sup>(112)</sup> for orthotropic plates.

#### 6.2.4.2 Brickwork with cracked perpends

It may be assumed that for brickwork with no tensile bond strength, cracking in the perpends is predominantly caused by bending parallel to the bedjoints. The finite element subdivision with simulated perpend cracking, described in Section 6.2.3.2, may be used to analyse a brickwork panel module subjected to twist. With reference to figures 6.11, 6.12, by symmetry, the displacements of the panel module boundary faces AA, BB, CC and DD may be calculated using equations (6.6). By using PROGRAM MFYDCP with the simulated cracked perpends shown in figure 6.8, an effective torsional stiffness for brickwork was calculated for various brick:mortar modular ratios (Table 6.6). The brick elastic modulus was  $20.0 \times 10^3$  MPa for all cases.

Modular Ratio $E_b : E_m$	Relative Torsional Stiffness <sup>(a)</sup> PROGRAM MFYDCP
1.0	0.906
2.0	0.909
5.0	0.928

(a) Torsional stiffness of brickwork having cracked perpends only relative to uncracked brickwork with the same modular ratio.

Table 6.6: Torsional Stiffness of Cracked Brickwork

The calculations using PROGRAM MFYDCP showed that as a result of cracking on the perpends, normal stresses, both tension and compression, might occur at the bedjoint-perpend junction in the bricks and that the magnitude of the normal stresses could be, locally, of the order of the shear stresses. This could indicate, therefore, that

once perpend cracking had occurred because of bending parallel to the bedjoints, tensile failure of the bricks due to normal stress concentration could be expected at the perpend-bedjoint intersection as a result of torsion. This type of failure may also be expected as a result of bending parallel to the bedjoints (Section 6.2.3.2).

#### 6.2.4.3 Brickwork with cracked perpend and cracked bedjoints

Cracking on both the perpend and bedjoint brick-mortar interfaces can be caused by applying an eccentric vertical compression load simultaneously with bending parallel to the bedjoints (Section 6.2.3.3). It may be assumed, as an approximation, that the action of twist does not contribute significantly to bedjoint and perpend cracking. Calculations using PROGRAM MFYDCP, in which the bedjoints are simulated as cracked up to one-half the panel thickness (figure 6.10(a)), Appendix E), showed that the relative torsional stiffnesses of cracked brickwork for various brick:mortar modular ratios were as shown in Table 6.7.

#### 6.2.4.4 Summary

An equivalent shear modulus for uncracked brickwork may be calculated by equation (6.8) which is similar to equation (6.4) proposed by Timoshenko<sup>(112)</sup> for shear in orthotropic plates. The calculated relative torsional stiffness values (Table 6.6) showed that the stiffness of the panel module (figure 6.1(b)) in which the perpend were cracked as a result of bending parallel to the bedjoints, was approximately nine-tenths the stiffness of the brickwork in its uncracked state. Simultaneous cracking of bedjoints and perpend (cracks on the same panel face) reduced the relative torsional stiffnesses in accordance with some function dependent upon the depth of the bedjoint crack (Table 6.7).

Relative Torsional Stiffness <sup>(a)</sup> – PROGRAM MFYDCP			
Modular Ratio $E_b:E_m$	Depth of Bedjoint Crack <sup>(b)</sup>		
	d/6	d/3	d/2
1.0	0.855	0.800	0.766
2.0	0.858	0.805	0.774
5.0	0.869	0.826	0.806

(a) Torsional stiffness of cracked brickwork relative to uncracked brickwork with the same modular ratio. Brick modulus  $20.0 \times 10^3$  MPa for all cases.

(b) Perpend and bedjoint cracks on same panel face (Section 6.2.3.3)

Table 6.7: Torsional Stiffness of Cracked Brickwork

### 6.3 EQUATION OF EQUILIBRIUM AND LOAD-DEFLECTION RELATIONSHIPS FOR A PLATE OF VARYING THICKNESS

#### 6.3.1 The Equation of Equilibrium

The coordinate axes shown on an element of a plate of varying thickness of dimensions  $dx$  by  $dy$  in figure 6.15(a) and the bending moments and shear forces shown in figure 6.15(b) define the positive sign conventions used throughout this section. (Note that the axis system differs from the set of axes used in Section 6.2.) The middle surface shown in figure 6.15(a) is defined so that it is always at the mid-distance between the negative- $z$  and positive- $z$  faces of the element. The in-plane resultant forces (figure 6.15(b)) are assumed to act at the middle surface at the element boundaries.

The equation of equilibrium for the element shown in figures 6.15(a) and 6.15(b) is –

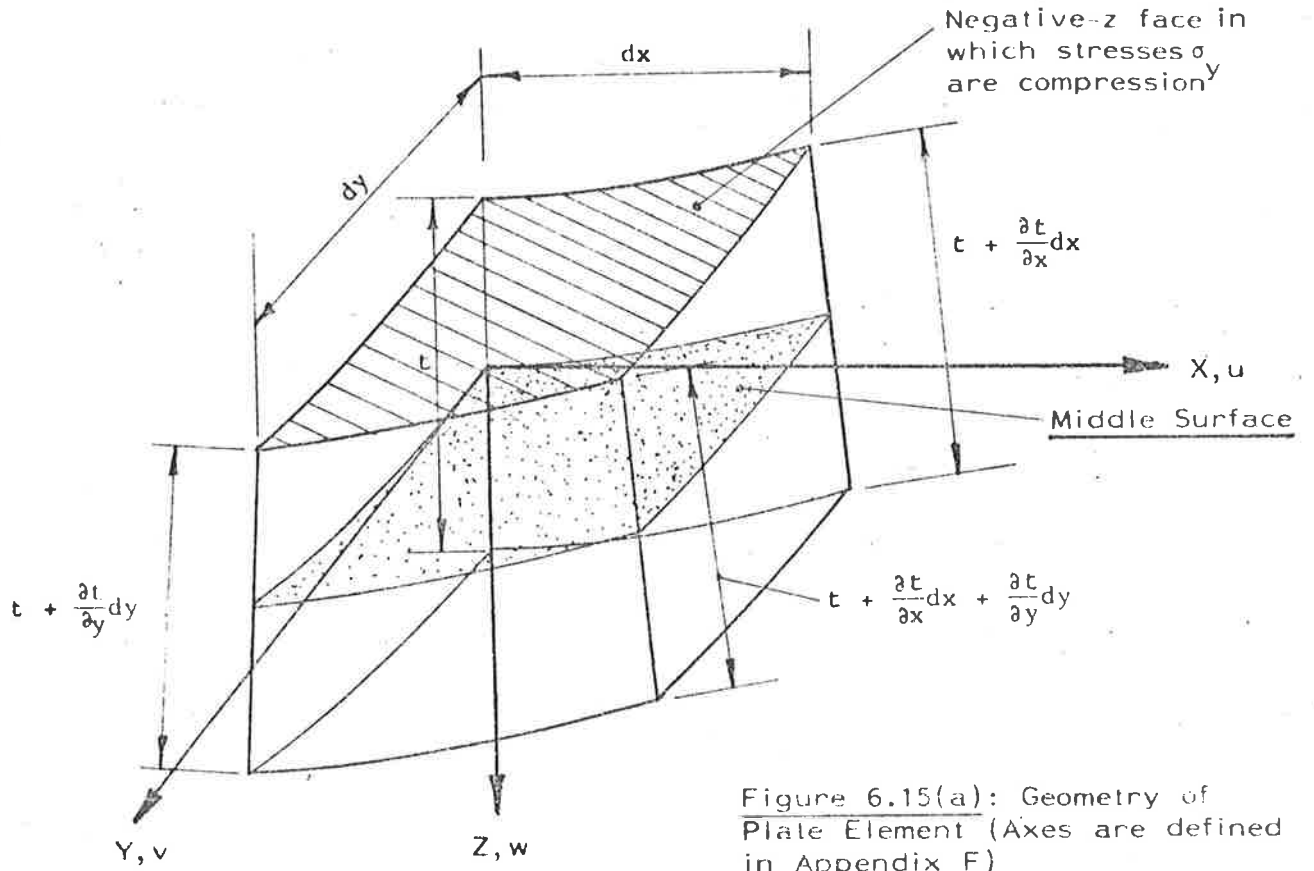


Figure 6.15(a): Geometry of Plate Element (Axes are defined in Appendix F)

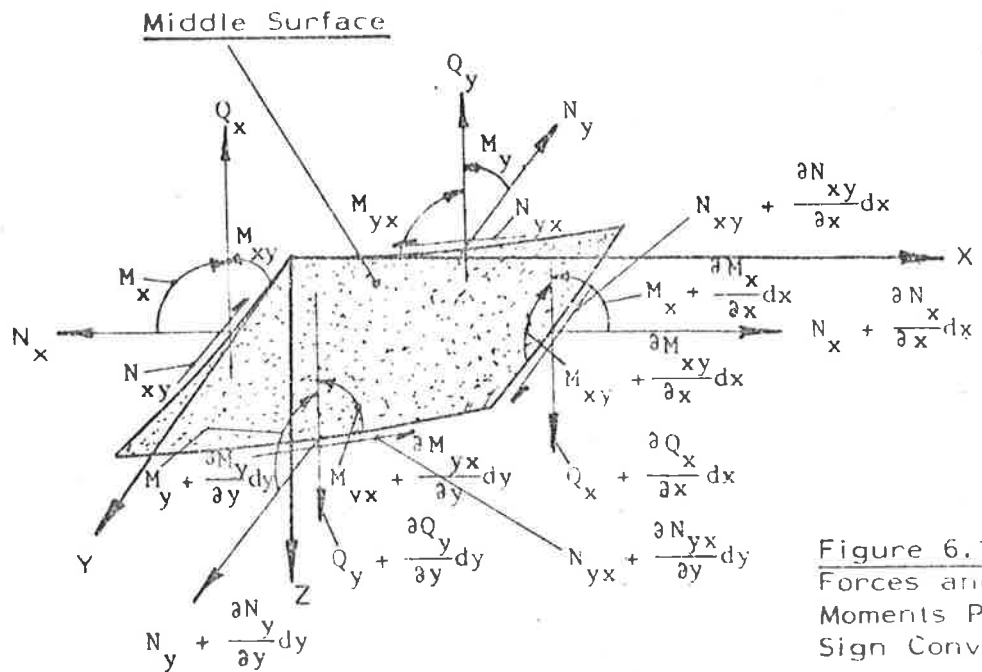


Figure 6.15(b): Forces and Moments Positive Sign Conventions

Figure 6.15: Varying Thickness Plate Element

$$\frac{\partial^2 M_x}{\partial x^2} + \frac{\partial^2}{\partial x \partial y} (M_{xy} + M_{yx}) + \frac{\partial^2 M_y}{\partial y^2} = -[q + N_x \left( \frac{\partial^2 w}{\partial x^2} + \frac{1}{2} \frac{\partial^2 t}{\partial x^2} \right) + N_y \left( \frac{\partial^2 w}{\partial y^2} + \frac{1}{2} \frac{\partial^2 t}{\partial y^2} \right) + 2 \cdot N_{xy} \left( \frac{\partial w}{\partial x \partial y} + \frac{1}{2} \frac{\partial t}{\partial x \partial y} \right)] \quad (6.9)$$

in which  $M_x$  is the moment per unit width of plate associated with normal stresses in the X direction

$M_y$  is the moment per unit width of plate associated with normal stresses in the Y direction

$M_{xy}$  and  $M_{yx}$  are the moments per unit width of plate associated with shear stresses parallel to the X-Y plane

$N_x$  is the normal force per unit width of plate in the X direction

$N_y$  is the normal force per unit width of plate in the Y direction

$N_{xy}$  is the shear force per unit width of plate parallel to the X-Y plane

$q$  is a uniformly applied pressure on the z-faces in the positive-z direction

$t$  is the element thickness.

Equation (6.9) is derived in Appendix F. If the element thickness is constant, equation (6.9) reduces to the plate equation (3.73) in Section 3.4.4, provided that account is taken of the different definitions for positive twisting moments.



### 6.3.2 Constitutive Relationships

Equation (6.9) can be applied to a plate element of varying thickness (figure 6.15(a)) when subjected to the forces shown in figure 6.15(b) irrespective of the material properties of the plate.

Timoshenko<sup>(112)</sup> described the analysis of a rectangular plate, isotropic in its material properties but with varying thickness (Section 3.4.4), and showed that, provided there was no abrupt change in plate thickness, the expressions for bending and twisting moments were similar to the equations for an isotropic plate of constant thickness, viz:

$$M_x = -D\left(\frac{\partial^2 w}{\partial x^2} + \nu \frac{\partial^2 w}{\partial y^2}\right) \quad (6.10(a))$$

$$M_y = -D\left(\frac{\partial^2 w}{\partial y^2} + \nu \frac{\partial^2 w}{\partial x^2}\right) \quad (6.10(b))$$

$$M_{xy} = M_{yx} = -D(1-\nu) \cdot \frac{\partial^2 w}{\partial x \partial y} \quad (6.10(c))$$

in which  $M_x$ ,  $M_y$ ,  $M_{xy}$  and  $M_{yx}$  are defined as in equation (6.9).

$$D \text{ is the plate stiffness} = \frac{Et^3}{12(1-\nu^2)} \quad (6.10(d))$$

in which  $E$  is Young's Modulus for the isotropic plate

$t$  is the plate thickness which varies throughout the plate

$\nu$  is Poisson's ratio.

Timoshenko also reviewed the analysis of anisotropic plates and suggested that the relationships between the stresses and strains for the case of plane stress in the X-Y plane could be represented by the following equations -

$$\sigma_x = E'_x \cdot \epsilon_x + E'' \cdot \epsilon_y \quad (6.11(a))$$

$$\sigma_y = E'_y \cdot \epsilon_y + E'' \cdot \epsilon_x \quad (6.11(b))$$

$$\tau_{xy} = G \gamma_{xy} \quad (6.11(c))$$

in which  $\sigma_x$  is normal stress in the X direction

$\sigma_y$  is normal stress in the Y direction

$\tau_{xy}$  is shear stress parallel to the X-Y plane

$\epsilon_x$  is normal strain in the X direction

$\epsilon_y$  is normal strain in the Y direction

$\gamma_{xy}$  is shear strain parallel to the X-Y plane

$E'_x$ ,  $E'_y$  and  $E''$  are constants related to the elastic

moduli  $E_x$  and  $E_y$  and Poisson's ratios  $\nu_{xy}$  and

$\nu_{yx}$

$G$  is the shear modulus.

The inverse formulation of equations (6.11) is -

$$\epsilon_x = \frac{\sigma_x}{E_x} - \nu_{xy} \cdot \frac{\sigma_y}{E_y} \quad (6.12(a))$$

$$\epsilon_y = \frac{\sigma_y}{E_y} - \nu_{yx} \cdot \frac{\sigma_x}{E_x} \quad (6.12(b))$$

$$\gamma_{xy} = \frac{\tau_{xy}}{G} \quad (6.12(c))$$

In equations (6.12), five constants,  $E_x$ ,  $E_y$ ,  $G$ ,  $\nu_{xy}$  and  $\nu_{yx}$  are needed to describe the elastic properties of the material. However, Timosehniko showed that only four of the constants are independent.

As in the analysis of brickwork walls and columns of varying thickness<sup>(96), (124)</sup>, with reference to figure 6.15(a), it may be assumed that plane sections normal to the z-face in which  $\sigma_y$  stresses are compressive remain plane throughout bending. Equations (6.12) can be used to obtain constitutive relationships similar to equations (6.10), that is<sup>(112)</sup> -

$$M_x = -\frac{E_x \cdot t^3}{12(1 - \nu_{xy} \cdot \nu_{yx})} \cdot \left( \frac{\partial^2 w}{\partial x^2} + \nu_{xy} \cdot \frac{\partial^2 w}{\partial y^2} \right) \quad (6.13(a))$$

$$M_y = -\frac{E_y \cdot t^3}{12(1 - \nu_{xy} \cdot \nu_{yx})} \cdot \left( \frac{\partial^2 w}{\partial y^2} + \nu_{yx} \cdot \frac{\partial^2 w}{\partial x^2} \right) \quad (6.13(b))$$

$$M_{xy} = M_{yx} = -\frac{G \cdot t^3}{6} \cdot \frac{\partial^2 w}{\partial x \partial y} \quad (6.13(c))$$

in which  $w$  is the displacement of the  $z$ -face in which stresses,

$\sigma_y$ , are compressive.

As an extension of equations (6.13), modulus functions  $E_x(t)$ ,  $E_y(t)$  and  $G(t)$  can be derived (Appendix F) which equate the moment-rotation characteristics of a plate of varying thickness to those for real brickwork, so that equations (6.13) become:

$$M_x = -\frac{E_x(t) \cdot t^3}{12(1 - \nu_{xy} \cdot \nu_{yx})} \cdot \left( \frac{\partial^2 w}{\partial x^2} + \nu_{xy} \cdot \frac{\partial^2 w}{\partial y^2} \right) \quad (6.14(a))$$

$$M_y = -\frac{E_y(t) \cdot t^3}{12(1 - \nu_{xy} \cdot \nu_{yx})} \cdot \left( \frac{\partial^2 w}{\partial y^2} + \nu_{yx} \cdot \frac{\partial^2 w}{\partial x^2} \right) \quad (6.14(b))$$

and instead of equation (6.13(c)),

$$(M_{xy} + M_{yx}) = -2 \frac{G(t) \cdot t^3}{6} \cdot \frac{\partial^2 w}{\partial x \partial y} \quad (6.14(c))$$

The functions  $E_x(t)$ ,  $E_y(t)$  and  $G(t)$  are described in Appendix F.

Equations (6.14) for an equivalent plate of varying thickness lead to the calculation of the deflections of a real brickwork panel. The thickness of the equivalent plate at any position in the panel can be calculated from the effective eccentricity of the vertical compression force in the real brickwork. If the effective eccentricity of the resultant vertical load is greater than  $d/6$ , the brickwork is assumed to be cracked on the bedjoints at that point. The equivalent

plate thickness is less than the panel thickness,  $d$ , and can be calculated as follows.

The magnitude of the bending moment,  $M_y$ , about the equivalent plate middle surface is given by

$$|M_y| = \left| \frac{N_y \cdot t}{6} \right| \quad (6.15(a))$$

in which  $N_y$  is the resultant compressive vertical force  
 $t$  is the equivalent plate thickness.

From equation (6.14(b)),

$$M_y = - \frac{E_y(t) \cdot t^3}{12(1 - \nu_{xy} \cdot \nu_{yx})} \cdot \left( \frac{\partial^2 w}{\partial y^2} + \nu_{yx} \cdot \frac{\partial^2 w}{\partial x^2} \right) \quad (6.14(b))$$

Substitution for  $M_y$  in equation (6.15(a)) leads to the result –

$$t = \left[ \frac{2}{E_y(t)} \cdot (1 - \nu_{xy} \cdot \nu_{yx}) \cdot \left| \frac{N_y}{C_y} \right| \right]^{\frac{1}{2}} \quad (6.15(b))$$

$$\text{in which } C_y = \left( \frac{\partial^2 w}{\partial y^2} + \nu_{yx} \cdot \frac{\partial^2 w}{\partial x^2} \right)$$

and  $\left| \frac{N_y}{C_y} \right|$  is the absolute value of the quotient ( $N_y/C_y$ ).

If the resultant vertical load in the brickwork acts within the kern region, the brickwork is not cracked on a bedjoint and the equivalent plate thickness is equal to the panel thickness,  $d$ . Equations (6.9), (6.14) and (6.15) can be solved by an iteration technique described in Section 6.4.

### 6.3.3 Finite Difference Formulation

Consider a wall panel supported on four sides and subdivided into a uniform rectangular finite difference mesh as shown in figure 6.16. In finite difference form; with central differences for bending moments  $M_x$  and  $M_y$  and an averaged first central difference for twisting moment terms  $(M_{xy} + M_{yx})$ , equations (6.14) at node I in figure 6.16 become –

$$M_x(I) \approx -\frac{E_x(t) \cdot t^3}{12(1-\nu_{xy} \cdot \nu_{yx})} \cdot \left[ \frac{w(m-1,n) - 2w(m,n) + w(m+1,n)}{\ell^2} + \nu_{xy} \cdot \frac{w(m,n-1) - 2w(m,n) + w(m,n+1)}{(\Omega \ell)^2} \right] \quad (6.16(a))$$

$$M_y(I) \approx -\frac{E_y(t) \cdot t^3}{12(1-\nu_{xy} \cdot \nu_{yx})} \cdot \left[ \frac{w(m,n-1) - 2w(m,n) + w(m,n+1)}{(\Omega \ell)^2} + \nu_{yx} \cdot \frac{w(m-1,n) - 2w(m,n) + w(m+1,n)}{\ell^2} \right] \quad (6.16(b))$$

$$(M_{xy} + M_{yx})(I) \approx -2 \cdot \frac{G(t) \cdot t^3}{6} \cdot \left[ \frac{w(m+1,n+1) - w(m-1,n+1) - w(m+1,n-1) + w(m-1,n-1)}{4\Omega \ell^2} \right] \quad (6.16(c))$$

The equilibrium equation (6.9) at node I in figure 6.16 can be expressed in finite element form by replacing the partial differential terms with the following expressions –

$$\frac{\partial^2 M_x}{\partial x^2} \approx \frac{M_x(m-1,n) - 2M_x(m,n) + M_x(m+1,n)}{\ell^2} \quad (6.17(a))$$

$$\frac{\partial^2}{\partial x \partial y} (M_{xy} + M_{yx}) \approx \frac{(M_{xy} + M_{yx})(m+1,n+1) - (M_{xy} + M_{yx})(m-1,n+1) - (M_{xy} + M_{yx})(m+1,n-1) + (M_{xy} + M_{yx})(m-1,n-1)}{4\Omega \ell^2} \quad (6.17(b))$$

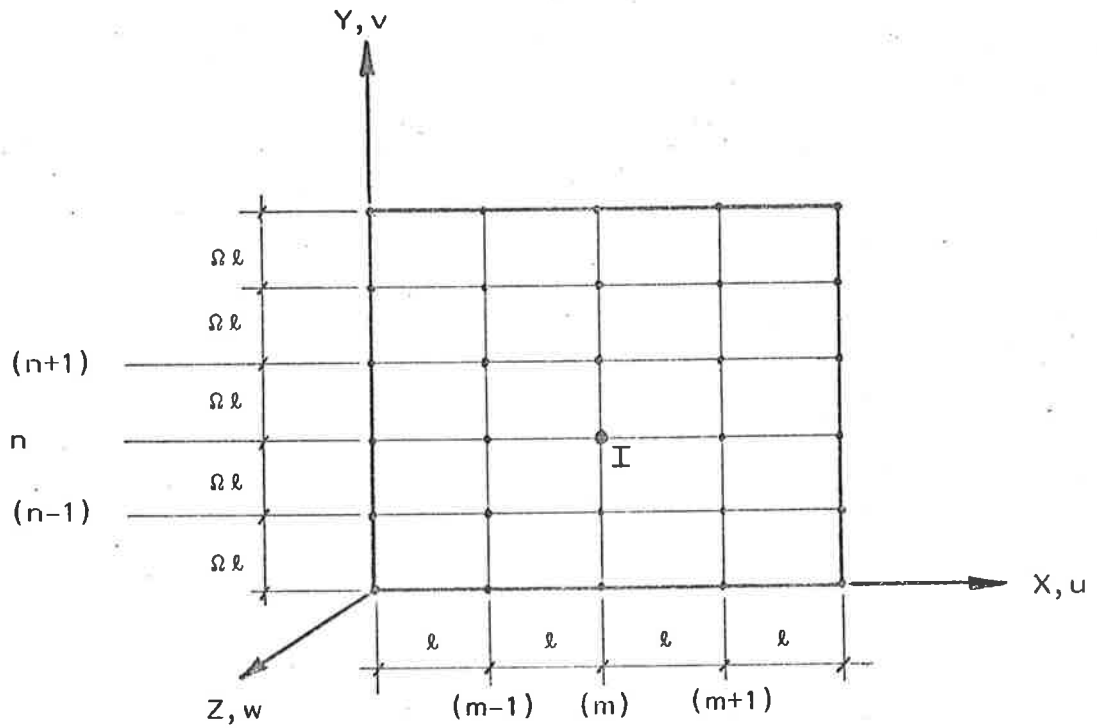


Figure 6.16: Finite Difference Mesh

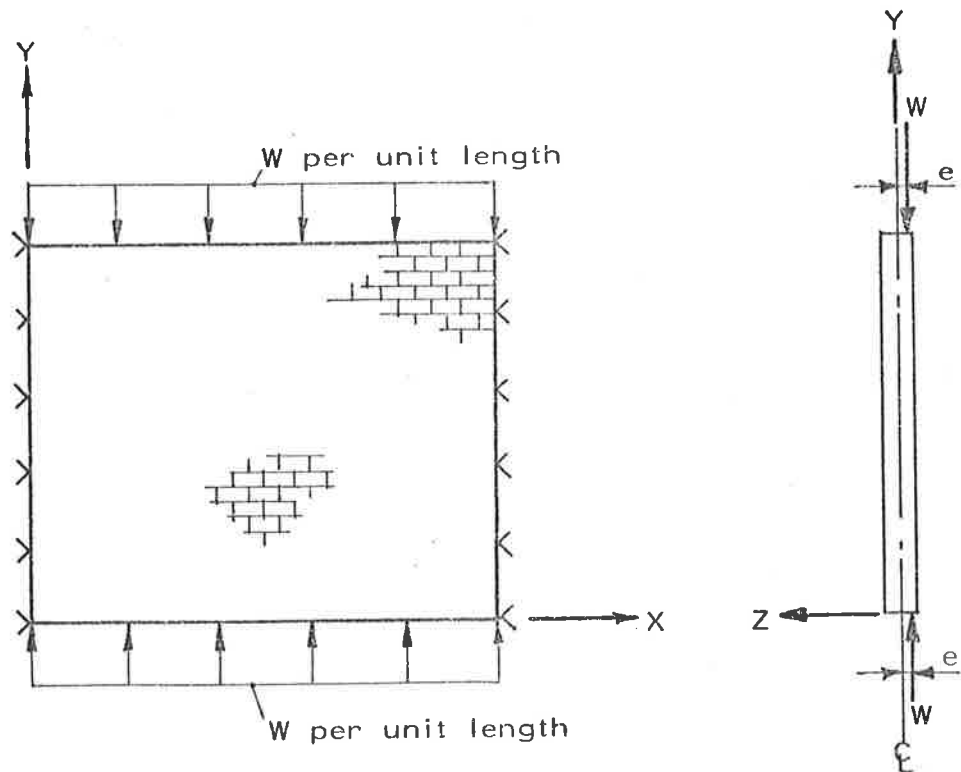


Figure 6.17: Panel Loading Details

$$\frac{\partial^2 M_y}{\partial y^2} = \frac{M_y(m, n-1) - 2M_y(m, n) + M_y(m, n+1)}{(\Omega l)^2} \quad (6.17(c))$$

$$N_x \left( \frac{\partial^2 w}{\partial x^2} + \frac{1}{2} \frac{\partial^2 t}{\partial x^2} \right) = N_x \left[ \frac{w(m-1, n) - 2w(m, n) + w(m+1, n)}{l^2} + \frac{t(m-1, n) - 2t(m, n) + t(m+1, n)}{2l^2} \right] \quad (6.17(d))$$

$$N_y \left( \frac{\partial^2 w}{\partial y^2} + \frac{1}{2} \frac{\partial^2 t}{\partial y^2} \right) = N_y \left[ \frac{w(m, n-1) - 2w(m, n) + w(m, n+1)}{(\Omega l)^2} + \frac{t(m, n-1) - 2t(m, n) + t(m, n+1)}{2(\Omega l)^2} \right] \quad (6.17(e))$$

$$2N_{xy} \left( \frac{\partial^2 w}{\partial x \partial y} + \frac{1}{2} \frac{\partial^2 t}{\partial x \partial y} \right) = 2N_{xy} \left[ \frac{w(m+1, n+1) - w(m-1, n+1) - w(m+1, n-1) + w(m-1, n-1)}{4\Omega l^2} + \frac{t(m+1, n+1) - t(m-1, n+1) - t(m+1, n-1) + t(m-1, n-1)}{8\Omega l^2} \right] \quad (6.17(f))$$

#### 6.3.4 Boundary Conditions

The boundary conditions considered in this thesis for slender brickwork panels are shown in figure 6.17. The panel is simply-supported on all four sides and the load eccentricity,  $e$ , is the same at the top and the base of the panel. The compressive force,  $W$  per unit length of panel, is a uniform load per unit length of wall so that the forces in equation (6.9) in Section 6.3.1 are —

$$\begin{aligned} N_x &= 0 \\ N_y &= -W \\ N_{xy} &= 0 \end{aligned} \quad (6.18)$$

Equation (6.9) becomes, therefore,

$$\begin{aligned} \frac{\partial^2 M_x}{\partial x^2} + \frac{\partial^2}{\partial x \partial y} (M_{xy} + M_{yx}) + \frac{\partial^2 M_y}{\partial y^2} \\ = -q + W \left( \frac{\partial^2 w}{\partial y^2} + \frac{1}{2} \frac{\partial^2 t}{\partial y^2} \right) \end{aligned} \quad (6.19)$$

The solution of equation (6.19), in a finite difference formulation, can be obtained using the grid shown in figure 6.18.

The number of rows and columns of finite difference points can be varied with the number of rows different from the number of columns. At the row of nodes,  $j=2$  in figure 6.18, the moment equations (6.16) in Section 6.3.3 become —

$$M_x(i,2) = \begin{cases} 0 & \text{for } i=2,7 \\ \frac{-E_x(t) \cdot t^3}{12(1-\nu_{xy} \cdot \nu_{yx})} \cdot \nu_{xy} \cdot \left[ \frac{w(i,1) + w(i,3)}{(\Omega l)^2} \right] & \text{for } i=3 \text{ to } 6 \end{cases} \quad (6.20(a))$$

$$M_y(i,2) = \begin{cases} 0 & \text{for } i=2,7 \\ \frac{-E_y(t) \cdot t^3}{12(1-\nu_{xy} \cdot \nu_{yx})} \cdot \left[ \frac{w(i,1) + w(i,3)}{(\Omega l)^2} \right] = \begin{cases} W \cdot e & \text{for } 0 < e \leq d/6 \\ \frac{W}{2} \left( \frac{d}{2} - e \right) & \text{for } d/6 < e < d/2 \end{cases} \end{cases}$$

for  $i=3$  to  $6$

(6.20(b))

$$(M_{xy} + M_{yx})(i,2) = -2 \cdot \frac{G(t) \cdot t^3}{6} \cdot \left[ \frac{w(i+1,3) - w(i-1,3) - w(i+1,1) + w(i-1,1)}{4\Omega l^2} \right]$$

for  $i=2$  to  $7$  (6.20(c))

The displacements of the fictitious nodes on row  $j=1$  can be calculated from equations (6.20(b)), so that —

$$w(i,1) = \begin{cases} 0 & \text{for } i=2,7 \\ -w(i,3) - \frac{12(1-\nu_{xy} \cdot \nu_{yx}) \cdot (\Omega l)^2 \cdot W \cdot e}{E_y(d) \cdot d^3} & \text{for } 0 < e \leq d/6 \\ -w(i,3) - \frac{12(1-\nu_{xy} \cdot \nu_{yx}) \cdot (\Omega l)^2 \cdot \left( \frac{W}{2} (d/2 - e) \right)}{E_y(t) \cdot t^3} & \text{for } d/6 < e < d/2 \end{cases} \left. \begin{array}{l} \text{for} \\ i=3 \\ \text{to } 6 \end{array} \right\} \quad (6.21)$$



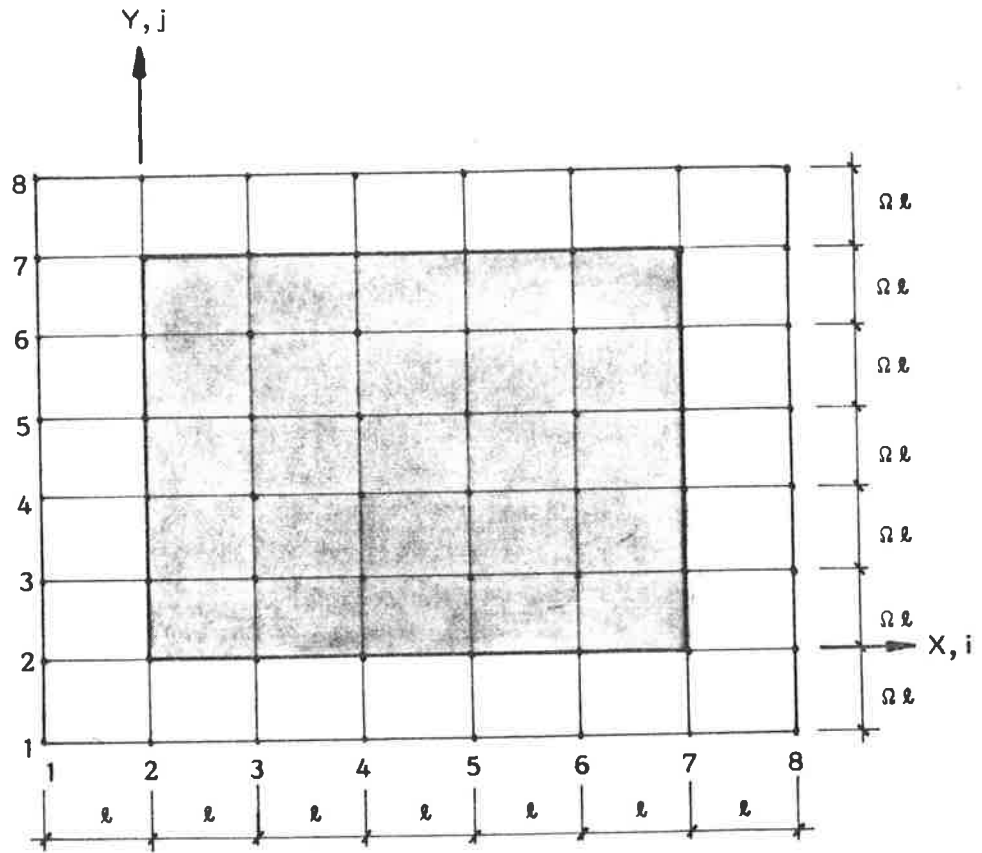


Figure 6.18: Finite Difference Mesh for Simply-supported Panel  
Showing Fictitious Nodes outside Panel Edges

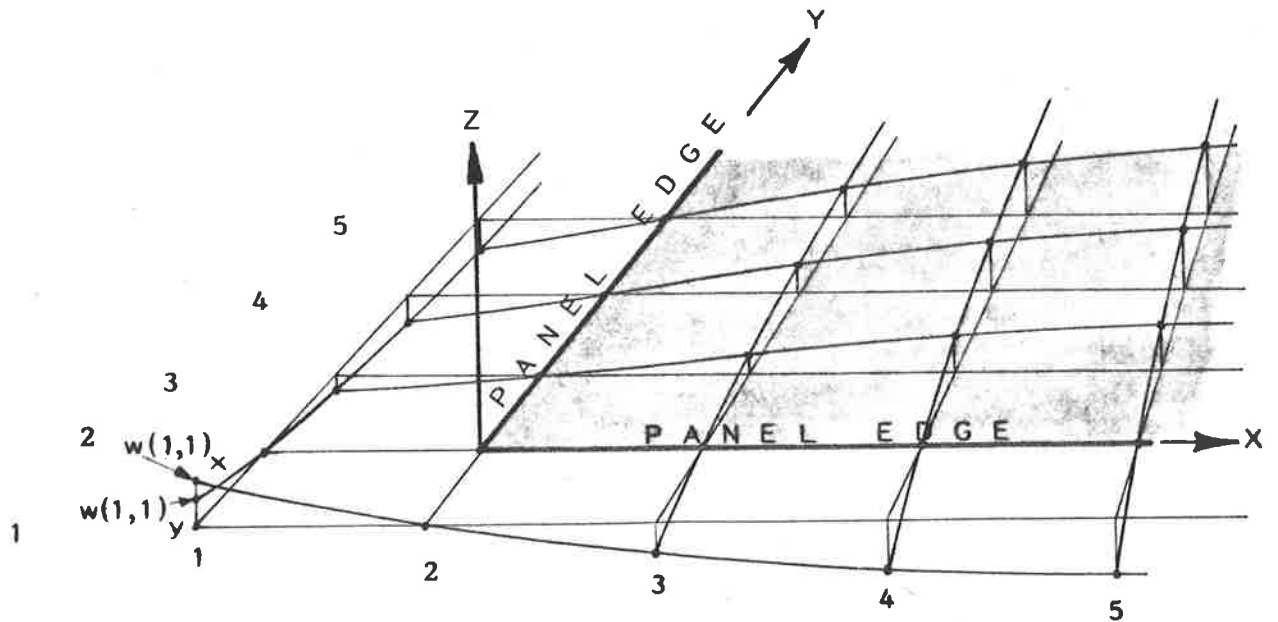


Figure 6.19: Quadratic Extrapolation for Displacement  
of Corner Fictitious Node

The displacements for nodes (1,3) and (8,3) are also required for the calculation of twisting moments ( $M_{xy} + M_{yx}$ ) on row  $j=2$ . At the simply-supported boundaries,  $M_x(2,3)$  and  $M_x(7,3)$  are zero, so that, from equation (6.16(a)),

$$\begin{aligned} w(1,3) &= -w(3,3) \\ w(8,3) &= -w(6,3) \end{aligned} \quad (6.22)$$

Equations similar to equations (6.20), (6.21) and (6.22) can also be derived for nodal row  $j=7$  (figure 6.18).

The twisting moments ( $M_{xy} + M_{yx}$ ), at the panel corner nodes (2,2), (7,2), (2,7) and (7,7) are also required, which implies that the displacements of fictitious corner nodes (1,1), (8,1), (1,8) and (8,8) must be calculated (equation (6.16(c))). The displacements of the fictitious corner nodes may be approximated by quadratic extrapolation of the edge fictitious nodes, as shown in figure 6.19. On the row  $j=1$ , it can be shown that for quadratic extrapolation on fictitious nodes —

$$w(1,1)_x = w(4,1) - 3w(3,1) \quad (6.23(a))$$

Similarly, on the column  $i=1$ , it can be shown that

$$w(1,1)_y = w(1,4) - 3w(1,3) \quad (6.23(b))$$

The mean of the two solutions  $w(1,1)_x$  and  $w(1,1)_y$  may be used in the calculations for ( $M_{xy} + M_{yx}$ ) at the panel corner node (2,2), so that —

$$w(1,1) = \frac{1}{2}[w(4,1) - 3w(3,1) + w(1,4) - 3w(1,3)] \quad (6.24)$$

with similar expressions for displacements  $w(8,1)$ ,  $w(1,8)$  and  $w(8,8)$ . The displacements,  $w$ , on the four panel edges are zero.

#### 6.4 SOLUTION PROCEDURE

Figure 6.18 (Section 6.3.4) shows a brickwork panel subdivided into a  $5 \times 5$  finite difference mesh in which the grid lines do not necessarily coincide with the mortar perpends and bedjoints. The subdivision is different from that for a brick wall (figure 4.15, Section 4.4) in which the nodes were specified to be at the mid-height of the mortar joints. The large number of mortar joints in a panel prohibited the placement of a node at every joint so that a grid size was selected (Section 6.5) which gave a compromise between the accuracy of the solutions and the time taken for computation.

The equilibrium equation (6.19) was applied at all the internal nodes in the panel, that is, all nodes excluding the nodes on the panel boundaries. At any node at which either perpend cracking or bedjoint cracking occurred, the equations for the bending and twisting moments changed with the depth of the bedjoint crack. The set of simultaneous equations generated for all the internal nodes, plus the equations at the boundaries, were non-linear and direct solutions could not be obtained. The method proposed for the solution of the equations was similar to the technique used for solving the non-linear equations for a brick wall (Section 4.4). The vertical uniform load,  $W$ , was applied incrementally and at each load increment, a Newton-Raphson method was used to find a consistent set of values for the nodal deflections,  $w$ , and the nodal effective thicknesses,  $t$ , such that the equilibrium equation (6.19) was satisfied to within a prescribed error at all nodes. As the ratio of the node displacement increments to load increment increased, the magnitude of the load increment was decreased. Panel buckling was deemed to have occurred if no configuration of displacements could be found for the incremented load.

Calculations were started with a small value of  $W$  and all node displacements,  $w$ , were set to zero. At each internal node, the effective panel thickness was calculated by equations (6.15) and the modulus functions  $E_x(t)$ ,  $E_y(t)$  and  $G(t)$  were evaluated (Appendix F). The bending moments  $M_x$  and  $M_y$  were calculated at all internal nodes and the twisting moments,  $(M_{xy} + M_{yx})$ , were calculated at all internal nodes and at all nodes on the boundary (Sections 6.3.3, 6.3.4).

An error term, given by rearranging equation (6.19), was calculated at each internal node  $I(m,n)$  as —

$$\begin{aligned} \xi(m,n) = & \frac{\partial^2 M_x(m,n)}{\partial x^2} + \frac{\partial^2}{\partial x \partial y} (M_{xy} + M_{yx})(m,n) \\ & + \frac{\partial^2 M_y(m,n)}{\partial y^2} + q - W \left( \frac{\partial^2 w}{\partial y^2} + \frac{1}{2} \frac{\partial^2 t}{\partial y^2} \right) \end{aligned} \quad (6.25)$$

In finite difference form (equations (6.17), figure 6.18), equation (6.25) is —

$$\begin{aligned} \xi(m,n) = & \frac{M_x(m-1,n) - 2M_x(m,n) + M_x(m+1,n)}{\ell^2} \\ & + \left[ \frac{(M_{xy} + M_{yx})(m+1,n+1) - (M_{xy} + M_{yx})(m-1,n+1)}{4\Omega\ell^2} \right. \\ & \left. - \frac{(M_{xy} + M_{yx})(m+1,n-1) - (M_{xy} + M_{yx})(m-1,n-1)}{4\Omega\ell^2} \right] \\ & + \frac{M_y(m,n-1) - 2M_y(m,n) + M_y(m,n+1)}{(\Omega\ell)^2} \\ & + q - W \left[ \frac{w(m,n-1) - 2w(m,n) + w(m,n+1)}{(\Omega\ell)^2} \right. \\ & \left. + \frac{t(m,n-1) - 2t(m,n) + t(m,n+1)}{2(\Omega\ell)^2} \right] \end{aligned} \quad (6.26)$$

The error term, equation (6.26), is a measure of the out-of-balance of force in the  $z$ -direction and is related to the displacement and force resultants in the equilibrium equation (6.19) at node  $I(m,n)$  (figure 6.18). The error terms at all nodes were grouped into an error vector  $\{\xi\}$ . In the solution procedure, if no component of  $\{\xi\}$  exceeded a limit, selected to be  $1.0 \times 10^{-6}$  (Newtons), the displaced shape of

of the panel was assumed to be in equilibrium with the external forces. If any component of  $\{\xi\}$  exceeded the limit of  $1.0 \times 10^{-6}$  (Newtons), a Newton-Raphson method of correction was applied until the desired accuracy was reached (Section 4.4.3).

The correction to displacements was calculated, for the  $k^{\text{th}}$  iteration, by the equations

$$[J]_k \{\Delta w\}_k = -\{\xi\}_k \quad (6.27)$$

$$\{w\}_{k+1} = \{w\}_k + \{\Delta w\}_k \quad (6.28)$$

In equation (6.27),  $[J]$  is the "Jacobian" of  $\{\xi\}$  and is a square matrix formed by the partial derivatives of the components of  $\{\xi\}$  with respect to the components of the solution vector,  $\{w\}$ . Elements of the "Jacobian" matrix were evaluated numerically by incrementing successively the solution vector,  $\{w\}$ , and calculating the increments of the error vector, as described in Section 4.4.3. Generally, the largest component of the error vector  $\{\xi\}$  was reduced to a value less than the selected limit in less than ten iteration cycles. Once equilibrium was attained for a specified load,  $W$ , the load was increased and new displacements were calculated using the iteration technique. A further increment in load was then applied, and so on, until a load was reached for which no displacements were calculated after one hundred iterations. The panel was deemed to have failed by buckling at that load.

## 6.5 RESULTS OF THE NUMERICAL METHOD

PROGRAM PANEL1, documented in Appendix G, has been used to calculate the buckling failure loads of a range of brickwork panels simply-supported on four sides. In this section, it is assumed that the material strength does not affect the failure mode of the panels;

brickwork panels which fail as a result of material failure are examined in detail in Chapter 8.

With reference to figure 6.17, the load is applied with equal eccentricity top and bottom and the panel length-to-height ratios vary between 1.0 and 10.0. The brick elastic modulus is arbitrarily  $16 \times 10^3$  MPa in all cases and the mortar is assumed to be linear with a modulus of  $8 \times 10^3$  MPa. The lateral pressure,  $q$ , on all panels is assumed to be zero. Buckling failure loads were calculated using two finite difference grids, 6 by 6 and 8 by 8 (figure 6.18), and the panel buckling failure load was calculated for each case by using a "delta-squared extrapolation" on the two sets of results. The resulting correction on the buckling loads for an eccentricity of  $d/12$ , calculated using an 8 by 8 grid, was approximately 3 percent for length-to-height ratio of 1.0 and approximately 1.5 percent for an  $l/h$  of 10.0. The corrections were similar for eccentricities of  $d/4$  and  $d/1000$ .

The calculated results, shown in figure 6.20, show that the buckling failure load decreases as the panel aspect ratio,  $l/h$ , increases and that for panels with aspect ratios greater than 5.0, the buckling failure load is within 30 percent of the buckling load of a wall of similar height supported top and bottom (Table 6.8).

In figure 6.20, it is evident that the buckling failure load of a brickwork panel decreases with increasing load eccentricity and that the failure load of a brickwork panel under near-axial load ( $d/1000$ ) is approximately equal to the failure load calculated using equation (3.79) derived for non-cracking panels of uniform thickness<sup>(112)</sup>. This shows that the buckling failure loads of brickwork panels subjected to vertical loads which are close to axial may be calculated by PROGRAM PANEL1.

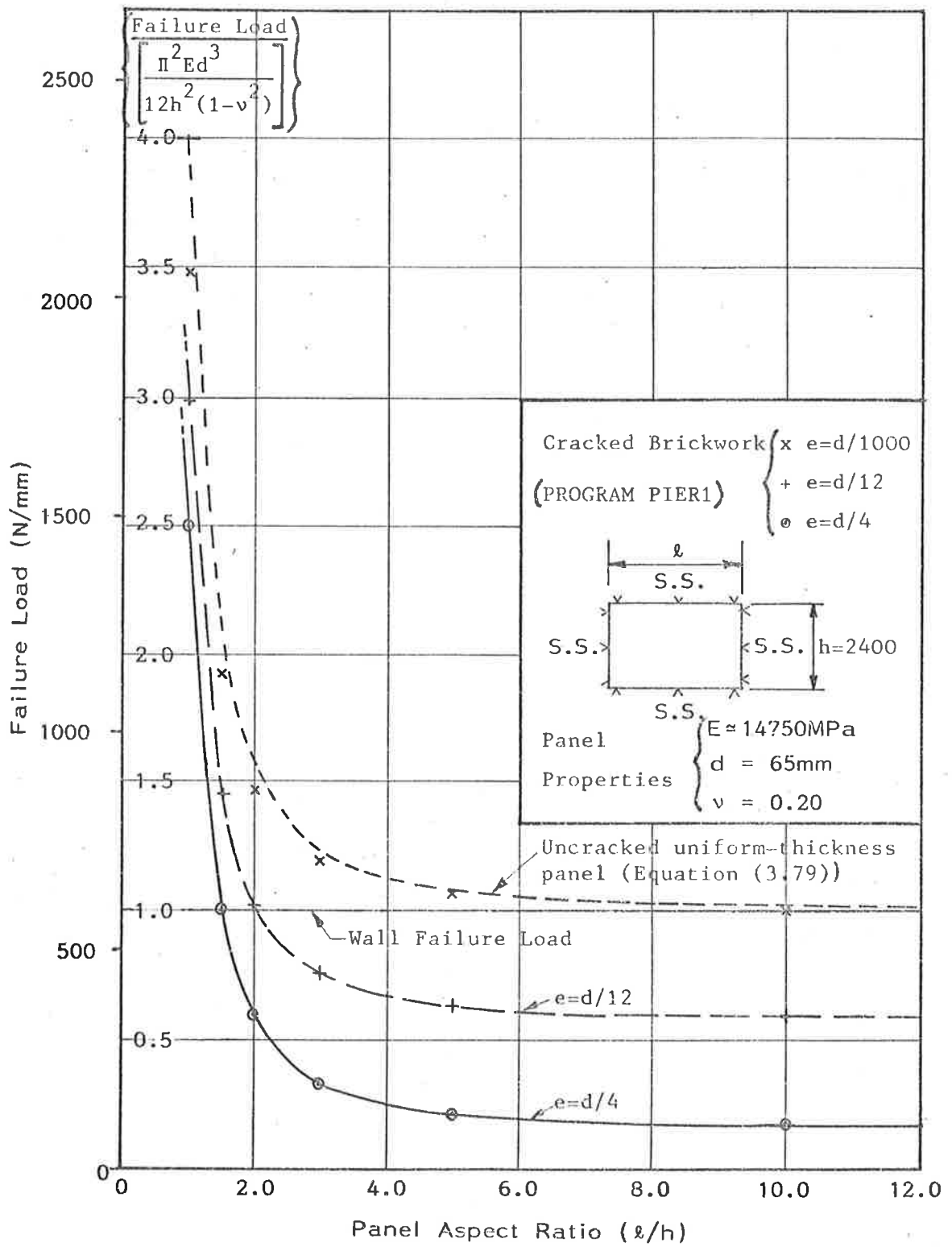


Figure 6.20: Buckling Failure Loads of Cracked Brickwork Panels

Load Eccentricity	Calculated Buckling Failure Load (N/mm)		
	(PROGRAM PANEL1) Aspect Ratio $l/h$		(PROGRAM PIER1) Wall/Column
	5.0	10.0	
d/1000	631	594	577
d/12	375	357	342
d/4	127	102	95

Table 6.8: Buckling Loads of Brickwork Panels and Walls

## 6.6 SUMMARY AND CONCLUSIONS

A method of analysis has been proposed in which the deformations of a brickwork panel supported on four sides and loaded by in-plane vertical compression forces may be calculated by replacing the brickwork with an equivalent plate of varying thickness. The bending and torsion stiffnesses of the equivalent plate have been calculated by analysing a brickwork module using a three-dimensional finite element program (PROGRAM MFYDCP) and the results have been incorporated into finite difference formulations of the plate equations in PROGRAM PANEL1.

The finite difference method permits the analysis of panels with various boundary conditions by altering the constraints on boundary nodes and the fictitious nodes generated outside the panel boundaries. The scope of PROGRAM PANEL1 may be extended to include a range of boundary conditions as well as initial imperfections in the panel, as in PROGRAM PIER1 (Appendix C).

PROGRAM PANEL1 has been applied to the analysis of brickwork panels constructed of 110mm x 65mm x 230mm bricks on edge, as in



the experimental tests described in Chapter 7. The calculated buckling failure loads for brickwork panels, summarized in figure 6.20, have not been obtained previously.

## 7. EXPERIMENTS ON BRICKWORK PANELS

### 7.1 INTRODUCTION

A series of experiments was carried out on small brickwork panels designed to check the finite element calculations described in Section 6.2.3. In addition, a full scale panel was tested as a particular case study in order to compare the predictions of the finite difference PROGRAM PANEL1 with actual panel behaviour.

The small brickwork panels were subjected to bending parallel to the bedjoints and the moment-curvature characteristics were determined both before as well as after cracking on the perpends had occurred. An axial vertical stress was applied to check the effect of axial stresses normal to the bedjoints on the behaviour of brickwork in horizontal bending.

PROGRAM PANEL1 was tested by loading a slender, simply-supported brickwork panel eccentrically top and bottom with a uniform vertical load. The development of the test apparatus constituted a significant part of the experiment because of the scale of the test and the quantity of data needed to obtain a meaningful interpretation of the structural action. Details of the test apparatus are presented and comparisons are made between measured deflections and the values calculated using PROGRAM PANEL1.

### 7.2 BRICKWORK PANELS SUBJECTED TO BENDING PARALLEL TO THE BEDJOINTS

Six brickwork panels, each six bricks long by five courses high, were constructed to test the following —

1. Page's<sup>(95)</sup> proposition that shear deformations in brickwork are not sensitive to the degree of compression normal to the bedjoint.
2. The proposition by Base and Baker<sup>(69)</sup> that the effective stiffness of uncracked brickwork subjected to bending parallel to the bedjoints may be calculated using equation (6.2).
3. The ratios of stiffness after cracking to stiffness before cracking in the perpends, as summarized in Table 6.3.
4. The method of calculation proposed by Sahlin<sup>(44)</sup> and Royen<sup>(88)</sup> which may be used to determine whether failure will occur by torsional shear failure on the bedjoints or by tensile failure in the bricks.

All bricks were selected to be approximately 230mm x 110mm x 65mm and were laid on-edge to give the panels a height-to-thickness ratio of 9.1. The mortar was 1 cement:1 lime:6 sand by volume with a water-to-cement ratio of 1.41 by weight. All bricks were solid and were selected to have no visible chips or cracks and were laid in a saturated surface-dry condition. All panels were cured in polythene sheeting for 21 days and subsequently were cured in ambient conditions.

Three bricks from the batch were tested<sup>(116)</sup> in compression using pairs of 30mm long strain gauges to determine the strains. The brick elastic modulus results are shown in Table 7.1.

Brick No.	Elastic Modulus ( $\times 10^3$ MPa)
1	21.9
2	21.7
3	19.6

Table 7.1: Brick Elastic Modulus

The mean brick elastic modulus was  $21.1 \times 10^3$  MPa with a coefficient of variation of 4.9 percent.

Six mortar prisms  $25\text{mm} \times 25\text{mm} \times 50\text{mm}$  were cast for each of the six panels constructed and one prism from each mortar batch was tested in compression to measure the mortar elastic modulus (Table 7.2).

Panel No.	Mortar Prism Elastic Modulus ( $\times 10^3$ MPa)
1	12.1
2	12.5
3	11.6
4	13.4
5	12.5
6	11.4

Table 7.2: Mortar Elastic Modulus

The mean mortar prism elastic modulus was  $12.3 \times 10^3$  MPa with a coefficient of variation of 5.4 percent.

Six brickwork prisms, each four bricks high, were constructed with the panels and were tested in axial compression to failure between 4mm sheets of plywood (Table 7.3).

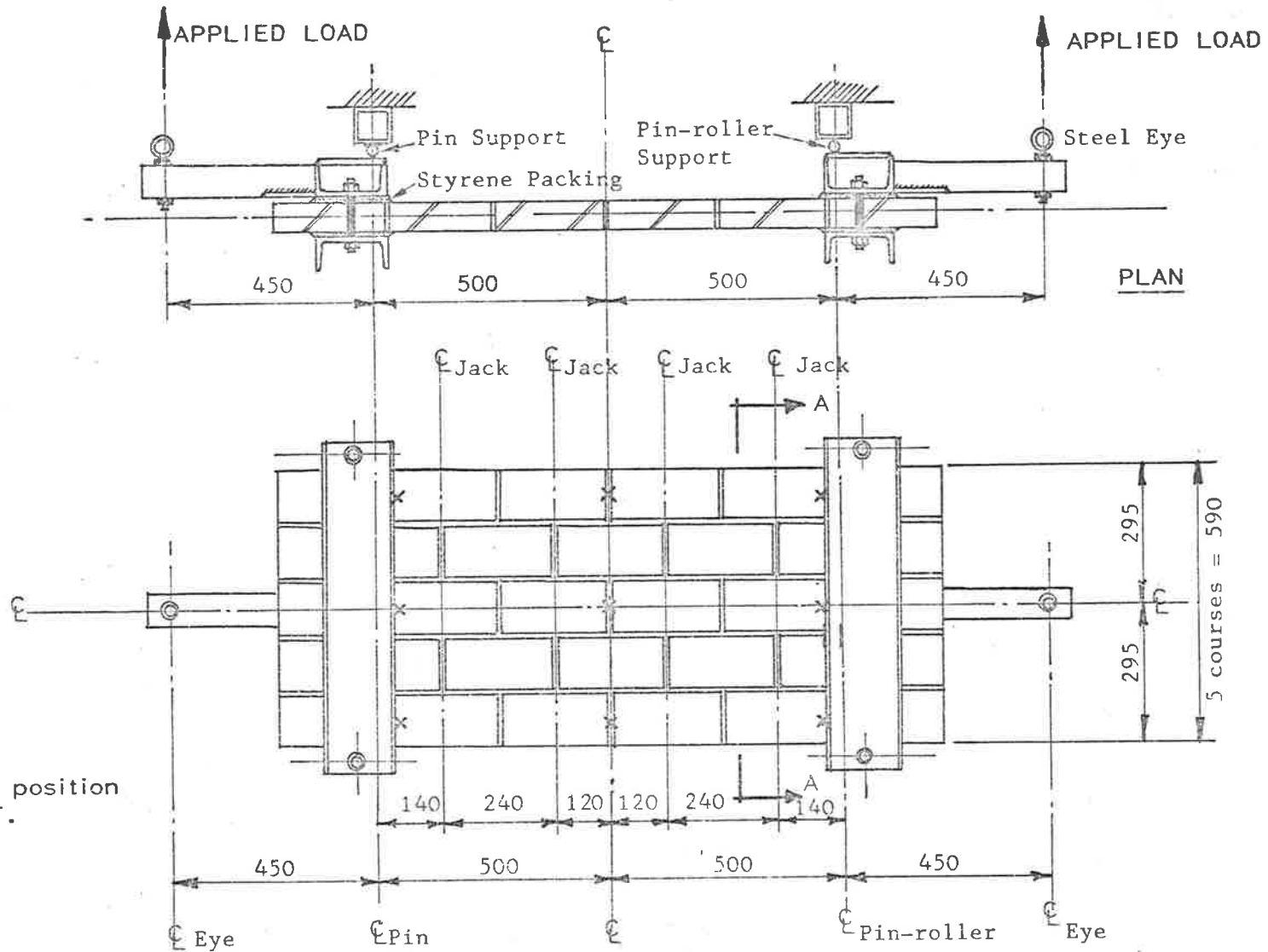
Prism No.	Axial Stress at Failure (MPa)	Ratio( $\frac{\text{Mean Elastic Modulus}^{(a)}}{\text{Failure Stress}}$ )
1	52.3	381
2	48.7	409
3	48.9	407
4	51.3	388
5	49.7	401
6	49.4	403

(a) Mean Elastic Modulus Values calculated from Tables 7.1 and 7.2 and equation (5.4).

The mean compression failure stress was 50.0MPa with a coefficient of variation of 3 percent and the mean ratio of mean elastic modulus to failure stress was 398 with a coefficient of variation of 3 percent.

Each panel was set up in the test apparatus shown in figures 7.1 so that a vertical axial load could be applied simultaneously with a uniform bending moment parallel to the bedjoints. Initially no vertical load was applied to the panel and the horizontal force at each loading point (figure 7.1(a)) was increased by increments to approximately 0.75KN. This produced a bending moment parallel to the bedjoints of approximately  $350 \times 10^3 \text{Nmm}$  which was insufficient to cause cracking in the perpends. The out-of-plane displacements of the panel were measured using linear voltage displacement transducers (L.V.D.T.) constructed to a multi-channel logger and the three curvatures (top, centre and bottom) in the horizontal plane were calculated at each load increment by using the computing facilities in the logger. The three curvatures were found to be within 5 percent of one another. A plot of applied moment against horizontal curvature is shown in figure 7.2(a) for curvature calculated on the horizontal centreline.

Subsequently, the panel was subjected to bending parallel to the bedjoints simultaneously with a vertical axial stress of 1.3MPa applied by the four hydraulic jacks (figure 7.1). A vertical stress of 2.6MPa was then applied simultaneously with the horizontal bending. The relationships between the applied moments and the panel curvatures in the horizontal plane, shown typically in figure 7.2, are summarized in Table 7.4.



SIDE ELEVATION (Jack Yokes Omitted for Clarity)

Figure 7.1(a): Small Panel Details

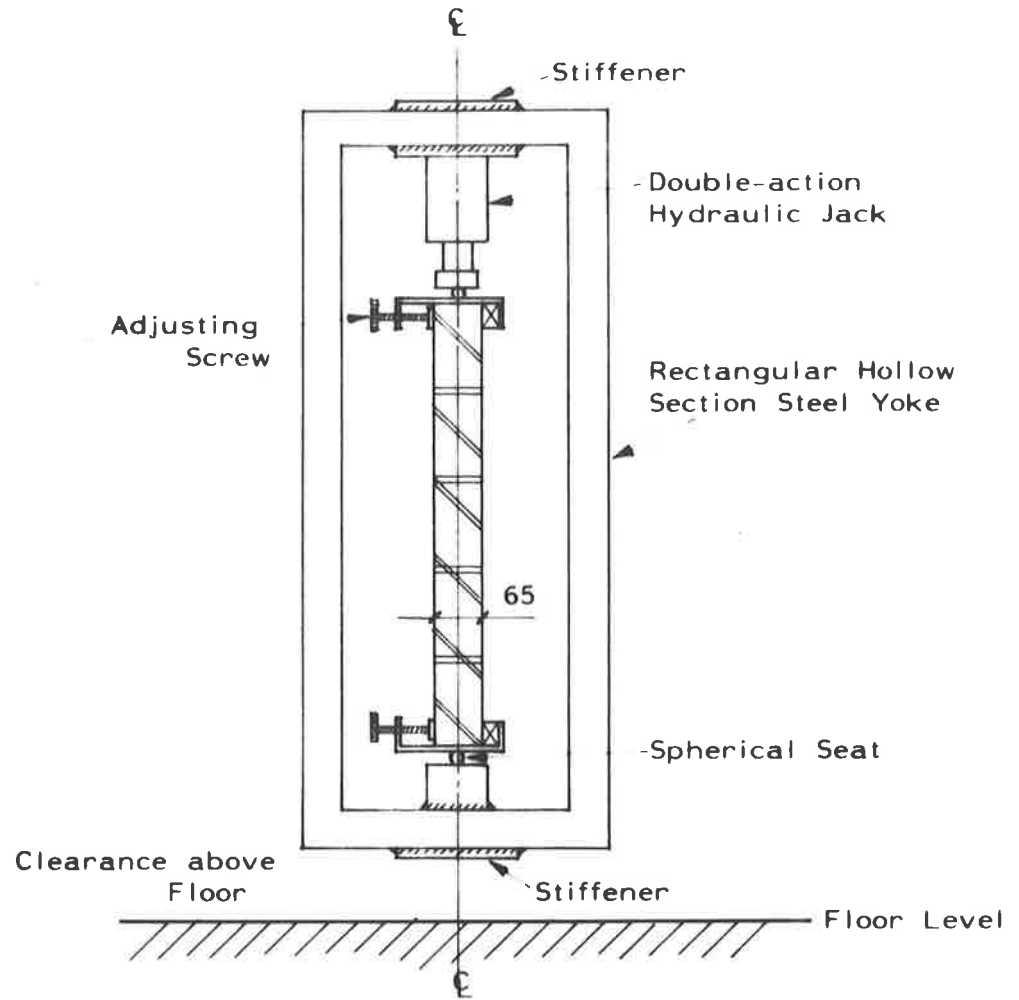


Figure 7.1(b): SECTION A-A

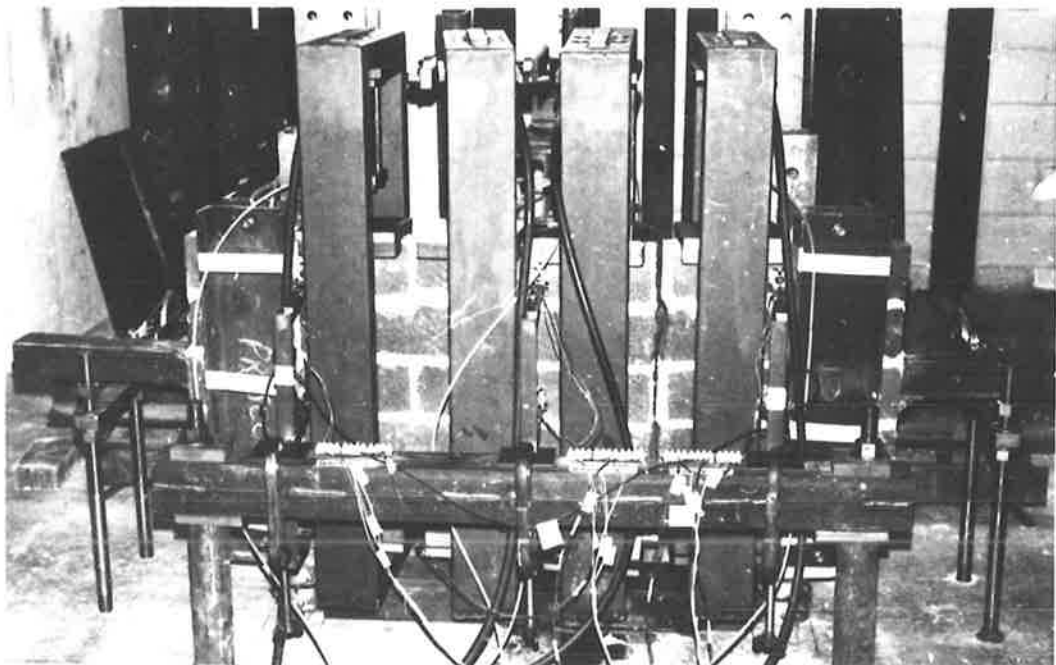


Figure 7.1(c): Side Elevation of Brickwork Panel

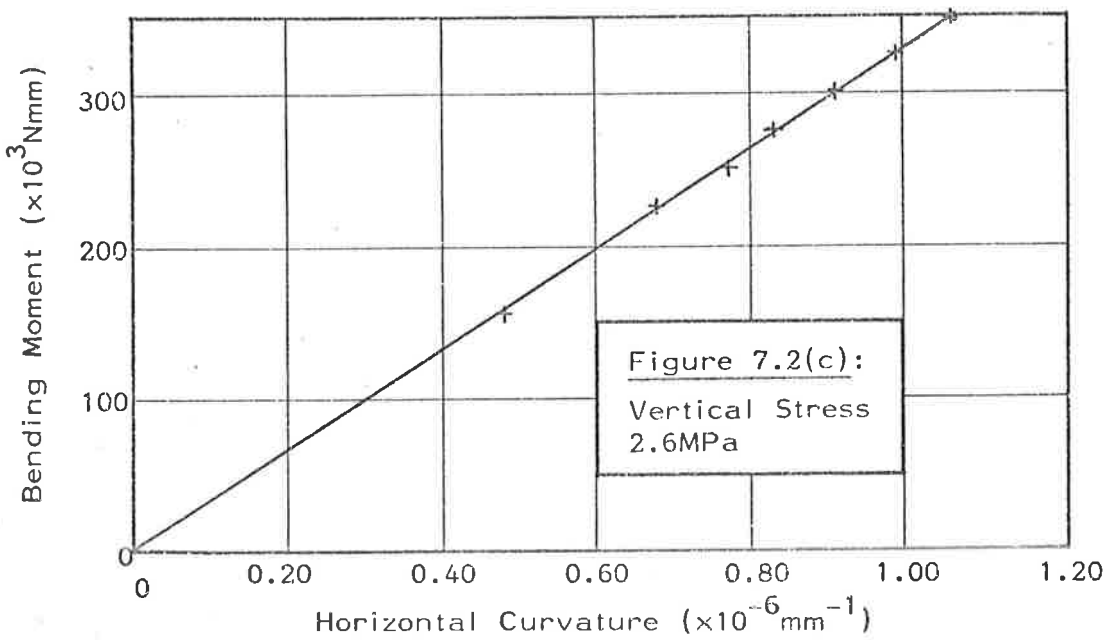
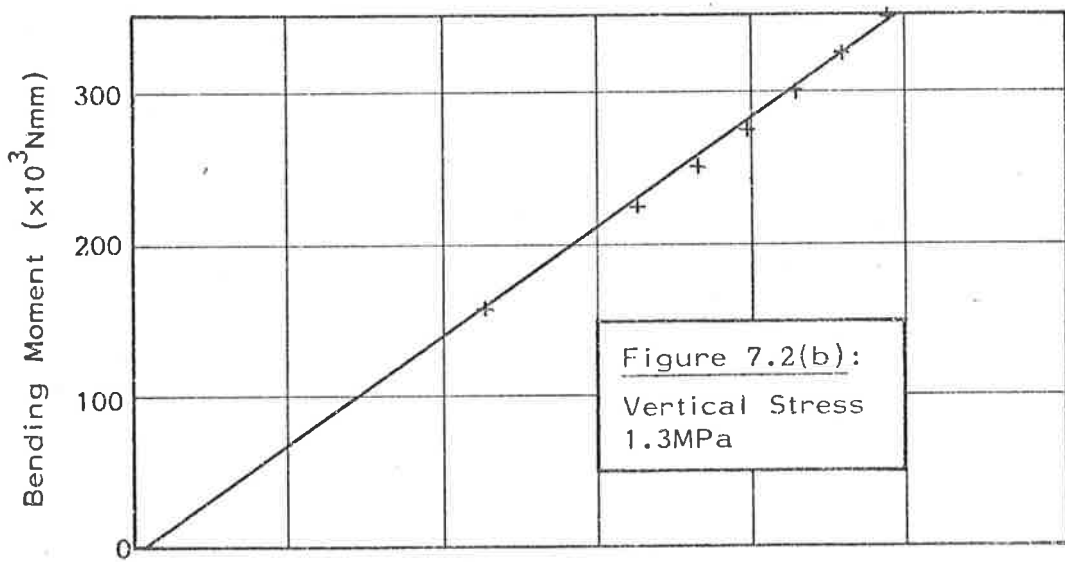
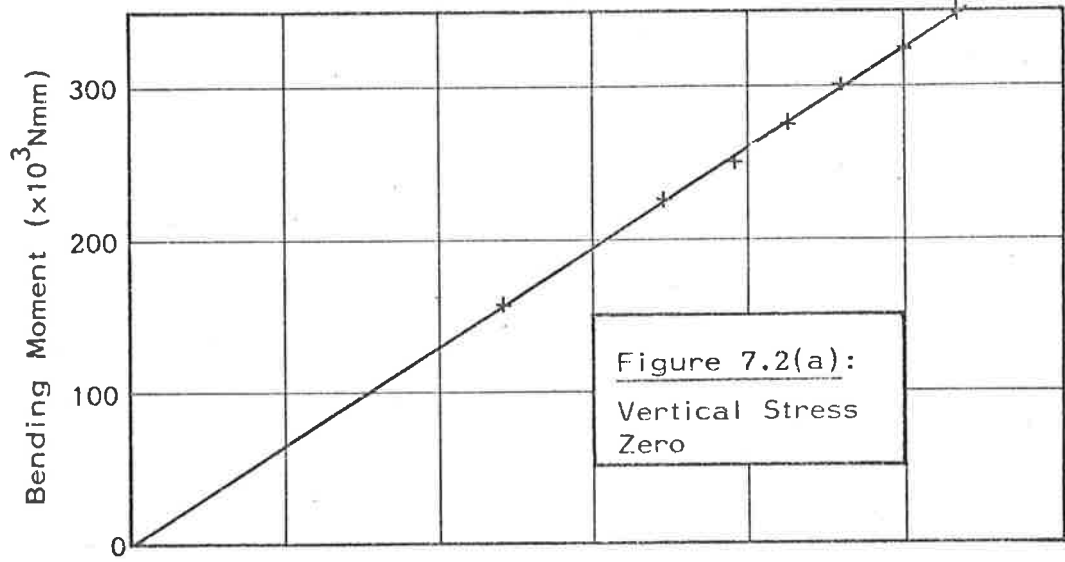


Figure 7.2: Moment-Curvature Relationship for Un-cracked Brickwork Panels



Panel No.	Applied Vertical Stress (MPa)		
	Zero	1.3	2.6
1	325	346	337
2	232	232	266
3	303	328	339
4	272	277	268
5	281	310	317
6	293	299	292

Table 7.4: Ratio of Applied Moment: Curvature in Horizontal Plane ( $\times 10^9 \text{Nmm}^2$ )

The results in Table 7.4 indicate that, statistically, the stiffness of the brickwork panels, when subjected to bending parallel to the bedjoints, was independent of the magnitude of the applied axial stress normal to the bedjoints. The mean effective stiffness of the panels was  $295 \times 10^9 \text{Nmm}^2$  with a coefficient of variation of 4.7 percent. The stiffness calculated using Base and Baker's<sup>(69)</sup> proposed equation (6.2) with the material properties summarized in Tables 7.1 and 7.2 is  $280 \times 10^9 \text{Nmm}^2$ , approximately 5 percent less than the experimental value.

Each panel was then loaded so that the bending parallel to the bedjoints caused cracking in the perpends. The moment-curvature relationships, shown typically in figure 7.3, are summarized for the six panels in Table 7.5.

A one-way analysis of variance on the results in Table 7.5 shows that the stiffness ratios SLOPE3:SLOPE1 and SLOPE4:SLOPE1 are statistically the same, but are different from the stiffness ratios SLOPE2:SLOPE1.

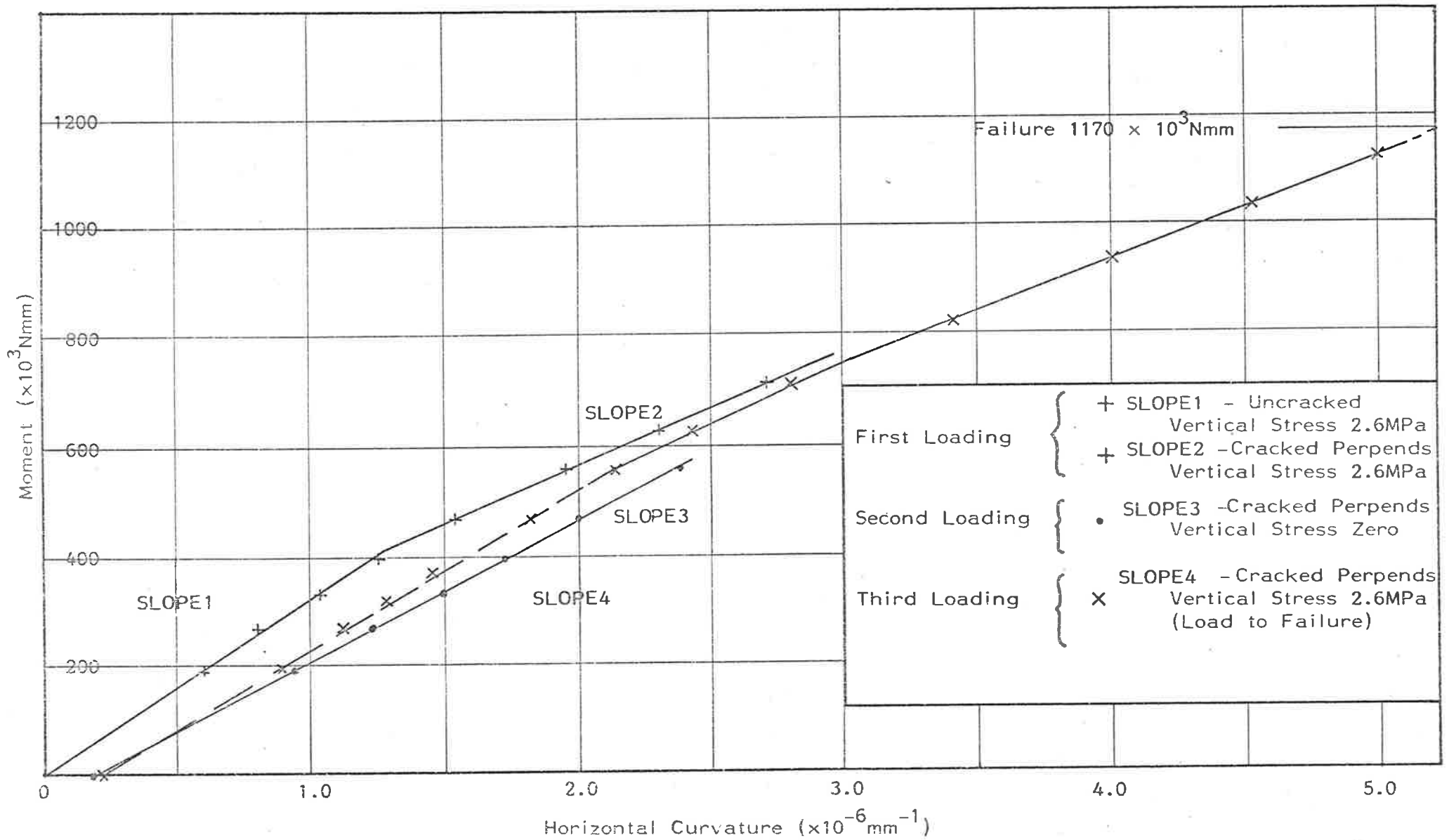


Figure 7.3: Moment-curvature Relationships for Small Panel No. 6 (Typical for all Panels tested)

Panel No.	Ratios of Slopes from Moment-Curvature Graphs <sup>(a)</sup>		
	SLOPE2:SLOPE1	SLOPE3:SLOPE1	SLOPE4:SLOPE1
1	0.65	0.86	0.81
2	0.70	0.79	0.78
3	0.67	0.89	0.84
4	0.85	0.76	0.78
5	0.68	0.78	0.77
6	0.66	0.90	0.88

(a) Definition of SLOPE1, etc. is shown in figure 7.3.

Table 7.5: Relative Horizontal Stiffnesses of Brickwork Panel

The mean of the stiffness ratios SLOPE3:SLOPE1 and SLOPE4:SLOPE1 is 0.82 with a coefficient of variation of 6 percent and the mean of the stiffness ratios SLOPE2:SLOPE1 is 0.70 with a coefficient of variation of 10 percent. The difference in the groups of stiffness ratios may be explained by an observed non-elastic behaviour of the panels in which the perpend cracks appear not to close completely as the panel is unloaded (figure 7.3). It is also significant that for the first loading, the panels were loaded from the uncracked to the cracked condition whereas for the subsequent tests, the panels were cracked throughout the entire loading range. The stiffness ratio computed for the panels as 0.77 (Table 6.3, Section 6.2.3.2) compares favourably with the results in Table 7.5, noting that the assumption of zero tensile bond made in the calculations corresponds more closely with the behaviour of a panel having pre-existent perpend cracks than that for a panel which is initially uncracked. It should be noted also that the experimentally-derived ratio proposed by Lawrence and Morgan<sup>(12)</sup> (equation (3.53)) differs from the results summarized in

Table 6.3 and 7.5 because the tests were conducted on panels of brick laid on flat with a geometry different from that of the panels in the present investigation.

The bending moments which produced failure and the maximum bending stresses (calculated on a gross panel section) are summarized in Table 7.6.

Panel No.	Failure Moment ( $\times 10^6 \text{Nmm}$ )	Failure Stress <sup>(a)</sup> (MPa)
1	1.40	3.37
2	0.90	2.17
3	1.13	2.72
4	1.08	2.60
5	0.95	2.29
6	1.17	2.82

(a) Failure stress calculated on gross panel section.

Table 7.6: Strengths of Brickwork Panels in Horizontal Bending

The mean failure stress was 2.66MPa with a coefficient of variation of 14.7 percent. Failure occurred in the panels with the formation of a vertical crack running through both the mortar perpends and the bricks (figure 7.4). An alternate mode of failure, proposed by Sahlin<sup>(44)</sup> and Royen<sup>(88)</sup> in which torsional shear failure occurs on the bedjoints, would have required a bending stress in the panel of 3.2MPa ( $\mu = 0.5$  in equation (3.43), Section 3.3.4.2). The mode of failure in the panels (figure 7.4) was thus not inconsistent with Sahlin's and Royen's conclusions. The position of the crack formation at a perpend-bedjoint intersection agrees with results obtained using PROGRAM MFYDCP (Section 6.2.2).

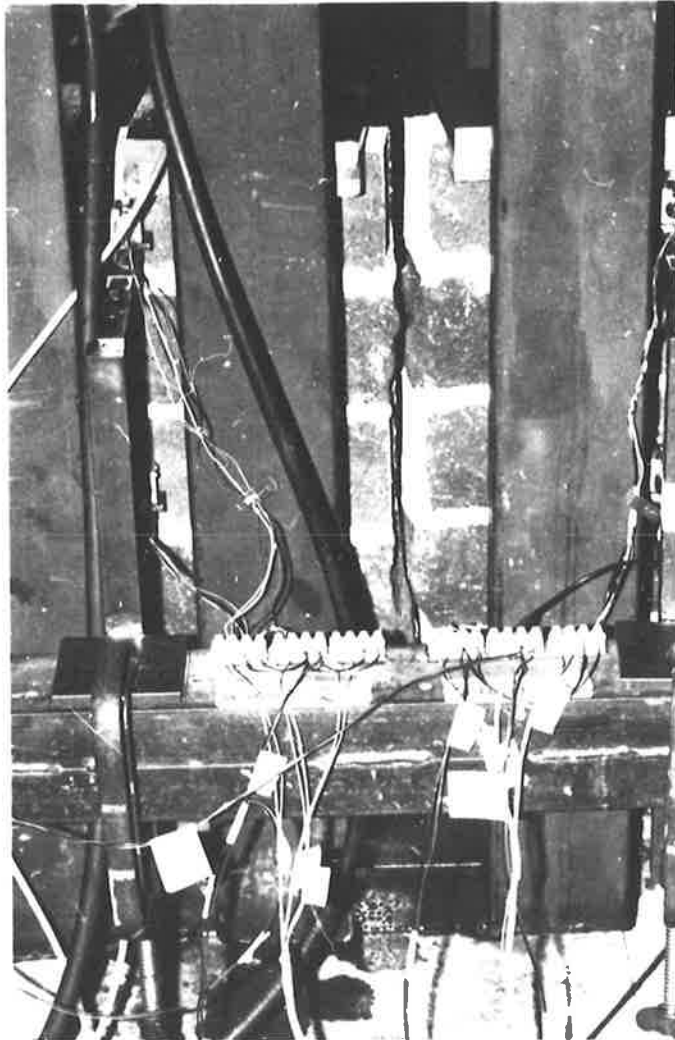


Figure 7.4: Brickwork Panel  
Failure Mode

The test results presented in this section support the propositions by Page<sup>(95)</sup> and Base and Baker<sup>(69)</sup> (as outlined at the beginning of this section) and show that the stiffness ratios, calculated by PROGRAM MFYDCP and summarized in Table 6.3 may be used to calculate the behaviour of complete brickwork panels.

### 7.3 A SIMPLY-SUPPORTED PANEL IN TWO-WAY BENDING

#### 7.3.1 Introduction

A full scale experiment was carried out on a brickwork panel approximately 3600mm long by 2400m high. The experiment was designed specifically to compare the theoretical behaviour predicted from PROGRAM PANEL1 (Appendix G) with test observations. For this purpose, idealized edge conditions and loading patterns were chosen rather than the less well identified conditions and patterns found in practice. The experiment may thus be regarded as a particular case study undertaken to indicate the order of accuracy that might be expected from the calculations.

The experimental apparatus was designed to meet the following criteria.

- (a) The load required to cause failure should be achievable with the test facilities available.
- (b) The panel should be free to rotate at its four supported edges with no out-of-plane movements at the edges (that is, simply-supported).
- (c) The load should be applied uniformly along the top and bottom edges with no load-shedding towards the vertical edges as the out-of-plane deflections increase.

In order to make the test results as extensive as possible, the test panel itself was designed —

- (a) To avoid excessive vertical compression (causing vertical splitting) so that failure might occur from lateral buckling.
- (b) To ensure that the mortar would not be stressed into the non-linear range in a state of triaxial compression.

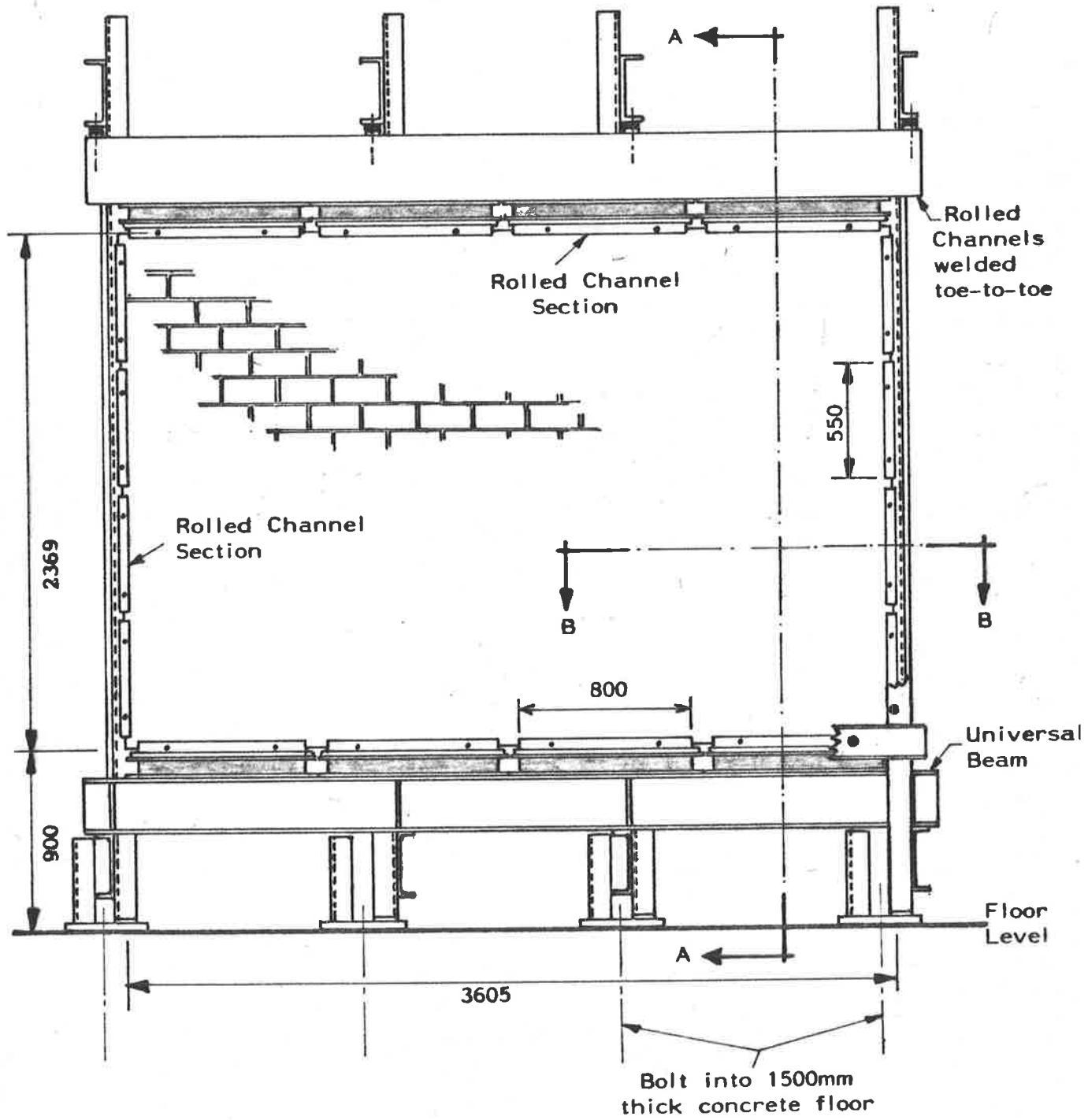
Preliminary calculations showed that a panel 65mm thick loaded at a nominal eccentricity of 20mm along both top and bottom edges might comply with the above conditions. Details of the test apparatus provided to meet the design criteria are given in the following sections.

### 7.3.2 Experimental Apparatus

#### 7.3.2.1 Panel support structure and loading frame

The elements of the steel support structure and loading frame are shown in figures 7.5(a) to (f). The support structure was erected on four fabricated steel bases attached to a 1.5 metre thick concrete strong floor by 38mm diameter high strength bolts (figure 7.5(a)). The superstructure, reaction and support frames, consisted of lengths of modular channel section system (300mm x 90mm x 10mm thick) designed for use on the concrete strong floor, with all lengths interconnected by high strength friction grip bolts (figure 7.5(b)). The loading frame consisted of two steel beams contained by the modular channel section superstructure (figure 7.5(b)). The base beam was an I-section stiffened at support points by vertical plate stiffeners and the top beam was a boxed steel beam fabricated from two lengths of rolled steel channel section welded toe-to-toe.

In order to provide for the design loading condition, hydraulic jacks were fabricated from 800mm lengths of rolled steel channel, over



NOTE: Jacks are shown shaded

Figure 7.5(a): East Elevation of Support Structure and Loading Frame (Steel Sections at Front Deleted for Clarity)



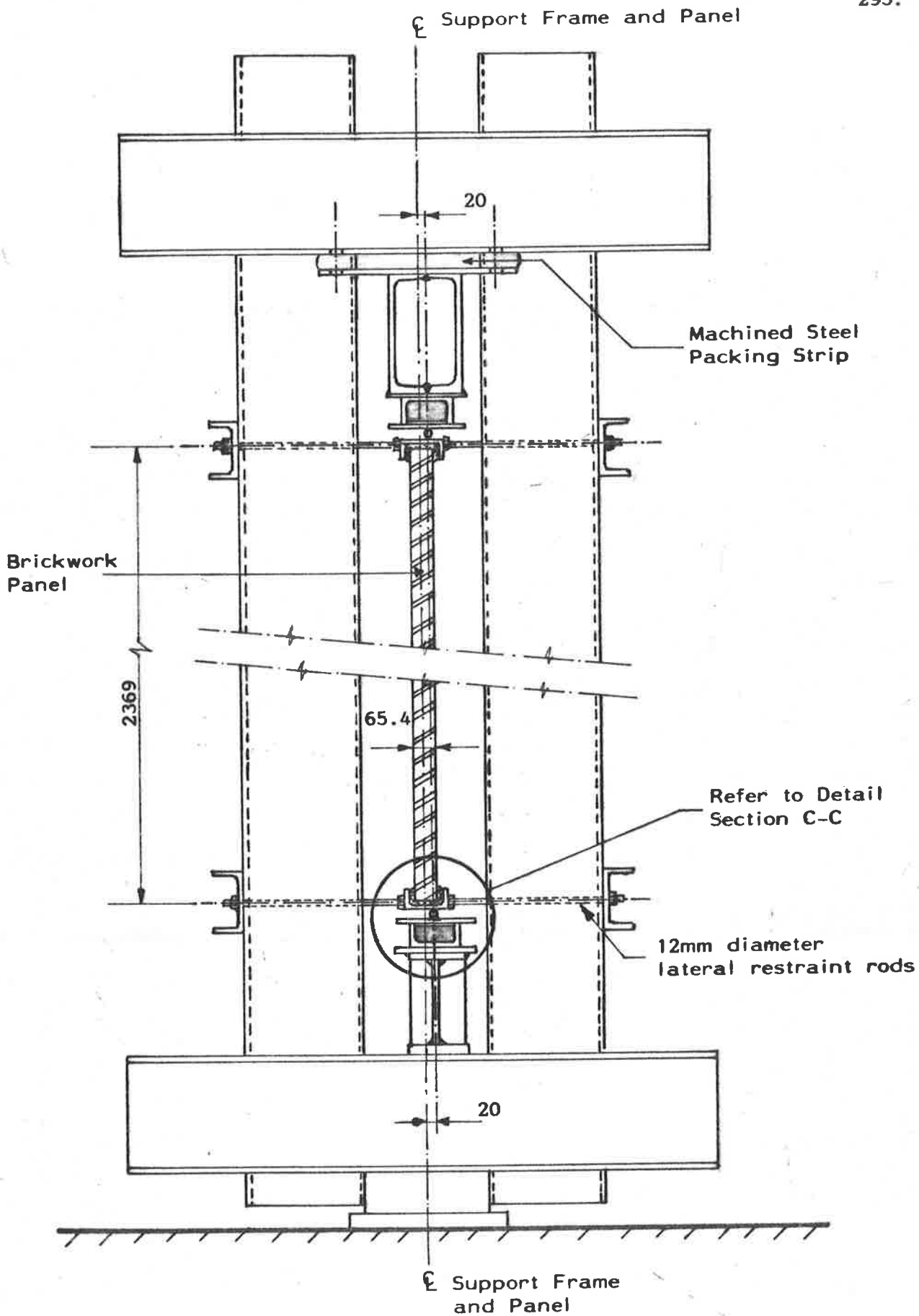


Figure 7.5(b): Section A-A Facing South (Showing Load Eccentricity)

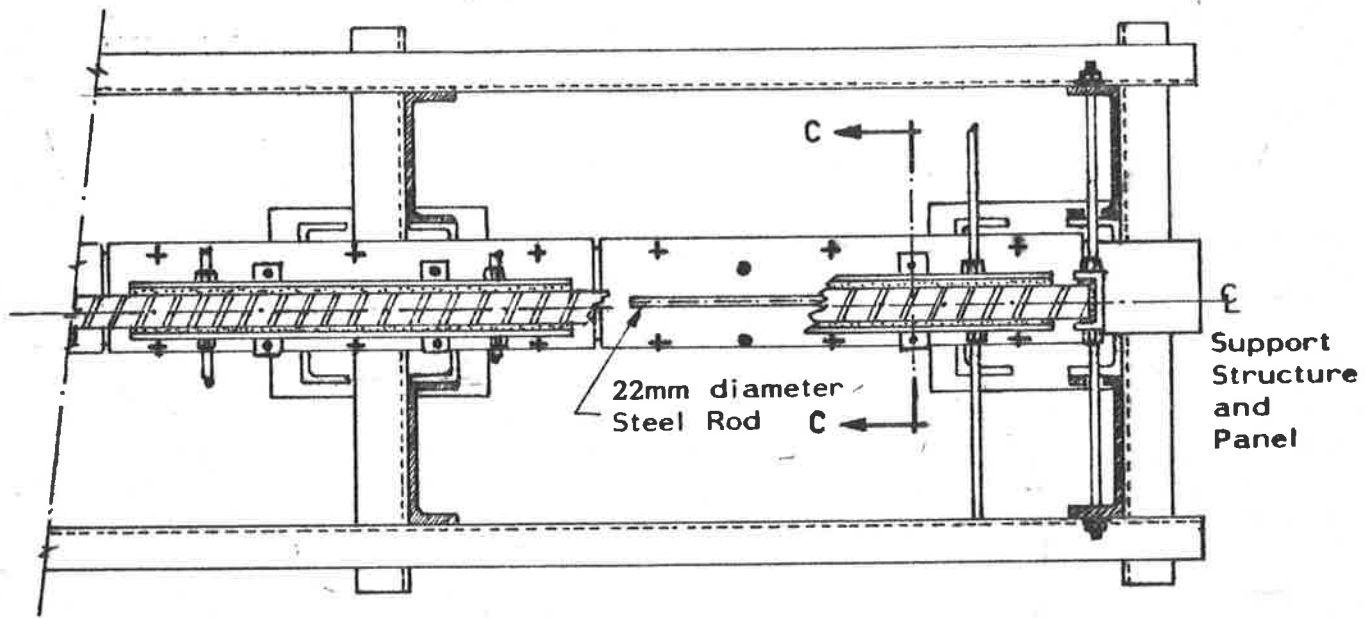


Figure 7.5(c): Section B-B

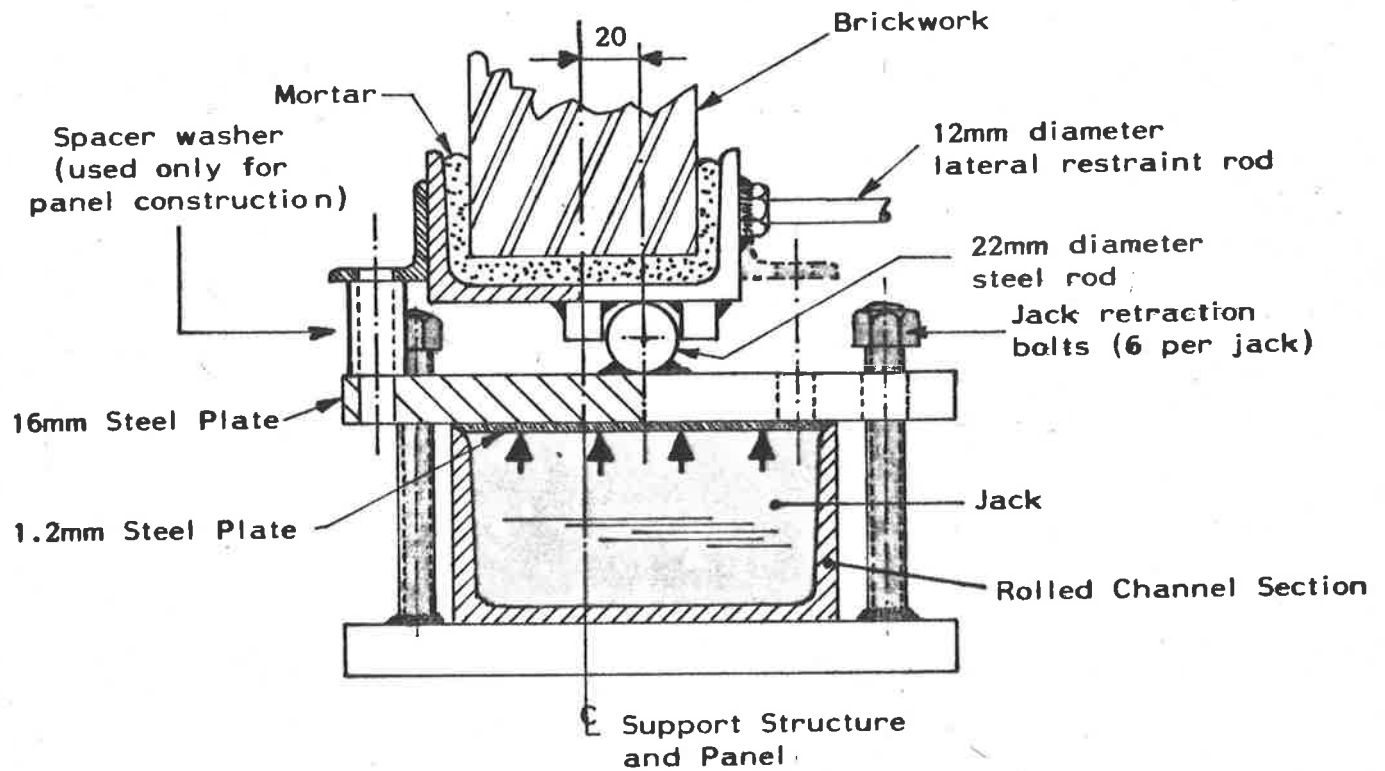


Figure 7.5(d): Section C-C (Jack Loading Details)

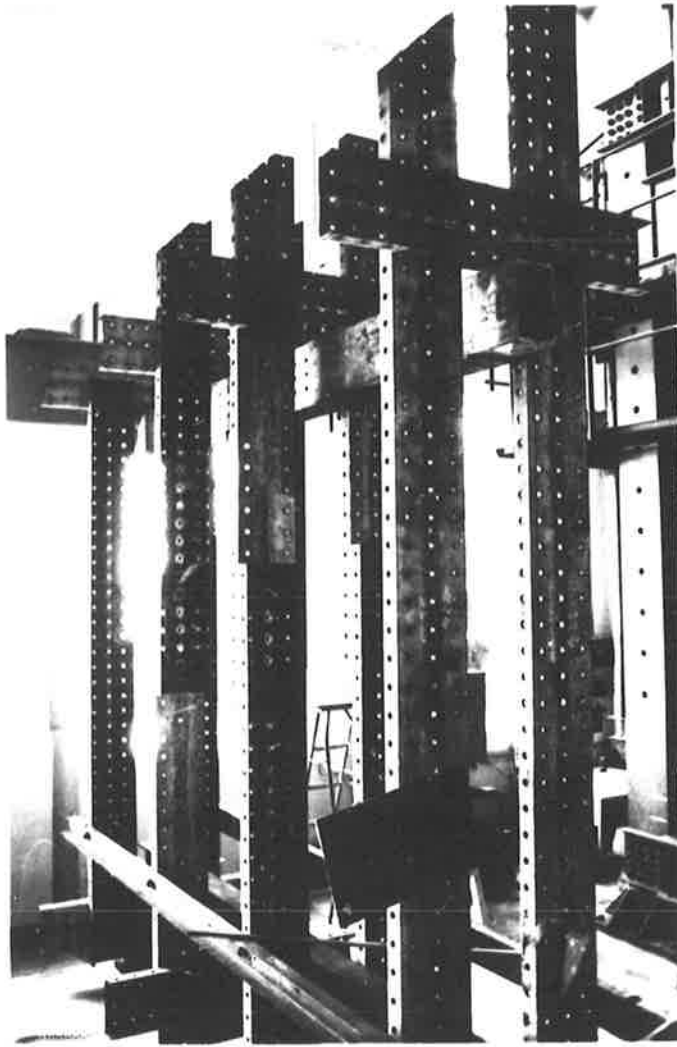


Figure 7.5(e): Steel Support Frame

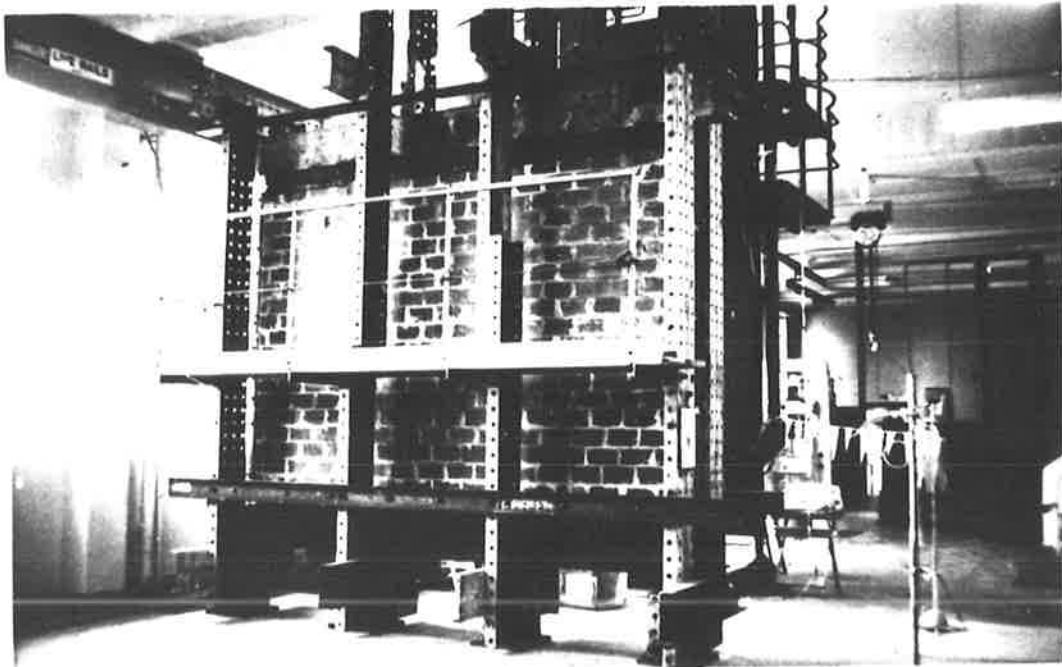


Figure 7.5(f): Elevation of Brickwork Panel  
(Prior to Construction of Instrumentation Frame)

the toes of which 1.2mm mild steel plate was welded, to form low-profile units (figures 7.5(b), 7.5(d)). The ends of the jacks were sealed by welding in 6mm steel plates. Eight jacks were used to load the panel, four at the base and four at the top (figure 7.5(a)). The load was applied to the panel eccentrically through lengths of mild steel rod offset nominally 20mm from the structure centreline (figures 7.5(b), 7.5(d)). The centreline of the jacks was thus coincident with the line of application of the load to the panel. Preliminary tests on a prototype jack showed that the jack top plates could extend by plastic yielding under load, so lengths of 16mm thick plate were placed between the 1.2mm plates and the 22mm diameter steel loading rods (figure 7.5(d)). To retract the jacks after the hydraulic pressure was released, six bolts per jack passed through this top plate and were welded to a base plate under each jack (figures 7.5(c), (d)).

The panel edges were restrained from out-of-plane displacement by building the brickwork into lengths of rolled steel channel section. The lengths of channel were, in turn, connected to the main support frame by lengths of steel rod, the diameter being determined by calculating the maximum expected lateral force at the panel edges. The resistance to rotation of the channel/rod edge support system was measured to be of the order of only 2.5 percent of the calculated stiffness of the panel against flexural rotation at its edge. The edge condition was thus considered to be essentially simply-supported. The position of the applied load relative to the panel middle surface was fixed additionally by welding lengths of square-section steel to the top and bottom edge channel supports (figure 7.5(d)).

### 7.3.2.2 Panel construction

All bricks used in the panel were solid extruded wire-cut clay bricks selected to be approximately 230mm x 115mm x 65mm (solid bricks of width 110mm were not available at the time of construction). A random sample of twelve bricks from the batch was measured giving mean brick dimensions of 231mm x 115mm x 65.4mm. The panel was constructed by laying nineteen courses of brickwork with the bricks on edge. The mortar was 1 cement:1 lime:6 sand by volume with a water-to-cement ratio of 1.29. The bricks were laid in a saturated surface-dry condition and each course of brickwork was laid against a double string line as shown in figure 7.6. The brickwork was built into the base channels and vertical edge support channels using the mortar as grout.

Six brickwork prisms, each of four bricks, were constructed to test the brickwork compressive strength. Six prisms, each of six bricks, were also built to test the brickwork bond strength of the bedjoints. Three mortar prisms 25mm x 25mm x 50mm were cast with each of the ten mortar batches used in the panel construction. All the brickwork was cured in polythene sheeting for 14 days after which the top edge channels were grouted to the brickwork using a mortar of 1 cement:3 sand by volume with a water-to-cement ratio of 0.53 by weight. The grout thickness above the brickwork was approximately 15mm (figures 7.7(a), 7.7(b)).

The measured height of the completed panel was 2369mm between the top and bottom edge restraints and the length was 3605mm (figure 7.5(a)). The mean measured eccentricity of the load at the base was 20.1mm and the top was 20.8mm; the overall mean of the measured load eccentricity (for use in PROGRAM PANEL1) was 20.5mm with a coefficient of variation of approximately 5 percent.

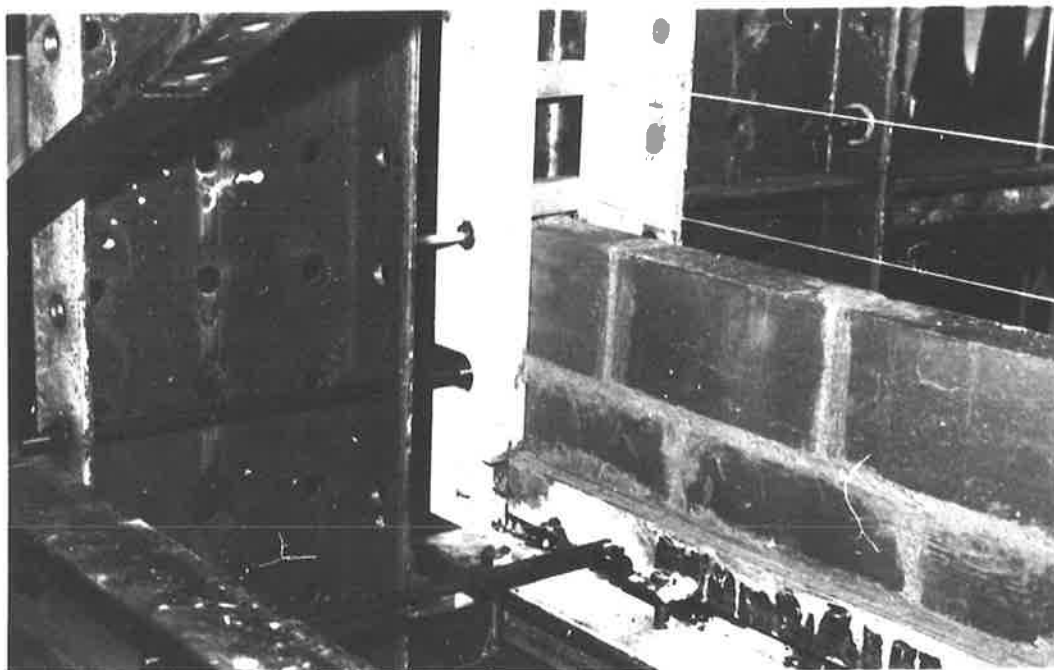


Figure 7.6: Method of Laying Bricks in Panel

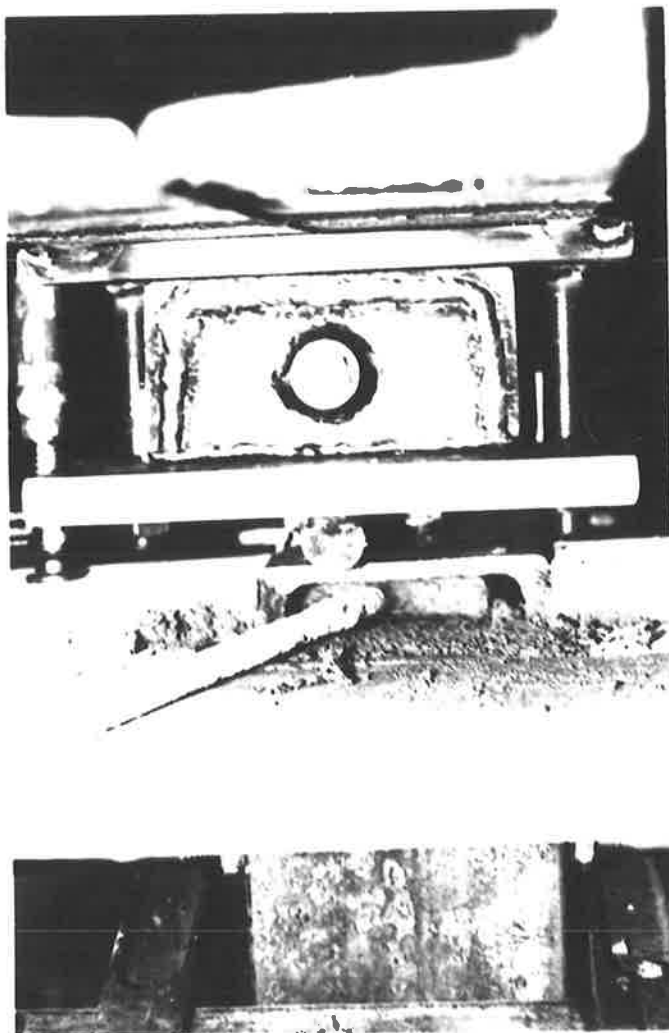


Figure 7.7(a):  
Grouting Procedure

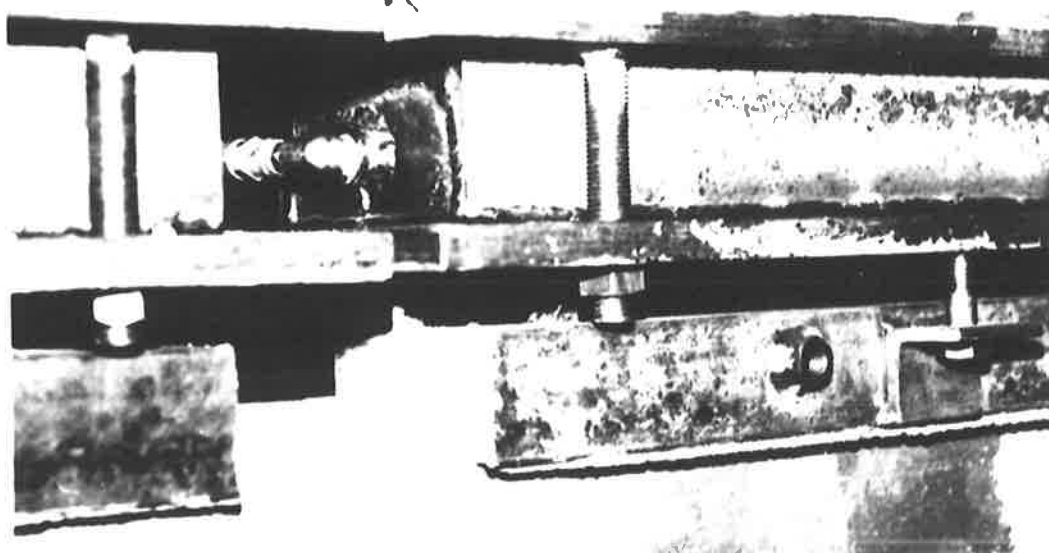


Figure 7.7(b): Grouting Completed

Figure 7.7: Grouting of Brickwork into Top  
Edge Channels

### 7.3.2.3 Jack calibration

Each of the low profile test hydraulic jacks (Section 7.3.2.1) was calibrated by placing the jack in a compression testing machine and displacing the thin plate by a prescribed amount by pressurizing the fluid in the jack. The reaction force applied by the compression machine was measured, and by taking sets of reaction force-jack pressure-jack displacement readings, a series of calibration curves for various values of thin plate displacement were obtained (figure 7.8). The curves for all of the eight jacks were closely coincident and showed that the displacement of each jack must be known to calculate the jack load. The displacements of the jacks were measured throughout the panel load tests by using two dial gauges at the mid-points of the long sides of each jack.

### 7.3.2.4 Instrumentation

Figure 7.9 shows the positions of strain gauges, dial gauges and linear voltage displacement transducers (L.V.D.T.) installed to measure strains and displacements in the panel under vertical load. All strain gauges on the brickwork were of 20mm gauge length and were fixed in pairs to opposite faces of the panel so that in-plane strains and bending strains could be measured on the panel vertical and horizontal centrelines and at one corner. 5mm gauge length strain gauges were fixed to four of the 12mm bolts restraining the panel from lateral movement so that the change in force in the bolts with changing vertical load could be measured.

The out-of-plane displacements of the panel edges were checked with eight L.V.D.T.'s and the displacements on the panel vertical and horizontal centrelines and at the panel quarter points were measured using nine dial gauges. The dial gauges and L.V.D.T.'s



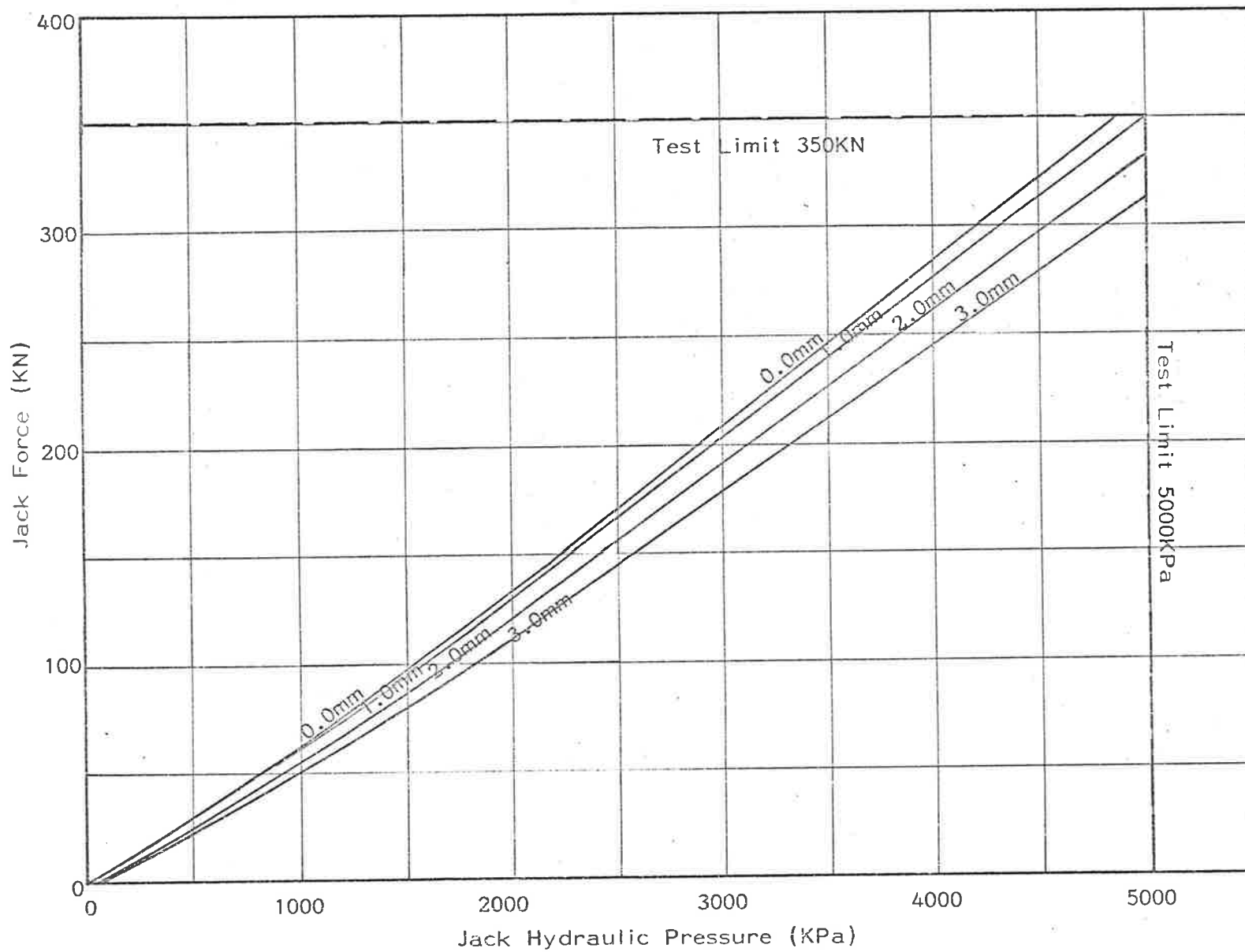
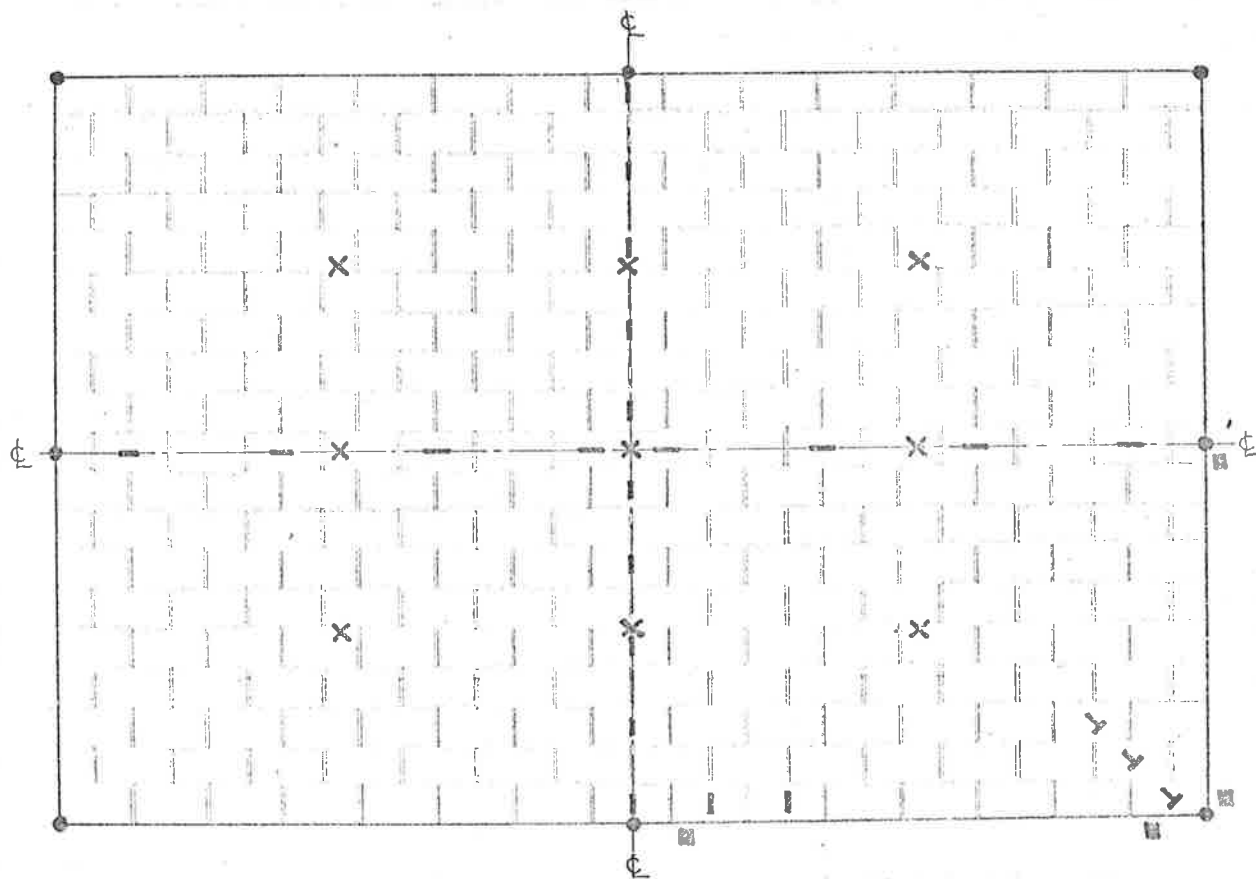


Figure 7.8: Jack Calibration Curves










- Legend:
- 



 Electrical Resistance Strain Gauge on Brick
  - 
 Electrical Resistance Strain Gauges on Steel Rods
  - 
 Linear Voltage Displacement Transducer (LVDT)
  - 
 Displacement Dial Gauge

Figure 7.9: Positions of Gauges on Brickwork Panel  
(East Elevation)

were fixed to an independent rigid frame mounted on the concrete floor separately from the panel support frame.

The pressure in the low-profile hydraulic jacks was monitored by connecting all jacks to a manifold which in turn was connected to a high output pressure transducer which was accurate to within 10KPa. The pressure was applied through a hand-operated high pressure hydraulic pump and was read directly on a digital voltmeter.

All the strain gauges and L.V.D.T. were connected to a computer-based data logger and the dial gauge readings were entered manually into the data-collection program. All data was reduced by computer as the test progressed to give a continuous assessment of the experimental behaviour of the panel. Figure 7.10 shows schematically the interconnections of all the instrumentation.

### 7.3.3 Brickwork Material Properties

Tests were conducted to determine the elastic moduli of the bricks, the mortar and the brickwork. Six bricks from the batch were tested in compression using pairs of 30mm gauge length strain gauges to determine strains. The brick elastic modulus results are given in Table 7.7.

The mean elastic modulus was  $9.4 \times 10^3$  MPa with a coefficient of variation of 23 percent.

Six mortar prisms, all from different mortar batches and chosen at random, were tested in compression to measure the mortar elastic modulus (Table 7.8). Six prisms only were tested because the effect of any error in determining the mortar modulus on the overall modulus of the brickwork is significantly less than the effect of error in determining the brick modulus.

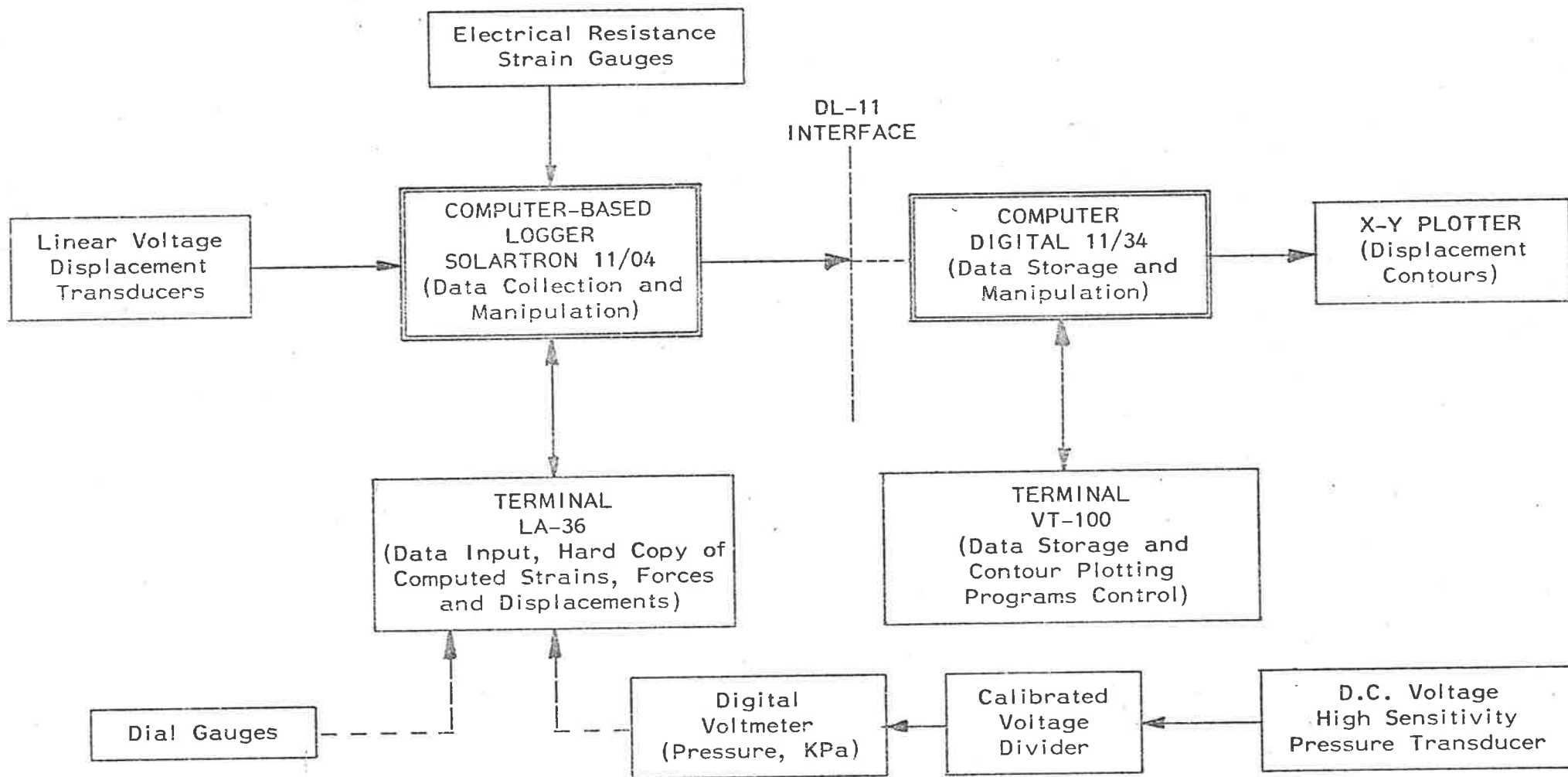


Figure 7.10: Instrumentation Block Diagram

Brick No.	Elastic Modulus ( $\times 10^3$ MPa)
1	10.3
2	6.6
3	8.2
4	9.0
5	13.6
6	8.7

Table 7.7: Brick Elastic Modulus

Prism Batch No.	Initial Tangent Modulus ( $\times 10^3$ MPa)
3	10.0
5	10.8
6	9.5
8	13.8
9	10.0
10	13.1

Table 7.8: Mortar Elastic Modulus

The mean mortar prism elastic modulus was  $11.2 \times 10^3$ MPa with a coefficient of variation of 15 percent.

The four-brick-high brickwork prisms were tested in axial compression and the axial shortening was measured across a height of three bricks and three mortar joints. Elastic modulus values calculated for the brickwork prisms are given in Table 7.9.

Brickwork Prism No.	Brickwork Elastic Modulus ( $\times 10^3$ MPa)
1	10.2
2	9.2
3	8.9
4	8.5
5	9.5
6	8.4

Table 7.9: Brickwork Elastic Modulus

The mean brickwork elastic modulus was  $9.1 \times 10^3$ MPa with a coefficient of variation of 7 percent. A brickwork modulus calculated using the results from Tables 7.7 and 7.8 in equation (5.4) is  $9.5 \times 10^3$ MPa with a coefficient of variation of approximately 20 percent. This value is consistent with the results in Table 7.9.

The six four-brick-high brickwork prisms were tested to failure in axial compression between sheets of 4mm thick plywood. The compressive strengths and elastic modulus-to-compressive strength ratios are summarized in Table 7.10.

Brickwork Prism No.	Compressive Strength (MPa)	Ratio( $\frac{\text{Elastic Modulus}^{(a)}}{\text{Compressive Strength}}$ )
1	25.1	406
2	27.6	333
3	25.7	346
4	25.7	331
5	28.7	331
6	23.9	351

(a) Elastic Modulus Values from Table 7.9.

Table 7.10: Brickwork Prism Compressive Strength

The mean compressive strength was 26.1MPa with a coefficient of variation of 6 percent and the mean ratio of elastic modulus to compressive strength was 350 with a coefficient of variation of 8 percent. The ratio of elastic modulus to compressive strength of brickwork is referred to in more detail in Chapter 8.

The six prisms of six bricks were tested for bond strength in a two-point load test, as shown in figure 7.11. The results of the tests are summarized in Table 7.11.

Brickwork Prism No.	Minimum Joint Bond Strength (MPa)
1	0.365
2	0.046
3	0.264
4	0.695
5	0.599
6	0.209

Table 7.11: Brickwork Flexural Bond Strength

The mean minimum joint bond strength for the six brickwork prisms was 0.363MPa. However, the scatter of results indicates that for a 95 percent confidence limit based on six tests, the flexural bond strength of the brickwork would be zero. The statistical analysis thus indicates that the assumption of zero flexural bond strength made in the theoretical analysis (PROGRAM PANEL1) is not unreasonable.

#### 7.3.4 Panel Experiment Results

A preliminary load test was conducted on the panel to check the apparatus and instrumentation and it was found that the lateral displacements presented the best method of assessing the panel

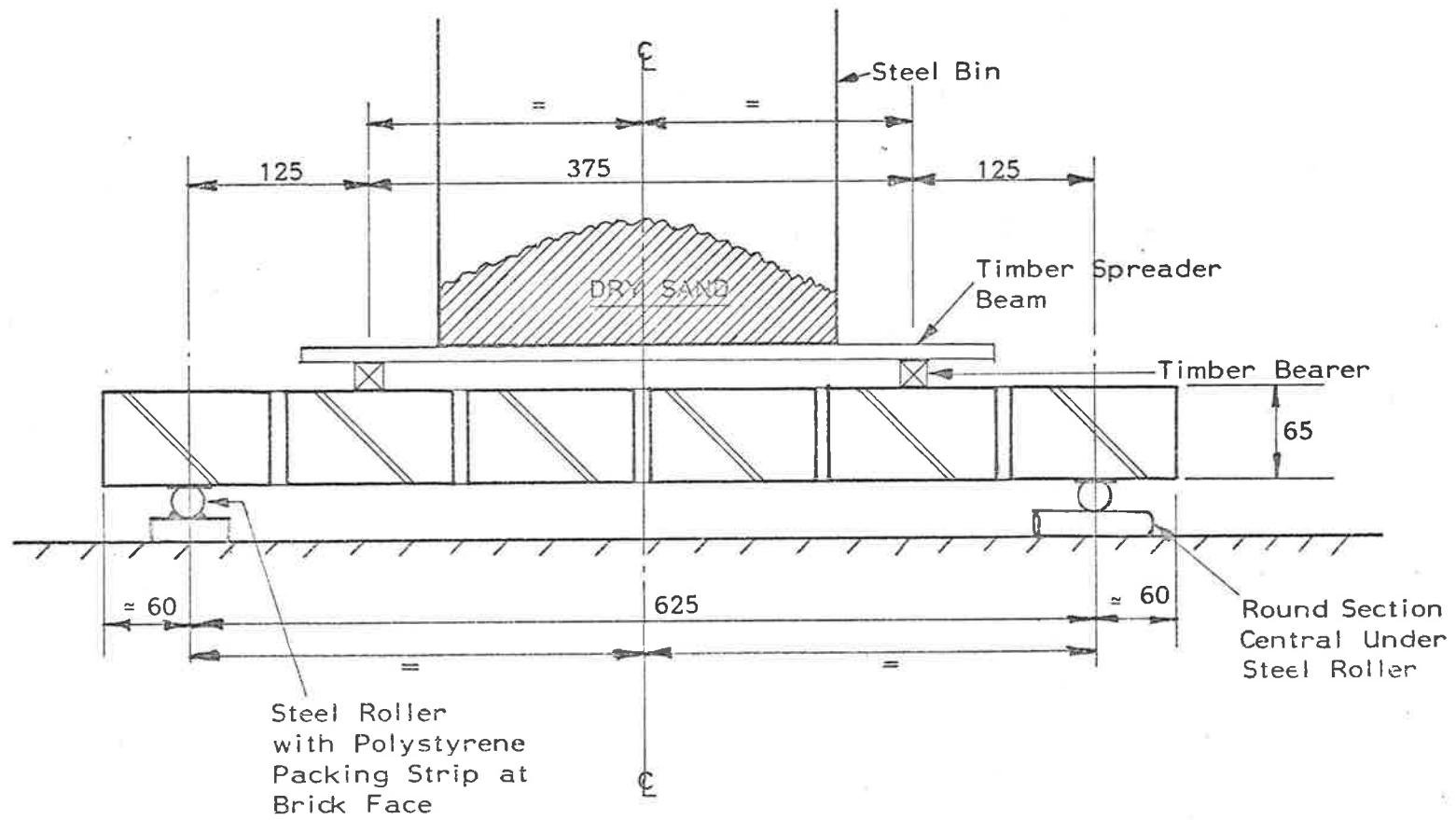


Figure 7.11: Test for Brickwork Bond Strength



behaviour. The strain gauges showed that the load-strain behaviour of the brickwork was linear at low load, but the measured strains could not be compared with the theoretical values because of the large variation in elastic modulus values among the bricks and also within the bricks themselves. Strain gauge readings on ten bricks in the panel (on the vertical centreline, figure 7.9) gave a mean elastic modulus for the bricks of  $11.5 \times 10^3$  MPa compared with  $9.4 \times 10^3$  MPa determined from brickwork prism tests (Table 7.7). The elastic modulus determined from the panel tests was used for all calculations using PROGRAM PANEL1 because the difference between the two test modulus values was within one standard deviation from the mean of the prism test results (Section 7.3.3) and the modulus determined from the panel test was calculated from the larger sample.

After the preliminary test, the panel was loaded incrementally to 55N per millimetre length of brickwork so that no debonding, or cracking, would have occurred at the brick-mortar interfaces. All the measured load-deformation characteristics were linear throughout the load range.

The panel was loaded subsequently in increments to a load of approximately 170N/mm length of brickwork and progressive cracking (brick-mortar debonding) was observed on loads greater than approximately 70N/mm. Comparisons between experimental and theoretical lateral displacements at the panel centre and quarter-points (figure 7.12) showed that during this loading phase from the uncracked to the cracked state, the measured lateral displacements initially were less than the calculated values (panel uncracked). However, once cracking was initiated, the differences between the measured and calculated displacements decreased. The test results in figure 7.12 showed that for loads less than approximately 130N/mm length of

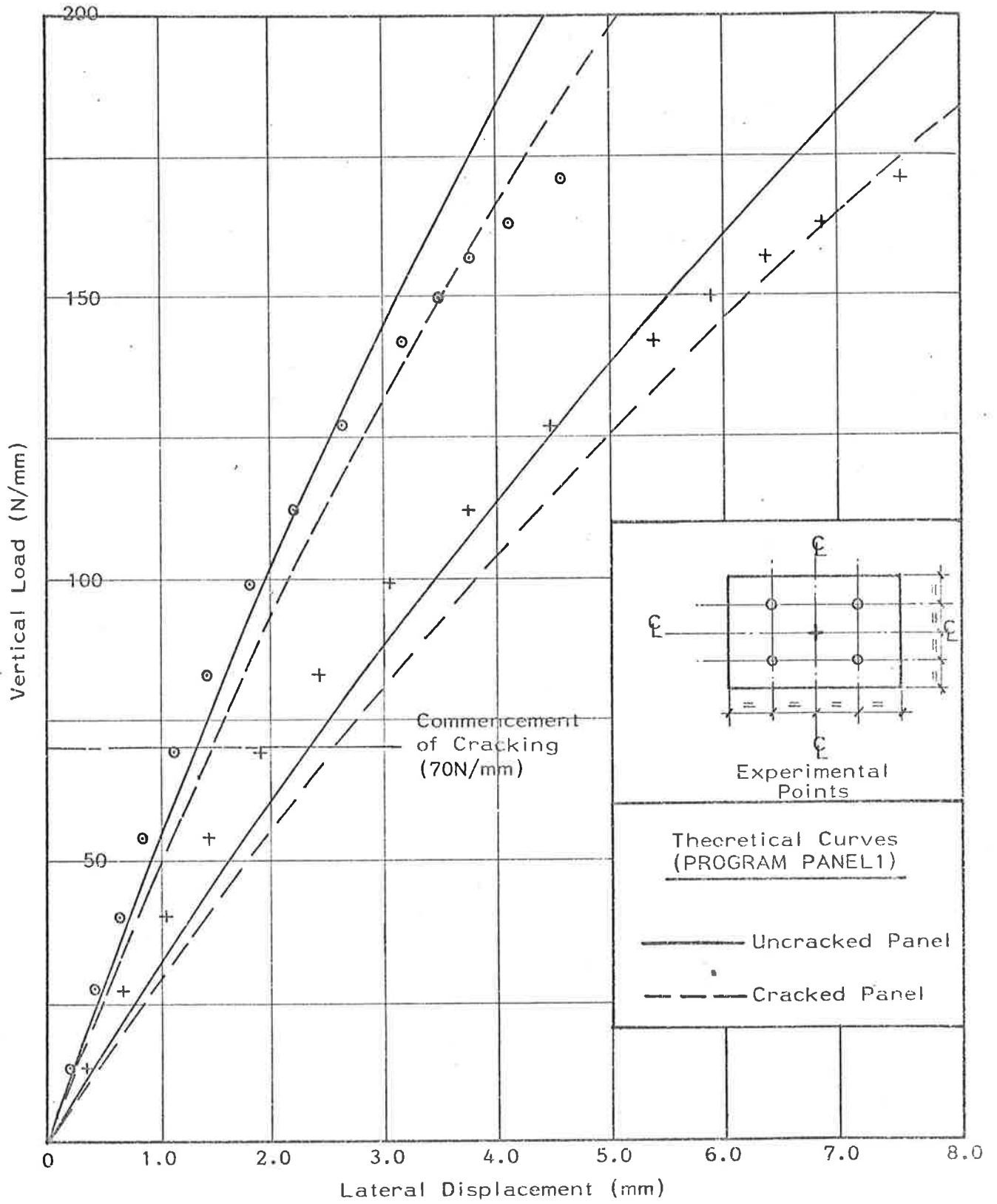


Figure 7.12: Comparison between Experimental and Calculated Lateral Displacements (Panel Initially Uncracked)

brickwork, the measured lateral displacements were consistently less than the calculated values by approximately 15 percent at the panel centre and by approximately 10 percent at the panel quarter-points. This percentage difference is less than the coefficient of variation of the brick elastic modulus, so that the agreement between the measured displacements and the computed values may be regarded as acceptable.

Once the load exceeded 130N/mm, some material non-linearity was evident as shown by sudden increases in the strains at two of the strain gauges. This material non-linearity, not incorporated into PROGRAM PANEL1, resulted in deflections larger than calculated values (figure 7.12).

The panel was unloaded and was then reloaded by increments of approximately 140N per millimetre length to brickwork. The load against central deflection curves for this test and the previous test in which the brickwork was initially uncracked are shown in figure 7.13. The results showed that for the cracked panel, the change in lateral displacement per unit load was approximately 20 percent greater than that for the uncracked panel; for the cracked panel, the slopes of the linear parts of the loading and unloading curves were approximately the same. Calculations using PROGRAM PANEL1 showed that the ratio of central displacements of cracked panel-to-uncracked panel was approximately 1.11 compared with 1.20 found in the test. The corresponding ratios at the panel quarter-points (figure 7.12) were 1.12 and 1.23 respectively. Further detailed research involving a number of tests on the progressive cracking of brickwork is required to ascertain confidence limits on these ratios.

The panel was loaded, finally, by increments to failure which occurred at a load of approximately 185N/mm length of brickwork. This

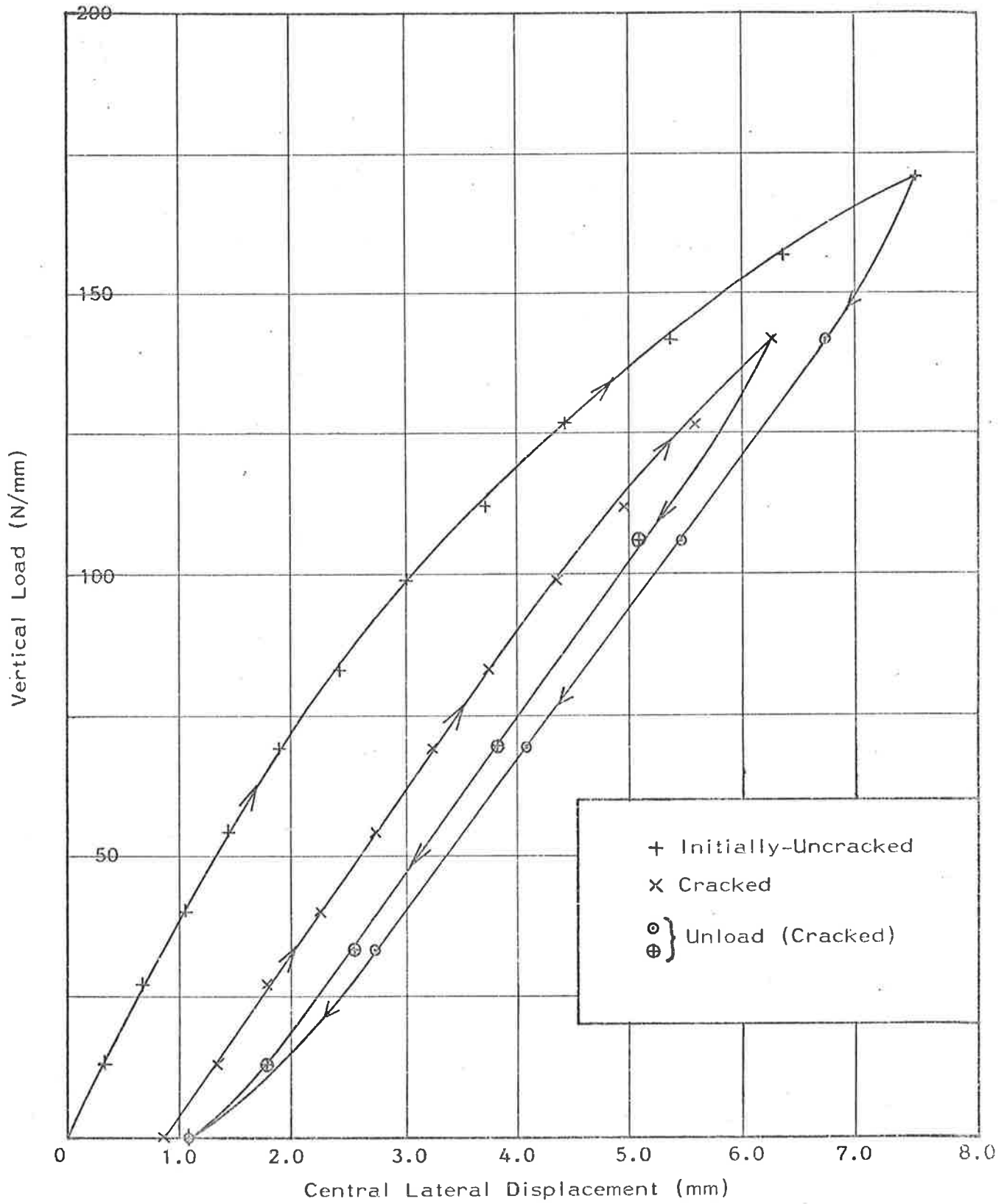


Figure 7.13: Load - Central Displacement Curves for Brickwork Panel

represented a total load on the panel of approximately 66 tonnes (670KN). The load-displacement characteristics are shown in figure 7.14 and the crack pattern at panel failure is shown in figure 7.15.

Failure was initiated by the formation of a crack through the bricks and along some of the mortar joints, at point 'A' in figure 7.15, which continued vertically through the brickwork to point 'B'. The load remained at approximately 10N/mm below the maximum load and the cracking developed further as the jack displacements were increased. Final collapse, at approximately 175N/mm, was caused by a lateral buckling failure of the central area of the panel acting essentially as a column isolated by the two vertical cracks from the vertical edge supports. The crack pattern at collapse (figure 7.15) was approximately symmetrical about the panel vertical and horizontal centrelines.

Figure 7.14 shows that the displacements agreed closely with calculated values for loads up to approximately 150N/mm after which non-linear material behaviour occurred. The deviation of the experimental displacements from calculated values was less at the quarter-points than at the panel centre (figure 7.14).

Contour plots of lateral displacements, plotted by the computer during the experiment (figures 7.16(a) to 7.16(c)) showed that the displacements were approximately symmetrical about the panel centrelines for the load values shown. By superimposing on one another during the test the three plots shown in figures 7.16(a) to (c), it was possible to confirm immediately that the relationship between load and displacement was closely linear throughout the panel. As the load was increased, a general non-linear behaviour in the panel became evident by plotting the displacement contours and comparing them as described above. Figure 7.17 shows that immediately prior to failure,

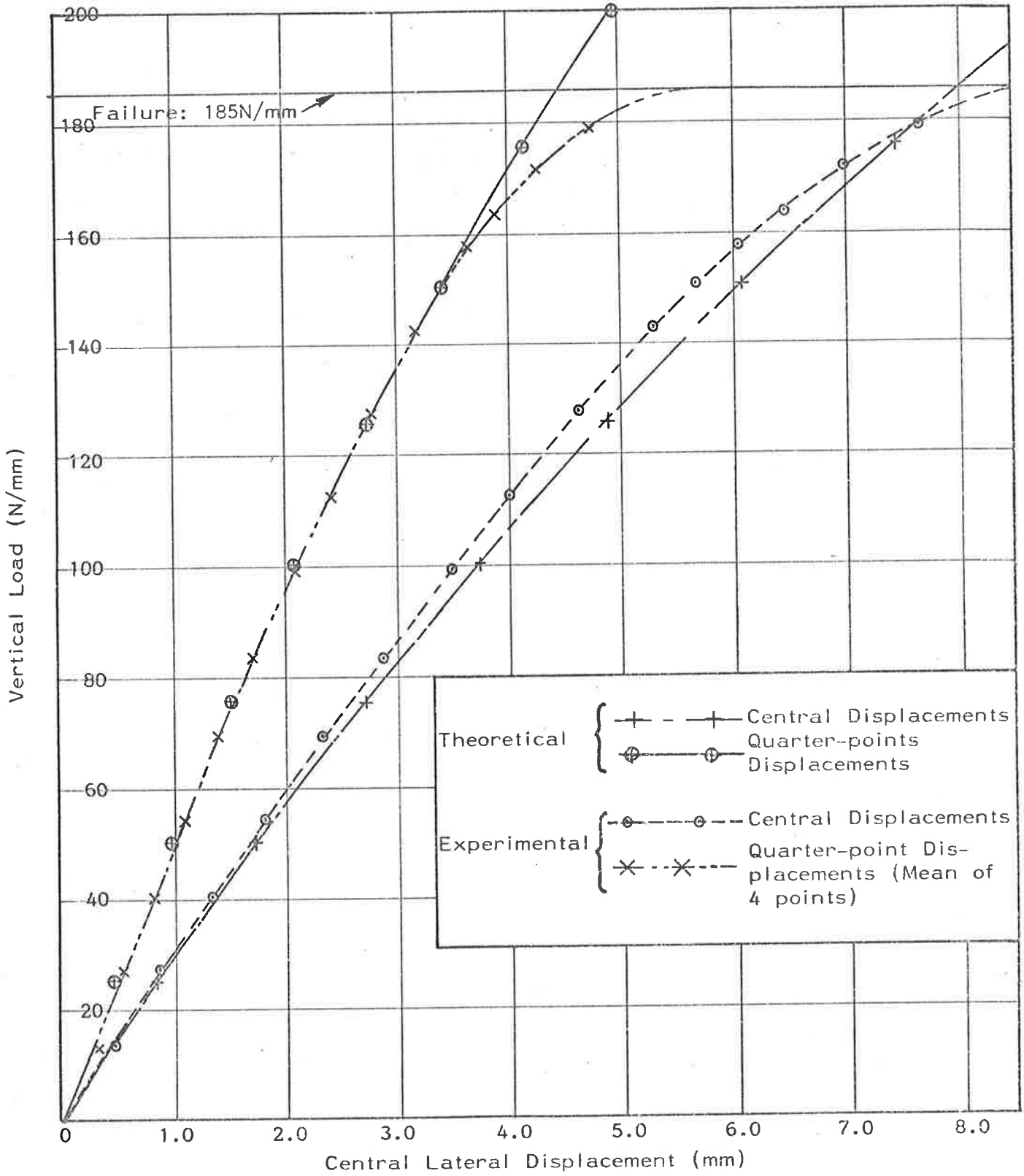


Figure 7.14: Lateral Displacements of Brickwork Panel

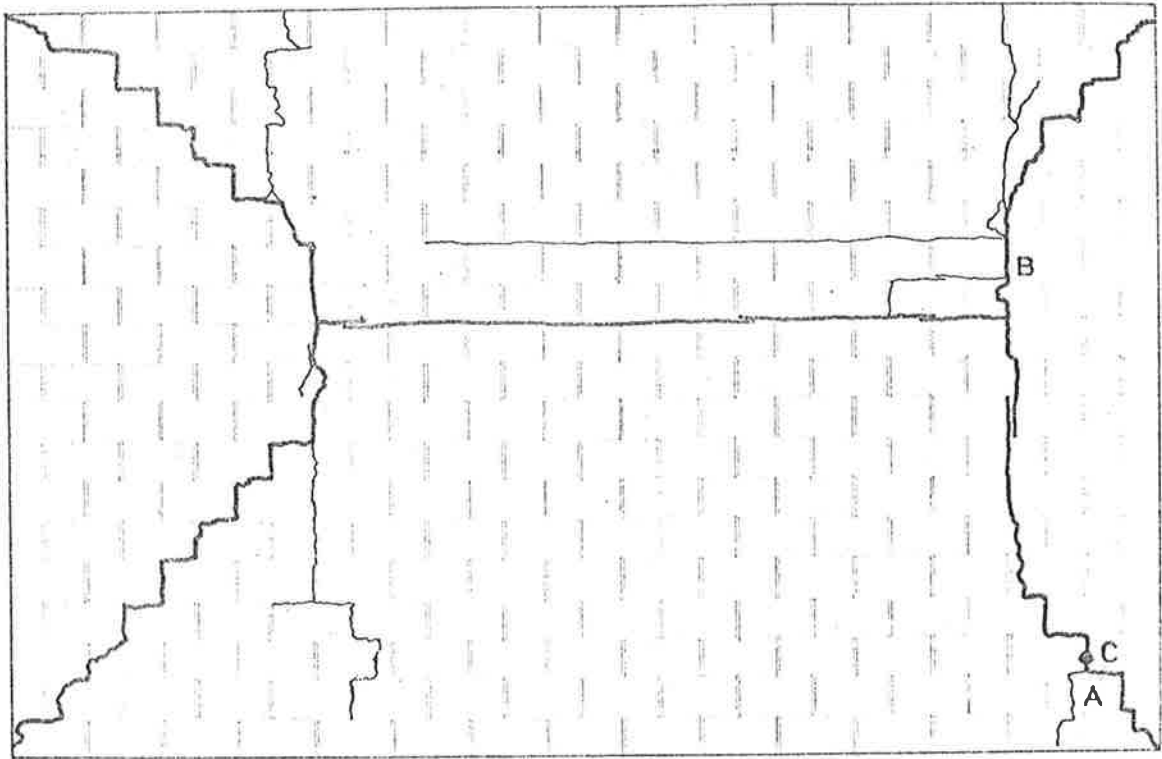


Figure 7.15(a): East Face

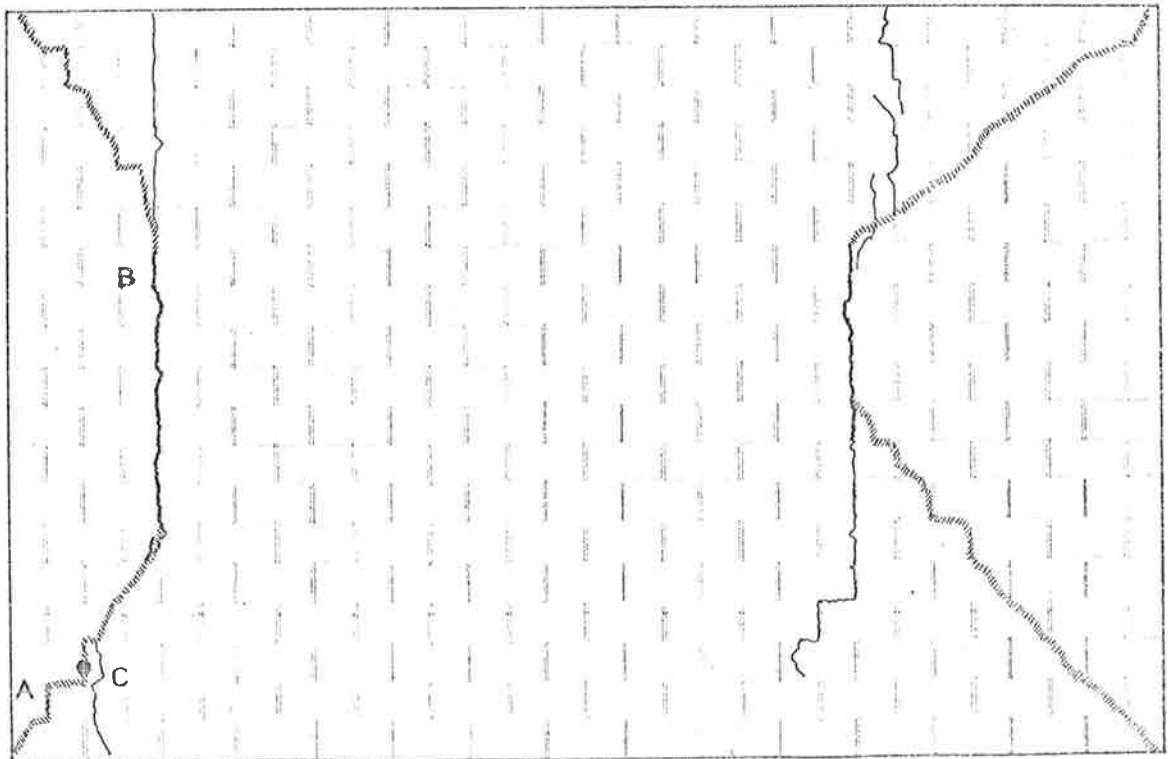


Figure 7.15(b): West Face (Hatching denotes brick spalling)

Figure 7.15: Crack Patterns in Brickwork Panel (refer to figure 7.5)

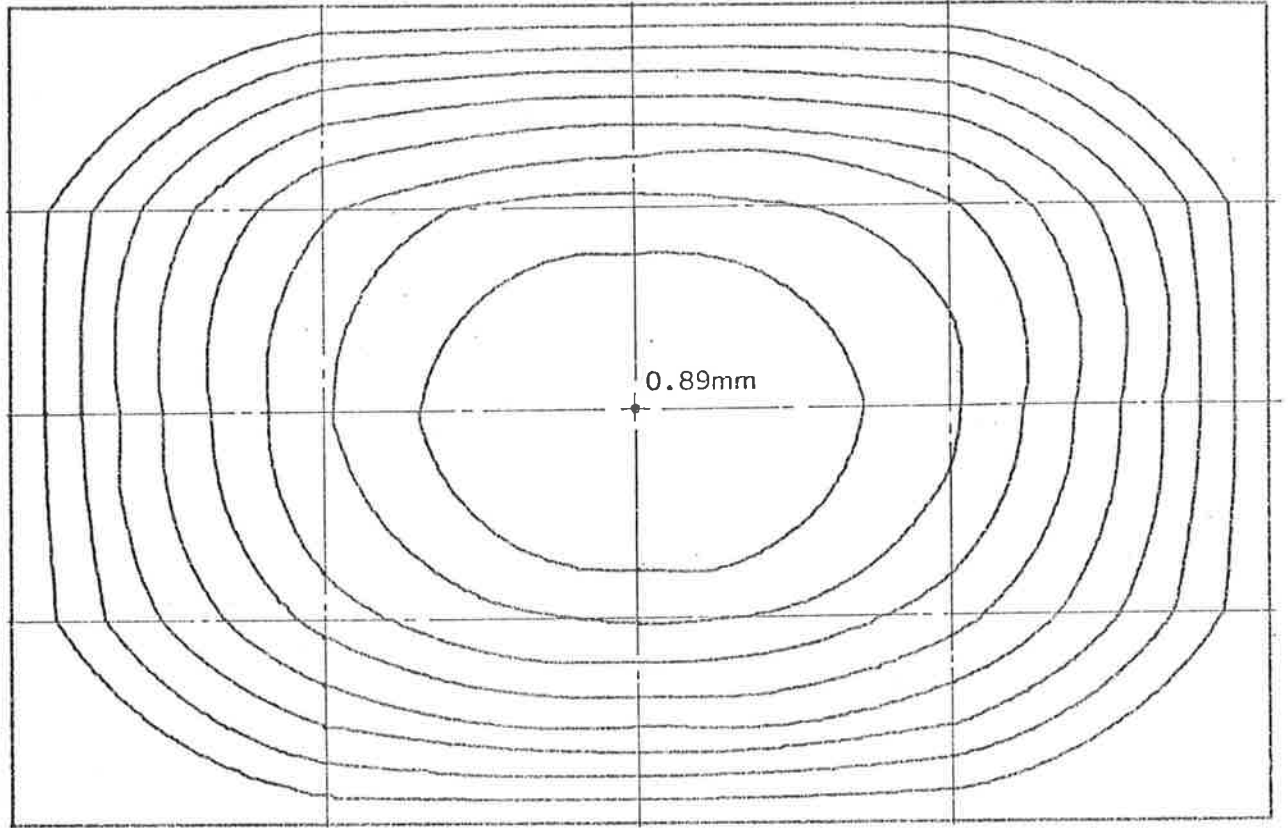


Figure 7.16(a): Lateral Displacement Contours for Load 27N/mm  
(Contour Intervals 0.10mm)

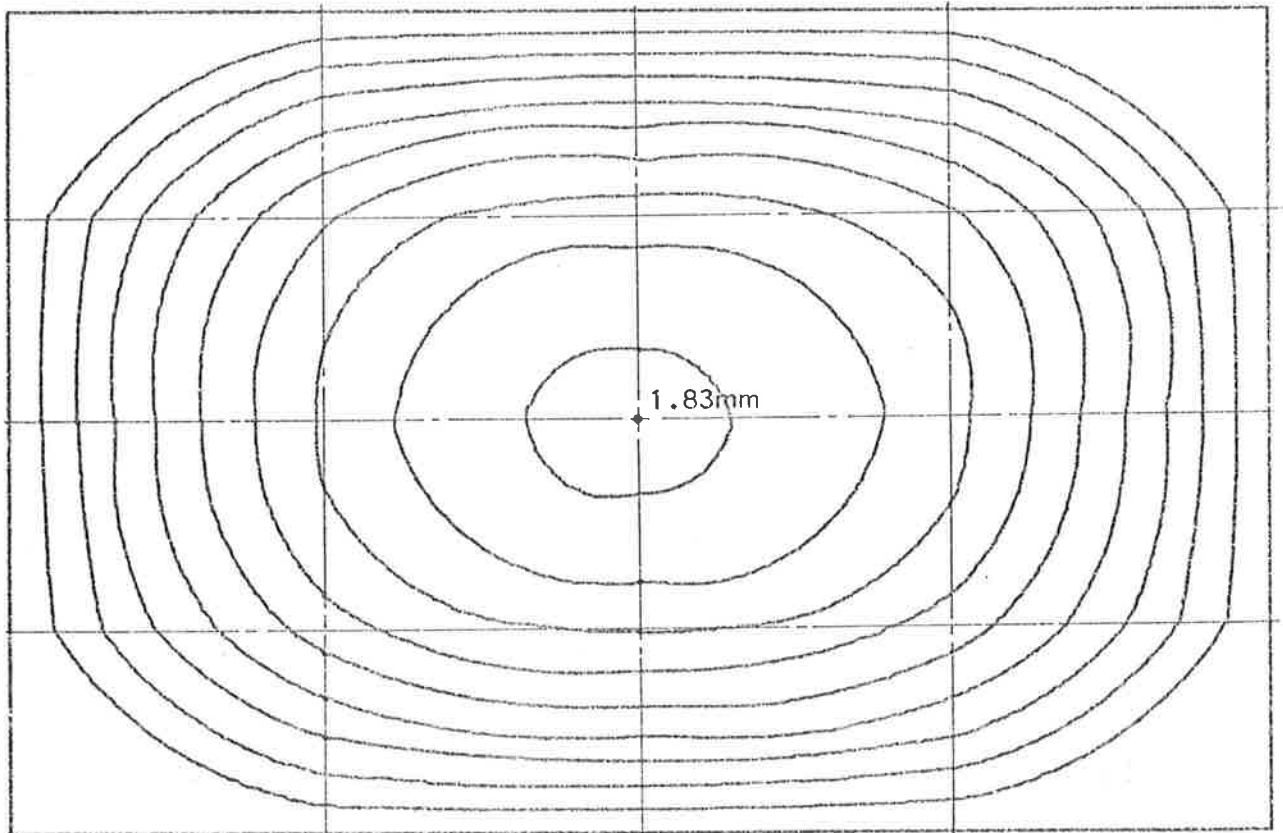


Figure 7.16(b): Lateral Displacement Contours for Load 54N/mm  
(Contour Interval 0.20mm)



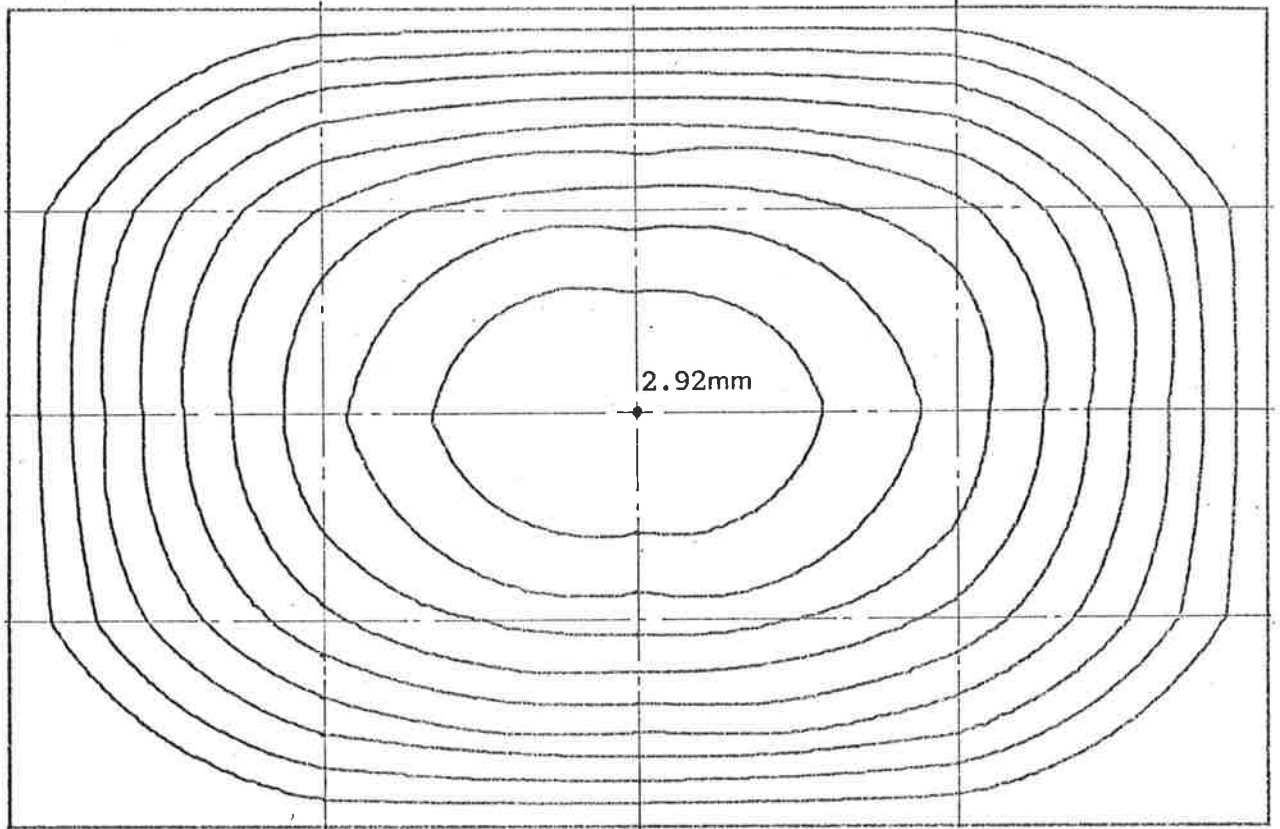


Figure 7.16(c): Lateral Displacement Contours for Load 83N/mm  
(Contour Interval 0.30mm)

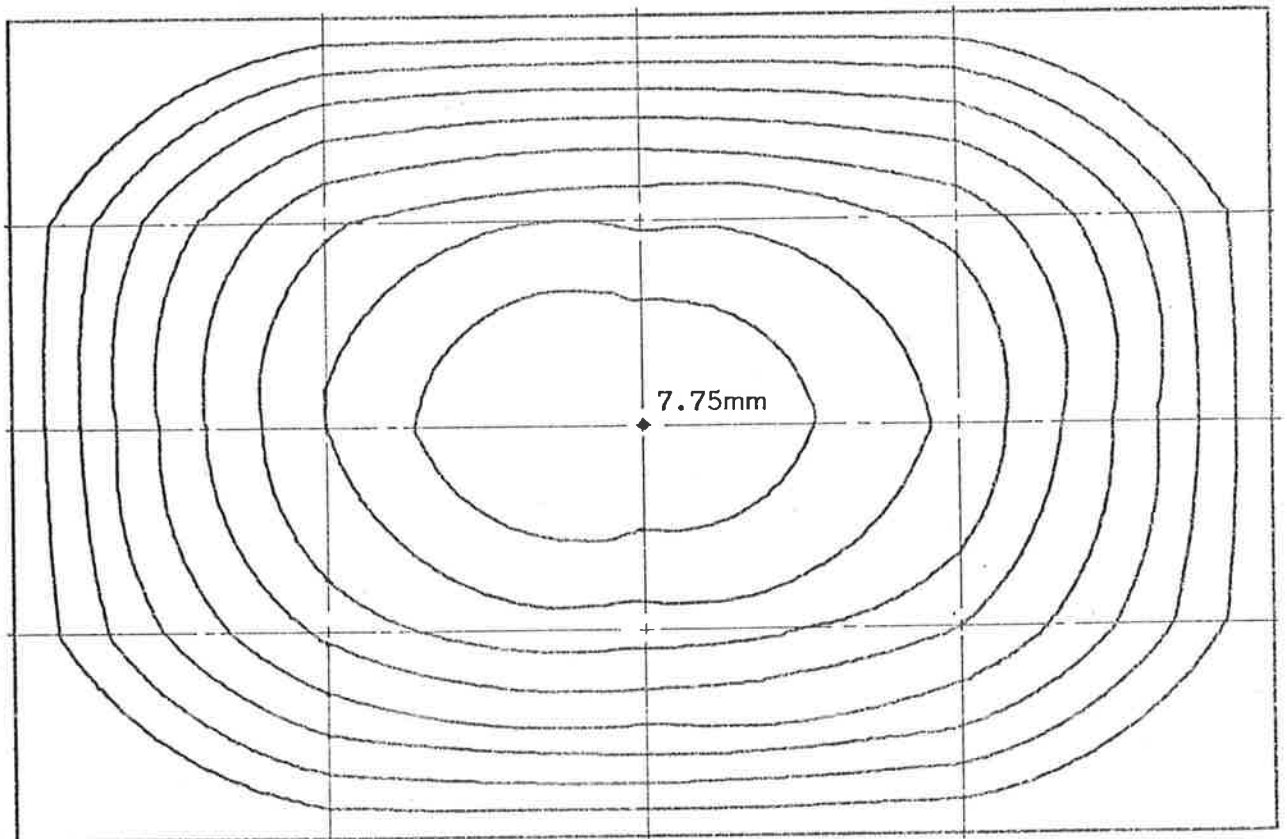


Figure 7.17: Lateral Displacement Contours for Load 178N/mm  
(Contour Interval 0.90mm)

the displacements were still approximately symmetrical about the panel centrelines and also indicates that the load was approximately symmetrical about the vertical centreline of the panel.

The cracking in the panel at a load of 185N/mm length of panel was associated with a tensile failure of the brickwork close to the panel corners, both through the bricks and on the brick-mortar interfaces, caused by normal tensile stresses at approximately 45 degrees to the bedjoints. The magnitude of the vertical load and its effective eccentricity, combined with corner twisting moments, can cause significant normal tensile stresses close to the panel corners<sup>(112)</sup>. No failure criterion for brickwork subjected to this combination of bending and pure twist is known to the author. However, an approximate method using the results of PROGRAM PANEL1 and the tensile strength of a brick, as proposed by Hendry<sup>(120)</sup>, may be used to predict this type of brickwork failure in the test panel as follows.

For a uniform vertical load  $W$  N/mm length of panel, the vertical compressive stress in the middle surface of the panel is -

$$\sigma_a = -\frac{W}{d} \quad (7.1)$$

in which  $d$  is the panel thickness ( $d = 65.4\text{mm}$ )

By assuming a Mohr's Circle distribution of normal stresses, noting that the brick and mortar elastic moduli are approximately equal, the component of the vertical stress,  $\sigma_a$ , at 45 degrees to the bedjoints is -

$$(\sigma_a)_{45} = \sigma_a \cdot \cos^2 \pi/4 = -\frac{W}{2d} \quad (7.2)$$

Results obtained from PROGRAM PANEL1 indicate that the brickwork cracks predominantly in the region of the panel centre. Therefore, since the brick and mortar moduli are approximately equal, it may

be assumed that bending moments at 45 degrees to the bedjoints, say  $(M_{xy})_{45}$ , associated with twisting moments,  $M_{xy}$  and  $M_{yx}$ , are -

$$(M_{xy})_{45} \approx \frac{1}{2}(M_{xy} + M_{yx}) \quad (7.3)$$

The maximum flexural stress associated with  $(M_{xy})_{45}$  -

$$(\sigma_{xy})_{45} = \frac{6}{d^2}(M_{xy})_{45} \approx \frac{3}{d^2}(M_{xy} + M_{yx}) \quad (7.4)$$

The vertical tensile stress,  $\sigma_b$ , caused by bending due to the eccentricity of the applied load may be calculated as -

$$\sigma_b = \frac{6}{d^2}We \quad (7.5)$$

in which  $W$  is the load per unit length of panel, and for a brick close to the top or bottom edge of the panel,  $e$  may be assumed to be equal to the eccentricity of the applied load (c.f. stress distributions shown in figures 4.6(a), (b)).

The component of the bending stress,  $\sigma_b$ , at 45 degrees to the bedjoints may be calculated, as for the axial stresses, as -

$$(\sigma_b)_{45} \approx \sigma_b \cdot \cos^2 \pi/4 = \frac{3We}{d^2} \quad (7.6)$$

Equations (7.2), (7.4) and (7.6) may be combined to give the maximum tensile stress in a brick at 45 degrees to the bedjoints. This stress, say,  $(\sigma_t)_{45}$ , may be calculated as -

$$(\sigma_t)_{45} = (\sigma_a)_{45} + (\sigma_b)_{45} + (\sigma_{xy})_{45} \quad (7.7)$$

That is,

$$(\sigma_t)_{45} = -\frac{W}{2d} \cdot (1 - \frac{6e}{d}) + \frac{3}{d} \cdot (M_{xy} + M_{yx}) \quad (7.8)$$

Equation (7.8) may be solved by iteration by using PROGRAM PANEL1 as follows.

Hendry<sup>(120)</sup> proposed a set of relationships between brick uniaxial compressive strengths and uniaxial tensile strengths as shown in figure 3.19. For example, according to Hendry, a brick with a compressive strength of 60MPa would have a tensile strength of approximately 3.5MPa. This value may be assumed for the tensile strength of the bricks in the experimental panel described above; that is  $(\sigma_t)_{45} = 3.5\text{MPa}$  in equation (7.8). A (16 x 8) mesh may be used in PROGRAM PANEL1 to calculate the twisting moments  $(M_{xy} + M_{yx})$  at point 'C' on the experimental failure line (figure 7.15) for any selected value of the vertical load, W per unit length of panel. It is found, by iteration, that equation (7.8) is satisfied at point 'C' when W is approximately 173N/mm length of panel; the corresponding value of  $(M_{xy} + M_{yx})$  is approximately 3280Nmm/mm.

That is, by using PROGRAM PANEL1, the vertical load at which the brickwork panel described in this section could be expected to fail in tension at 45 degrees to the bedjoints, close to a panel corner, is approximately 173N/mm length of panel. This may be compared with 185N/mm failure load measured in the panel experiment.

### 7.3.5 Summary

A case study has been described of a full scale brickwork panel approximately 2400mm high x 3600mm long x 65mm thick loaded vertically at an eccentricity nominally 20mm at both the top and the bottom. Statistically, the results obtained from the case study are consistent with results obtained using the finite difference theory for brickwork panels proposed in Chapter 6. In addition, an approximate

method has been presented for predicting the failure of brickwork panels in which bending at 45 degrees to the bedjoints may be significant. The failure load calculated for the case study by using this method agrees closely with the experimental result.

Further research is required involving a range of brickwork panels before definite conclusions can be drawn concerning the validity of PROGRAM PANEL1. Factors to be considered include the effects on panel behaviour of the load eccentricity, the degree of fixity at the panel edges and material constitutive and strength properties. Other factors to be considered include initial deviations of a brickwork panel from a plane and poor quality brickwork due to inferior workmanship.

However, the theoretical work proposed in Chapter 6 and incorporated into PROGRAM PANEL1 appears to provide a method for predicting the behaviour of brickwork panels subjected to uniform vertical load. Experimental results summarized in this chapter indicate that PROGRAM PANEL1 could be used as the basis of a comprehensive parametric study carried out to investigate the sensitivity of the strength of brickwork panels to the factors mentioned above.

## 8. COMPARISONS OF THEORETICAL RESULTS WITH DESIGN CODE SPECIFICATIONS

In Chapters 4 and 5 it has been shown that PROGRAM PIER1 (Appendix C) may be used to calculate the failure loads of brickwork walls subjected to eccentric vertical loads. Parameters which may affect the failure loads include the brickwork elastic properties, the brickwork compressive strength which in turn depends on the mortar compressive strength in triaxial compression, the top and base support conditions and the initial deviations of the wall from a vertical plane. It will be appreciated that a comprehensive parametric study of the above effects on wall failure loads is beyond the scope of this thesis. However, a general indication is given in this chapter of typical results which may be obtained from such a study by presenting wall failure loads calculated for one type of brickwork by using PROGRAM PIER1. The effects of various end conditions and deviations from vertical straightness are investigated and comparisons are made between the calculated failure loads and failure loads which form the basis of various Design Codes.

In Chapters 6 and 7 PROGRAM PANEL1 (Appendix G) has been used to calculate the strength of brickwork panels when simply-supported on four sides and subjected to eccentric uniform vertical line loads. In contrast to PROGRAM PIER1, PROGRAM PANEL1 calculates a panel failure load on the assumption that the brickwork remains linearly elastic; the analysis of brickwork panels with non-linear material properties is beyond the scope of this thesis. Possible criteria which may be used in PROGRAM PANEL1 are summarized in Section 8.2. Failure loads are presented for one type of brickwork only and, in order to place the calculated results in perspective, the panel

failure loads are compared with wall failure loads and such relevant Code Design requirements as exist at present.

### 8.1 BRICKWORK WALLS - PROGRAM PIER1

Calculated failure loads are given in the following sections for walls with various conditions of end load eccentricity, end fixity and initial deviations from vertical straightness. All computations use the brickwork properties summarized in Table 8.1.

Material Property	Reference(s)
Brick Compressive Strength, 60MPa ( $\sigma_c$ )	Assumption for typical bricks
Mortar, 1:1:6 by Volume	Assumption for typical mortar
Brick Elastic Modulus, $18 \times 10^3$ MPa ( $E_b$ )	Sahlin <sup>(44)</sup> , Figure 3.1
Brick Tensile Strength, 3.5MPa ( $\sigma_t$ )	Hendry <sup>(120)</sup> , Figure 3.19
Brickwork Compressive Strength, 26MPa ( $\sigma_c$ )	Hendry <sup>(120)</sup> , Figure 3.19
<u>Non-linear Mortar Modulus Coefficients:</u>	
Initial Tangent Modulus, $8.0 \times 10^3$ MPa ( $E_m$ )	Assumption, Chapter 5
$n = 1.5$	Assumption, Section 5.2.2, Figure D.3
$K = 6.752$	Equation (B.2)

Table 8.1: Material Properties for Parametric Study on Brickwork Walls

A further assessment of consistency of the assumed material properties may be made by calculating the ratio -

$$\chi = \left( \frac{E_{br}}{\sigma_c} \right) \quad (8.1)$$

in which  $E_{br}$  is the initial tangent modulus of the brickwork (MPa)  
 $\sigma_c$  is the brickwork compressive strength (MPa).

Hendry<sup>(120)</sup> has reported experimental results which show that typically  $\chi$  may vary between approximately 400 and 800. (These reported values of  $\chi$  may be compared with mean experimental values of 398 and 350 (Tables 7.3 and 7.10 respectively) and a mean value of 500 for the wall experiments (Sections 5.2.2.3, Appendix D).) The value of  $\chi$  for the materials summarized in Table 8.1 is 604, thus indicating that the material assumed properties are representative of the properties of real bricks and mortar.

### 8.1.1 Walls Loaded with Equal End Eccentricities in One-way Bending

Figure 8.1 shows wall failure loads plotted non-dimensionally as a fraction of the compressive strength of a short brickwork wall. The end load eccentricities are assumed to be equal, pinned both top and bottom, and initial deviations from vertical straightness are taken to be zero. Failure loads are shown for eccentricities of zero,  $d/50$ ,  $d/6$  and  $d/3$  for wall height-to-thickness ratios (slenderness ratios) up to 40, calculated for brick-on-flat brickwork with 10mm thick mortar bedjoints. The failure loads of end eccentricities of  $d/50$ ,  $d/6$  and  $d/3$  were calculated using PROGRAM PIER1. However, PROGRAM PIER1 cannot be used for the calculation of axial failure loads because lateral displacements of a wall prior to failure are zero; the axial failure loads may be estimated as follows.

For linear materials, the maximum wall load per unit length, in a non-dimensional form, may be taken to be the lower value obtained from equations (8.2) and (8.3). That is,

$$\frac{P_f}{\sigma_c d} = \frac{\pi^2}{12 \sigma_c} \cdot \frac{E_{br}}{(h/d)^2} \quad (8.2)$$



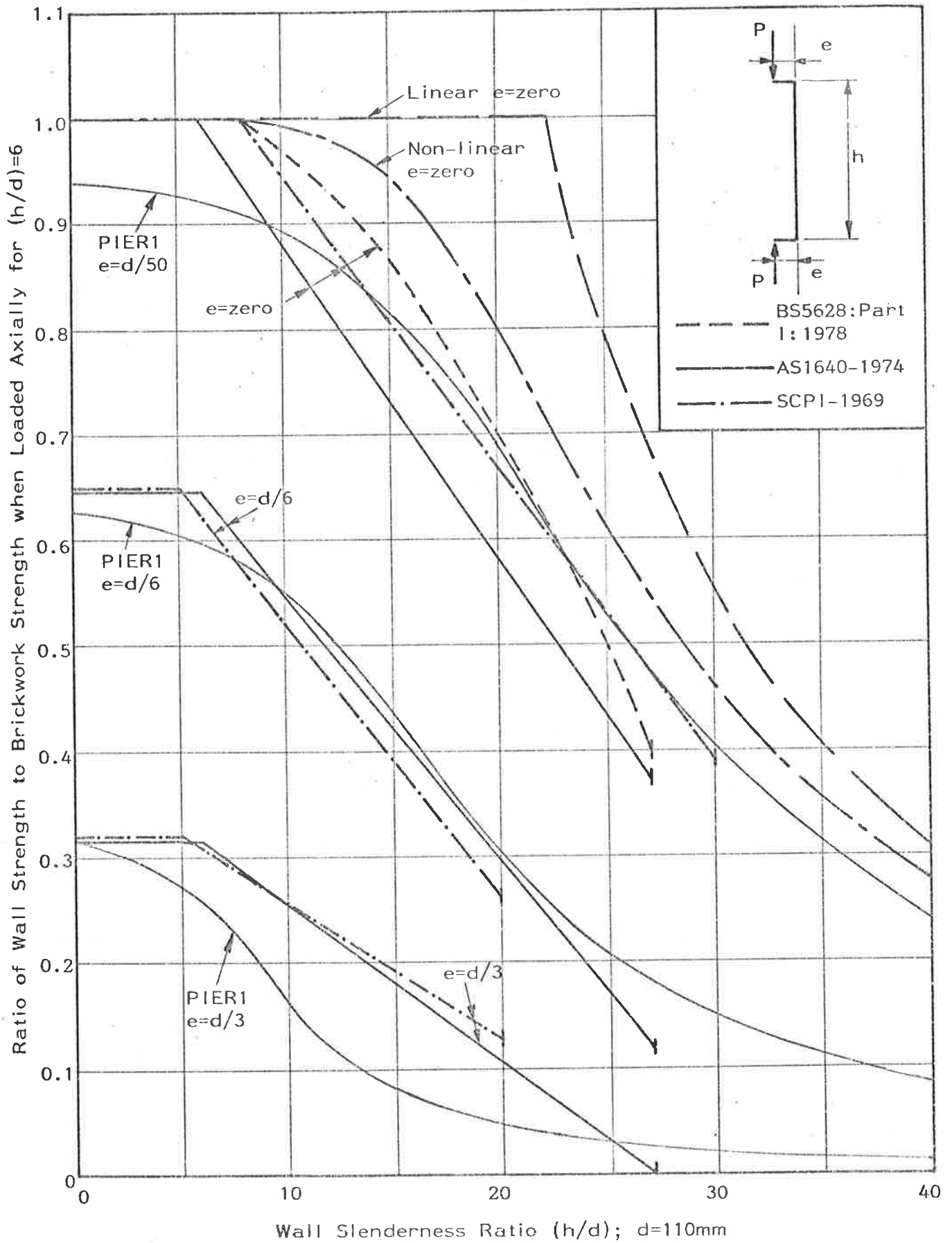


Figure 8.1: Failure Loads for Walls Loaded at Equal End Eccentricities

in which  $E_{br}$  is the initial tangent modulus of the brickwork  
 $d$  is the wall thickness  
 $h$  is the wall height  
 $\sigma_c$  is the brickwork compressive strength

$$\text{or } \frac{P_f}{\sigma_c d} = 1.0 \quad (8.3)$$

In equation (8.2), the initial tangent modulus of the brickwork may be calculated from equation (3.47).

Results obtained using equations (8.2) and (8.3), shown in figure 8.1, indicate a sharp transition between brickwork compression failure (vertical splitting) and wall buckling failure at a slenderness ratio of 22.3. This sharp transition has not been observed in experiments (Hendry<sup>(120)</sup>); the reasons can be appreciated by considering the effects of the non-linear behaviour of brickwork.

For brickwork constructed from linear elastic bricks and non-linear mortar, the wall failure loads for zero load eccentricity may be estimated using a tangent modulus approach. The mortar stress-strain relationship may be assumed to be —

$$\sigma = E_m (\epsilon - K\epsilon^n) \quad (B.1)$$

in which  $E_m$  is the mortar initial tangent modulus

$K, n$  are constants (Appendix B).

When the stress in axially loaded brickwork is  $\sigma_a$  and the uniform strain in the mortar is  $\epsilon_a$ , the mortar tangent modulus is

$$E_a^t = \left. \frac{d\sigma}{d\epsilon} \right|_{\epsilon=\epsilon_a} = E_m (1 - nK\epsilon_a^{n-1}) \quad (8.4)$$

From equation (3.47), the average modulus for the brickwork at stress  $\sigma_a$  is given by —

$$E_{br,a} = E_b \cdot \left[ \frac{H + b}{H + b \left( \frac{b}{t} \right) \frac{E_b}{E_a}} \right] \quad (8.5)$$

in which  $E_b$ ,  $H$ ,  $b$ ,  $t$  are as defined in figure 6.5 and  $E_a^t$  is as defined in equation (8.4).

The critical buckling load per unit length of a pin-ended wall for which the elastic modulus is  $E_{br,a}$  is thus —

$$P_{cr} = \frac{\pi^2 (E_{br,a}) d^3}{12h^2} \quad (8.6)$$

in which  $h$  and  $d$  are as defined above.

The nominal critical buckling stress becomes, therefore —

$$\sigma_{cr} = \frac{\pi^2}{12} \cdot \frac{E_{br,a}}{(h/d)^2} \quad (8.7)$$

Equations (B.1), (8.4), (8.5) and (8.7) must be solved by iteration because the strain in the mortar,  $\epsilon_a$ , is not known initially. By Newton-Raphson iteration, a failure curve may be obtained for axially-loaded non-linear brickwork walls which fail by buckling (figure 8.1). As can be seen, this method, which uses an equivalent tangent modulus, gives results which fit well in the region between a linear material analysis with zero eccentricity, and a non-linear analysis with an eccentricity of  $d/50$ .

In contrast the the curve obtained for linear brickwork, the smoothness of the non-linear curve in figure 8.1 reflects the transition in wall failure from brickwork compression failure (vertical splitting) to a buckling failure mode<sup>(120)</sup>.

Figure 8.1 indicates that for non-linear brickwork walls constructed from materials specified in Table 8.1 and loaded at eccentricities of  $d/6$  or less, the wall strength decreases rapidly as the slenderness ratio increases. In addition, the strength of walls loaded

at an eccentricity of  $d/50$  remains greater than approximately 25 percent of the brickwork compressive strength for slenderness ratios up to 40. However, this level of strength in walls of high slenderness is not shown in the results obtained for brickwork walls loaded at an eccentricity of  $d/3$ . For such walls the load capacity decreases from approximately 30 percent of the brickwork compressive strength at a slenderness ratio of 2 to less than 5 percent for slenderness ratios greater than 20.

Also plotted in figure 8.1 are the load capacities of brickwork walls as calculated by using the recommendations of Design Codes S.C.P.I.-1969<sup>(127)</sup>, BS5628: Part 1: 1978<sup>(24)</sup> and AS1640-1974<sup>(4)</sup>. It should be noted that BS5628: Part 1: 1978 (Section 32, Table 7) may be applied only to the axially-loaded walls in figure 8.1 because the load is equally-eccentric at the ends. The Code failure loads agree closely with the calculated values for load eccentricities of zero and  $d/6$ , but the calculated wall capacities for an eccentricity of  $d/3$  are less than the Code loads by as much as 50 percent of the Code values for a range of slenderness ratios. The results for eccentricities less than  $d/6$  indicate that structural brickwork design and construction may be restricted unnecessarily by specifying the maximum allowable wall slenderness ratio to be 27<sup>(4), (24)</sup> or 30<sup>(127)</sup>. Code limitations on slenderness ratios will be discussed further in this chapter as results are presented which show some on the effects of wall failure loads of various end conditions and initial deviations from vertical straightness.

### 8.1.2 Walls Loaded with Unequal End Eccentricities

Figures 8.2, 8.3 and 8.4 are plotted non-dimensionally and show wall failure loads as functions of wall slenderness. All brickwork materials are assumed to have the properties summarized in Table 8.1

and the walls are subjected to the loading conditions described in Table 8.2.

Figure No.	Wall Support Conditions		Load Eccentricities <sup>(a), (b)</sup>	
	Top <sup>(c)</sup>	Base	Top	Base
8.2	Pin-roller	Pin	e	zero
8.3	Pin-roller	Fixed	e	-
8.4	Pin-roller	Pin	e	-0.75e

(a)  $e = \text{zero}, d/50, d/6, d/3$

(b)  $d = 110\text{mm}$

(c) A pin-roller at a top support provides translational restraint in the horizontal direction only.

Table 8.2: Wall Support and Loading Conditions

Figure 8.2 shows that the load capacities of walls loaded axially at the base and loaded at the top at eccentricities of  $d/3$  or less depend essentially on the brickwork compressive strength for slenderness ratios of 15 or less. For slenderness ratios greater than 15, the wall strengths decrease as a result of slenderness effects which cause wall failure by lateral buckling rather than material failure. Figure 8.2 indicates also that the strength of a wall with a slenderness ratio of 40, when loaded at a top eccentricity of  $d/50$ , is approximately 25 percent of the strength of an axially-loaded short (slenderness less than 6) brickwork wall.

Failure loads calculated using the Swiss Rule, as specified in clause # 4.13.3.4 of the Australian Code AS1640-1974<sup>(4)</sup>, differ considerably from values calculated using PROGRAM PIER1. This shows that the Code requirements may not be conservative for walls in which the top load eccentricity is greater than  $d/6$ . Failure loads calculated

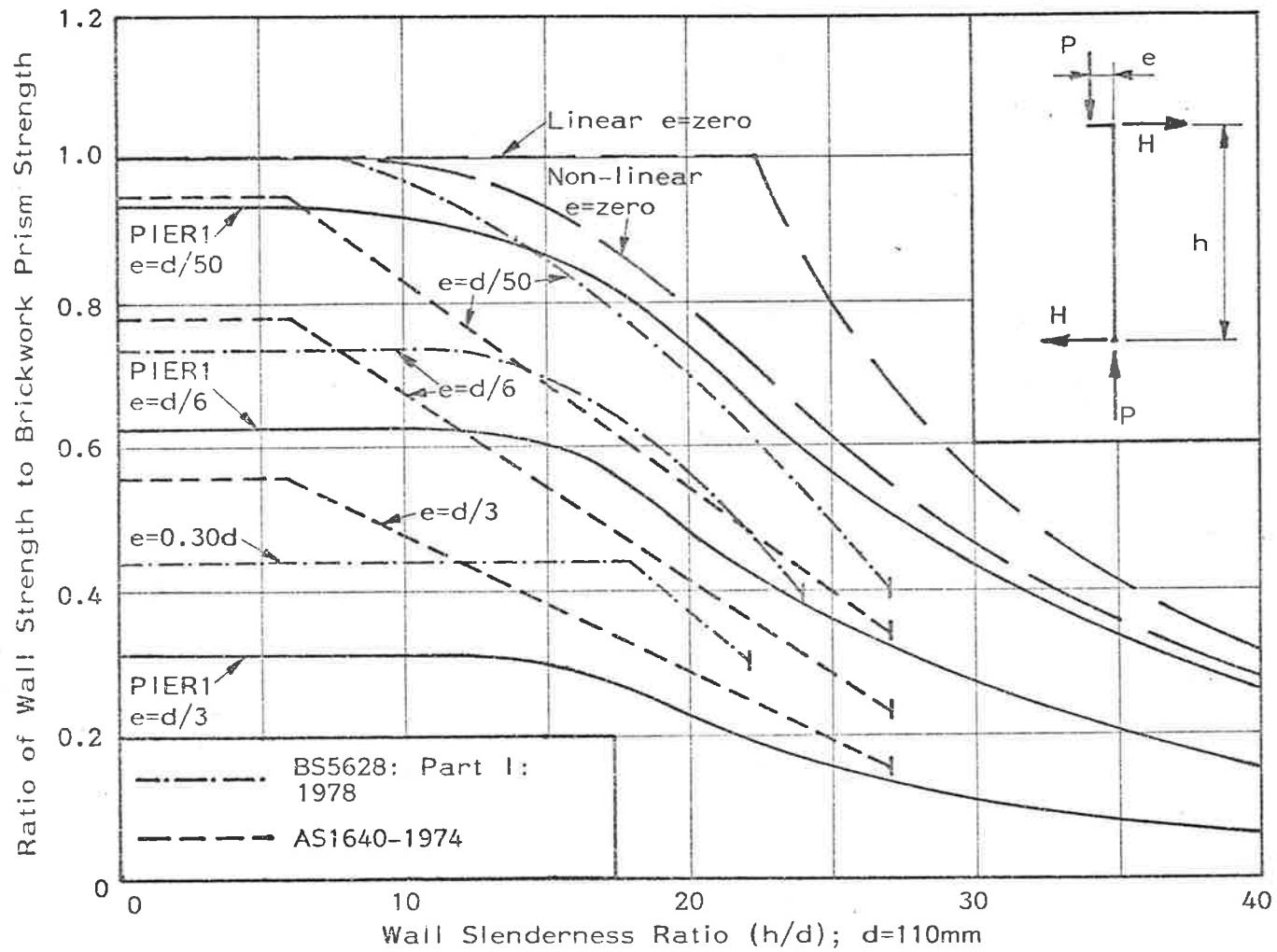


Figure 8.2: Failure Loads of Walls Loaded Eccentrically at the Top and Concentrically at the Base

using BS5628: Part 1: 1978<sup>(24)</sup> (maximum load eccentricity  $0.30d$ ) also differ from the computed values but are closer than values calculated by the Swiss Rule.

Figure 8.3 shows the load capacity curves for walls fixed against rotation at the base and loaded eccentrically at the top. In practical terms, the curves may be used to estimate the load capacities of single-storey brick-on-flat walls sitting on rigid concrete raft footings. The calculated results shown in figure 8.3 indicate that the load capacities of such walls, when loaded at eccentricities of  $d/3$  or less, depend only on the brickwork compressive strength and the load eccentricity for slenderness ratios of 20 or less. In addition, for a given load eccentricity, the strength of a wall with a slenderness ratio of 40 is approximately one half the strength of a wall with a slenderness ratio of 6 or less. Figure 8.3 also shows that failure loads calculated using # 4.13.3.4 of AS1640-1974 may be non-conservative for load eccentricities of  $d/6$  or greater.

In figure 8.4, plots are given for the load capacities of walls free to rotate at both ends loaded eccentrically on opposite sides of the wall centreline (Table 8.2). The curves show that the failure loads for an eccentricity of  $d/50$  agree closely with the load capacities of axially-loaded walls with slenderness ratios between 15 and 40; the load capacities for walls loaded at  $d/6$  and  $d/3$  are almost constant for slenderness ratios of 20 or less. Wall load capacities calculated using AS16140-1974 show that the Code requirements may be non-conservative for load eccentricities between  $d/3$  and  $d/50$ .

### 8.1.3 Effect of Initial Imperfections

Initial imperfections, or deviations from vertical straightness, may result from poor workmanship. Clause # 5.5.3 of Australian Standard AS1640-1974<sup>(4)</sup> permits a maximum deviation from vertical

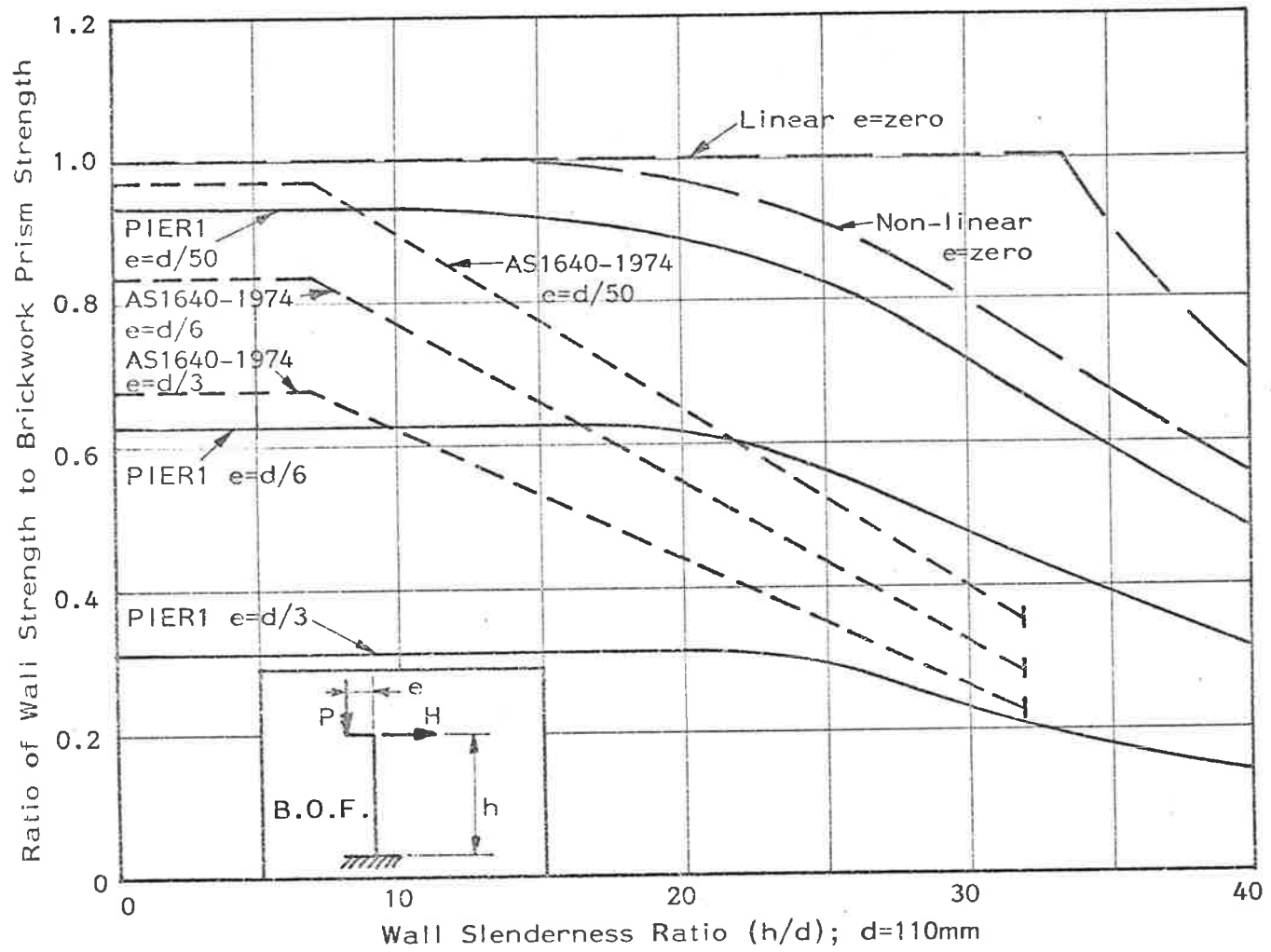


Figure 8.3: Failure Loads of Fixed Base Brick-on-flat Walls Loaded Eccentrically at the Top



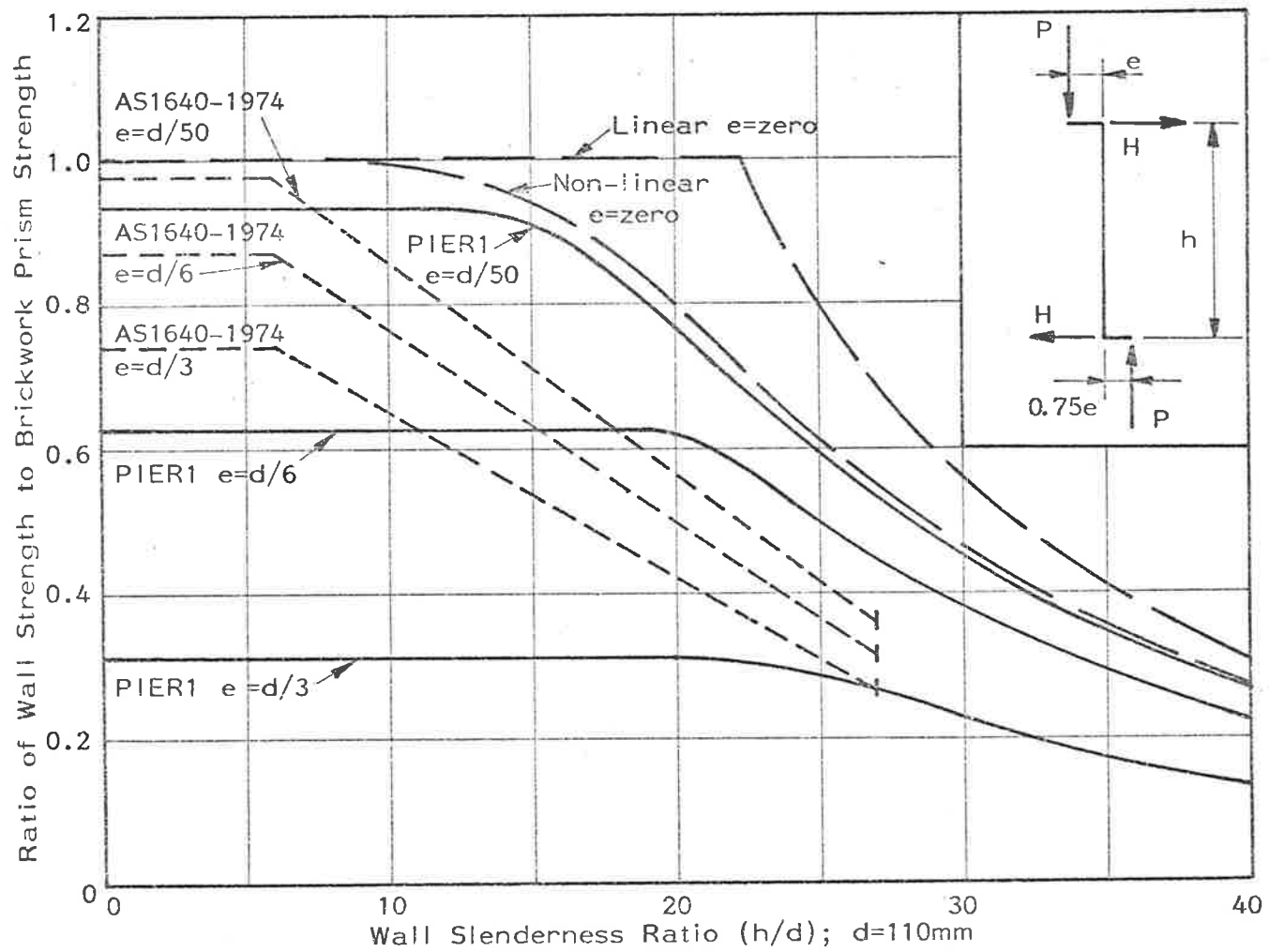


Figure 8.4: Failure Loads of Walls Loaded Eccentrically on Opposite Sides of the Wall Centreline

straightness within a storey of 6mm for every 3 metres of height; that is, a maximum deviation from vertical straightness of  $h/500$ .

Figure 8.5 shows the effects on wall load capacity of initial deviations of zero,  $h/800$  (3mm for each 2400mm height) and  $h/400$  (6mm for each 2400mm height). The walls are assumed to be loaded with equal end eccentricities and the shape of the initial imperfections is assumed to be bilinear with the maximum deviation at wall mid-height. PROGRAM PIER1 can also be used to analyse any arbitrary pattern of initial deviations.

The results plotted in figure 8.5 show that for a slenderness ratio of 20, the load capacity of a wall loaded at an eccentricity of  $d/50$  may be approximately 80 percent of the capacity of a wall initially straight; if the initial imperfection is  $h/400$ , for a slenderness ratio of 40, the capacity ratio is approximately 65 percent. The load capacities of walls loaded at eccentricities of  $d/6$  are also reduced by the assumed initial imperfections but the wall failure loads calculated using AS1640-1974 appear to be only slightly non-conservative for most slenderness ratios.

#### 8.1.4 Summary

Figures 8.1 and 8.5 show that for walls loaded at equal end eccentricities of  $d/6$  or less, Code specifications<sup>(4), (24), (127)</sup> agree closely with wall failure loads calculated using PROGRAM PIER1 for the brickwork materials summarized in Table 8.1. However, the effects of initial deviations from vertical straightness may cause Code specifications to become slightly non-conservative because they do not give the expected factor of safety. The results shown in figures 8.1 to 8.5 also indicate that for walls loaded at eccentricities greater than  $d/6$ , the load capacities calculated by using Code coefficients

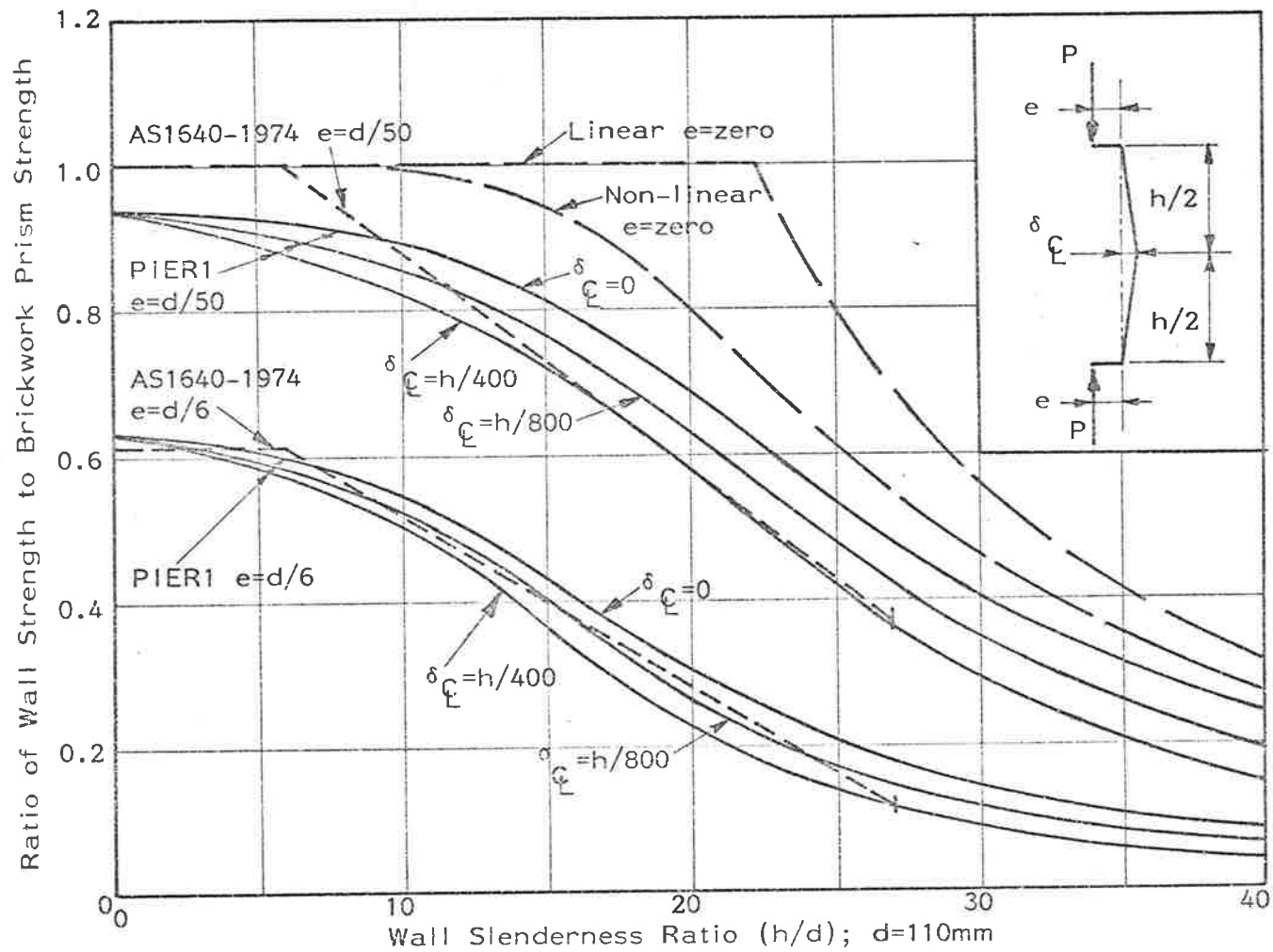


Figure 8.5: Failure Loads of Walls with Initial Imperfections

and the Swiss Rule, where relevant, may be significantly greater than the wall failure loads calculated using PROGRAM PIER1.

#### 8.1.5 Brick-on-edge Partition Walls

It was stated in Chapter 1 that one of the aims of this investigation was to study the strength of slender brick-on-edge walls used as partition walls in domestic construction. Figure 8.6 shows the load capacities of such walls assuming that the supporting rigid footing restrains the base of the wall against rotation. The results, which are close to those shown in figure 8.3 for brick-on-flat walls, indicate that a brick-on-edge wall may support significant loads even at a slenderness ratio of 40 provided that the load at the top acts within the middle third of the wall section. Figure 8.6 also shows that limiting the slenderness ratios to 32 or less, as required by AS1640-1974<sup>(4)</sup>, may be unnecessarily restrictive. However, in the formulation of design rules for such slender walls, it would be prudent to make some allowances for the effects of initial imperfections and the possibility of small lateral loads which may arise accidentally. In addition, as with brick-on-flat walls built on a rigid base (figure 8.3), the load capacities calculated by using AS1640-1974 specifications may be non-conservative for some load eccentricities, as indicated, where the eccentricity exceeds  $d/6$ .

## 8.2 BRICKWORK PANELS IN TWO-WAY BENDING - PROGRAM PANEL1

In this section, it is demonstrated that the load capacity of brickwork walls may be significantly increased by restraining the vertical edges against lateral translation. This may be achieved in domestic construction by the intersecting of walls at the corners of rooms. In such a situation the brickwork will behave as a panel

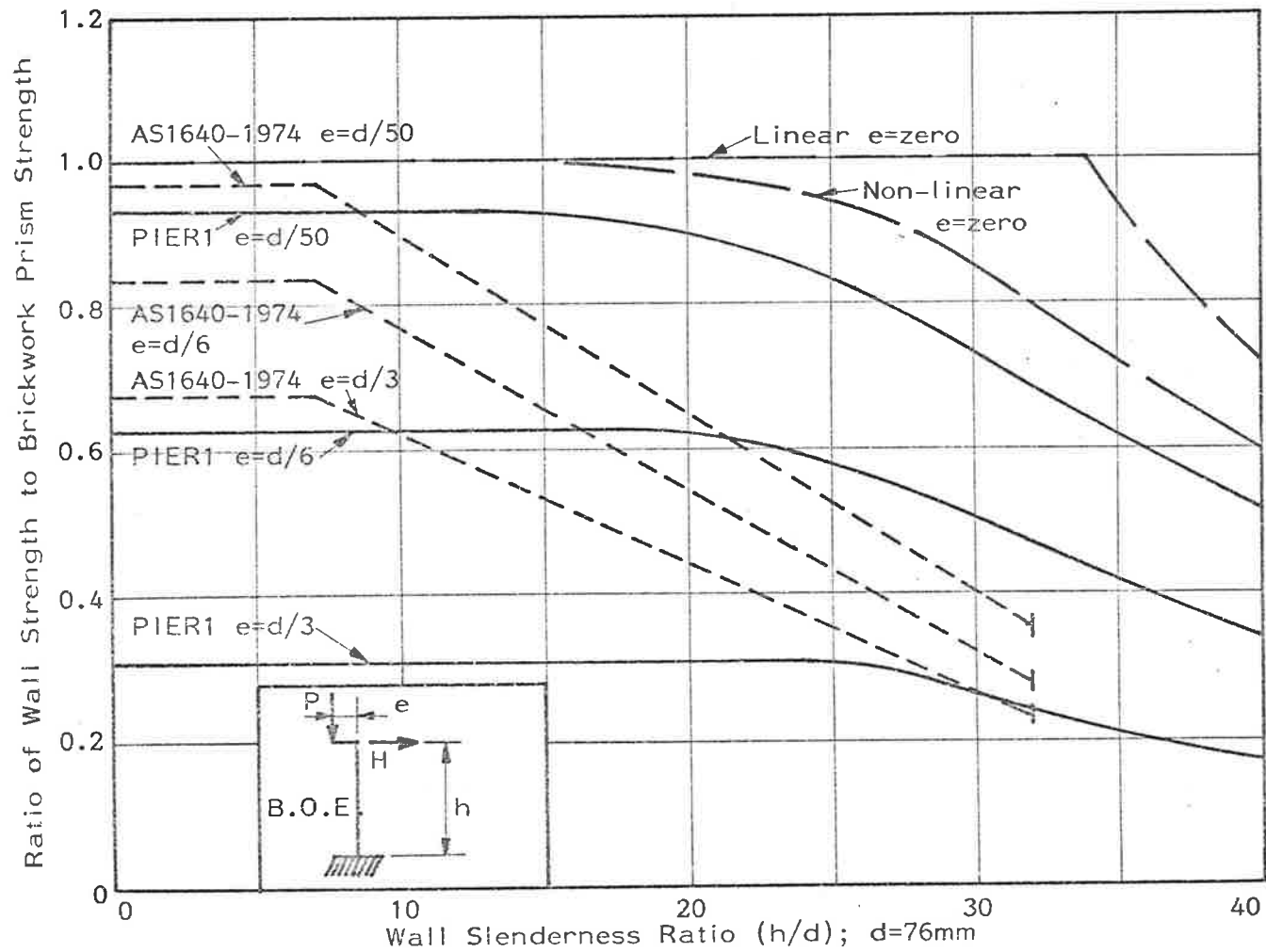


Figure 8.6: Failure Loads of Brick-on-edge Partition Walls

(Chapter 6) rather than as a wall supported only at the top and at the base.

The brickwork material properties are assumed to be as specified in Table 8.1 with the exception of the mortar elastic modulus which is taken as constant at  $8.0 \times 10^3$  MPa. All brickwork panels are assumed to be simply-supported on four sides and are loaded uniformly and eccentrically both at the top and at the base (Appendix G, figure G.1). PROGRAM PANEL1 has been written so that a uniform lateral load may be applied in combination with the vertical load (Appendix G), but, because the modes of failure may be complex<sup>(69)</sup>, no results are presented in this chapter for panels subjected to combined loading conditions.

Three possible modes of failure are shown in figure 8.7. The vertical splitting failure (figure 8.7(a)) is associated with excessive vertical compression (Section 3.3.2) and may occur in the brickwork when the maximum normal vertical stress per unit length of panel is equal to the brickwork compressive strength,  $\sigma_c$ , so that --

$$\sigma_c = \frac{W_f}{d} \left( 1 + \frac{6e(m,n)}{d} \right) \quad (8.8)$$

in which  $W_f$  is the failure load per unit length of panel

$d$  is the panel thickness

$e(m,n)$  is the load eccentricity at a typical node  $(m,n)$  in the panel.

Figure 8.7(b) shows the mode of failure expected as a result of excessive bending parallel to the bedjoints (Section 7.2) provided that the vertical precompression is sufficient to prevent bond shear failure on the bedjoints at the brick-mortar interfaces (Sahlin<sup>(44)</sup>, Base and Baker<sup>(69)</sup>, Section 3.3.4.2). It may be assumed that the brick transverse bending strength,  $\sigma_{bt}$ , is equal to the brick normal tensile

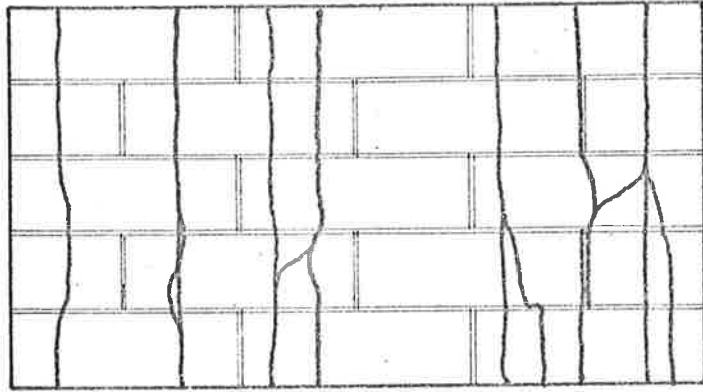


Figure 8.7(a): Vertical Compression Failure (Vertical Splitting)

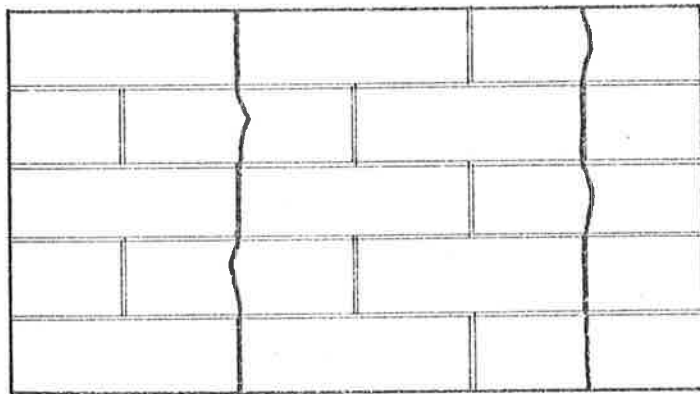


Figure 8.7(b): Failure in Flexure due to Horizontal Bending

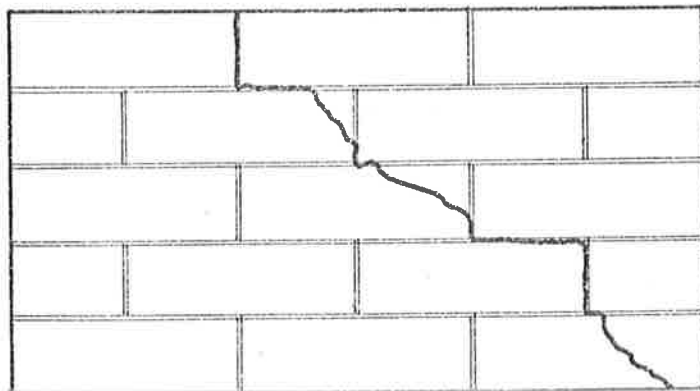


Figure 8.7(c): Torsional Cracking Failure at 45 degrees to the Bedjoints

Figure 8.7: Modes of Failure for a Brickwork Panel

strength,  $\sigma_t$  (Table 8.1), so that equation (3.46)<sup>(44)</sup> may be written as –

$$0.5\sigma_t \leq \sigma_{xx,f} \leq \sigma_t \quad (8.9)$$

in which  $\sigma_{xx,f}$  is a brickwork bending stress per unit height of panel at failure and may be calculated as –

$$\sigma_{xx,f} = \frac{6M_{xx,f}}{d^2} \quad (8.10)$$

In equation (8.10),  $M_{xx,f}$  is the failure bending moment, per unit height of panel, parallel to the bedjoints (Chapter 6) and  $d$  is the panel thickness.

A value for the failure stress,  $\sigma_{xx,f}$ , must be chosen arbitrarily because of a lack of experimental data. However, as was shown in Section 3.3.4.4, a practical estimate of  $\sigma_{xx,f}$  would be –

$$\sigma_{xx,f} = 0.75 \sigma_t \quad (8.11)$$

Therefore, from equations (8.10) and (8.11), the bending moment per unit height of panel at which the failure mode shown in figure 8.7(b) may be expected is –

$$M_{xx,f} = 0.125 \sigma_t d^2 \quad (8.12)$$

Failure at 45 degrees to the bedjoints adjacent to a panel corner (figure 8.7(c)) may be calculated by using equation (7.8) (Section 7.3). It may be assumed for practical purposes that  $(\sigma_t)_{45} = \sigma_t$  approximately, so that the failure load,  $W_f$ , may be calculated by iteration by using –

$$(\sigma_t)_{45} = \sigma_t = -\frac{W_f}{2d} \left(1 - \frac{6e}{d}\right) + \frac{3}{d^2} \left| (M_{xy} + M_{yx}) \right| \quad (7.8)$$

in which  $e$ ,  $d$ ,  $M_{xy}$ ,  $M_{yx}$  are defined in Section 7.3.



The three failure conditions prescribed by equations (8.8), (8.12) and (7.8) may be incorporated into PROGRAM PANEL1 in order to calculate the least value of the vertical load at which either material failure occurs or the panel fails by lateral buckling.

### 8.2.1 Panels Loaded with Equal Load Eccentricities

The relative stiffness of cracked brickwork subjected to bending parallel to the bedjoints (Section 6.2.3) and the relative torsional stiffness of cracked brickwork (Section 6.2.4) have been calculated for bricks 230mm x 110mm x 65mm laid on edge as used in the test panel. Figure 8.8 shows the failure loads, plotted non-dimensionally, for panels 2400mm high constructed from standard bricks 230mm x 110mm x 76mm laid on edge. It may be assumed, for practical purposes, that the relative bending and torsion stiffnesses for such cracked brickwork are as given in Chapter 6.

The results indicate that for aspect ratios  $l/h$  less than 1.0, panels loaded at eccentricities of  $d/1000$  carry approximately the same load per unit length as a short brickwork prism loaded in axial compression. This result is supported by experiments on brickwork panels (Hendry<sup>(120)</sup>). Figure 8.8 shows that panel load capacity decreases as the panel aspect ratio (length-to-height ratio) increases between 1.0 and 3.0, but, nevertheless, panel strength exceeds the strength of a linear material wall with the same height-to-thickness ratio.

Results obtained by assuming linear material properties show that a panel loaded at an eccentricity of  $d/6$  fails at one-half the brickwork compressive strength if the panel aspect ratio is less than 0.5. For panels with aspect ratios greater than 0.5, the load capacity decreases rapidly to approximately 23 percent of the brickwork compressive strength. In addition, the calculations show that panels

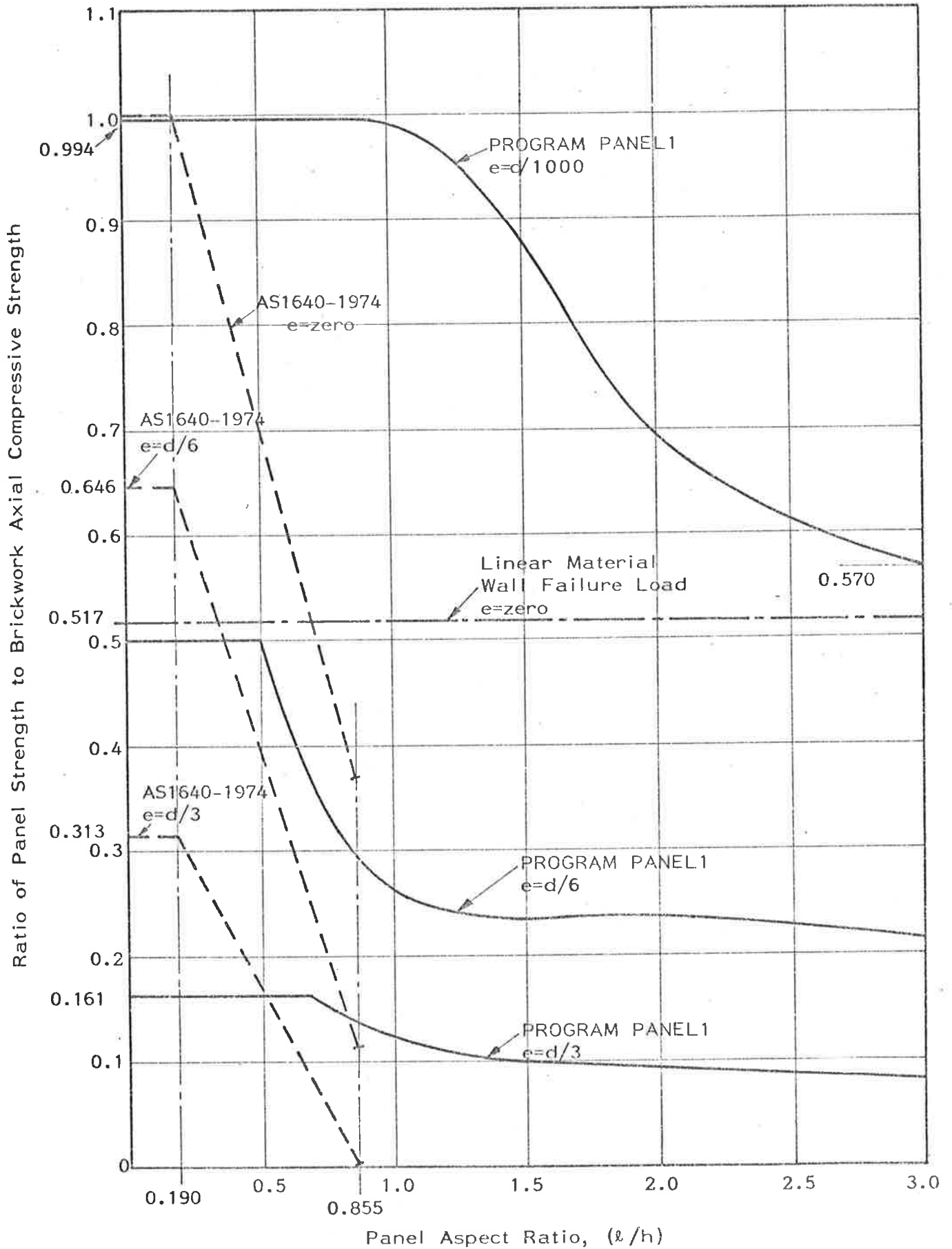


Figure 8.8: Failure Loads for Panels Simply-supported on Four Sides (Brick-on-edge Construction)

with aspect ratios greater than approximately 0.6, when loaded at an eccentricity of  $d/6$ , fail due to excessive horizontal bending stress as determined by equation (8.12).

Brickwork panels of aspect ratios less than approximately 0.7, loaded at an eccentricity of  $d/3$ , fail due to excessive horizontal bending stresses at the top and base supports caused by cracking on the bedjoints combined with the effects of forces associated with a relatively high value of Poisson's ratio ( $\nu = 0.20$ ). However, for all panels investigated with aspect ratios greater than 0.7, the calculated load capacities are determined by the loads at which tensile failure occurs at 45 degrees to the bedjoints adjacent to a panel corner (equation (7.8)).

Australian Standard AS1640-1974 states that the slenderness ratio of a brickwork panel shall be determined by the smaller value of the ratios  $l/d$  and  $h/d$ , and specifies that the slenderness ratio shall not exceed 27. For a brick-on-edge panel of height 2400mm, as used in the computations in this section, the slenderness ratio  $h/d$  is 31.6. However, if the length of such a panel is less than 2052mm, the Code rules may be applied and the load capacities may be calculated. The results are shown in figure 8.8. The Code results are similar to the panel load capacities calculated by PROGRAM PANEL1 for load eccentricities of  $d/6$ , but at eccentricities of  $d/1000$  and  $d/3$  the two sets of values differ considerably. Figure 8.8 shows clearly that for panels with aspect ratios greater than 0.5, the Code load capacities are conservative and take no account of the reserve of strength in a panel beyond the strength of a wall with the same height-to-thickness ratio.

## 9. SUMMARY AND RECOMMENDATIONS

Structural brickwork, as an engineered system, must be designed by using the rules of structural mechanics together with a knowledge of the strengths of its component materials. In order to facilitate the design procedure, practical simplifications may be made and summarized in the form of Code rules, but, initially at least, the true behaviour of brickwork when subjected to various forces and deformations should be understood.

Codes of Practice can only be formulated in the light of the available knowledge. The overall behaviour of brickwork structures, in which the wall and floor elements are assumed to act compositely, is reasonably well appreciated; for example, it is known that the cantilever method of analysis for wind loads (Section 2.2) generally leads to a safe structure. Experience has also shown that the even distribution of loads among all the wall elements is desirable in structural brickwork. However, in the past, the diversity of research and the variability of component materials for brickwork, as reviewed in Chapter 3, made it difficult to assess and compare many of the published results. Recently, Khoo and Hendry<sup>(117)</sup> have developed a fundamental theory for predicting brickwork material strength in compression and Base and Baker<sup>(60)</sup> have summarized the elastic properties of uncracked brickwork in the linear elastic ranges of the brick and mortar materials.

It is also noted in Chapter 3 that theoretical investigations conducted in the past on the strength of brickwork walls have been based on the assumptions that a wall behaves as a column regardless of its vertical edge support conditions and that no tension stresses can exist in the brickwork column<sup>(96), (97)</sup>. These simplifying

assumptions do not reflect the actual behaviour of real brickwork and, as a consequence, past theoretical studies have led to inaccurate and generally conservative predictions for wall strengths.

The work presented in this thesis has approached more closely the real behaviour of brickwork walls by observing that even for a stress distribution in which there are no tensile stresses at the brick-mortar interfaces, the tensile stresses in the bricks themselves can be significant. In Chapter 4, it is shown that cracking occurs at discrete intervals on the brick-mortar interfaces, with the extent of the cracking in the bedjoints depending on the position of the line of action of the resultant compression load relative to the wall centre-line. The reduction in brickwork flexural stiffness caused by the cracking is determined by using a two-dimensional finite element analysis to calculate the moment-rotation characteristics of a cracked brickwork module consisting of two half-height bricks plus one mortar bedjoint. The resulting characteristics are used to develop load-deflection relationships for a homogeneous isotropic varying-thickness column equivalent to the real brickwork. The load capacities of eccentrically-loaded brickwork walls are calculated by solving the equivalent-column equations, written in finite difference form, by using a Newton-Raphson method.

Chapter 5 contains a description of experiments from which was determined the elastic modulus of a brickwork prism subjected to eccentric vertical compression; the test results are shown to agree with analytical results proposed by Base and Baker<sup>(69)</sup>. In addition, results obtained from the method of analysis developed in Chapter 4 are shown to agree with results obtained from experiments conducted on a slender steel block column and a series of brickwork walls of varying slenderness ratio.

In Chapter 6, brickwork panels simply-supported on four sides and subjected to vertical eccentric load are analysed by determining the bending and torsion stiffness of a three-dimensional brickwork module using a three-dimensional finite element method of analysis. Load-deflection relationships are developed for an equivalent plate of varying thickness, analogous to the equivalent column of varying thickness for a wall, in order to represent the behaviour of a real brickwork panel. By writing the load-deflection equations in finite difference form, load capacities are calculated for eccentrically-loaded simply-supported brickwork panels.

Chapter 7 describes tests conducted on small brickwork panels subjected to horizontal bending. Results obtained from the experiments for the reduction in brickwork bending stiffness caused by cracking agree closely with values given by the finite element analysis in Chapter 6. In addition, a full scale test of a slender simply-supported brickwork panel loaded eccentrically top and bottom is described in detail. Results obtained from the experiment show that the equivalent plate analysis developed in Chapter 6 can be used for calculating the load capacities of vertically-loaded brickwork panels.

In Chapter 8, PROGRAM PIER1 has been used in a parametric study of the load capacities of brickwork walls. Wall load capacities calculated by PROGRAM PIER1 differ significantly in some instances from load capacities calculated using Code recommendations (figures 8.1 to 8.6), thus indicating that revision of some Code recommendations may be required. For example, the Swiss Rule, clause # 4.13.3.4 in AS1640-1974<sup>(4)</sup>, can lead to non-conservative load capacities for some types of wall with slenderness ratios up to 27. In addition, results obtained from PROGRAM PIER1 indicate that the maximum allowable wall slenderness ratio could be increased to permit brick-on-edge walls in domestic construction to act as load-bearing elements.

PROGRAM PANEL1 has been used to calculate the load capacities of brickwork panels, simply-supported on four sides, loaded at equal eccentricities top and bottom. PROGRAM PANEL1 could be extended further for use in a more general study of the load capacities of brickwork panels if the following were included –

- (i) The relative stiffness factors, calculated using a finite element method of analysis, for bricks laid in various practical bonding patterns subjected to horizontal bending or pure torsion.
- (ii) Non-linear mortar behaviour.
- (iii) Initial imperfections due to poor workmanship.
- (iv) Failure criteria, determined experimentally, for brickwork subjected to combined compression, bending and torsion.
- (v) The degree of fixity on panel edge supports.

A general parametric study of brickwork panels should necessarily determine the sensitivity of the panel load capacity to the factors listed above. In addition, theoretical predictions should be checked against experimental results from tests on full-sized panels. Other more general aspects of structural brickwork subjected to vertical loads which could be investigated to gain a more comprehensive understanding of brickwork behaviour include –

- (i) The true distribution of vertical loads along the lengths of structural brickwork walls and panels.
- (ii) The extent of the interaction between walls and floor slabs and the resulting effects on vertical load eccentricity.
- (iii) The combined effects of vertical and horizontal loads on brickwork panels (as distinct from walls, which are understood

(Hendry<sup>(15)</sup>)). This may be investigated initially using PROGRAM PANEL1, but this topic is considered to be beyond the scope of this thesis.

- (iv) Seismic loading as it affects the stability of slender brick walls and panels.
- (v) The effects of cavity wall construction on wall stiffness and strength.
- (vi) The effect of coring on brickwork stiffness.

Initially, however, PROGRAM PIER1 and PROGRAM PANEL1 may be used confidently as a basis for modifying existing Code recommendations related to the design of vertically-loaded slender brickwork walls and panels.



APPENDIX A

THE BRICK CURVATURE FUNCTION,  $\alpha$  (EQUATION (4.2))

A.1 A METHOD FOR CALCULATING THE CURVATURE RATIO FUNCTION,  $\alpha$

This section describes one method which may be used to calculate the curvature ratio function,  $\alpha$ , in equation (4.2).

It may be assumed that there exists a function  $\alpha_1(e_o/d, h_b/d)$  such that —

$$\alpha_1(e_o/d, h_b/d) = A(h_b/d) + B(h_b/d)(e_o/d) + C(h_b/d)(e_o/d)^2 + D(h_b/d)(e_o/d)^3 \quad (\text{A.1})$$

in which  $A(h_b/d)$ ,  $B(h_b/d)$ ,  $C(h_b/d)$ ,  $D(h_b/d)$  are cubic polynomial functions of  $(h_b/d)$ . Using the results in Table 4.1 (Section 4.2.2), the values of the functions  $A(h_b/d)$ ,  $B(h_b/d)$ ,  $C(h_b/d)$  and  $D(h_b/d)$ , can be found for each value of  $(h_b/d)$  by a least-squares approximation (Table A.1). For the calculation, it can be assumed that the value of the function  $\alpha_1(e_o/d, h_b/d)$  is 1.000 for  $(h_b/d) = 0.050$  (one-half a mortar joint aspect ratio).

$(h_b/d)$	$A(h_b/d)$	$B(h_b/d)$	$C(h_b/d)$	$D(h_b/d)$
0.000	1.00	0	0	0
0.050	1.00	0	0	0
0.691	0.521	5.93	-24.0	33.6
1.447	0.406	7.75	-35.6	62.4
2.00	0.311	9.47	-46.4	85.7

Table A.1: Coefficients for Function  $\alpha_1(e_o/d, h_b/d)$

Assume also that there exists a function  $\alpha_2(e_o/d, h_b/d)$  such that —

$$\alpha_2(e_o/d, h_b/d) = E(e_o/d) + F(e_o/d)(h_b/d) + G(e_o/d)(h_b/d)^2 + H(e_o/d)(h_b/d)^3 \quad (\text{A.2})$$

in which  $E(e_o/d)$ ,  $F(e_o/d)$ ,  $G(e_o/d)$ ,  $H(e_o/d)$  are cubic polynomial functions of  $(e_o/d)$ . The values of these functions for each value of  $(e_o/d)$ , using the results in Table 4.1, are summarized in Table A.2.

$(e_o/d)$	$E(e_o/d)$	$F(e_o/d)$	$G(e_o/d)$	$H(e_o/d)$
0.167	1.000	0	0	0
0.208	1.000	0.0201	0.00837	-0.00466
0.250	1.000	-0.00582	0.0974	-0.0319
0.292	1.001	-0.0696	0.242	-0.0716
0.333	1.003	-0.134	0.428	-0.122
0.375	1.003	-0.172	0.676	-0.188

Table A.2: Coefficients for Function  $\alpha_2(e_o/d, h_b/d)$

Functions  $A(h_b/d)$ ,  $B(h_b/d)$ ,  $C(h_b/d)$ ,  $D(h_b/d)$  can be expressed as cubic polynomials in  $(h_b/d)$  by using the values of the functions, summarized in Table A.1, in a least-squares approximation (the five values for each of  $A(h_b/d)$ ,  $B(h_b/d)$ ,  $C(h_b/d)$  and  $D(h_b/d)$  are sufficient for a least-squares approximation). The four functions may be written as —

$$\begin{Bmatrix} A(h_b/d) \\ B(h_b/d) \\ C(h_b/d) \\ D(h_b/d) \end{Bmatrix} = \begin{bmatrix} 1.03 & -1.18 & 0.799 & -0.193 \\ -0.324 & 14.4 & -9.51 & 2.38 \\ 1.22 & -54.0 & 31.6 & -8.23 \\ -1.39 & 60.8 & -18.8 & 5.11 \end{bmatrix} \begin{Bmatrix} 1 \\ (h_b/d) \\ (h_b/d)^2 \\ (h_b/d)^3 \end{Bmatrix} \quad (\text{A.3})$$

Similarly, the functions  $E(e_o/d)$ ,  $F(e_o/d)$ ,  $G(e_o/d)$ ,  $H(e_o/d)$  can be expressed as cubic polynomials in  $(e_o/d)$ , so that —

$$\begin{Bmatrix} E(e_o/d) \\ F(e_o/d) \\ G(e_o/d) \\ H(e_o/d) \end{Bmatrix} = \begin{bmatrix} 1.03 & -0.328 & 1.23 & -1.40 \\ -1.19 & 14.5 & -54.3 & 61.2 \\ 0.789 & -9.43 & 31.1 & -18.2 \\ -0.181 & 2.26 & -7.74 & 4.48 \end{bmatrix} \begin{Bmatrix} 1 \\ (e_o/d) \\ (e_o/d)^2 \\ (e_o/d)^3 \end{Bmatrix} \quad (\text{A.4})$$

Equation (A.2) can be written as -

$$\alpha_1(e_o/d, h_b/d) = [1(e_o/d)(e_o/d)^2(e_o/d)^3] [S] \begin{Bmatrix} 1 \\ (h_b/d) \\ (h_b/d)^2 \\ (h_b/d)^3 \end{Bmatrix} \quad (\text{A.5})$$

in which [S] is the 4x4 matrix in equation (A.3).

Similarly, equation (A.2) can be written as -

$$\alpha_2(e_o/d, h_b/d) = [1(h_b/d)(h_b/d)^2(h_b/d)^3] [T] \begin{Bmatrix} 1 \\ (e_o/d) \\ (e_o/d)^2 \\ (e_o/d)^3 \end{Bmatrix} \quad (\text{A.6})$$

in which [T] is the 4x4 matrix in equation (A.4).

If the fitted functions  $\alpha_1(e_o/d, h_b/d)$  and  $\alpha_2(e_o/d, h_b/d)$  fit the data in Table 4.1 exactly, the right-hand side of equation (A.5) will be the transposed form of the right-hand side of equation (A.6).

That is,

$$[S] = [T]^T \quad (\text{A.7})$$

in which  $[T]^T$  is the transposed matrix of [T].

Inspection of equations (A.3) and (A.4) shows that equation (A.7) is not satisfied because the functions  $\alpha_1(e_o/d, h_b/d)$  and  $\alpha_2(e_o/d, h_b/d)$  are calculated by a least-squares approximation to the data on the assumption that both functions are cubic polynomials in  $(e_o/d)$  and  $(h_b/d)$ .

As an approximation, it may be assumed that a 4x4 matrix for equations (A.3) and (4.2) may be calculated as follows —

$$[R] = \frac{1}{2} \{ [S] + [T]^T \} \quad (A.8)$$

That is,

$$[R] = \begin{bmatrix} 1.03 & -1.18 & 0.794 & -0.187 \\ -0.326 & 14.4 & -9.47 & 2.32 \\ 1.22 & -54.1 & 31.3 & -7.98 \\ -1.39 & 61.0 & -18.5 & 4.79 \end{bmatrix} \quad (A.9)$$

A scale model representing the function  $\alpha(e_o/d, h_b/d)$  is shown in figure A.1.

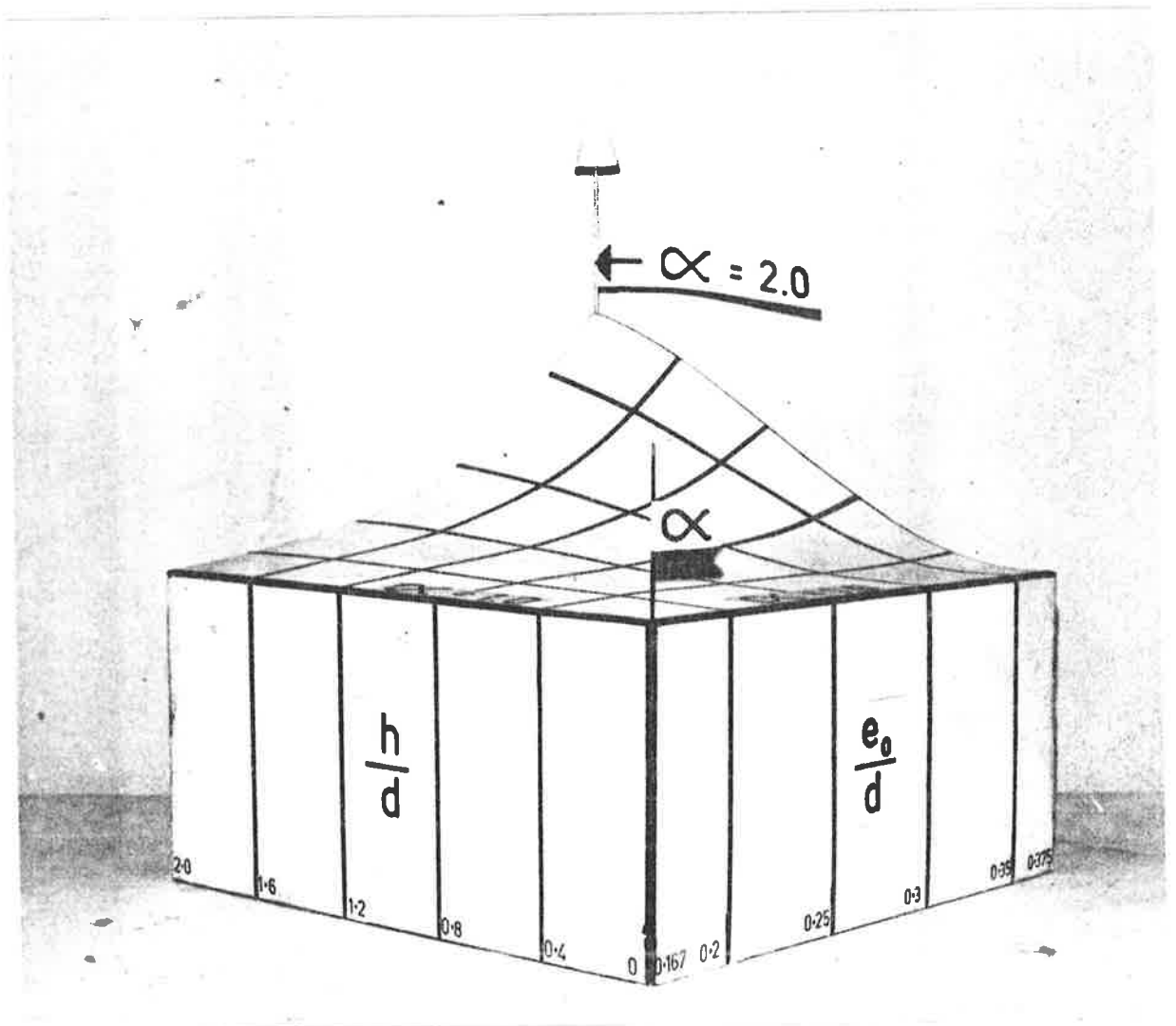


Figure A.1: Scale Model of Function,  $\alpha (e_o/d, h_b/d)$

APPENDIX B  
AN IDEALIZED NON-LINEAR MORTAR SUBJECT TO  
ECCENTRIC COMPRESSION

**B.1 A STRESS-STRAIN RELATIONSHIP FOR NON-LINEAR MORTAR**

Assume that the stress-strain relationship for a non-linear mortar is —

$$\sigma = E_m (\epsilon - K\epsilon^n) \quad (B.1)$$

in which  $E_m$  is the initial tangent modulus

$\sigma$  is normal stress parallel to the applied load

$\epsilon$  is strain parallel to the applied load

$K$  and  $n$  are constants.

Assume that  $\sigma_c$  is the maximum normal stress attained by the mortar at strain  $\epsilon_c$  (figure B.1).

Parameters  $\epsilon_c$  and  $K$  in equation (B.1) may be calculated as follows. At the maximum stress  $\sigma_c$ ,  $\frac{d\sigma}{d\epsilon} = 0$ , so that, from equation (B.1),

$$E_m (1 - nK\epsilon_c^{n-1}) = 0$$

That is,

$$K = \frac{1}{n\epsilon_c^{n-1}} \quad (B.2)$$

This value of  $K$  can be substituted into equation (B.1) at the point  $\sigma = \sigma_c$  and  $\epsilon = \epsilon_c$  to give —

$$\epsilon_c = E_m \left( \epsilon_c - \frac{\epsilon_c}{n} \right)$$

so that —

$$\epsilon_c = \frac{n\sigma_c}{E_m(n-1)} \quad (B.3)$$

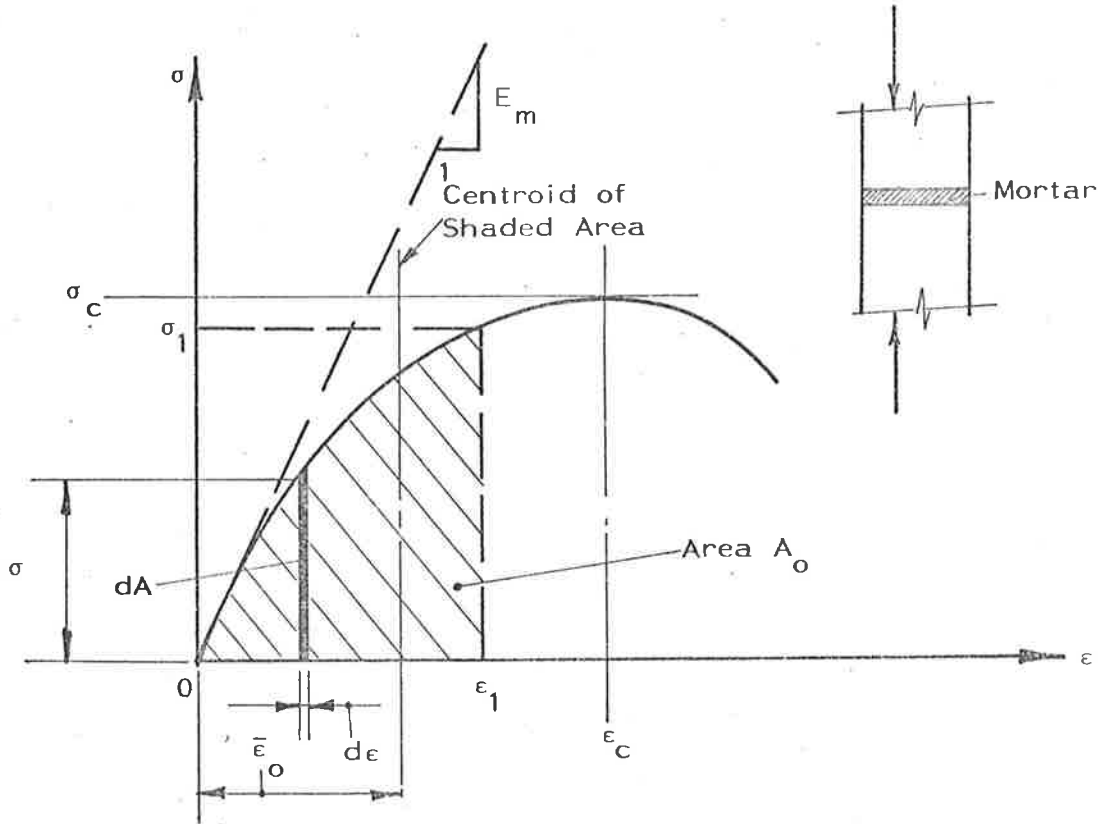


Figure B.1: Stress-strain Relationship for Non-linear Mortar (Bedjoint Cracked)

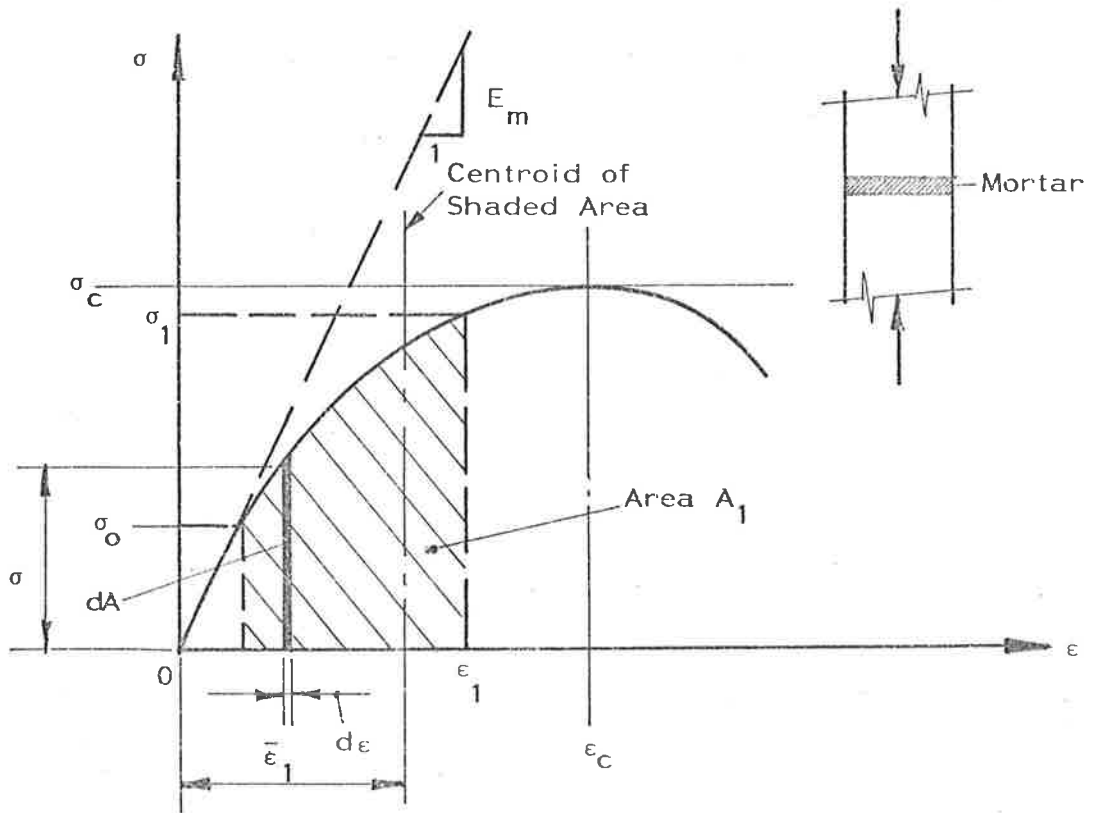


Figure B.2: Stress-strain Relationship for Non-linear Mortar (Bedjoint Uncracked)

By choosing values of  $\sigma_c$  and  $n(n>1)$ , the parameters  $\epsilon_c$  and  $K$  may be calculated from equations (B.2) and (B.3).

## B.2 GEOMETRIC PROPERTIES OF STRESS-STRAIN CURVE

The shaded area under the curve in figure B.1 is -

$$\begin{aligned}
 A_o &= \int dA \\
 &\approx \int_0^{\epsilon_1} \sigma d\epsilon \\
 &= \int_0^{\epsilon_1} E_m (\epsilon - K\epsilon^n) d\epsilon \\
 \therefore A_o &= E_m \left( \frac{\epsilon_1^2}{2} - \frac{K}{(n+1)} \cdot \epsilon_1^{n+1} \right) \quad (B.4(a))
 \end{aligned}$$

The first moment of area of the shaded portion under the curve in figure B.1 about the axis origin, 0, is -

$$\begin{aligned}
 (FMA)_o &= \int \epsilon dA \\
 &\approx \int_0^{\epsilon_1} \epsilon \sigma d\epsilon \\
 &= \int_0^{\epsilon_1} E_m (\epsilon^2 - K\epsilon^{n+1}) d\epsilon \\
 \therefore (FMA)_o &= E_m \left( \frac{\epsilon_1^3}{3} - \frac{K}{(n+2)} \cdot \epsilon_1^{n+2} \right) \quad (B.4(b))
 \end{aligned}$$

From equations (B.4(a)) and (B.4(b)), the distance to the centroid of the shaded portion under the curve from the axis origin, 0, is -

$$\bar{\epsilon}_o = \frac{(FMA)_o}{A_o} = \frac{E_m \left( \frac{\epsilon_1^3}{3} - \frac{K}{(n+2)} \cdot \epsilon_1^{n+2} \right)}{E_m \left( \frac{\epsilon_1^2}{2} - \frac{K}{(n+1)} \cdot \epsilon_1^{n+1} \right)}$$

$$\therefore \bar{\epsilon}_0 = \frac{\frac{2}{3} \epsilon_1 - \frac{2K}{(n+2)} \epsilon_1^n}{1 - \frac{2K}{(n+1)} \epsilon_1^{n-1}} \quad (\text{B.5})$$


---

Assume that the shaded area under the stress-strain curve does not include the origin, 0, but lies in the strain range  $[\epsilon_0, \epsilon_1]$  (figure B.2). The area of the shaded portion under the curve in figure B.2 is —

$$\begin{aligned} A_1 &= \int dA \\ &\approx \int_{\epsilon_0}^{\epsilon_1} \sigma d\epsilon \\ &= \int_{\epsilon_0}^{\epsilon_1} E_m (\epsilon - K\epsilon^n) d\epsilon \end{aligned}$$

$$\therefore A_1 = E_m \left\{ \frac{1}{2} (\epsilon_1^2 - \epsilon_0^2) - \frac{K}{(n+1)} (\epsilon_1^{n+1} - \epsilon_0^{n+1}) \right\} \quad (\text{B.6(a)})$$


---

The first moment of area of the shaded portion under the curve in figure B.2 about the axis origin, 0, is —

$$\begin{aligned} (\text{FMA})_1 &= \int \epsilon dA \\ &\approx \int_{\epsilon_0}^{\epsilon_1} \epsilon \sigma d\epsilon \\ &= \int_{\epsilon_0}^{\epsilon_1} E_m (\epsilon^2 - K\epsilon^{n+1}) d\epsilon \end{aligned}$$

$$\therefore (\text{FMA})_1 = E_m \left\{ \frac{1}{3} (\epsilon_1^3 - \epsilon_0^3) - \frac{K}{(n+2)} (\epsilon_1^{n+2} - \epsilon_0^{n+2}) \right\} \quad (\text{B.6(b)})$$


---

From equations (B.6(a)) and (B.6(b)), the distance to the centroid of the shaded portion under the curve in figure B.2 from the axis origin, 0, is —



$$\bar{\epsilon}_1 = \frac{E_m \cdot \left\{ \frac{1}{3} \cdot (\epsilon_1^3 - \epsilon_0^3) - \frac{K}{(n+2)} \cdot (\epsilon_1^{n+2} - \epsilon_0^{n+2}) \right\}}{E_m \cdot \left\{ \frac{1}{2} \cdot (\epsilon_1^2 - \epsilon_0^2) - \frac{K}{(n+1)} \cdot (\epsilon_1^{n+1} - \epsilon_0^{n+1}) \right\}}$$

$$\bar{\epsilon}_1 = \frac{\frac{2}{3} \cdot (\epsilon_1^3 - \epsilon_0^3) - \frac{2K}{(n+2)} \cdot (\epsilon_1^{n+2} - \epsilon_0^{n+2})}{(\epsilon_1^2 - \epsilon_0^2) - \frac{2K}{(n+1)} \cdot (\epsilon_1^{n+1} - \epsilon_0^{n+1})} \quad (B.7)$$

### B.3 LOAD-CURVATURE RELATIONSHIPS

#### B.3.1 Partially Cracked Section

Assume that the stress and strain distributions on a partially cracked mortar bedjoint at each brick-mortar interface are as shown in figure B.3.

The total load per unit length,  $P$ , from geometry (figures B.1 and B.3) and equation (B.4(a)) is -

$$P = E_m \cdot \left( \frac{\epsilon_1^2}{2} - \frac{K}{(n+1)} \cdot \epsilon_1^{n+1} \right) \cdot \frac{d_c}{\epsilon_1} \quad (B.8)$$

Also from geometry (figures B.1 and B.3) and equation (B.5),

$$d_p = (\epsilon_1 - \bar{\epsilon}_0) \cdot \frac{d_c}{\epsilon_1} \quad (B.9)$$

For equation (B.9),  $d_p$  can be calculated from static equilibrium as -

$$d_p = \left( \frac{\text{Moment about the Compression Edge}}{\text{Total Load per unit Length}} \right) \quad (B.10)$$

The curvature of the uncracked part of the mortar is

$$\left( \frac{1}{R} \right)' = \frac{\epsilon_1}{d_c} \quad (B.11)$$

Equations (B.8), (B.9) and (B.10) can be used to calculate  $\epsilon_1$  and  $d_c$  which are required in equation (B.11) for the calculation of the non-linear mortar curvature.

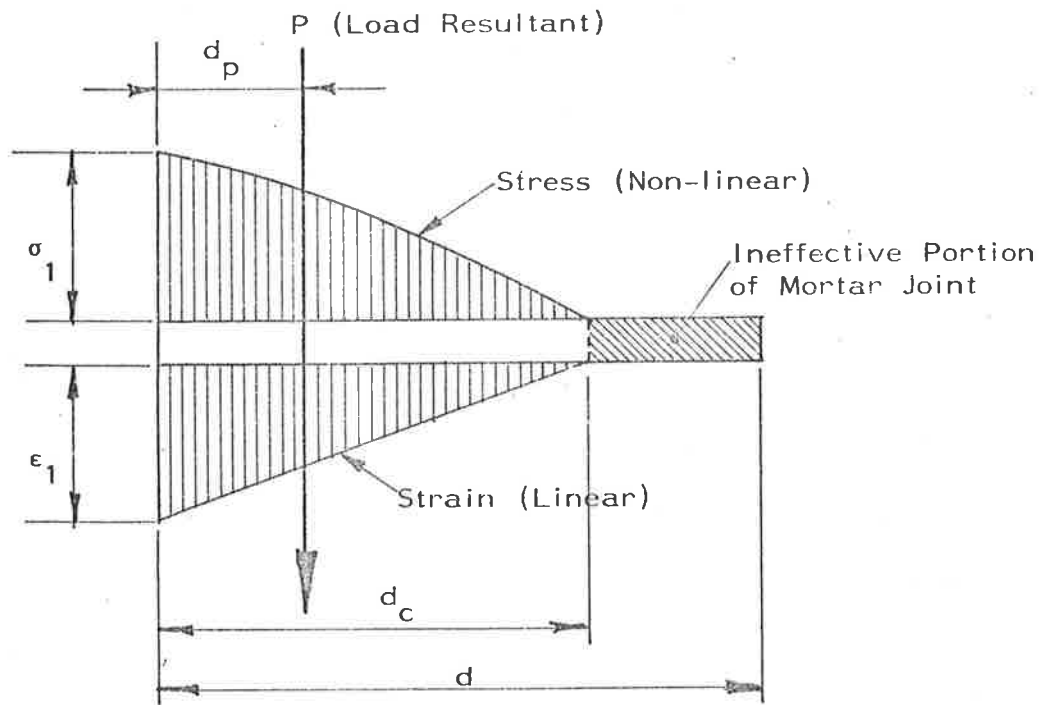


Figure B.3: Partially Cracked Mortar Joint  
(Non-linear Mortar)

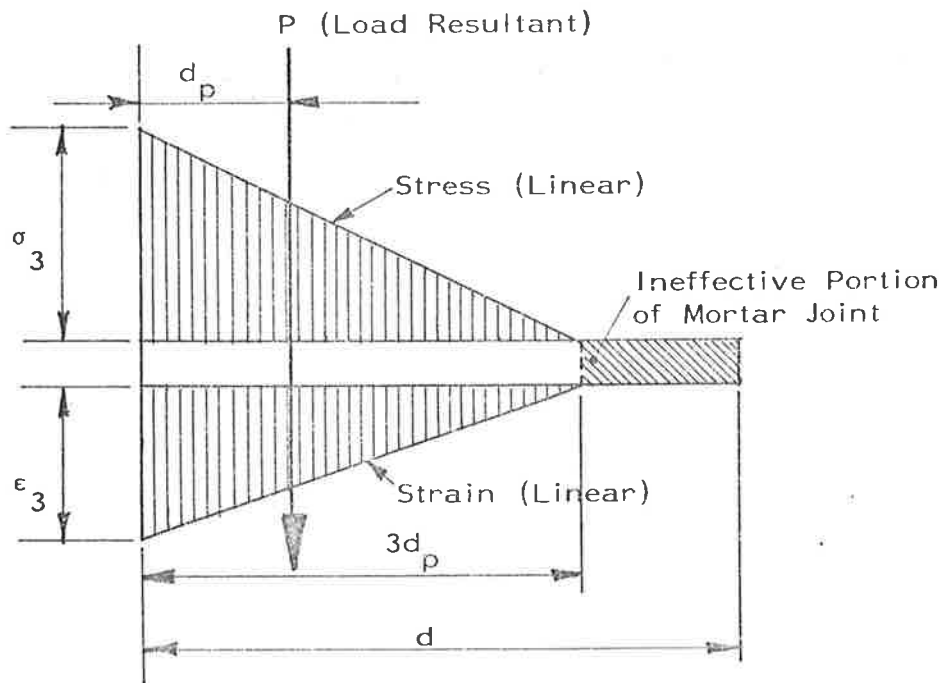


Figure B.4: Partially Cracked Mortar Joint  
(Linear Mortar)

### B.3.1 Solution Procedure

The parameters  $\epsilon_1$  and  $d_c$  may be calculated by using a Newton-Raphson technique. Arbitrary approximately-correct values for  $\epsilon_1$  and  $d_c$  may be chosen and used in equation (B.8), rewritten as follows.

$$T = P - E_m \left( \frac{\epsilon_1^2}{2} - \frac{A}{(n+1)} \cdot \epsilon_1^{n+1} \right) \cdot \frac{d_c}{\epsilon_1} \quad (\text{B.12})$$

in which  $T$  is an error term caused by approximations  $\epsilon_1$  and  $d_c$ . Similarly, equation (B.9) may be rewritten as –

$$V = d_p - (\epsilon_1 - \bar{\epsilon}_0) \cdot \frac{d_c}{\epsilon_1} \quad (\text{B.13})$$

in which  $V'$  is an error term caused by approximations  $\epsilon_1$  and  $d_c$ . If the values of  $T$  and  $V$  in equations (B.12) and (B.13) exceed prescribed limitations because of incorrect values of  $\epsilon_1$  and  $d_c$ , a series of Newton-Raphson corrections can be applied successively until the desired accuracy is reached.

For a function of a single variable  $y = f(x)$ , an approximate solution,  $x_1$ , of the equation  $f(x) = 0$ , giving  $y_1 - f(x_1) = \Delta y_1$ , is generally improved by calculating –

$$x_2 = x_1 - \frac{\Delta x_1}{f'(x_1)} \quad (\text{B.14})$$

The corresponding Newton-Raphson correction for the simultaneous equations (B.12) and (B.13), for the  $i^{\text{th}}$  iteration, can be calculated from –

$$\begin{Bmatrix} \Delta \epsilon_1 \\ \Delta d_c \end{Bmatrix} = -[J]_i^{-1} \begin{Bmatrix} T \\ V \end{Bmatrix}_i \quad (\text{B.15})$$

so that –

$$\begin{Bmatrix} \epsilon_1 \\ d_c \end{Bmatrix}_{i+1} = \begin{Bmatrix} \epsilon_1 \\ d_c \end{Bmatrix}_i + \begin{Bmatrix} \Delta \epsilon_1 \\ \Delta d_c \end{Bmatrix}_i \quad (\text{B.16})$$

In equation (B.15),  $[J]$  is the "Jacobian" matrix of the functions  $T(\epsilon_1, d_c)$  and  $V(\epsilon_1, d_c)$ , and is formed from the partial derivatives of the components  $T$  and  $V$  of the error vector  $\begin{Bmatrix} T \\ V \end{Bmatrix}$  with respect to the components of the solution vector  $\begin{Bmatrix} \epsilon_1 \\ d_c \end{Bmatrix}$ .

That is,

$$[J] = \begin{bmatrix} \frac{\partial T}{\partial \epsilon_1} & \frac{\partial T}{\partial d_c} \\ \frac{\partial V}{\partial \epsilon_1} & \frac{\partial V}{\partial d_c} \end{bmatrix} \quad (B.17)$$

The elements of the "Jacobian" matrix can be calculated numerically by incrementing successively the components of the solution vector  $\begin{Bmatrix} \epsilon_1 \\ d_c \end{Bmatrix}$  by approximately 0.01 percent and calculating the resulting increments of the error vector  $\begin{Bmatrix} T \\ V \end{Bmatrix}$  as follows.

$$[J] \approx \begin{bmatrix} \frac{\Delta T}{\Delta \epsilon_1} & \frac{\Delta T}{\Delta d_c} \\ \frac{\Delta V}{\Delta \epsilon_1} & \frac{\Delta V}{\Delta d_c} \end{bmatrix} \quad (B.18)$$

After several iterations, the error vector  $\begin{Bmatrix} T \\ V \end{Bmatrix}$  can be reduced to within prescribed limits to give the solution vector  $\begin{Bmatrix} \epsilon_1 \\ d_c \end{Bmatrix}$ . Generally, closure to acceptable levels has been attained within ten iteration cycles.

### B.3.2 Relationships between Curvatures for Non-linear and Linear Mortars

#### B.3.2.1 Cracked Section

##### (i) Load Resultant Outside Kern

If the resultant of the distributed load are outside the kern, the stress and strain distributions for the non-linear and linear mortars

as shown in figures B.3 and B.4 respectively. It has been shown that the curvature of the non-linear mortar given by equation (B.1) is—

$$\left(\frac{1}{R}\right)' = \frac{\epsilon_1}{d_c} \quad (\text{B.11})$$

in which  $\epsilon_1$  and  $d_c$  are calculated iteratively as described above.

Assume that  $d_p$ ,  $P$  and  $E_m$  are identical for both the non-linear mortar and the linear mortar shown in figures (B.3) and (B.4) respectively. The curvature of the linear mortar (figure B.4) is —

$$\left(\frac{1}{R}\right)_m = \frac{\epsilon_3}{3d_p} \quad (\text{B.19})$$

The load resultant in figure B.4 is —

$$P = \frac{1}{2} \cdot \sigma_3 \cdot 3d_p$$

in which  $\sigma_3 = E_m \cdot \epsilon_3$

$$\therefore \left(\frac{1}{R}\right)_m = \frac{2P}{9E_m d_p^2} \quad (\text{B.20})$$

The ratio of the two curvatures  $\left(\frac{1}{R}\right)'$  and  $\left(\frac{1}{R}\right)_m$  is (equations (B.11), (B.20)) —

$$\rho = \frac{\left(\frac{1}{R}\right)'}{\left(\frac{1}{R}\right)_m} = \frac{9}{2} \cdot \frac{\epsilon_1}{d_c} \cdot \frac{d_p^2}{P} \cdot E_m \quad (\text{B.21})$$

## (ii) Load Resultant Inside Kern

It should be noted that for a non-linear mortar defined by equation (B.1), the section can be partially cracked for cases in which the load resultant is inside the kern. However, a linear mortar is uncracked for this case and the stress and strain distributions for the non-linear and linear mortars are as shown in figures B.3 and B.5 respectively.

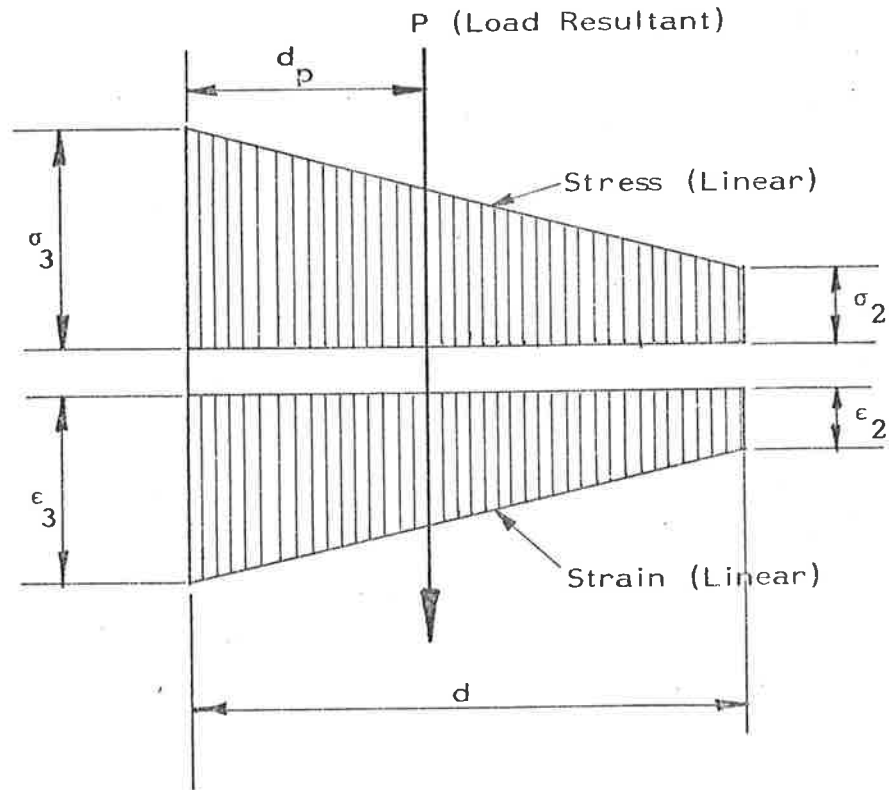


Figure B.5: Uncracked Mortar Joint (Linear Mortar)

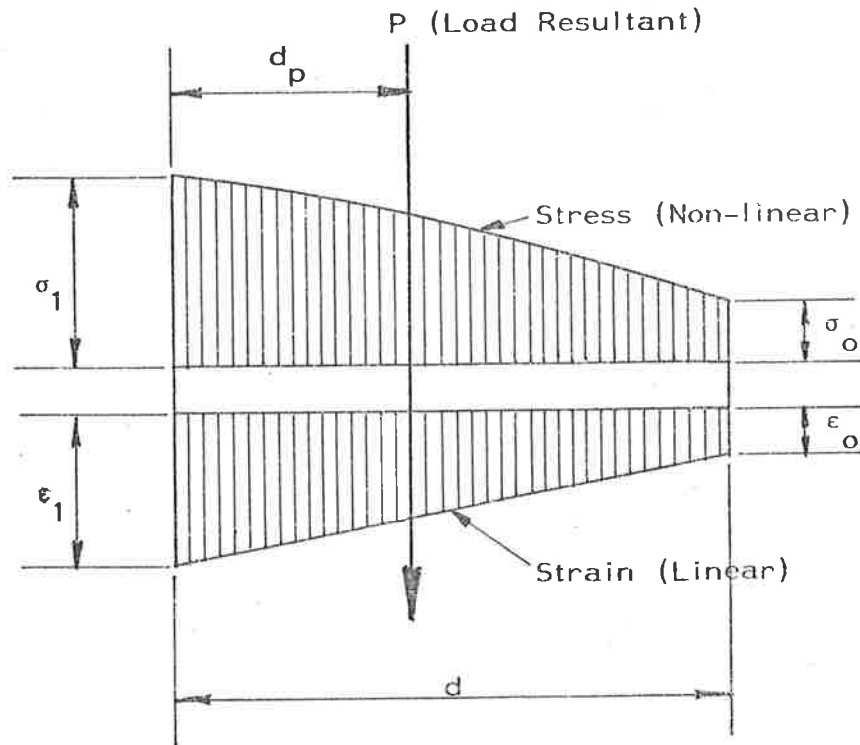


Figure B.6: Uncracked Mortar Joint (Non-linear Mortar)

The curvature of the non-linear mortar is —

$$\left(\frac{1}{R}\right)' = \frac{\epsilon_1}{d_c} \quad (\text{B.11})$$

Assume that  $d_p$ ,  $P$  and  $E_m$  are identical for both the non-linear mortar and the linear mortar shown in figures B.3 and B.5 respectively. The curvature of the linear mortar (figure B.5) is —

$$\left(\frac{1}{R}\right)_m = \frac{(\epsilon_3 - \epsilon_2)}{d} \quad (\text{B.22})$$

$$\text{But } \epsilon_3 = \frac{1}{E_m} \cdot \frac{P}{d} \cdot \left\{ 1 + \frac{6}{d} \left( \frac{d}{2} - d_p \right) \right\}$$

$$\text{and } \epsilon_2 = \frac{1}{E_m} \cdot \frac{P}{d} \cdot \left\{ 1 - \frac{6}{d} \left( \frac{d}{2} - d_p \right) \right\}$$

$$\therefore \epsilon_3 - \epsilon_2 = \frac{1}{E_m} \cdot \frac{P}{d} \cdot \left\{ \frac{12}{d} \left( \frac{d}{2} - d_p \right) \right\}$$

Equation (B.22) becomes —

$$\left(\frac{1}{R}\right)_m = \frac{\epsilon_3 - \epsilon_2}{d} = \frac{1}{E_m} \cdot \frac{12P}{d^3} \left( \frac{d}{2} - d_p \right) \quad (\text{B.23})$$

Hence, the ratio of the two curvatures  $\left(\frac{1}{R}\right)'$  and  $\left(\frac{1}{R}\right)_m$  is (equations (B.11), (B.23))—

$$p = \frac{\left(\frac{1}{R}\right)'}{\left(\frac{1}{R}\right)_m} = \frac{\epsilon_1}{d_c} \cdot \frac{d^3}{12P} \cdot \left( \frac{d}{2} - d_p \right)^{-1} \cdot E_m \quad (\text{B.24})$$

In general, in equation (B.24)  $p \gg 1$ .

### B.3.2.2 Uncracked section

Assume that a bedjoint of a non-linear mortar, defined by equation (B.1), is uncracked and that the stress distribution is as shown in figure B.6.

The total load per unit length, P, from geometry (figures B.2 and B.6) and equation (B.6(a)) is -

$$P = E_m \left\{ \frac{1}{2} (\epsilon_1^2 - \epsilon_0^2) - \frac{K}{(n+1)} \cdot (\epsilon_1^{n+1} - \epsilon_0^{n+1}) \right\} \cdot \frac{d}{(\epsilon_1 - \epsilon_0)} \quad (\text{B.25})$$

Also, from geometry (figures B.2 and B.6) and Equation (B.7),

$$d_p = (\epsilon_1 - \bar{\epsilon}_1) \cdot \frac{d}{(\epsilon_1 - \epsilon_0)} \quad (\text{B.26})$$

For equation (B.26),  $d_p$  can be calculated from static equilibrium as -

$$d_p = \left( \frac{\text{Moment about the Compression Edge}}{\text{Total Load}} \right) \quad (\text{B.10})$$

The curvature of the mortar bedjoint is -

$$\left( \frac{1}{R} \right)' = \frac{(\epsilon_1 - \epsilon_0)}{d} \quad (\text{B.27})$$

Equations (B.10), (B.25) and (B.26) can be used to calculate  $\epsilon_1$  and  $\epsilon_0$  which are required in equation (B.27) for the non-linear mortar curvature.

The parameters  $\epsilon_1$  and  $\epsilon_0$  may be calculated by using a Newton-Raphson technique similar to that described in Section B.3.1. Equation (B.25) can be rewritten as -

$$Q = P - E_m \left\{ \frac{1}{2} (\epsilon_1^2 - \epsilon_0^2) - \frac{K}{(n+1)} \cdot (\epsilon_1^{n+1} - \epsilon_0^{n+1}) \right\} \cdot \frac{d}{(\epsilon_1 - \epsilon_0)} \quad (\text{B.28})$$

Equation (B.26) can be rewritten as -

$$S = d_p - (\epsilon_1 - \bar{\epsilon}_1) \cdot \frac{d}{(\epsilon_1 - \epsilon_0)} \quad (\text{B.29})$$



In equations (B.28) and (B.29), Q and S are error terms caused by approximations to  $\epsilon_0$  and  $\epsilon_1$ . As described in Section B.3.1, solutions to  $\epsilon_0$  and  $\epsilon_1$  can be found as successive approximations by calculating a "Jacobian" matrix [J] such that -

$$[J] = \begin{bmatrix} \frac{\partial Q}{\partial \epsilon_0} & \frac{\partial Q}{\partial \epsilon_1} \\ \frac{\partial S}{\partial \epsilon_0} & \frac{\partial S}{\partial \epsilon_1} \end{bmatrix} \approx \begin{vmatrix} \frac{\Delta Q}{\Delta \epsilon_0} & \frac{\Delta Q}{\Delta \epsilon_1} \\ \frac{\Delta S}{\Delta \epsilon_0} & \frac{\Delta S}{\Delta \epsilon_1} \end{vmatrix} \quad (B.30)$$

The solution vector  $\begin{Bmatrix} \epsilon_0 \\ \epsilon_1 \end{Bmatrix}$  can be found by successive increment vectors  $\begin{Bmatrix} \Delta \epsilon_0 \\ \Delta \epsilon_1 \end{Bmatrix}$  which satisfy the relationship at the  $i^{\text{th}}$  step -

$$\begin{Bmatrix} \Delta \epsilon_0 \\ \Delta \epsilon_1 \end{Bmatrix}_i = - [J]_i^{-1} \begin{Bmatrix} Q \\ S \end{Bmatrix}_i \quad (B.31)$$

so that

$$\begin{Bmatrix} \epsilon_0 \\ \epsilon_1 \end{Bmatrix}_{i+1} = \begin{Bmatrix} \epsilon_0 \\ \epsilon_1 \end{Bmatrix}_i + \begin{Bmatrix} \Delta \epsilon_0 \\ \Delta \epsilon_1 \end{Bmatrix}_i \quad (B.32)$$

It has been found that, generally, the solution vector is obtained to an acceptable accuracy within ten iteration cycles.

If there is no cracking on the bedjoints, the stress and strain distributions for the non-linear mortar defined by equation (B.1) are as shown in figure B.6. The stress distribution for a linear mortar is shown in figure B.5. The curvature of the non-linear mortar is -

$$\left(\frac{1}{R}\right)' = \frac{(\epsilon_1 - \epsilon_0)}{d} \quad (B.27)$$

in which  $\epsilon_0$  and  $\epsilon_1$  are calculated by iteration as described above.

Assume that  $d_p$ , P and  $E_m$  are identical for both the non-linear mortar and the linear mortar shown in figures B.6 and B.5 respectively. The curvature of the linear mortar (figure B.5) is -

$$\left(\frac{1}{R}\right)_m = \frac{(\epsilon_3 - \epsilon_2)}{d} \quad (\text{B.22})$$

As shown in Section B.31,

$$\left(\frac{1}{R}\right)_m = \frac{1}{E_m} \cdot \frac{12P}{d^3} \cdot \left(\frac{d}{2} - d_p\right) \quad (\text{B.23})$$

Hence, the ratio of the two curvatures  $\left(\frac{1}{R}\right)'$  and  $\left(\frac{1}{R}\right)_m$  is (equations B(27), (B.23)) -

$$\rho = \frac{\left(\frac{1}{R}\right)'}{\left(\frac{1}{R}\right)_m} = \frac{d^2}{12P} \cdot (\epsilon_1 - \epsilon_0) \cdot \left(\frac{d}{2} - d_p\right)^{-1} \cdot E_m \quad (\text{B.33})$$

In general, in equation (B.33)  $\rho \gg 1$ .

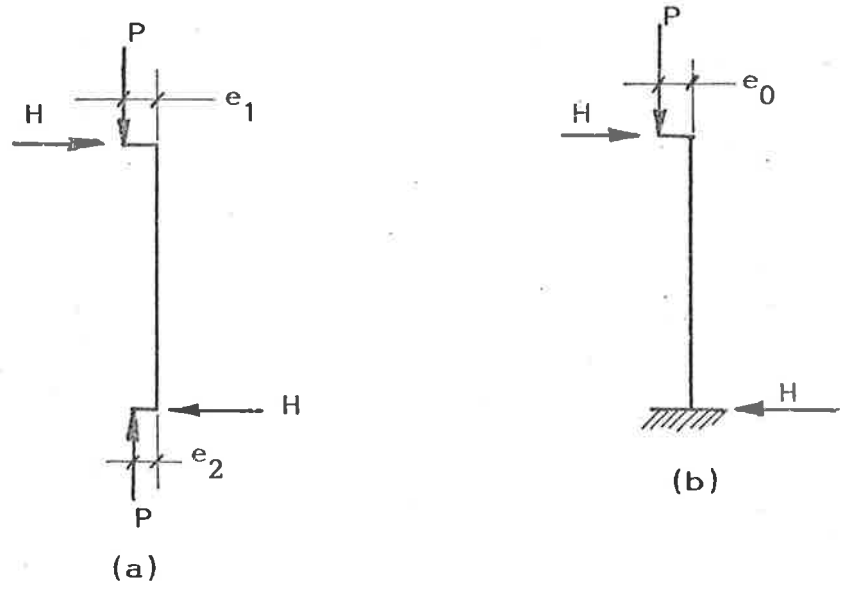
APPENDIX CBRICKWORK WALLS IN ONE-WAY BENDING -- PROGRAM PIER1

## C.1 THE SCOPE OF PROGRAM PIER1

PROGRAM PIER1 was a finite difference method of solution to calculate the behaviour of brickwork walls in one-way bending in which discrete cracking may occur at the brick-mortar interfaces. The types of problems which may be solved by PROGRAM PIER1 are as follows.

- (a) A pin-end wall subjected to an eccentric vertical load with either equal or unequal eccentricities top and bottom (figure C.1(a)). The eccentricities  $e_1$  and  $e_2$  are chosen and the load is incremented to calculate the column failure load.
- (b) A wall with a perfectly fixed base and a "pin-roller" top support (figure 4.14) loaded eccentrically at the top (figure C.1(b)). The load eccentricity,  $e_0$ , is chosen and the load is incremented to calculate column failure.
- (c) A pin-end wall subjected to equally-eccentric vertical load, both top and bottom (figure C.1(c)). The load,  $P_f$  per unit length, is chosen and the eccentricity is incremented to calculate the column failure eccentricity.
- (d) A wall with a perfectly fixed base and a "pin-roller" top support (figures 4.14, C.1(d)). The load,  $P_f$  per unit length, is chosen and the eccentricity is incremented to calculate the column failure eccentricity.

For all of the cases above, the brick stress-strain characteristic is linear. The mortar-strain relationship may be either linear or non-linear as <sup>(106)</sup> —



(For  $e_1=e_2$ ,  $H=0$ )

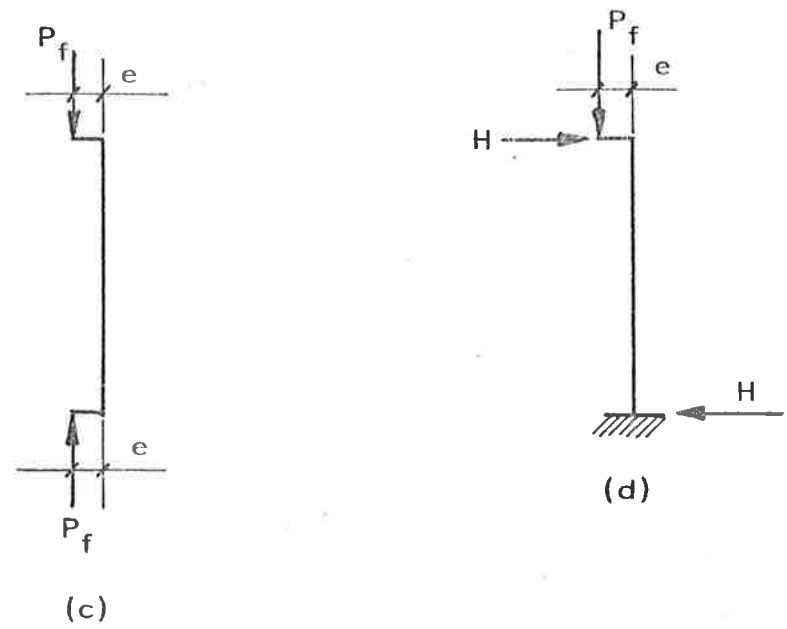


Figure C.1: Cases which may be Solved by using PROGRAM PIER1 (refer to text)

$$\sigma = E_m (\epsilon - K \epsilon^n) \quad (B.1)$$

in which  $E_m$  is the initial tangent modulus

$K, n$  are constants (Appendix B)

For all cases, the horizontal reactions,  $H$  per unit length, may be calculated by the solution method described in Section 4.3.

In real brickwork, poor bricklaying methods may produce walls which are not straight vertically. Effects of this type of poor workmanship may be calculated by PROGRAM PIER1 by specifying initial deviations from vertical straightness at each finite difference node (figures 4.13, 4.15).

Details of input data for PROGRAM PIER1 are given in the following section.





```

C      READ(5,4) IPEO,ITYPE
      4 FORMAT(2I1)
      IF(ITYPE.EQ.1) WRITE(6,900)
      IF(ITYPE.NE.1) WRITE(6,899)
899  FORMAT(1H1,15X,*----- LINEAR MORTAR PROBLEM -----*,///)
900  FORMAT(1H1,15X,*----- NON-LINEAR MORTAR PROBLEM -----*,///)
C      READ BASE SUPPORT CONDITION FLAG,"IS"
      READ (5,58) IS
      58 FORMAT(I1)
      IF(IS.EQ.1) WRITE(6,115)
      IF(IS.NE.1) WRITE(6,116)
      115 FORMAT(1H0,15X,*COLUMN BASE IS PINNED*//)
      116 FORMAT(1H0,15X,*COLUMN BASE IS FIXED*//)
      IF(IPEO.EQ.1) GO TO 10
C      IPEO EQ 1 IMPLIES ECCENTRICITY IS SPECIFIED
C      IPEO NE 1 IMPLIES LOAD IS SPECIFIED
C      READ FOR ECCENTRICITY INCREMENTS
      READ(5,5) E, D,WL,N,P
      5 FORMAT(F6.0,F6.2,F8.2,I5,F6.1)
      WRITE(6,3) E,D,WL,N
      3 FORMAT(1H0,15X,*---THIS PROGRAM INCREMENTS THE LOAD ECCENTRICITY E
      *0---*//
      *6X,*YOUNGS MODULUS OF BRICK IS *,F6.0,* MPA*//
      *6X,*THICKNESS OF WALL IS *,F6.2,* MM*//
      *6X,*HEIGHT OF WALL IS *,F8.2,* MM*//
      *6X,*NUMBER OF WALL SEGMENTS IS *,I5//)
      WRITE(6,13) P
      13 FORMAT(6X,*LOAD VALUE IS *,F6.1//)
      GO TO 11
      10 CONTINUE
C      READ FOR LOAD INCREMENTS
      READ(5,2) E,D,WL,N,TEO,BEO
      2 FORMAT(F6.0,F6.2,F8.2,I5,2F10.3)
      WRITE(6,12) E,D,WL,N
      12 FORMAT(1H0,15X,*---THIS PROGRAM INCREMENTS THE LOAD P ---*//
      *6X,*YOUNGS MODULUS OF BRICK IS *,F6.0,* MPA*//
      *6X,*THICKNESS OF WALL IS *,F6.2,* MM*//
      *6X,*HEIGHT OF WALL IS *,F8.2,* MM*//
      *6X,*NUMBER OF WALL SEGMENTS IS *,I5//)
      WRITE(6,6) TEO
      6 FORMAT(6X,*LOAD ECCENTRICITY IS *,F10.3,* MM AT TOP OF COLUMN*)
      IF(IS.EQ.1) WRITE(6,14) BEO
      14 FORMAT(6X,*LOAD ECCENTRICITY IS *,F10.3,* MM AT BASE OF COLUMN*//)
      11 CONTINUE
C      READ BRICKWORK PARAMETERS
      READ(5,8) PHB,PHM,PNB,IXN
      8 FORMAT(F6.2,F6.2,F6.2,I2)
      IF(IXN.EQ.0) IXN=1
      WRITE(6,9) PHB,PHM,PNB,IXN
      9 FORMAT(1H0,5X,*BRICK HEIGHT IS *,F6.2,* MM*//
      *6X,*MORTAR THICKNESS IS *,F6.2,* MM*//
      *6X,*MODULAR RATIO AT ZERO STRESS IS *,F6.2 //
      *6X,*NO. OF BRICKS PER F.D. ELEMENT IS *,I5 //)
C
C      INITIALIZE CONSTANTS AND ARRAYS
C

```



```

H=0.
HH=0.
KL=0
MS=40
NS=40
MO=1
DEAL=0.0001
DO 1 ISK = 1,MS
EO(ISK)=0.
EOP(ISK)=0.
PW(ISK)=0.
W(ISK)=0.
WE(ISK)=0.
QA(ISK)=0.
RA(ISK)=0.
PPL(ISK)=0.
PLAT(ISK)=0.
SLOT(ISK)=0.
PNBM(ISK)=PNB
DC(ISK)=D
EMX(ISK)=0.0001
SEM(X)=0.001
TEM(X)=0.001
SDC(ISK)=D
TDC(ISK)=D
EMN(ISK)=0.
SEMN(ISK)=0.
TEMN(ISK)=0.
RR(ISK)=0.
R(ISK)=0.
DO 7 ITK = 1,MS
RS(ISK,ITK)=0.
PWP(ISK,ITK)=0.
SP(ISK,ITK)=0.
7 CONTINUE
1 CONTINUE
DMAX=D/6
IF(ITYPE.NE.1) GO TO 901
EM=E/PNB
READ(5,131) AE,PT
131 FORMAT(F10.3,F5.2)
WRITE(6,132) EM,AE,PT
132 FORMAT(1H0,5X,*INITIAL MORTAR MODULUS IS *,F6.0,* MPA*/
*6X,*NON-LINEARITY CONSTANTS ARE----*/
*12X,*K = *,F10.3/12X,*N = *,F5.2)
901 CONTINUE
HD=PHB/D
X=(PHB+PHM)*IXN
C CHECK WHETHER TENSION FIELD STIFFENING EFFECT IS
C INCLUDED IN PROBLEM
READ(5,21) ITFS
21 FORMAT(I1)
IF(ITFS.EQ.0) GO TO 22
C ITFS EQ 0 IMPLIES TENSION FIELD STIFFENING IS IN PROGRAM
WRITE(6,23)
23 FORMAT(1H0,5X,*---NO TENSION FIELD STIFFENING IN THIS PROBLEM---*)
GO TO 24

```

```

22 CONTINUE
C   CALCULATE MATRIX A(4X1)=MATRIX R X MATRIX H-TRANSPOSE
    HD1=HD $ HD2=HD*HD $ HD3=HD**3
    A(1)=1.03-1.18*HD1+0.794*HD2-0.187*HD3
    A(2)=-0.326+14.4*HD1-9.47*HD2+2.32*HD3
    A(3)=1.22-54.1*HD1+31.3*HD2-7.98*HD3
    A(4)=-1.39+61.0*HD1-18.5*HD2+4.79*HD3
    WRITE(6,25)
25 FORMAT(1H0,5X,*---TENSION FIELD STIFFENING IS IN THIS PROBLEM---*)
24 CONTINUE
C   CALCULATE EULER BUCKLING LOAD FOR WALL WITH PIN ENDS
    CALL EULER(E,D,WL,PHB,PHM,PNB,PCR)
C   READ INITIAL IMPERFECTIONS AT NODES
    READ(5,59) (EP(IAT),IAT=1,16)
59 FORMAT(16F5.2)
    READ(5,65) (EP(JAT),JAT=17,32)
65 FORMAT(16F5.2)
    READ(5,68) (EP(KAT),KAT=33,40)
68 FORMAT(8F5.2)
    NP=N+1
    WRITE(6,60)
60 FORMAT(1H1,5X,*NODE NO.*,20X,*INITIAL IMPERFECTION (MM)* ///)
    DO 61 IA = 1,NP
    WRITE(6,62) IA,EP(IA)
62 FORMAT(1H0,8X,I2,35X,F5.2)
61 CONTINUE
    IF(ITYPE.EQ.1) WRITE(6,999)
999 FORMAT(1H1,8X,*LOAD*,3X,*NODE*,3X,*STRAIN IN MORTAR*,
12X,*STRAIN IN MORTAR*,3X,*UNCRACKED DEPTH*/8X,* (N/MM)*,
29X,* ( MAX. COMP. )*,4X,* ( MIN. COMP. )*,7X,* ( MM )*/)
    IF(IPEO.NE.1) GO TO 40
    GO TO 41
40 TEO=0. $ BEO=0.
41 CONTINUE
    DO 63 IB = 1,NP
    EO(IB)=TEO+EP(IB)
63 CONTINUE
    IF(IPEO.NE.1) GO TO 44
C   INITIALIZE LOAD INCREMENT PO
    READ(5,800) IP,PO
800 FORMAT(I1,F9.3)
    IF(IP.NE.0) GO TO 801
    PO=0.1*(D/2-TEO)/(D/2)*PCR
801 CONTINUE
    P=0.
    PP=0.
44 CONTINUE
    DO 200 NK = 1,40
    FIN=0.
    IR=0
    MP=1
C   ALLOW FOR EXTRAPOLATION
    DO 74 KD = 1,NP
    WE(KD)=W(KD)
    SEMX(KD)=TEMX(KD)
    SDC(KD)=TDC(KD)
    SEMN(KD)=TEMN(KD)

```

```

74 CONTINUE
C   REDUCE LOAD/ECCENTRICITY INCREMENT TO AVOID FAILURE
    DO 150 NO = 1,500
C   THIS LOOP ALLOWS FOR CHANGE IN DELP
    DO 50 KO = 1,NP
      W(KO)=PW(KO)
      TEMX(KO)=EMX(KO)
      TDC(KO)=DC(KO)
      TEMN(KO)=EMN(KO)
50 CONTINUE
    IF(NK.EQ.1) GO TO 77
C   EXTRAPOLATE FOR W AND H
    CALL EXTRAP(MP,NP,D,PW,WE,H,HA,IS,SEMX,EMX,SDC,DC,SEMN,EMN,NK,
1ITYPE)
77 CONTINUE
    IF(IPEO.NE.1) GO TO 42
C   CALCULATE THE LOAD INCREMENT DELP
    DELP=1./MO*PO
    P=P+DELP
    GO TO 43
42 CONTINUE
C   CALCULATE THE ECCENTRICITY INCREMENT DELEO
    DELEO=D/(6.*MO)
    DO 64 JA = 1,NP
      EO(JA)=EO(JA)+DELEO
64 CONTINUE
43 CONTINUE
C   CALCULATE HORIZONTAL REACTION H FOR COLUMN PINNED BOTH TOP AND BOTTOM
    IF(IS.EQ.1) H=(EP(1)+TEO-EP(NP)-BEO)/(X*N)*P
    DO 110 II = 1,10
C   CALCULATE PHYSICAL PROPERTIES AT ALL NODES
    IF(ITYPE.NE.1) CALL PHYSP1(NP,D,EO,PW,ECC,RIN,P,DMAX,H,X)
    IF(ITYPE.EQ.1) CALL PHYSP2(NP,D,EO,PW,ECC,RIN,P,DMAX,H,X,PNBM,AE,
1PT,EM,EMX,DC,E,KL,EMN)
    IF(KL.GE.200) GO TO 80
C   CALCULATE PKO AT ALL NODES
    CALL KON(NP,P,EO,PW,H,X,DMAX,D,PKO,PHB,PNBM,PHM,A,ITFS)
    IF(NK.NE.1) GO TO 101
C   SET UP MATRICES C AND CK
C   AT FIRST ITERATION COLUMN IS ASSUMED UNCRACKED
    IL=1
    CALL MATCOM(IS,N,X,E,RIN,NP,H,P,EO,PW,DMAX,C,CK,ECC,D,MS,IL,NK,
*PKO,PHB,PHM,PNBM)
C   CALCULATE DISPLACEMENTS BY GAUSSIAN REDUCTION
    CALL DISPL(N,C,CK,IS,H,PW,MS,EP,X,NP)
C   CHECK VALIDITY OF SOLUTIONS FOR RUNAWAY DISPLACEMENTS
    DO 87 KC = 1,NP
      IF(PW(KC).GT.1000.) GO TO 80
      EC=(P*(EO(KC)+PW(KC))-H*X*(KC-1))/(P)
      EC=ABS(EC)
      IF(EC.GE.0.95*D/2) GO TO 80
87 CONTINUE
C   CHECK VALIDITY OF MAX STRAIN AND EFFECTIVE WIDTH
C   BOTH MUST BE NON-NEGATIVE
    DO 187 KKA = 1,NP
      IF(EMX(KKA).LT.0.) GO TO 80
      IF(DC(KKA).LT.0.) GO TO 80

```

```

      IF(EMN(KKA).LT.0.) GO TO 80
187 CONTINUE
C   CALCULATE NEW PHYSICAL PROPERTIES
      IF(ITYPE.NE.1) CALL PHYSP1(NP,D,EO,PW,ECC,RIN,P,DMAX,H,X)
      IF(ITYPE.EQ.1) CALL PHYSP2(NP,D,EO,PW,ECC,RIN,P,DMAX,H,X,PNBM,AE,
      1PT,EM,EMX,DC,E,KL,EMN)
      IF(KL.GE.200) GO TO 80
C   CALCULATE PKO AT ALL NODES
      CALL KON(NP,P,EO,PW,H,X,DMAX,D,PKO,PHB,PNBM,PHM,A,ITFS)
C   CHECK EQUILIBRIUM OF COLUMN
      CALL EQUIL(N,RIN,PW,ECC,E,P,X,FIN,D,DMAX,H,IS,EO,IR,RR,R,PKO)
C   APPLY NEWTON-RAPHSON ITERATION TO ALL W AND H
101 CONTINUE
      DO 100 IL = 1,50
      IR=1
C   CHANGE W VALUES ONE AT A TIME
      DO 27 IT = 2,N
      PA(IT)=PW(IT)
      DO 16 IY = 2,NP
      RID(IY)=RIN(IY)
16 CONTINUE
      PW(IT)=PW(IT)+DEAL
C   CALCULATE NEW I-VALUES
      IF(ITYPE.NE.1) CALL PHYSP1(NP,D,EO,PW,ECC,RIN,P,DMAX,H,X)
      IF(ITYPE.EQ.1) CALL PHYSP2(NP,D,EO,PW,ECC,RIN,P,DMAX,H,X,PNBM,AE,
      1PT,EM,EMX,DC,E,KL,EMN)
      IF(KL.GE.200) GO TO 80
C   CALCULATE PKO AT ALL NODES
      CALL KON(NP,P,EO,PW,H,X,DMAX,D,PKO,PHB,PNBM,PHM,A,ITFS)
C   CHECK EQUILIBRIUM OF COLUMN
      CALL EQUIL(N,RIN,PW,ECC,E,P,X,FIN,D,DMAX,H,IS,EO,IR,RR,R,PKO)
C   CALCULATE CHANGE IN ERROR TERM ---STORE IN ARRAY RS
      JY=IT-1
      DO 28 KX = 1,N
      RS(KX,JY)=(RR(KX)-R(KX))/DEAL
28 CONTINUE
C   RESTORE ORIGINAL VALUES TO W
      PW(IT)=PA(IT)
      DO 17 IX = 2,NP
      RIN(IX)=RID(IX)
17 CONTINUE
27 CONTINUE
C   IF COLUMN IS PINNED H IS PROPORTIONAL TO LOAD P AND NOT
C   ALTERED BY NEWTON-RAPHSON PROCEDURE
      IF(IS.EQ.1) GO TO 20
C   IS = 1 IMPLIES PIN ENDS
C   CHANGE VALUE OF H
      HB=H
      DO 18 IW = 2,NP
      RID(IW)=RIN(IW)
18 CONTINUE
      H=H+DEAL
C   CALCULATE NEW I-VALUES
      IF(ITYPE.NE.1) CALL PHYSP1(NP,D,EO,PW,ECC,RIN,P,DMAX,H,X)
      IF(ITYPE.EQ.1) CALL PHYSP2(NP,D,EO,PW,ECC,RIN,P,DMAX,H,X,PNBM,AE,
      1PT,EM,EMX,DC,E,KL,EMN)
      IF(KL.GE.200) GO TO 80

```

```

C   CALCULATE PKO AT ALL NODES
      CALL KON(NP,P,EO,PW,H,X,DMAX,D,PKO,PHB,PNBM,PHM,A,ITFS)
C   CHECK EQUILIBRIUM OF COLUMN
      CALL EQUIL(N,RIN,PW,ECC,E,P,X,FIN,D,DMAX,H,IS,EO,IR,RR,R,PKO)
C   CALCULATE CHANGE IN ERROR TERM --- STORE IN ARRAY RS
      DO 29 KW = 1,N
        RS(KW,N)=(RR(KW)-R(KW))/DEAL
29  CONTINUE
C   RESTORE ORIGINAL VALUES TO H
      H=HB
      DO 19 IV = 2,NP
        RIN(IV)=RID(IV)
19  CONTINUE
20  CONTINUE
      IR=0
C   SOLVE EQUATIONS TO GIVE NEW VALUES OF W AND H
      CALL NEWGRAPH(N,RS,R,DPW,PW,H,MS,P,IL,PWP)
C   CHECK VALIDITY OF SOLUTIONS FOR RUNAWAY DISPLACEMENTS
C   OR OSCILLATORY DISPLACEMENT MODES
      DO 86 KD = 2,N
        IF(ABS(PW(KD)).LT.0.1*DMAX) GO TO 86
        IF(ABS(PW(KD)).GT.D) GO TO 80
        IF(W(KD)/PW(KD).LT.0.) GO TO 80
        EC=(P*(EO(KD)+PW(KD))-H*X*(KD-1))/(P)
        IF(ABS(EC).GE.0.95*D/2) GO TO 80
86  CONTINUE
C   CHECK VALIDITY OF MAX STRAIN AND EFFECTIVE SECTION
C   EMX AND DC MUST BOTH BE NON-NEGATIVE
      DO 186 KKB = 1,NP
        IF(EMX(KKB).LT.0.) GO TO 80
        IF(DC(KKB).LT.0.) GO TO 80
        IF(EMN(KKB).LT.0.) GO TO 80
186 CONTINUE
C   CHECK EQUILIBRIUM BEFORE NEW ITERATION IS COMMENCED
C   CALCULATE PHYSICAL PROPERTIES AT ALL NODES
      IF(ITYPE.NE.1) CALL PHYSP1(NP,D,EO,PW,ECC,RIN,P,DMAX,H,X)
      IF(ITYPE.EQ.1) CALL PHYSP2(NP,D,EO,PW,ECC,RIN,P,DMAX,H,X,PNBM,AE,
1PT,EM,EMX,DC,E,KL,EMN)
      IF(KL.GE.200) GO TO 80
C   CALCULATE PKO AT ALL NODES
      CALL KON(NP,P,EO,PW,H,X,DMAX,D,PKO,PHB,PNBM,PHM,A,ITFS)
      CALL EQUIL(N,RIN,PW,ECC,E,P,X,FIN,D,DMAX,H,IS,EO,IR,RR,R,PKO)
      IF(FIN.EQ.0.) GO TO 100
C   FIN GT 0. IMPLIES EQUILIBRIUM TO DESIRED ACCURACY
      GO TO 15
100 CONTINUE
C   NEWTON-RAPHSON ITERATION HAS NOT REACHED SOLUTION
C   ONE OR MORE OF SOLUTION HYPERSURFACES HAS SLOPE DISCONTINUITY
C   SHIFT P OR EO HYPERSURFACE TO ALLOW SOLUTION
      IF(IPEO.NE.1) GO TO 71
      P=P+1
      GO TO 110
71  CONTINUE
      ET=0.01*D
      DO 72 JJ = 1,NP
        EO(JJ)=EO(JJ)+ET
72  CONTINUE

```

```

110 CONTINUE
    WRITE(6,160) P,EO(1)
160 FORMAT(1H1,10X,*COLUMN EQUATIONS ARE ILL-CONDITIONED AT *
    1*LOAD = *,F10.3,* N/MM LENGTH OF WALL*/1H0,30X,
    2*TOP LOAD ECCENTRICITY IS *,F10.3,* MM*/1H0,25X,
    3*-----RUN PROGRAM WITH ALTERED LOAD(ECCENTRICITY) PATH-----*)
    STOP " PROGRAM ENCOUNTERED ILL-CONDITIONED EQUATIONS "
80 DO 70 JO = 1,NP
    PW(JO)=W(JO)
    EMX(JO)=TEMX(JO)
    DC(JO)=TDC(JO)
    EMN(JO)=TEMN(JO)
70 CONTINUE
    IF(IPEO.NE.1) GO TO 45
    P=PP
    H=HH
    GO TO 48
45 DO 66 JD = 1,NP
    EO(JD)=EOP(JD)
66 CONTINUE
    H=HH
48 CONTINUE
C THIS LOOP DECREASES THE INCREMENT IN P OR EO
    MO=MO*2
    MP=MP*2
    IF(IPEO.NE.1) GO TO 49
    IF(DELP.LT.0.1) GO TO 35
    GO TO 51
49 IF(DELEO.LT.0.01) GO TO 55
51 CONTINUE
150 CONTINUE
    STOP "500 ITERATIONS INSUFFICIENT"
15 CONTINUE
C FAILURE HAS NOT OCCURRED IF THIS STEP IS REACHED
C INCREASE LOAD/LOAD ECCENTRICITY
    IF(IPEO.NE.1) GO TO 52
    PP=P
    HA=HH
    HH=H
    GO TO 53
52 DO 67 IF = 1,NP
    EOP(IF)=EO(IF)
67 CONTINUE
    HA=HH
    HH=H
    GO TO 54
53 CONTINUE
C CALCULATE STRESS AT COMPRESSION FACE AT ALL NODES
    IF(ITYPE.NE.1) CALL STRESS1(NP,P,D,EO,PW,SMAX,H,X)
    IF(ITYPE.EQ.1) CALL STRESS2(NP,AE,PT,EMX,E,PNB,SMAX)
C ALLOCATE VALUES FOR PLOTTING AND PRINTING
    PPL(NK)=P
    DO91 KA=1,NP
    PWP(NK,KA)=PW(KA)
    SP(NK,KA)=SMAX(KA)
91 CONTINUE
    IF(ITYPE.NE.1) GO TO 92

```

```

      IF(IS.EQ.1) NPQ=(NP+1)/2
      IF(IS.NE.1) NPQ=4*N/10
      WRITE(6,1000) P, NPQ, EMX(NPQ), EMN(NPQ), DC(NPQ)
1000 FORMAT(1H0,5X,F8.2,I5,5X,E12.3,5X,E12.3,5X,F12.4)
      92 CONTINUE
      IF(DELP.LT.0.1) 35,34
      54 IF(DELEO.LT.0.01) GO TO 55
      34 CONTINUE
      200 CONTINUE
C   COMPLETED NK LOOP LEADS TO NK TOO LARGE BY ONE
      NK=NK-1
      WRITE(6,37)
      37 FORMAT(1H0,25X,*WALL FAILURE NOT ATTAINED IN 40 ITERATIONS*/)
      IF(IPEO.NE.1) STOP
      GO TO 36
      35 CONTINUE
      WRITE(6,88) P,H
      88 FORMAT(1H0,30X,*WALL FAILURE LOAD IS *,F8.2,* N/MM* / 1H0,30X,
      **MAX. HORIZONTAL REACTION IS *,F8.4, * N/MM*)
      36 CONTINUE
C   PRINT DISPLACEMENTS AND STRESSES FOR CRITICAL NODE(S)
      CALL PRINT(NP,NX,NK,PWP,SP,PPL,NS)
C   PLOT CRITICAL NODE(S) FOR DEFLECTION AND STRESS
      CALL DPLOT(NK,NP,QA,PPL,PWP,PLAT,NS)
      CALL SPLOT(NK,NP,RA,PPL,SP,SLOT,NS)
      GO TO 56
      55 EOD=D/EO(1)
      WRITE(6,57) P,EOD
      57 FORMAT(1H0,25X,*FOR LOAD OF *,F6.1,* MAX. ECCENTRICITY IS D /*,F8
      *.5)
      56 CONTINUE
      END
      SUBROUTINE EULER(E,D,WL,PHB,PHM,PNB,PCR)
C
C   CALCULATE EQUIVALENT WALL ELASTIC MODULUS FOR FULL SECTION
C
      EQ=E*(PHB+PHM)/(PHB+PNB*PHM)
      BI=D**3/12
      PCR=3.141592**2*EQ*BI/WL**2
      WRITE(6,4) PCR
      4 FORMAT(1H0,5X,*CRITICAL BUCKLING LOAD FOR PIN-END WALL IS *,F8.2,
      1* N/MM LENGTH*/)
      RETURN
      END
      SUBROUTINE EXTRAP(MP,NP,D,PW,WE,H,HA,IS,SEM,EMX,SDC,DC,SEM,
      *EMN,NK,ITYPE)
      DIMENSION PW(1),WE(1),SEM(1),EMX(1),SDC(1)
      DIMENSION DC(1),SEM(1),EMN(1)
C   EXTRAPOLATE ON ALL W
      DO 73 KC = 1,NP
      IF(PW(KC).EQ.0.) GO TO 76
      WMULT=1.+(1.-WE(KC)/PW(KC))/MP
      PW(KC)=PW(KC)*WMULT
      GO TO 73
      76 PW(KC)= -WE(KC)/MP
      73 CONTINUE
C   EXTRAPOLATE ON H

```

```

      IF(IS.EQ.1) GO TO 72
C   IS.EQ.1 IMPLIES PIN ENDS
      HMULT=1.+(1.-HA/H)/MP
      H=H*HMULT
72  CONTINUE
      IF(NK.EQ.2) GO TO 77
      IF(ITYPE.NE.1) GO TO 77
C   EXTRAPOLATE ON MAX STRAIN EMAX
      DO 74 KD = 1,NP
      EMULT=1.+(1.-SEM(KD)/EMX(KD))/MP
      EMX(KD)=EMX(KD)*EMULT
74  CONTINUE
C   EXTRAPOLATE ON EFFECTIVE SECTION DC
      DO 75 KE = 1,NP
      IF(EMN(KE).GT.0.) GO TO 75
C   EMN GT ZERO IMPLIES SECTION IS NOT CRACKED AND DC EQ D
      DMULT=1.+(1.-SDC(KE)/DC(KE))/MP
      DC(KE)=DC(KE)*DMULT
75  CONTINUE
C   EXTRAPOLATE ON EMIN
      DO 78 KF = 1,NP
      IF(DC(KF).NE.D) GO TO 78
      IF(EMN(KF).EQ.0.) GO TO 78
C   DC NE D IMPLIES SECTION IS CRACKED AND EMIN IS ZERO
      EMULT=1.+(1.-SEM(KF)/EMN(KF))/MP
      EMN(KF)=EMN(KF)*EMULT
78  CONTINUE
77  CONTINUE
      RETURN
      END
      SUBROUTINE PHYSP1(NP,D,EO,PW,ECC,RIN,P,DMAX,H,X)
      DIMENSION RIN(1),PW(1),ECC(1),EO(1)
      DO 51 J = 1,NP
      ECC(J)=D/2.-EO(J)-PW(J)
      EC=(P*(EO(J)+PW(J))-H*X*(J-1))/P
      ABSEC=ABS(EC)
      IF(ABSEC.LT.DMAX) GO TO 40
      RIN(J)=(3.*(D/2.-ABSEC)**3/12.
      GO TO 51
40  RIN(J)=D**3/12.
51  CONTINUE
      RETURN
      END
      SUBROUTINE PHYSP2(NP,D,EO,PW,ECC,RIN,P,DMAX,H,X,
      *PNBM,AE,PT,EM,EMX,DC,E,KL,EMN)
      DIMENSION RIN(1),PW(1),ECC(1),EO(1),PNBM(1),EMX(1)
      DIMENSION DC(1),EMN(1)
      DIMENSION DP(40),XX(2,2),ICF(40)
      DO 50 J = 1,NP
      ECC(J)=D/2.-EO(J)-PW(J)
      EC=EO(J)+PW(J)-H*X*(J-1)/P
      ABSEC=ABS(EC)
      IF(ABSEC.LT.DMAX.OR.DC(J).EQ.D) ICF(J)=1
      IF(ABSEC.GE.DMAX.OR.DC(J).LT.D) ICF(J)=0
C
C   ABSEC EQ ZERO IMPLIES AXIAL LOAD AT NODE J
C

```



```

      IF(ABSEC.EQ.0.) RIN(J)=D**3/12
      IF(ABSEC.EQ.0.) GO TO 50
      IF(ICF(J).NE.1) ICF(J)=0
C    CHECK WHETHER CRACKING IS BEING INITIATED
      IF(EMN(J).LT.0.) ICF(J)=0
      IF(EMN(J).LT.0.) EMN(J)=0.
      DP(J)=D/2-ABSEC
      DO 150 KP = 1,5
      IF(ICF(J).EQ.1) GO TO 160
      DO 300 KL = 1,200
      EMN(J)=0.
      EBAR=(2./3*EMX(J)-(2.*AE)/(2+PT)*EMX(J)**PT)/
* (1.-(2.*AE)/(1+PT)*EMX(J)**(PT-1))
      T=P-EM*(EMX(J)*EMX(J)/2-AE/(PT+1)*EMX(J)**(PT+1))
**DC(J)/EMX(J)
      V=DP(J)-(EMX(J)-EBAR)*DC(J)/EMX(J)
      IF(ABS(T).LT.0.01.AND.ABS(V).LT.0.001) GO TO 400
      DO 200 ILO = 1,2
      IF(ILO.EQ.1) EX=EMX(J)+0.001
      IF(ILO.EQ.1) DS=DC(J)
      IF(ILO.EQ.2) EX=EMX(J)
      IF(ILO.EQ.2) DS=DC(J)+0.1
      EBAR=(2./3*EX-(2.*AE)/(2+PT)*EX**PT)/(1.-(2.*AE)/
* (1+PT)*EX**(PT-1))
      DT=P-EM*(EX*EX/2-AE/(PT+1)*EX**(PT+1))*DS/EX
      DV=DP(J)-(EX-EBAR)*DS/EX
      IF(ILO.EQ.2) GO TO 100
      XX(1,1)=(DT-T)/0.001
      XX(2,1)=(DV-V)/0.001
      GO TO 200
100  XX(1,2)=(DT-T)/0.1
      XX(2,2)=(DV-V)/0.1
200  CONTINUE
      DETXX=XX(1,1)*XX(2,2)-XX(1,2)*XX(2,1)
      DEMX=(-T*XX(2,2)+V*XX(1,2))/DETXX
      DDC=(T*XX(2,1)-V*XX(1,1))/DETXX
C    CHECK WHETHER ITERATION LEADS TO NEGATIVE STRAIN EMX ( INVALID )
      IF((EMX(J)+DEMX).LE.0.) DEMX=0.
      EMX(J)=EMX(J)+DEMX
      DC(J)=DC(J)+DDC
300  CONTINUE
      WRITE(6,1000) P
1000 FORMAT(1H0,5X,*CONSISTENT CRACKED SECTION NOT FOUND FOR
1 LOAD =*,F12.4,* N/MM*)
      RETURN
400  CONTINUE
      IF(DC(J).GT.1.001*D) ICF(J)=1
      IF(ICF(J).EQ.1) DC(J)=D
      IF(ICF(J).EQ.1) GO TO 160
C    CALCULATE EFFECTIVE MORTAR MODULUS AND VALUE OF RIN
      IF(ABSEC.LT.DMAX) GO TO 201
      PNBM(J)=E*(4.5*DP(J)*DP(J)*EMX(J))/(DC(J)*P)
      RIN(J)=(3.*DP(J))**3/12
      GO TO 50
201  CONTINUE
      PNBM(J)=E/(12.*P/D**3*(0.5*D-DP(J))*DC(J)/EMX(J))
      RIN(J)=D**3/12

```

```

      GO TO 50
160 CONTINUE
C   SET EMIN GREATER THAN ZERO BUT NOT EQUAL TO EMAX ( IF REQUIRED )
      IF(EMN(J).EQ.0.) EMN(J)=0.00001
      EDEL=1.0E-06
      IF(EMN(J).EQ.EMX(J)) EMX(J)=EMX(J)+EDEL
C
C   LOOP 500 CALCULATES EMAX AND EMIN FOR UNCRACKED SECTION
C
      DO 500 KL = 1,200
      EBAR=(2./3*(EMX(J)**3-EMN(J)**3)-2.*AE/(PT+2)*(EMX(J)**(PT+2)
      *-EMN(J)**(PT+2)))/(EMX(J)*EMX(J)-EMN(J)*EMN(J)-2.*AE/
      *(PT+1)*(EMX(J)**(PT+1)-EMN(J)**(PT+1)))
C   CALCULATE ERROR TERMS Q AND S
      Q=P-EM*(0.5*(EMX(J)*EMX(J)-EMN(J)*EMN(J))-AE/(PT+1)*(EMX(J)**
      *(PT+1)-EMN(J)**(PT+1)))*D/(EMX(J)-EMN(J))
      S=DP(J)-(EMX(J)-EBAR)*D/(EMX(J)-EMN(J))
      IF(ABS(Q).LT.0.01.AND.ABS(S).LT.0.001) GO TO 600
      DO 700 ILP = 1,2
      IF(ILP.EQ.1) EX=EMX(J)+EDEL
      IF(ILP.EQ.1) EN=EMN(J)
      IF(ILP.EQ.2) EX=EMX(J)
      IF(ILP.EQ.2) EN=EMN(J)+EDEL
      EBAR=(2./3*(EX**3-EN**3)-2.*AE/(PT+2)*(EX**(PT+2)-EN**(PT+2)))/
      *(EX*EX-EN*EN-2.*AE/(PT+1)*(EX**(PT+1)-EN**(PT+1)))
C   CALCULATE CHANGE IN ERROR TERMS DQ AND DS
      DQ=P-EM*(0.5*(EX*EX-EN*EN)-AE/(PT+1)*(EX**(PT+1)-EN**(PT+1)))
      *D/(EX-EN)
      DS=DP(J)-(EX-EBAR)*D/(EX-EN)
      IF(ILP.EQ.2) GO TO 800
      XX(1,1)=(DQ-Q)/EDEL
      XX(2,1)=(DS-S)/EDEL
      GO TO 700
800 XX(1,2)=(DQ-Q)/EDEL
      XX(2,2)=(DS-S)/EDEL
700 CONTINUE
      DETXX=XX(1,1)*XX(2,2)-XX(1,2)*XX(2,1)
      DEMX=(-Q*XX(2,2)+S*XX(1,2))/DETXX
      DEMN=(Q*XX(2,1)-S*XX(1,1))/DETXX
C   CHECK WHETHER ITERATION LEADS TO NEGATIVE STRAIN EMX ( INVALID )
      IF((EMX(J)+DEMX).LE.0.) DEMX=0.
      EMX(J)=EMX(J)+DEMX
      EMN(J)=EMN(J)+DEMN
C   IF EMN(J) IS LESS THAN OR EQUAL TO ZERO, LIBRARY EXPONENTIATION
C   ROUTINE XTOY WILL NOT WORK FOR REAL EXPONENTS
      IF(EMN(J).LE.0.) EMN(J)=0.00001
500 CONTINUE
C   IF, AT COMPLETION OF LOOP 500, EMN(J) IS EQUAL TO 0.00001,
C   CRACKED SECTION ANALYSIS SHOULD BE USED
C   IF, HOWEVER, PROGRAM REACHES END OF LOOP 500 AND STRAINS ARE
C   NOT CALCULATED, FLAG IS SET TO REDUCE LOAD INCREMENT
      IF(EMN(J).NE.0.00001) RETURN
C   SET FLAGS FOR CRACKED SECTION ANALYSIS
      ICF(J)=0
      EMN(J)=0.
150 CONTINUE
      STOP "SECTION PROPERTIES NOT CALCULATED"

```

```

600 CONTINUE
C   CALCULATE EFFECTIVE MORTAR MODULUS AND VALUE OF RIN
    IF(DP(J).EQ.D/2) GO TO 850
    PNB(M)=E*D*D*(EMX(J)-EMN(J))/(12.*P*(D/2-DP(J)))
850 RIN(J)=D**3/12
50 CONTINUE
    RETURN
    END
    SUBROUTINE KON(NP,P,EO,PW,H,X,DMAX,D,PKO,PHB,PNBM,PHM,A,ITFS)
    DIMENSION PW(1),PKO(1),EO(1),A(4),PNBM(1)
    DO 61 JB = 1,NP
C   CALCULATE EFFECTIVE ECCENTRICITY
    EC=(P*(EO(JB)+PW(JB))-H*X*(JB-1))/(P)
    ABSEC=ABS(EC)
    IF(ABSEC.LE.DMAX) GO TO 67
    IF(ITFS.NE.0) GO TO 67
    ED=ABSEC/D
    ED1=ED $ ED2=ED*ED $ ED3=ED**3
    PEC=A(1)+ED1*A(2)+ED2*A(3)+ED3*A(4)
    PKN=1./PEC
    GO TO 62
67 PKN=1.
62 CONTINUE
    PKO(JB)=(PKN*PHB+PNBM(JB)*PHM)/(PHB+PHM)
61 CONTINUE
    RETURN
    END
    SUBROUTINE EQUIL(N,RIN,PW,ECC,E,P,X,FIN,D,DMAX,H,IS,EO,IR,RR,R,
*PKO)
    DIMENSION RIN(1),PW(1),ECC(1),RR(1),R(1)
    DIMENSION PKO(1),EO(1)
    ERR = 0.
    ERRAL=0.000001
    NQ=N+1
    DO 30 KM = 2,NQ
    JI = KM-1 $ JK = KM + 1
    IF(KM.NE.NQ) GO TO 75
    IF(IS.EQ.1) GO TO 31
C   IS = 1 IMPLIES PINNED BASE
    PW(JK)=PW(JI)
75 EC=(P*(EO(KM)+PW(KM))-H*X*(KM-1))/(P)
    ABSEC=ABS(EC)
    IF(ABSEC.LT.DMAX) GO TO 37
    IF(EC.LT.0.) GO TO 38
    ERROR=E*RIN(KM)/P*(PW(JK)+PW(JI)-2.*PW(KM))/X**2+PKO(KM)*(.5*ECC(K
*M)+.5*H*JI*X/P)
    IF(IR.EQ.0) GO TO 41
    RR(JI)=ERROR
    GO TO 31
41 R(JI)=ERROR
    ERROR=ABS(ERROR)
    IF(ERROR.LE.ERR) GO TO 31
    ERR = ERROR
    GO TO 31
38 ERROR=E*RIN(KM)/P*(PW(JK)+PW(JI)-2.*PW(KM))/X**2+PKO(KM)*(-.5*(D-E
*CC(KM))+.5*H*JI*X/P)
    IF(IR.EQ.0) GO TO 43

```

```

RR(JI)=ERROR
GO TO 31
43 R(JI)=ERROR
ERROR=ABS(ERROR)
IF(ERROR.LE.ERR) GO TO 31
ERR=ERROR
GO TO 31
37 ERROR=E*RIN(KM)/P*(PW(JK)+PW(JI)-2.*PW(KM))/X**2+PKO(KM)*((D/2-ECC
*(KM))-H*JI*X/P)
IF(IR.EQ.0) GO TO 45
RR(JI)=ERROR
GO TO 31
45 R(JI)=ERROR
ERROR=ABS(ERROR)
IF(ERROR.LE.ERR) GO TO 31
ERR=ERROR
31 CONTINUE
30 CONTINUE
IF(IR.EQ.1) GO TO 16
IF(ERR.GT.ERRAL) GO TO 16
FIN=ERR
16 CONTINUE
RETURN
END
SUBROUTINE MATCOM(IS,N,X,E,RIN,NP,H,P,EO,PW,DMAX,C,CK,ECC,D,MS,
*IL,NK,PKO,PHB,PHM,PNBM)
DIMENSION RIN(1),PW(1),C(MS,1),CK(1),ECC(1)
DIMENSION PKO(1),EO(1),PNBM(1)
DO 20 IXA = 1,MS
DO 21 IXB = 1,MS
C(IXA,IXB)=0.
21 CONTINUE
20 CONTINUE
PK=(PHB+PNBM(1)*PHM)/(PHB+PHM)
C SET UP EQUATION MATRIX C WITH FIXED TERMS
NA=N-1 $ NB=N-2
C(1,1)=2.
C(1,2)=-1.
C(NA,NB)=-1.
C(NA,NA)=2.
IF(IS.EQ.1) GO TO 6
C(N,NA)=-2.
6 CONTINUE
DO 55 I = 2,NB
IF=I-1 $ IG=I+1
C(I,IF)=-1.
C(I,I)=2.
C(I,IG)=-1.
55 CONTINUE
DO 52 K = 2,NP
KJ=K-1 $ KL = K+1
C ASSUME COLUMN IS UNCRACKED FOR FIRST ITERATION
IF(NK.NE.1) GO TO 14
IF(IL.NE.1) GO TO 14
DI=D**3/12
DO 53 LP = 1,NP
PKO(LP)=PK

```

```

RIN(LP)=DI
53 CONTINUE
GO TO 58
14 CONTINUE
EC=(P*(EO(K)+PW(K))-H*X*(K-1))/(P)
ABSEC=ABS(EC)
IF(ABSEC.GE.DMAX) GO TO 56
58 CK(KJ)=P*(D/2-ECC(K))*X**2/(E*RIN(K))*PKO(K)
GO TO 52
56 IF(EC.LT.0.) GO TO 57
CK(KJ)=X**2/(E*RIN(K))*(.5*P*ECC(K))*PKO(K)
GO TO 52
57 CK(KJ)=X**2/(E*RIN(K))*(-.5*P*(D-ECC(K))*PKO(K)
52 CONTINUE
IF(IS.EQ.1) GO TO 10
DO 12 IN = 1,N
IM=IN+1
C ASSUME COLUMN IS UNCRACKED FOR FIRST ITERATION
IF(NK.NE.1) GO TO 15
IF(IL.NE.1) GO TO 15
PKO(IM)=PK
RAN=X**2/(E*DI)*X*IN
GO TO 13
15 CONTINUE
EC=(P*(EO(IM)+PW(IM))-H*X*(IM-1))/(P)
ABSEC=ABS(EC)
RAN=X**2/(E*RIN(IM))*X*IN
IF(ABSEC.LT.DMAX) GO TO 13
C(IN,N)=-.5*RAN*PKO(IM)
GO TO 12
13 C(IN,N)=RAN*PKO(IM)
12 CONTINUE
10 CONTINUE
RETURN
END
SUBROUTINE DISPL(N,C,CK,IS,H,PW,MS,EP,X,NP)
DIMENSION C(MS,1),CK(1),PW(1),EP(1)
ND=N-2
DO 57 IT = 1,ND
DIV=C(IT,IT) $ IV=IT+1
DO 58 IR = 1,N
C(IT,IR)=C(IT,IR)/DIV
C(IV,IR)=C(IV,IR)+C(IT,IR)
58 CONTINUE
CK(IT)=CK(IT)/DIV
CK(IV)=CK(IV)+CK(IT)
57 CONTINUE
NE=N-1
DUV=C(NE,NE)/2
DO 59 IW = 1,N
C(NE,IW)=C(NE,IW)/DUV
C(N,IW)=C(N,IW)+C(NE,IW)
59 CONTINUE
CK(NE)=CK(NE)/DUV
CK(N)=CK(N)+CK(NE)
C MATRICES ARE NOW REDUCED
C BACK-SUBSTITUTE FOR VALUES OF W AND H

```

```

IF(IS.NE.1) H=CK(N)/C(N,N)
PW(N)=(CK(NE)-C(NE,N)*H)/2
DO 61 NO = 1,ND
NR=N-NO
NRI=NR-1 $ NRJ=NR+1
PW(NR)=CK(NRI)-C(NRI,NR)*PW(NRJ)-C(NRI,N)*H
61 CONTINUE
RETURN
END
SUBROUTINE NEWGRAPH(N,RS,R,DPW,PW,H,MS,P,IL,PWP)
DIMENSION RS(MS,1),R(1),DPW(1),PW(1)
DIMENSION PWP(MS,1)
IPT=N-1
DO 51 LB = 2,N
LA=LB-1
IF(RS(LB,LA).EQ.0.) GO TO 51
C THIS IMPLIES NO REDUCTION IS REQUIRED ON ROW LB
RMULT=-RS(LA,LA)/RS(LB,LA)
DO 53 LC = 1,N
RS(LB,LC)=RS(LB,LC)*RMULT
RS(LB,LC)=RS(LB,LC)+RS(LA,LC)
53 CONTINUE
R(LB)=R(LB)*RMULT
R(LB)=R(LB)+R(LA)
51 CONTINUE
C BACKSUBSTITUTE
IF(RS(N,N).EQ.0.) GO TO 54
DELH=-R(N)/RS(N,N)
GO TO 55
54 DELH=0.
55 CONTINUE
IF(RS(IPT,IPT).EQ.0.) GO TO 56
DPW(N)=(-R(IPT)-RS(IPT,N)*DELH)/RS(IPT,IPT)
GO TO 57
56 DPW(N)=0.
57 CONTINUE
NR=N-2
DO 58 NC = 1,NR
MR=N-NC
MSI=MR-1 $ MSJ=MR+1
IF(RS(MSI,MSI).EQ.0.) GO TO 59
DPW(MR)=(-R(MSI)-RS(MSI,MR)*DPW(MSJ)-RS(MSI,N)*DELH)/RS(MSI,MSI)
GO TO 58
59 DPW(MR)=0.
58 CONTINUE
C CALCULATE NEW VALUES OF W AND H
DO 61 MT = 2,N
PW(MT)=PW(MT)+DPW(MT)
61 CONTINUE
H=H+DELH
RETURN
END
SUBROUTINE STRESS1(NP,P,D,EO,PW,SMAX,H,X)
DIMENSION PW(1),SMAX(1),EO(1)
C
C THIS ROUTINE CALCULATES STRESSES FOR LINEAR MORTARS ONLY
C

```

```

DO 53 JT=1, NP
DAX=D/6
EC=(P*(EO(JT)+PW(JT))-H*X*(JT-1))/(P)
ABSEC=ABS(EC)
IF(ABSEC.LT.DAX) GO TO 41
SMAX(JT)=2./3*(P)/(D/2-ABSEC)
GO TO 53
41 SMAX(JT)=(P)*(1./D+6./D**2*ABSEC)
53 CONTINUE
RETURN
END
SUBROUTINE STRESS2(NP, AE, PT, EMX, E, PNB, SMAX)
DIMENSION EMX(1), SMAX(1)
C
C THIS ROUTINE CALCULATES STRESSES FOR NON-LINEAR MORTARS ONLY
C
DO 60 JA = 1, NP
SMAX(JA)=E/PNB*(EMX(JA)-AE*EMX(JA)**PT)
60 CONTINUE
RETURN
END
SUBROUTINE PRINT(NP, NX, NK, PWP, SP, PPL, NS)
DIMENSION NX(1), PWP(NS, 1), SP(NS, 1), PPL(1)
C PRINT DISPLACEMENTS AND STRESSES FOR ALL NODES
DO 69 IX = 1, 2
XL=0.
IF(IX.EQ.2) GO TO 68
50 CONTINUE
WRITE(6, 64)
64 FORMAT(1H1, 50X, *DISPLACEMENTS*/1H0, 2X, *LOAD*, 65X, *NODES*)
GO TO 61
68 CONTINUE
WRITE(6, 62)
62 FORMAT(1H1, 40X, *MAX. COMPRESSIVE STRESS*/1H0, 2X, *LOAD*, 65X, *NODES*
* )
61 CONTINUE
IF(NP.GT.21) GO TO 80
DO 65 KP = 1, NP
65 NX(KP)=KP
WRITE(6, 66) (NX(KT), KT=1, NP)
66 FORMAT(8X, 21I6/)
GO TO 81
80 CONTINUE
DO 82 JP = 1, NP
T=JP/2.
JS=INT(T)
VR=T-JS
IF(VR.EQ.XL) GO TO 82
IF(XL.NE.0.)GO TO 90
JS=JS+1
90 CONTINUE
NX(JS)=JP
82 CONTINUE
WRITE(6, 66) (NX(JT), JT=1, JS)
81 CONTINUE
IF(IX.EQ.2) GO TO 67
IF(NP.GT.21) GO TO 84

```

```

DO 73 KV = 1, NK
WRITE(6, 74) PPL(KV), (PWP(KV, KW), KW=1, NP)
74 FORMAT(1H0, F6.1, 2X, 21F6.3/)
73 CONTINUE
GO TO 69
84 CONTINUE
IF(XL.EQ.0.5) GO TO 91
DO 85 KZ = 1, NK
WRITE(6, 86) PPL(KZ), (PWP(KZ, KW), KW=1, NP, 2)
86 FORMAT(1H0, F6.1, 2X, 21F6.3/)
85 CONTINUE
GO TO 94
91 CONTINUE
DO 92 KZ = 1, NK
WRITE(6, 93) PPL(KZ), (PWP(KZ, KW), KW=2, NP, 2)
93 FORMAT(1H0, F6.1, 2X, 21F6.3/)
92 CONTINUE
94 CONTINUE
IF(XL.EQ.0.5) GO TO 69
XL=0.5
GO TO 50
67 CONTINUE
IF(NP.GT.21) GO TO 87
DO 76 KX=1, NK
WRITE(6, 77) PPL(KX), (SP(KX, KY), KY=1, NP)
77 FORMAT(1H0, F6.1, 2X, 21F6.2/)
76 CONTINUE
GO TO 69
87 CONTINUE
IF(XL.EQ.0.5) GO TO 95
DO 88 KZ=1, NK
WRITE(6, 89) PPL(KZ), (SP(KZ, KY), KY=1, NP, 2)
89 FORMAT(1H0, F6.1, 2X, 21F6.3/)
88 CONTINUE
GO TO 98
95 CONTINUE
DO 96 KZ = 1, NK
WRITE(6, 89) PPL(KZ), (SP(KZ, KY), KY=2, NP, 2)
96 CONTINUE
98 CONTINUE
IF(XL.EQ.0.5) GO TO 69
XL=0.5
GO TO 68
69 CONTINUE
RETURN
END
SUBROUTINE DPLOT(NK, NP, QA, PPL, PWP, PLAT, NS)
DIMENSION QA(1), PPL(1), PWP(NS, 1), PLAT(1)
C FIND NODE(S) WITH MAX. DISPLACEMENT
DIS=0. $MA=1
DO 92 NA = 1, NK
DO 93 NB = 1, NP
DISP=PWP(NA, NB)
IF(DISP.LT.DIS) GO TO 93
DIS=DISP
93 CONTINUE
92 CONTINUE

```

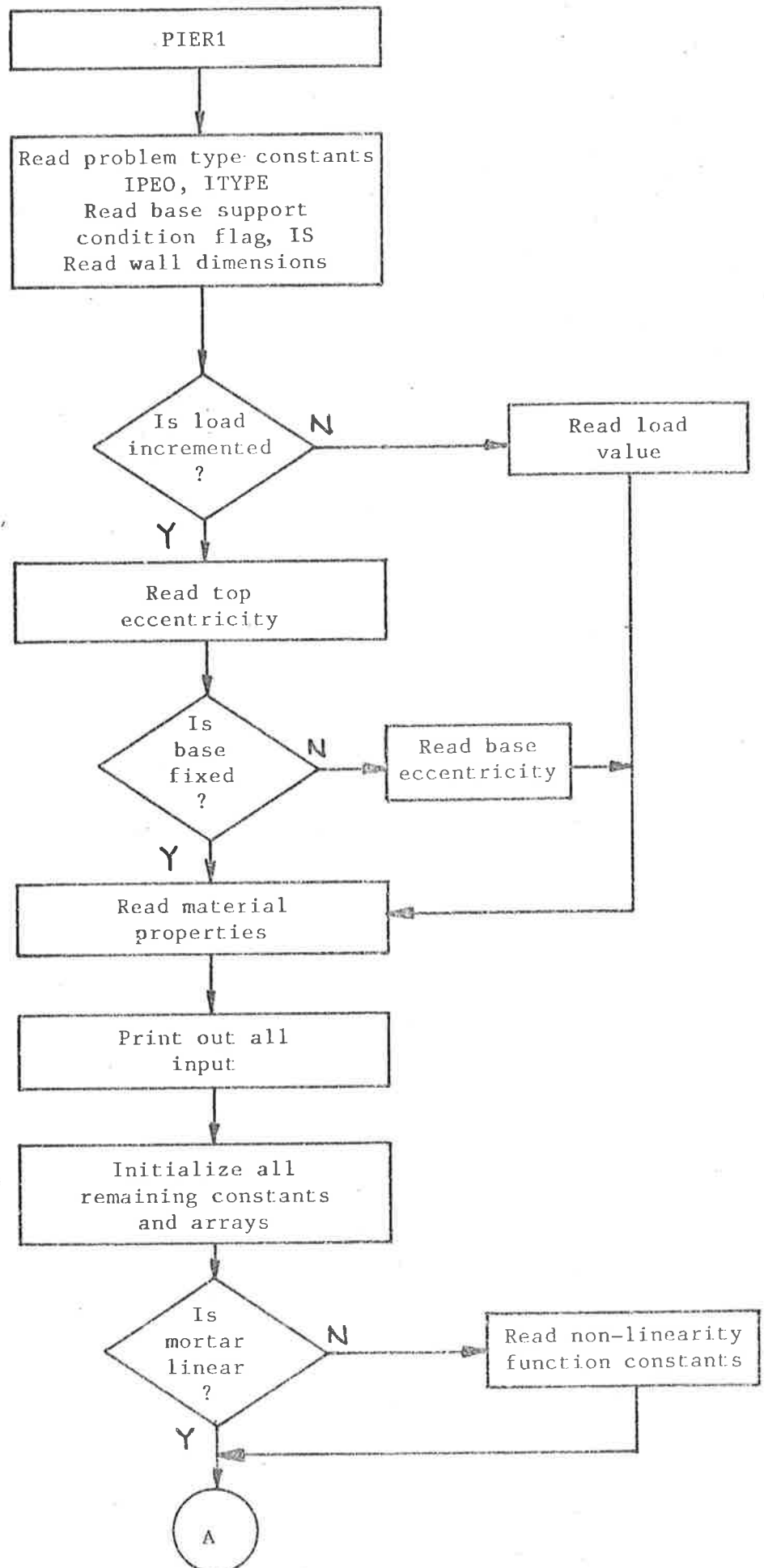


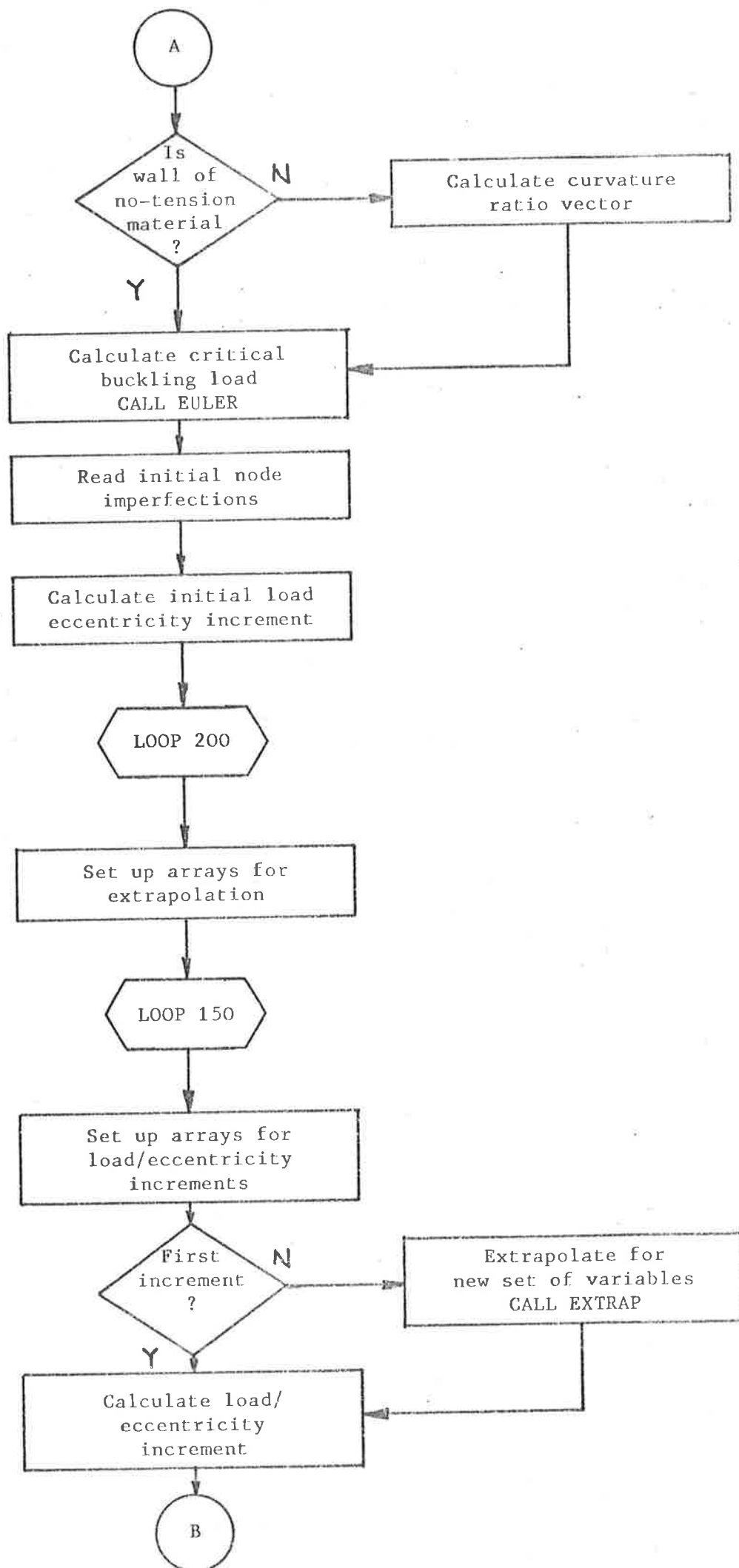
```

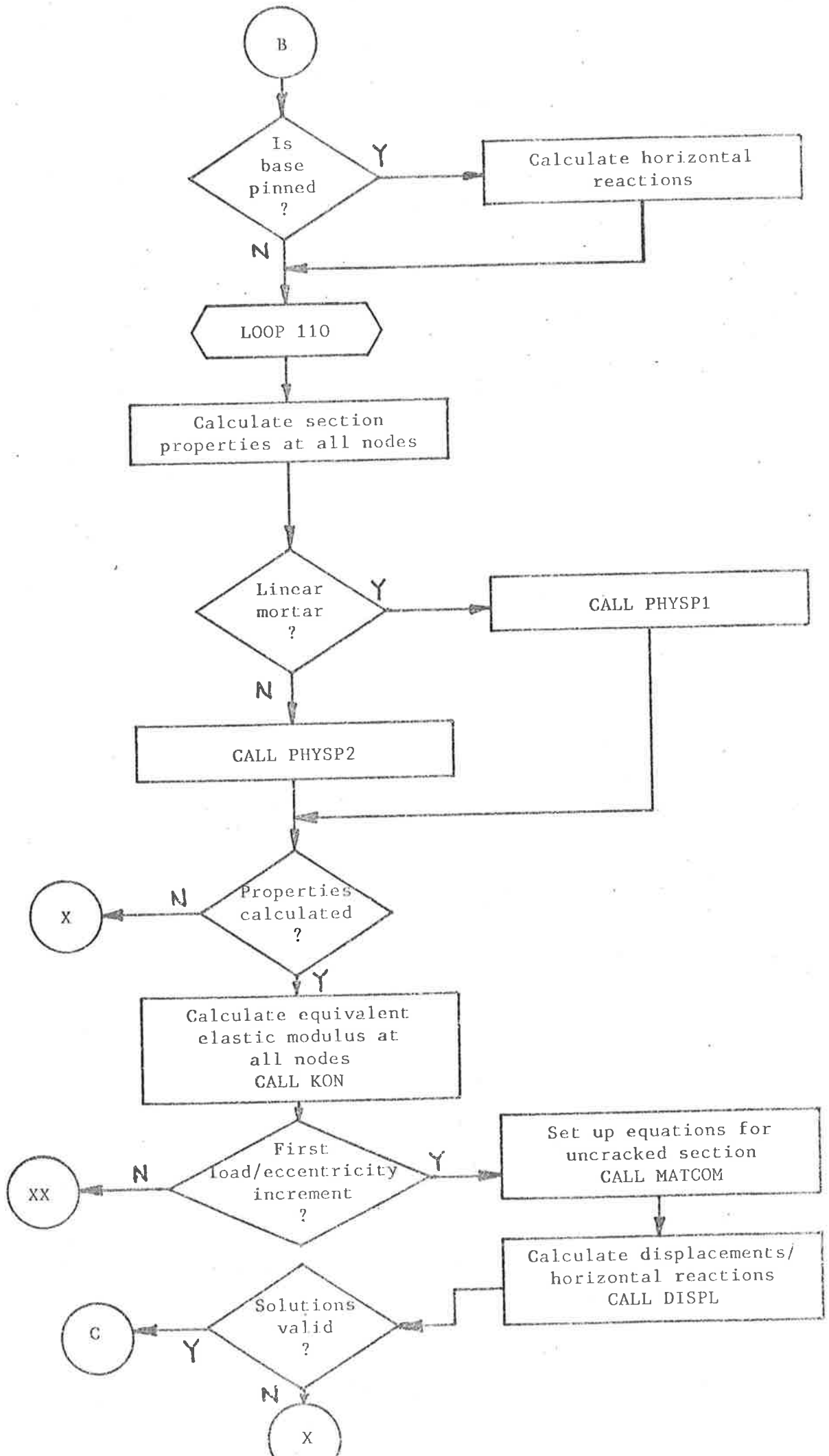
DO 94 NC = 1, NK
DO 95 ND = 1, NP
DOS=PWP(NC, ND)
IF(DOS.EQ.DIS) GO TO 96
95 CONTINUE
GO TO 94
96 QA(MA)=ND
MA=MA+1
94 CONTINUE
C PLOT DISPLACEMENT OF CRITICAL NODE(S)
DO 97 IB = 1, 5
NF = QA(IB)
IF(NF.EQ.0.) GO TO 97
DO 98 IC = 1, NK
98 PLAT(IC)=PWP(IC, NF)
CALL QIKPLOT(PLAT, PPL, -40, 14H*DISPLACEMENT*, 6H*LOAD*, -1)
WRITE(6, 44) NF
44 FORMAT(1H0, 30X, *CRITICAL NODE IS NODE NO. *, I3/)
97 CONTINUE
RETURN
END
SUBROUTINE SPLOT(NK, NP, RA, PPL, SP, SLOT, NS)
DIMENSION RA(1), PPL(1), SP(NS, 1), SLOT(1)
C FIND NODE(S) WITH MAX. STRESS
TIS=0. $ MB=1
DO 22 LA = 1, NK
DO 23 LB = 1, NP
STRS=SP(LA, LB)
IF(STRS.LT.TIS) GO TO 23
TIS=STRS
23 CONTINUE
22 CONTINUE
DO 24 LC = 1, NK
DO 25 LD = 1, NP
TOS=SP(LC, LD)
IF(TOS.EQ.TIS) GO TO 26
25 CONTINUE
GO TO 24
26 RA(MB)=LD
MB=MB+1
24 CONTINUE
C PLOT STRESS AT CRITICAL NODE(S)
DO 27 LE = 1, 5
LF=RA(LE)
IF(LF.EQ.0) GO TO 27
DO 28 LG = 1, NK
28 SLOT(LG)=SP(LG, LF)
CALL QIKPLOT(SLOT, PPL, -40, 8H*STRESS*, 6H*LOAD*, -1)
WRITE(6, 45) LF
45 FORMAT(1H0, 30X, *CRITICAL NODE IS NODE NO. *, I3/)
27 CONTINUE
RETURN
END

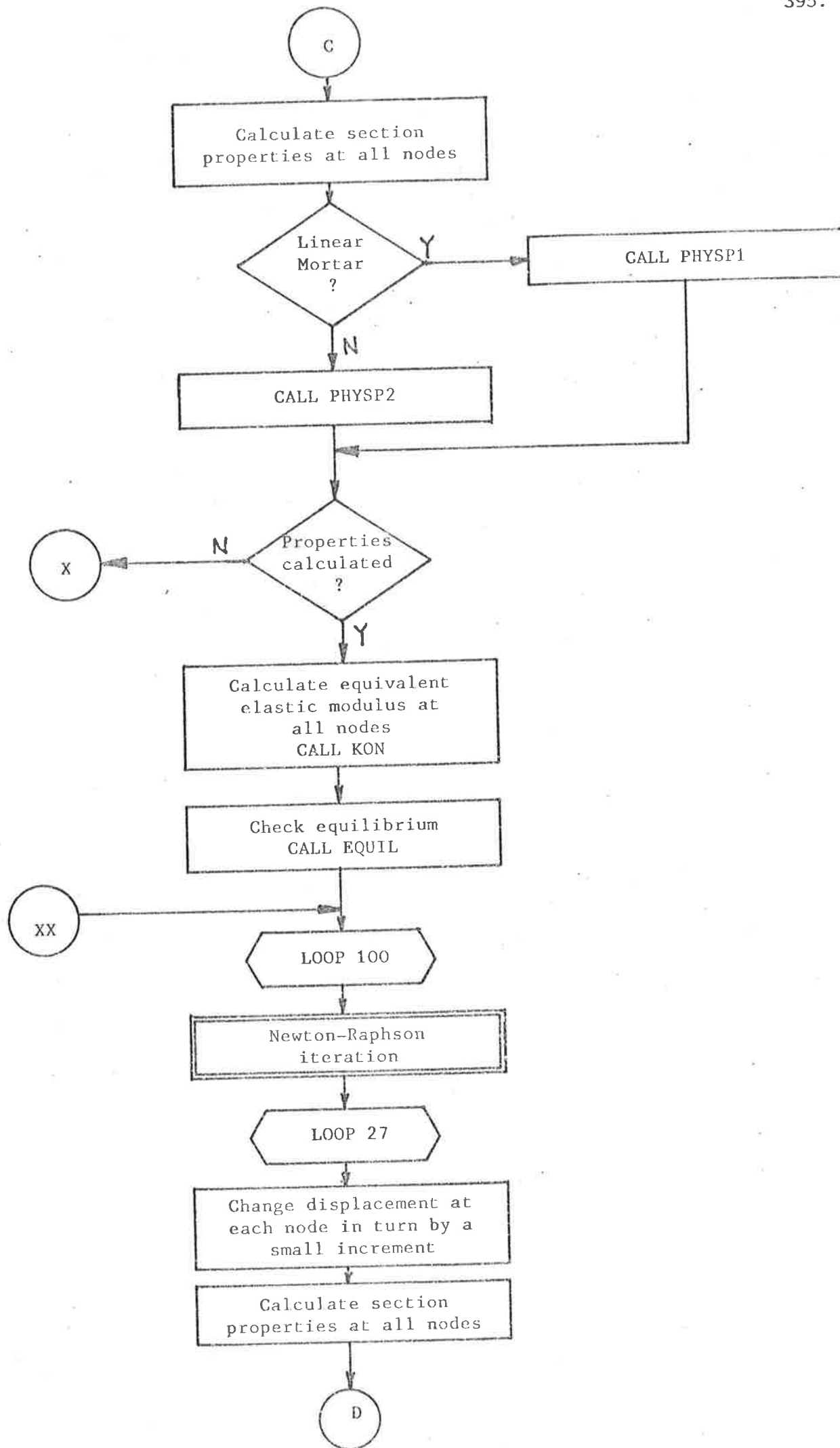
```

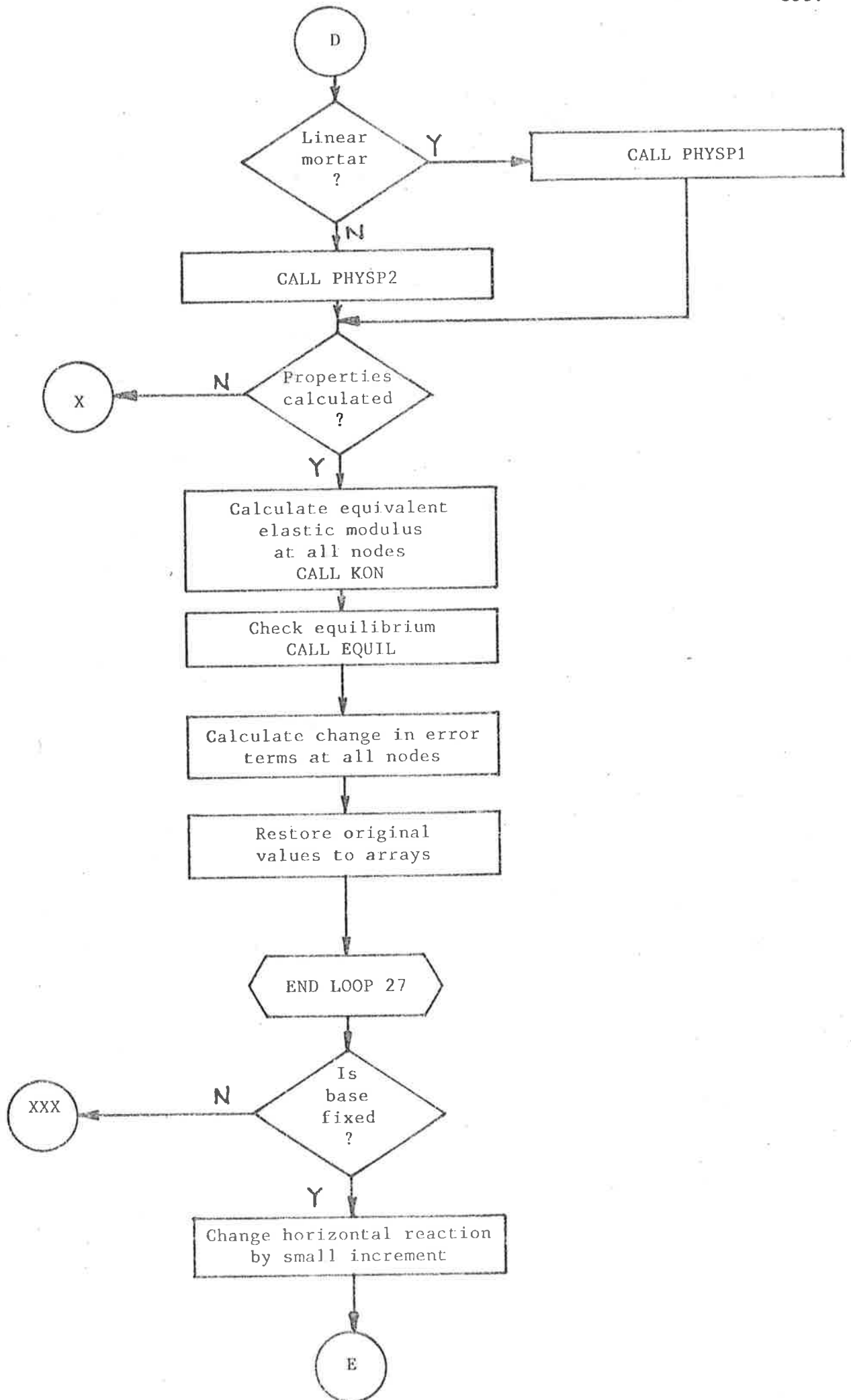
## C.3 FLOW CHARTS FOR PROGRAM PIER1

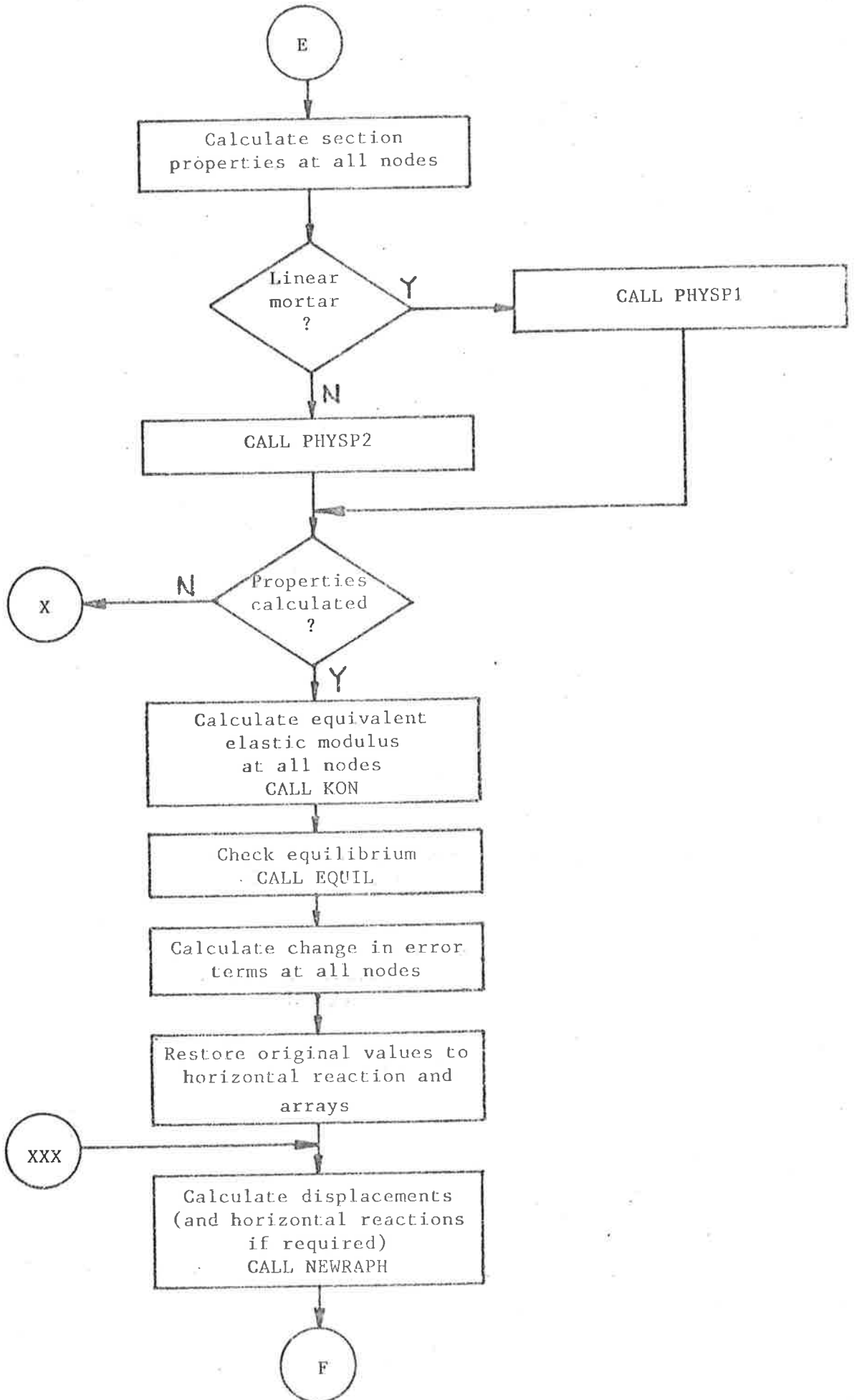


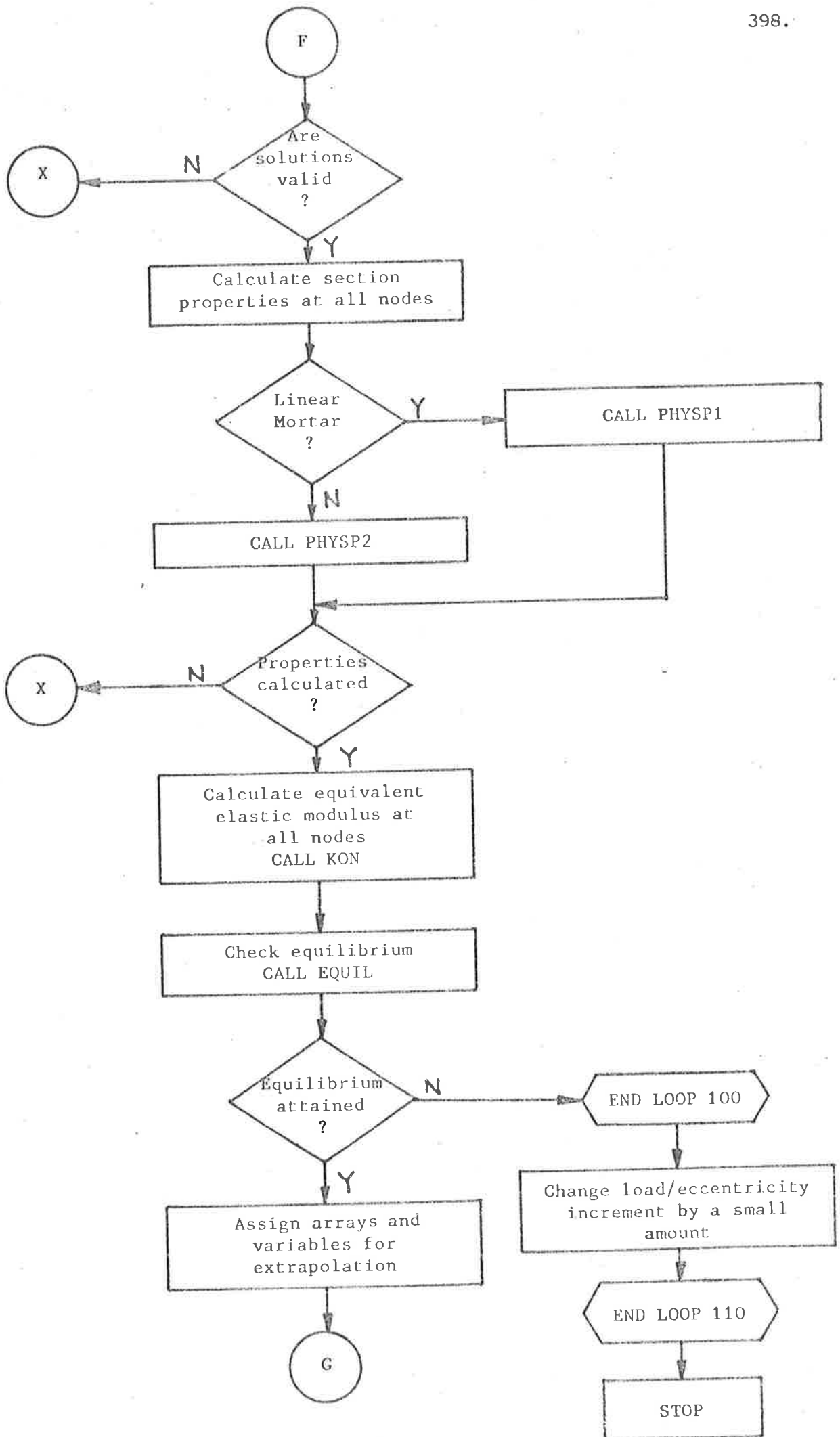




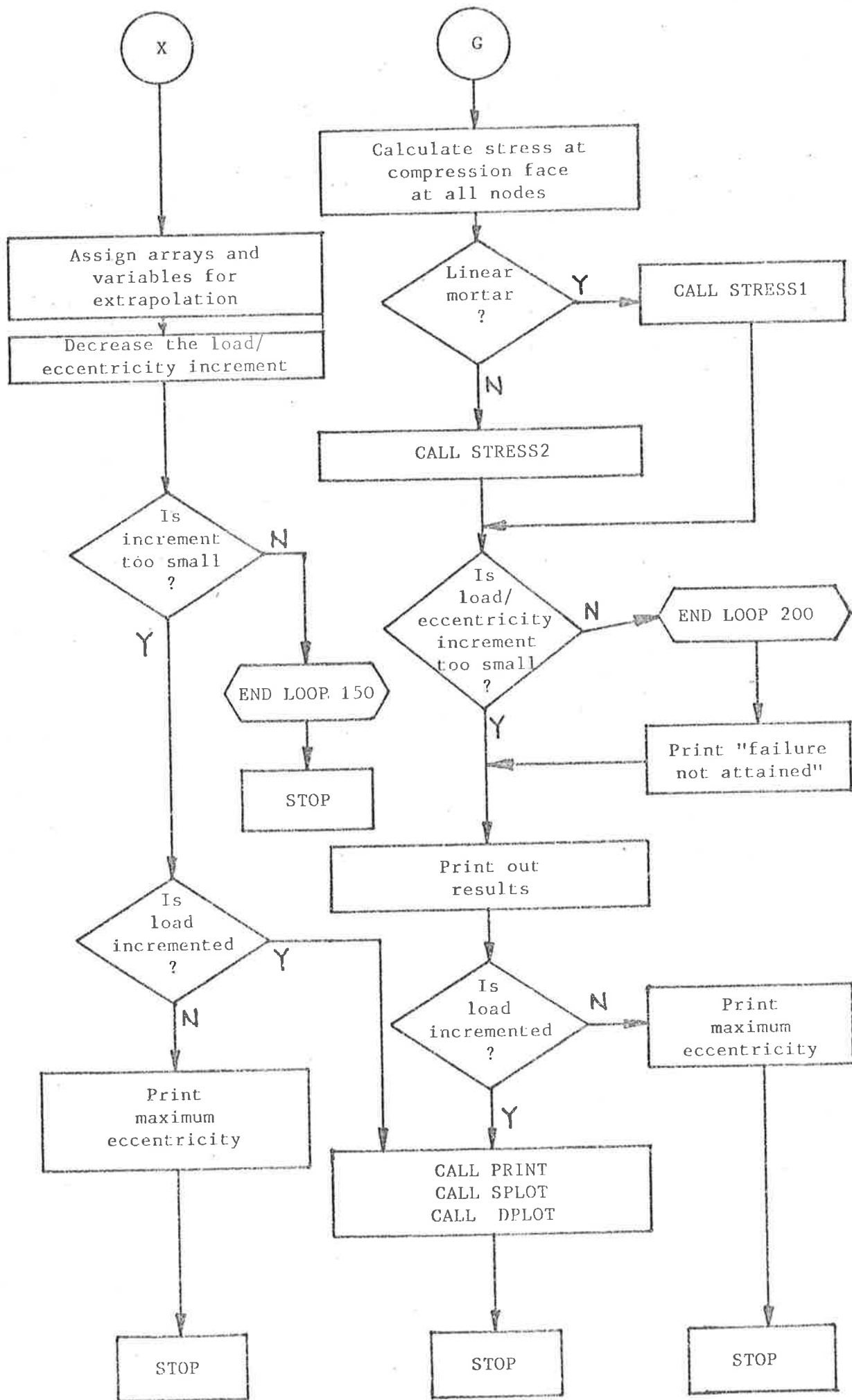


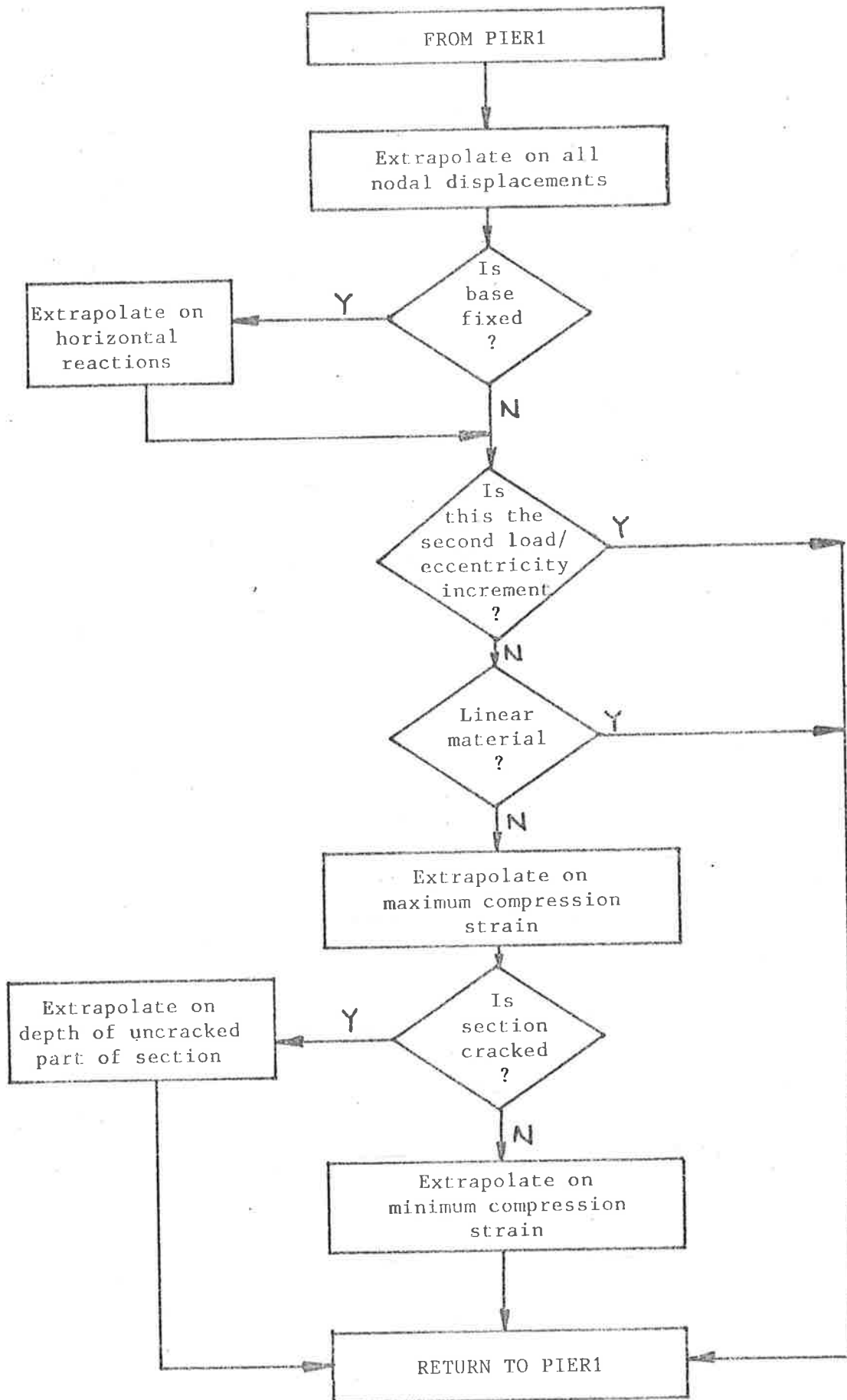




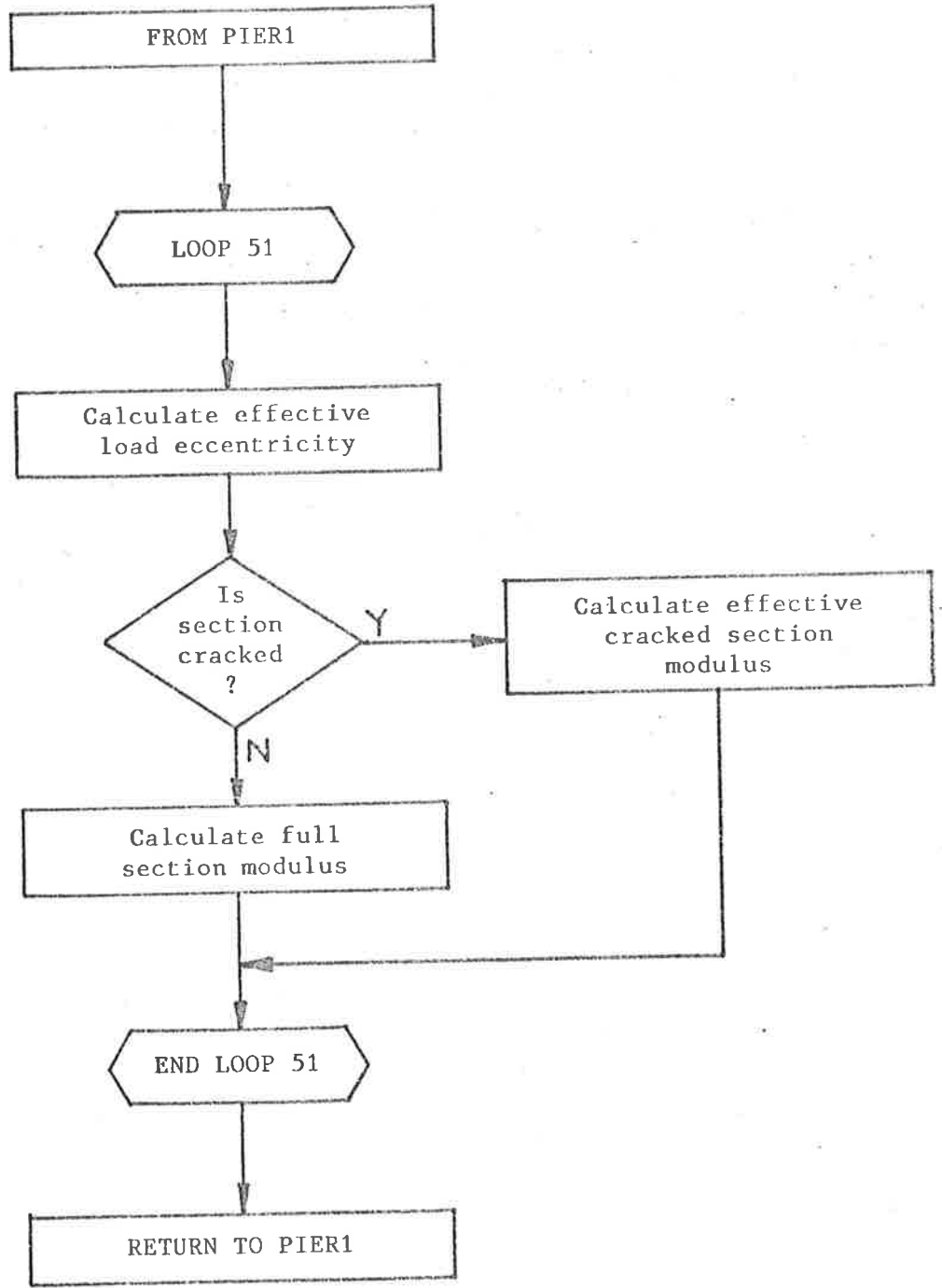






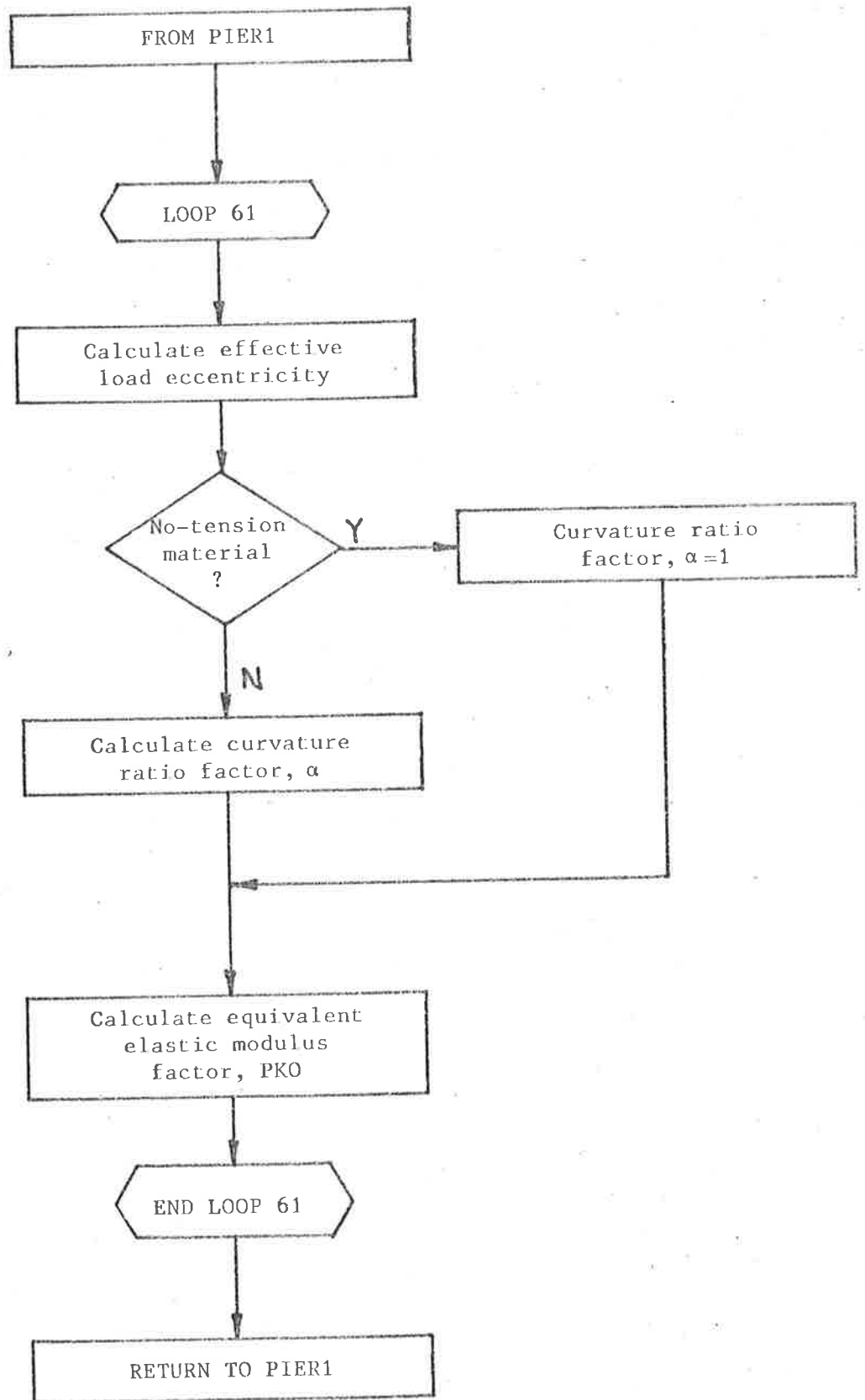


SUBROUTINE EXTRAP

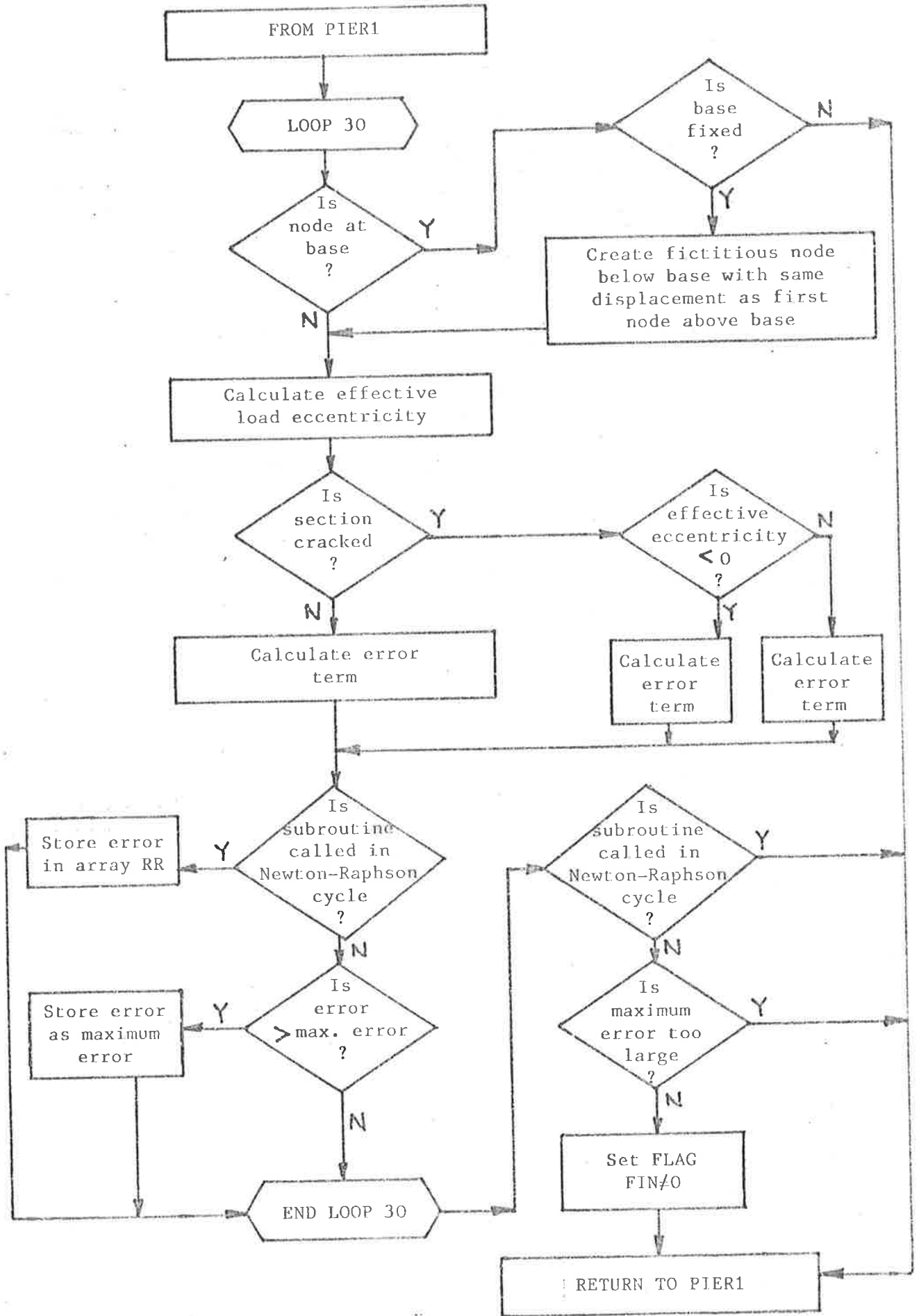


SUBROUTINE PHYSP1

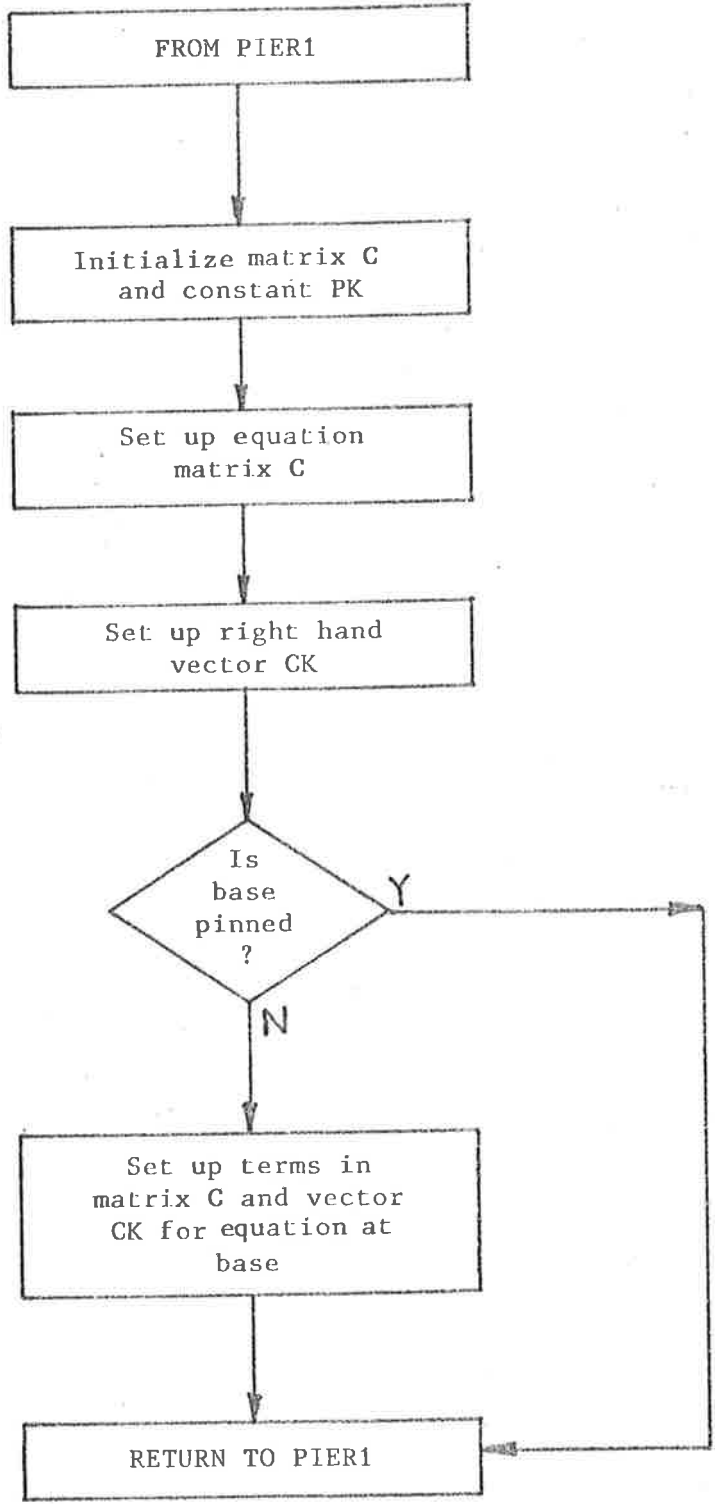




SUBROUTINE KON



SUBROUTINE EQUIL



SUBROUTINE MATCOM

MISCELLANEOUS SUBROUTINES

SUBROUTINE EULER: Calculates Critical Buckling Load of Pin-ended Wall.

SUBROUTINE DISPL: A Gauss Reduction routine on Matrix C and Vector CK Set up in MATCOM.

SUBROUTINE NEWGRAPH: A Gauss Reduction routine on Matrix RS and Vector R Set up by EQUIL and PIER1 in the Newton-Raphson Cycle.

SUBROUTINE STRESS1: Stresses for Linear Mortar.

SUBROUTINE STRESS2: Stresses for Non-linear Mortar.

SUBROUTINE PRINT: Routine for Output of Displacements and Stresses.

SUBROUTINE DPLOT: CYBER\* Plot of Displacements of Node with Maximum Displacement.

SUBROUTINE SPLOT: CYBER\* Plot of Stresses at Node with Maximum Stress.

\* NOTE: Plotting Routine in PROGRAM PIER1 is called QIKPLOT.



APPENDIX D  
BRICKWORK PRISM TESTS AND NON-LINEAR  
PROPERTIES OF MORTAR (Section 5.2.2.4(b))

Six brickwork prisms were constructed from the same batches of materials as the eight walls and cured identically with the walls (figure 5.12(a)). Each prism comprised four bricks and three mortar joints. All prisms were tested concurrently with the walls in a 5000KN capacity compression testing machine, two prisms axially, two prisms at an equal end eccentricity of 12.5mm ( $d/6$ ) and two prisms at an equal end eccentricity of 25.0mm ( $d/3$ ). All prisms were loaded through pin blocks both top and bottom (figure D.1) and the rotations at the mid-heights of the end bricks were measured on the eccentrically-loaded prisms. The failure loads and failure modes for the six prisms are summarized in Table D.1 and the vertical splitting failure modes of prisms 1 and 2 are shown in figure D.2. Vertical splitting occurred for a load eccentricity of  $d/6$  and brick spalling failure was evident at a load eccentricity of  $d/3$  (Table D.1).

Prism No.	Load Eccentricity (mm)	Failure Load (KN)	Failure Mode
1	zero	570	Vertical Splitting
2	zero	595	Vertical Splitting
3	12.5	270	Vertical Splitting
4	12.5	395	Vertical Splitting
5	25.0	184	Brick Spalling on Comp. Face
6	25.0	164	Brick Spalling on Comp. Face

Table D.1: Compression Failure of Brickwork Prisms

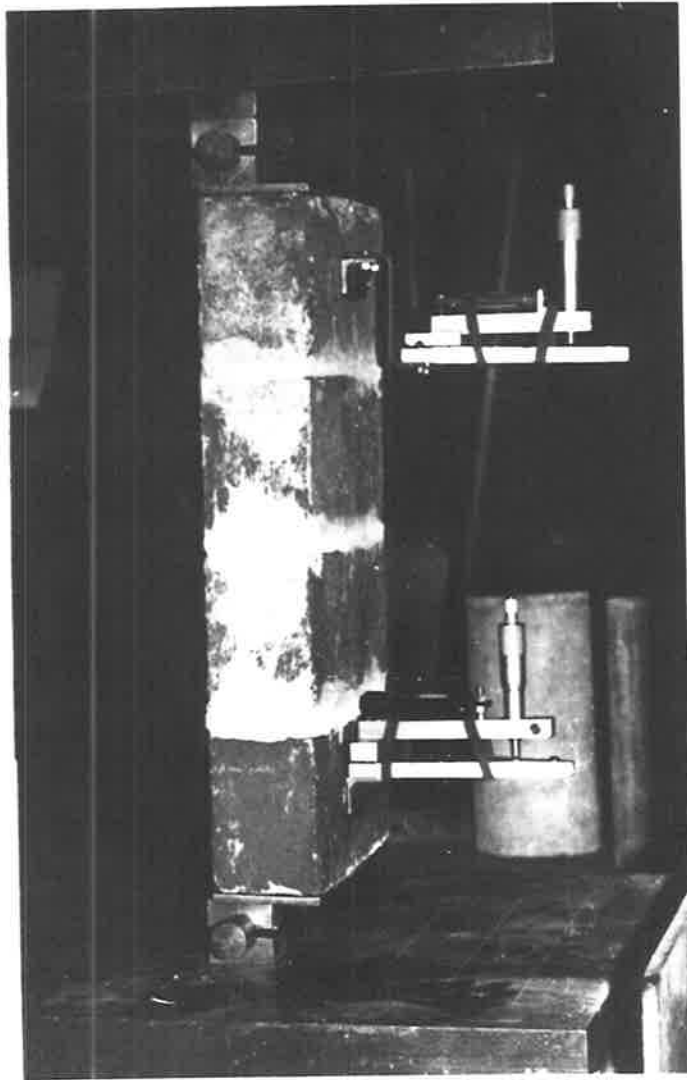


Figure D.1: Brickwork Prism  
Subjected to Eccentric Load

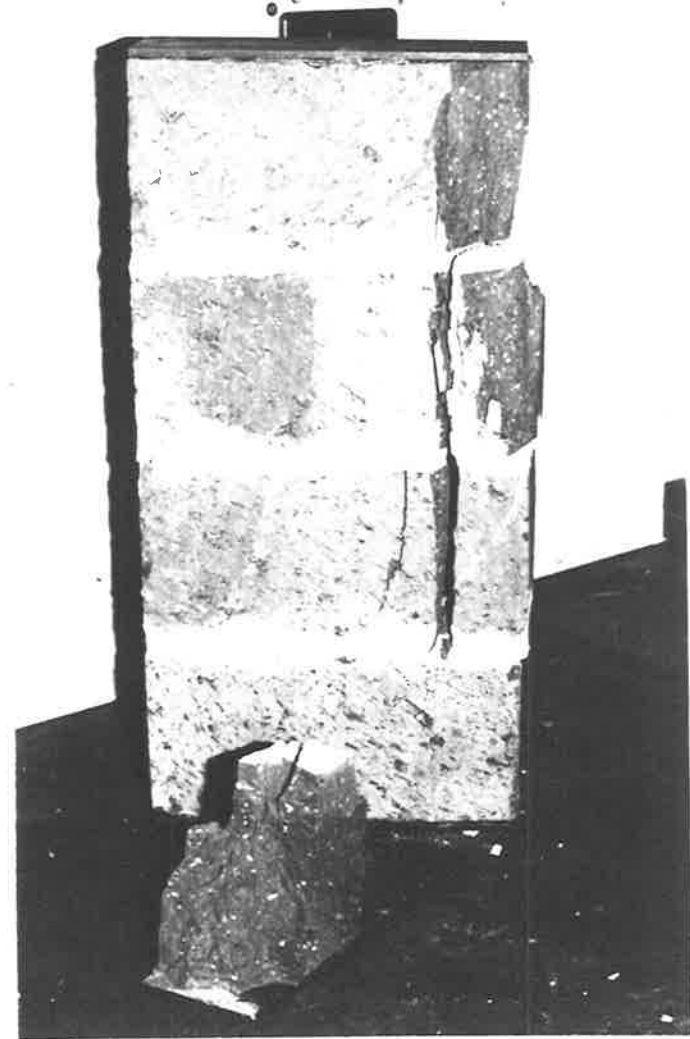


Figure D.2: Failure of Brickwork  
Prisms in Axial Compression (Prism 1  
at Rear)

The minimum axial stress at which failure occurred was 33.0MPa (prism 1, Table D.1) which may be chosen to be the crushing strength,  $\sigma_c$ , of the mortar in the brickwork.<sup>(117)</sup> An initial mortar modulus of  $8.3 \times 10^3$ MPa may be used (Section 5.2.2.3) and the non-linear stress-strain relationship may be assumed to be –

$$\sigma_m = E_m (\epsilon - K \epsilon^n) \quad (B.1)$$

in which  $E_m$  is  $8.3 \times 10^3$ MPa.

By using equations (B.2) and (B.3) in Appendix B, values of the coefficient, K, in equation (B.1) may be calculated for assumed values of exponent, n. Values of K, together with values of crushing strain,  $\epsilon_c$ , are shown in Table D.2 for various n. Equation (B.1) is plotted for the exponents, n, in figure D.3.

Exponent, n	Coefficient, K	Strain, $\epsilon_c (\times 10^{-3})$
3.0	9371	5.964
2.0	62.88	7.952
1.5	6.104	11.93
1.2	1.759	23.86

Table D.2: Constants in Equation (B.1) for Various Exponents, n

Although the rotations of the brickwork prisms were measured for the cases of eccentric loading, a comparison could not be made with calculated rotation values because the small number of bricks measured (three bricks in each of two prisms) was not a sufficient statistical sample (Section 5.2.2.3).

If an experimental program were to be carried out to test the non-linear behaviour of mortar in brickwork, a sample of at least six brickwork prisms should be tested axially to give an estimate of

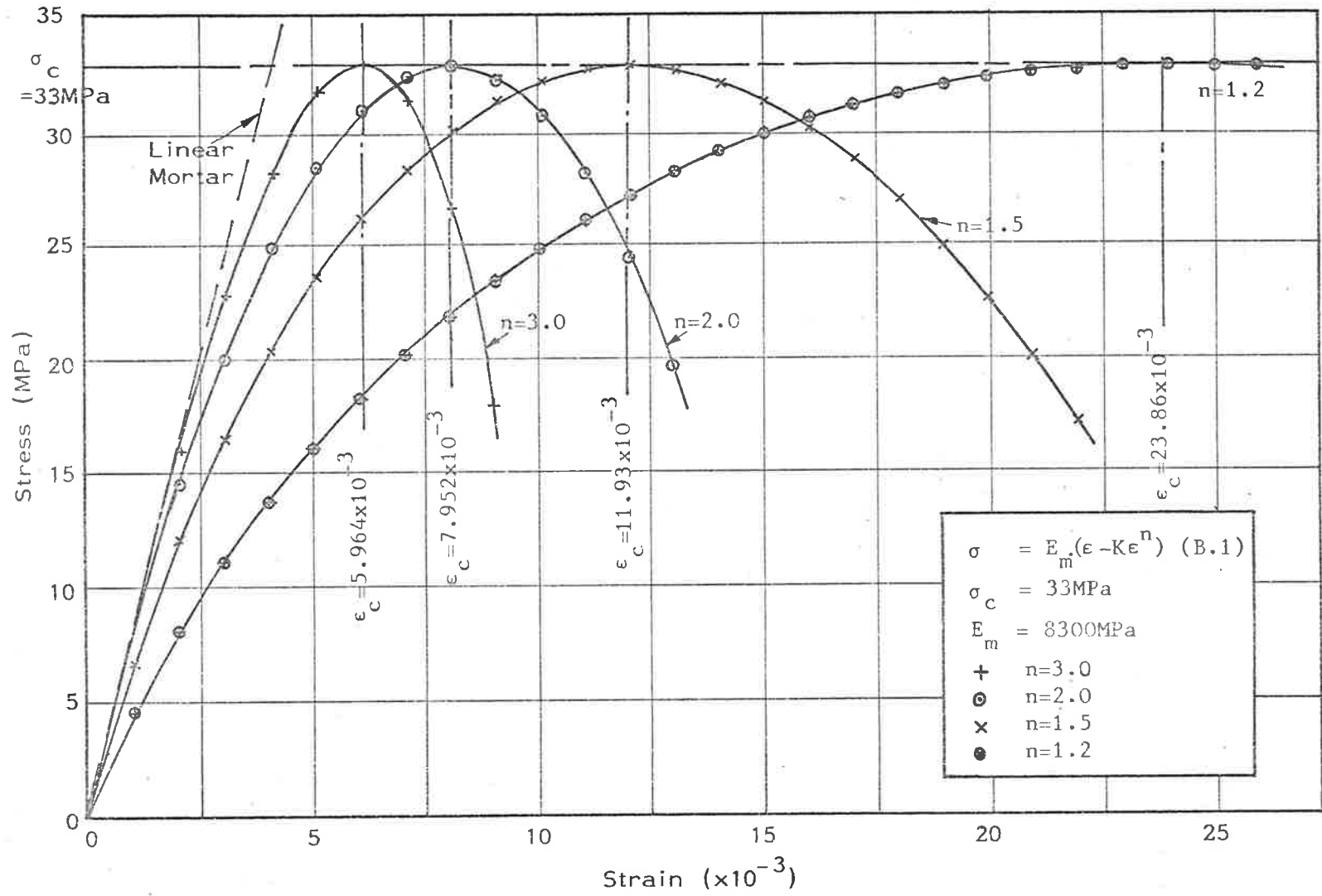


Figure D.3: Stress-strain Curves for Non-linear Mortars

the minimum axial crushing strength,  $\sigma_c$ , and six prisms should be tested at each chosen eccentricity to give a statistical comparison with the non-linear mortar analysis in PROGRAM PIER1.

APPENDIX E  
THREE-DIMENSIONAL FINITE ELEMENT  
PROGRAM MFYDCP

### E.1 INTRODUCTION

The stiffness of brickwork in bending and torsion may be affected by discrete cracking at the brick-mortar interfaces on the bedjoints and perpends (Sections 6.2.2, 6.2.3 and 6.2.4). The effects of such cracking may be calculated by using a three-dimensional finite element analysis. Commercially-produced packages may be expensive, if obtainable, and, because they are usually general purpose programs, they may require the capacity of virtual memory computers to solve large problems, say, of thirty elements or more. However, large problems requiring three-dimensional isoparametric elements may be solved using conventional core-storage computers by transferring data between central memory and disk storage as required. Such problems may be solved efficiently in terms of total calculation time by optimizing the total data transfer time.

Cheung and Yeo<sup>(126)</sup> described a two-dimensional finite element program in which a front-solver method was used to minimize the amount of data required in central memory at any time. Yeo extended the method to a three-dimensional version of the program, "MFY3D" (the program is unpublished) in which one of the three displacement vectors at each node was calculated at each step of the front-solver technique. The modified version of PROGRAM MFY3D (PROGRAM MFYDCP, Section E.3) also uses a front-solver method, but all three nodal displacements are calculated at each step by using 3x3 matrices throughout the equation reduction and backsubstitution stages. The total execution

time for PROGRAM MFYDCP as determined by the program control cards, was approximately 35 percent of that of PROGRAM MFY3D for the problem described in the following section; the total execution time for PROGRAM MFYDCP was approximately 40 minutes.

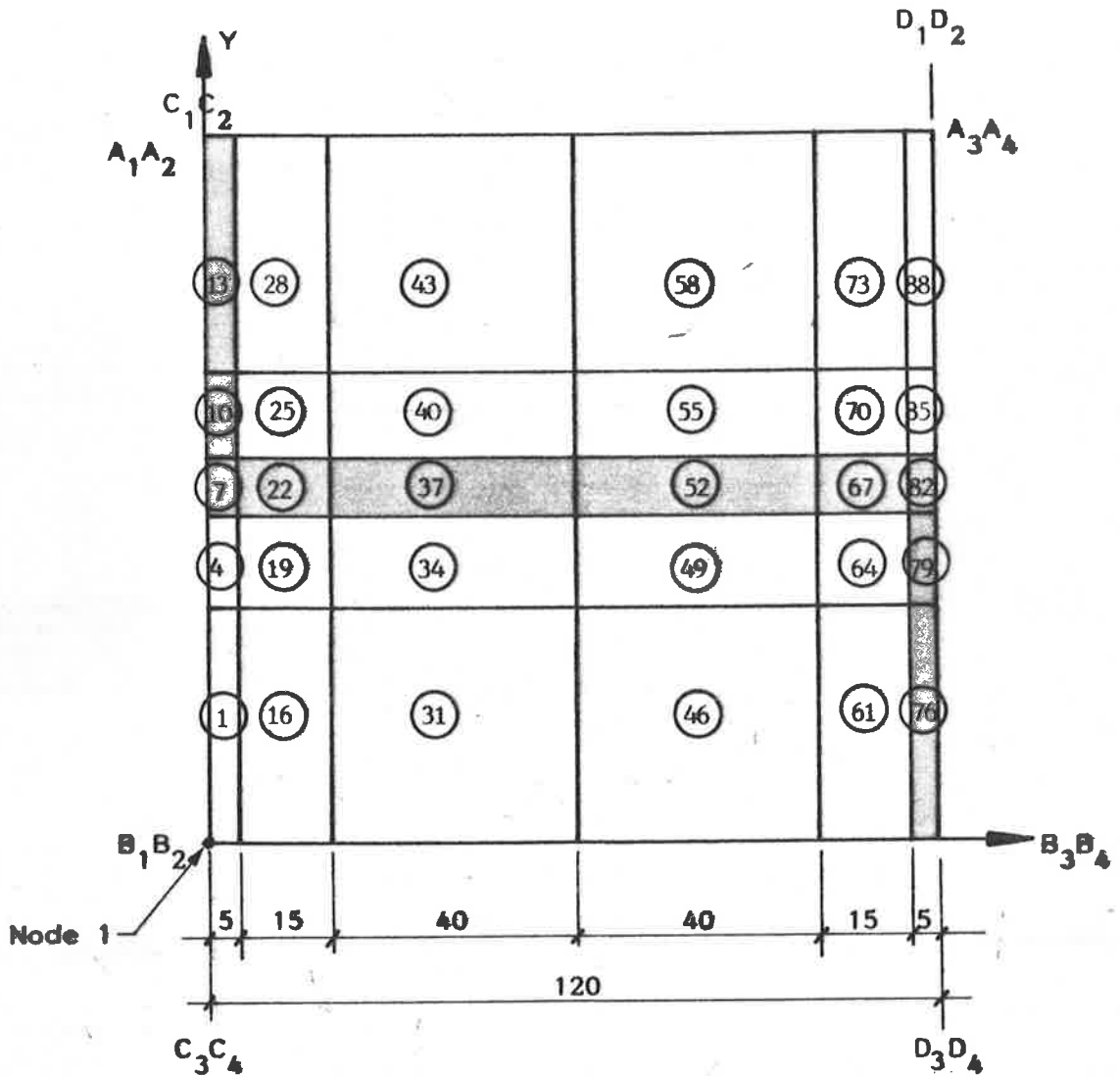
## E.2 THE FINITE ELEMENT SUBDIVISION

Figures E.1 and E.2 show the finite element subdivision of the panel module described in Chapter 6 (figure 6.1(b)). The elements close to the brick-mortar interfaces are specified to be smaller than other elements so that displacements and stresses may be calculated accurately in the regions of possible cracking.

Element definitions may be generated by computer but the uncoupled nodes on the perpends (Section 6.2.3, figure E.2) must be included into the input data file manually.

The element subdivision shown in figures E.1 and E.2 require a front width of 240 equation coefficients for uncracked brickwork. The front width for brickwork with both perpend and bedjoint cracking is 258 coefficients. PROGRAM MFYDCP (Section E.3) requires a central memory area (on a CYBER 173 computer) of approximately 130K (octal) and requires a disk storage space of approximately 900,000 words.

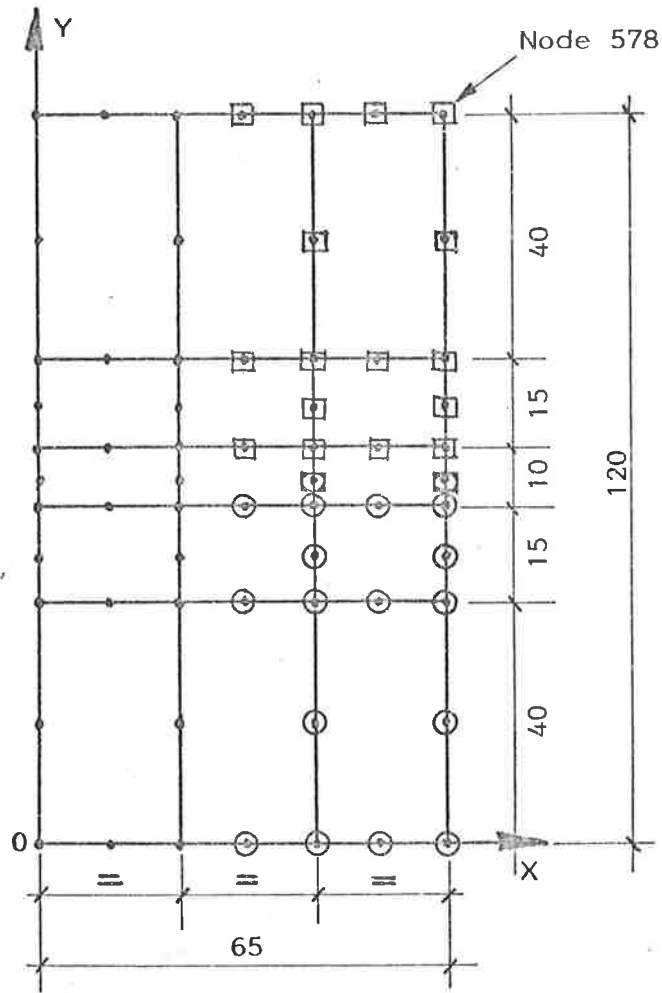
A skeleton flow chart for PROGRAM MFYDCP is presented in Section E.4.



Mortar is shown Shaded  
Element Numbers are Circled

**Figure E.1: Side Elevation of Panel Module (Section 6.2.1)  
Showing Finite Element Subdivision**





- ⊙ Uncoupled Nodes on section plane  $z=5$
  - ⊠ Uncoupled Nodes on section plane  $z=115$
- } refer to figure E.1

Figure E.2: End Elevation of Panel Module (Section 6.2.1) showing Finite Element Subdivision and Uncoupled Nodes for the Analysis of Horizontal Bending (Section 6.2.3) and Torsion (Section 6.2.4)

## E.3 LISTING OF PROGRAM MFYDCP

```

PROGRAM MFYDCP(INPUT=65,OUTPUT=65,TAPE5=INPUT,TAPE6=OUTPUT,TAPE2,
1          TAPE3,TAPE4,TAPE20=0,TAPE21=0)

```

```

COMMON/MFY1/XX(20),YY(20),ZZ(20)
COMMON/MFY2/WTFUN(3),VECTLC(3)
COMMON RS(60),AW(9),S(1830),SHP(20),X(20),Y(20),Z(20),CW(9)
COMMON PIVOT(3,3),PINVOT(3,3),CFACT(3,3),DFACT(3,3)
COMMON DX(20),DY(20),DZ(20),U(20),V(20),W(20),SIGMA(6),D(12)
COMMON NELDES(20),NELDEF(20)
COMMON DISP(120,3),REACT( 9,3),NREACT( 9),MAT( 90)
COMMON LDEST(700),LDEF( 91,20),CORD(700,3)
COMMON YM(5),PR(5),WT(5),AYM(5),EXPN(5),GG(5),APR(5)
COMMON SRS(260),SS(15000),REQ(2000),LREQ(300)
COMMON NDISP(120,4),DISPL(700,3),NW(260),JW(260),NDISPZ(200,4)
COMMON XREQ(260),YREQ(260),ZREQ(260),XRAQ(260),YRAQ(260),ZRAQ(260)
COMMON YMOD,PRAT,WEIGHT,AYMOD,AGG,EXPAN,WX,WY,WZ,XL,YL,ZL
COMMON NVABZ,MAXDIS,NIC,LIV,NNODZ,NSNW,NFNW,MAXNDZ,MAXNEL,NEL,NTN
COMMON MTM,MAXFW,MAXREQ,MAXNW,MAXNOD,MAXMAT,MAXSS
COMMON DETJ,NPUT,IPRINC,NPRINC,NRULE,LIN,NSTOP
COMMON L20,L21,NK,KMAX,KS,KF

```

```

C          *****
C          *
C          *   PROGRAM MFYDCP IS A REVISED VERSION OF A *
C          *   THREE-DIMENSIONAL FINITE ELEMENT PROGRAM *
C          *   ( PROGRAM MFY3D ) WRITTEN BY MICHAEL F YEO *
C          *   AT THE UNIVERSITY OF ADELAIDE, *
C          *   SOUTH AUSTRALIA *
C          *
C          *   THIS REVISED VERSION WAS WRITTEN BY *
C          *   DAVID C. PAYNE AS PART OF THE REQUIREMENTS *
C          *   OF A DOCTOR OF PHILOSOPHY DEGREE AT THE *
C          *   UNIVERSITY OF ADELAIDE ( SUBMITTED 1982 ) *
C          *
C          *   THE PROGRAM USES 90 20-NODE ISOPARAMETRIC *
C          *   3-DIMENSIONAL ELEMENTS TO ANALYSE THE *
C          *   BENDING OF BRICKWORK IN STRETCHER BOND *
C          *   AND HAS BEEN WRITTEN FOR A CYBER 173 *
C          *   COMPUTER FOR WHICH THE MAXIMUM CM IS *
C          *   150K AND THE MAXIMUM DISK STORAGE SPACE *
C          *   IS 900 000 WORDS *
C          *
C          *   NO DOCUMENTATION ON INPUT DATA REQUIREMENTS *
C          *   IS GIVEN IN THIS PROGRAM *
C          *
C          *   THE 17 LINES OF COMMON STATEMENTS LISTED *
C          *   ABOVE ARE REQUIRED IN ALL SUBROUTINES EXCEPT *
C          *   SUBROUTINE CLOKIT(N). FOR CONVENIENCE IN *
C          *   LISTING THE PROGRAM, THE COMMON STATEMENTS *
C          *   ARE ABBREVIATED TO THE FOLLOWING---- *
C          *
C          *   ** INSERT 17 LINES OF COMMON STATEMENTS *
C          *   HERE ** *
C          *****

```

C  
C  
C  
C

INITIALIZE PROGRAM VARIABLES

```

MAXRCT=0
MAXFW=0
NRULE=3
MAXMAT=1
NPUT=0
IPRINC=0
NPRINC=0
MAXNEL=0
MAXNOD=0
NVABZ=3
NNODZ=20
MAXSS=15000
MAXREQ=2000
MAXDIS=0
MAXNDZ=0
MAXNW=260
CALL CLOKIT(1)
CALL INDAT
CALL CLOKIT(2)
CALL PREFNT
CALL CLOKIT(3)
CALL STIFN
CALL CLOKIT(4)
CALL FRONT
CALL CLOKIT(5)
CALL BAKSUB
CALL CLOKIT(6)
CALL STRESS
STOP
END
SUBROUTINE ASMBLE

```

\*\* INSERT 17 LINES OF COMMON STATEMENTS HERE \*\*

C  
C  
C

```

DO 26 KK = 1,NK
N1=0
DO 24 INOD=1,NNODZ
IDES=NELDES(INOD)
I1=(IDES-1)*NVABZ
I2=(INOD-1)*NVABZ
IF(KK.NE.1) GO TO 4
DO 3 I=1,NVABZ
SRS(I1+I)=SRS(I1+I)+RS(I2+I)
3 CONTINUE
4 DO 23 JNOD=INOD,NNODZ
JDES=NELDES(JNOD)
I3=(JDES-1)*NVABZ
I4=(JNOD-1)*NVABZ
DO 22 I=1,NVABZ

```

```

ISS=I1+I
NW(ISS)=1
IS=I2+I
DO 20 J=1,NVABZ
JSS=I3+J
IF(IDES.GT.JDES) GO TO 19
JS=I4+J
IF(IS.GT.JS) GO TO 20
N1=N1+1
LOC=JW(ISS)+JSS-ISS
IF(LOC.LT.KS.OR.LOC.GT.KF) GO TO 20
LOC=LOC-KS+1
SS(LOC)=SS(LOC)+S(N1)
GO TO 20
19 N1=N1+1
LOC=JW(JSS)+ISS-JSS
IF(LOC.LT.KS.OR.LOC.GT.KF) GO TO 20
LOC=LOC-KS+1
SS(LOC)=SS(LOC)+S(N1)
20 CONTINUE
22 CONTINUE
23 CONTINUE
24 CONTINUE
IF(KK.EQ.NK) GO TO 26
BUFFER OUT(L21,1) (SS(1),SS(MAXSS))
IF(UNIT(L21)) 11,12,13
11 CONTINUE
BUFFER IN(L20,1) (SS(1),SS(MAXSS))
KS=KS+MAXSS
KF=KF+MAXSS
IF(UNIT(L20)) 14,12,13
14 CONTINUE
26 CONTINUE
CALL RESETT
RETURN
12 STOP
13 STOP
END
SUBROUTINE BAKSUB

```

\*\* INSERT 17 LINES OF COMMON STATEMENTS HERE \*\*

C  
C  
C

```

DO 300 NEL=1,MAXNEL
MEL=MAXNEL+1-NEL
WRITE(6,1005) MEL
DO 299 IN=1,NNODZ
N1=NNODZ+1-IN
NIC=-LDEF(MEL,N1)
IF(NIC.LE.0) GO TO 299
IF(NTN.NE.0) GO TO 219
BACKSPACE 2
READ(2) MTM,NTN,REQ,LREQ
BACKSPACE 2

```

```

219 MTM=MTM-NVABZ
    NSNW=LREQ(MTM+1)
    NFNW=LREQ(MTM+2)
    LIV=LREQ(MTM+3)
    NTN=NTN-NVABZ
    DO 230 I = 1,NVABZ
C   OVERWRITE XREQ WITH REDUCED RIGHT HAND SIDE COEFFICIENTS
    NTN=NTN+1
    XREQ(I)=REQ(NTN)
230 CONTINUE
C   EXTRACT MATRIX PIVOT FROM REQ
    NPIVOT=NTN-NVABZ+3*(LIV-NFNW)
    DO 221 J = 1,NVABZ
    DO 222 K = 1,NVABZ
    NPIVOT=NPIVOT+1
    PINVOT(J,K)=REQ(NPIVOT)
    REQ(NPIVOT)=0.0
222 CONTINUE
221 CONTINUE
    N2=NTN-NVABZ+3*(NSNW-NFNW-1)
    NTN=N2
    DO 225 J = NSNW,NFNW,NVABZ
C   EXTRACT MATRIX FOR BACKSUBSTITUTION FROM REQ
    DO 226 I = 1,NVABZ
    DO 227 K = 1,NVABZ
C   OVERWRITE MATRIX CFACT
    N2=N2+1
    CFACT(I,K)=REQ(N2)
227 CONTINUE
226 CONTINUE
    DO 228 L = 1,NVABZ
    DO 229 I = 1,NVABZ
    XREQ(L)=XREQ(L)-CFACT(L,I)*SRS(J+I-1)
229 CONTINUE
228 CONTINUE
225 CONTINUE
    DO 231 I = 1,NVABZ
    SMULT=0.
    DO 232 J = 1,NVABZ
    SMULT=SMULT+PINVOT(I,J)*XREQ(J)
232 CONTINUE
    SRS(LIV+I)=SMULT
    DISPL(NIC,I)=SMULT
231 CONTINUE
    LIV=LIV+1
    CALL POSTCN
299 CONTINUE
300 CONTINUE
C   RESTORE ELEMENTS OF CFACT TO ZERO
    DO 233 I = 1,NVABZ
    DO 234 J = 1,NVABZ
    CFACT(I,J)=0.0
234 CONTINUE
233 CONTINUE
    RETURN
1005 FORMAT(///,5X,18HREACTIONS ELEMENT ,I3)

```

END  
BLOCK DATA

C  
C  
C  
C  
C

\*\* INSERT 17 LINES OF COMMON STATEMENTS HERE \*\*

DATA XX/1.0,1.0,1.0,0.0,-1.0,-1.0,-1.0,0.0,1.0,1.0,-1.0,-1.0,1.0,  
1 1.0,1.0,0.0,-1.0,-1.0,-1.0,0.0/  
DATA YY/-1.0,0.0,1.0,1.0,1.0,0.0,-1.0,-1.0,-1.0,1.0,1.0,-1.0,-1.0,  
1 0.0,1.0,1.0,1.0,0.0,-1.0,-1.0/  
DATA ZZ/-1.0,-1.0,-1.0,-1.0,-1.0,-1.0,-1.0,-1.0,0.0,0.0,0.0,0.0,  
1 1.0,1.0,1.0,1.0,1.0,1.0,1.0,1.0/  
DATA WTFUN/0.5555555556,0.8888888889,0.5555555556/  
DATA VECTLC/-0.77459666924,0.0,0.77459666924/  
END  
SUBROUTINE CHK(N)

C  
C  
C  
C  
C

\*\* INSERT 17 LINES OF COMMON STATEMENTS HERE \*\*

10 IF(N.GE.KS.AND.N.LE.KF) GO TO 20  
BUFFER OUT(L21,1) (SS(1),SS(MAXSS))  
IF(UNIT(L21)) 11,12,13  
11 CONTINUE  
BUFFER IN(L20,1) (SS(1),SS(MAXSS))  
KS=KS+MAXSS  
KF=KF+MAXSS  
IF(UNIT(L20)) 14,12,13  
14 CONTINUE  
GO TO 10  
20 N=N-KS+1  
RETURN  
12 STOP  
13 STOP  
END  
SUBROUTINE CLOKIT(N)

C  
C

CALL SECOND(ASECS)  
WRITE(6,1000) N,ASECS  
1000 FORMAT(1H0,5X,\*LOCATION = \*,I3,10X,\*TIME = \*,F10.3,\* SECS\*)  
RETURN  
END  
SUBROUTINE DMAT(I1)

\*\* INSERT 17 LINES OF COMMON STATEMENTS HERE \*\*

C  
C  
C

YMOD=YM(I1)

```

PRAT=PR(I1)
WEIGHT=WT(I1)
AYMOD=AYM(I1)
AGG=GG(I1)
EXPAN=EXPN(I1)
APRAT=APR(I1)
IF(AYMOD.EQ.0.0) AYMOD=YMOD
IF(APRAT.EQ.0.0) APRAT=PRAT
IF(AGG.EQ.0.0) AGG=YMOD/(2.0*(1.0+PRAT))
A1=1.0+PRAT
A2=YMOD/AYMOD
A3=(1.0-PRAT-2.0*A2*APRAT*APRAT)
A4=A1*A3
D(1)=YMOD*(1.0-A2*APRAT*APRAT)/A4
D(2)=YMOD*(PRAT+A2*APRAT*APRAT)/A4
D(3)=YMOD*APRAT/A3
D(4)=D(2)
D(5)=D(1)
D(6)=D(3)
D(7)=D(3)
D(8)=D(6)
D(9)=AYMOD*(1.0-PRAT)/A3
D(10)=YMOD/(2.0*(1.0+PRAT))
D(11)=AGG
D(12)=AGG
RETURN
END
SUBROUTINE FRONT

```

\*\* INSERT 17 LINES OF COMMON STATEMENTS HERE \*\*

C  
C  
C

```

DIMENSION CIS(3,3),CSJ(3,3)
REWIND 2
REWIND 4
DO 1 I=1,MAXFW
NW(I)=0
1 CONTINUE
JW(1)=1
DO 2 I=2,MAXFW
JW(I)=JW(I-1)+MAXFW+2-I
2 CONTINUE
CALL SETUP
MTM=0
NTN=0
DO 42 NEL=1,MAXNEL
READ(4) S,RS,NELDEF,NELDES
WRITE(6,13) NEL
13 FORMAT(10X,*LAST EL. READ NO.*,I5)
CALL CLOKIT(7)
CALL ASMBLE
CALL CLOKIT(8)
NSNW=1
NFW=MAXFW

```

```

DO 40 NOD=1, NNODZ
NIC=-NELDEF(NOD)
IF(NIC.LE.0) GO TO 40
LIN=NELDES(NOD)
C SET START FLAG NSNW FOR NODE VECTOR NW ( FIRST NON-ZERO ROW )
9 IF(NW(NSNW).NE.0) GO TO 10
NSNW=NSNW+1
GO TO 9
C SET FINISH FLAG NFNW FOR NODE VECTOR NW ( LAST NON-ZERO ROW )
10 IF(NW(NFNW).NE.0) GO TO 11
NFNW=NFNW-1
GO TO 10
C START AND FINISH FLAGS FOR NODE NIC ARE SET
11 CALL PRECON
LIV=(LIN-1)*NVABZ
N13=NTN+1
IF((NTN+(NFNW+2-NSNW)*3).LT.MAXREQ) GO TO 12
WRITE (2) MTM,NTN,REQ,LREQ
MTM=0
NTN=0
N13=1
C EXTRACT THREE EQUATIONS AT NODE NIC FROM STIFFNESS MATRIX SS
C STORE EACH ROW IN MATRICES XREQ,YREQ ZREQ IN TURN
C START BY STORING GROUPS OF THREE DOWN "COLUMN" UP TO PIVOT MATRIX
12 NXN=0
NYN=0
NZN=0
IREQ=1
IF((LIV+1).EQ.NSNW) GO TO 8
C FIRST NON-ZERO MATRIX IS ON DIAGONAL
DO 24 IAI = NSNW,LIV,3
IF(NW(IAI).EQ.0) GO TO 62
C NW EQ 0 IMPLIES ROWS AND COLUMNS IAI,IAI+1,IAI+2 ARE ALL ZERO
DO 25 I = 1,NVABZ
II=IAI+I-1
GO TO ( 26,27,28 ),I
26 DO 29 J = 1,NVABZ
NXN=NXN+1
N5=JW(II)+LIV-II+J
CALL CHK(N5)
XREQ(NXN)=SS(N5)
IF(NXN.GT.MAXNW) WRITE(6,1060)
SS(N5)=0.0
29 CONTINUE
GO TO 25
27 DO 30 K = 1,NVABZ
NYN=NYN+1
N5=JW(II)+LIV-II+K
CALL CHK(N5)
YREQ(NYN)=SS(N5)
IF(NYN.GT.MAXNW) WRITE(6,1060)
SS(N5)=0.0
30 CONTINUE
GO TO 25
28 DO 31 L = 1,NVABZ
NZN=NZN+1

```



```

N5=JW(II)+LIV-II+L
CALL CHK(N5)
ZREQ(NZN)=SS(N5)
SS(N5)=0.0
31 CONTINUE
25 CONTINUE
GO TO 24
62 DO 63 JF = 1,NVABZ
    NXN=NXN+1
    NYN=NYN+1
    NZN=NZN+1
    XREQ(NXN)=YREQ(NYN)=ZREQ(NZN)=0.0
63 CONTINUE
24 CONTINUE
    IREQ=NXN+1
C   STORE PIVOT MATRIX
C   FIRST STORE FIRST ROW AND THEN REMAINDER OF MATRIX XREQ
C   THEN STORE SECOND ROW PAST DIAGONAL AND REMAINDER OF MATRIX YREQ
C   FINALLY STORE THIRD ROW AT DIAGONAL AND REMAINDER OF MATRIX ZREQ
8 DO 32 J = 1,NVABZ
    II=LIV+J
    DO 36 K = J,NVABZ
        N5=JW(II)+K-J
        CALL CHK(N5)
        GO TO ( 33,34,35 ),J
33 NXN=NXN+1
    XREQ(NXN)=0.
    PIVOT(J,K)=SS(N5)
    SS(N5)=0.0
    GO TO ( 36,37,38 ),K
37 NYN=NYN+1
    PIVOT(K,J)=PIVOT(J,K)
    YREQ(NYN)=0.0
    GO TO 36
38 NZN=NZN+1
    PIVOT(K,J)=PIVOT(J,K)
    ZREQ(NZN)=0.
    GO TO 36
34 NYN=NYN+1
    YREQ(NYN)=0.0
    PIVOT(J,K)=SS(N5)
    SS(N5)=0.0
    IF(K.EQ.J) GO TO 36
    NZN=NZN+1
    PIVOT(K,J)=PIVOT(J,K)
    ZREQ(NZN)=0.
    GO TO 36
35 NZN=NZN+1
    ZREQ(NZN)=0.
    PIVOT(J,K)=SS(N5)
    SS(N5)=0.0
36 CONTINUE
C   STORE REMAINDER OF ROW ( LIV+J ) IN ARRAYS XREQ,YREQ,ZREQ
    IF((LIV+NVABZ).EQ.NFNW) GO TO 32
C   PIVOT IS LAST NON-ZERO MATRIX ON DIAGONAL
    N6=JW(II)+NVABZ-J+1

```

```

N7=JW(II)+NFW-II
DO 39 N18 = N6,N7
N8=N18
GO TO (41,43,44),J
41 NXN=NXN+1
CALL CHK(N8)
XREQ(NXN)=SS(N8)
IF(NXN.GT.MAXNW) WRITE(6,1060)
SS(N8)=0.0
GO TO 39
43 NYN=NYN+1
CALL CHK(N8)
YREQ(NYN)=SS(N8)
IF(NYN.GT.MAXNW) WRITE(6,1060)
SS(N8)=0.0
GO TO 39
44 NZN=NZN+1
CALL CHK(N8)
ZREQ(NZN)=SS(N8)
IF(NZN.GT.MAXNW) WRITE(6,1060)
SS(N8)=0.0
39 CONTINUE
32 CONTINUE
C LEFT HAND SIDE OF THREE EQUATIONS FOR NODE NIC ARE NOW STORED
C IN CORE IN ARRAYS XREQ,YREQ AND ZREQ
C SORT COEFFICIENTS FOR ALL 3X3 MATRICES AND STORE AS GROUPS OF
C 1X9 IN ARRAY REQ FOR STORAGE ON TAPE2
IR=(LIV+1-NSNW)/3
IF(IR.EQ.0) GO TO 51
C IR EQ 0 IMPLIES FIRST NON-ZERO MATRIX FOR EQUATIONS AT NODE NIC
C IS ON MAIN DIAGONAL
DO 45 IL = 1,IR
IN=IL-1
IS=IN*NVABZ
DO 46 IK = 1,NVABZ
IV=IS+IK
DO 47 IT = 1,NVABZ
NTN=NTN+1
GO TO (48,49,50),IT
48 REQ(NTN)=XREQ(IV)
GO TO 47
49 REQ(NTN)=YREQ(IV)
GO TO 47
50 REQ(NTN)=ZREQ(IV)
47 CONTINUE
46 CONTINUE
45 CONTINUE
C STORE PIVOT POSITIONS IN REQ AS ALL ZERO
51 DO 52 IJ = 1,NVABZ
DO 58 JI = 1,NVABZ
IF(IJ.EQ.1.AND.JI.EQ.1) N9=NTN
NTN=NTN+1
REQ(NTN)=0.0
58 CONTINUE
52 CONTINUE
C STORE REMAINDER OF 3X3 MATRICES PAST PIVOT IN REQ

```

```

IF((LIV+NVABZ).EQ.NFNW) GO TO 53
N1=LIV+NVABZ+1
DO 54 II = N1,NFNW,NVABZ
IREQ=IREQ+NVABZ
DO 59 JJ = 1,NVABZ
DO 60 KK = 1,NVABZ
LL=IREQ+KK-1
NTN=NTN+1
GO TO (55,56,57),JJ
55 REQ(NTN)=XREQ(LL)
GO TO 60
56 REQ(NTN)=YREQ(LL)
GO TO 60
57 REQ(NTN)=ZREQ(LL)
60 CONTINUE
59 CONTINUE
54 CONTINUE
53 DO 61 IJ = 1,NVABZ
NW(LIV+IJ)=0
NTN=NTN+1
C STORE RIGHT HAND SIDE OF THREE EQUATIONS FOR NODE NIC
REQ(NTN)=SRS(LIV+IJ)
C SET RIGHT-HAND SIDE MATRIX SRS ELEMENTS TO ZERO
SRS(LIV+IJ)=0.
61 CONTINUE
LREQ(MTM+1)=NSNW
LREQ(MTM+2)=NFNW
LREQ(MTM+3)=LIV
MTM=MTM+NVABZ
C RESET ARRAY SS FOR EQUATION REDUCTION
CALL RESETT
C REDUCE SET OF THREE EQUATIONS TO ELIMINATE NODE NIC
C CALCULATE THE INVERSE OF MATRIX PIVOT
C CALCULATE THE DETERMINANT OF MATRIX PIVOT
DPIVOT=PIVOT(1,1)*(PIVOT(2,2)*PIVOT(3,3)-PIVOT(2,3)*PIVOT(3,2))
1 -PIVOT(2,1)*(PIVOT(1,2)*PIVOT(3,3)-PIVOT(1,3)*PIVOT(3,2))
2 +PIVOT(3,1)*(PIVOT(1,2)*PIVOT(2,3)-PIVOT(1,3)*PIVOT(2,2))
IF(DPIVOT.EQ.0.0) WRITE(6,1050) NEL,NIC
IF(DPIVOT.EQ.0.0) STOP
C CALCULATE COFACTORS FOR INVERSE MATRIX PINVOT
COFACT1=PIVOT(2,2)*PIVOT(3,3)-PIVOT(2,3)*PIVOT(3,2)
COFACT2=PIVOT(1,1)*PIVOT(3,3)-PIVOT(1,3)*PIVOT(3,1)
COFACT3=PIVOT(1,1)*PIVOT(2,2)-PIVOT(1,2)*PIVOT(2,1)
COFACT4=-PIVOT(2,1)*PIVOT(3,3)+PIVOT(2,3)*PIVOT(3,1)
COFACT5=-PIVOT(1,1)*PIVOT(3,2)+PIVOT(1,2)*PIVOT(3,1)
COFACT6=PIVOT(2,1)*PIVOT(3,2)-PIVOT(2,2)*PIVOT(3,1)
C CALCULATE MATRIX PINVOT----INVERSE OF MATRIX PIVOT
PINVOT(1,1)=COFACT1/DPIVOT
PINVOT(2,1)=PINVOT(1,2)=COFACT4/DPIVOT
PINVOT(3,1)=PINVOT(1,3)=COFACT6/DPIVOT
PINVOT(2,2)=COFACT2/DPIVOT
PINVOT(3,2)=PINVOT(2,3)=COFACT5/DPIVOT
PINVOT(3,3)=COFACT3/DPIVOT
N2=0
C STORE MATRIX CIS NEEDED FOR REDUCTION OF EQUATIONS AT NODE NIC
DO 64 J = NSNW,NFNW,NVABZ

```

```

        IF(J.EQ.(LIV+1)) GO TO 68
        IF(J.GT.(LIV+NVABZ)) GO TO 65
        DO 66 I = 1, NVABZ
            N2=N2+1
            CIS(1, I)=XREQ(N2)
            CIS(2, I)=YREQ(N2)
            CIS(3, I)=ZREQ(N2)
66     CONTINUE
        GO TO 166
65     CONTINUE
        DO 67 K = 1, NVABZ
            N2=N2+1
            CIS(K, 1)=XREQ(N2)
            CIS(K, 2)=YREQ(N2)
            CIS(K, 3)=ZREQ(N2)
67     CONTINUE
166    CONTINUE
C     POSTMULTIPLY CIS BY PINVOT
        DO 69 I = 1, NVABZ
            DO 70 K = 1, NVABZ
                DO 71 L = 1, NVABZ
                    CFACT(I, K)=CFACT(I, K)+CIS(I, L)*PINVOT(L, K)
71     CONTINUE
70     CONTINUE
69     CONTINUE
        N3=N2-NVABZ
        N4=0
C     STORE MATRIX CSJ NEEDED FOR REDUCTION OF EQUATIONS
        DO 94 JJ = J, NFNW, NVABZ
C     (LIV+1) EQ JJ IMPLIES PIVOT IS AT JJ
        IF(JJ.EQ.(LIV+1)) GO TO 75
        IF(JJ.GT.(LIV+NVABZ)) GO TO 73
        DO 74 I = 1, NVABZ
            N3=N3+1
            CSJ(I, 1)=XREQ(N3)
            CSJ(I, 2)=YREQ(N3)
            CSJ(I, 3)=ZREQ(N3)
74     CONTINUE
        GO TO 72
73     CONTINUE
        DO 76 KK = 1, NVABZ
            N3=N3+1
            CSJ(1, KK)=XREQ(N3)
            CSJ(2, KK)=YREQ(N3)
            CSJ(3, KK)=ZREQ(N3)
76     CONTINUE
72     CONTINUE
C     PREMULTIPLY CSJ BY MATRIX CFACT
        DO 77 LA = 1, NVABZ
            DO 78 LB = 1, NVABZ
                DO 79 LC = 1, NVABZ
                    DFACT(LA, LB)=DFACT(LA, LB)+CFACT(LA, LC)*CSJ(LC, LB)
79     CONTINUE
78     CONTINUE
77     CONTINUE
C     STORE VALUES OF DFACT IN ARRAYS XRAQ, YRAQ, ZRAQ

```

```

C   AND RESET MATRIX DFACT TO ZERO
      DO 80 LD = 1, NVABZ
        N4=N4+1
        XRAQ(N4)=DFACT(1, LD)
        YRAQ(N4)=DFACT(2, LD)
        ZRAQ(N4)=DFACT(3, LD)
        DFACT(1, LD)=DFACT(2, LD)=DFACT(3, LD)=0.
80   CONTINUE
      GO TO 94
75   N3=N3+NVABZ
94   CONTINUE
      N6=0
      N7=1
      N8=2
C   REDUCE ELEMENTS OF STIFFNESS MATRIX SS
      JA=J+NVABZ-1
      DO 81 LL = J, JA
        JL=LL-J+1
        DO 82 LK = LL, NFNW
          DO 83 LJ = 1, NVABZ
            IF(LK.NE.(LIV+LJ)) GO TO 83
            GO TO 82
83   CONTINUE
          N5=JW(LL)+LK-JL
          CALL CHK(N5)
          GO TO (85,86,87), JL
85   N6=N6+1
          SS(N5)=SS(N5)-XRAQ(N6)
          GO TO 82
86   N7=N7+1
          SS(N5)=SS(N5)-YRAQ(N7)
          GO TO 82
87   N8=N8+1
          SS(N5)=SS(N5)-ZRAQ(N8)
82   CONTINUE
81   CONTINUE
C   REDUCE RIGHT HAND SIDE OF THREE EQUATIONS FOR NODE NIC
C   EXTRACT THE THREE ELEMENTS OF MATRIX SRS FOR NODE NIC
      N10=NTN-NVABZ
      DO 88 LS = 1, NVABZ
        JP=J+LS-1
        DO 89 LT = 1, NVABZ
          NA=N10+LT
          SRS(JP)=SRS(JP)-CFACT(LS, LT)*REQ(NA)
89   CONTINUE
88   CONTINUE
C   RESET MATRICES CFACT AND DFACT TO ZERO
      DO 92 IK = 1, NVABZ
        DO 93 JK = 1, NVABZ
          CFACT(IK, JK)=0.0
          DFACT(IK, JK)=0.0
93   CONTINUE
92   CONTINUE
      GO TO 64
68   CONTINUE
      N2=N2+NVABZ

```

```

4 CONTINUE
C STORE INVERSE OF MATRIX PIVOT (PINVOT) IN ARRAY REQ
  DO 90 JS = 1,NVABZ
  DO 91 JT = 1,NVABZ
  N9=N9+1
  REQ(N9)=PINVOT(JS, JT)
91 CONTINUE
90 CONTINUE
C ALL EQUATIONS HAVE NOW BEEN REDUCED BY EQUATIONS FOR NODE NIC
C THREE EQUATIONS FOR NODE NIC HAVE BEEN STORED IN ARRAY REQ
  CALL RESETT
40 CONTINUE
  CALL CLOKIT(9)
42 CONTINUE
  RETURN
1050 FORMAT(//5X,26HZERO DETERMINANT FOR PIVOT,/,5X,
111HELEMENT NO.,I5,/,5X,8HNODE NO.,I8)
1060 FORMAT(//5X,36HMATRICES XREQ,XRAQ,ETC.ARE TOO SMALL)
  END
  SUBROUTINE INDAT

  ** INSERT 17 LINES OF COMMON STATEMENTS HERE **
C
C
C
  DIMENSION HEAD(9)
  1 READ(5,1002) ICODE,NCODE
  2 WRITE(6,1083) ICODE,NCODE
  IF(ICODE.EQ.99) RETURN
  GO TO(100,150,200,250,300,350,400),ICODE
100 READ(5,1002) ICODE,NCODE,HEAD
  IF(ICODE.NE.0) GO TO 2
  WRITE(6,1003) HEAD
  GO TO 100
150 READ(5,1004) IPRINC,NPRINC,NPUT
  WRITE(6,1005) IPRINC,NPRINC,NPUT
  GO TO 1
200 GO TO(201,210),NCODE
201 READ(5,1006) ICODE,NCODE,NMAT,YMOD,PRAT,WEIGHT,EXPAN,AYMOD,APRAT,
  1 AGG
  IF(ICODE.NE.0) GO TO 2
  WRITE(6,1007) NMAT,YMOD,PRAT,WEIGHT,EXPAN,AYMOD,APRAT,AGG
  YM(NMAT)=YMOD
  PR(NMAT)=PRAT
  WT(NMAT)=WEIGHT
  EXPN(NMAT)=EXPAN
  AYM(NMAT)=AYMOD
  APR(NMAT)=APRAT
  GG(NMAT)=AGG
  GO TO 201
210 READ(5,1014) ICODE,NCODE,NMAT,(NW(I),I=1,14)
  IF(ICODE.NE.0) GO TO 2
  WRITE(6,1015) NMAT,(NW(I),I=1,14)
  IF(MAXMAT.LT.NMAT) MAXMAT=NMAT
  DO 220 I=1,14

```

```

NIC=NW(I)
IF(NIC.EQ.0) GO TO 210
MAT(NIC)=NMAT
220 CONTINUE
GO TO 210
250 READ(5,1006) ICODE,NCODE,NIC,COX,COY,COZ
IF(ICODE.NE.0) GO TO 2
WRITE(6,1007) NIC,COX,COY,COZ
CORD(NIC,1)=COX
CORD(NIC,2)=COY
CORD(NIC,3)=COZ
GO TO 250
300 NEL=0
301 NEL=NEL+1
READ(5,1018) ICODE,NCODE,(LDEF(NEL,I),I=1,14)
IF(ICODE.NE.0) GO TO 302
READ(5,1004) (LDEF(NEL,I),I=15,20)
WRITE(6,1015) NEL,(LDEF(NEL,I),I=1,20)
MAXNEL=NEL
GO TO 301
302 DO 305 NEL=1,MAXNEL
DO 304 LNOD=1,NNODZ
IF(MAXNOD.LT.LDEF(NEL,LNOD)) MAXNOD=LDEF(NEL,LNOD)
304 CONTINUE
305 CONTINUE
GO TO 2
350 NCOUNT=0
GO TO(351,360),NCODE
351 NCOUNT=NCOUNT+1
READ(5,1026) ICODE,NCODE,(NDISP(NCOUNT,I),I=1,4),
1 (DISP(NCOUNT,I),I=1,3)
IF(ICODE.NE.0) GO TO 2
WRITE(6,1027) (NDISP(NCOUNT,I),I=1,4),(DISP(NCOUNT,I),I=1,3)
MAXDIS=NCOUNT
GO TO 351
360 READ(5,1008) ICODE,NCODE,NFIXX,NFIXY,NFIXZ,(NW(I),I=1,14)
IF(ICODE.NE.0) GO TO 2
WRITE(6,1009) NFIXX,NFIXY,NFIXZ,(NW(I),I=1,14)
DO 365 I=1,14
IF(NW(I).EQ.0) GO TO 360
NCOUNT=NCOUNT+1
NDISPZ(NCOUNT,4)=NW(I)
NDISPZ(NCOUNT,1)=NFIXX
NDISPZ(NCOUNT,2)=NFIXY
NDISPZ(NCOUNT,3)=NFIXZ
MAXNDZ=NCOUNT
365 CONTINUE
GO TO 360
400 NCOUNT=0
401 NCOUNT=NCOUNT+1
READ(5,1006) ICODE,NCODE,NREACT(NCOUNT),(REACT(NCOUNT,I),I=1,3)
IF(ICODE.NE.0) GO TO 2
WRITE(6,1007) NREACT(NCOUNT),(REACT(NCOUNT,I),I=1,3)
MAXRCT=NCOUNT
GO TO 401
1002 FORMAT(2I2,1X,9A8)

```

```

1003 FORMAT(6X,9A8)
1004 FORMAT(10X,6I5)
1005 FORMAT(11X,6I5)
1006 FORMAT(2I2,1X,I5,7E10.4)
1007 FORMAT(6X,I5,7E10.3)
1008 FORMAT(2I2,1X,3I1,2X,14I5)
1009 FORMAT(6X,3I1,2X,14I5)
1014 FORMAT(2I2,1X,15I5)
1015 FORMAT(6X,15I5,/,11X,6I5)
1018 FORMAT(2I2,6X,14I5)
1026 FORMAT(2I2,1X,3I1,2X,I5,5X,3F10.5)
1027 FORMAT(6X,3I1,2X,I5,5X,3F10.5)
1083 FORMAT(1X,2I2)
      END
      SUBROUTINE JACOB(I1)

```

\*\* INSERT 17 LINES OF COMMON STATEMENTS HERE \*\*

C  
C  
C

```

      DO 5 I=1,9,
      CW(I)=0.0
5  CONTINUE
      A1=1.0-XL*XL
      A2=1.0-YL*YL
      A3=1.0-ZL*ZL
      DO 100 I=1,20
      A7=XL*XX(I)+1.0
      A8=YL*YY(I)+1.0
      A9=ZL*ZZ(I)+1.0
      GO TO(10,20,10,30,10,20,10,30,40,40,
1      40,40,10,20,10,30,10,20,10,30),I
10 A6=A7+A8+A9-5.0
      DX(I)=A8*A9*(A6+A7)*XX(I)*0.125
      DY(I)=A7*A9*(A6+A8)*YY(I)*0.125
      DZ(I)=A7*A8*(A6+A9)*ZZ(I)*0.125
      SHP(I)=A6*A7*A8*A9*0.125
      GO TO 90
20 DX(I)=A2*A9*XX(I)*0.25
      DY(I)=-A7*A9*YL*0.5
      DZ(I)=A2*A7*ZZ(I)*0.25
      SHP(I)=A2*A7*A9*0.25
      GO TO 90
30 DX(I)=-A8*A9*XL*0.5
      DY(I)=A1*A9*YY(I)*0.25
      DZ(I)=A1*A8*ZZ(I)*0.25
      SHP(I)=A1*A8*A9*0.25
      GO TO 90
40 DX(I)=A3*A8*XX(I)*0.25
      DY(I)=A3*A7*YY(I)*0.25
      DZ(I)=-A8*A7*ZL*0.5
      SHP(I)=A3*A7*A8*0.25
90 CW(1)=CW(1)+DX(I)*X(I)
      CW(2)=CW(2)+DX(I)*Y(I)
      CW(3)=CW(3)+DX(I)*Z(I)

```



```

    CW(4)=CW(4)+DY(I)*X(I)
    CW(5)=CW(5)+DY(I)*Y(I)
    CW(6)=CW(6)+DY(I)*Z(I)
    CW(7)=CW(7)+DZ(I)*X(I)
    CW(8)=CW(8)+DZ(I)*Y(I)
    CW(9)=CW(9)+DZ(I)*Z(I)
100 CONTINUE
    DETJ=CW(1)*(CW(5)*CW(9)-CW(8)*CW(6))+
1      CW(2)*(CW(7)*CW(6)-CW(4)*CW(9))+
2      CW(3)*(CW(4)*CW(8)-CW(7)*CW(5))
    IF(DETJ.GT.0.0) GO TO 110
    WRITE(6,1000) NEL,DETJ
    NSTOP=1
110 RDETJ=1.0/DETJ
    AW(1)=(CW(5)*CW(9)-CW(6)*CW(8))*RDETJ
    AW(2)=(CW(3)*CW(8)-CW(2)*CW(9))*RDETJ
    AW(3)=(CW(2)*CW(6)-CW(3)*CW(5))*RDETJ
    AW(4)=(CW(6)*CW(7)-CW(4)*CW(9))*RDETJ
    AW(5)=(CW(1)*CW(9)-CW(3)*CW(7))*RDETJ
    AW(6)=(CW(3)*CW(4)-CW(1)*CW(6))*RDETJ
    AW(7)=(CW(4)*CW(8)-CW(5)*CW(7))*RDETJ
    AW(8)=(CW(2)*CW(7)-CW(1)*CW(8))*RDETJ
    AW(9)=(CW(1)*CW(5)-CW(2)*CW(4))*RDETJ
    IF(I1.EQ.1) RETURN
    DO 200 I=1,20
    DXI=DX(I)
    DYI=DY(I)
    DZI=DZ(I)
    DX(I)=AW(1)*DXI+AW(2)*DYI+AW(3)*DZI
    DY(I)=AW(4)*DXI+AW(5)*DYI+AW(6)*DZI
    DZ(I)=AW(7)*DXI+AW(8)*DYI+AW(9)*DZI
200 CONTINUE
    RETURN
1000 FORMAT(//,5X,28HNEGATIVE OR ZERO DETERMINANT,/,5X,8HELEMENT ,I5,
1      12H DETERMINANT,2X,E10.3)
    END
    SUBROUTINE MULT1

```

\*\* INSERT 17 LINES OF COMMON STATEMENTS HERE \*\*

C  
C  
C

```

    N=0
    WAIT=WX*WY*WZ*DETJ
    DO 20 I=1,NNODZ
    DXI=DX(I)*WAIT
    DYI=DY(I)*WAIT
    DZI=DZ(I)*WAIT
    DO 15 J=I,NNODZ
    DXJ=DX(J)
    DYJ=DY(J)
    DZJ=DZ(J)
    S(N+1)=S(N+1)+DXI*DXJ
    S(N+2)=S(N+2)+DXI*DYJ
    S(N+3)=S(N+3)+DXI*DZJ

```

```

S(N+4)=S(N+4)+DYI*DYJ
S(N+5)=S(N+5)+DYI*DZJ
S(N+6)=S(N+6)+DZI*DZJ
N=N+6
IF(I.EQ.J) GO TO 15
S(N+1)=S(N+1)+DYI*DXJ
S(N+2)=S(N+2)+DZI*DXJ
S(N+3)=S(N+3)+DZI*DYJ
N=N+3
15 CONTINUE
20 CONTINUE
RETURN
END
SUBROUTINE MULT2

```

\*\* INSERT 17 LINES OF COMMON STATEMENTS HERE \*\*

C  
C  
C

```

N=0
DO 40 I=1, NNODZ
DO 30 J=I, NNODZ
S1=S(N+1)
S2=S(N+2)
S3=S(N+3)
S4=S(N+4)
S5=S(N+5)
S6=S(N+6)
IF(I.EQ.J) GO TO 20
S7=S(N+7)
S8=S(N+8)
S9=S(N+9)
S(N+1)=S1*D(1)+S4*D(10)+S6*D(12)
S(N+2)=S2*D(2)+S7*D(10)
S(N+3)=S3*D(3)+S8*D(12)
S(N+4)=S7*D(4)+S2*D(10)
S(N+5)=S4*D(5)+S1*D(10)+S6*D(11)
S(N+6)=S5*D(6)+S9*D(11)
S(N+7)=S8*D(7)+S3*D(12)
S(N+8)=S9*D(8)+S5*D(11)
S(N+9)=S6*D(9)+S4*D(11)+S1*D(12)
N=N+9
GO TO 30
20 S(N+1)=S1*D(1)+S4*D(10)+S6*D(12)
S(N+2)=S2*(D(2)+D(10))
S(N+3)=S3*(D(3)+D(12))
S(N+4)=S4*D(5)+S1*D(10)+S6*D(11)
S(N+5)=S5*(D(6)+D(11))
S(N+6)=S6*D(9)+S4*D(11)+S1*D(12)
N=N+6
30 CONTINUE
40 CONTINUE
RETURN
END
SUBROUTINE MULT3

```

\*\* INSERT 17 LINES OF COMMON STATEMENTS HERE \*\*

C  
C  
C

```

DO 1 I=1,9
CW(I)=0.0
1 CONTINUE
DO 10 I=1,NNODZ
CW(1)=CW(1)+DX(I)*U(I)
CW(2)=CW(2)+DX(I)*V(I)
CW(3)=CW(3)+DX(I)*W(I)
CW(4)=CW(4)+DY(I)*U(I)
CW(5)=CW(5)+DY(I)*V(I)
CW(6)=CW(6)+DY(I)*W(I)
CW(7)=CW(7)+DZ(I)*U(I)
CW(8)=CW(8)+DZ(I)*V(I)
CW(9)=CW(9)+DZ(I)*W(I)
10 CONTINUE
SIGMA(1)=CW(1)*D(1)+CW(5)*D(2)+CW(9)*D(3)
SIGMA(2)=CW(1)*D(4)+CW(5)*D(5)+CW(9)*D(6)
SIGMA(3)=CW(1)*D(7)+CW(5)*D(8)+CW(9)*D(9)
SIGMA(4)=(CW(2)+CW(4))*D(10)
SIGMA(5)=(CW(6)+CW(8))*D(11)
SIGMA(6)=(CW(3)+CW(7))*D(12)
RETURN
END
SUBROUTINE PLOAD

```

\*\* INSERT 17 LINES OF COMMON STATEMENTS HERE \*\*

C  
C  
C

```

DO 50 NOD=1,NNODZ
NIC=NELDEF(NOD)
DO 49 I=1,MAXRCT
IF(NIC.NE.NREACT(I)) GO TO 49
II=(NOD-1)*NVABZ
DO 45 J=1,NVABZ
RS(II+J)=RS(II+J)+REACT(I,J)
45 CONTINUE
NREACT(I)=0
49 CONTINUE
50 CONTINUE
RETURN
END
SUBROUTINE POSTCN

```

\*\* INSERT 17 LINES OF COMMON STATEMENTS HERE \*\*

C  
C  
C

```

DIMENSION RACTN(3)

```

```

DO 232 I=1,NVABZ
  RACTN(I)=0.0
232 CONTINUE
  IF(MAXDIS.EQ.0) GO TO 251
  DO 250 I=1,MAXDIS
  IF(NIC.NE.NDISP(I,4)) GO TO 250
  DO 240 J=1,NVABZ
  IF(NDISP(I,J).EQ.0) GO TO 240
  DSP=DISP(I,J)
  N1=LIV+J-1
  IF(ABS(SRS(N1)).GT.ABS(DSP/1.0E15)) WRITE(6,1400)
  RACTN(J)=-SRS(N1)*1.0E+50
  SRS(N1)=DSP
  DISPL(NIC,J)=DSP
240 CONTINUE
  WRITE(6,1200) NIC,RACTN
250 CONTINUE
251 IF(MAXNDZ.EQ.0) RETURN
  DO 270 I=1,MAXNDZ
  IF(NIC.NE.NDISPZ(I,4)) GO TO 270
  DO 260 J=1,NVABZ
  IF(NDISPZ(I,J).EQ.0) GO TO 260
  N1=LIV+J-1
  RACTN(J)=-SRS(N1)*1.0E+50
  IF(ABS(SRS(N1)).GT.1.0E-15) WRITE(6,1400)
  SRS(N1)=0.0
  DISPL(NIC,J)=0.0
260 CONTINUE
  WRITE(6,1200) NIC,RACTN
  RETURN
270 CONTINUE
  RETURN
1200 FORMAT(/,6X,I5,3(5X,E10.3))
1400 FORMAT(42H1BIG SPRING STIFFNESS IS NOT LARGE ENOUGH.,/,
1 68H ERRORS ARE ALMOST CERTAIN TO OCCUR DUE TO FIXITY BEING INEFFE
2CTIVE.,/,1H0)
  END
  SUBROUTINE PRECON

```

\*\* INSERT 17 LINES OF COMMON STATEMENTS HERE \*\*

C  
C  
C

```

IF(MAXDIS.EQ.0) GO TO 175
DO 170 I=1,MAXDIS
IF(NIC.NE.NDISP(I,4)) GO TO 170
DO 160 J=1,NVABZ
IF(NDISP(I,J).EQ.0) GO TO 160
DSP=DISP(I,J)
N1=(LIN-1)*NVABZ+J
DO 140 K=NSNW,N1
N2=JW(K)
N4=N2+N1-K
CALL CHK(N4)
SRS(K)=SRS(K)-DSP*SS(N4)

```

```

140 CONTINUE
    SS(N4)=1.0E+50
    IF(N1.EQ.NFNW) GO TO 159
    N3=N1+1
    DO 150 K=N3,NFNW
    N4=N2-N1+K
    CALL CHK(N4)
    SRS(K)=SRS(K)-DSP*SS(N4)
150 CONTINUE
159 CONTINUE
    CALL RESETT
160 CONTINUE
170 CONTINUE
175 IF(MAXNDZ.EQ.0) RETURN
    DO 190 I=1,MAXNDZ
    IF(NIC.NE.NDISPZ(I,4)) GO TO 190
    DO 180 J=1,NVABZ
    IF(NDISPZ(I,J).EQ.0) GO TO 180
    N1=(LIN-1)*NVABZ+J
    N2=JW(N1)
    CALL CHK(N2)
    SS(N2)=1.0E+50
180 CONTINUE
    CALL RESETT
190 CONTINUE
    RETURN
    END
    SUBROUTINE PREFNT

```

\*\* INSERT 17 LINES OF COMMON STATEMENTS HERE \*\*

C  
C  
C

```

    DO 1 I=1,MAXNW
    NW(I)=0
1 CONTINUE
    DO 10 NEL=1,MAXNEL
    DO 5 I=1,NNODZ
    NIC=LDEF(NEL,I)
    LDEST(NIC)=NEL
5 CONTINUE
10 CONTINUE
    DO 20 NIC=1,MAXNOD
    NEL=LDEST(NIC)
    IF(NEL.EQ.0) GO TO 20
    DO 15 I=1,NNODZ
    IF(LDEF(NEL,I).NE.NIC) GO TO 15
    LDEF(NEL,I)=-NIC
    LDEST(NIC)=0
    GO TO 20
15 CONTINUE
20 CONTINUE
    DO 100 NEL=1,MAXNEL
    DO 50 I=1,NNODZ
    NIC=IABS(LDEF(NEL,I))

```

```

IF(LDEST(NIC).NE.0) GO TO 50
DO 30 J=1,MAXNW
IF(NW(J).NE.0) GO TO 30
LDEST(NIC)=J
NW(J)=NIC
IF(MAXFW.LT.J) MAXFW=J
GO TO 50
30 CONTINUE
WRITE(6,1000)
STOP
50 CONTINUE
DO 70 I=1,NNODZ
NIC=LDEF(NEL,I)
IF(NIC.GT.0) GO TO 70
N1=LDEST(-NIC)
NW(N1)=0
70 CONTINUE
100 CONTINUE
MAXFW=MAXFW*NVABZ
WRITE(6,1001) MAXFW
RETURN
1000 FORMAT(62H,1MAXIMUM FRONT WIDTH DURING PREFNT EXCEEDS LENGTH OF NW
1VECTOR)
1001 FORMAT(/////,5X,19HMAXIMUM FRONT WIDTH,2X,I3)
END
SUBROUTINE RESETT

```

C  
C  
C  
C  
C

\*\* INSERT 17 LINES OF COMMON STATEMENTS HERE \*\*

```

10 IF(KF.EQ.KMAX) GO TO 20
BUFFER OUT(L21,1) (SS(1),SS(MAXSS))
IF(UNIT(L21)) 11,12,13
11 CONTINUE
BUFFER IN(L20,1) (SS(1),SS(MAXSS))
KS=KS+MAXSS
KF=KF+MAXSS
IF(UNIT(L20)) 14,12,13
14 CONTINUE
GO TO 10
20 BUFFER OUT(L21,1) (SS(1),SS(MAXSS))
REWIND L20
IF(UNIT(L21)) 15,12,13
15 CONTINUE
REWIND L21
LEN=L20
L20=L21
L21=LEN
KS=1
KF=MAXSS
BUFFER IN(L20,1) (SS(1),SS(MAXSS))
IF(UNIT(L20)) 16,12,13
16 CONTINUE

```

```

    RETURN
12 STOP
13 STOP
    END
    SUBROUTINE SETUP
C
C
** INSERT 17 LINES OF COMMON STATEMENTS HERE **
C
C
C
C
    NK=(JW(MAXFW)/MAXSS)+1
    DO 10 I = 1,NK
    BUFFER OUT(20,1) (SS(1),SS(MAXSS))
    IF(UNIT(20)) 11,12,13
11 CONTINUE
    BUFFER OUT(21,1) (SS(1),SS(MAXSS))
    IF(UNIT(21)) 14,12,13
14 CONTINUE
10 CONTINUE
C NO MORE MATRIX SS ----- WRITE END OF FILE ON TPAE20,TAPE21
    ENDFILE20
    ENDFILE21
    REWIND 20
    REWIND 21
    BUFFER IN(20,1) (SS(1),SS(MAXSS))
    L20=20
    L21=21
    KS=1
    KF=MAXSS
    KMAX=NK*MAXSS
    IF(UNIT(20)) 15,12,13
15 CONTINUE
    RETURN
12 STOP
13 STOP
    END
    SUBROUTINE STIFN

** INSERT 17 LINES OF COMMON STATEMENTS HERE **
C
C
C
    REWIND 4
    IF(MAXMAT.EQ.1) CALL DMAT(1)
    DO 900 NEL =1,MAXNEL
    NCHK=0
    DO 1 I=1,60
    RS(I)=0.0
1 CONTINUE
    DO 2 I=1,1830
    S(I)=0.0
2 CONTINUE
    IF(MAXMAT.EQ.1) GO TO 3

```

```

    I1=MAT(NEL)
    CALL DMAT(I1)
  3 DO 10 J=1,NNODZ
    NIC=IABS(LDEF(NEL,J))
    NELDES(J)=LDEST(NIC)
    NELDEF(J)=NIC
    X(J)=CORD(NIC,1)
    Y(J)=CORD(NIC,2)
    Z(J)=CORD(NIC,3)
  10 CONTINUE
    IF(MAXRCT.NE.0) CALL PLOAD
    DO 100 JA=1,NRULE
    XL=VECTLC(JA)
    WX=WTFUN(JA)
    DO 90 JB=1,NRULE
    YL=VECTLC(JB)
    WY=WTFUN(JB)
    DO 80 JC=1,NRULE
    ZL=VECTLC(JC)
    WZ=WTFUN(JC)
    CALL JACOB(0)
    CALL MULT1,
  80 CONTINUE
  90 CONTINUE
  100 CONTINUE
    CALL MULT2
    WRITE(4) S,RS,(LDEF(NEL,J),J=1,NNODZ),NELDES
  900 CONTINUE
    IF(NSTOP.EQ.0) RETURN
    WRITE(6,1000)
    STOP
  1000 FORMAT( 50H1ILLCONDITIONING OR GEOMETRY OR DEFINITION ERRORS.,/,
    1 22H EXECUTION TERMINATED.)
    END
    SUBROUTINE STRESS

```

\*\* INSERT 17 LINES OF COMMON STATEMENTS HERE \*\*

C  
C  
C

```

    WRITE(6,1000)
    DO 10 I=1,MAXNOD
    WRITE(6,1001) I,(DISPL(I,J),J=1,NVABZ)
  10 CONTINUE
    IF(NPUT.EQ.0) GO TO 20
    N1=MAXNOD*7
    IF(N1.LE.MAXSS) GO TO 11
    NPUT=0
    WRITE(6,2000)
    GO TO 20
  11 DO 12 I=1,N1
    SS(I)=0.0
  12 CONTINUE
  20 DO 100 NEL=1,MAXNEL
    IF(MAXMAT.EQ.1) GO TO 25

```

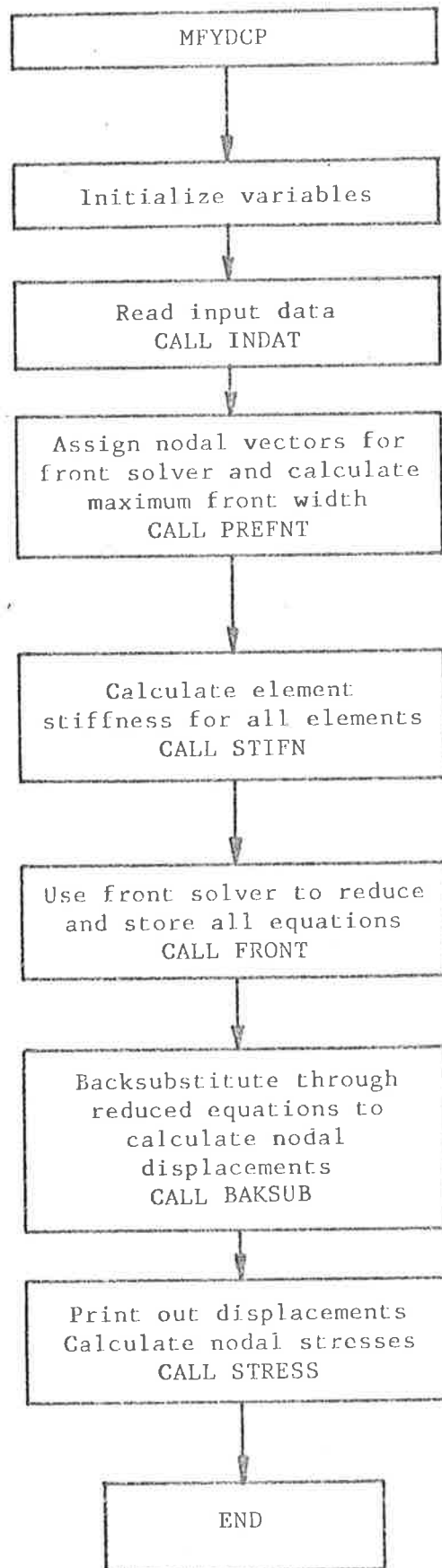


```

      N2=MAT(NEL)
      CALL DMAT(N2)
25  CONTINUE
      DO 30 NOD=1, NNODZ
      N3=IABS(LDEF(NEL, NOD))
      NELDEF(NOD)=N3
      X(NOD)=CORD(N3, 1)
      Y(NOD)=CORD(N3, 2)
      Z(NOD)=CORD(N3, 3)
      U(NOD)=DISPL(N3, 1)
      V(NOD)=DISPL(N3, 2)
      W(NOD)=DISPL(N3, 3)
30  CONTINUE
      DO 50 NOD=1, NNODZ
      XL=XX(NOD)
      YL=YY(NOD)
      ZL=ZZ(NOD)
      CALL JACOB(0)
      CALL MULT3
      NIC=NELDEF(NOD)
      IF(NPUT.EQ.0) GO TO 50
      N4=(NIC-1)*7
      DO 40 I=1, 6
      SS(N4+I)=SS(N4+I)+SIGMA(I)
40  CONTINUE
      SS(N4+7)=SS(N4+7)+1.0
50  CONTINUE
100 CONTINUE
      IF(NPUT.EQ.0) RETURN
      N5=-7
      WRITE(6, 1004)
      DO 150 NOD=1, MAXNOD
      N5=N5+7
      DIV=SS(N5+7)
      IF(DIV.EQ.0.0) GO TO 150
      DO 140 I=1, 6
      SIGMA(I)=SS(N5+I)/DIV
140 CONTINUE
      WRITE(6, 1003) NOD, SIGMA
150 CONTINUE
      RETURN
1000 FORMAT(20H1NODAL DISPLACEMENTS, /,
1       7X, 4HNODE, 8X, 6HX-COMP, 9X, 6HY-COMP, 9X, 6HZ-COMP)
1001 FORMAT(6X, I5, 3(5X, E10.3))
1003 FORMAT(/, 1X, I10, 3X, 6(2X, F10.1))
1004 FORMAT(23H1AVERAGE NODAL STRESSES, //,
1       7X, 4HNODE, 6X, 9HSIGMA X-X, 3X, 9HSIGMA Y-Y, 3X, 9HSIGMA Z-Z, 5X,
2       7HTAU X-Y, 5X, 7HTAU Y-Z, 5X, 7HTAU X-Z)
2000 FORMAT( 65H1INSUFFICIENT SPACE IN SS VECTOR TO ALLOW NODAL STRESS
1AVERAGING., /, 21H AVERAGING CANCELLED.)
      END

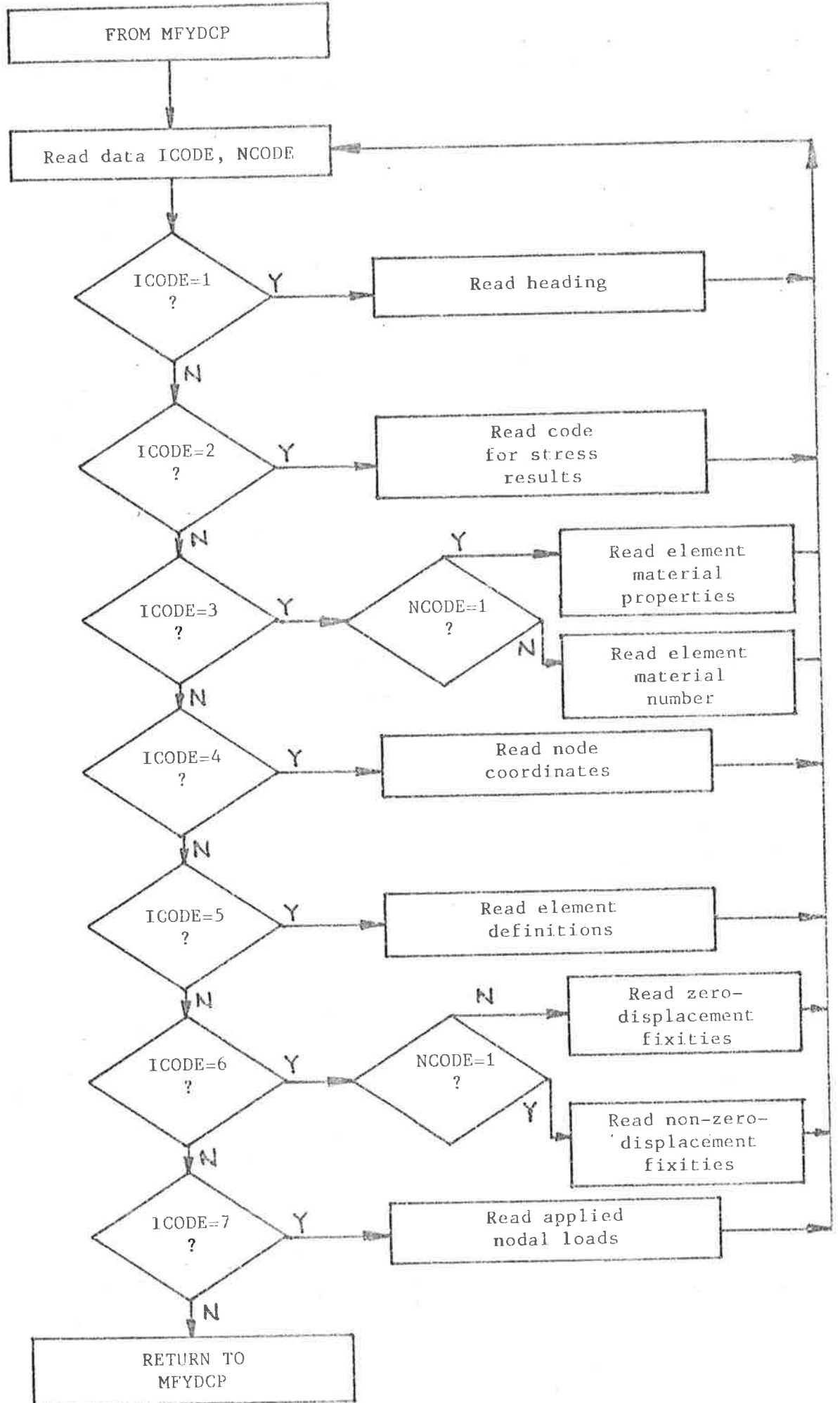
```

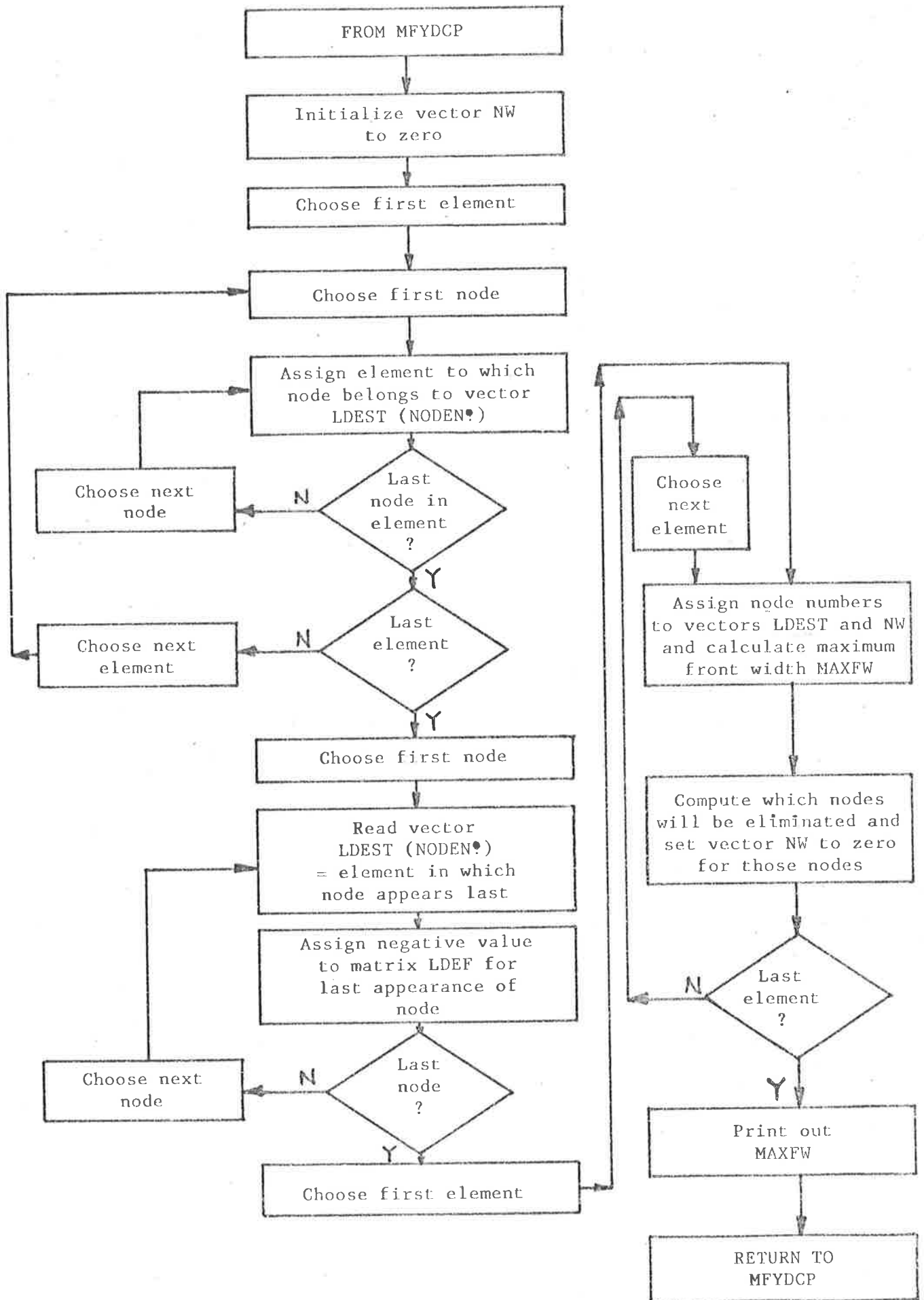
## E.4 SKELETON FLOW CHART FOR PROGRAM MFYDCP



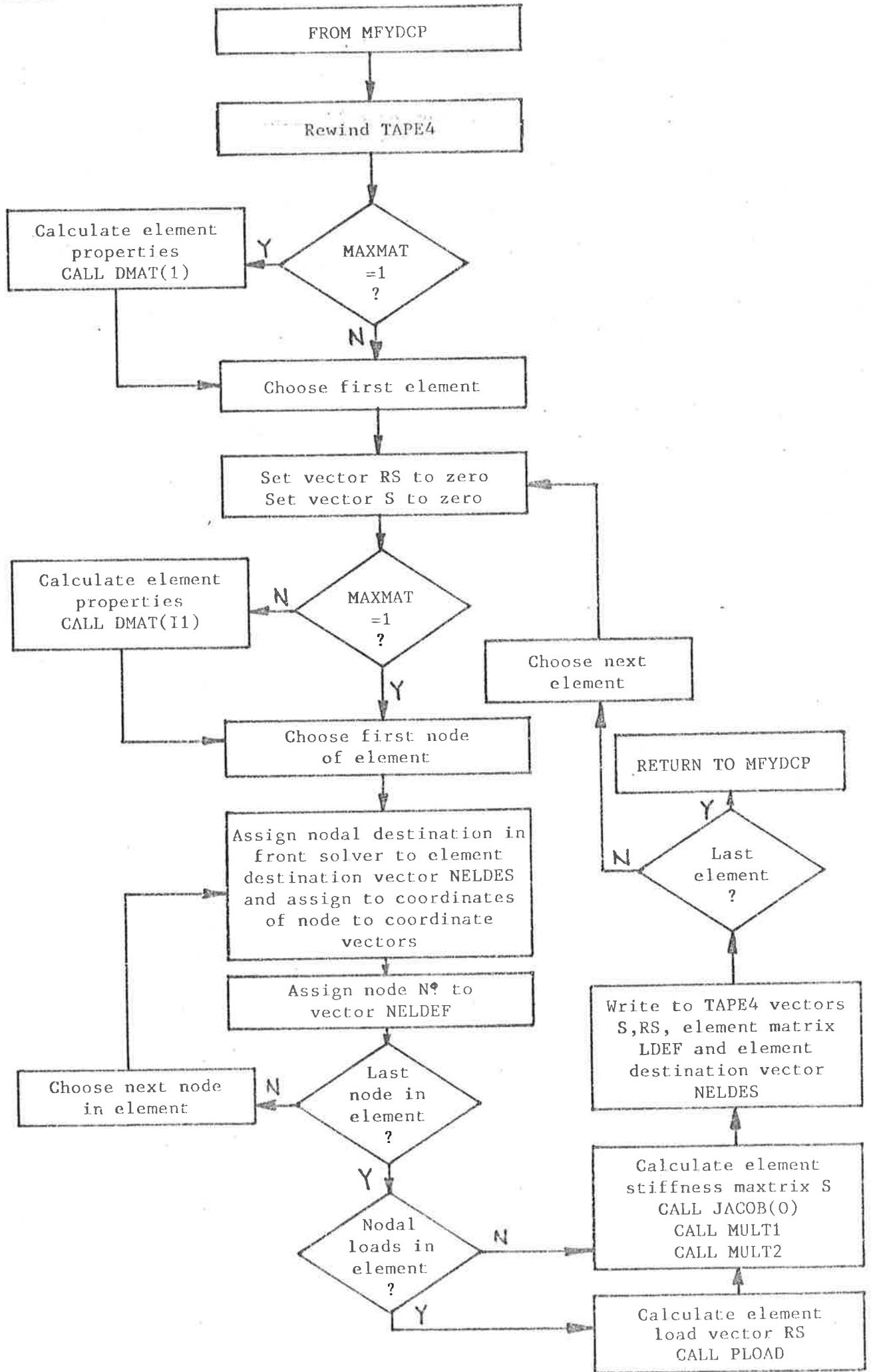
MAIN PROGRAM MFYDCP

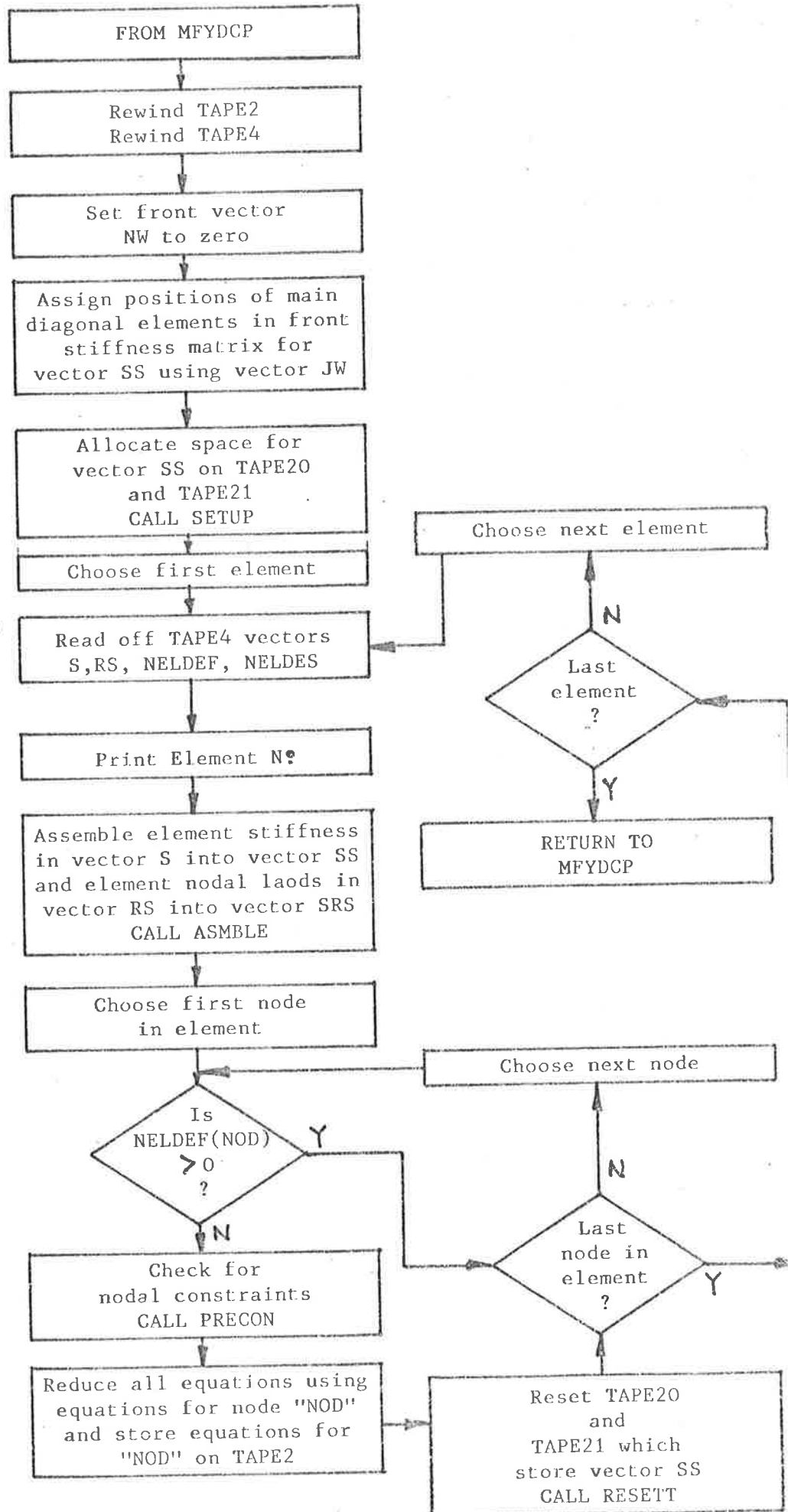
SUBROUTINE INDAT

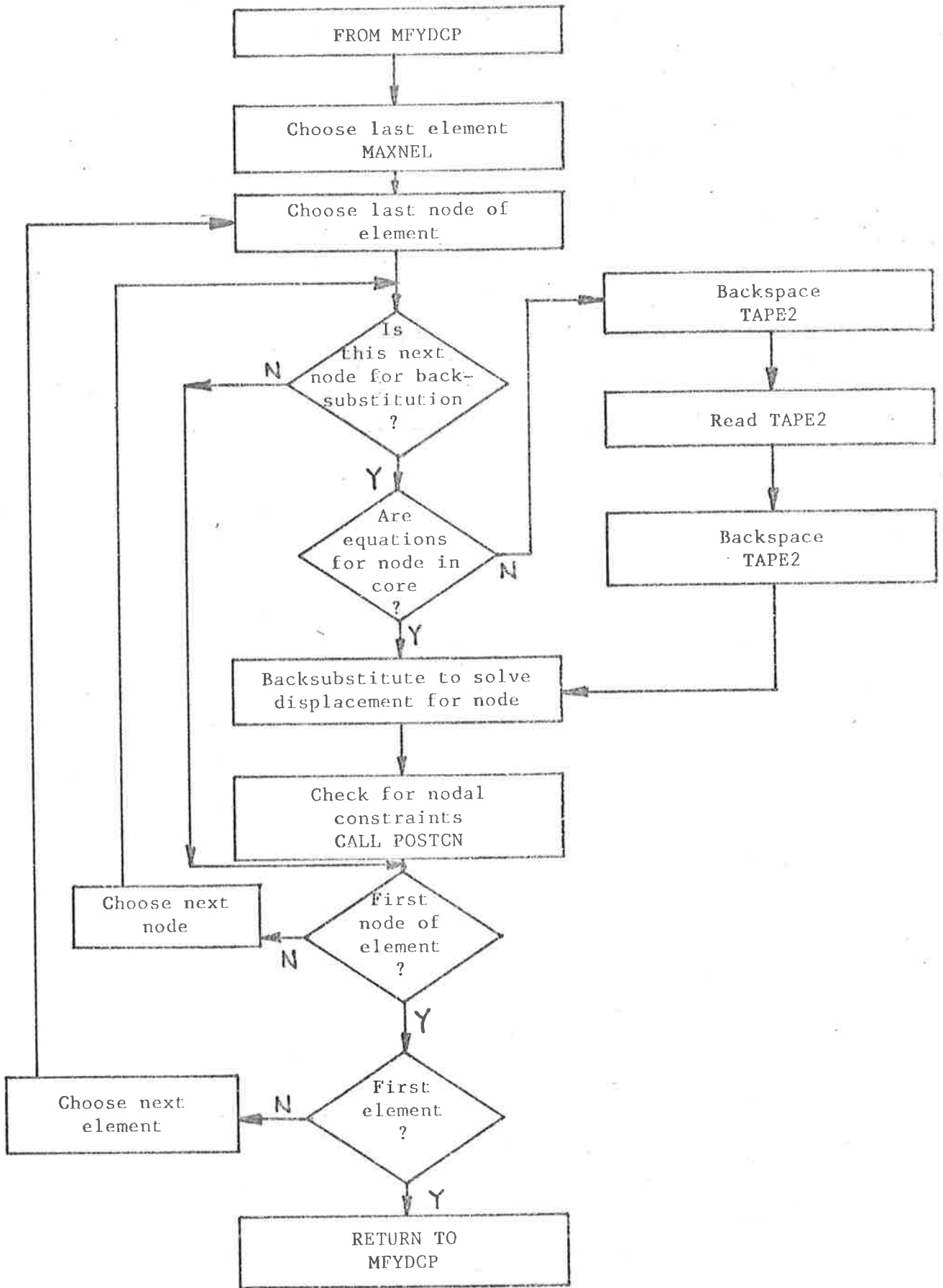




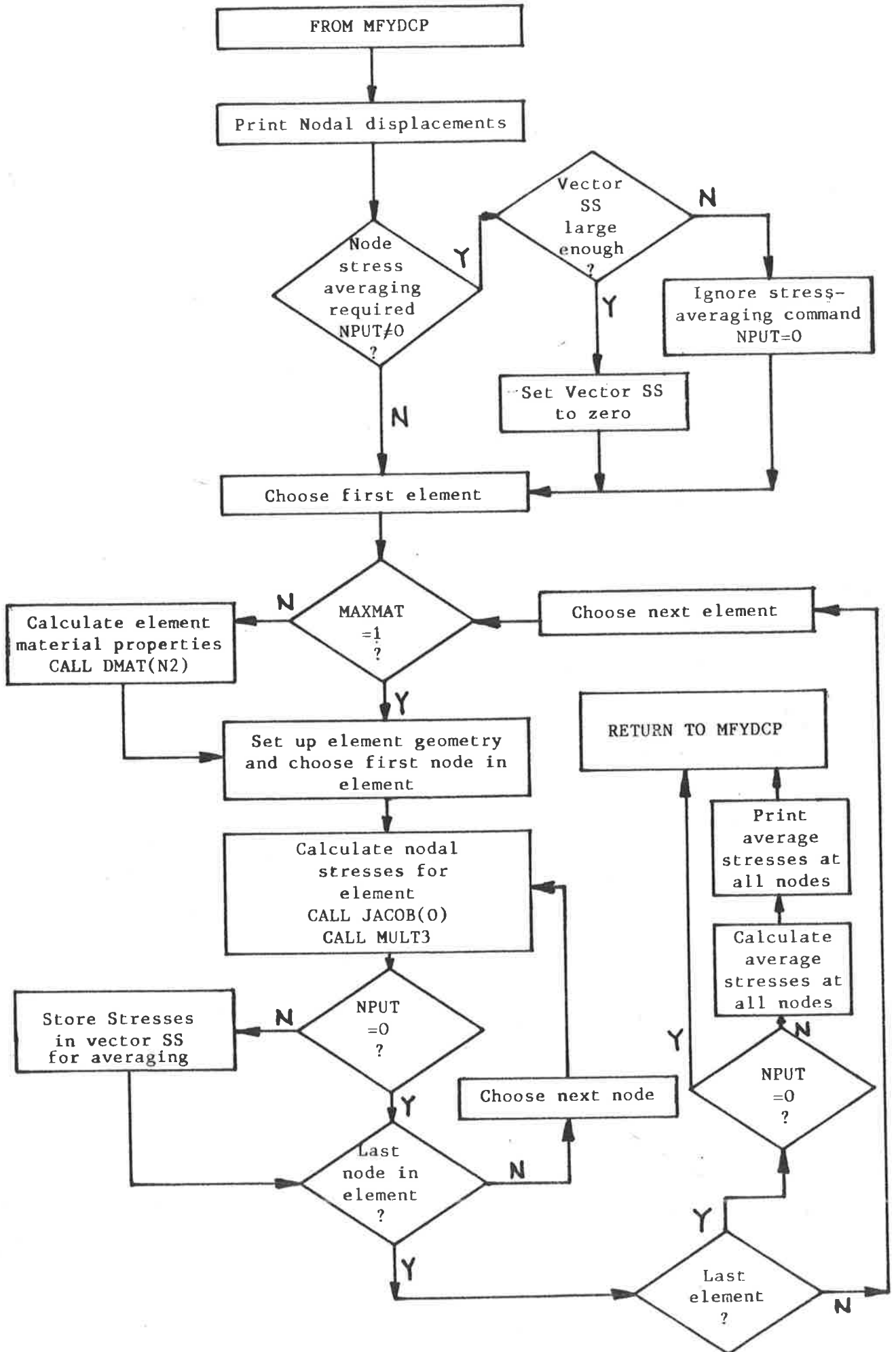
SUBROUTINE STIFN







SUBROUTINE STRESS





APPENDIX F  
DERIVATION OF PANEL EQUATIONS

F.1 THE EQUILIBRIUM EQUATION (6.9)

For the equivalent plate of varying thickness (figure F.1(a)), a coordinate system may be chosen with its origin at the middle thickness (middle surface) of the plate; the Z axis may be chosen to be perpendicular to the outer (negative-z) face of the element with the X and Y axes parallel to the (undeflected) outer face. This coordinate system may be chosen because the sections of the panel initially plane and normal to the outer face remain so during panel deflection (c.f. columns<sup>(96), (97)</sup>), whereas the middle surface can undergo additional rotations as the depth of cracking varies with loading.

Bending moments  $M_x$  and  $M_y$  (figure F.1(b)) are defined to be positive if caused by tensile normal stresses  $\sigma_x$  or  $\sigma_y$  acting on a positive X or Y face respectively and at positive z. Twisting moments  $M_{xy}$  and  $M_{yx}$  are defined to be positive if caused by shear stresses on a positive X or Y face acting in a positive Y or X direction respectively at positive z. The displacements in the X, Y, Z directions are u, v, and w respectively.

(a) Moment Equilibrium

Take moments about the X axis and neglect high order curvature effects, so that —

$$\frac{\partial M_{xy}}{\partial x} dx dy - (Q_y + \frac{\partial Q_y}{\partial y} dy) dy \cdot dx + \frac{\partial M_y}{\partial y} dy \cdot dx = 0$$

By neglecting second order terms,

$$\frac{\partial M_{xy}}{\partial x} - Q_y + \frac{\partial M_y}{\partial y} = 0 \tag{F.1}$$

Similarly, by taking moments about the Y axis,

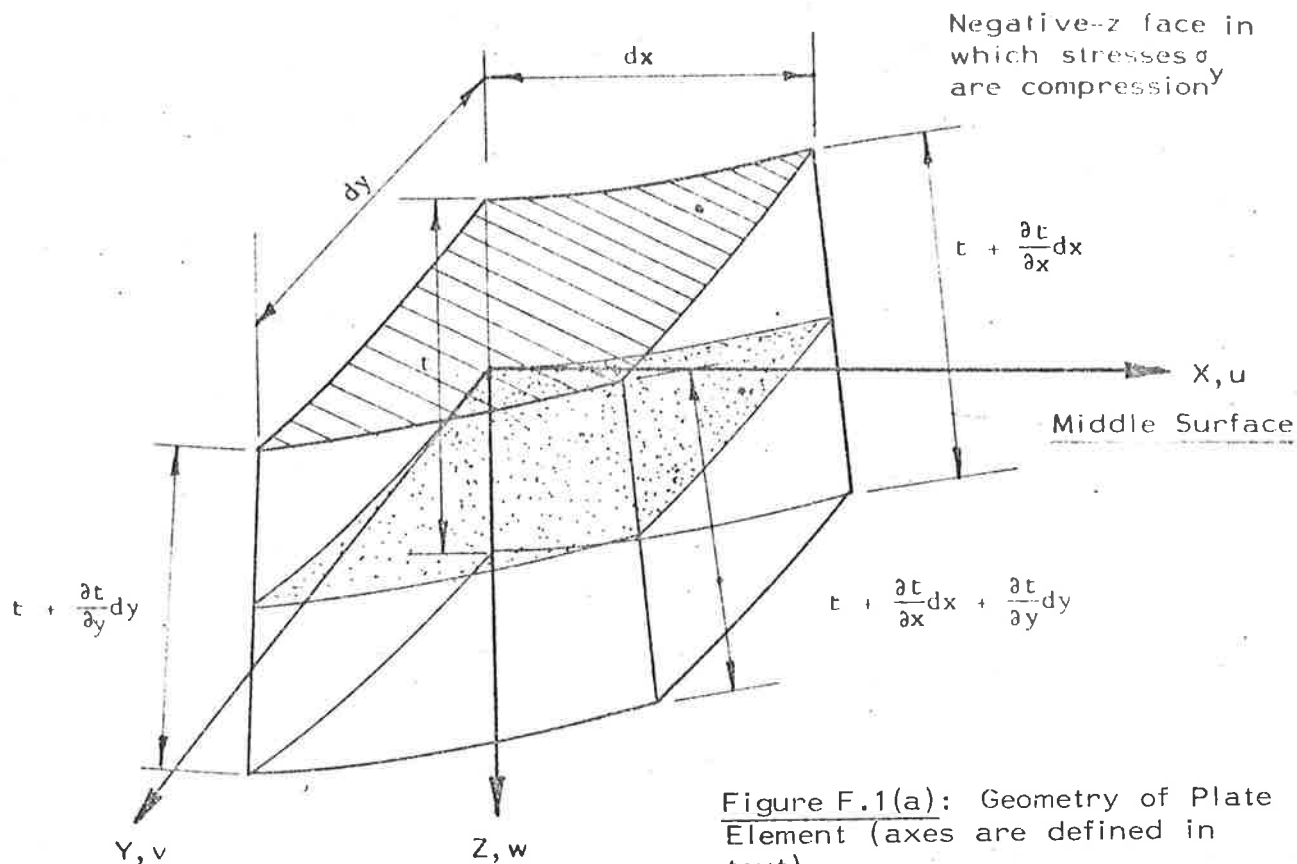


Figure F.1(a): Geometry of Plate Element (axes are defined in text)

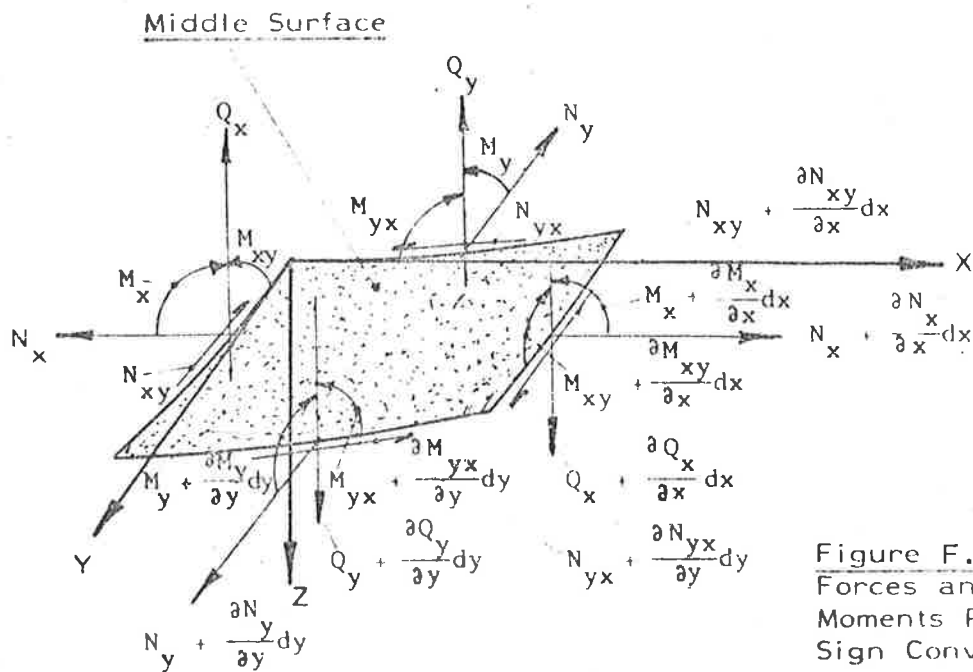


Figure F.1 (b): Forces and Moments Positive Sign Conventions

Figure F.1: Varying Thickness Plate Element

$$\frac{\partial M_{yx}}{\partial y} - Q_x + \frac{\partial M_x}{\partial x} = 0 \quad (\text{F.2})$$

(b) Force Equilibrium

(i)  $\sum$  Forces in X direction is zero, so that -

$$\frac{\partial N_x}{\partial x} + \frac{\partial N_{yx}}{\partial y} = 0 \quad (\text{F.3})$$

(ii)  $\sum$  Forces in Y direction is zero, so that -

$$\frac{\partial N_{xy}}{\partial x} + \frac{\partial N_y}{\partial y} = 0 \quad (\text{F.4})$$

(iii)  $\sum$  Forces in Z direction is zero.

The forces in the Z direction are made up of several components.

(a) Considering the shear forces in figure F.1(b), if the uniform lateral pressure is  $q$ , then the component of forces in the Z direction is -

$$\left( \frac{\partial Q}{\partial x} + \frac{\partial Q}{\partial y} + q \right) dx dy \quad (\text{F.5(a)})$$

(b) The projection of X-directed forces in the Z-direction can be calculated by observing that the slope of the middle surface on the negative-X face in the X direction is  $\left( \frac{\partial w}{\partial x} + \frac{1}{2} \frac{\partial t}{\partial x} \right)$  and on the positive-X face as  $\left[ \left( \frac{\partial w}{\partial x} + \frac{1}{2} \frac{\partial t}{\partial x} \right) + \frac{\partial}{\partial x} \left( \frac{\partial w}{\partial x} + \frac{1}{2} \frac{\partial t}{\partial x} \right) dx \right]$ . Therefore the component of X-directed forces in the Z-direction is -

$$-N_x dy \left( \frac{\partial w}{\partial x} + \frac{1}{2} \frac{\partial t}{\partial x} \right) + \left( N_x + \frac{\partial N_x}{\partial x} dx \right) \left( \frac{\partial w}{\partial x} + \frac{1}{2} \frac{\partial t}{\partial x} + \frac{\partial}{\partial x} \left( \frac{\partial w}{\partial x} + \frac{1}{2} \frac{\partial t}{\partial x} \right) dx \right) dy$$

By neglecting high order terms, this expression becomes -

$$N_x \left( \frac{\partial^2 w}{\partial x^2} + \frac{1}{2} \frac{\partial^2 t}{\partial x^2} \right) dx dy + \frac{\partial N_x}{\partial x} \left( \frac{\partial w}{\partial x} + \frac{1}{2} \frac{\partial t}{\partial x} \right) dx dy \quad (\text{F.5(b)})$$

Similarly, projection of the normal forces  $N_y$  on the Z axis gives the expression –

$$N_y \left( \frac{\partial^2 w}{\partial y^2} + \frac{1}{2} \frac{\partial^2 t}{\partial y^2} \right) dx dy + \frac{\partial N_y}{\partial y} \left( \frac{\partial w}{\partial y} + \frac{1}{2} \frac{\partial t}{\partial y} \right) dx dy \quad (\text{F.5(c)})$$

(c) For the projection of the shearing forces  $N_{xy}$  on the Z-axis, the slopes of the middle surface in the Y-direction on the two opposite X faces of the element (figure F.1(a)) are –

$$\left( \frac{\partial w}{\partial y} + \frac{1}{2} \frac{\partial t}{\partial y} \right) \text{ on the negative-X face}$$

$$\text{and} \quad \left( \frac{\partial w}{\partial y} + \frac{1}{2} \frac{\partial t}{\partial y} \right) + \frac{\partial}{\partial x} \left( \frac{\partial w}{\partial y} + \frac{1}{2} \frac{\partial t}{\partial y} \right) dx \text{ on the positive-X face.}$$

Hence, the projection of the shearing forces  $N_{xy}$  on the Z-axis is equal to

$$N_{xy} \left( \frac{\partial^2 w}{\partial x \partial y} + \frac{1}{2} \frac{\partial^2 t}{\partial x \partial y} \right) dx dy + \frac{\partial N_{xy}}{\partial x} \left( \frac{\partial w}{\partial y} + \frac{1}{2} \frac{\partial t}{\partial y} \right) dx dy \quad (\text{F.5(d)})$$

(d) Similarly, the projection of the shearing forces  $N_{yx}$  on the Z-axis is –

$$N_{yx} \left( \frac{\partial^2 w}{\partial x \partial y} + \frac{1}{2} \frac{\partial^2 t}{\partial x \partial y} \right) dx dy + \frac{\partial N_{yx}}{\partial y} \left( \frac{\partial w}{\partial x} + \frac{1}{2} \frac{\partial t}{\partial x} \right) dx dy \quad (\text{F.5(e)})$$

By substituting  $N_{yx} = N_{xy}$ , the total expression for the projection of all forces on the Z-axis from equations (F.5(a)) to (F.5(e)) is –

$$\begin{aligned} & \left[ \frac{\partial Q_x}{\partial x} + \frac{\partial Q_y}{\partial y} + q + N_x \left( \frac{\partial^2 w}{\partial x^2} + \frac{1}{2} \frac{\partial^2 t}{\partial x^2} \right) + \frac{\partial N_x}{\partial x} \left( \frac{\partial w}{\partial x} + \frac{1}{2} \frac{\partial t}{\partial x} \right) + N_y \left( \frac{\partial^2 w}{\partial y^2} + \frac{1}{2} \frac{\partial^2 t}{\partial y^2} \right) \right. \\ & + \frac{\partial N_y}{\partial y} \left( \frac{\partial w}{\partial y} + \frac{1}{2} \frac{\partial t}{\partial y} \right) + 2N_{xy} \left( \frac{\partial^2 w}{\partial x \partial y} + \frac{1}{2} \frac{\partial^2 t}{\partial x \partial y} \right) + \frac{\partial N_{xy}}{\partial x} \left( \frac{\partial w}{\partial y} + \frac{1}{2} \frac{\partial t}{\partial y} \right) \\ & \left. + \frac{\partial N_{xy}}{\partial y} \left( \frac{\partial w}{\partial x} + \frac{1}{2} \frac{\partial t}{\partial x} \right) \right] dx dy = 0 \quad (\text{F.6}) \end{aligned}$$

By inspection, from equations (F.3) and (F.4), the following relationships may be used to eliminate terms from equation (F.6) –

$$\frac{\partial N_x}{\partial x} \left( \frac{\partial w}{\partial x} + \frac{1}{2} \frac{\partial t}{\partial x} \right) + \frac{\partial N_{xy}}{\partial y} \left( \frac{\partial w}{\partial x} + \frac{1}{2} \frac{\partial t}{\partial x} \right) = 0 \quad (\text{F.7(a)})$$

$$\frac{\partial N_y}{\partial y} \left( \frac{\partial w}{\partial y} + \frac{1}{2} \frac{\partial t}{\partial y} \right) + \frac{\partial N_{xy}}{\partial x} \left( \frac{\partial w}{\partial y} + \frac{1}{2} \frac{\partial t}{\partial y} \right) = 0 \quad (\text{F.7(b)})$$

As well, from equation (F.1), 
$$\frac{\partial Q_x}{\partial x} = \frac{\partial^2 M_x}{\partial x^2} + \frac{\partial^2 M_{yx}}{\partial x \partial y} \quad (\text{F.7(c)})$$

and from equation (F.2), 
$$\frac{\partial Q_y}{\partial y} = \frac{\partial^2 M_y}{\partial y^2} + \frac{\partial^2 M_{xy}}{\partial x \partial y} \quad (\text{F.7(d)})$$

With reference to section 6.2.4 on brickwork torsion, in general  $M_{xy} \neq M_{yx}$ , so that, from equations (F.6) and (F.7(a)) to (F.7(d)), the equation of equilibrium is -

$$\begin{aligned} \frac{\partial^2 M_x}{\partial x^2} + \frac{\partial^2}{\partial x \partial y} (M_{xy} + M_{yx}) + \frac{\partial^2 M_y}{\partial y^2} &= -q - N_x \left( \frac{\partial^2 w}{\partial x^2} + \frac{1}{2} \frac{\partial^2 t}{\partial x^2} \right) \\ &= N_y \left( \frac{\partial^2 w}{\partial y^2} + \frac{1}{2} \frac{\partial^2 t}{\partial y^2} \right) - 2N_{xy} \left( \frac{\partial^2 w}{\partial x \partial y} + \frac{1}{2} \frac{\partial^2 t}{\partial x \partial y} \right) \end{aligned} \quad (\text{6.9})$$

## F.2 MODULUS FUNCTIONS $E_x(t)$ , $E_y(t)$ , $G(t)$

The brickwork modulus functions  $E_x(t)$ ,  $E_y(t)$  and  $G(t)$  (Section 6.3.2) may be derived by using the results of the finite element calculations described in Section 6.2. The functions  $E_x(t)$ ,  $E_y(t)$  and  $G(t)$  modify the stiffnesses of the an equivalent varying thickness plate to simulate the stiffnesses of cracked brickwork.

### F.2.1 Function $E_x(t)$ (Section 6.2.3)

Provided that forces  $N_x$  and  $N_{xy}$  are zero —

$$E_x(t) = C_x \cdot E_b \cdot \left[ \frac{H(L + p) + \frac{b}{(E_b/E_m)}}{L + \frac{(E_b/E_m)p}{E_m}} \right] \quad (F.8)$$

in which  $E_b$  is brick modulus

$E_m$  is mortar modulus

$H$  is brick height

$b$  is bedjoint thickness

$p$  is perpend thickness

$L$  is brick length

$$\text{and } C_x = \begin{cases} 1.0 & \text{for uncracked perpends} \\ 0.75 \cdot \left(\frac{d}{t}\right)^3 & \text{for cracked perpends (bricks 110mm x 65mm x} \\ & \text{230mm laid on edge)} \end{cases}$$

It should be noted that in the derivation of equation (F.8), brick-to-mortar modular ratios varied between 1.0 and 10.0 (Tables 6.3, 6.4).

### F.2.2 Function $E_y(t)$ (Sections 4.3.1, 6.2.2)

$$E_y(t) = E_b \cdot \left[ \frac{(b + H)}{\left(\frac{H}{\alpha}\right) + \left(\frac{E_b}{E_m}\right) \cdot b} \right] \quad (F.9)$$

in which  $\alpha$  is a curvature ratio factor defined in Chapter 4.

In terms of the equivalent plate thickness at any point —

$$\alpha = \begin{cases} 1.0 & \text{for } t=d \\ \{1 \ t_o \ t_o^2 \ t_o^3\} [R] \begin{Bmatrix} 1 \\ r_o \\ r_o^2 \\ r_o^3 \end{Bmatrix} & \text{for } t < d \end{cases} \quad (\text{F.10})$$

in which  $t_o = \left(\frac{d/2 - t/3}{d}\right)$

[R] is a 4x4 matrix derived in Appendix A (equation (A.3))

$r_o = (H/d)$

H is the brick height

d is the brickwork thickness.

### F.2.3 Function G(t) (Section 6.2.4)

It may be assumed (figure 6.14) that for brick-to-mortar modular ratios between 1.0 and 10.0, functions  $F_1(E_b:E_m)$  and  $F_2(E_D:Em)$  (equations (6.7(a)), (6.7(b)) respectively) are equal. That is -

$$\frac{1}{2} \left( \frac{\bar{M}_{yz} + \bar{M}_{zy}}{\bar{M}} \right) = \left[ \frac{E_y}{E_b} \cdot \frac{E_z}{E_b} \right]^{\frac{1}{2}}$$

in which  $\bar{M}_{yz}$  is the total twisting moment on each Y force of the panel module defined in figures 6.1(b), 6.11

$\bar{M}_{zy}$  is the total twisting moment on each Z face of the panel module defined in figures 6.1(b), 6.11.

$\bar{M}$  is the total twisting moment on each of the Y and Z faces for a brick:mortar modular ratio of 1.0

$E_y$  is an effective elastic modulus for brickwork as defined by equation (4.21)

$E_z$  is an effective elastic modulus for brickwork as defined by equation (6.2)

$E_b$  is the brick elastic modulus.

From plate theory<sup>(112)</sup>, it can be shown that –

$$\bar{M} = -(H+b) \frac{E_b \cdot d^3}{(1-\nu_b)} \cdot (1-\nu_b) \cdot \frac{\partial^2 \bar{x}}{\partial y \partial z} \quad (F.12)$$

in which  $d$  is the panel thickness (= 65mm in this case)

$\nu_b$  is the brick Poisson's ratio

$\bar{x}$  is brick displacement in the X direction (figure 6.11)

$H, b$  are defined as for equation (F.8)

Equation (F.11) may be written as –

$$(\bar{M}_{yz} + \bar{M}_{zy}) = \frac{2\bar{M}}{E_b} [E_y \cdot E_z]^{\frac{1}{2}} \quad (F.13)$$

Equations (F.12) and (F.13) together give –

$$\frac{1}{(H+b)} \cdot (\bar{M}_{yz} + \bar{M}_{zy}) = -2[E_y \cdot E_z]^{\frac{1}{2}} \cdot \frac{d^3}{12(1+\nu_b)} \cdot \frac{\partial^2 \bar{x}}{\partial y \partial z} \quad (F.14)$$

Equation (F.14) is similar to the equation for twisting moments of a homogeneous plate<sup>(112)</sup> in which –

$$G = \frac{[E_y \cdot E_z]^{\frac{1}{2}}}{2(1+\nu_b)} \quad (6.8)$$

Results summarized in Tables 6.6 and 6.7 for brick-to-mortar modular ratios between 1.0 and 5.0 indicate that the torsional stiffness of cracked brickwork is approximately 85 percent of the stiffness of uncracked brickwork. Therefore, in equation (6.14(c)), the torsional stiffness,  $G(t)$ , for cracked brickwork may be expressed as –

$$G(t) = 0.85 \cdot G \cdot \left(\frac{d}{t}\right)^3 \quad (F.15)$$

since the equivalent plate thickness,  $t$ , may be less than the uncracked plate thickness,  $d$ , and perpendicular cracking occurs throughout the panel defined in figure 6.17.



That is, for the axis system defined in Section 6.3, the torsional stiffness for cracked brickwork for equation (6.14(c)) is -

$$G(t) = 0.85 \left(\frac{d}{t}\right)^3 \sqrt{\frac{E_x(t)_{t=d} \cdot E_y(t)_{t=d}}{2(1 + \nu_b)}} \quad (F.16)$$

in which  $E_x(t)_{t=d}$ ,  $E_y(t)_{t=d}$  may be calculated from equations (F.8) and (F.9) respectively

$\nu_b$  is the brick Poisson's ratio.

Equation (F.16) may be applied to bricks 110mm x 65mm x 230mm laid in common stretcher bond (figures 6.1(a), 6.1(b)), and for brick-to-mortar modular ratios between 1.0 and 5.0.

APPENDIX GBRICKWORK PANELS IN TWO-WAY BENDING - PROGRAM PANEL1

## G.1 THE SCOPE OF PROGRAM PANEL 1

PROGRAM PANEL1 uses a finite difference method to analyse a brickwork panel simply-supported on four sides. Such a panel may be loaded at equal eccentricities top and bottom by a uniform line load and may be loaded simultaneously by a uniform lateral pressure (figure G.1).

Both the brick and mortar materials are assumed to have linear stress-strain characteristics and stress-related failure criteria may be assumed (Section 8.2). Documentation of input data requirements is given in the following section and a skeleton flow chart is presented in Section G.3.

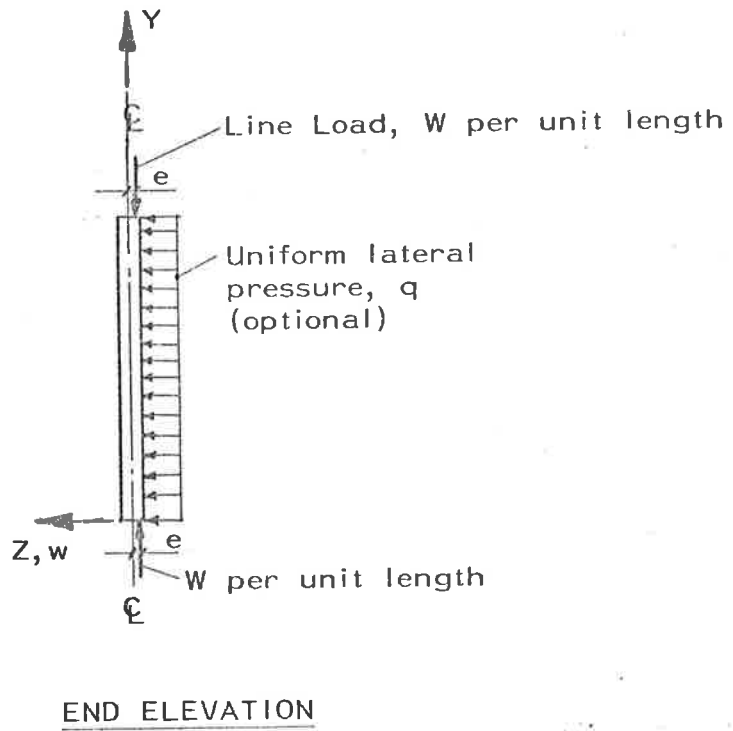
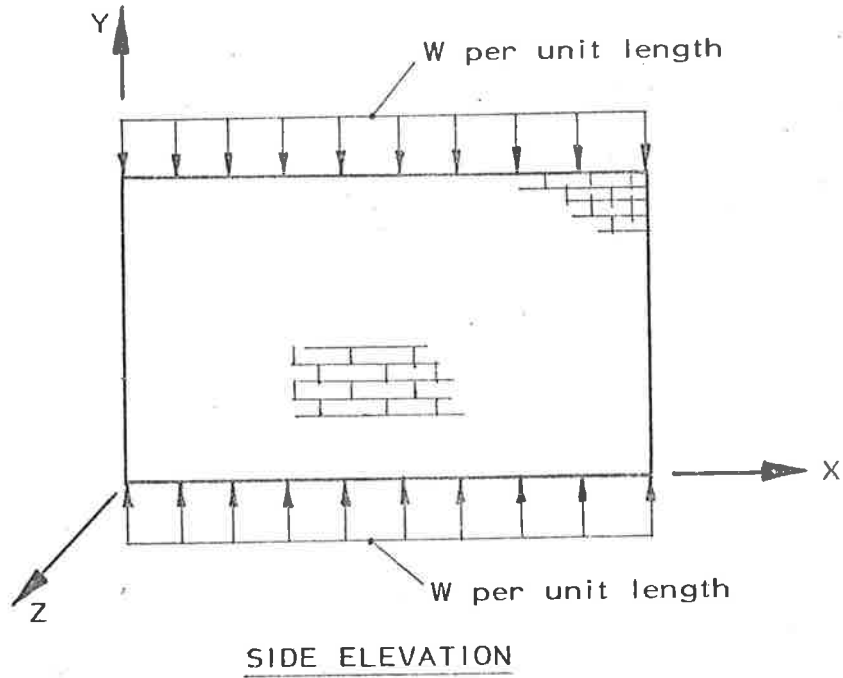


Figure G.1: Simply-supported Brickwork Panel showing Load Conditions for PROGRAM PANEL1



```

C      *      PERPEND THICKNESS, F10.3 ( MM )      *
C      *      BRICK HEIGHT, F10.3 ( MM )          *
C      *      BEDJOINT THICKNESS, F10.3 ( MM )    *
C      *      LINE 4: PANEL THICKNESS, F10.4 ( MM ) *
C      *      F.D. ELEMENT DIM.(X-DIR.), F10.4 ( MM ) *
C      *      LOAD ECCENTRICITY, F10.4 ( MM )     *
C      *      LINE 5: RATIO ALPHA, F5.3           *
C      *      NO. ELEMENTS IN X-DIR.(16), I5      *
C      *      NO. ELEMENTS IN Y-DIR.(8), I5      *
C      *      LINE 6: BRICK MODULUS, F8.0 ( MPA ) *
C      *      MORTAR MODULUS, F8.0 ( MPA )       *
C      *      BRICKWORK SHEAR MODULUS, F8.0 ( MPA ) *
C      *      ( ---IF ZERO, IS AUTO. GENERATED--- ) *
C      *      POISSONS RATIOS, UXY,UYX,UB, 3F8.3 *
C      *      LINE 7: BRICKWORK COMPRESSIVE STRENGTH, F6.2(MPA) *
C      *      BRICK TENSILE STRENGTH, F6.2 ( MPA ) *
C      *      STRENGTH TEST FLAG; I2 ( 1=YES,0=NO ) *
C      *      *
C      *****

```

```

MS=19
MRS=11
MO=1
NPLOT=0
IFAIL=0

```

```

C
C
C

```

READ PROBLEM TYPE, INITIAL LOADS AND PANEL CONSTANTS

```

READ(5,1) ITYPE
1 FORMAT(I1)
IF(ITYPE.EQ.0) WRITE(6,60)
IF(ITYPE.EQ.1) WRITE(6,61)
IF(ITYPE.EQ.2) WRITE(6,62)
60 FORMAT(1H1,15X,*---- SOLID PANEL PROBLEM ----*/)
61 FORMAT(1H1,15X,*---- NO-TENSION-MATERIAL PANEL PROBLEM*
1* ----*/)
62 FORMAT(1H1,15X,*---- CRACKED BRICKWORK PANEL PROBLEM ----*/)
READ(5,10) PNY,Q
10 FORMAT(F10.4,F10.6)
WRITE(6,11) PNY,Q
11 FORMAT(1H0,5X,*VERTICAL LOAD IS *,F10.4,* N/MM LENGTH*
1* OF WALL*/,1H0,5X,*LATERAL LOAD IS *,F10.6,* MPA*)
READ(5,2) XB,XP,HB,HM
2 FORMAT(4F10.3)
WRITE(6,3) XB,XP,HB,HM
3 FORMAT(1H0,5X,*BRICK LENGTH IS *,F10.3,* MM*/,1H0,5X,
1*MORTAR PERPEND THICKNESS IS *,F10.3,* MM*/,1H0,5X,
2*BRICK HEIGHT IS *,F10.3,* MM*/,1H0,5X,*MORTAR BEDJOINT*
3* THICKNESS IS *,F10.3,* MM*)
READ(5,14) T,XH,EO
14 FORMAT(3F10.4)
WRITE(6,15) T,XH,EO
15 FORMAT(1H0,5X,*PANEL THICKNESS IS *,F10.4,* MM*/,1H0,5X,
1*HORIZONTAL DIMENSION OF FINITE DIFFERENCE ELEMENT IS *,
2F10.4,* MM*/,1H0,5X,*VERTICAL LOAD ECCENTRICITY IS *,F10.4,

```

```

3* MM*)
  READ(5,12) ALPHA,M,N
12 FORMAT(F5.3,2I5)
  WRITE(6,13) ALPHA,M,N
13 FORMAT(1H0,5X,*RATIO ALPHA IS *,F5.3,/,1H0,5X,*NO. OF*
  1* FINITE DIFFERENCE ELEMENTS IN HORIZONTAL */25X,
  2*DIRECTION IS *,I5,/,1H0,5X,*NO. OF FINITE DIFFERENCE*
  3* ELEMENTS IN VERTICAL DIRECTION IS *,I5)
  READ(5,90) EB,EM,GXY,UXY,UYX,UB
90 FORMAT(3F8.0,3F8.3)
  READ(5,114) CMFAIL,SIGT,ISTFLG
114 FORMAT(2F6.2,I2)
  IF(ISTFLG.EQ.0) GO TO 116
  WRITE(6,115) CMFAIL,SIGT
115 FORMAT(1H0,5X,*BRICKWORK COMPRESSIVE STRENGTH IS SPECIFIED TO BE *
  1,F6.2,* MPA*/1H0,5X,*BRICK TENSILE STRENGTH IS SPECIFIED TO BE *,
  2F6.2,* MPA*)
  GO TO 117
116 WRITE(6,118)
118 FORMAT(1H0,5X,*---NO MATERIAL STRENGTH TESTS IN THIS PROGRAM---*)
117 CONTINUE

C
C   CALCULATE EX FOR TRANSVERSE BENDING ( REF. BASE,BAKER )
C
  EX=EB*(HB*(XB+XP)/(XB+EB/EM*XP)+HM*EM/EB)/(HB+HM)
  WRITE(6,4) EX
  4 FORMAT(1H0,5X,*EQUIVALENT TRANSVERSE ELASTIC MODULUS IS *,
  *F10.0,* MPA*)

C
C   CALCULATE EQUIVALENT MODULUS FOR UNCRACKED VERTICAL BENDING
C
  EY=EB*(HB+HM)/(HB+EB/EM*HM)
C   CALCULATE SHEAR MODULUS IF REQUIRED
  IF(GXY.NE.0.) GO TO 64
  GXY=SQRT(EX*EY)/(2.*(1.+UB))
64 CONTINUE
  WRITE(6,91) EB,EM,GXY,UXY,UYX,UB
91 FORMAT(1H0,5X,*BRICK YOUNGS MODULUS IS *,F10.0,* MPA*,
  1/,1H0,5X,*MORTAR YOUNGS MODULUS IS *,F10.0,* MPA*,/,1H0,5X,
  2*BRICKWORK SHEAR MODULUS IS *,F10.0,* MPA*,/,
  31H0,5X,*BRICKWORK POISSONS RATIO UXY IS *,F10.3,/,1H0,5X,
  4*BRICKWORK POISSONS RATIO UYX IS *,F10.3,/,1H0,5X,*BRICK *
  5*POISSONS RATIO UB IS *,F10.3,/,1H1)

C
  IF(ITYPE.NE.2) GO TO 63
C   CALCULATE MATRIX AA FOR TENSION-FIELD STIFFENING
C
  HD=HB/T $ HD1=HD $ HD2=HD*HD $ HD3=HD**3
  AA(1)=1.03-1.18*HD1+0.794*HD2-0.187*HD3
  AA(2)=-0.326+14.4*HD1-9.47*HD2+2.32*HD3
  AA(3)=1.22-54.1*HD1+31.3*HD2-7.98*HD3
  AA(4)=-1.39+61.0*HD1-18.5*HD2+4.79*HD3
63 CONTINUE

C
C   INITIALIZE LOAD INCREMENT CONSTANTS
C

```

```

      DELPNY=PNY
      SPNY=0.
C
C   SET UP FINITE DIFFERENCE GRID CONSTANTS
C
      MN=M+1 $ MNO=M+2 $ MNOP=M+3
      NP=N+1 $ NPQ=N+2 $ NPQR=N+3
      MNT=(M-1)*(N-1)
C
C   SET MATRICES TO ZERO
C
      DO 92 JT = 1,MRS
      DO 93 JS = 1,MS
      W(JS, JT)=0.
      PW(JS, JT)=0.
      DW(JS, JT)=0.
      WE(JS, JT)=0.
      BMX(JS, JT)=0.
      BMY(JS, JT)=0.
      BMXY(JS, JT)=0.
      PKX(JS, JT)=0.
      PKY(JS, JT)=0.
      PKXY(JS, JT)=0.
      SKX(JS, JT)=0.
      SKY(JS, JT)=0.
      SKXY(JS, JT)=0.
      ET(JS, JT)=0.
      BT(JS, JT)=0.
93 CONTINUE
92 CONTINUE
      DO 94 JW = 1,MNT
      DO 95 JV = 1,MNT
      RS(JV, JW)=0.
      A(JV, JW)=0.
      AINV(JV, JW)=0.
95 CONTINUE
      R(JW)=0.
      RR(JW)=0.
94 CONTINUE
C
C   INITIALIZE SECTION THICKNESS AND ELASTIC MODULUS FACTORS
C   AT ALL NODES
C
      DO 65 JIL = 2,NPQ
      DO 66 JAK = 2,MNO
      ET(JAK, JIL)=T
      PKX(JAK, JIL)=1.
      PKXY(JAK, JIL)=1.
      PKY(JAK, JIL)=(HB+HM)/(HB+EB/EM*HM)
66 CONTINUE
65 CONTINUE
C
C   CALCULATE ELASTIC MODULUS FACTORS PKY AT TOP AND
C   BOTTOM BOUNDARIES
C
      DO 6 IL = 3,MN

```

```

C
C CHECK WHETHER TENSION-STIFFENING IS REQUIRED
C IF YES, CALCULATE EFFECTIVE MODULUS FACTORS PKY
C
  IF(ITYPE.NE.2) GO TO 5
  IF(E0.LE.T/6.) GO TO 5
  TE=E0/T
  TE1=TE $ TE2=TE*TE $ TE3=TE**3
  PEC=AA(1)+TE1*AA(2)+TE2*AA(3)+TE3*AA(4)
  PKY(IL,2)=PKY(IL,NPQ)=(HB+HM)/(1./PEC*HB+EB/EM*HM)
  GO TO 6
5 PKY(IL,2)=PKY(IL,NPQ)=(HB+HM)/(HB+EB/EM*HM)
6 CONTINUE

C
C CALCULATE EFFECTIVE THICKNESS AT TOP AND BOTTOM SUPPORTS
C
  DO 9 IRA = 3,MN

C
C CHECK WHETHER SECTION IS CRACKED ON BEDJOINT
C
  IF(ITYPE.EQ.0) GO TO 8
  IF(E0.LE.T/6.) GO TO 8
  ET(IRA,2)=ET(IRA,NPQ)=3.*(T/2.-E0)
  GO TO 9
8 ET(IRA,2)=ET(IRA,NPQ)=T
9 CONTINUE

C
C CALCULATE EFFECTIVE THICKNESS AT VERTICAL SUPPORTS
C
  DO 7 IRC = 2,NPQ
  ET(2,IRC)=ET(MNO,IRC)=T
7 CONTINUE

C
C NEWTON-RAPHSON ITERATION PROCEDURE BEGINS AT THIS STAGE
C
  DO 100 LP = 1,100

C
C THIS LOOP INCREMENTS THE LOAD PNY
C CALCULATE DISPLACEMENTS BY ITERATION ALLOWING FOR CRACKING
C ( IF REQUIRED )
  DO 99 IJK = 1,20
C ITERATE TO CALCULATE CONSISTENT SET OF DISPLACEMENTS, CURVATURES
C AND TENSION STIFFENING FACTORS ( IF REQUIRED )
  DO 98 JIK = 1,10
C CALCULATE EFFECTIVE THICKNESS AT ALL NODES ( IF REQUIRED )
  IF(ITYPE.NE.0) CALL PHYSP(NP,MN,XH,ALPHA,UYX,UXY,PNY,T,W,ET,MS,
  *PKX,PKY,PKXY,AA,EB,EM,HB,HM,ITYPE)
C CALCULATE BENDING MOMENTS AT ALL NODES
  CALL BEND(M,MN,MNO,MNOP,N,NP,NPQ,NPQR,I1,I2,XH,ALPHA,UYX,UXY,
  *EX,GXY,E0,T,PNY,W,ET,BMX,BMY,BMXY,MS,PKX,PKY,PKXY,EB,ITYPE)
98 CONTINUE
C CALCULATE THE ERROR TERM AT ALL NODES
  CALL ERROR(NP,MN,XH,ALPHA,Q,PNY,W,ET,BMX,BMY,BMXY,RR,MS,ITYPE)
  ERR=0.
  DO 16 LX = 1,MNT
  R(LX)=RR(LX)

```



```

C   CALCULATE MAXIMUM ERROR TERM TO CHECK END OF ITERATION
      ER=ABS(R(LX))
      IF(ER.GT.ERR) ERR=ER
16  CONTINUE
C
C   CHECK VALUE OF MAXIMUM ERROR TERM
C   ITERATION IS COMPLETED IF MAX ERR IS LESS THAN 1.0E-06
C
      IF(ERR.LT.1.0E-06) GO TO 110
C
C   USE MODIFIED NEWTON-RAPHSON METHOD TO CALCULATE DISPLACEMENTS
C
      DEAL=0.001
C
C   CHANGE NODAL DISPLACEMENTS EACH IN TURN BY DEAL
C   CALCULATE EFFECT OF CHANGE IN ERROR TERM AT ALL NODES
C
      NRS=0
      DO 17 LY = 3,NP
      DO 18 LZ = 3,MN
      WSAVE=W(LZ,LY)
C   SAVE ORIGINAL VALUES OF EFFECTIVE THICKNESS AND STIFFENING COEFFICIENT
      DO 19 IV = 3,NP
      DO 20 JV = 3,MN
      BT(JV,IV)=ET(JV,IV)
      SKX(JV,IV)=PKX(JV,IV)
      SKY(JV,IV)=PKY(JV,IV)
      SKXY(JV,IV)=PKXY(JV,IV)
20  CONTINUE
19  CONTINUE
      NRS=NRS+1
      W(LZ,LY)=W(LZ,LY)+DEAL
C   CALCULATE NEW EFFECTIVE THICKNESS AT ALL NODES ( IF REQUIRED )
      IF(ITYPE.NE.0) CALL PHYSP(NP,MN,XH,ALPHA,UYX,UXY,PNY,T,W,ET,MS,
      *PKX,PKY,PKXY,AA,EB,EM,HB,HM,ITYPE)
C   CALCULATE NEW BENDING MOMENTS AT ALL NODES
      CALL BEND(M,MN,MNO,MNOP,N,NP,NPQ,NPQR,I1,I2,XH,ALPHA,UYX,UXY,
      *EX,GXY,EO,T,PNY,W,ET,BMX,BMY,BMXY,MS,PKX,PKY,PKXY,EB,ITYPE)
C   CALCULATE NEW ERROR TERMS AT ALL NODES
      CALL ERROR(NP,MN,XH,ALPHA,Q,PNY,W,ET,BMX,BMY,BMXY,RR,MS,ITYPE)
C   REASSIGN ORIGINAL DISPLACEMENT FUNCTION VALUES
      W(LZ,LY)=WSAVE
      DO 21 IW = 3,MN
      DO 22 JW = 3,NP
      ET(IW,JW)=BT(IW,JW)
      PKX(IW,JW)=SKX(IW,JW)
      PKY(IW,JW)=SKY(IW,JW)
      PKXY(IW,JW)=SKXY(IW,JW)
22  CONTINUE
21  CONTINUE
C
C   SET UP JACOBIAN MATRIX RS FOR NEWTON-RAPHSON ITERATION
      DO 23 MRS = 1,MNT
      RS(MRS,NRS)=(RR(MRS)-R(MRS))/DEAL
23  CONTINUE
18  CONTINUE

```

```

17 CONTINUE
C
C   TRANSFER MATRIX RS INTO MATRIX A FOR INVERSION
C
      DO 34 KAR = 1,MNT
      DO 35 KAT = 1,MNT
      A(KAR,KAT)=RS(KAR,KAT)
35 CONTINUE
34 CONTINUE
C
C   INVERT MATRIX A
C
      CALL MINV(A,AINV,MNT)
C
C   CALCULATE INCREMENTAL CHANGES IN DISPLACEMENTS ( DW )
C
      DO 36 KAL = 1,MNT
      X=0.
      DO 37 KAK = 1,MNT
      X=X+AINV(KAL,KAK)*(-R(KAK))
37 CONTINUE
      KBL=KAL-1
      KAP=KBL/(M-1)
      KBP=3+KAP
      KAS=KBL-(M-1)*KAP
      KASS=3+KAS
      DW(KASS,KBP)=X
36 CONTINUE
C
C   CALCULATE NEW DISPLACEMENTS AT ALL NODES
C   CHECK FOR NEGATIVE DISPLACEMENTS ( INVALID )
C
      DO 38 LTA = 3,MN
      DO 39 LTB = 3,NP
      W(LTA,LTB)=W(LTA,LTB)+DW(LTA,LTB)
      IF(W(LTA,LTB).LT.0.) GO TO 120
39 CONTINUE
38 CONTINUE
C
C   CHECK THAT SECONDARY MODE OF DISPLACEMENT IS NOT ATTAINED ( INVALID )
C
      DO 24 JXL = 2,NPQ
      DO 25 IXL = 2,MNO
      MC=M/2+2 $ NC=N/2+2
      IF(W(IXL,JXL).GT.(1.05*W(MC,NC))) GO TO 120
25 CONTINUE
24 CONTINUE
99 CONTINUE
C
C   END OF INNER ITERATION LOOP
C
      WRITE(6,40) PNY
40 FORMAT(1H0,5X,*AT LOAD PNY = *,F10.3,* N/MM */6X,*EQUILIBRIUM IS *
      **NOT ATTAINED AFTER TWENTY ITERATIONS*)
      GO TO 130
120 WRITE(6,41)

```

```

41 FORMAT(1H0,5X,*MATHEMATICAL FAILURE HAS OCCURRED*)
130 CONTINUE
    DPNY=DELPNY/MO
    IF(DPNY.GT.-1.0) GO TO 140
C
C   DECREASE THE LOAD INCREMENT ADDED TO PNY
C   REASSIGN DISPLACEMENT VALUES ASSOCIATED WITH LOAD SPNY
C
    PNY=SPNY
    DO 42 JLP = 2, NPQ
    DO 43 ILP = 2, MNO
    W(ILP, JLP)=PW(ILP, JLP)
43 CONTINUE
42 CONTINUE
    MO=MO*2
    PNY=PNY+DELPNY/MO
C
C   EXTRAPOLATE FOR NEW DISPLACEMENTS AT NEW LOAD PNY
C
    CALL EXTRAP(NPQ, MNO, MO, W, WE, MS)
    GO TO 100
110 WRITE(6, 54)
    54 FORMAT(1H1, 25X, *EQUILIBRIUM HAS BEEN ATTAINED*)
C
C   CHECK FOR MATERIAL FAILURE
C
    IF(ISTFLG.EQ.0) GO TO 170
    CALL MATFAIL(MNO, NPQ, T, SIGT, IFAIL, PNY, CMFAIL, EO, BMX, BMY,
1BMXY, ET, MS)
    IF(IFAIL.EQ.0) GO TO 170
    IF(IFAIL.EQ.1) WRITE(6, 121)
    IF(IFAIL.EQ.2) WRITE(6, 122)
    IF(IFAIL.EQ.3) WRITE(6, 123)
121 FORMAT(1H0, 20X, *TENSILE FAILURE DUE TO BENDING X-X*)
122 FORMAT(1H0, 20X, *BRICKWORK COMPRESSIVE FAILURE*)
123 FORMAT(1H0, 20X, *TENSILE FAILURE AT 45 DEGREES TO BEDJOINTS*)
    IFAIL=0
    GO TO 130
170 CONTINUE
C
C   PRINT OUT PLATE DISPLACEMENTS
C
    WRITE(6, 44) PNY
44 FORMAT(1H0, 10X, *NODAL DISPLACEMENTS (MM) FOR PNY = *, F10.3,
1* N/MM ARE ----*)
    DO 45 II = 2, NPQ
    WRITE(6, 52) (W(JJ, II), JJ=2, MNO)
45 CONTINUE
C
C   STORE DISPLACEMENTS OF CENTRE NODE FOR LOAD-DISPLACEMENT PLOT
C
    NPLOT=NPLOT+1
    PLAT(NPLOT)=-PNY
    PLOT(NPLOT)=W(MC, NC)
C
C   PRINT OUT BENDING MOMENTS AT ALL NODES
C

```

```

WRITE(6,180) PNY
180 FORMAT(1H0,10X,*BENDING MOMENTS MX ( NMM/MM ) FOR PNY = *,F10.3,
1* N/MM ARE ---*)
DO 181 II = 2, NPQ
WRITE(6,52) (BMX(JJ,II),JJ=2,MNO)
181 CONTINUE
WRITE(6,182) PNY
182 FORMAT(1H0,10X,*BENDING MOMENTS MY ( NMM/MM ) FOR PNY = *,F10.3,
1* N/MM ARE ---*)
DO 183 II = 2, NPQ
WRITE(6,52) (BMY(JJ,II),JJ=2,MNO)
183 CONTINUE
WRITE(6,184) PNY
184 FORMAT(1H0,10X,*TWISTING MOMENTS (MX+MYX) ( NMM/MM ) FOR PNY *
1*= *,F10.3,* N/MM ARE ---*)
DO 185 II = 2, NPQ
WRITE(6,52) (BMXY(JJ,II),JJ=2,MNO)
185 CONTINUE
WRITE(6,186) PNY
186 FORMAT(1H0,10X,*NODE EFFECTIVE THICKNESSES ( MM ) FOR PNY = *,
1F10.3,* N/MM ARE ---*)
DO 187 II = 2, NPQ
WRITE(6,52) (ET(JJ,II),JJ=2,MNO)
187 CONTINUE
C
C STORE VALUES OF LOAD AND DISPLACEMENT IN CASE OF FAILURE AT NEW LOAD
C
C SPNY=PNY
C STORE VALUES OF PW IN WE FOR EXTRAP AND VALUES OF W IN PW
DO 46 JOP = 2, NPQ
DO 47 IOP = 2, MNO
WE(IOP,JOP)=PW(IOP,JOP)
PW(IOP,JOP)=W(IOP,JOP)
47 CONTINUE
46 CONTINUE
C INCREASE LOAD VALUE PNY
PNY=PNY+DELPNY/MO
C EXTRAPOLATE FOR DISPLACEMENTS AT NEW LOAD PNY
CALL EXTRAP(NPQ,MNO,MO,W,WE,MS)
100 CONTINUE
C
C END OF MAIN ITERATION LOOP
C
C WRITE(6,48)
48 FORMAT(1H0,10X,*FAILURE NOT ATTAINED AFTER 100 ITERATION *
**LOAD INCREMENTS*)
GO TO 150
140 PNY=SPNY
WRITE(6,49) PNY
49 FORMAT(1H1,////10X,*-----*,
1/,20X,*FAILURE LOAD IS *,/
2,25X,F10.3,/,17X,*N/MM LENGTH OF PANEL*,/,
310X,*-----*)
C
C PLOT DISPLACEMENT OF WALL CENTRE NODE
C

```

```

CALL QIKPLOT(PLOT,PLAT,-40,14H*DISPLACEMENT*,6H*LOAD*,-1)
150 CONTINUE
52 FORMAT(1H0,5X,10F12.3)
END
SUBROUTINE PHYSP(NP,MN,XH,ALPHA,UYX,UXY,PNY,T,W,ET,MS,
*PKX,PKY,PKXY,AA,EB,EM,HB,HM,ITYPE)
DIMENSION W(MS,1),ET(MS,1)
DIMENSION AA(4),PKX(MS,1),PKY(MS,1),PKXY(MS,1)
PLX=0.
C
C CALCULATE CURVATURE CURVY AND NEW EFFECTIVE THICKNESS AT ALL NODES
C
DO 10 LF = 3,NP
LR=LF-1 $ LS=LF+1
DO 11 LE = 3,MN
LG=LE-1 $ LH=LE+1
DO 13 LY = 1,10
CURVY=(W(LE,LR)-2.*W(LE,LF)+W(LE,LS))/(XH*ALPHA)**2
*+UYX*(W(LG,LF)-2.*W(LE,LF)+W(LH,LF))/(XH*XH)
ACURVY=ABS(CURVY)
IF(ACURVY.LT.1.0E-50) GO TO 12
PVY=PNY/CURVY
APVY=ABS(PVY)
BPVY=2.*(1.-UXY*UYX)/(PKY(LE,LF)*EB)*APVY
CPVY=SQRT(BPVY)
IF(CPVY.GT.T) CPVY=T
ET(LE,LF)=CPVY
GO TO 16
12 ET(LE,LF)=T
16 CONTINUE
C
C CALCULATE NEW VALUES OF ELASTIC MODULUS FACTORS PKX,PKY AND PKXY
C ( IF REQUIRED )
C
IF(ITYPE.EQ.1) GO TO 11
C ITYPE EQ 1 IMPLIES NO-TENSION MATERIAL
ED=(0.5*T-ET(LE,LF)/3.)/T
IF(ED.LE.1./6.) PLY=1.
IF(ED.LE.1./6.) GO TO 15
ED1=ED $ ED2=ED*ED $ ED3=ED**3
PLY=AA(1)+ED1*AA(2)+ED2*AA(3)+ED3*AA(4)
IF(ABS(PLY-PLX).LE.1.0E-09) GO TO 15
PLX=PLY
13 CONTINUE
WRITE(6,14)
14 FORMAT(1H0,5X,*PKY IS NOT FOUND AFTER 10 ITERATIONS*)
15 PKY(LE,LF)=(HB+HM)/(1./PLY*HB+EB/EM*HM)
PKX(LE,LF)=0.75*(T/ET(LE,LF))**3
PKXY(LE,LF)=0.85*(T/ET(LE,LF))**3
11 CONTINUE
10 CONTINUE
C
C CALCULATE NEW VALUES OF TWIST FACTOR PKXY AT TOP
C AND BOTTOM BOUNDARIES ( IF REQUIRED )
C
IF(ITYPE.EQ.1) GO TO 18

```

```

DO 17 ITW = 3,MN
PKXY(ITW,2)=0.85*(T/ET(ITW,2))**3
PKXY(ITW,NP+1)=0.85*(T/ET(ITW,NP+1))**3
17 CONTINUE
18 CONTINUE
RETURN
END
SUBROUTINE BEND(M,MN,MNO,MNOP,N,NP,NPQ,NPQR,I1,I2,XH,ALPHA,UYX,
*UXY,EX,GXY,EO,T,PNY,W,ET,BMX,BMY,BMXY,MS,PKX,PKY,PKXY,EB,ITYPE)
DIMENSION W(MS,1),ET(MS,1),BMX(MS,1),BMY(MS,1),BMXY(MS,1)
DIMENSION PKX(MS,1),PKY(MS,1),PKXY(MS,1)

```

C  
C  
C

CALCULATE BENDING MOMENTS AT TOP AND BOTTOM BOUNDARIES

C  
C

```

DO 12 IJ = 3,MN
IF(ITYPE.EQ.0) GO TO 17
C ITYPE EQ 0 IMPLIES SOLID PANEL PROBLEM
IF(EO.GT.T/6.) GO TO 13
17 BMY(IJ,2)=BMY(IJ,NPQ)=-PNY*EO
GO TO 14
13 CONTINUE
BMY(IJ,2)=BMY(IJ,NPQ)=-0.5*PNY*(T/2.-EO)
14 CONTINUE

```

C  
C  
C  
C  
C

CALCULATE VALUES OF DISPLACEMENTS OF FICTITIOUS NODES FOR  
CALCULATION OF BMXY TWISTING MOMENTS TOP AND BOTTOM  
( BMXY IS THE \*SUM\* OF TWISTING MOMENTS MXY AND MYX )

```

W(IJ,1)=-W(IJ,3)-BMY(IJ,2)*(XH*ALPHA)**2*(12.*(1.-UXY*UYX))/
*(EB*PKY(IJ,2)*ET(IJ,2)**3)
W(IJ,NPQR)=-W(IJ,NP)-BMY(IJ,NPQ)*(XH*ALPHA)**2
***(12.*(1.-UXY*UYX))/(EB*PKY(IJ,NPQ)*ET(IJ,NPQ)**3)
12 CONTINUE

```

C  
C  
C

CALCULATE BENDING MOMENTS BMX AND BMY AT ALL INTERNAL NODES

C  
C

```

DO 10 NF = 3,NP
NR=NF-1 $ NS=NF+1
DO 11 NE = 3,MN
NG=NE-1 $ NH=NE+1
BY=(W(NE,NR)-2.*W(NE,NF)+W(NE,NS))/(XH*ALPHA)**2
*+UYX*(W(NG,NF)-2.*W(NE,NF)+W(NH,NF))/(XH*XH)
BMY(NE,NF)=-EB*PKY(NE,NF)*ET(NE,NF)**3/(12.*(1.-UXY*UYX))*BY
BX=(W(NG,NF)-2.*W(NE,NF)+W(NH,NF))/(XH*XH)
*+UXY*(W(NE,NR)-2.*W(NE,NF)+W(NE,NS))/(XH*ALPHA)**2
BMX(NE,NF)=-EX*PKX(NE,NF)*ET(NE,NF)**3/(12.*(1.-UXY*UYX))*BX
C CALCULATE TWISTING MOMENTS AT INTERNAL NODE (NE,NF)
C ( BMXY IS THE *SUM* OF TWISTING MOMENTS MXY AND MYX )
BXY=(W(NH,NS)-W(NG,NS)-W(NH,NR)+W(NG,NR))/(4.*ALPHA*XH*XH)
BMXY(NE,NF)=-2.*GXY*PKXY(NE,NF)*ET(NE,NF)**3/6.*BXY
11 CONTINUE
10 CONTINUE

```

C  
C  
C

CALCULATE BENDING MOMENTS BMX AT TOP AND BOTTOM BOUNDARIES

```

DO 18 KL = 3,MN

```

```

BX=UXY*(W(KL,3)+W(KL,1))/(XH*ALPHA)**2
TX=UXY*(W(KL,NP)+W(KL,NPQR))/(XH*ALPHA)**2
BMX(KL,2)=-EX*T**3/(12.*(1.-UXY*UYX))*BX
BMX(KL,NPQ)=-EX*T**3/(12.*(1.-UXY*UYX))*TX
18 CONTINUE
C
C   CALCULATE APPROXIMATE DISPLACEMENTS OF FICTITIOUS CORNER NODES
C
W(1,3)=-W(3,3)
W(MNOP,3)=-W(MN,3)
W(1,NP)=-W(3,NP)
W(MNOP,NP)=-W(MN,NP)
W(1,4)=-W(3,4)
W(MNOP,4)=-W(MN,4)
W(1,N)=-W(3,N)
W(MNOP,N)=-W(MN,N)
I1=1 $ I2=1
CALL CORNER(M,MN,MNO,N,NP,NPQ,I1,I2,W,MS)
I1=MNOP $ I2=1
CALL CORNER(M,MN,MNO,N,NP,NPQ,I1,I2,W,MS)
I1=1 $ I2=NPQR
CALL CORNER(M,MN,MNO,N,NP,NPQ,I1,I2,W,MS)
I1=MNOP $ I2=NPQR
CALL CORNER(M,MN,MNO,N,NP,NPQ,I1,I2,W,MS)
C
C   CALCULATE TWISTING MOMENTS BMXY AT TOP AND BOTTOM BOUNDARIES
C   ( BMXY IS THE *SUM* OF TWISTING MOMENTS MXY AND MYX )
C
DO 15 IK = 2,MNO
IKA=IK-1 $ IKB=IK+1
BXY=(W(IKB,3)-W(IKA,3)-W(IKB,1)+W(IKA,1))/(4.*ALPHA*XH*XH)
TXY=(W(IKB,NPQR)-W(IKA,NPQR)-W(IKB,NP)+W(IKA,NP))/(4.*ALPHA*XH*XH)
BMXY(IK,2)=-2.*GXY*PKXY(IK,2)*ET(IK,2)**3/6.*BXY
BMXY(IK,NPQ)=-2.*GXY*PKXY(IK,NPQ)*ET(IK,NPQ)**3/6.*TXY
15 CONTINUE
C
C   CALCULATE TWISTING MOMENTS BMXY AT VERTICAL SUPPORTS
C   ( BMXY IS THE *SUM* OF TWISTING MOMENTS MXY AND MYX )
C
DO 16 JK = 3,NP
JKA=JK-1 $ JKB=JK+1
VLXY=2.*(W(3,JKB)-W(3,JKA))/(4.*ALPHA*XH*XH)
VRXY=2.*(W(MN,JKA)-W(MN,JKB))/(4.*ALPHA*XH*XH)
BMXY(2,JK)=-2.*GXY*PKXY(2,JK)*ET(2,JK)**3/6.*VLXY
BMXY(MNO,JK)=-2.*GXY*PKXY(MNO,JK)*ET(MNO,JK)**3/6.*VRXY
16 CONTINUE
RETURN
END
SUBROUTINE ERROR(NP,MN,XH,ALPHA,Q,PNY,W,ET,BMX,BMY,BMXY,RR,MS
1,ITYPE)
DIMENSION W(MS,1),ET(MS,1),BMX(MS,1),BMY(MS,1),BMXY(MS,1),RR(1)
C
C   CALCULATE ERROR TERM AT ALL INTERNAL NODES
C
KX=0
DO 10 LB = 3,NP

```

```

      LA=LB-1 $ LC=LB+1
      DO 11 KB = 3,MN
      KA=KB-1 $ KC=KB+1
      KX=KX+1
C
C   CALCULATE ELEMENTS OF ERROR TERM SEPARATELY
C
C   D2MXDX2
      DMX=(BMX(KA, LB)-2.*BMX(KB, LB)+BMX(KC, LB))/(XH*XH)
C
C   D2MYDY2
      DMY=(BMY(KB, LA)-2.*BMY(KB, LB)+BMY(KB, LC))/(XH*ALPHA)**2
C
C   D2(MXY+MYX)DXDY
      DMXY=(BMXY(KC, LC)-BMXY(KA, LC)-BMXY(KC, LA)+BMXY(KA, LA))/
      *(4.*ALPHA*XH*XH)
C
C   D2WBARDY2
      DWBAR=(W(KB, LA)-2.*W(KB, LB)+W(KB, LC)+0.5*(ET(KB, LA)-2.*ET(KB, LB)
      *+ET(KB, LC)))/(XH*ALPHA)**2
C
C   COMBINE TERMS TO GIVE TOTAL ERROR TERM
C
      RR(KX)=DMX+DMXY+DMY+Q+PNY*DWBAR
11 CONTINUE
10 CONTINUE
      RETURN
      END
      SUBROUTINE EXTRAP(NPQ,MNO,MO,W,WE,MS)
      DIMENSION W(MS, 1),WE(MS, 1)
C
C   EXTRAPOLATE ON ALL DISPLACEMENTS IN ARRAY W
C
      DO 10 KD = 2, NPQ
      DO 11 KC = 2, MNO
      IF(W(KC, KD).EQ.0.) GO TO 12
      WMULT=1.+(1.-WE(KC, KD)/W(KC, KD))/MO
      W(KC, KD)=W(KC, KD)*WMULT
      GO TO 11
12 W(KC, KD)=-WE(KC, KD)/MO
11 CONTINUE
10 CONTINUE
      RETURN
      END
      SUBROUTINE MINV(A,AINV,MNT)
      DIMENSION A(MNT, 1),AINV(MNT, 1)
C
C   MATRIX INVERSION BY GAUSS-JORDAN METHOD ( AFTER P. C. WANG )
C
      DO 10 I = 1, MNT
      DO 10 J = 1, MNT
      AINV(I, J)=0.

```



```

      IF(I.EQ.J) AINV(I,J)=1.0
10  CONTINUE
      EPS=1.0E-08
      DO 12 I = 1,MNT
        K=I
        IF(I-MNT) 13,14,13
13  IF(A(I,I)-EPS) 16,17,14
16  IF(-A(I,I)-EPS) 17,17,14
17  K=K+1
      DO 18 J = 1,MNT
        AINV(I,J)=AINV(I,J)+AINV(K,J)
18  A(I,J)=A(I,J)+A(K,J)
      GO TO 13
14  DIV=A(I,I)
      DO 19 J=1,MNT
        AINV(I,J)=AINV(I,J)/DIV
19  A(I,J)=A(I,J)/DIV
      DO 12 MM = 1,MNT
        DELT=A(MM,I)
        IF(ABS(DELT)-EPS) 12,12,20
20  IF(MM-I) 21,12,21
21  DO 22 J = 1,MNT
        AINV(MM,J)=AINV(MM,J)-AINV(I,J)*DELT
22  A(MM,J)=A(MM,J)-A(I,J)*DELT
12  CONTINUE
      RETURN
      END
      SUBROUTINE CORNER(M,MN,MNO,N,NP,NPQ,I1,I2,W,MS)
      DIMENSION W(MS,1)

```

C  
C  
C

CALCULATE DISPLACEMENTS OF FICTITIOUS CORNER NODES

```

      IF(I1.EQ.1) GO TO 10
      NO=M $ N1=MN $ N2=MNO
      GO TO 11
10  NO=4 $ N1=3 $ N2=2
11  CONTINUE
      W1=W(NO,I2)-3.*W(N1,I2)+3.*W(N2,I2)
      IF(I2.EQ.1) GO TO 12
      LO=N $ L1=NP $ L2=NPQ
      GO TO 13
12  LO=4 $ L1=3 $ L2=2
13  CONTINUE
      W2=W(I1,LO)-3.*W(I1,L1)+3.*W(I1,L2)
      W(I1,I2)=0.5*(W1+W2)
      RETURN
      END
      SUBROUTINE MATFAIL(MNO,NPQ,T,SIGT,IFAIL,PNY,CMFAIL,EO,
1BMX,BMY,BMXY,ET,MS)
      DIMENSION BMX(MS,1),BMY(MS,1),BMXY(MS,1),ET(MS,1)

```

C  
C  
C  
C  
C  
C

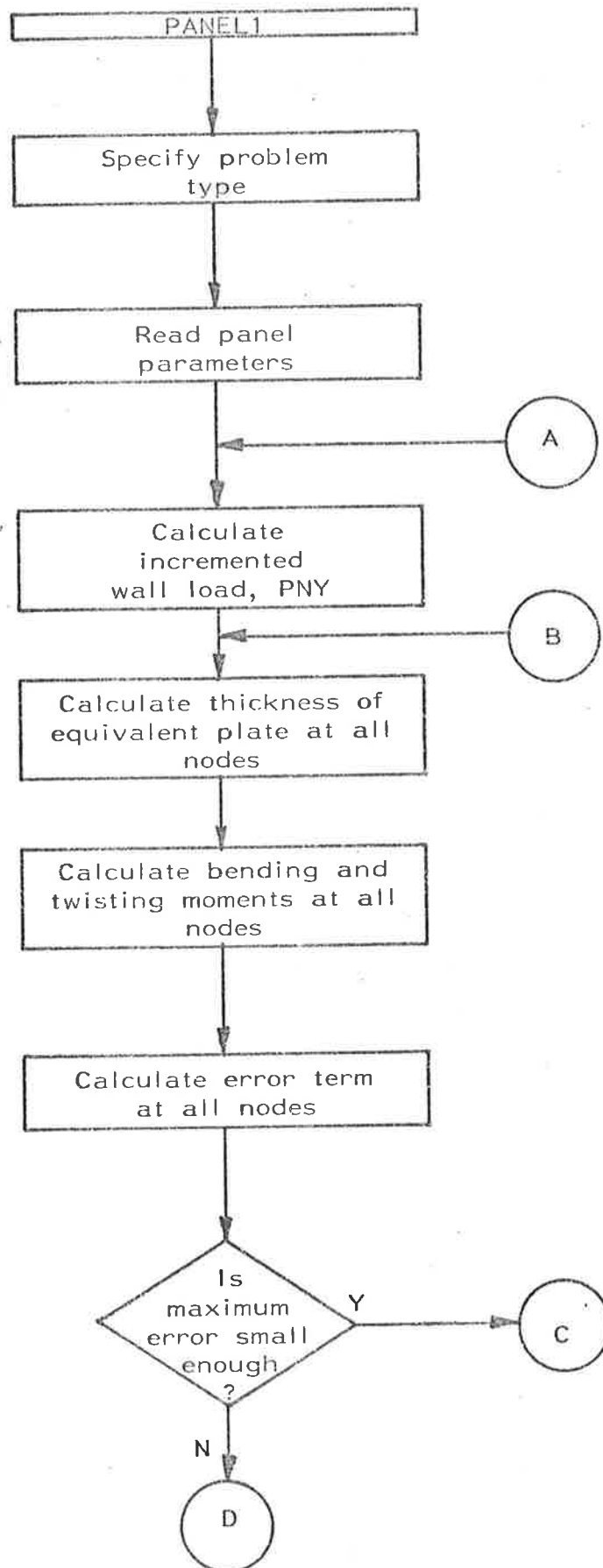
THIS SUBROUTINE CHECKS FOR MATERIAL FAILURE IN ANY OF THREE MODES ---  
 1. TENSILE FAILURE IN BRICKWORK DUE TO BENDING X-X  
 2. VERTICAL SPLITTING FAILURE ---THE COMPRESSIVE STRENGTH  
 OF THE BRICKWORK MUST BE KNOWN OR ASSUMED. LINEAR MATERIAL  
 ELASTIC PROPERTIES ARE ASSUMED.

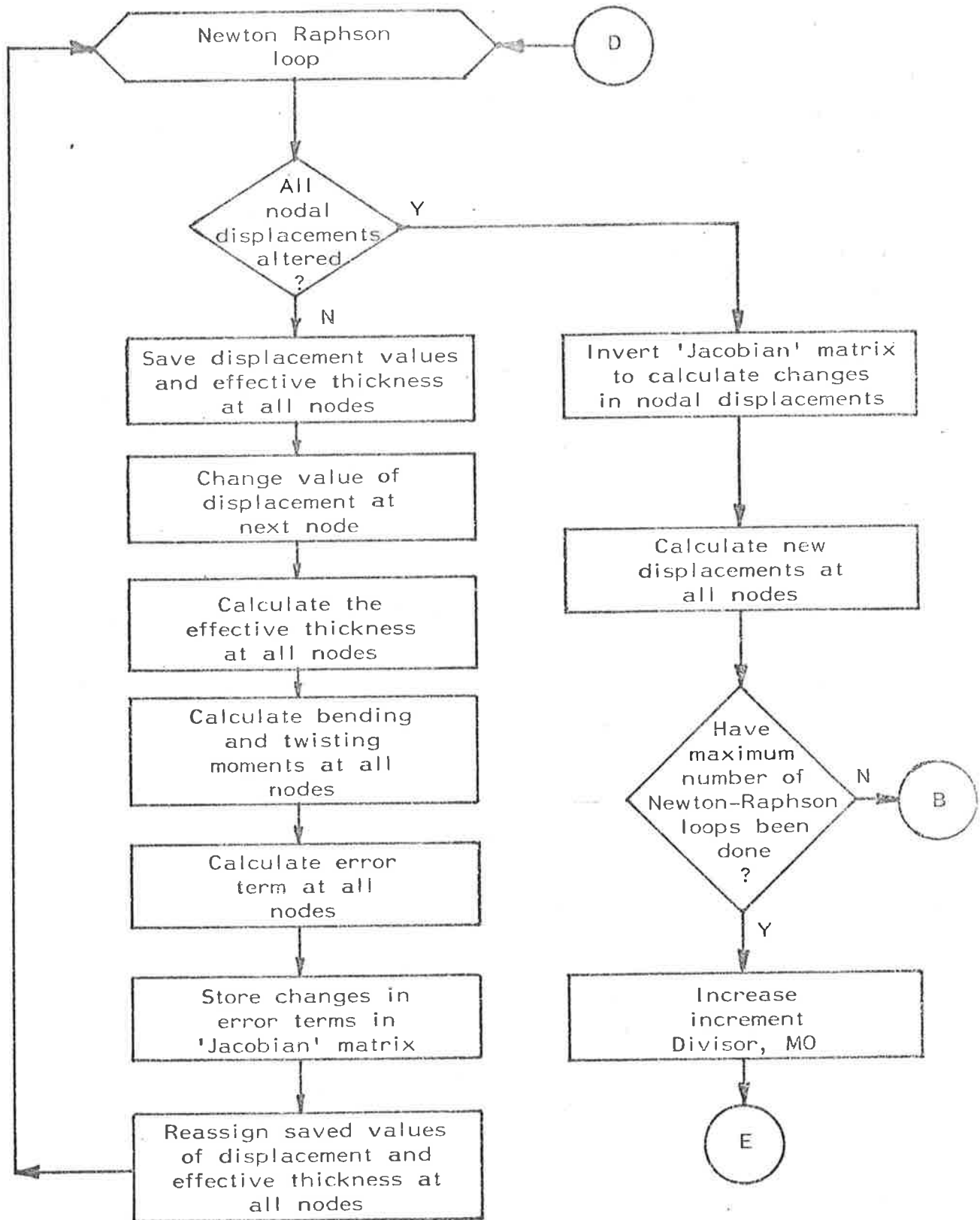
```

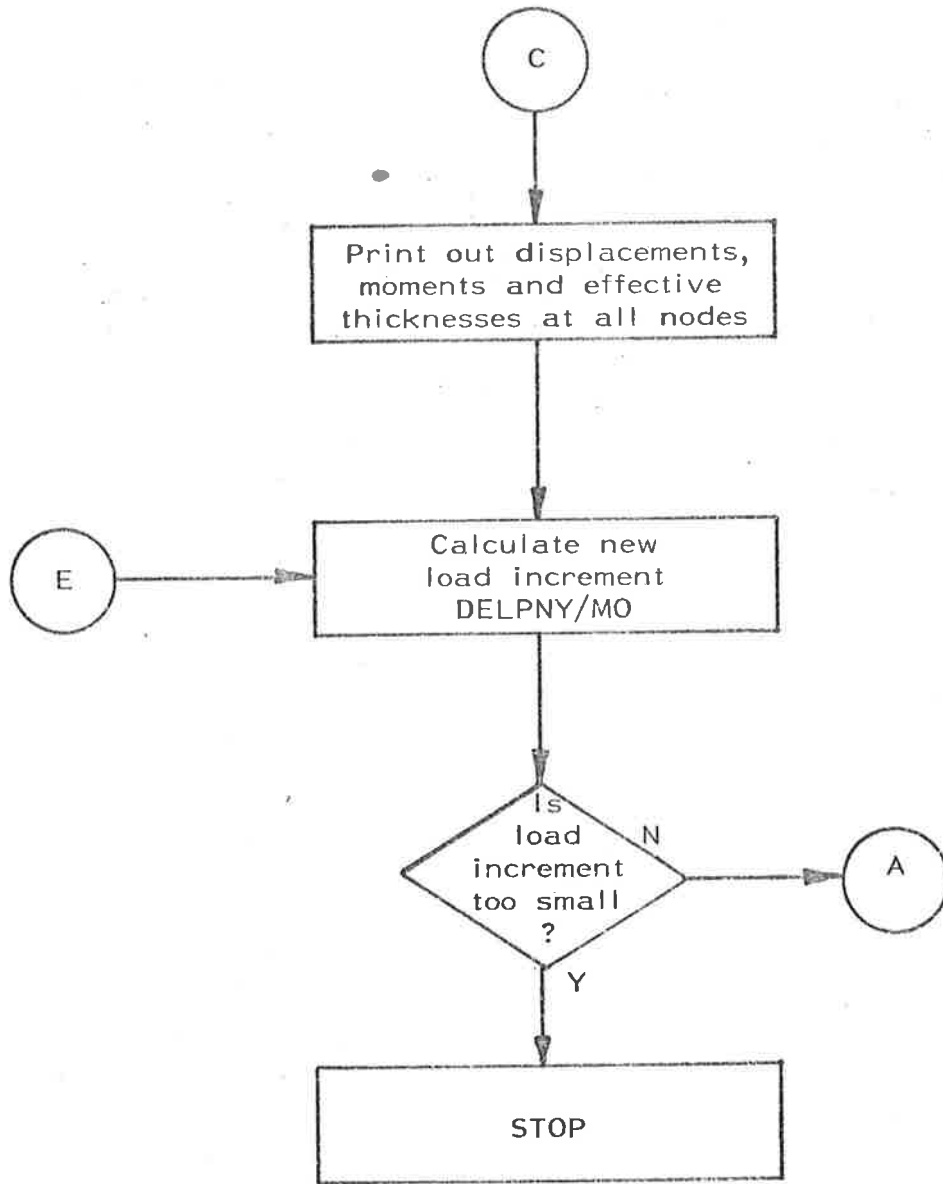
C      3.  TENSILE FAILURE AT 45 DEGREES TO THE BEDJOINTS ---- A CHECK
C          IS MADE AT AN INTERNAL NODE CLOSEST TO A PANEL CORNER
C
C
C      MODE 1.---CHECK FOR TENSILE FAILURE DUE TO BENDING X-X
C
C          DO 10 I = 2,MNO
C          DO 11 J = 2, NPQ
C          SIGX=BMX(I,J)*6./(T*T)
C          IF(SIGX.GE.0.75*SIGT) IFAIL=1
11 CONTINUE
10 CONTINUE
C
C      MODE 2.---CHECK FOR VERTICAL SPLITTING FAILURE
C
C          DO 12 I = 2,MNO
C          DO 13 J = 2, NPQ
C          IF(ET(I,J).LT.T) GO TO 14
C          SIGY=-PNY/T+6.*BMY(I,J)/(T*T)
C          GO TO 15
14 SIGY=-2.*PNY/ET(I,J)
15 CONTINUE
C          IF(SIGY.GE.CMFAIL) IFAIL=2
13 CONTINUE
12 CONTINUE
C
C      MODE 3.---CHECK FOR TENSILE FAILURE AT 45 DEGREES TO THE BEDJOINTS
C
C          SIGXY=PNY/(2.*T)*(1.-6.*EO/T)+3./(T*T)*ABS(BMXY(3,3))
C          IF(SIGXY.GE.SIGT) IFAIL=3
C
C      MATERIAL FAILURE FLAG IFAIL IS NOW SET
C
C          RETURN
C          END

```

## G.3 SKELETON FLOW CHART FOR PROGRAM PANEL1







### BIBLIOGRAPHY

1. FITCHEN, J., The Construction of Gothic Cathedrals, Oxford, 1961.
2. HEYMAN, J., "The Stone Skeleton", Int. Journal Solids Structures, 1966, Vol. 2, pp. 249-279.
3. de COULOMB, C.A., "Essai sur une application des règles de maximis et minimis à quelques problèmes de statique, relatifs à l'architecture", Memoires de Mathématique et de Physique présentés à l'Academie Royale des Sciences, p. 343, 1773.
4. AS6140-1974 SAA Brickwork Code, Standards Association of Australia.
5. FRANCIS, A.J., "The SAA Brickwork Code: The Research Background", Civ. Eng. Trans. Inst. Eng. Aust., Oct. 1969, Vol. C.E.11, No. 2, pp. 165-176.
6. HALLER, P., "The Technological Properties of Brick Masonry in High Buildings", Schweizerische Bauzeitung, Vol. 76, No. 28, 1958, pp. 411-419 (Technical Translation 792, National Research Council of Canada, Ottawa, 1959).
7. HALLER, P., "Load Capacity of Brick Masonry", Proc. Int. Conf. on Masonry Structural Systems, Austin, Texas, 1967.
8. HALLQUIST, A., "Lateral Loads on Masonry Walls", Reprint 172, Norwegian Building Research Institute, 1970.
9. HENDRY, A.W., "The Lateral Strength of Unreinforced Brickwork", The Structural Engineer, Feb. 1973, No. 2, Vol. 51, pp. 43-51.
10. SATTI, K.M.H., Model Brickwork Wall Panels Under Lateral Loading", Ph.D. Thesis, Edinburgh, 1972.
11. BAKER, L.R., "Structural Action of Brickwork Panels Subjected to Wind Loads", Journal of the Aust. Ceram. Soc., Vol. 9, No. 1, May 1973.

12. LAWRENCE, S.J. and MORGAN, J.W., "Investigations of the Properties of Small Brickwork Panels in Lateral Bending", E.B.S. Dept. of Housing and Construction, Technical Record TR/52/75/418 Sydney, Australia, 1975.
13. BRADSHAW, R.E. and ENTWISLE, F.D., "Wind Forces on Non-loadbearing Brickwork Panels", CPTB Technical Note, Vol. 1, No. 6, May 1965.
14. WEST, H.W.H., HODGKINSON, H.R., and WEBB, W.F., "The Resistance of Clay Brick Walls to Lateral Loading", Proc. Fourth Symposium on Loadbearing Brickwork, Brit. Ceram. Soc., 1971.
15. MORTON, J. and HENDRY, A.W., "A Theoretical Investigation of the Strength of Brick Walls with Precompression", Proc. Fourth Symposium on Loadbearing Brickwork, Brit. Ceram. Soc., 1971.
16. HENDRY, A.W., "Wind Load Analysis of Multi-Storey Brickwork Structures", B.D.A. Research Note, Vol. 1, No. 3, Jan. 1971.
17. LEUNG, Y.T. and CHEUNG, Y.K., "A New Frame Super-element in Static and Dynamic Analysis", Seventh Australasian Conference on the Mechanics of Structures and Materials, Univ. Western Aust., May 1980.
18. THOMAS, K., "Essex University. Construction of Tower Blocks in Calculated Loadbearing Brickwork", CPTB Technical Note, Vol. 1, No. 12, Jan. 1967.
19. SOANE, A.J.M., "Model Analysis of Essex University Tower Block", CPTB Technical Note, Vol. 1, No. 1, Jan. 1967.
20. KRANTZ, D., Calculated Brick Bearing Wall Construction - What? Why? How?, Advance Press, Perth, W.A., 1968.
21. HENDRY, A.W., "Summary of Research and Design Philosophy for Bearing Wall Structures", Journal of the American Concrete Institute, June 1979, No. 6, Proc. V76, pp. 723-737.

22. MORTON, J. and HENDRY, A.W., "A Theoretical Investigation of the Lateral Strength of Brick Walls with Precompression", Proc. Brit. Ceram. Soc., No. 21, 1974, pp. 181-194.
23. SUTHERLAND, R.J.M., "Stability of Masonry Structures", Proc. Second Canadian Masonry Symposium, Ottawa, Canada, 1980, pp. 197-219.
24. "Code of Practice for Structural Use of Masonry, Part 1. Unreinforced Masonry", B.S. 5628: Part 1: 1978, British Standards Institution, London, 1978.
25. BUBB, C.T.J., "Introduction to the Draft Code for the Design of Earthquake Resistant Buildings", National Committee on Earthquake Engineering, Seminars on Earthquake Engineering, Standards Association of Australia, 1974.
26. AS2121-1979, SAA Earthquake Code, Standards Association of Australia.
27. KATEIVA, G.A., "The Effects of the Meckering Earthquake on Engineered Brick Structures in Perth, Western Australia", SIBMAC Proc., Stoke-on-Trent, England, 1970, pp. 365-368.
28. MAYES, R.L. and CLOUGH, R.W., "A Literature Survey - Compressive, Tensile, Bond and Shear Strength of Masonry", Earthquake Engineering Research Center, University of California, 1975.
29. PLUMMER, H.C. and BLUME, J.A., Reinforced Brick Masonry and Lateral Force Design, Structural Clay Products Institute, Washington, D.C., 1953.
30. DAVEY, N. and THOMAS, F.G., "The Structural Uses of Brickwork", Inst. Civil Engineers, Structural and Building Engineering Division, Paper No. 24, 1950.
31. PAGE, A.W., "Structural Brickwork - a Literature Review", Engineering Bulletin CE4 1973, University of Newcastle, N.S.W. Australia.



32. AS1225-1980, "Burnt Clay and Shale Building Bricks", Standards Association of Australia.
33. AS1653-1974, "Calcium Silicate Bricks", Standards Association of Australia.
34. AS1346-1974, "Concrete Building Bricks", Standards Association of Australia.
35. AS1226-1980, "Methods of Sampling and Testing Burnt Clay and Shale Building Bricks", Standards Association of Australia.
36. GRIMM, C.T., "Strength and Related Properties of Brick Masonry", Journal of the Structural Division ASCE, ST 1, January 1975, pp. 217-232.
37. GRENLEY, D.G., CATTANEO, L.E. and PFRANG, E.O., "Effect of Edge Load on Flexural Strength of Clay Masonry Systems Utilizing Improved Mortars", Proc. Int. Conf. on Masonry Structural Systems, Austin, Texas, 1967.
38. BAKER, I.O., A Treatise on Masonry Construction, John Wiley and Sons, New York, 1909.
39. McBURNEY, J.W. and LOVEWELL, C.E., "Strength, Water Absorption and Weather Resistance of Building Bricks Produced in the United States", Proc. ASTM, Vol. 33, Part II, 1933.
40. MONK, C.B., "A Historical Survey and Analysis of the Compressive Strength of Brick Masonry", Structural Clay Products Research Foundation, Research Report No. 2, Geneva, Ill., 1967.
41. SCHELLBACH, G., "The Influence of Perforation on the Load-bearing Capacity of Hollow Brick Masonry Structures", SIBMAC Proceedings, British Ceramic Research Association, Stoke-on-Trent, England, 1971, p. 50.
42. WEST, H.W.H., HODGKINSON, H.R. and DAVENPORT, S.T.E., "The Performance of Walls built of Wire Cut Bricks With and Without Perforations", British Ceramic Research Association, Special Publication No. 60, 1968.

43. BS 3921: 1965, "Bricks and Blocks of Fired Brickearth, Clay or Shale", British Standards Institution.
44. SAHLIN, S., Structural Masonry, Prentice-Hall, Inc., 1971.
45. NEVANDER, L.E., Provningar av Tegelmurverk (Tests on Brick Walls), Tegel, No. 5, Stockholm, 1954.
46. HILSDORF, H.K., "Untersuchungen über die Grundlagen der Mauerwerksfestigkeit", Bericht Nr. 40, Materialprüfungsamt für das Bauwesen der Technischen Hochschule, München, 1965.
47. "Compressive, Transverse and Racking Strength Tests of Four-inch Brick Walls, Structural Clay Products Research Foundation, Research Report No. 9, Geneva, Ill., 1965.
48. GLANVILLE, W.H. and BARNETT, P.W., "Mechanical Properties of Bricks and Brickwork Masonry", Dept. Scientific and Industrial Research Building Research, Special Report No. 22, H.M. Stationery Office, London, 1934.
49. PSALTIS, P.G., Variations in Properties of Bricks, Undergraduate Report, University of Newcastle, 1977 (unpublished).
50. SCRIVENER, J.C. and WILLIAMS, D., "Compressive Behaviour of Masonry Prisms", Proc. 3rd Australasian Conference on the Mechanics of Structures and Materials, University of Auckland, August 1971.
51. PLOWMAN, J.M., "The Modulus of Elasticity of Brickwork", Proc. British Ceramic Society, No. 4, Stoke-on-Trent, England, 1965, pp. 37-44.
52. AS A123-1963, "Mortar for Masonry Construction", Standards Association of Australia.
53. AS1465-1974, "Dense Natural Aggregates for Concrete", Standards Association of Australia.
54. Clay Products No. 4, Feb. 1964 - Mortar for Bricklaying, Brick Development Research Institute, Melbourne, Australia.

55. American Society for Testing Materials. Part 9: "Cement; Lime; Gypsum", Book of ASTM Standards, 1967.
56. BS 822, 1201: 1965, "Specification for Aggregates from Natural Sources for Concrete (including Granolithic)", British Standards Institution.
57. AS1315-1974, "Portland Cement", Standards Association of Australia.
58. AS1672-1974, "Building Limes", Standards Association of Australia.
59. American Society for Testing Materials, 1973, C91, "Specifications for Masonry Cement".
60. ISBERNER, A.W., "Properties of Masonry Cement Mortars", Proc. Int. Conf. on Masonry Structural Systems, ICMSS, Austin, Texas, 1967.
61. HOGBERG, E., "Mortar Bond", National Swedish Institute for Building Research, Report No. 40, Stockholm, 1967.
62. PALMER, L.A. and PARSONS, D.A., "Permeability Tests of 8-in. Brick Wallethes", ASTM Proceedings, Vol. 34, Part II, p. 419, Washington, 1934.
63. HOATH, S.B.A., LEE, H.N. and RENTON, K.H., "The Effect of Mortars on the Strength of Brickwork Cubes", Proc. SIBMAC, Stoke-on-Trent, England, 1970.
64. RITCHIE, T. and DAVISON, J.I., "Cement-Lime Mortars", Building Research, Ottawa, Technical Paper (183), 10, 1964.
65. American Society for Testing Materials, "Mortars for Unit Masonry", C270-68, 1968.
66. "Methods of Testing Mortars", 8th Draft 68/3502, 1968.; British Standards Institution.

67. GILLARD, R. and LEE, H.N., "Testing of Building Mortars Using the New British Standard Methods", Proc. ASTM Symposium, Atlantic City, N.J., 1969.
68. LENCZNER, D., "Strength and Elastic Properties of the 9-in. Brickwork Cube", Trans. British Ceramic Society, Vol. 65, 1966, pp. 363-382.
69. BASE, G.D. and BAKER, L.R., "Fundamental Properties of Structural Brickwork", Journal of the Aust. Ceramic Society, Vol. 9, No. 1, May 1973.
70. "Compressive and Transverse Strength Tests for Eight-inch Brick Walls", Structural Clay Products Research Foundation, Research Report No. 10, Geneva, Ill., 1966.
71. "Compressive and Transverse Strength of Five-inch Brick Walls", Structural Clay Products Research Foundation, Research Report No. 8, Geneva, Ill., 1965
72. STANG, A.H., PARSONS, D.E. and McBURNEY, J.W., "Compressive Strength of Clay Brick Walls", U.S. Bureau of Standards, Journal of Research 1929, Vol. 3, No. 4, pp. 507-571 (Research Report No. 108).
73. BASE, G.D., "Compression Tests on Six Single-leaf Brick Walls", University of Melbourne, Department of Civil Engineering, Report of Investigation No. ST 78/66, April 1968.
74. ANDERSON, G.W., "Stack-bonded Small Specimens as Design and Construction Criteria", Proc. SIBMAC, Stoke-on-Trent, England, 1970.
75. BROCKER, O., "Steinfestigkeit und Wandfestigkeit", Betonstein-Zeitung 27, Heft 3, p. 120, 1961.
76. American Society for Testing and Materials 1973, C67, Sampling and Testing Brick, Part 12.

77. HILSDORF, H.K., "Investigation into the Failure Mechanism of Brick Masonry in Axial Compression", Proc. Int. Conf. on Masonry Structural Systems, Austin, Texas, 1967.
78. FRANCIS, A.J., HORMAN, C.B. and JERREMS, L.E., "The Effect of Joint Thickness and Other Factors on the Compressive Strength of Brickwork", Proc. SIBMAC, Stoke-on-Trent, England, 1970.
79. DAVIS, R.E., "Report of Masonry Tests - 1929 Series", Clay Products Institute, 1930, unpublished (Reference No. 29, p. 40).
80. SINHA, B.P. and HENDRY, A.W., "The Effect of Brickwork Bond on the Loadbearing Capacity of Brick Walls", Proc. Brit. Ceram. Soc., No. 11, July, 1965.
81. RICHART, F.E., BRANDTZAEG, A. and BROWN, R.L., "A Study of the Failure of Concrete under Combined Compressive Stresses", Bulletin 185, University of Illinois, Engineering Experiment Station, 1928.
82. American Society for Testing Materials, 1973, E149, Test for Bond Strength of Mortar to Masonry Units.
83. YOUL, V.A. and FOSTER, P.K., "Miniature Tensile and Panel Flexure Properties of Brickwork", Proc. Int. Conf. on Masonry Structural Systems, Austin, Texas, 1967.
84. PLUMMER, H.C. and REARDON, L.J., Principles of Brick Engineering, Handbook of Design, Structural Clay Products Institute, Washington, D.C., 1939.
85. SINHA, B.P. and HENDRY, A.W., "Further Investigations of Bond Tension, Bond Shear and the Effect of Precompression on the Shear Strength of Model Brick Masonry Couplets", Brit. Ceram. Research Assoc., Tech. Note No. 80, 1966.
86. MURTHY, C.K. and HENDRY, A.W., "Preliminary Investigations of the Shear Strength of one-sixth scale Model Brickwork", Brit. Ceram. Research Assoc., Technical Note No. 65, Feb. 1965.

87. HAMID, A.A. and DRYSDALE, R.G., "Behaviour of Brick Masonry under Combined Shear and Compression Loading", Proc. Second Canadian Masonry Symposium, Ottawa, Canada, 1980.
88. ROYEN, N., "Dimensionering av Murar med hänsyn tagen till Friktion och Vidhäftning" (Design of Masonry Walls, Accounting for Friction and Bond), Häfte 9, Byggmästaren, Stockholm, 1936.
89. TIMOSHENKO, S., Strength of Materials, McGraw-Hill Book Co., New York, 3rd Edition, 1955.
90. BAKER, L.R., "Lateral Loading of Masonry Panels", Structural Design of Masonry, Clay and Concrete, Cement and Concrete Assoc., Australia, 1980.
91. LAWRENCE, S.J., "Flexural Strength of Brickwork Normal to and Parallel to the Bed Joints", Journal of the Aust. Ceram. Soc., Vol. 11, No. 1, pp.5-6, May 1975.
92. POLYAKOV, S.V., "Masonry in Framed Buildings", Gosudatst Vennse Izdatel' stvo Literature po Straitel 'stvu' i Arkhitekture", Moscow, 1956. (Translated by Building Research Station and Published by National Lending Library for Science and Technology, Boston Spa, England).
93. POWELL, B. and HODGKINSON, H.R., "The Determination of Stress/Strain Relationship for Brickwork", Proc. Fourth Int. Brick Masonry Conference, Brugge, 1976.
94. WATSTEIN, D. and ALLEN, M.H., "Structural Performance of Clay Masonry Assemblages Built with High-bond Organic-Modified Mortars", Proc. SIBMAC, Stoke-on-Trent, England, 1970.
95. PAGE, A.W., "A Model for the In-plane Deformation and Failure of Brickwork", Engineering Bulletin CE8, March 1978, University of Newcastle, N.S.W., Australia.

96. ANGERVO, K., "Über die Knickung und Tragfähigkeit eines excentrisch Pfeilers ohne Zugfestigkeit" (On the Buckling and Bearing Capacity of an Eccentrically Compressed Pillar without Tensile Strength), Staatliche Technische Forschungsanstalt Finnland; Publication 26, Helsinki, 1954.
97. CHAPMAN, J.C. and SLATFORD, J., "The Elastic Buckling of Brittle Columns", Proc. Inst. Civ. Eng., Vol. 107, No. 6, 1957. (Paper No. 6147, 1956.)
98. YOKEL, F.Y., "Stability and Load Capacity of Members with No Tensile Strength", Proc. ASCE Structural Division, Vol. 97, ST7, July 1971, pp. 1913-1926.
99. FRISCH-FAY, R., "Stability of Masonry Piers", Int. Journal Solids Structures, Vol. 11, 1975.
100. FRISCH-FAY, R., "Stability Functions for Structural Masonry", Int. Journal Solids Structures, Vol. 13, 1977, pp. 381-393.
101. CHEN, W.F. and ATSUTA, T., "Strength of Eccentrically Loaded Walls", Int. Journal Solids Structures, Vol. 9, 1973, pp. 1283-1300.
102. MONK, C.B., "Column Action of Clay Masonry Walls", Proc. Int. Conf. on Masonry Structural Systems, Austin, Texas, 1967.
103. RISAGER, S., "The Buckling Load of Linear Elastic Walls without Tensile Strength", Proc. SIBMAC, Stoke-on-Trent, England, 1970.
104. TESHAYE, E. and BROOME, T.H., "Effect of Weight on Stability of Masonry Walls", Journal ASCE Structural Division, Vol. 103, No. ST5, May 1977, pp. 961-970.
105. CRANSTON, W.B. and ROBERTS, J.J., "The Structural Behaviour of Concrete Masonry - Reinforced and Unreinforced", The Structural Engineer, Vol. 11, No. 54, November 1976, pp. 423-436.

106. CONTALDO, M., FAELLA, C. and MAZZOLANI, P.M., "The Numerical Simulation for the Prevision of the Load-carrying Capacity of Masonry Structures", Proc. VIBMAC, Washington, D.C., 1979.
107. JAMES, J.A., "Eccentrically Loaded Single-leaf Storey-height Walls", Building Development Laboratories Ltd., Report No. W/BDRI/1, June 1975, Perth, Australia.
108. JAMES, J.A., "Eccentrically Loaded Single-leaf Storey-height Walls - Stage 2", Building Development Laboratories Ltd., Report No. W/BDRI/2, August 1976, Perth, Australia.
109. JAMES, J.A., "Eccentrically Loaded Single-leaf Storey-height Walls - Stage 3", Building Development Laboratories Ltd., Report No. W/BDRI/3, November 1977, Perth, Australia.
110. MARTIN, R.H. and NETTLE, R., "Axial and Flexural Strength of Slender Brick Walls", Civil Engineering Dept., University of Adelaide, 1974 (unpublished).
111. HENDRY, A.W., "Workmanship Factors in Brickwork Strength", B.D.A. Technical Note, Vol. 1, No. 6, November 1972.
112. TIMOSHENKO, S.P. and WOINOWSKY-KRIEGER, S., "Theory of Plates and Shells", Second Edition, McGraw-Hill, 1959.
113. OLSSON, R.G., "Beigung der Richteckplatte bei linear veränderlicher Beigungsteifigkeit", Ing. Arch., Vol. 5, 1934, p. 363.
114. NAKAGAWA, K., "Note on the Bending of Rectangular Plates with Variable Thickness", Transactions of JSCE, Applied Mechanics and Structure Engineering Division, Vol. 8, 1976, pp. 37, 38.
115. SINHA, B.P. and HENDRY, A.W., "Compressive Strength of Axially Loaded Brick Walls Stiffened along their Vertical Edges", Proc. VIBMAC, Washington, D.C., 1979.



116. BUSHNELL, S.D. and MIDDLEMIS, H., "Lateral Bending Effects in Brick Wall Panels", Civil Engineering Dept., University of Adelaide, 1980 (unpublished).
117. KHOO, C.L. and HENDRY, A.W., "A Failure Criterion for Brickwork in Axial Compression", Proc. Third International Brick Masonry Conference (L. Foertig, K. Gobel ed.) Essen, 1973, pp.139-145.
118. KHOO, C.L. and HENDRY, A.W., "Strength Tests on Brick and Mortar under Complex Stresses for the Development of a Failure Criterion for Brickwork in Compression", Proc. British Ceramic Society, Vol. 21, 1973, pp 57-66.
119. KHOO, C.L., A Failure Criterion for Brickwork in Axial Compression, Ph.D. Thesis, University of Edinburgh, 1972.
120. HENDRY, A.W., Structural Brickwork, The Macmillan Press Ltd., London, 1981.
121. LAWRENCE, S.J., "The Flexural Behaviour of Brickwork", Proceedings of the North American Masonry Conference, Boulder, Colorado, August 1978.
122. WEST, H.W.H., "The Flexural Strength of Clay Masonry determined from Wallethe Specimens", Proc. Fourth International Brick Masonry Conference, Brugge, 1976, Paper 4.a.6.
123. HASAN, S.S. and HENDRY, A.W., "Effect of Slenderness and Eccentricity on the Compressive Strength of Walls", Proc. Fourth International Brick Masonry Conference, Brugge, 1976, Paper 4.d.3.
124. PAYNE, D.C., SVED, G. and BROOKS, D.S., "Numerical Analysis of Brick Columns Subject to Axial and Lateral Loads", Proc. Seventh Australasian Conference on the Mechanics of Structures and Materials, Perth, Aust., May 1980.
125. Analysis Civil Engineering Structures (ACES), South Australian Public Service, Adelaide, Aust., 1979.

126. CHEUNG, Y.K. and YEO, M.F., A Practical Introduction to Finite Element Analysis, Pitman Publishing Ltd., 1979.
127. Recommended Practice for Engineered Brick Masonry, Structural Clay Products Institute, Maclean, Virginia, 1969.